

1258519

THE UNITED STATES OF AMERICA

TO ALL TO WHOM THESE PRESENTS SHALL COME:

UNITED STATES DEPARTMENT OF COMMERCE

United States Patent and Trademark Office

December 09, 2004

THIS IS TO CERTIFY THAT ANNEXED HERETO IS A TRUE COPY FROM THE RECORDS OF THE UNITED STATES PATENT AND TRADEMARK OFFICE OF THOSE PAPERS OF THE BELOW IDENTIFIED PATENT APPLICATION THAT MET THE REQUIREMENTS TO BE GRANTED A FILING DATE.

APPLICATION NUMBER: 60/519,681

FILING DATE: *November 13, 2003*

RELATED PCT APPLICATION NUMBER: PCT/US04/33089

Certified by



Jon W Dudas

Acting Under Secretary of Commerce
for Intellectual Property
and Acting Director of the U.S.
Patent and Trademark Office

BEST AVAILABLE COPY

PROVISIONAL APPLICATION FOR PATENT COVER SHEET

This is a request for filing a PROVISIONAL APPLICATION FOR PATENT under 37 CFR 1.53(c).

Express Mail Label No. ET730094938US

INVENTOR(S)					
Given Name (first and middle (if any))		Family Name or Surname		Residence (City and either State or Foreign Country)	
Michael E. Gordon P.		Nanna Bierwagen		Moorhead, Minnesota Fargo, North Dakota	
<input type="checkbox"/> Additional inventors are being named on the _____ separately numbered sheets attached hereto					
TITLE OF THE INVENTION (500 characters max)					
COATING SYSTEMS					
Direct all correspondence to: CORRESPONDENCE ADDRESS					
<input type="checkbox"/> Customer Number <input type="text"/>					
OR					
<input checked="" type="checkbox"/> Firm or Individual Name		Peter Rogalskyj, Esq.			
Address		Rogalskyj & Weyand, LLP			
Address		P.O. Box 44			
City		Livonia	State	New York	ZIP 14487-0044
Country		United States	Telephone	585-346-1004	Fax 585-346-1001
ENCLOSED APPLICATION PARTS (check all that apply)					
<input checked="" type="checkbox"/> Specification		Number of Pages 810		<input type="checkbox"/> CD(s), Number <input type="text"/>	
<input type="checkbox"/> Drawing(s)		Number of Sheets <input type="text"/>		<input type="checkbox"/> Other (specify) <input type="text"/>	
<input type="checkbox"/> Application Data Sheet. See 37 CFR 1.76					
METHOD OF PAYMENT OF FILING FEES FOR THIS PROVISIONAL APPLICATION FOR PATENT					
<input checked="" type="checkbox"/> Applicant claims small entity status. See 37 CFR 1.27.				FILING FEE AMOUNT (\$)	
<input type="checkbox"/> A check or money order is enclosed to cover the filing fees					
<input checked="" type="checkbox"/> The Director is hereby authorized to charge filing fees or credit any overpayment to Deposit Account Number 50-0772				\$80.00	
<input type="checkbox"/> Payment by credit card. Form PTO-2038 is attached.					
The invention was made by an agency of the United States Government or under a contract with an agency of the United States Government.					
<input type="checkbox"/> No.					
<input checked="" type="checkbox"/> Yes, the name of the U.S. Government agency and the Government contract number are: U.S. Air Force Office of Scientific Research Grant No. F49620-99-1-0283					

Respectfully submitted,

SIGNATURE

Peter Rogalskyj

Date

11/13/2003

TYPED or PRINTED NAME

Peter Rogalskyj

REGISTRATION NO.

38,601

(if appropriate)

Docket Number:

047.00060 (RFT-118)

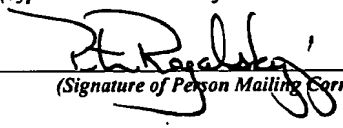
TELEPHONE

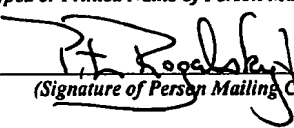
585-346-1004

USE ONLY FOR FILING A PROVISIONAL APPLICATION FOR PATENT

This collection of information is required by 37 CFR 1.51. The information is required to obtain or retain a benefit by the public which is to file (and by the USPTO to process) an application. Confidentiality is governed by 35 U.S.C. 122 and 37 CFR 1.14. This collection is estimated to take 8 hours to complete, including gathering, preparing, and submitting the completed application to the USPTO. Time will vary depending upon the individual case. Any comments on the amount of time you require to complete this form and/or suggestions for reducing this burden, should be sent to the Chief Information Officer, U.S. Patent and Trademark Office, U.S. Department of Commerce, P.O. Box 1450, Alexandria, VA 22313-1450. DO NOT SEND FEES OR COMPLETED FORMS TO THIS ADDRESS. SEND TO: Mail Stop Provisional Application,

If you need assistance in completing the form, call 1-800-PTO-9199 and select option 2.

CERTIFICATE OF MAILING BY "EXPRESS MAIL" (37 CFR 1.10) Applicant(s): Nanna et al.			Docket No. 047.00060 (RFT-118)
Serial No. To Be Assigned	Filing Date Herewith	Examiner Not Assigned	Group Art Unit Not Assigned
Invention: COATING SYSTEMS			
I hereby certify that the following correspondence: <div style="border: 1px solid black; padding: 10px; margin: 10px 0;">Provisional Application for Patent Cover Sheet (1 page) (in duplicate)</div> <p style="text-align: center;"><i>(Identify type of correspondence)</i></p> <p>is being deposited with the United States Postal Service "Express Mail Post Office to Addressee" service under 37 CFR 1.10 in an envelope addressed to: Commissioner for Patents, P.O. Box 1450, Alexandria, VA 22313-1450 on</p> <p style="text-align: center;"><u>November 13, 2003</u> <i>(Date)</i></p> <div style="text-align: center; margin-top: 20px;"><u>Peter Rogalskyj</u> <i>(Typed or Printed Name of Person Mailing Correspondence)</i>  <i>(Signature of Person Mailing Correspondence)</i> <u>ET730094938US</u> <i>("Express Mail" Mailing Label Number)</i></div>			
Note: Each paper must have its own certificate of mailing.			

CERTIFICATE OF MAILING BY "EXPRESS MAIL" (37 CFR 1.10) Applicant(s): Nanna et al.			Docket No. 047.00060 (RFT-118)	
Serial No. To Be Assigned	Filing Date Herewith	Examiner Not Assigned	Group Art Unit Not Assigned	
Invention: COATING SYSTEMS				
<p>I hereby certify that the following correspondence:</p> <div style="border: 1px solid black; padding: 10px; margin: 10px 0;"> Provisional Patent Application (810 pages) </div> <p style="text-align: center;"><i>(Identify type of correspondence)</i></p> <p>is being deposited with the United States Postal Service "Express Mail Post Office to Addressee" service under 37 CFR 1.10 in an envelope addressed to: Commissioner for Patents, P.O. Box 1450, Alexandria, VA 22313-1450 on</p> <div style="display: flex; justify-content: space-between; align-items: flex-end; margin-top: 20px;"> <div style="text-align: center;"> <u>November 13, 2003</u> <i>(Date)</i> </div> <div style="text-align: center; width: 40%;"> <u>Peter Rogalskyj</u> <i>(Typed or Printed Name of Person Mailing Correspondence)</i>  <i>(Signature of Person Mailing Correspondence)</i> <u>ET730094938US</u> <i>("Express Mail" Mailing Label Number)</i> </div> </div>				
Note: Each paper must have its own certificate of mailing.				

This Page Is Inserted by IFW Operations
and is not a part of the Official Record

BEST AVAILABLE IMAGES

Defective images within this document are accurate representations of the original documents submitted by the applicant.

Defects in the images may include (but are not limited to):

- BLACK BORDERS
- TEXT CUT OFF AT TOP, BOTTOM OR SIDES
- FADED TEXT
- ILLEGIBLE TEXT
- SKEWED/SLANTED IMAGES
- COLORED PHOTOS
- BLACK OR VERY BLACK AND WHITE DARK PHOTOS
- GRAY SCALE DOCUMENTS

IMAGES ARE BEST AVAILABLE COPY.

**As rescanning documents *will not* correct images,
please do not report the images to the
Image Problem Mailbox.**

TITLE: COATING SYSTEMS

INVENTORS: Michael E. Nanna
Gordon P. Bierwagen

DOCKET NO.: 046.00060 (RFT-118)

COATING SYSTEMS

The present application contains 19 parts, labeled Part I through Part XIX. Certain aspects and embodiments of the present invention are described in Part I through Part XIX. Each of the references set forth in each of Parts I through XIX is hereby incorporated by reference.

Although preferred embodiments of the present invention are depicted and described in detail hereinbelow in Parts I through XIX of the present application, it will be apparent to those skilled in the relevant art that various modifications, additions, substitutions and the like can be made without departing from the spirit of the invention, and these modifications, additions, substitutions, and the like are, therefore, considered to be within the scope of the present invention.

PART I

Certain aspects and embodiments of the present invention are described in the following text.

Description of Mg-rich Coating System and Polymeric Binder Material

The magnesium-rich coating system for Al alloys consists of the following components:

- 1) Pigmentary magnesium (powder) with proprietary surface (oxide) treatment developed by Eckart (ECKA Granulate GmbH & Co. KG), Fürth/Bavaria. A pigmentary magnesium mixture is used in the "metal-rich primer component",

consisting of at least one particle size distribution (PSD): a) sub micron/micron particulate at $(0.01\text{ }\mu\text{m}) < \text{PSD} < (20\text{ }\mu\text{m})$ diameter, and b) micron/micro sized particulate at $(20\text{ }\mu\text{m}) < \text{PSD} < (0.4\text{ micrometers})$ in diameter. Mixtures of different PSDs are known to account for different degrees of efficiency/protective action when used as a sacrificial anode in a cathodic protect coating system. Where the physical units assigned to the particulate range over a scale of $(\mu\text{m (microns)} = 10^{-6}\text{ meters})$ and $(\text{micrometers} = 10^{-3}\text{ meters})$. It is also surmised that surface treatment of the magnesium powder (via incorporation of an oxide layer over the pigment is modified with a surfactant which acts to 'hydrophobically' seal the surface of the magnesium oxide to prevent ingress or adsorption of water), thus this surface treatment acts to stabilize the metal, i.e., decrease its reactivity, which allows it to be utilized in a convenient form as a manufacturing material in these coating systems.

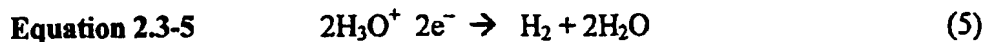
- 2) The Mg-rich primers (magnesium powder loaded primer) is formulated (physically filled with powder) in the vicinity or at the primer coating's 'critical pigment volume concentration' (CPVC) for the purpose of maximizing the cathodic protection effect observed in these coatings via (sacrificial anode). See Appendix 2-A. In addition, loading the primer with a Mg-metal concentration at or near CPVC has the additional effect of extending the corrosion control of these coatings by action of filling with magnesium oxide/hydroxide corrosion byproducts which protect an aluminum alloy of underlying substrate by 'barrier' action.
- 3) A methodology for preferential treatment of the smaller particle size distribution fraction of Mg powder, i.e. $\text{PSD} < 20\text{ }\mu\text{m}$, used in conjunction with a larger $\text{PSD} > 20\text{ }\mu\text{m}$, similar to the pigmentary Mg powders used in Chapter 5 thesis (Michael Nanna). For example, the magnesium powder Eckagranules PK-31 has a $(\text{PSD} < 30\text{ }\mu\text{m})$ that would be treated with cerium(III)nitrate solution, while the a magnesium powder such as PK-51 $(\text{PSD} > 30\text{ }\mu\text{m})$ would not receive treatment. Based upon the observation by Mansfeld that Mg treated with cerium(III) preferentially formed hydroxides before the Mg metal did when exposed to a NaCl environment. Mansfeld *et al.*, showed that the corrosion protection of cerium conversion coatings formed on pure magnesium and a magnesium alloy, WE43, was studied by D.C. polarization and A.C. impedance techniques. REMS coatings were observed to show reduced dissolution of magnesium in a pH 8.5 buffer solution. This was ascribed to the formation of protective magnesium hydroxy corrosion products and mixed rare

earth/magnesium oxide/ hydroxides. It was observed that protection continued until REMS coatings were consumed by the formation of magnesium corrosion products. The importance of this methodology lies in its ability to reduce the overall PSD of the Mg-powder incorporated into the primer coating which is important for the following reasons: 1) a reduced PSD yields a primer with a thinner film thickness and more uniform coating; 2) flammability / fire retardance of the coating is increased by reducing the mass of Mg metal that may incinerate, (smaller PSD Mg-powders are better wet by due to more even distribution of silane modified polymeric binder than large PSDs), and 3) formulation and application of smaller PSD Mg-powders are easier due to the more spherical geometry of the powders. Recalling that the model used to approximate CPVC relies on the volume of a sphere which more accurately represents the geometry of the fine PSD Mg-powders as opposed to a more "oblongated-swarf" geometry observed in the larger PSD, (PSD>80 μ m) powders.

- 4) As previously discussed in Chapter 2.3, (see thesis Nanna), central to the preservation of the β -Al(OH)₃ bayerite / γ -AlOOH(s) boehmite interface in the presence of copper cathodic sites has been the application of REMS such as cerium. These REMS, when incorporated as a film or coating, have also shown to inhibit the primary reduction reaction occurring on the surface of Al alloys containing copper at pH's circa ~ 8.5, (which is at the upper stability limit for Al according to Pourbaix diagrams previous section 2.1 (see thesis Mike Nanna), by precipitation of rare earth hydroxides/oxides. In addition, when used in conjunction with magnesium, they also show a similar activity by the precipitation of rare earth hydroxides/oxides at the surface of magnesium thus inhibiting corrosion of the magnesium metal by preferentially forming oxides/hydrides.

As a means by which to control the afore mentioned "burn-out" due to localized depletion of micron sized Mg powder in the vicinity of cathodic sites of the Al alloy, nano-particle cerium should be incorporated into the primer interface as a means by which to moderate excessive magnesium consumption directly at the Al / primer interface, as depicted in Figure 8.5, below. Figure 8.5, below, depicts a Mg-rich coating over Al 2024 T-3 with nano-particle cerium incorporated into the interface. It is surmised that the presence of cerium would forestall the consumption of micron sized Mg powder, (particle sizes < 20 μ m), and in so doing extend the actual period the coating functions as a cathodic coating, i.e., the potential difference due to cathodic current, as depicted in Figure 3.11, (see thesis Mike Nanna), would be extended. Therefore, the effect of moderating consumption of Mg-powder closest to the Cu-cathodic sites should be similar to that of formulating the coating at the PVC which was shown to best extend the coating's cathodic lifetime. This was shown to occur in Chapter 3, i.e., the magnitude of the negative potential (OCP) remained larger over an extended period for the Mg-rich primer that was formulated at its CPVC. The electrochemical interpretation ascribed to such an effect would be that extended cathodic protection would be due to the more even distribution and consumption of sacrificial anode that feeds the hydrogen evolution reaction, Equ.

2.3-5, which has been implicated as the major reduction reaction occurring in such an alkaline environment.¹



It would also be surmised that another approach taken to achieve a similar effect would be to simply treat the Al 2024 T-3 surface with cerium(III)nitrate $\text{Ce}(\text{NO}_3)_3$, as described in the literature by Yu and Cao^[2] and then apply the Mg-rich coating. In this approach the Al surface would receive an anodization treatment, by any such means previously described in Chapter 2.3, and then the cerium(III)nitrate solution applied followed by application of Mg-rich primer according to the methodology described in this thesis.

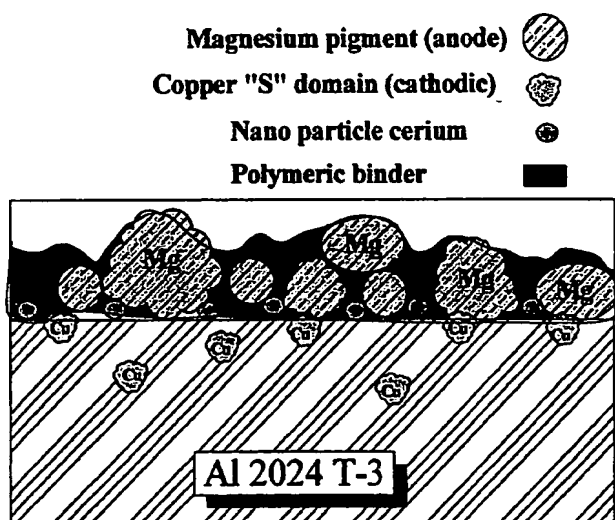


Figure 8.5, Illustrative scheme for proposed Mg-rich coating system with nano particle cerium incorporated at Al / Coating interface.

- 5) The polymeric binder material was developed specifically for the magnesium rich coating system due to its ability to withstand slightly elevated pH levels that occur as a result of generation of magnesium corrosion byproducts. In addition, the polymeric binder component of the primer is an integral part of the multi-layer silane modified 'hybrid' coating system (see chapter 4, thesis Mike Nanna).

The polymeric binder consists of a mixture of polyisocyanate prepolymer, or oligomers of diphenylmethane diisocyanate (MDI) Desmodur™ E23-A from Bayer Corp; or oligomers of hexamethylene diisocyanate (HMDI) Desmodur™ N-3300; or any polyisocyanate prepolymer containing reactive NCO functional group whether it be aromatic or aliphatic in nature. The second ingredient in the polymeric material consists of an epoxy prepolymer such as Epon 1001X type, as reviewed in Chapter 2.9, or any "taffy process" epoxy resin containing both

The polymerization reactions in this experiment were assumed to have been initiated at the Al surface where M-O-S-R-NH₂ bonds were assumed to have formed upon application of the N-beta-(aminoethyl)-gamma-aminopropyltrimethoxysilane, from which it is assumed a (M~Al, and R-NH₂) structure formed at the surface of the substrate and was extending into the bulk upon addition of 1) MC-PUR; 2) (7-PQ-6-ol) crosslinker according to Figures 5.10 -to- 5.12, below:³

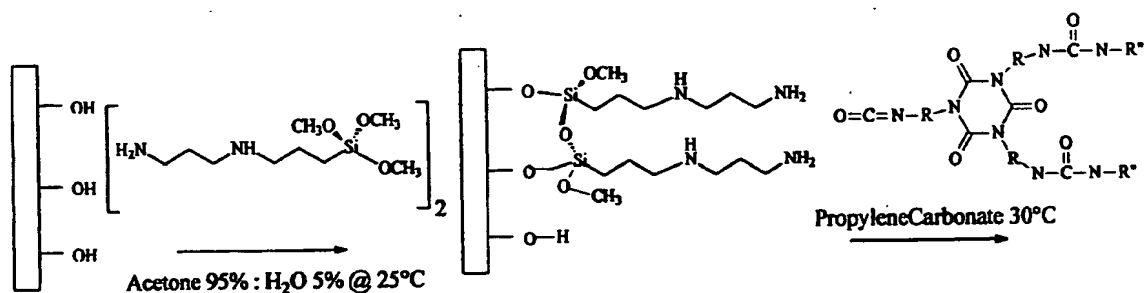


Figure 5.10: Initial sol reaction with surface hydroxyls and β -(aminoethyl)- γ -amino propyl trimethoxysilane

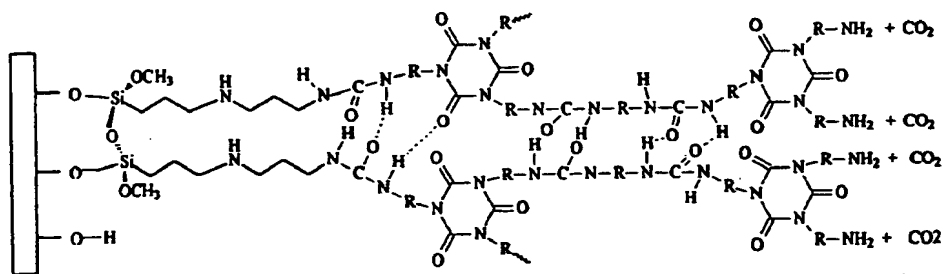
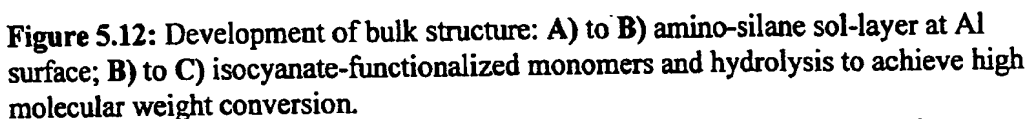
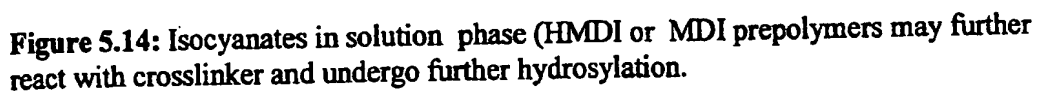
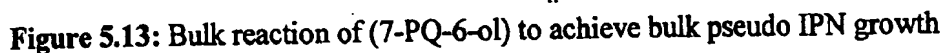


Figure 5.11: Terminal surface amines reacting with MC-PUR isocyanates in solution phase (HMDI or MDI prepolymers) to form second layer over M~Al, and R-NH₂).



The crosslinker (used in both Epoxy- HMDI and Epoxy- MDI hybrids) (7-PQ-6-ol) (Figure 5.12, center) synthesized in these laboratories, was added to promote bulk polymerization throughout the IPN matrix. In addition, from spectroscopic analysis Chapter 4,



- 6 -

5.12 Summary Multi-layer Surface

The multi layer silane modified polyurea provides a means whereby the properties of polymers/ macromolecules adsorbing at a metal surface can be tailored to match those of the polymer in bulk. Based upon this assumption, a conformation approach, involving pretreatment with a dilute polymeric material, as suggested by Funke

, was pursued as a means by which to improve the adhesive properties of a coating.

In addition, two other methods have been suggested and incorporated into this scheme as well: 1) use of reactive molecules of low molecular weight organ-silane (N-beta-(aminoethyl)-gamma-aminopropyl trimethoxysilane), which after physical or chemical adsorption can be connected by crosslinking or improving the molecular adaptation to the metal surface structure; 2) by incorporating small reactive, mobile binder molecules, (polyisocyanate prepolymer) which may which may be crosslinked after adsorption, i.e., polyurea multi layer. Figure 5.15, below, depicts the effect of cooperative functional groups at promoting good interactions between polymeric material and areas surrounding a potentially flawed metallic surface that have been filled in with polymeric material.

Appendix 2-A Critical Pigment Volume Concentration (CPVC)

The CPVC calculation can be approached intuitively in terms of the relationship between two associated components: 1) the oil absorption (OA) value, and 2) the configuration / packing factor of the pigment(s). Generally, it is the largest pigment in the particle size distribution that exerts the largest effect on the CPVC of the coating. As an intuitive example of what the CPVC calculation means an example of a hypothetical coating system consisting of polymeric binder and one pigment, a 100% solids system will be examined. It will be assumed that this hypothetical coating will consist of a polymer and pigment properly dispersed at the coating's CPVC. From which an OA value was ascertained, given in grams oil to 100 grams pigment; this yields a volume of oil which is a surrogate for the polymeric binder. The next component is the pigment's packing factor, which gives its configuration and the associated maximum volume at its packed configuration. Putting two plus two together the volume of oil adsorbed (from OA determination) is associated with the volume of pigment at its maximum packing configuration which results in the CPVC when indexed according to Equ. 2.6-8, below.

Generally, the confusion associated with CPVC calculations often arises due to the fact that it involves a maximum packing configuration, such as that for simple spheres, as opposed to just the maximum pigment volume at the OA run-up end-point. The previous sections have demonstrated the mechanics and parameters associated with the critical pigment volume concentration (CPVC). Essentially, the difference between PVC and CPVC is that PVC can be measured, according to the equation below; while CPVC can not be measured it must be determined.

- a) PVC is the pigment *volume* content of a coating that contains a binder and at least one pigment. The PVC serves as a *volume* index for the ratio of pigment(s) to binder in a coating.

Equation 2.6-8

$$PVC = \frac{\sum_{i=1}^n Pigments_i}{\sum_{i=1}^n Pigments_i + \sum_{i=1}^n Binder} \times 100 \quad (8)$$

- b) CPVC is the *coatings* critical pigment volume concentration which refers to the transition point above or below which substantial differences in the appearance and behavior of a paint film will be encountered. Overall, it is the most pigment you can put into a cured film without air voids forming due to an insufficiency of the continuous phase polymer matrix. Moreover, many coatings properties catastrophically change at the CPVC.

¹ Emley, E.F., Principles of Magnesium Technology, Pergamon Press, Oxford, (1966)

² Yu, X., and Cao, C., *Thin Solid Films*, Vol. 423 Pp. 252–256 (2003)

³ Kohli, P., and Blanchard, G.J., *Langmuir*, Vol. 16, pp. 4655-4661 (2000)

PART II

Certain aspects and embodiments of the present invention are described in the following text and figures.

Magnesium Powder Filled Primers for Cathodic Protection of 2024 T-3 Aluminum Alloy

Abstract

500 hours direct exposure of 2024 T-3 aluminum panels to Prohesion cycling in Harrison's solution causes rapid corrosion of the alloy to occur. Coating the alloy with an epoxy primer filled with 20 micron sized magnesium powder, at or above CPVC (critical pigment volume concentration) cathodically protects the alloy for up to 2,000 hours. Cathodic protection of a primed panel appears to occur in two distinct stages, initially, closely packed metal particles connect in the primer to form a conductive path thus circulating charge. Gradually, as the surface of the metal is oxidized porous hydroxides, and possibly conductive, $[\text{MgO}, \text{Mg}(\text{OH})_2]$ [brucite] domains grow and interconnect providing a path for charge to flow, thus extending the period of protection of the alloy's surface. However, once depleted of brucite structure the remaining coating rapidly begins to fail as magnesium sulfate [hexahydrite] salt accumulates at the interface .

Introduction

Magnesium powder filled epoxy primers have been formulated above and below CPVC, then subjected to Prohesion cycling in Harrison's solution to emulate acid rain conditions. Upon initial exposure the acidic ($\text{pH} \sim 4.5$) solution quickly attacks magnesium metal yielding hydrogen gas H_2 , the metal oxide MgO , and brucite the metal's hydroxide $\text{Mg}(\text{OH})_2$. (1) Primer PVC (pigment volume concentration) was found to strongly influence integrity of exposed primer coatings. (2) High PVC metal content primers contain more surface metal available to serve as sacrificial anode, thus elevating PVC far above CPVC extends galvanic protection to both binder and alloy, however, lower available binder concentration at the metal anode surface caused poor adhesion between primer and interface. Poorly encapsulated magnesium in a sulfate solution quickly forms a high volume of interlaced hydroxide extending over the metal's surface. (3) Lower PVC metal load primers develop lower surface hydroxide coverage thus are prone to develop aluminum oxides sooner when alloy surface is damaged or exposed. Formulating primers near CPVC causing particles to pack and connect thereby increasing the coatings effectiveness to serve as a sacrificial anode. Elevating the PVC of a primer above CPVC increases the exposed anode surface area, more anode metal delivers more protection. Primers formulated far above

CPVC lack sufficient binder required to effectively encapsulate the metal, as a result connectivity and volume of brucite formed over the surface is greater and more uniform. However, equilibrium eventually favors formation of magnesium sulfate hydrate salts hexahydrate $[(\text{MgSO}_4) \cdot 6 \text{H}_2\text{O}]$, found to precipitate and accumulate at the interface between primer and alloy. (3) In turn, accumulation of hexahydrate salt at the alloy interface corresponds to a loss of passivity and evolution of the flakey porous oxide structure corresponding to the oxide observed in figure 1-C at 1,000-hours Prohesion exposure. Once the metal has been depleted by conversion to oxide the remaining binder, at the alloy interface, ruptures and fragments from compressive forces exerted by expanding salt structures. Studies have shown the course of events for the corrosion process of magnesium powder filled epoxy primers follows three distinct events. (3)

1. EDX spectrum show initial formation of magnesium carbonate hydrates at the liquid/vapor interface, dypingite $[\text{Mg}_5(\text{CO}_3)_4(\text{OH})_2 \cdot 8\text{H}_2\text{O}]$ & hydromagnesite $[\text{Mg}_5(\text{CO}_3)_4(\text{OH})_2 \cdot 4\text{H}_2\text{O}]$ fluffy white carbonate powder formation extends up to the first 500 hours of exposure.
2. Over a more extended period of exposure, formation of magnesium hydroxides due to oxidation from acid exposure forms extensive thin crystalline domains of brucite needles $[\text{Mg}(\text{OH})_2]$. Note during this time period the aluminum alloy remains cathodically protected, scribed lines remain clear.
3. Ultimately, failure delamination corresponds to the accumulation of hexahydrate $[(\text{MgSO}_4) \cdot 6 \text{H}_2\text{O}]$ salt at the interface. At which time the interface rapidly covers with aluminum oxide and the coating binder quickly decomposes.

Overall, failure occurs when magnesium has been depleted from the binder matrix and sufficient hexahydrate salts have accumulated at the alloy interface to cause decomposition of the binder. It is believed that during the first two stages of the process the Al alloy substrate is cathodically protected.

Epoxy Binders

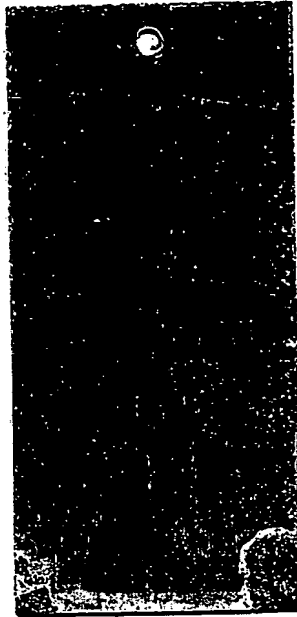
Coatings formulated with magnesium powder for cathodic protection of the aluminum alloy have two distinct disadvantages,

1. Blistering and delamination occurs at alloy interface as hydrogen gas evolves when magnesium metal is oxidized by acid.
2. Adhesion of high metal volume content coating to the alloy surface requires excellent wetting of both magnesium and alloy surfaces.

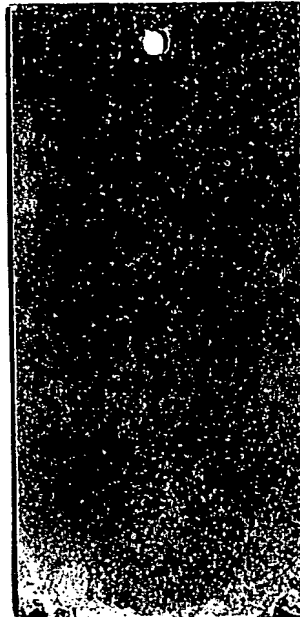
Ambient temperature cure epoxy/amide systems tend to wet pigments well and as a result yield superior adhesion to aluminum alloys, for example, the combination of Epicure 3115 & Epon 1001cx (5) is often used in epoxy lacquers for high solids primers. Epoxies cured with polyamides have poor acid and chemical resistance, (6) and as a result tend to develop blisters and delaminate after brief periods of exposure. Ambient cure polyamines used as epoxy curatives yield improved acid/base and chemical resistance, e.g. DEN-439 & Ancamine 2422 (7) but due to development of extensive crosslink density lack flexibility and as a result their adhesion to metal is severely compromised. In addition, polyamines based on primary amines are high surface tension liquids, circa 40–45 dyne-cm making them slightly incompatible with epoxy resins and poor pigment wetting agents limiting their utility to formulations below CPVC. Two-component epoxy coatings formulated with primary amines tend to develop highly cross-link structures and as a result high internal stress accumulate in the coating over time. Development of high internal stresses directly reduces the epoxy binder's adhesion to alloy substrate. Thus far, neither epoxy binder system has performed well enough as a stand alone for magnesium powder. Overall, ambient cure epoxy binders encapsulate pigments well and form films but lack the versatility required to bind large particle size high metal PVC coatings to an aluminum alloy interface.

Bare Aluminum

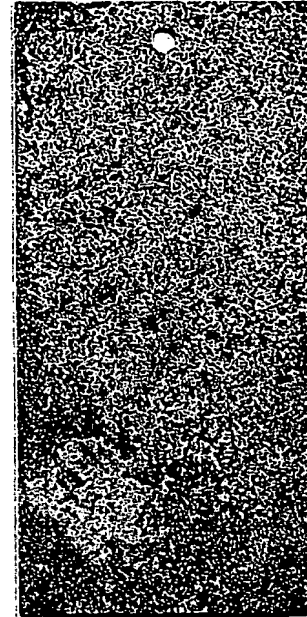
Bare 2024 T-3 aluminum panels were subjected to Prohesion cycling in dilute Harrison's solution for 1000 hours. Six, untreated 2024 T-3 panels were subjected to Prohesion cycling for up to 1000 hours upon which time testing was terminated due to extensive corrosion of the alloy. Initially, and up to 500 hours of exposure the panels were characterized by slow formation of micron sized clusters of oxide and the initiation and growth of pits that filled with a white, passive aluminum oxide Al_2O_3 . This oxide was found to be slightly adherent and in localized clusters, thus characterized by a Pilling-Bedworth ratio of 1.5 for that oxide. (8) The Pilling-Bedworth ratio is a ratio of the specific volume of metal oxide developed to specific volume of the metal itself. A P-B ratio of less than one indicates the metal develops a fluffy, penetrable, porous oxide, such as magnesium oxide with a P-B of 0.85. A P-B ratio greater than one yields a higher volume of oxide that is a passive more closely packed compressed structure such as Al_2O_3 . Finally, after 500 hours exposure no remnant of passive Al_2O_3 layer appears to exist the entire surface has been extensively consumed by pitting and replaced by a gray, non-adherent, oxide flake. This non-adherent oxide can be characterized by a Pilling-Bedworth ratio similar to that of iron rust Fe_3O_2 of around three, this very high ratio of oxide to metal in its atomic lattice structure causes high internal compressive forces to develop as the oxide grows. Oxides are characterized as having high compressive and poor tensile strengths thus by nature leaving them prone to flake from the surface as they grow.



1-a Unexposed 2024 T-3



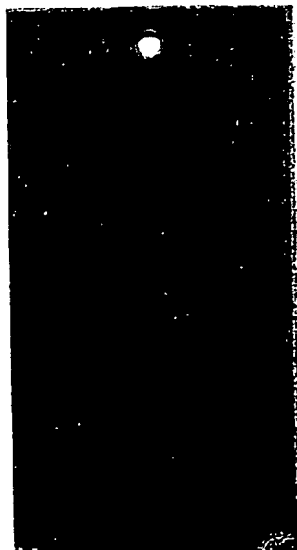
1-b 500-hrs. 2024 T-3



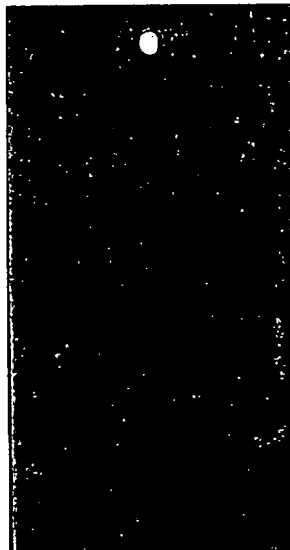
1-c 1000-hrs. 2024 T-3

Organo-Silane Treated 2024 T-3

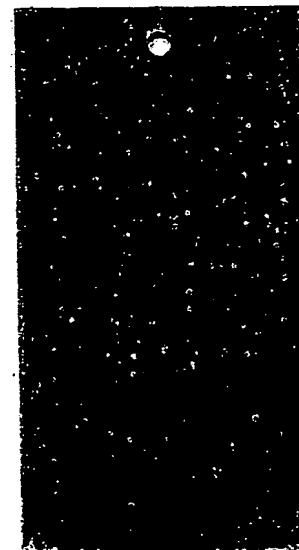
Primers formulated at high PVCs with epoxy binders tend to lack adhesion to 2024 T-3 aluminum surface. An organo-silane adhesion promoter was synthesized and applied to 2024 T-3 and subsequently exposed to Prohesion cycling. Six panels were treated with a 10% solution of a silane modified quinone. The panels were cured 48 hours at 40°C, whereupon a strongly adherent, solvent resistant sub-micron film formed. After 1000 hours exposure white oxide clusters pits sparsely form over the surface. Surface treated panels arrested the corrosion process by physically blocking dissolution, thereby moderating the corrosion process.



2-a Unexposed, Silane treated 2024 T-3



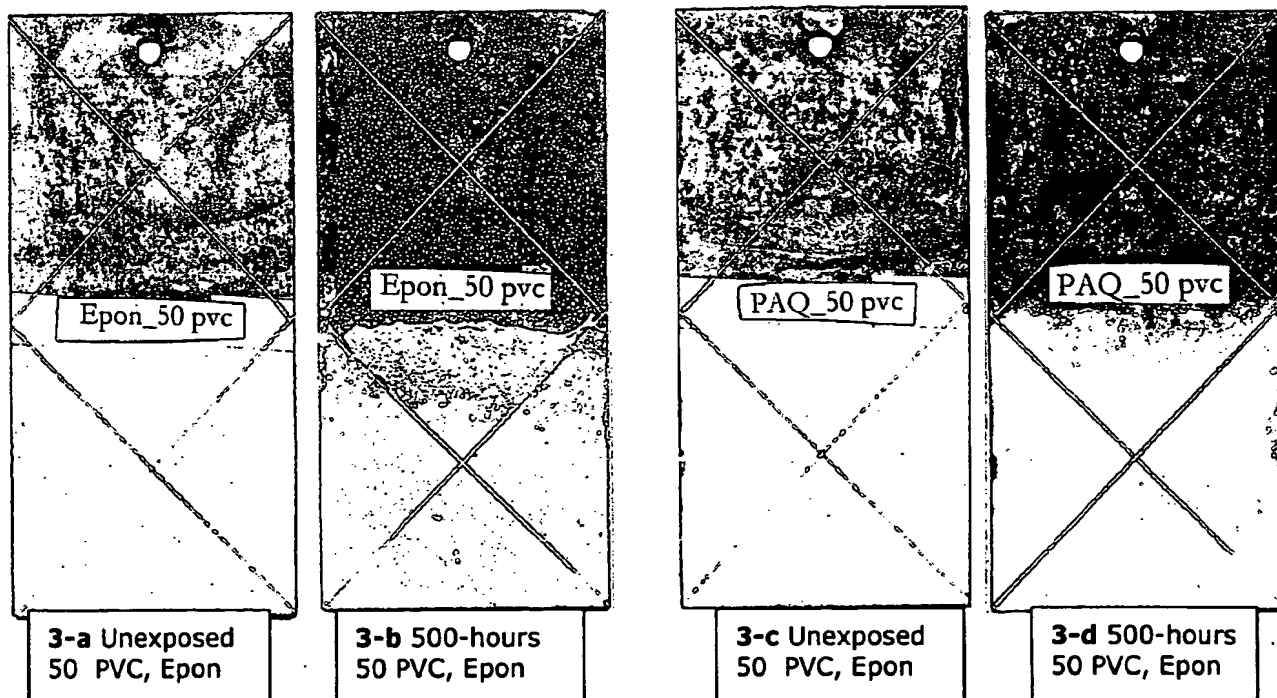
2-b 500-hrs. Silane treated 2024 T-3

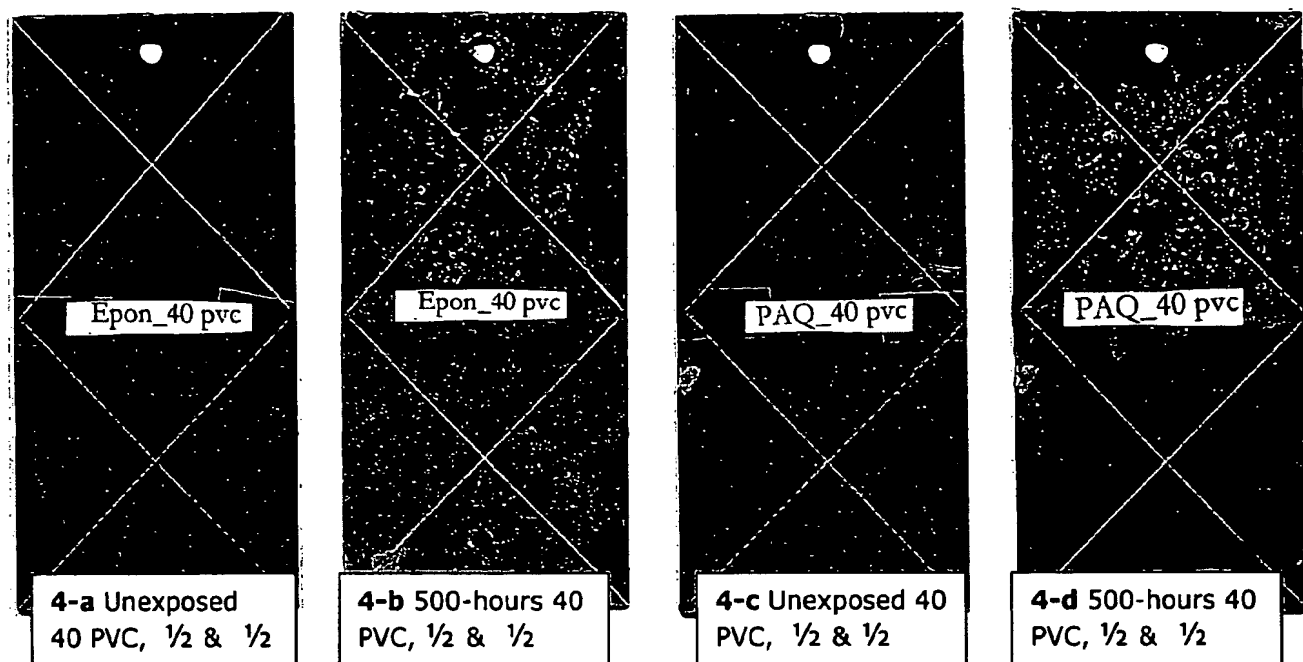


2-c 1000-hrs. Silane treated 2024 T-3

Magnesium Filled Primers

The purpose of the magnesium powder filled primer is to provide cathodic protection to the 2024 T-3 alloy without physically blocking the aluminum surface. Primers formulated above CPVC block less surface than those below CPVC. It has been observed in past studies that those primers formulated above CPVC provide longer periods of protection simply because there is more anode available. Physically blocking the surface occludes cathodic protection when contact between anode and cathode is interrupted. Primers formulated below CPVC, circa 40 PVC are effective at blocking surface and providing limited local cathodic protection so long as the coating itself remains integral and intact. However, once the coating is damaged and the surface exposed cathodic protection becomes limited to the local concentration of magnesium anode at the site of fracture. If the metal is well encapsulated galvanic protection terminates resulting in oxide ingress and lifting about the damaged area. Primers formulated with epoxy binders well above CPVC are prone to lifting and delamination as adhesion to the surface is poor as a result of epoxy binder preferentially wetting the smaller spherical pigment particles to minimize surface free energy as opposed to wetting a lower energy flat alloy surface. PVC effect illustrated below, series of magnesium primer panels prepared in epoxy binders polyamine (PAQ), and polyamide (EPON), with and without organo-silane surface treatment.





50 PVC Panels

Top row, previous page, two sets of panels before and after 500 hours Prohesion cycling with top section of panels organo-silane treated. Scribed lines of treated section partially filling with aluminum oxide while untreated section scribe lines remained clear. Note presence of white magnesium oxide, Brucite, magnesium hydroxide covering the surface of the untreated. Panels were stowed with silane treated sections set into base of the storage rack allowing drainage from upper untreated portion to accumulate and precipitate on treated portions. The crystalline precipitate covering silane treated panels was identified by x-ray diffraction to be the magnesium sulfate hydrate salt, Hexahydrate. Hexahydrate accumulation was observed to be due to precipitation from liquid drops at liquid/vapor interface.

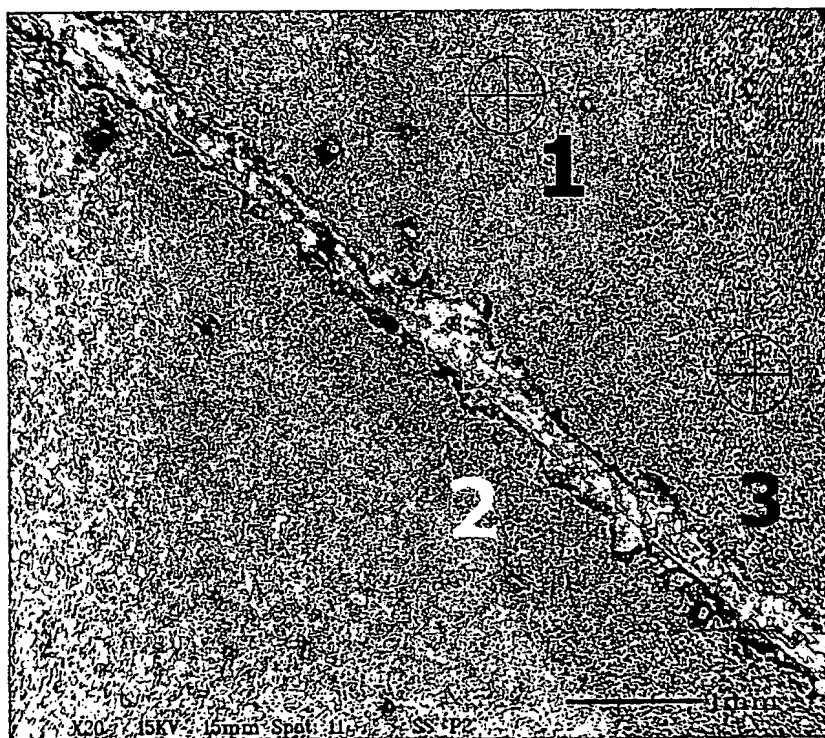
40 PVC Panels

Bottom row, previous page, two sets of panels before and after 500 hours cycling identical treatment as above. Scribed lines of both silane treated portions filled packed solid with aluminum oxide while both sets of untreated panels scribe lines remain clear. Hexahydrate accumulation, darkened areas, over surface of treated portion where untreated panels drained. Brucite white oxide covering surface of untreated portions no lifting under scribes. PVC effect between 40 and 50 samples shows the scribed lines over silane treated portions of the 40 PVC to be packed with aluminum oxide, whereas, for the 50 PVC panels lines contained sparse areas filled with oxide.

Exposed Primer Panel

SEM and corresponding EDX energy disperse x-ray diffraction spectra of three areas of a 50 PVC primer with 20-micron powder at 500 hours exposure revealed different chemical compositions at the panel surface as a function of exposure.

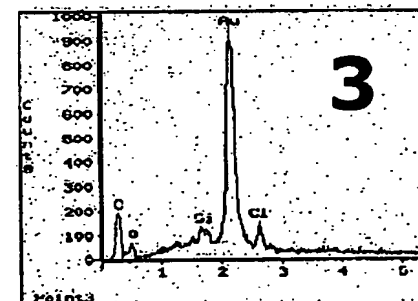
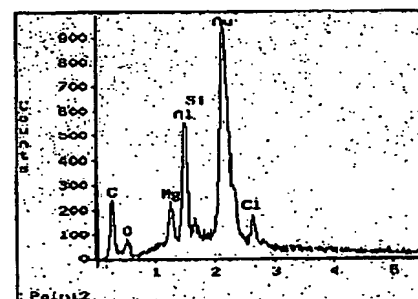
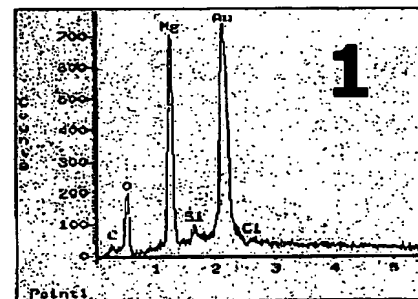
SEM and EDX of area one (1) correspond to white Brucite structure emanating directly from metal in the primer, binder still in tact, fine, needle crystalline structure covering the face of the coating. It is believed that Brucite is an intermediate equilibrium structure formed at the metal surface as a result of magnesium being oxidized by acid. During the first 500 hours of exposure all of the metal available at the surface is oxidized and converted to Brucite, proceeding after 500 hours the structure continues to grow at the expense of the metal anode. SEM and EDX of area three (3) correspond to the epoxy binder matrix depleted of magnesium and Brucite. Distinct demarcation reveals depletion of metal anode starting at the edges of the panel and following an ingress toward the more electrically connected metal rich center. SEM and EDX of area two (2) correspond to the scribed bare 2024 T-3 panel. Higher resolution SEM photomicrographs show the surface to be relatively clear and unblemished by aluminum oxide on a sub-micron scale. EDX spectrum reveals components essential and proportional to magnesium carbonate present on surface.



Title: 201218 105 500 HRS
Comment: LOW MAG

Date: 12-27-2000 Time: 15:17
Filename: 2707.TIF

Figure 5, SEM 20x, 500 hr exposed 2024 T-3 primer panel. Figures 5-1,2,3 adjunct EDX spectra



- 1) White oxide area magnesium hydroxide Brucite over magnesium metal. Note magnesium, oxygen and aluminum. Minimum carbon is detected.
- 2) Scribed area with no epoxy matrix, nor magnesium metal present. Spectrum shows carbon, oxygen magnesium and aluminum. Possible presence of dypingite, magnesium carbonate structure over aluminum surface.
- 3) Magnesium depleted epoxy matrix, spectrum shows aluminum, carbon and oxygen in almost equal proportion and intensity to spectrum "2" above.

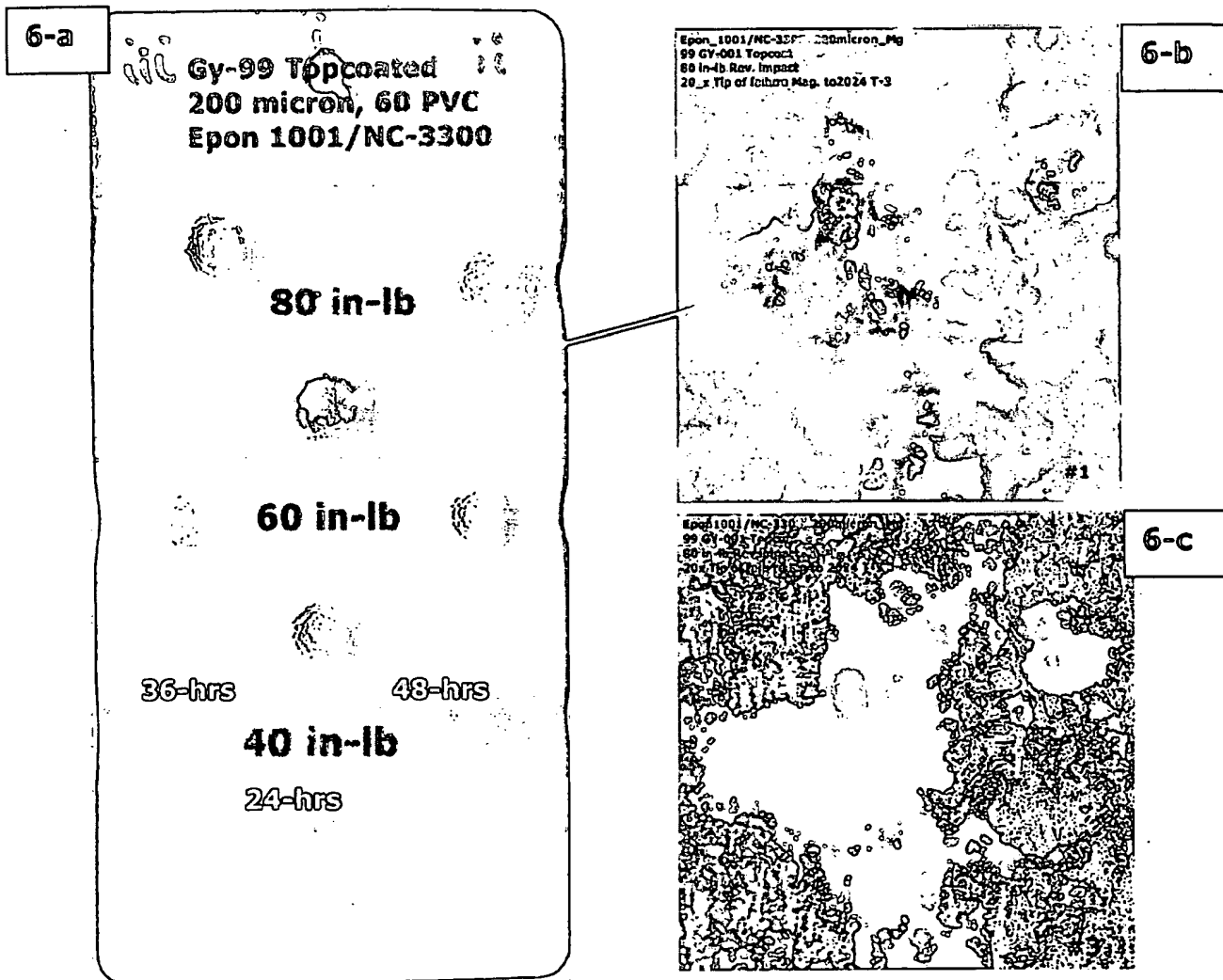
In summation, it was observed the salts generated during first 1000 hours of exposure did not degrade neither binder nor alloy surface. With reference to the SEM and EDX of area 2, the presence of magnesium carbonate at the unblemished bare alloy surface reveals that hydrated magnesium carbonate does not attack and degrade the passive aluminum oxide layer, and its presence on the surface suggests that it participates in the overall cathodic protection mechanism.

Topcoated Panels

Deft 99 GY-001 Base & Catalyst "Extended Life fluoropolymer Topcoat" was applied to alloy panels formulated with Eckart 200 micron 099/00 magnesium powder. Elevated PVCs require excellent primer adhesion. Primers formulated with 200 micron, (average) particle size magnesium powder above CPVC tend to fare poorly in reverse impact. Poor reverse impact resistance in cathodic coatings has been a good indication of early coating delamination during Prohesion cycling studies. Larger average particle size magnesium powders tend to be coarse and fare poorer in reverse impact than smaller 20micron size powders. Coarse particles, over 380 micron size, in turn leave the high PVC topcoat prone to failure. Smaller particle sized magnesium powders yield a higher exposed surface area and higher reactivity. The ideal primer will be comprised of a balance of the two at some ideal thickness.

Figure Deft GY-99 70 micron thick film topcoat over 200 micron thick film primer with 200 micron average particle size magnesium powder. Reverse impact results for 24, 36, and 48hour topcoat cure time. Figures 20x depth profile images at site of reverse impact failure, indentation of exposed aluminum panel reveals remnants of polymer binder and large magnesium particles adhered to panel surface. Polymer binder component from primer the red colored substance appears not to preferentially wet the magnesium pigment, or aluminum alloy surfaces to a high degree. Instead it appears to localize and collect and form discontinuous domains between both surfaces. The apparent improvement in reverse impact resistance over time may be related to loss of retained solvent from applied topcoat underscoring some degree of adhesion loss caused by solvent from the topcoat penetrating to the surface.

Figure 6-a: Reverse impact top-coated aluminum panel at 24, 36, & 48 hr cure. Figures 6-b & 6-c Profile view of failure locus at panel tip adherent metal and polymer



Polymer binder for primers

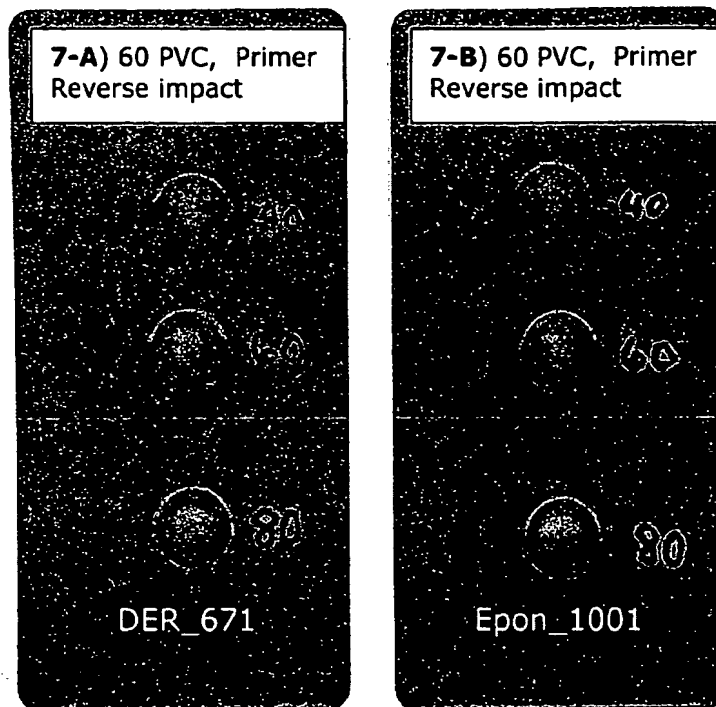
High PVC extended lifetime topcoats simply provide surface protection over an extended time period. They must remain integral and not fail or degrade. Primers essentially provide the coating's integral guts it connects both surface and substrate and arrests drastically different effects occurring in two separate but interconnected environments. Primers formulated for cathodic protection require a polymer binder that wets metal well, retains flexibility, maintains solvent and acid resistance, provide, and in addition are not easily hydrolyzed by caustic salts.

Aromatic moisture cure polyisocyanates are commercially available materials for application to high pH concrete surfaces thus making them suitable as an ideal

binder system for magnesium powder filled primers for cathodic protection. (9)
The polyisocyanate binder utilized in these systems forms both urethane and urea linkages at a stoichiometric ratio of 5 to 1. In order of stability to caustic high pH conditions these urethane/urea coatings rank above polyamides and are similar to polyamines. (10)

Epoxies for ambient cure primers include novolac, bisphenol A or F as the commercially available binders of choice for cathodic primers. Polyamines and polyamides are the workhorse curatives for ambient cure epoxy coatings. In either case, high cross-link density contribution from primary amine content leads to poor adhesion and flexibility due to internal stress accumulation over an extended time scale. Addition of mono-functional diluents such as CGE (cresylglycidal ether) or BPA reduces high cross-link density and improves flexibility, however, comes with a reduction in chemical resistance and substrate/pigment wetting. A more common practice is to add a mono-functional epoxidized linseed oil diluent, Union Carbide "Flexol" plasticizer which greatly enhances substrate/pigment wetting and flexibility at lower concentrations than GCE. However, neither approach leads to solvent resistance. Secondary amines and nucleophiles of similar reactivity are believed to be more suitable as curatives for epoxies used in cathodic primers filled with magnesium powder. It has been observed that green organo-metallic compounds, possibly salts, of magnesium have formed in epoxies cured with polyamines high in primary amine content. Formation of organo-metallic magnesium compounds presents both problems as well as opportunities to formulating cathodic coatings. Currently, a moisture cure binder system is being developed that utilizes magnesium powder to catalyze a reaction between an aromatic polyisocyanate and ambient moisture. Reaction kinetics of the polyisocyanate have been observed to be dependent on both polarity of carrier solvent and magnesium powder particle size, where a smaller 20 micron average particle size 099/99 has been found to be far more reactive than the 200 micron average 099/00 powder.

Figure 7-A & B , reverse impact results for primed panels containing Eckart 099/00, 200 micron sized magnesium powder at 60 PVC with current hybrid polyisocyanate/epoxy binder system. Similar results were obtained using two commercially available epoxy resins DER 671PM, panel '7-A' and Epon 1001cx,



panel '7-B'. Both resins Taffy process at 450 to 550 EEW. The coating carrier solvent was a xylol /acetone mix, spray applied, single coat approximately 200 micron film thickness. Reverse impact indentations from top to bottom 40, 60, and 80 lb-inch respectively. Overall, the panels with Epon 1001cx had slightly better adhesion possibly a result of better wetting of the non-polar stearate treated magnesium powder surface. Solvent effect may have played a role as the Epon resin was cut in non-polar xylene, while the DER-671PM cut in more polar DOWANOL PM, (propyleneglycol monomethylether). Coating failure at 80 lb-inch from the surface indicates mechanical limits of the polymer binder at that PVC have been greatly exceeded. The 60 lb-in results appear to be the more attainable practical limit for a top-coated panel with a 200 micron sized magnesium powder.

Summary

Aluminum is an amphoteric metal and corrodes under both acid low pH and alkaline high pH conditions. A Pourbaix diagram gives the thermodynamic relationship between aluminum metal/oxide/hydroxide stability in solution typically over a pH range from 0 to 14. The Pourbaix diagram for pure aluminum shows the metal forms a passive oxide layer over a pH range of 3.5 to 9. However, the presence of coherent copper microstructure in 2024 T-3 alloy

renders it more susceptible to corrosion at a slightly higher pH than 3.5. Dilute Harrison solution with a pH~4.5 is acidic and readily oxidizes this aluminum alloy. In a cathodic coating, magnesium serves as the sacrificial anode and as the anode is consumed, depending on the conditions, oxides and hydroxides are generated that tend to be progressively more alkaline. The alkalinity depends upon the nature and concentration of anion present. Thus far three dominant salts have been observed to occur during exposure carbonate, hydroxide, and sulfate each in turn progressively more alkaline. It is believed that the carbonate and hydroxide salts of magnesium help protect the passive layer of the alloy and participate in the cathodic protection mechanism while highly soluble sulfate salts appear benign to the alloy in the presence of abundant Mg^{2+} . Meaning there is no evidence that magnesium hydroxides (hexahydrate) damages the aluminum passive layer. However, once the primer has been depleted of Mg^{2+} soluble sulfate anion drives the dissolution of aluminum and the alloy corrodes at the rate seen in figures 1-a to 1-3.

Addition of an organo-silane to the surface of the aluminum appeared to physically block the surface and retard migration of electrolyte and dissolution of aluminum. Figures 2-a to 2-c moderated corrosion effect, no soluble organo-silane salts appeared to form in presence of aluminum cation, only small domains of aluminum oxide emanating from surface. Figure 2-c gives a qualitative measure as to size and progression of aluminum oxide on the surface that causes disbonding of adhered silane as the underlying metal is dissolved.

The complete coating system for cathodic protection of 2024 T-3 aluminum with a magnesium powder primer begins at the alloy interface with an organo-silane adhesion promoter that is integral to the binder itself. A moisture cure aromatic isocyanate binder comprises the backbone of the primer polymer adding high chemical and alkaline resistance improved adhesion, flexibility, and wetting of both pigment and alloy surface. Ideal magnesium particle size distribution should range from 10 to 200 microns. As-submicron sized magnesium is rapidly consumed and acts to over accelerate cure of primer binder.

References

- 1) D. Elizer and A. Antonyraj, Unusual Behavior of Magnesium an ZM Anodes in Aqueous Electrolytes at High Concentrations, Corrosion, April 2001, Pp. 334-345
- 2) M. Nanna, G.P. Bierwagen, Unpublished work shown at IAB poster session, North Dakota State University, October 1999

- 3) J. Genesca, L. Betancourt, and C. Rodriguez, Electrochemical Behavior of a Magnesium Galvanic Anode Under ASTM Test Method G-97-89 Conditions, Corrosion, July 1996, Pp. 502 – 507
- 4) M. Nanna, G.P. Bierwagen, Unpublished work FSCT Poster session , Chicago, October, 2000, & IAB poster session, North Dakota State University, October 2000
- 5) S. Sumner, Resolution Performance Inc./Epon resins, personal communication, September 1999 & Shell Epon resin formulation guide.
- 6) M. Nanna, Departmental Seminar Presentation, North Dakota State University, April, 2001
- 7) Ancamine 2224 Curing Agent bulletin/guide, Air Products Inc., Hamilton Blvd. Allentown, PA, 1998
- 8) D. R. Asklund, The Science and Engineering of Materials, Alternate Edition, PWS Publishers, 1985, Pp. 510-511
- 9) R.R. Roesler, Personal Communication, NDSU, June 8, 20001
- 10) R.R. Roesler, Polyurethanes for Coatings, Bayer Corporation, June 1999, Pp. 32-36

PART III

Certain aspects and embodiments of the present invention are described in the following text and figures.

MG-RICH COATINGS AS CR-FREE PRIMERS FOR AL 2024 T-3

Abstract:

Environmentally allowable alternative coatings to chromate pigments and pretreatments for corrosion control of Al alloy 2024 T-3, commonly used in aircraft, were designed, formulated and tested as primer coatings that provide protection using particulate Mg pigmentation. The system was developed in a manner analogous to Zn-rich primer coatings used for the protection of steel. In the current study four coating polymer systems were examined as possible candidates as Mg-rich polymer matrices for cathodic protect coatings. The first two polymer systems were 1) a commercially available moisture cure aromatic polyisocyanate based upon 4-4'-diphenylmethane diisocyanate, and 2) a standard liquid bisphenol-A epoxy resin cured with a fatty acid polyamide. The solvent system for the first two was a 70:30 xylene/MEK (methyl ethyl ketone) mixture. The third and fourth coating polymer matrices were experimental organosilane modified polyisocyanate-epoxy hybrids, based on two commercially available moisture cure polyisocyanate oligomers, one aromatic and one aliphatic. The epoxy was a popular EEW~500 bisphenol-A resin, and the solvent system for both hybrid coating polymers was propylene carbonate. Mg-rich primers were formulated with 50-micron average particle size magnesium powder, near to the critical pigment volume concentration (CPVC) for this system. They were spray applied to Q-Panel Al 2024 T-3, then subsequently top-coated with Extended Lifetime Topcoat™,* a military aircraft topcoat currently gaining wide acceptance. Scribed coatings systems have been subjected to Prohesion™ exposure in dilute Harrison's solution for up to 5,000 hours. These coatings were the first non-chromated coatings to satisfy 3000 hours of such exposure and remain shiny and undamaged in the scribe area, only showing damage at about 4800 hours. The corrosion byproducts generated in the scribe areas during Prohesion™ exposure were examined by Energy Dispersive X-ray Analysis (EDXA) and the local pH of the coating was determined by the nature of the salt formed as a function of exposure conditions and time.

I. Introduction:

A. Initial Motivation

Following by analogy the formulation of Zn-rich primer coatings for the protection of steel, the formulation of Mg-rich primer coatings for protection of aluminum alloys has been examined in this laboratory. This work has as its motivation the protection of high strength aircraft Al alloys such as 2024 T-3 and 7075 T-6 without the use of chromate-based pretreatments or chromate pigments. This class of alloys, whose high strength is based on phase separated intermetallic compounds within the bulk alloy, have proved resistant to efforts to develop corrosion protective (pretreatment + coating) systems that do not contain any Cr, a metal whose compounds are notorious for their toxicity and carcinogenicity.¹ Further, any aircraft painting or repainting operation that utilizes Cr-based pretreatments generates large amounts of hazardous waste which can be handled properly only at great cost.²

* Deft, Inc., 17451 Von Karman Ave., Irvine, CA 92614

The basic principles of Zn-rich primer coatings are as follows:^{3,4}

1. Coatings are either organic or inorganic in nature (see ref. 3 for further discussion).
2. They are pigmented with particulate Zn, in either spherical or flake form.
3. The PVC of the Zn pigment in the coating should exceed the CPVC in order for the coating to properly provide sacrificial/cathodic protection to the underlying steel substrate. Under these conditions, the Zn particles are all in mutual contact as well as in electrical contact with the steel substrate.
4. The mode of protection by these coatings is sacrificial as long as the Zn is electrically connected to the steel as the Zn is more anodic (reactive) than Fe (major constituent of steel) in the electrochemical series, and then the mixed Zn oxides formed in the sacrificial oxidation fill damaged areas and also sometimes passivate the steel surface by their basic nature. There is some evidence that the electrical connectivity of the Zn particles carries over from the PVC = CPVC (circa 60-70% by volume) to PVC = Volume Percolation Threshold for Zn (~30% by volume for spherical particles), so some sacrificial protection occurs over this range even while the Zn is being consumed by sacrificial oxidation.⁵ The percolation threshold for flake pigments may be different depending on particle alignment.
5. The organic or inorganic matrix of the coating must be stable under the basic environment created by the zinc oxide, hydroxide, etc, formed from the oxidation of Zn in the presence of electrolyte. It must also adhere well to the steel alloys and be stable in a corroding environment.
6. These primer coatings must be top-coated to function properly and have a long field lifetime. When used properly, these primers provide almost as much protection to steel as galvanizing. With a topcoat, they provide both barrier and damage (sacrificial/cathodic) protection to steel substrates.

As work in this lab and others⁶ had shown that satisfactory corrosion protection was not available for Al 2024 T-3 without the use of chromates, many alternate options for protecting this alloy have been considered by this lab and others, including plasma polymer layers⁷ and conducting polymers^{8,9}. Because of the availability of particulate Mg appropriate for use as a pigment in coatings,¹⁰ it was decided to examine the possibility of designing Mg-rich coatings that would protect 2024 T-3 in a manner analogous to Zn protecting iron alloys (steel). There were two confounding features of considering Mg for cathodic protection of Al versus Zn for cathodic protection of Fe. The first was that particulate Mg can be a fire hazard, but this concern was alleviated by the manner in which Mg pigment was delivered by Eckart*. Their particulate Mg has a thin oxide layer that stabilizes it against further oxidation and is shipped already dispersed in an inert organic solvent. The second concern was that the oxidation products of Mg, MgO and its various hydroxides in hydrated form, would create such basic conditions that Al would undergo basic corrosion** as is indicated in its Pourbaix diagram.¹¹ Fe is mostly passive under basic conditions, so this is not a valid consideration for Zn over steel. As shown below, the natural Mg oxidation products do not give a high enough pH to corrode and dissolve Al, so this concern was also alleviated.

* Eckart GmbH, Kaiserstrasse 30, Furth D-90763, Germany

** We thank Prof. J. Frankel of the Dept. of Materials Science at The Ohio State Univ., Columbus OH for pointing this fact out to us.

B. Further Considerations

The primary goal of this Mg-rich technology was the development of a new type of primer for Al alloys and a resultant coating system that is suitable for objects whose structural components are made up of Al 2024 T-3 or other corrosion prone aluminum alloys. The system needed to be easy to apply and repair, and eliminate all use of chromate pretreatments and chromate pigments altogether, if used as the total coating system, by providing cathodic protection to the alloy. In addition, cyanide and other toxic substances are also used in most methods for chromate pretreatments. The secondary goal in this study has been to successfully employ coating matrix polymers with an environmentally acceptable solvent formulation, such as propylene carbonate, so that VOC regulations were met.

II. Proof of Concept: Initial Electrochemical and Exposure Studies

A. Open Circuit Potential and Early EIS Studies

The initial electrochemical studies of several of the initial Mg-rich primers formulated in our laboratory were studies of the primer over Al 2024 T-3 immersed in 3% NaCl solution. The open circuit potential (OCP) and the electrochemical impedance spectroscopy (EIS) spectra of the various primers as formulated in an epoxy-polyamide polymer matrix. The data presented below are for three of these primers based on ECKA Mg at 50, 56 and 60% PVC. These data indicate that the most effective protection from just the primer is at 56% PVC, and this is the CPVC for this system.

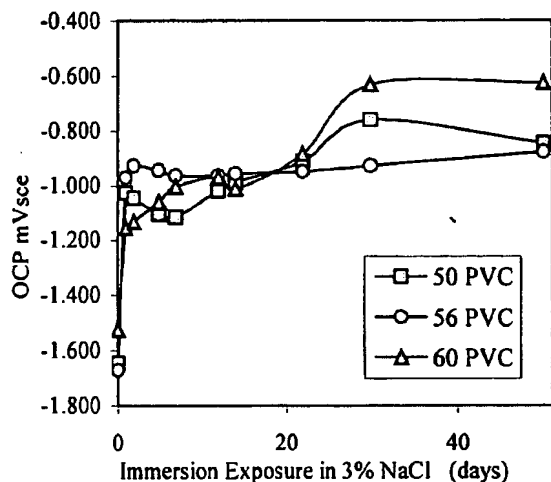


Figure 1. Open circuit potential SCE vs PVC of Mg-rich epoxy/polyamide primers at pH= 6.2 in 3% NaCl ⁽⁶⁾

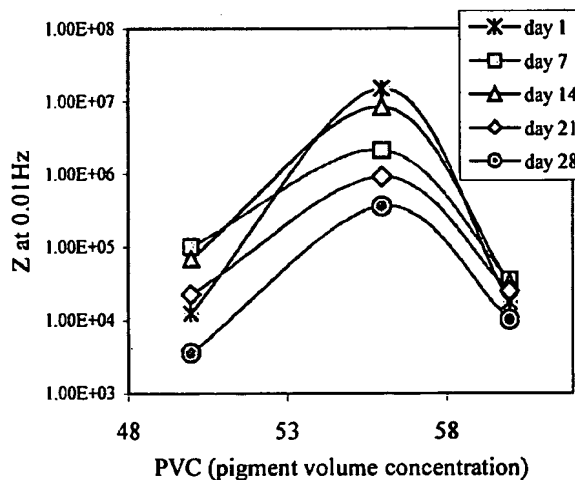


Figure 2. |Z| modulus at 0.01Hz vs PVC of Mg-rich epoxy/polyamide primers at pH= 6.2 in 3% NaCl ⁽⁶⁾

Figure 1 gives (OCP) vs. exposure time for Mg-rich primers, at 50, 56, and 60% PVC in a polyamide/epoxy coating polymer exposed to 3% NaCl solution at pH \approx 6.2. Interpretation of the events is as follows. Initial OCP values for the three sets correspond to a single electron transfer

* The primer binder was a 2K epoxy-polyamide: Epon®1001cx and Ancamide® 2353 at stoichiometric ratios

potential for Mg metal, $E_{Mg} \approx -1.50V$ to $-1.60 V_{SCE}$, and the primers appear to be acting like bare Mg¹². Subsequently, over a 24 hour period, Mg and the Al alloy polarize to a mixed potential, E_{mix} , corresponding to the galvanic corrosion potential, E_{corr} ¹³ at which the Mg is still sacrificially protecting the Al 2024 whose OCP is $-0.68 V$ vs. saturated calomel electrode (SCE). The observed mixed potential for Mg and Al alloy in 3% NaCl was found to be about $E_{mix} \approx -0.90 V$ to $-1.00 V_{SCE}$. OCP values extending beyond the initial 24-hour period varied according to primer PVC. The initial lower mixed potential value, E_{mix} , figure 1, for the 50% PVC sample is thought to be due to the lower effective active metal area as a result of higher polymer coverage at the Mg/Al alloy interface. Initially, the Mg-anode dominates the OCP. The gradual rise in OCP for the 50% PVC sample toward $E_{Al-2024} \approx -0.68mV_{SCE}$ is assumed to be due to reactive consumption of the exposed Mg in this system and the disbonding of epoxy coating polymer from the cathode surface. The gradual decrease in OCP of the 50% PVC sample toward $E_{mix} \approx -0.90 V$ to $-1.00 V_{SCE}$ is thought to be due to resistance polarization by the formation and packing of Mg oxides in the coating. The initial and continuous decrease in OCP of the 60% PVC sample is concluded to be due to a higher void volume in the primer as well as a higher cathode area at the primer alloy interface. The OCP of the 56% PVC sample quickly arrives at the $E_{mix} \approx -0.90 V$ to $-1.00 V_{SCE}$ value and remains constant for the duration of the test time period. Thus, it is assumed that the 56% PVC primer corresponds to the critical pigment volume concentration for the primer. Therefore, suggesting cathodic protection of the Al alloy due to Mg metal occurs most effectively at or near CPVC.¹⁴

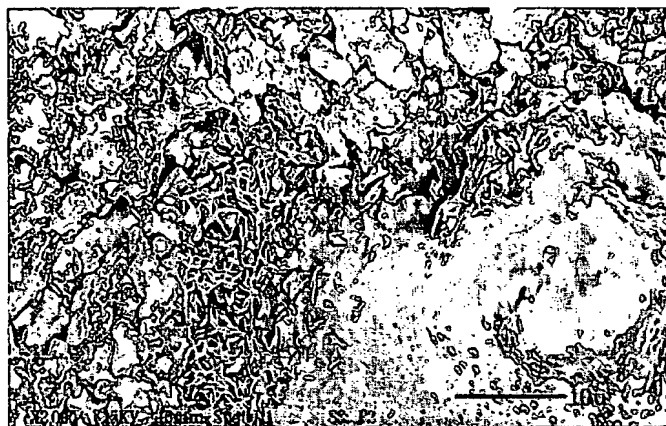
Figure 2 gives the $|Z|$ modulus versus exposure time as measured in 3% NaCl solution at $pH \approx 6.2$ on 50, 56, and 60% PVC Mg-rich primers. This figure demonstrates the effect of PVC at CPVC for Mg-rich primers. The Z modulus values for the 56 PVC samples yielded a higher impedance modulus over the 28-day period suggesting proper formulation at or near the critical pigment volume concentration, which is required to ensure close packing of Mg pigment with minimum resistance from the polymer matrix of the system, but with polymer matrix content sufficient enough to ensure good substrate wetting and reasonable physical properties from the primer.

B. Initial Exposure Studies Using the Prohesion™ Cycle

Prohesion™ cyclic exposure in dilute Harrison's solution with no topcoat follows three distinct events:

1. EDXA spectra have revealed formation of magnesium carbonate hydrates at the primer liquid/vapor interface, dypingite $[Mg_5(CO_3)_4(OH)_2 \cdot 8H_2O]$ & hydromagnesite $[Mg_5(CO_3)_4(OH)_2 \cdot 4H_2O]$. These salts have been observed only to be present up to the first 500 hours of exposure for all non top-coated primed Mg-rich panels tested.
2. For exposure times beyond 500-hours cause brucite $[Mg(OH)_2]$ domains to form and subsequently extend throughout the bulk of the primer. During this time the aluminum alloy remains cathodically protected as scribed lines remain unblemished.
3. For exposure times greater than 1300 hours, primer failure and film delamination corresponds to the accumulation of hexahydrate $[(MgSO_4) \cdot 6 H_2O]$ compound at the interface. Failure occurs, Figure 3, when Mg-metal and brucite structure have been depleted from the coating polymer matrix and sufficient hexahydrate salts have accumulated at the alloy interface. At which time the coating polymer ruptures and fragments from compressive forces exerted by hexahydrate structures.

In the first 24 hours of exposure to salt fog solution with atmospheric CO₂, magnesium forms magnesium carbonate compound, Mg₃(OH)₅*CO₃, which is replaced by a more densely packed magnesium hydroxide Mg(OH)₂ pseudo-hexagonal crystal structure. The rosette structure observed in the magnesium epoxy primer scanning electron microscopy (SEM) images shown in Figure 3 is consistent with *brucite* magnesium hydroxide Mg(OH)₂ (acicular needle) crystal formed in Prohesion exposure.



Title: EPOXY - MG COATING Date: 02-24-2000 Time: 16:11
Comment: SAMPLE 200138 HIGHEST MG LEVEL Filename: 1138.TIF

Figure 3. Underside of exposed Mg-rich primer with magnesium salts 1) Hexahydrite, (upper left), 2) Brucite rosette structure (center), and 3) epoxy binder (lower right)

Further observations were made on the Mg-rich primers exposed to Prohesion cyclic salt fog with dilute Harrison's solution:

- 1) White oxide area magnesium hydroxide (brucite) formed over magnesium metal and energy dispersed X-ray analysis (EDXA) measurements indicated the presence of magnesium, oxygen and aluminum with a minimum amount of carbon detected.
- 2) In the scribed area with no epoxy matrix or magnesium metal originally present, EDXA spectra show carbon, oxygen, magnesium and aluminum with possible presence of dypingite (magnesium carbonate) structure over the exposed aluminum surface.

Table 1. Magnesium salts solubility pH

Salt (designation)		K _{sp}	H ₂ O g/100ml	pH
Mg(OH) ₂	<i>Brucite</i>	2.5 x 10 ⁻¹² *	7.8 x 10 ⁻⁴	10.7 ~ 11 **
MgCO ₃ 5* H ₂ O	<i>Magnesite</i>	3.8 x 10 ⁻⁶ *	0.002 ***	8.0 ~ 8.8 ***
MgSO ₄ 6* H ₂ O	<i>Hexahydrite</i>	(soluble)	95 ***	6 ~ 9 ***

* CRC Handbook of Chemistry and Physics, 68th Ed., Boca Raton, FL (1987-88)

** Shand, M., Magnesium Hydroxide -A safer alternative to Caustic Soda, Premiere Chemicals, 5/9/02

*** Seelig, B.D., Salinity and Sodicty in North Dakota Soils, EB-57, North Dakota Extension Service, May 2000

In summary, Table I gives the relative pH, the solubility product, and the water solubility for magnesium salts identified in EDXA spectra. It was observed that the salts generated during the first 1000 hours of exposure generated local pH in damaged areas which did not degrade either the coating polymer or the alloy surface.

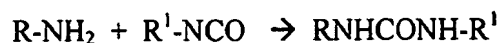
C. Conclusions of Preliminary Feasibility Studies

These results were obtained from a simple Mg-rich coating based on an off-the-shelf (OTS) polymer system with no optimization efforts. They showed that the oxidation products of the Mg pigment in an exposure environment, fairly typical of what an actual system might see in field exposure, did not cause basic corrosion of the Al 2024 T-3 alloy. Further, the Mg-rich system did provide a type of cathodic protection to the Al 2024 T-3, giving the system significant corrosion protection properties in a completely Cr-free system. The research studies now proceed to improvement of the coating polymer system and additional formulation studies.

III. Formulation Improvement by Coating Polymer Design and Preparation

A. Coating Polymer Selection

It has been well documented that the best deterrent to adhesion failure in organic coatings lies in developing the right chemical interactions between the coating polymer, pigment, coating layers, and their metallic substrates.¹⁵ The most effective strategy, thus far, has been to develop coatings whose polymer matrix hydrophilicity decreases during cure as the polymer matrix coating undergoes film formation and solidifies. Organofunctional silanes are commonly used as coupling agents and adhesion promoters in epoxide and urethane paints to improve their initial, wet, and recovery adhesion to aluminum surfaces. The "Reversible Hydrolytic Bond Mechanism Theory", discussed by Walker¹⁶, proposes the reversible breaking and reformation of stressed bonds between a coupling agent and the substrate, which allows stress relaxation without the loss of adhesion when water is present. It is argued that when Si-O-metal bond is broken by intrusion of water, the bond will be capable of reforming with some recovery in adhesion.¹⁷ Chemical reactions between organofunction silanes and some component of a polymeric coating polymer is expected to occur between a N-beta-aminoethylaminopropyl-trimethoxysilane (A-1120), $\text{NH}_2(\text{CH}_2)_2 \text{NH}(\text{CH}_2)_3\text{Si}(\text{CH}_3)_3$ [$\text{R} \equiv (\text{CH}_2)_2 \text{NH}(\text{CH}_2)_3\text{Si}(\text{CH}_3)_3$], and a substituted isocyanate group to form initially a substituted urea



and then further react with another isocyanate group to form a biuret.^{18,19} Alkoxy silanes can hydrolyze in a multi-step process with water to form silane triols.²⁰



2-ethyl-3-ethoxypropionate (EEP) is primarily used as a retarder in coatings containing polyisocyanates as it possesses slight water solubility, not toxic, low vapor pressure, (inhalation unlikely), little effect skin contact. In this coating system EPP has been found to be an effective retarder when used at about 15% on total solvent system. Propylene carbonate (PC) is commonly used

as a urethane prepolymer viscosity reducer.²¹ PC is the primary carrier solvent used in this system, it is used as both a polar activator and wetting agent, (polar activators function by disrupting weak Van der Waal forces) which in turn enhances silane reactivity at the aluminum surface. Propylene carbonate wets both aluminum and magnesium powder and is an excellent solvent for both the epoxy and polyisocyanate. Improved solvent evaporation from films cast using a PC and EEP solvent mix appears due to an azeotropic effect between PC, EEP and the particular polymeric binder system. Films cast from other oxygenated ketone solvents were found to require heating to 40°C to drive out solvent as all other oxygenated ketone solvent mixtures caused beading of PC over the surface of the coating film. Both solvents have been found suitable in Mg-rich coatings with organo-functional silanes and polyisocyanates such as hexamethylene diisocyanate (HMDI). Moisture-cure polyurethanes (MC-PUR's), such as diphenylmethane diisocyanate (MDI) Desmodur® E23-A from Bayer Corp., are used as coating polymers in Zinc-rich coatings applied to refurbishing of steel structures and require photo-active aromatic solvents that are environmentally unacceptable.²³

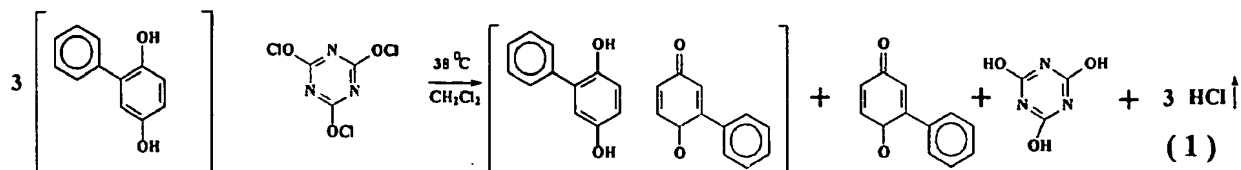
B. Hybrid Coating Polymer (Organic-inorganic Non-Covalent IPN Materials)

Non-covalent interpenetrating network (IPN) materials incorporate a low loading of inorganic phase into polymers ranging from polyacrylates, polyesters, to polyimides and nylons. The lower inorganic loading helps promote effective interfacial interactions between the organic-inorganic phases of the material without sacrificing interfacial bonding. An interpenetrating polymer network (IPN) polymer alloys consist of two or more distinct crosslinked polymer networks held together by permanent entanglements.²⁴ Frisch *et al.*²⁵ first reported simultaneous interpenetrating networks (SINs) composed of a polyurethane (PU) combined with an epoxy resin. The epoxy-urethane reaction occurs when the secondary hydroxyl group in the epoxy backbone is reacted with an isocyanate which gives rise to the hybrid structure of such SINs.²⁶ Epoxy resins and modified epoxy systems generally yield excellent heat resistance, mechanical properties and adhesion. However the same secondary hydroxyls that introduce polarity, which is beneficial for adhesion and pigment wetting, also yield undesired high viscosities in polar solvent systems. End-capping free hydroxyls or addition of a high percentage of reactive diluent to reduce viscosity can cause film brittleness, shrinkage and compromise film quality. The overall objective of this work is to produce a silane modified *non-covalent IPN* with a more flexible, lower viscosity oligomer.

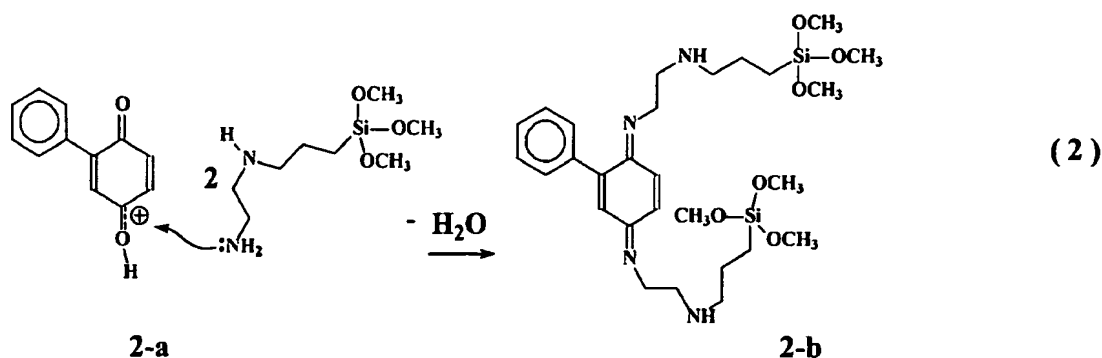
C. Preparation of Silane modified Poly(Ureoxy) 'Epoxy-Urethane' with Crosslinked Structure

Phenyl-hydroquinone, and trichloroisocyanuric acid, obtained from Aldrich, and N-beta-(aminoethyl)-gamma-aminopropyltrimethoxysilane Silquest®* (A-1120), supplied graciously by Witco OSi Specialties, were used as received. Phenyl-hydroquinone is gently oxidized in tetrahydrofuran (THF) to phenyl quinone and the spent oxidizer (isocyanuric acid) is filtered out. The first reaction (1) yields an 60% conversion to phenyl-hydroquinone with a remainder of 40% starting material (phenyl hydroquinone), the product is essentially quin-hydrone.

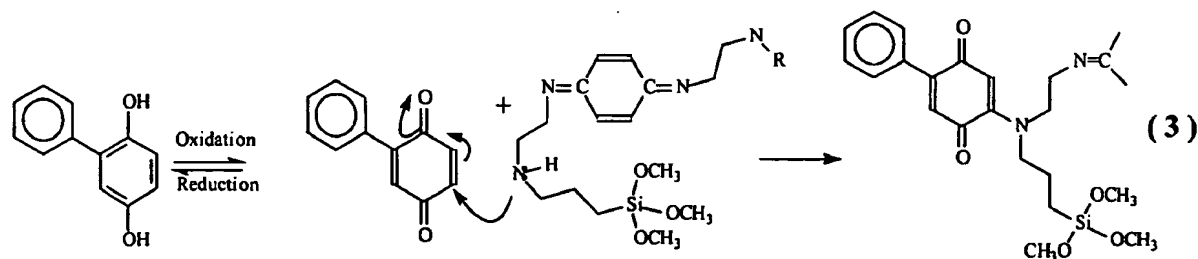
* Silquest® registered trademark of OSi Specialties, Crompton Corporation, 771 Old Saw Mill River Road, Tarrytown, NY 10591, USA



The product mix from reaction 1 was identified as a 60:40 ratio using UV-VIS, by examining n ranging from 10: 90 to 90:10 of phenyl-hydroquinone (Aldrich) maximum abs. 290nm, phenyl-quinone (Sigma-Aldrich) maximum abs. 360nm. The second reaction product (2) results from nucleophilic attack on the α,β unsaturated phenyl-quinone carbonyl moiety by the primary amine of β -amino-(aminoethyl)- γ -aminopropyltrimethoxysilane under acidic conditions. The reaction is carried out under acidic conditions in EEP/propylene carbonate solvent mixture and the resulting N,N''-Bis (2,5-phenyl) benzoquinone Diimine is observed to form preferentially.²⁷ Product 2b (Red solid) examined with FTIR 2913, 1578 (C=N), 1479, 1270, 1060, 695 cm^{-1} ; ^{13}C -NMR δ (CDCl_3), 25°C): 29.6, 42.7, 66.1, 117.9, 127.4, 135.2, 140.7, 149.8; ^1H -NMR δ (CDCl_3), 25°C): 7.24 (s,H), 7.37 (q,4H) 7.40 (q, 4H), 7.44 (d, 2H); 6.62 (d, 2H), 6.85 (s, 4H), 3.56 (s broad, OH), 2.129 (s, 6H). Note, after 72 hours equilibration, 3.56 (s broad, OH) disappears from ^1H -NMR spectrum (indication of oxidation of phenylhydroquinone to phenylbenzoquinone). FTIR corroborates with diminished (C=N) 1578 cm^{-1} and the appearance of (C=O) 1660 cm^{-1} quinone. The proposed mechanism phenylhydroquinone is easily oxidized in the presence of the propylethylenediamine moiety and in turn undergoes Michael addition as depicted in reaction 3.



The intermediate product from reaction (2) may in turn react through secondary amine with oxidized hydroquinone, oxidized by isocyanate present, and yield a phenylquinone-N,N'' Bis (2,5-phenyl) benzoquinone Diimine.²⁸



3a

The salient feature of the synthesis is that it yields both imine and quinone moieties in the polymeric binder. Imines function as (contact corrosion inhibitors) when used with inhibitive pigments such as zinc, aluminum, zinc oxide, modified ZnO, and calcium ion-exchanged amorphous silica gel.³⁰ Imines protect metal surfaces as the nitrogen has electrons that are attracted to polar metal surfaces, while the rest of the molecule remains hydrophobic and repels water to significantly retard corrosion.³¹ Nikles et al.²⁸, found that "amine-quinone polymers could displace water from the surface of iron, making it hydrophobic..., then they would inhibit corrosion." The inhibiting effect can be attributed to the abundance of π electrons on the nitrogen that can interact with the d-orbitals of the metal to coordinate the bond.³²

The presence of imine and quinone functionality in poly(ureoxy) films can be followed by FTIR spectroscopy. Imine functionality shows a red color with a characteristic (C=N) 1578cm^{-1} absorption, while quinone functionality shows a yellow color with characteristic (C=O) 1660cm^{-1} absorption. Figure 4 shows four reflectance curves taken from 2-mil poly(ureoxy) coatings on Al 3015 panels. The characteristic reflectance of each curve can be related to the chemical composition of the dominant functional group present in the coating. It can be used as an indication of whether the imine functionality or the quinone functionality is present. For example, coating SE-23A_3_15 has a high yellow reflectance and denotes a non-propylene carbonate solvent system coating where no imine functionality is present. Coating PCE-23A_3_15, yields red reflectance, the same formulation with propylene carbonate as the carrier solvent, shows green adsorption circa 520nm indicating the presence of the imine functional group. Coatings PCE-23A_15_11 and PCE-23A_8_2, both reddish-brown, are similar poly(ureoxy) coatings formulated at higher (NCO/OH) and lower (NCO/OH) ratios respectively with an excess of amine over SE-23A_3_15 and PCE-23A_3_15. It is proposed that excess amine shifts equilibrium to favor imine formation as opposed to exclusively quinone formation as in SE-23A_3_15. By judicious solvent selection, the nature and quantity of the functional groups in the polymer binder can be controlled.

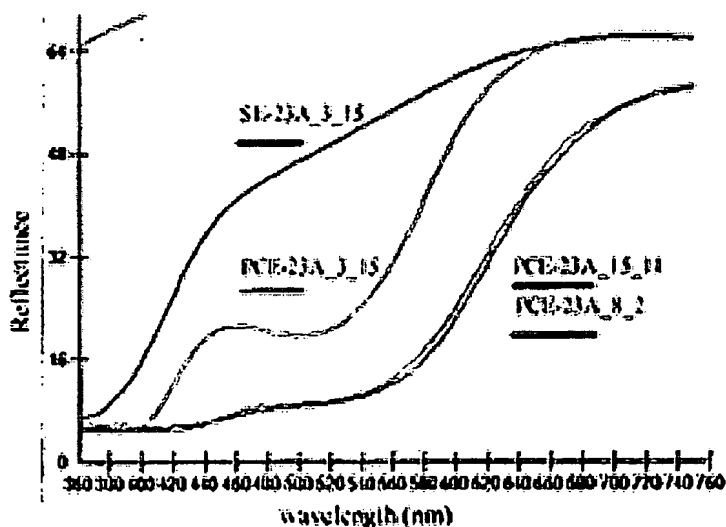


Figure 4 Reflectance curves for 2-mil films of poly(ureoxy) coatings on Al 3015 panels. SE_23A_3_15 (2-methoxyethyl acetate) solvent; PCE_23-A_3_15 (propylene carbonate) Solvent; PCE-23A_15_11 (propylene carbonate) solvent, high (NCO/OH) ratio, high amine; PCE-23A_8_2 (propylene carbonate) solvent, lower (NCO/OH) ratio, high amine.

D. Coating Formulations

Formulation	Material s
-------------	------------

#1) MC-PUR	Desmdodure® E23-A, Bentone® 34, Eckagranules® PK 31, Anti Terra U, Aromatic 100/Xylol
#2) Epoxy-Polyamide	Epon® 862, Epicure® 3115, Aerosil R202, Eckagranules® PK 31, Anti Terra U, Aromatic 100/Xylol,
#3) Hyb-EA23	Desmdodure® E23-A, Aerosil R202 , Eckagranules® PK 31, Epon® 1001CX, Propylene Carbonate/Methoxy Acetate
#4) Hyb-N3300	Desmdodure® NC-3300, Aerosil R202 , Eckagranules® PK 31, Epon® 1001CX, Propylene Carbonate/Methoxy Acetate

IV. Mg-rich Coatings Formulation and Characterization Studies

* Desmodure® registered trade mark of Bayer Co. 100 Bayer Rd., Pittsburgh, PA, 15205-9741

- 33 -

Magnesium powder bulk density was determined by measuring the powder's density after ultrasonic treatment for 45 minutes. Sonication improved dispersion of the pigmentary Mg, yielding a higher bulk density value than reported by the manufacturer. Critical pigment volume concentration (CPVC) for each primer was first crudely determined from oil/powder rub-ups.³⁴ Magnesium powder, 50 μm average diameter, (Eckagranules™ PK 31) was provided by Eckart Inc. and was used as received.

B. Characterization of Mg-rich Coatings Properties

1. Panel and Film Preparation

The primers based on the materials, given in Table 2, were prepared using conventional techniques: the pigment was dispersed in a polymer solvent mix and Bentone-Gel™, or Aerosil, was added to the letdown mix. Viscosity was adjusted by dilution and adjusted with a No.4 Ford cup to 24 seconds. Primers were applied to lightly wire brushed 6" x 3" Al 2024 T3 Q-panels™, rinsed and degreased with methoxy-acetate, immersed in a 10% phosphoric acid solution for 60 seconds, and then rinsed with distilled water. Mg-rich coatings were applied with a touch-up spray gun at an adjusted air pressure of 60 psi. The coatings ambient cured at 20° C for 14 days. The average primer film thickness was measured with Elco-meter at 1.8 +/-0.2 mils. Primed panels were top coated with Extended Lifetime™ Topcoat. The average topcoat film thickness was measured at 1.2 +/-0.2 mils. Polymer film samples for further mechanical testing were cast over a Teflon™ sheet. Moisture cured films were exposed at 80% relative humidity at 50 ° C for 7 days, while epoxy-polyamide films were cured for 14 days at 50 ° C, and hybrid polymer films were ambient cured at 25 ° C for 7 days.

C. Testing of Mg-rich Coatings

1. Mechanical Properties of Mg-Rich Coatings

All mechanical testing was performed according to the following ASTM standards: reverse impact resistance (ASTM D 2794-84), pull-off adhesion (ASTM D 4541-85), and tensile properties (ASTM D 2370-82). For reverse impact and pull-off adhesion, three sets of measurements were made per sample and at least six per sample in tensile tests. Tensile properties were measured using an Instron™ model 5542 with Merlin (2) software. The dimensions of films in tensile test were 0.06 to 0.20 mm in thickness, 12 mm in width and at least 40 mm in length. A crosshead speed of 20mm/min was used to determine elongation-at-break, tensile modulus, and tensile strength. The mean and standard deviation for each polymer sample set is reported. DMTA measurements were made with a Rheometrics model 3-E dynamic mechanical analyzer.

2. Flammability Testing of Mg-Rich Coatings

Six inch strips were cut from top-coated Mg-rich Al panels and subjected to a modified flammability test, referenced in document IPC-SM840B paragraph 3.6.3 and 4.4.8. Also refer to test method 2.3.10.1 and the U.L.-94 flammability specification using a Bunsen burner, tube length 4", I.D. 0.37" with methane gas at equivalent 1000 BTU/Ft³. The test was further modified by scribing an X over the entire length of the surface of each sample strip to expose the magnesium metal in the primer.

3. Exposure Testing

Prohesion™ exposure was performed according to ASTM test method B117. Top-coated Mg-rich panels were prepared by covering panel backside and edges with 3M electroplater's tape and edges were then sealed with a 2-K industrial epoxy from Aldrich. Top-coated panels were scribed through the entire coating with a carbide tip glass scribe, forming an X pattern, thus exposing the Al surface.

V. Test Results

1. Mechanical Properties of Mg-rich Coatings

Table 3 shows the mechanical properties of the primer coatings as a function of PVC and for pull-off adhesion as a function of exposure time in a solution of 3 % NaCl for a duration of 4 weeks. The pull off-adhesion is sensitive measurement that can differentiate between coatings that develop a reversible breaking and reformation of stressed bonds without the loss of adhesion when water is present. In the conventional coating systems, high VOC coatings MC-PUR and epoxy-polyamide initial pull-off adhesion were comparable to the hybrid coatings. However, without the silane-coupling agent these two coating systems failed wet adhesion in spite of both the polymer matrix's hydrophobic nature. The reverse impact results suggest coatings formulated near CPVC require a coating polymer with a high tensile modulus.

Table 3
Mechanical Properties of Mg-Rich coatings

Coating	PVC	MC-PUR	Epoxy-Polyamide	HyE23-A	HyN3300
Pull-off adhesion (lb _f /in. ²)					
(initial)	(50% PVC)	150	90	175	100
	(55% PVC)	200	80	150	175
	(60% PVC)	140	50	150	175
(5 week exposure 3% NaCl)					
	(50% PVC)	80	25	400	200
	(55% PVC)	30	35	300	225
	(60% PVC)	90	25	350	400
Reverse Impact (inch-lb.)					
	(50% PVC)	30	0	30	60
	(55% PVC)	30	10	10	60
	(60 %PVC)	30	20	0	60

Tensile tests were conducted on coating polymer film- strips with no visible voids. Table 4 gives a summary of the measured tensile properties of coating polymer films:

Table 4
Mechanical properties of coating polymer films

Polymer Film	Elongation at-break (%)	Tensile strength (MPa)	Tensile modulus (Mpa)
MC-PUR	8.0 ± 0.3	25 ± 6	825 ± 110
Epoxy-polyamide	18.0 ± 0.1	5 ± 0.9	150 ± 50
N3300 (MC-PUR)	5.0 ± 0.1	45 ± 7	1250 ± 90
Hyb-N3300	6.0 ± 0.3	56 ± 9	1800 ± 50
Hyb-E23-A	4.5 ± 0.2	50 ± 5	1500 ± 50

2. Viscoelastic Properties of Coating Polymers

The material's mechanical loss or damping is given by the quantity $\tan \delta$ that is the ratio of its out of phase deformation to in phase deformation (E''/E'). The maximum in the $\tan \delta$ is used to identify the glass transition temperature T_g of the polymer.²⁹ The measured viscoelastic properties for the three coating polymers in table 5 reveal a wide range of variation in T_g and elastic storage modulus E' (minimum). The significant differences in reported glass transition temperatures are assumed to be related to the individual coating polymer composition and free-volume. Crosslink density calculated from (E') at $T_g + 50^\circ\text{C}$, where ν_e is the elastically effective crosslink density.³⁰

$$\nu_e = 3 E' / RT (T + T_g)$$

Table 5
Viscoelastic properties of binder films

Binder	T_g ($^\circ\text{C}$)	Crosslink density ν_e (mol/cm ³)	E' (Pa) minimum
MC-PUR	159	5.8×10^{-4}	6.6×10^5
Epoxy-polyamide	65	2.1×10^{-3}	2.0×10^7
Hyb-N3300	96	1.3×10^{-3}	1.3×10^7
Hyb-E23-A	100	6.9×10^{-4}	6.9×10^6

3. Flammability

Figure 5 Flammability test for topcoated samples exposed directly to blue-cone tip of Bunsen flame for 30 seconds. From left to right for the Hyb-N3300, the Hyb-E23-A, the MC PUR E23-A, and the Epoxy-Polyamide. The least affected was the Hyb-N3300 coating at 60% PVC as the magnesium in the coating did not burn and only slight incineration of the polymer matrix occurred. The Hyb-E23-A @ 60 PVC coating gave the appearance of black soot indicating a higher degree of coating polymer incineration with only slight magnesium powder involvement. Two conventional coatings, formulated at 60% PVC, incinerated after 15 seconds exposure. The sequence of events leading to failure, in chronological order, are as follows: loss of adhesion and lifting from the substrate occurring within the first 10 seconds about the cut and scribed areas, rapid discoloration and coating polymer incineration at 15 seconds, and finally ignition and combustion of magnesium powder occurring at 20 seconds exposure. Overall, there was no difference in result between scribed and unscribed samples.

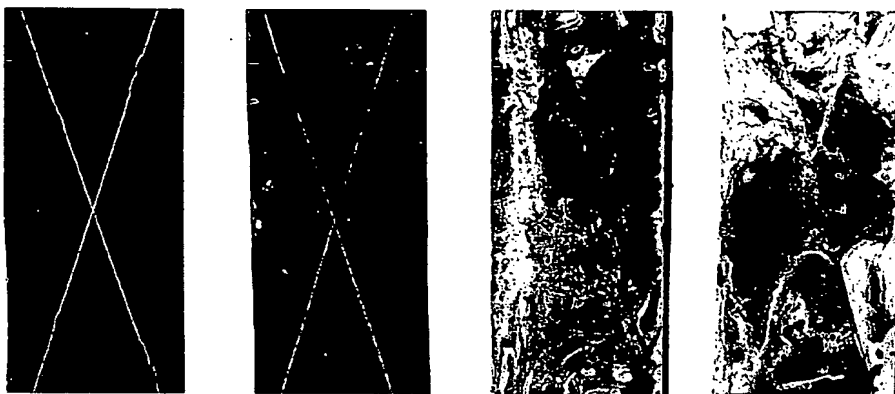
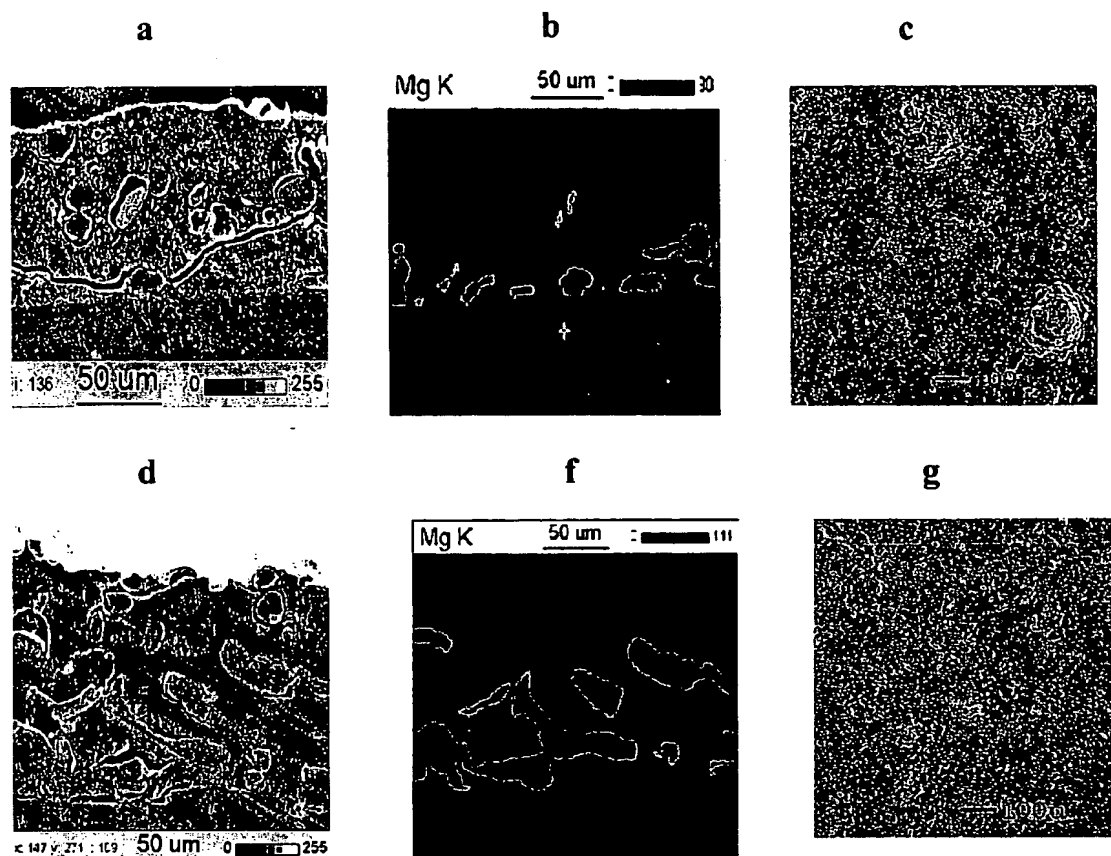


Figure 5 - modified UL-94 flammability test. Left two panels Hyb-N3300, and HybE23-A (hybrid binders), right two panels MC-PUR and Epoxy-Polyamide

4. Micrographs SEM and X-Ray Fluorescence

The physical structure and features of the final coating system, primer plus topcoat, are strongly influenced by chemical interactions between the coating polymer, pigment, coating layers, and the metallic substrate. For example in figure 6a, the MC PUR E23-A Mg-rich primer with ELT fluorinated polyurethane topcoat shows a distinct fissure as a boundary line runs between primer and topcoat. The defect may have originated as a result of film formation effects along the base of the topcoat film. Figure 6b gives an XRDA map of the magnesium metal distribution in the primer at the alloy surface. Figure 6c is a SEM topological scan at 50-x of the topcoated surface, which reveals a coarse profile as expected from a matte coating (the ELT) over a very high PVC primer. The structural features revealed in figures 6 a,b, and c suggest that magnesium powder was poorly wetted by this coating polymer which resulted in a poor primer film structure. In sharp contrast figures 6 d, e, and f, taken of the Hybrid E23-A primer and topcoat system, reveal a well-formed integral primer structure with close packed magnesium particles in the primer, along with a smoother more homogeneous surface profile from the topological scan in 6 f. Samples were assembled on aluminum mounts and coated with gold using a Technics Hummer II sputter coater. Images were obtained using a JEOL JSM-6300 Scanning Electron Microscope. X-ray information was obtained by a ThermoNoran EDX detector using a VANTAGE Digital Acquisition Engine.



Figures 6a, b, d, and e are SEM cross section profiles of MC-PUR Mg-rich primer and topcoat and Hyb-E23-A respectively. Figures VII b and f correspond to X-ray fluorescence specific to magnesium counts (in red) for MC-PUR Mg-rich primer and topcoat and Hyb-E23-A.

Discussion of Results

Flammability Results

The utility of a coating lies in its inherent ability to protect a substrate from environmental degradation. A coating that supplies the potential to incinerate the very structure it has been designed to protect is worthless. Early in this work it was realized that conventional binder systems only promoted magnesium powder incineration when subjected to flammability exposure, which resulted in emphasis on developing a non-incinerating Mg-rich polymer vehicle. Results from the flammability tests revealed that once the conventional coating had disbonded from the Al substrate the paint burned with magnesium incinerating. Both hybrid coatings were found to firmly adhere to Al substrate even after 30 seconds exposure to direct flame, thus preventing incineration. Conventional binders evolved black soot when burned while hybrid binders did not evolve soot.

Mechanical Property Results

The mechanical properties of the Hybrid coatings were superior to the conventional coatings in pull-off adhesion after 5-week exposure to 3% NaCl solution. The tensile properties of the Hyb-N3300 and Hyb-E23A were both superior to their parent moisture cure Desmodure® N3300 and E-23A films in addition to the epoxy-polyamide coating. These results suggest an improved hybrid silane modified poly(ureoxy) binder to be a superior vehicle for active metal filled primers. Viscoelastic DMTA measurements show the Hyb-N3300 and E-23A both possess higher (E') elastic modulus while retaining a moderate T_g , thus supporting the formation of elastically effective crosslink networks with good chemical resistance and modulus.

Prohesion® Exposure Results

Prohesion™ exposure in dilute Harrison solution, (NH_4SO_4) acid rain emulation, resulted in Mg-Rich coatings with conventional binders maintaining clean scribes for up to 2,000 hours, and those formulated with hybrid binders realized clean scribes from 3,000 to 4,800 hours exposure. It is proposed that the nature of the topcoat's porosity influences the kinetic dissolution of magnesium metal in the Mg-Rich vehicle.

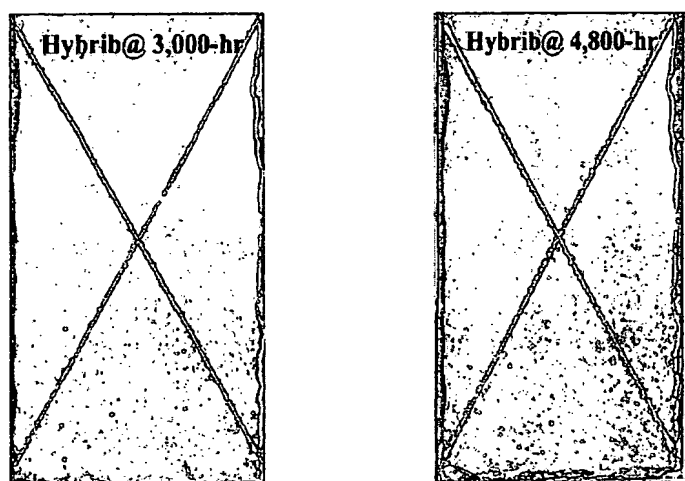


Figure 6a and b, Prohesion™ results for Al 2024 T-3 panels with Mg-Rich primer (Hyb-N3300) with ELT™ topcoat at a) 3000 and b) 4,800 hours exposure.

Conclusion

The impetus for this research has been to deliver a simplistic but effective coating system for cathodic protection of aluminum alloy structures comprised of environmentally acceptable components. The solvents used in this coating system are EEP and PC both classified as *non-Haps*, (non hazardous air pollutants). The major emphasis in polymer binder matrix development lies in harnessing the anti-corrosive properties inherent to the imine substituted benzoquinone and amine substituted phenyl quinone intermediates. The importance of a suitable polymeric matrix lies in its resistance to acid degradation in the presence of an active metal such as magnesium. Previous studies in our laboratories show that both polyamine/polyamide and fatty acid polyamide cured epoxy lacquers used as vehicles

for Mg-rich primers were susceptible to acid degradation, and that epoxy resins cured with amine-quinone curatives greatly increased acid resistance of the polymer matrix. An excellent electrochemical analysis, by Ellingson¹³, was performed on Mg-rich primers formulated from polyamide-epoxy lacquers in our laboratories. This electrochemical study has aided insight and understanding of the basic mechanism accounting for cathodic protection of Al 2024 T-3 alloys by Mg-rich coatings. Similar future electrochemical studies must, however, be tailored to the more acid resistant polymer binder matrices and their relationships to PVC and CPVC in the presence of an active metal.

The following conclusions can be reached based on this study:

1. The (Mg-rich primers + Extended Life Topcoat) coatings systems are the first non-chromated coatings systems to satisfy 3000 hours of such exposure and remain shiny and undamaged in the scribe area, only showing damage at about 4800 hours.
2. The degradation of Mg-rich coatings in acid-rain atmospheres was found to be controlled by the nature of the salts formed and was found not to be deleterious to the Al substrate.
3. A superior, room temperature cure, polymer matrix was synthesized by first reacting an amino-functional silane with an α,β unsaturated phenyl quinone. The silane modified imine/quinone serves as the effective intermediate which can be incorporated into both the epoxy and urethane portions of the polymer's organic matrix.
4. Incorporation of a silane modified organic-inorganic Non-Covalent IPN with multi-functional crosslink potential yields a superior polymer system adding many desired properties including burn-flame resistance, adhesion, mechanical properties, total system performance, and durability.

The overall objective of the foregoing study has been to examine magnesium pigments as a potential raw material for use in anticorrosive Mg-rich primers and to determine the underlying relationships between primer coating polymer, magnesium PVC, and corrosion by-products formed. It also aims at establishing how and if they may detrimentally affect the aluminum alloy during service. The significance of all these findings is that a more extensive knowledge base has been developed and tested on materials, formulation techniques, and application of coatings formulated with magnesium powders for cathodic protection of aluminum alloys. These results can now be compared and contrasted to coatings that both parallel and differ from existing Zinc-rich coating systems, which have been used extensively to provide cathodic protection to steel structures. In summary, while the full optimization of this technology is yet to be realized, a wide range of possibilities and variations in coating polymer components exist, making this a most interesting and valuable raw material for use in achieving corrosion control with environmentally benign coating systems.

References and Literature Cited

-
- ¹ J. Janata, D.Baer, G.P.Bierwagen, H.Birnbaum, R. Buchheit, O.Davenport, H.Isaacs, F.Hedberg, M.Kendig, F.Mansfeld, B.Miller, A.Wieckowski, & J.Wilkes, "Issues Related to Chromium Replacement," presented at 187th Meeting of The Electrochemical Society, May 21-26, 1995, Reno, Nevada
- ² R.L.Twite, G.P.Bierwagen, "Review of Alternatives to Chromate for Corrosion Protection of Aluminum Aerospace Alloys," Prog. Org. Coatings, 33 (1998) 91-100
- ³ C. Hare, "Corrosion Control of Steel by Organic Coatings," Ch. 55 in *Uhlig's Corrosion Handbook*, 2nd Edition. R. W. Review, Editor, John Wiley & Sons, New York (2000) pp.1023-1038

- ⁴ S. Felix, R. Barajas, J.M.Bastidas, M. Morcillo & S. Feliu, "Study of Protections Mechanism of Zinc-Rich paints by Electrochemical Impedance Spectroscopy," in *Electrochemical Impedance Spectroscopy, ASTM STP 1188*, J.R.Scully, D.C.Silverman, & M. Kendig, eds., Amer. Soc. Testing and Materials (ASTM), Philadelphia, PA (1993) pp. 438-449
- ⁵ S. Böhm, R.J. Holness, H.N. McMurray and D.A. Worsley, "Charge percolation and sacrificial protection in zinc-rich organic coatings," Eurocorr 2000, Queen Mary and Westfield College, London, 10th-14th September 2000
- ⁶ Joseph H. Osborne, Kay Y. Blohowiak, S. Ray Taylor, Chad Hunter, Gordon P. Bierwagen, Brenden Carlsion, Dan Bernard, and Michael S. Donley, "Testing and Evalation of Non-Chromated Coating Systems for Aerospace Applications," *Prog. Organic Coatings*, 41 (2001) 217-225
- ⁷ H.K.Yasuda, C.M.Reddy, Q.S.Yu, J. Deffeyes, G.P.Bierwagen & L.He, "Effect of Scribing on Corrosion Test Results," *Corrosion*, 57, (2001) 29-34
- ⁸ Jie He, Victoria Johnston Gelling, Dennis E. Tallman, Gordon P. Bierwagen and Gordon G. Wallace, "Conducting Polymers and Corrosion III: A Scanning Vibrating Electrode Study of Poly(3-Octyl Pyrrole) on Steel and Aluminum," *J. Electrochem. Soc.*, 147 (2000) 3667-3672
- ⁹ D.E.Tallman, Y. Pae, & G.P.Bierwagen, "Conducting Polymers and Corrosion 2: Polyaniline on Aluminum Alloys," *Corrosion*, 56 (2000) 401-410
- ¹⁰ Information from Eckart GmbH, Kaiserstrasse 30, Fürth D-90763, Germany and technical references therein
- ¹¹ Jones D. A. Jones, *Principles and Prevention of Corrosion*, 2nd Ed., Prentice-Hall, Upper Saddle River, NJ (1996), Ch. 2
- ¹² Song G., Atrens A., StJohn D., Nairn J., Li Y., "The Electrical Corrosion of Pure Magnesium in 1N NaCl," *Corrosion Science*, Vol. 39, Pp 5, 855-875, (1997)
- ¹³ Lisa Ellingson, "Corrosion Studies for the Protection of Aluminum Alloys and Outdoor Bronze," Masters Thesis, North Dakota State University, June 2001
- ¹⁴ Hare C.H., and Wright S.J., "Anti-Corrosive Primers Based on Zinc Flake," *J Coatings Tech*, 54, No. 693, (1982) 65-76
- ¹⁵ W.Funke, "Problems and Progress in Organic Coatings Science and Technology," *Progress in Organic Coatings*, 31 (1997) 5-9
- ¹⁶ Walker, P., "Organo Silanes As Adhesion Promoters for Organic Coatings," *Journal of Coatings Technology*, Vol. 52, No. 670, November 1980, Pp. 49-61.
- ¹⁷ Rosen M.R., "From Treating Solution to Filler Surface and Beyond The Life History of a Silane Coupling Agent," *J. Coatings Technology*, 50 (1978) (No.644) 70 - 82
- ¹⁸ Dusek, K., Spirkova, M., Havlicek, I., "Network Formation of Polyurethanes due to Side Reactions," *Macromolecules*, Vol. 23, Issue 6, 19 March, 1990, Pp. 1774 - 1781
- ¹⁹ Vanderbuilt, B. M., and Clayton, R.E., *Ind. Eng. Chemistry*. No 4(1965), 18
- ²⁰ Bjorksten, J., and Valger, L.L., *Mod. Plastics*, 29 (1952) 124
- ²¹ BASF Tech data sheet, BASF Co. Chemicals Division 3000 Continental Drive-North Mt. Olive, NJ, (www.basf.com)
- ²² BASF Tech data sheet, BASF Co. Chemicals Division 3000 Continental Drive-North Mt. Olive, NJ, (www.basf.com)
- ²³ Schwindt, J., "Moisture-Cured, Polyurethane-Based, Surface Tolerant Coatings: An Economical Alternative for Corrosion Control," Technical literature from Bayer AG, Leverkusen, Germany, (2000)
- ²⁴ L.H.Sperling, *Interpenetrating Polymer Networks and Related Materials*, Plenum, New York (1981)
- ²⁵ H.L.Frisch & D. Klempner, *Polymer Eng. Sci.*, 14 (1974) 646
- ²⁶ K.H. Hseih & T.H.Han, J., *Polymer Sci. Part B: Polymer Physics*, 28 (1990) 623
- ²⁷ Bakola-Christianopolou, Maria N., Silyation-desilylation of quines and their derivatives, *Appl. Organometallic Chemistry*, Vol. 15, Pp. 889-900, (2001)
- ²⁸ Han M., Nikles D.E., Amine-Quinone Polyurethanes Containing N-Alkylated Amine-Quinone Monomers, *J. Polymer Sci: Part A: Polymer Chemistry*, Vol 38, 3284- 3292 (2000)
- ²⁷ Hare C., *Protective Coatings – Fundamentals of Chemistry and Composition*, Technology Publishing Co., Pittsburgh, PA, (1994) ch. 15& 16,
- ²⁹ Prenosil M., Volatile Corrosion Inhibitor Coatings, CORTEC Co., Suppliment to Materials Performance, January 2001, Pp 14-17
- ³⁰ Y.I. Kuznetsov, et al., Inhibiting Action and Adsorption of Beta-Aminoketones on Metals, *Zassschita-Metalov*, 32, 5, (1966) Pp. 528 - 533
- ³¹ Vaccaro, E. & Scola D.A., *Proc Am Chem Soc Div, Polymer Mater Sci Eng* 1998, 78, Pp 9-10
- ³² Hare C., *Protective Coatings – Fundamentals of Chemistry and Composition*, Technology Publishing Co., Pittsburgh, PA, (1994) ch. 15& 16,
- ³³ G.P.Bierwagen, R.S.Fishman, T. Storsved, & J. Johnson, "Recent Studies of Particle Packing in Organic Coatings," *Prog. Organic Coatings*, 35(1999) 1-10

-
- ³⁵ Heijboer J., "Modulus and Damping of Polymers in Relation to Their Structure," Br. Polymer J., 1969, vol. 1, January
- ³⁴ L.W. Hill, J. Coatings Technology, vol 64, No. 808, (1992), Pp 29

PART IV

Certain aspects and embodiments of the present invention are described in the following text and figures.

Binders for Mg-Rich Coatings as Cr-free Primers for Al 2024T-3

ABSTRACT

Mg-rich coatings with exceptional resistance to corrosion were formulated for cathodic protection of aluminum 2024 T-3 alloy. Coating the 2024 T-3 alloy with an polyamide epoxy or aromatic polyisocyanate primer filled with 20 to 200 micron sized magnesium powder, at or above CPVC (critical pigment volume concentration), protected scribed areas of the alloy for up to 2,000 hours in Prohesion™ exposure. Top-coating the Mg-rich primers with an Extended Lifetime™ extended protection up to about 3,000 hours. Mg-rich coatings formulated with an epoxy-polyisocyanate-silane 'hybrid' binder and top coated with an Extended Lifetime™ coating protected scribed areas for up to 4,500 hours. In addition, coatings formulated with the hybrid binder were found to be fire retardant at elevated magnesium PVC's (pigment volume concentrations).

INTRODUCTION

Primers formulated for cathodic protection require a polymer binder that wets metal, retains flexibility, maintains solvent and acid resistance, and remains insensitive to wide fluctuations in pH. Magnesium powder filled epoxy primers formulated above and near to CPVC, were subjected to Prohesion™ cycling in Harrison's solution to emulate acid rain conditions. Initial exposure of the uncoated primer to an acidic (pH~4.5) solution quickly attacks magnesium metal generating hydrogen gas H_2 the metal's oxide MgO , and brucite the metal's hydroxide $Mg(OH)_2$.¹ Primer PVC was found to strongly influence integrity of exposed primer coatings.

High PVC metal content primers containing more available surface metal were better able to serve as sacrificial anodes and lasted longer by extending protection to both binder and alloy.²

Cathodic protection of a primed panel appears to occur in two distinct stages, initially, closely packed metal particles connect in the primer to form a conductive, sacrificial path. Gradually, as the surface of the Mg-metal is oxidized porous hydroxides, $[\text{MgO}, \text{Mg}(\text{OH})_2]$ [brucite] domains grow and interconnect providing a medium for electrolyte to penetrate and maintain electrical connectivity with the primer. As long as the Mg metal can be kept in contact with the Al surface, cathodic protection of the alloy remains in effect, the cathodic protection still takes place, but the reactive consumption of the Mg is slowed considerably. Overall, it is not the surface of the coating that is important but the bulk of the primer. Figure 1. By putting on a topcoat, as the system is actually used in the field, acid dissolution of the Mg metal in the primer is minimized, thereby confining oxidation-reduction processes to an electrically connected coating within the primer layer.

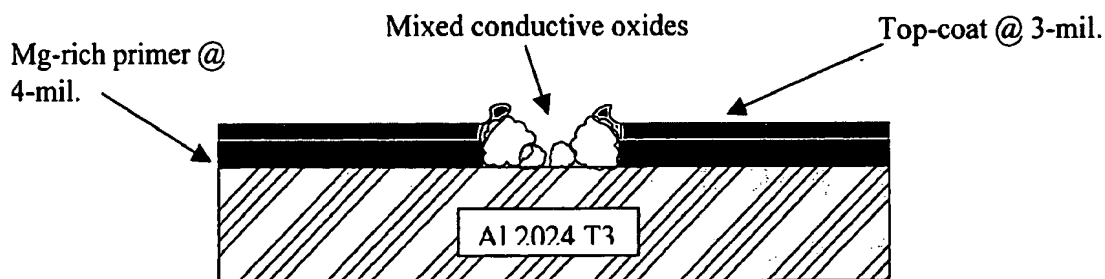


Figure 1. Cathodic protection of top-coated Mg-rich coating over Al 2024 T-3 lengthy exposure to Harrison's solution. Porous mixed oxides of aluminum, copper, and magnesium remaining electrically connected to bulk of primer. So long as the binder is not degraded cathode area remains small relative to a larger electrically connected Mg-rich anode

PRIMER PROHESION EXPOSURE

Our previous studies on Mg-rich primers reveal the corrosion process for primers exposed to Prohesion™ exposure in dilute Harrison's solution with no topcoat follow three distinct events.³

1. EDX spectra have revealed formation of magnesium carbonate hydrates at the primer liquid/vapor interface, dypingite $[\text{Mg}_5(\text{CO}_3)_4(\text{OH})_2 \cdot 8\text{H}_2\text{O}]$ & hydromagnesite $[\text{Mg}_3(\text{CO}_3)_4(\text{OH})_2 \cdot 4\text{H}_2\text{O}]$. These salts have been observed only to be present up to the first 500 hours of exposure for all non top-coated primed Mg-rich panels tested.
2. At exposure times beyond 500-hours brucite $[\text{Mg}(\text{OH})_2]$ domains form and subsequently extend throughout the bulk of the primer during which time the aluminum alloy remains cathodically protected as scribed lines remain unblemished.
3. At exposure times greater than 1500 hours, primer failure and film delamination corresponds to the accumulation of hexahydrite $[(\text{MgSO}_4) \cdot 6\text{H}_2\text{O}]$ salt at the interface. Failure occurs, figure 2, when Mg-metal and brucite structure have been depleted from the binder matrix and sufficient hexahydrite salts have accumulated at the alloy interface. At which time the binder ruptures and fragments from compressive forces exerted as the less porous but more expansive hexahydrite salt structures grow.³



Title: EPOXY - MG COATING

Comment: SAMPLE 200138 HIGHEST MG LEVEL

Date: 02-24-2000 Time: 16:11

Filename: 1138.TIF

Figure 2. Underside of exposed Mg-rich primer with magnesium salt emanations

PRIMER OPEN CIRCUIT POTENTIAL MEASUREMENTS

Figure 3. open circuit potential (OCP) diagram for Mg-rich primers, at 50, 56, and 60 PVC in a polyamide/epoxy binder exposed to 3% NaCl solution at pH \approx 6.2. Initial OCP values for the three sets correspond to a single electron transfer potential for Mg metal, $E_{Mg} \approx -1.50V$ to $-1.60 V_{SCE}$ is assumed to have occurred.⁴ Subsequently, over a 24 hour period, Mg and the Al alloy polarizes to a mixed potential, E_{mix} , corresponding to the galvanic corrosion potential, E_{corr} , at which both metals corrode.⁵ The observed mixed potential for Mg and Al alloy in 3% NaCl was found to be about $E_{mix} \approx -0.90 V$ to $-1.00 V_{SCE}$. OCP values extending beyond the initial 24 hour period varied according to primer PVC.

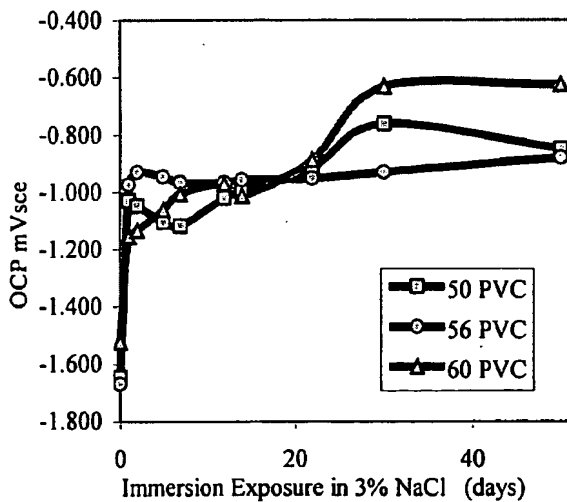


Figure 3. Open circuit potential SCE vs PVC of Mg-rich epoxy/polyamide primers at pH=6.2 in 3% NaCl ⁽⁶⁾

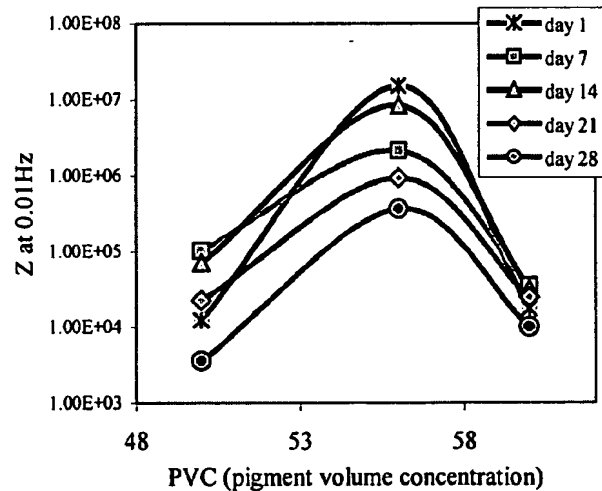


Figure 4. $|Z|$ modulus at 0.01Hz vs PVC of Mg-rich epoxy/polyamide primers at pH= 6.2 in 3% NaCl ⁽⁶⁾

The initial lower mixed potential value, E_{mix} , figure 3, for the 50 PVC sample is thought to be due to the lower cathode area as a result of higher binder coverage at the Mg Al alloy interface. Initially, the Mg-anode dominates the OCP. The gradual rise in OCP for the 50 PVC sample

toward $E_{Al-2024T3} \approx -0.68mV_{SCE}$ is thought to be due to water sorption and the disbonding of epoxy binder from the cathode surface. The gradual decrease in OCP of the 50 PVC sample toward $E_{mix} \approx -0.90 \text{ V}$ to -1.00 V_{SCE} is thought to be due to resistance polarization by the formation and packing of Mg oxides in the coating. The initial and continuous decrease in OCP of the 60 PVC sample is thought to be due to a higher void volume in the primer as well as a higher cathode area at the primer alloy interface. The OCP of the 56 PVC sample quickly arrives at the $E_{mix} \approx -0.90 \text{ V}$ to -1.00 V_{SCE} value and remains constant for the duration of the test time period. Thus, it is assumed that the 56 PVC primer corresponds to the critical pigment volume concentration for the primer.⁷ Thus, suggesting cathodic protection of the Al alloy due to Mg metal occurs most effectively at or near CPVC.⁷ |Z| modulus versus time measurements made in 3% NaCl solution at pH ≈ 6.2 on 50, 56, and 60 PVC Mg-rich primers, figure 4, demonstrates the effect of PVC at CPVC for Mg-rich primers. The Z modulus values for the 56 PVC samples yielded a higher complex modulus over the 28 day period suggesting judicious formulation at or near the critical pigment volume concentration is required to ensure close packing of Mg pigment with minimum encapsulation, but with vehicle content sufficient enough to ensure good substrate wetting and reasonable physical properties from the primer.

MAGNESIUM POWDER ANODE

Magnesium rich primer coatings may be viewed analogously to zinc rich systems, in that, as long as there is sufficient electrical conduction within the continuous film at the interface the aluminum alloy must remain protected so long as magnesium is available for corrosion. However, unlike zinc, magnesium metal has a density of 1.738 g/cm^3 and its micron sized powders, physically less dense, have bulk densities ranging from 0.87 to 0.67 g/cm^3 . In sharp

contrast to zinc metal that has a density of 7.133 g/cm^3 , a denser pigment, with bulk densities in the range 4.56 to 5.20 g/cm^3 , depending on the polydispersity of the zinc spheres. As a result of its higher density zinc powders tend to settle and cause considerable heterogeneities in many film applications.⁷ Generally, organic binders used in cathodic primer systems have densities ranging from 1.0 g/cm^3 for polyisocyanates to 1.10 g/cm^3 for typical polyamide-BPAepoxies, and when cut in a suitable solvent the densities of these vehicles approaches that of the magnesium powder leaving the coatings less susceptible to film application heterogeneities. Eckart GmbH, ECKATM metallic magnesium powder produced from p-magnesium 99.95 % to DIN 17800 with Mg content @ 96% and MgO (magnesium oxide) content @ 4%. The Pilling-Bedworth ratio, (Askeland, 1985)⁸ is the ratio of the specific volume of metal oxide per atom to the volume of the metal per atom. Metals with a P-B ratio of less than one develop a fluffy, penetrable, non-protective, porous oxide that occupies less volume than the metal itself, such as magnesium oxide with a P-B of 0.80. Metals with a P-B ratio greater than one yield a higher volume of oxide that is a passive more closely packed compressed structure such as Al_2O_3 or Zinc oxide, ZnO , with a Pilling-Bedworth ratio of 1.60.⁸ Zinc rich coatings require that the flakes or the dust be in a close contact proximity in order to establish electrical conductivity. In organic vehicles, the outer surface of zinc oxide has been characterized as forming a “dielectric vehicle sheath”, (Hare and Wright, 1982)⁷, composed of zinc oxide and organic binder. It should be noted that the higher P-B ratio for zinc and its oxide yields a more compressed, less permeable dielectric vehicle sheath about the metal itself. While magnesium and its oxide with a lower P-B ratio yields the less compressed, more permeable oxide structure that may not form a dielectric vehicle sheath analogous to that formed around zinc.

While Magnesium's oxide, MgO , is not conductive, brucite $\text{Mg}(\text{OH})_2$, its hydroxide is conductive⁹ and has been observed to form a passive layer in Mg-rich primers exposed to dilute Harrison's solution.³ Figure 5. depicts the nature of relative contact areas and dielectric vehicle sheaths formed around both magnesium and zinc powders.

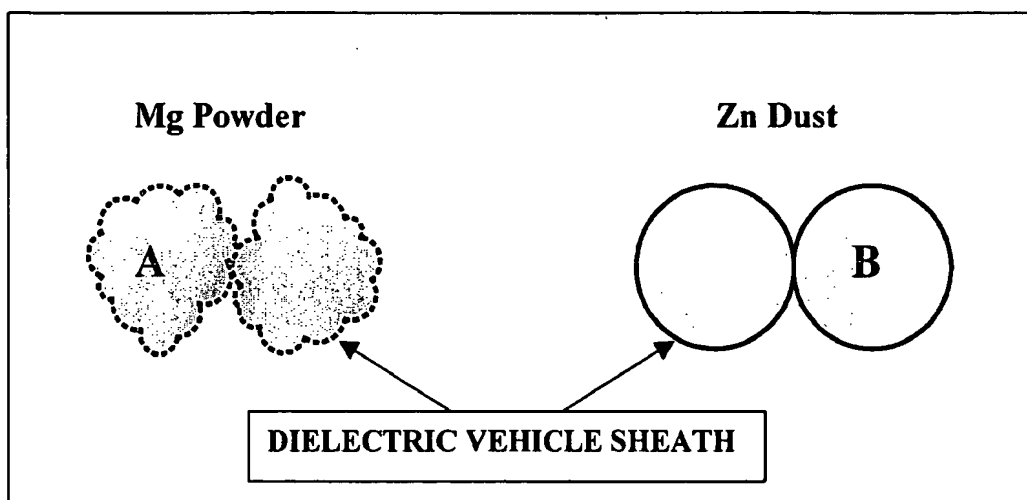


Figure 5. Contact areas and dielectric sheath films between particles of magnesium powder (A) with a more porous open oxide and zinc dust (B) with its less permeable closed oxide. (Adapted from Hare and Wright, 1982)⁷

COATING FORMULATION

Primer critical pigment volume concentration, (Bierwagen, 1990)¹⁰, was estimated from 1) plastic limit determination by addition of resin to pigment. 2) manufacturer's reported bulking value and 3) Particle volume fraction determination using optical particle counting. Primers were formulated using conventional techniques, pigment was dispersed in a resin solvent mix and Bentone-Gel™ was added to the letdown mix. Viscosity was adjusted with a No.4 Ford cup at 24 seconds. Primers were applied to lightly wire brushed Al 2024 T3 Q-panels™ by conventional atomized spray and allowed to ambient cure at 20° C for five days. The average primer film thickness was measured at 4 mils with an average coefficient of variation of 10%. Primed panels

were topcoated with Deft Extended Lifetime™ top-coat. The average topcoat film thickness was measured at 3 mils with an average coefficient of variation at 5%.

PRIMER BINDERS

Three coating polymer systems were evaluated as vehicles for Mg-rich primers, two were commercially available products and the other an experimental epoxy-urethane-silane hybrid developed in this laboratory. The moisture cure aromatic polyisocyanate, Desmodure™ A-23, used is classified as forming both urethane and urea linkages at a stoichiometric ratio of 5 to 1. The ambient cure epoxy/polyamine was liquid BPA Epon™ 828 with an (epoxide equivalent weight) EEW \approx 188 and a Mannich base Epicure™-3251 polyalkylamines with an AHEW (amine hydrogen equivalent weight) \approx 55. The reaction was catalyzed with 5% nonylphenol based upon total epoxy resin weight. The experimental epoxy-urethane-silane was composed of 60% epoxy resin and 40% aliphatic polyisocyanate, forming both urethane and urea linkages in a ratio of approximately 4 to 1. Trimethoxysilane was added as an adhesion promoter.

TEST PROCEDURES

Test primers formulated at CPVC, with 90micron average size magnesium powder, were applied to Al 2024 T-3 aluminum Q-panels™ and topcoated with Deft Extended Lifetime™ top-coat. Modified Flammability test reference document IPC-SM840B paragraph 3.6.3 and 4.4.8, also refer to test method 2.3.10.1 and the U.L.-94 flammability specification. Using a Bunsen burner, tube length 4", I.D. 0.37" with methane gas at equivalent 1000 BTU/Ft³. Prohesion™ exposure testing ASTM test method B117 using Cleveland Humidity Cabinet (Q-Panel Co.), at 60° C water temperature. Electrochemical impedance spectroscopy (EIS) and open circuit potential experiments were performed with a GAMRY Instruments PC-4 board System with Gamry framework™ software version 3.1, EN120 and DC-105. DSC experiments were run on a Perkin-Elmer DSC-7 using Pyrrus™ software.

MODIFIED FLAMMABILITY TEST

A Modified Flammability test was performed on Mg-rich coatings applied to Al 3015 substrate. Topcoated Mg-rich sample strips with dimensions 1" by 6" formulated at CPVC ~ 65 pigment volume concentration with magnesium powder and one of three binders were subjected directly to blue cone of the Bunsen burner flame for 30 seconds.

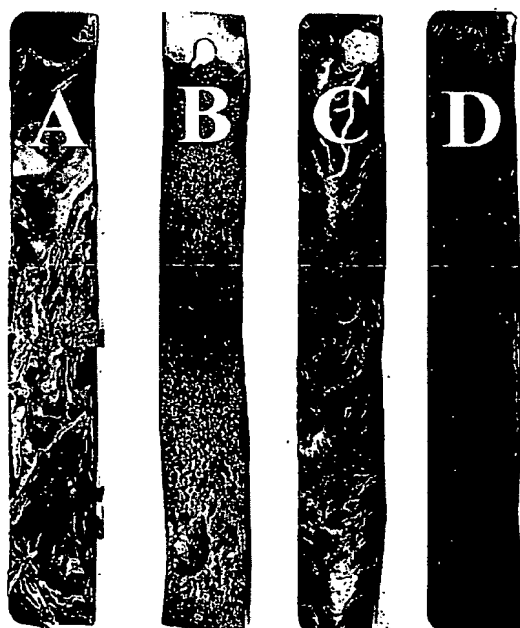


Figure 6. 1"x 6" metal filled coating strips at (CPVC) exposed to flame 30 seconds.

Binder Flammability 30 second Burn Duration



**Hybrid Binder slightly charred
Did not sustain combustion**



**Epoxy/polyamide Binder
Sustained combustion**

Figure 7. 1"x 6" Organic binder strips exposed to flame 30 seconds.

Figure 6. Results from modified UL-94 flammability test, topcoated strips (A) Mannich base/BPA epoxy sample sustained combustion of Mg metal (FAILED TEST); (B) Zinc-rich dust epoxy sample, did not sustain combustion (PASSED TEST); (C) aromatic polyisocyanate sample sustained combustion of Mg metal (FAILED TEST); (D) hybrid epoxy-polyisocyanate sample did not sustain combustion of magnesium (PASSED TEST).

Figure 7. Results from modified flammability test for organic binders on Al 3015 panel strips (A) hybrid epoxy-polyisocyanate binder at 4-mils; (B) polyamide/BPA epoxy binder at 4 mils.

PROHESION EXPOSURE RESULTS

Q-Panel™ Al 2024 T-3 panels were primed with Mg-rich primer at CPVC film thickness of 4 mil and subsequently topcoated with Extended Lifetime™ topcoat at 3mil. A carbide tipped glass scribe was used to cut scribes marks through the coated panels. Panels were covered with electroplater's tape and the front borders sealed with a polysulfide epoxy curative. Panels were subsequently subjected up to 4,500 hours of Prohesion™ exposure in dilute Harrison's solution at pH~4.0.

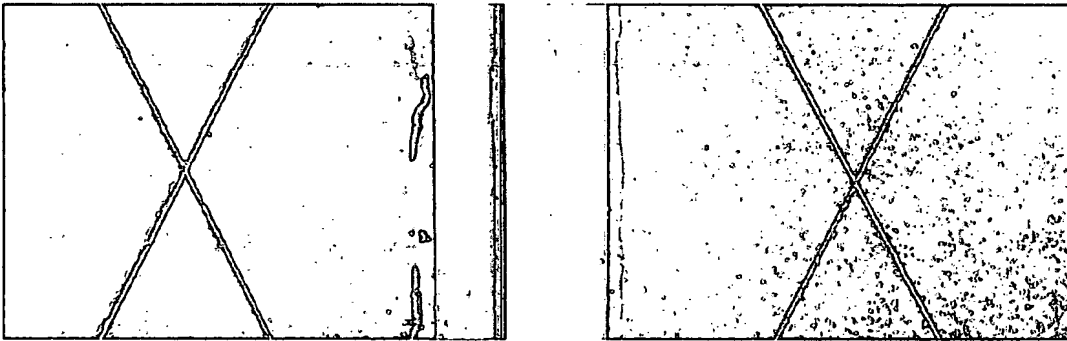


Figure 8. Hybrid epoxy-polyisocyanate topcoated with Extended Lifetime™ topcoat Prohesion™ exposure at 2,500 hours for Mg-rich primer at 4 mils and topcoat at 3 mils.

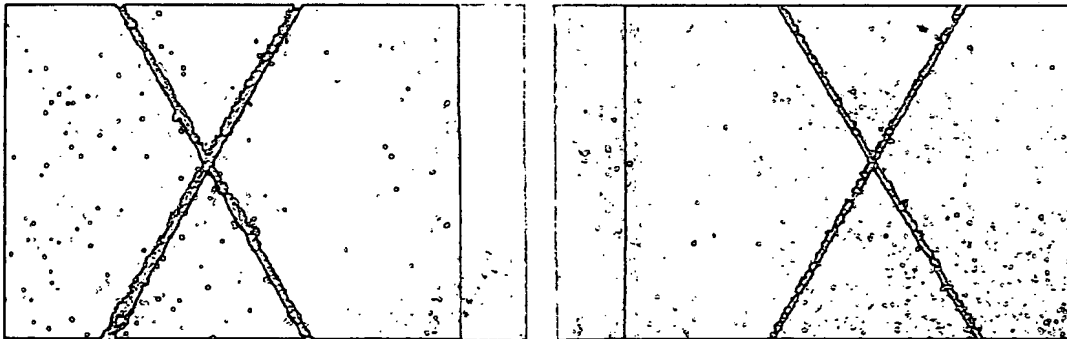
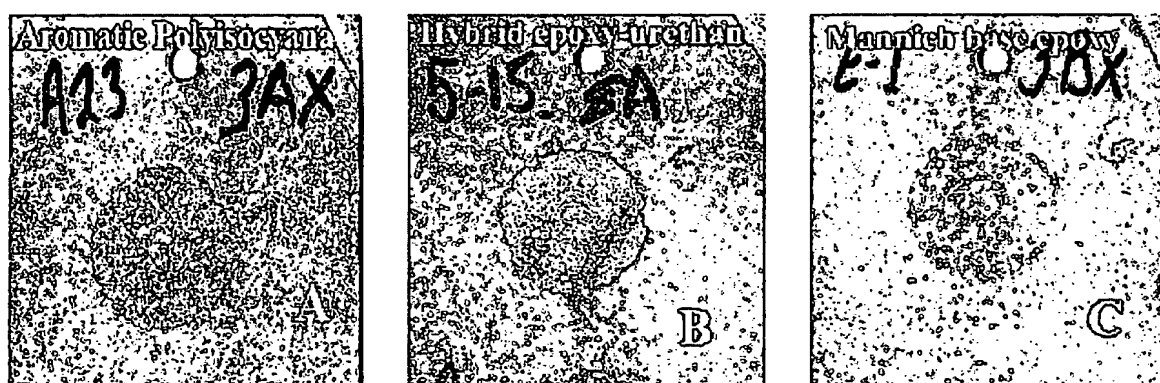


Figure 9. Hybrid epoxy-polyisocyanate topcoated with Extended Lifetime™ topcoat Prohesion™ exposure at 4,500 hours for Mg-rich primer at 4 mils and topcoat at 3 mils.

ELECTROCHEMICAL IMPEDANCE SPECTROSCOPY

Cylindrical electrode cells were mounted over samples with 1.0 cm diameter scribes cut through the coating exposing Al 2024 T-3 surface. Cylinders were filled with electrolytes of the following compositions 1) Neutral at 3.0% weight NaCl at pH =6.2; 2) Acidic at 3% weight NaCl adjusted to pH = 2.2 with HCl; 3) Basic at 3% weight NaCl adjusted to pH= 12.75 with NaOH. Impedance measurements were carried out using a Gamry PC4/300TM electrochemical measurement system. The amplitude of the signal perturbation was 10mV (rms) with a frequency sweep from 0.01Hz to 10kHz. Measurements were made over an 11-day time period with test intervals on the 1st, 2nd, 4th, 7th, and 11th day.

DATA FOR BASIC CONDITIONS



Figures 10 A, B, & C: Topcoated Mg-rich Al 2024 T-3 after 11 days EIS in basic 3% NaCl

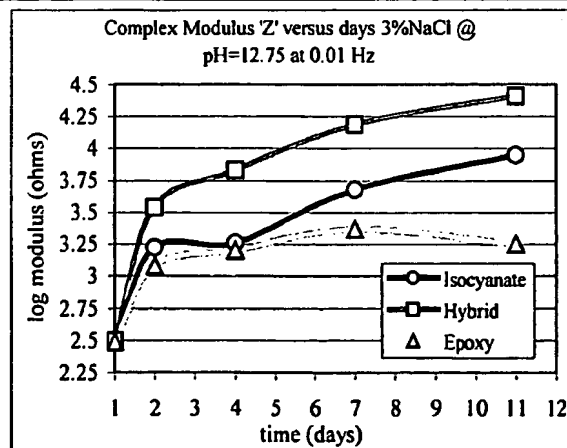


Figure11. Complex modulus vs time (basic)

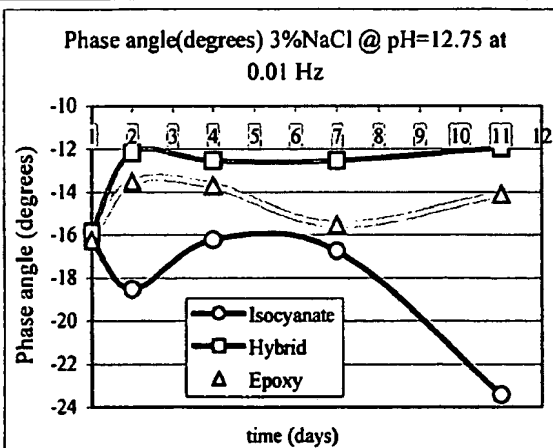
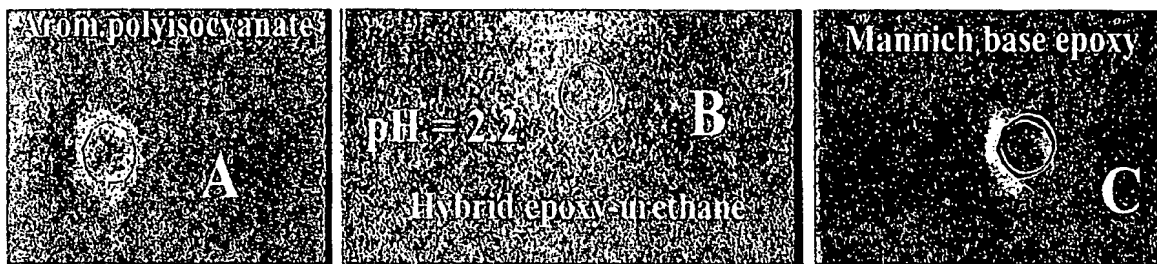


Figure12. Phase angle vs time (basic)

DATA FOR ACIDIC CONDITIONS



Figures 13 A, B, & C: Topcoated Mg-rich Al 2024 T-3 after 11 days EIS in acidic 3% NaCl

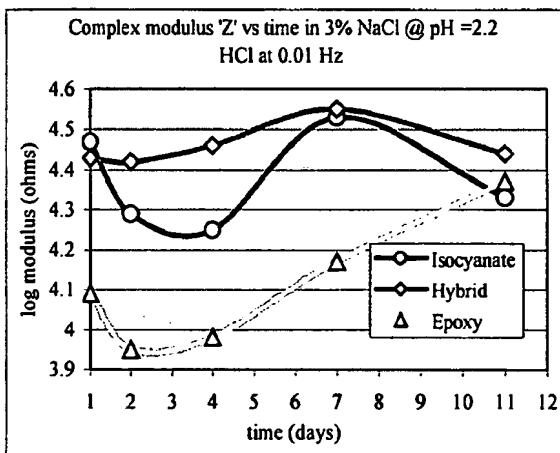


Figure14. Complex modulus vs time (acidic)

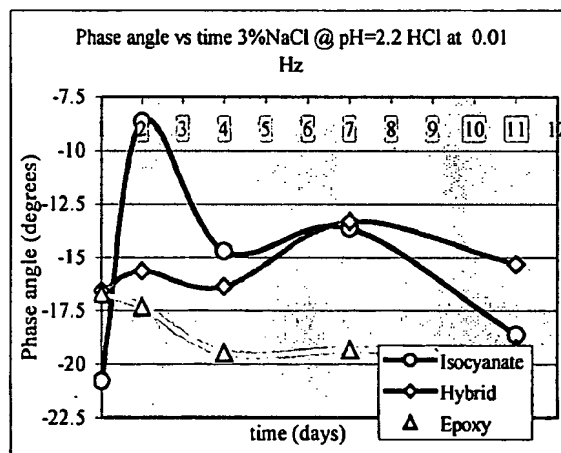


Figure15. Phase angle vs time (acidic)

DATA FOR NEUTRAL CONDITIONS

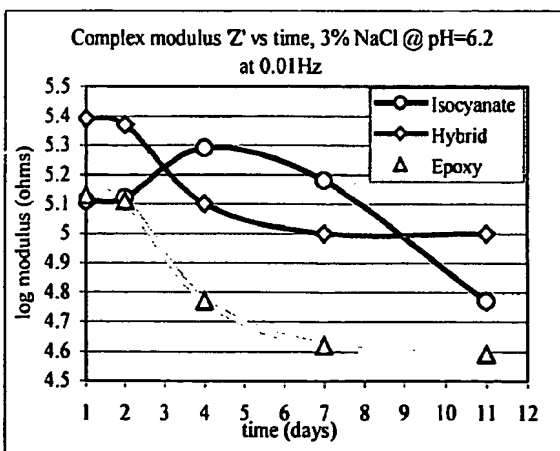


Figure16. Complex modulus vs time (neutral)

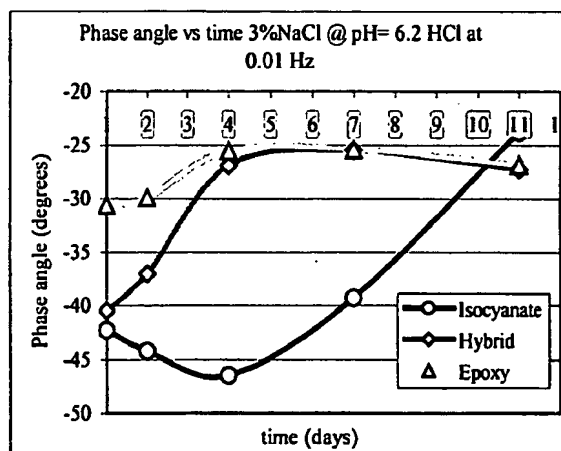


Figure17. Phase angle vs time (neutral)

DISCUSSION EIS RESULTS

Basic 3% NaCl solution at pH= 12.75

A partially protective film forms on magnesium's surface in 1N NaCl and has been found to play an important role in electrochemical corrosion.¹¹ Magnesium's hydroxide has a stability range (pH range 11 to 13).¹ Figures 10A, B, & C show 11 day exposure results for Mg-rich topcoated Al 2024 T-3 panels in 3% NaCl solution adjusted with NaOH to pH = 12.75. Adjunct EIS measurements for complex modulus and phase angle for panels in figures 10A, B, & C for figures 11 and 12 respectively. Starting with figure 10A, aromatic polyisocyanate, white precipitate from NaOH base, possibly a magnesium ion deposition, appears to have deposited in pits over the exposed surface of the coating. Figure 11, the measured impedance, complex modulus log(ohms) at 0.01Hz, increased after an initial 24 hour exposure. The phase angle, figure 12, became more negative -16 to -24 degrees as time progressed indicating an overall capacitive effect probably due to water uptake and related effects. Usually, when this feature occurs at the low frequency end of the spectrum it is indicative of electrolyte penetration and the formation of pitting corrosion.¹² Figure 10B, hybrid epoxy-polyisocyanate, shows white precipitate deposit evenly accumulated over the exposed surface of the coating. The complex modulus for the coating log(ohms) at 0.01 Hz starts initially 2.5 and increases to 4.3 after 10 days exposure. However, the phase angle of the hybrid coating, unlike the aromatic polyisocyanate, decreases from an initial value of -16 to -12 degrees during the first 48 hours of exposure, and then remained constant up to the eleventh-day, suggesting that only the resistive contribution to Z , and no capacitive effect due to electrolyte penetration occurs. Figure 10C, Mannich base epoxy, failed due to complete blistering over the entire surface of the exposed area. The complex modulus for the epoxy coating log(ohms) at 0.01 Hz started initially 2.5 and

increased to 3.2 until the eleventh day of exposure. The phase angle for the epoxy coating, like the Hybrid, also initially decreased from an initial value of -16 to -13.5 degrees, during the first 48 hours of exposure, and then fell back again to -16 degrees until the seventh day where it once again decreased to a lower value of -12 degrees. The observed dip in the phase angle for the Mannich base epoxy coating may be indicative of blister propagation occurring between day three and seven upon which time the blister had propagated to the edge of the cylinder where the coating was physically compressed by the o-ring against the panel.

Acidic 3% NaCl solution at pH= 2.2

Reference one states that "Thermodynamics and the E -pH diagram predict that there should be no film on the magnesium surface in solution with a pH value less than 10 because of the instability of the film in such solutions. However, even though the film is thermodynamically unstable at low pH values, the dissolution kinetics are slower than the formation kinetics."¹ It might be assumed that the film formation kinetics at pH = 2.2 are faster than film dissolution kinetics. Figures 14, and 15 provide relative EIS data at 0.01 Hz for complex modulus Z and phase angle for the corrosion behavior of the three samples in figure 13A, B, and C, in acidified conditions at pH = 2.2. The corrosion behavior of the three samples is observed to be similar to that of the same samples in basic conditions at pH= 12.75. Overall, the polyisocyanate fared better than the Mannich base epoxy which blistered and delaminated to the same extent as it did in basic conditions. The corrosion behavior of the Hybrid epoxy-polyisocyanate was similar to that of the sample in basic conditions best overall.

Neutral 3% NaCl solution at pH= 6.2

A NaCl solution at pH = 6.2, considered to be a less aggressive environment, does not allow a continuous stable "protective hydroxide" skin to form on magnesium surface. Therefore, the film dissolution rate should be higher in an acidic solution than in an alkaline solution.¹

All coating samples tested in 3% NaCl solution at neutral pH = 6.2 appeared to be visually unaffected by exposure as there were no visible defects observed over any of the exposed areas. EIS spectra, figures 16 and 17, data collected at 0.01Hz, indicate a higher corrosion level to have occurred in all samples. It may be assumed that dissolution kinetics of the magnesium hydroxide film may be faster at pH = 6.2 than film formation of the hydroxide. An interpretation for the lack of visible corrosion damage at the surface of any of the coatings tested in 3% NaCl at pH = 6.2 for 11 days may be indicative of the presence of a more extensive electrically connected larger anode area to a smaller localized scribed cathode area.

Al 2024 T-3 PULL OFF ADHESION

Figure 18. ASTM-4551 direct pull-off adhesion using an Elco-meter™ gives a measure of force in (lb/in²) required cause decohesion of the coating from the Al 2024T-3 substrate.

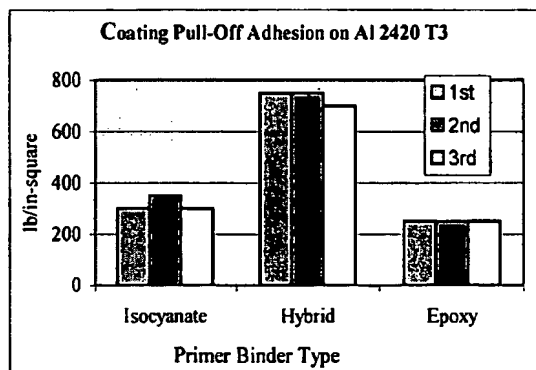


Figure 18. Pull off adhesion for Mg-rich topcoated with Extended Lifetime™ topcoat force vs coating type

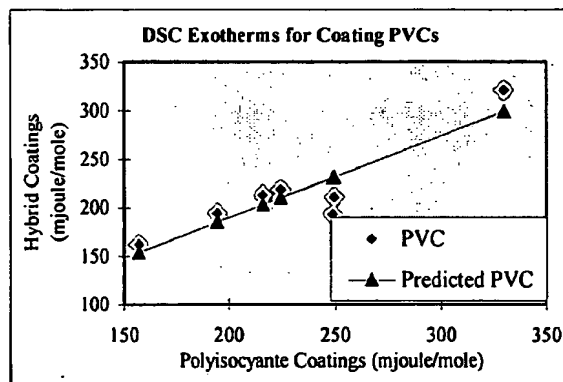


Figure 19. Correlation of PVC exotherm for topcoated Mg-rich coatings 1) Hybrid binder vs 2) Aromatic polyisocyanate

CORRELATION OF COATING PVC TO DSC DATA

Figure 19. Correlation of Mg-rich coating PVC to DSC (differential scanning calorimetry) data. DSC scans were generated from 10mg samples from two binders (1) Hybrid and (2) Aromatic polyisocyanate with Mg powder formulated at PVCs of 67, 60, 50, 40, 30, 20, and 0 and topcoated the ELT. Crimped samples were run at a heating rate of 30°/min. and heated over a

temperature range of 25°C to 450°C in air. Higher exotherm values were obtained for coatings that had primers with less pigment. The coating with a PVC of zero corresponded to the largest observed exotherm. Figure 19. gives the correlation for exotherms due to organic content in coating as a function of PVC in both binders. Regression statistics yielded a multiple $R \sim 0.9$, and an R square ~ 0.82 for the seven observations. The data implies organic content can be accurately correlated to Coating PVC, for Mg-rich systems, when film thickness is controlled.

SUMMARY

Magnesium-rich coatings in three organic binders were applied to Q-panel™ Al 2024 T-3 at critical pigment volume concentrations and topcoated with Deft Extended Lifetime™ topcoat then exposed to Prohesion™ exposure in dilute Harrison' solution for up to 4,500 hours. Binder stability was found to be strongly influenced by the presence of magnesium metal and it's hydroxide, e.g., blistering observed at high and low pH's due to binder failure. It is believed Mg-rich coatings protect the AL 2024 T-3 surface in an analogous way that Zinc-rich coatings protect steel. However, the polydisperse nature of magnesium powder with its more varied particle size distribution permits a higher packing factor, (Lee, 1970)¹³, than the zinc dust powders. In addition, the nature of magnesium's porous oxide with a B-P ratio of 0.80 yields more available surface area to electrolyte for the formation of a conductive hydroxide that has a lower dielectric strength when wet by an organic binder. Organic binders, such as epoxies with high dielectric constants appear to yield poorer cathodic coating systems in aggressive conditions that vary widely in pH. The aromatic polyisocyanate binder was better than the epoxy binder possibly due to its lower dielectric from isocyanate and urea linkages. Best performance was realized from the epoxy-polyisocyanate-silane hybrid binder as it appeared to have some inorganic character. This was shown by lower flammability, better stability in extreme acid and base conditions, as well as higher direct pull-off adhesion from the lightly wire-brushed Al 2420

T-3 panel. In summary, we have shown that cathodic protection of Al 2024 T-3 can be achieved simply by applying a Mg-rich primer formulated at CPVC, with an appropriate organic, or organic-silane modified binder with some given grade of magnesium powder to be used as the sacrificial anode. Of presently available aircraft topcoat systems, Deft's Extended Lifetime™ topcoat performed the best in combination with these Mg-rich primers.

References

- 1) Song G., Atrens A., St. John D., Nairin J., Li Y., The Electrical Corrosion of Pure Magnesium in 1N NaCl, Corrosion Science, Vol. 39, Pp 5, 855-875, (1997)
- 2) M. E. Nanna, and G.P. Bierwagen, Unpublished work shown at student poster session, North Dakota State University, October 1999
- 3) M.E. Nanna, and G.P. Bierwagen, Unpublished work FSCT Poster session, Chicago, October, 2000, & IAB poster session, North Dakota State University, October 2000
- 4) Natta Lopez-Buisan, M.G., Evidence of Two Anodic Processes in the Polarization Curves of Magnesium in Aqueous Media, Corrosion, Vol. 57, No.8, Pp. 712 – 720, (2001)
- 5) Jones D. A., Principles and Prevention of Corrosion, 2nd Ed., (1996), Pp. 444-447
- 6) Lisa Ellingson, Corrosion Studies for the Protection of Aluminum Alloys and Outdoor Bronze, Masters Thesis, North Dakota State University, June 2001
- 7) Hare C.H., and Wright S.J., Anti-Corrosive Primers Baased on Zinc Flake, Journal of Coatings Technology, Vol. 54, No. 693, Pp. 65 to 76, Oct. (1982)
- 8) Askeland D.R., The Science and Engineering of Materials, Alternate Ed. Pp. 510 to 512, PWS Publishers, (1985)
- 9) J. Genesca, L. Betancourt, and C. Rodriguez, Electrochemical Behavior of a Magnesium Galvanic Anode Under ASTM Test Method G-97-89 Conditions, Corrosion, July 1996, Pp. 502 – 507
- 10) Bierwagen G.P., Re-examination of the CPVC as a Transition Point in the Properties of Coatings, Polymeric Materials Science and Engineering, Proceedings of the ACS Division of Polymeric Materials Science and Engineering, Vol. 63, Pp. 186 – 189, (1990)

- 11) Song G., Atrens A., and Dargush M., Corrosion Sci., Vol. 41, Pp 249, (1999)
- 12) M. Han, H. Bie, G.W. Warren, D.E. Nikles, Amine-Quinone Polimides as Coatings that Protect Iron Against Corrosion, Mat. Res. Soc. Symp. Vol. 629, (2000), 17.1 to 17.6
- 13) Lee D.I., Packing of Spheres And Its Effect On the Viscosity of Suspensions, Journal of Coatings Technology, Vol. 42, No. 550, Pp.579 -587, (1970)

PART V

Certain aspects and embodiments of the present invention are described in the following text and figures.

Magnesium Powder Epoxy Primers for 2024 T-3 Al

Introduction:

The purpose of this study is to evaluate magnesium metal filled epoxy primers as possible chromate replacement technology for protecting the surface of 2024 T-3 aluminum. The thesis of the study is based upon cathodically protecting the surface of an aluminum alloy with magnesium metal while inhibiting passivation with an organic partner agent. Micron sized magnesium metal powder at concentrations above CPVC (critical pigment concentration) serves as the sacrificial anode while a PAQ (polyaminoquinone) oligomer serves as the organic inhibitor partner. Initial studies revealed that primers without PAQ inhibitor with PVCs between 55 and 70 quickly delaminated after 500- hours prohesion exposure in dilute Harrison's solution. The failure can be attributed to an excess accumulation of magnesium salts Brucite $Mg(OH)_2$ (within the coating) and Hexahydrite $MgSO_4 \cdot 6H_2O$ (under the coating). Studies with PAQ oligmer in high PVC primers reveal that film delamination as a result Hexahydrite formation beneath the coating does not occur.

Magnesium: is a very active metal it develops a negative galvanic potential when immersed in an electrolyte in seawater at -1.67 volts while that of most aluminum alloys fall between -1.0 to -0.75 volts. When any two metals are coupled together in an electrolyte the one with the more negative or active corrosion potential has the excess activity of electrons which are lost to the more positive alloy. The galvanic potential for 2024 T-3 has been reported at -0.67 volts slightly higher as a result of the 4.4% copper in the alloy leaving a potential difference between 2024 T-3 alloy and magnesium at -1.0 volt.

2024 T-3 aluminum (Al-4.4Cu1.5 Mg-0.6 Mn) is a high strength precipitation hardened grade aluminum alloy used extensively in aerospace applications. It is prone to corrosion due to Intermetallic S-phase (Al₃MgCu) particles that set up galvanic cells at high pH's with the Al matrix. The result causes aluminum dealloying as copper is redistributed over its surface, these copper particles then serve as preferential sites for the reduction of oxygen and dissolution of the metal. The dealloying process results in nanoporous Cu-rich remnants that induce metal depletion and pitting about the periphery of the aluminum grain boundaries.

Eckart G.m.b.H. 099/99
< 18 micron sized Mg powder



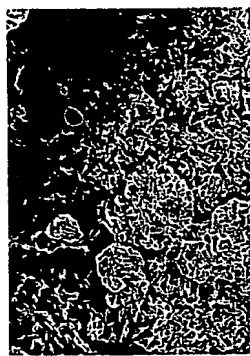
200 x image of 099/99Mg Powder

SEMs of Exposed

Surface Evolution and residence of Magnesium salts on surface and within primer



600 hr exposure Surface: Dypingite $(Mg_3(CO_3)_2(OH)_2 \cdot 4H_2O)$ & Hydromagnesite $(Mg_5(CO_3)_4(OH)_2 \cdot 4H_2O)$



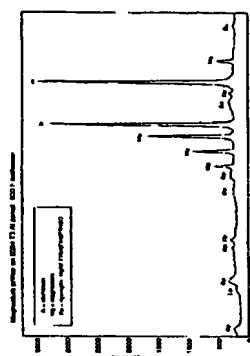
1300 hr exposure Surface & Interior: Brucite $(Mg(OH)_2)$ broad line absorption corresponds to fine crystalline domains.



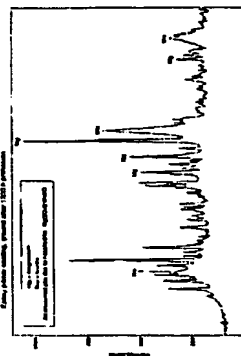
1300 hr exposure lifted underside: Brucite $(Mg(OH)_2)$ rosettes with Hexahydrite plate enantiomorphs

X-Ray Diffraction Patterns

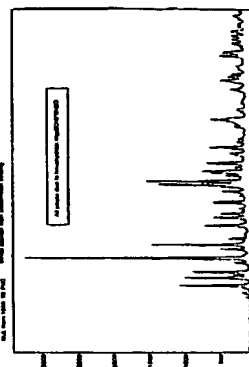
The mechanism of magnesium powder epoxy primer degradation on 2024 T-3 exposed to a dilute Harrison's solution prohesion test can be determined by the crystalline structures of hydroxides and hydrates of magnesium as a function of exposure time.



Surface of exposed Primer 600-hours



Ground up Primer exposed 1300-hours



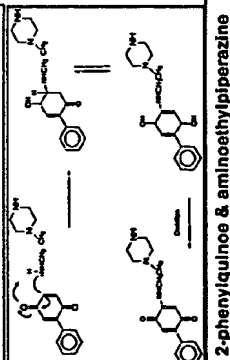
Underside of Primer exposed 1300-hours

Synthesis: PAQ diamines

Phenyl quinone amine oligomers
Poly (amino-quinone) (PAQ) polymers have been prepared from 2-phenyl-quinone and various diamines and studied in coatings by Reddy and Erhan (1). The *in situ* reaction is classified as a 1,4-addition which produces

substituted hydroquinones that can be reoxidized by a simple electron transfer with any suitable oxidizer. All quinoidal intermediates are capable of the addition reactions (including double additions) the PAQ reactions are seen as ECE processes. (2) Initially, Reddy and Erhan prepared PAQ polymers with Calcium hypochlorite. Vanideswaren, Bell & Nikles(3) prepared (AQM) amine quinone monomers in copper II chloride dihydrate. We have found trichloro-isocyanuric acid to be an effective oxidizer for this reaction. 2-phenylhydroquinone in THF is quickly oxidized to a green 2-phenylquinone.

Oxidative Amination Mechanism

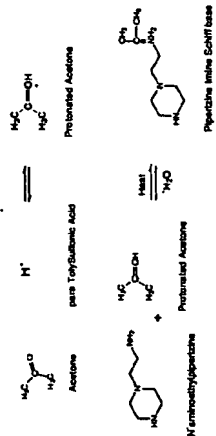


2-phenylquinone & aminoethyloperazine

PAQ Inhibitor Curative

Organic inhibition physically blocks the metal surface. The overall effect is to lower the reaction rate on the surface which lowers the corrosion current density. Organic inhibitors used in the protection of oil pipelines are diamines, polyamines, imidazoline.(4) In our studies Jeffamine D-400 poly(oxypropylene) diamine, was reacted with 2- phenyl-quinone and three amines an asymmetric amine (AEP) aminoethyloperazine, and two symmetric diamines (DCH-99) diaminocyclohexane, (mpDA) metaphenyldiamine.

Synthesis: Ketimine



Work Horse Curative

The resulting ketimine was used as a sole curative in the first study on PVC effect, the piperazine salt of toluene sulfonic acid a side reaction product was separated and used as a catalyst for the type1 BPA epoxy resin used in the study. The low AHEW of the resulting curative gave high epoxy to amine ratio for improved adhesion to aluminum.

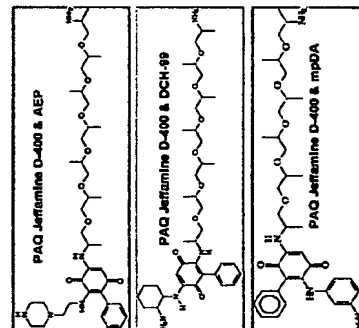
Physical Properties of Coatings from Study #1 PVC variation only

Coating	Hardness (K)	Modulus (GPa)	Adhesion (MPa)	Impact (J/m²)	Thermal Stability (°C)
Control	12-14	1.2-1.4	1.2-1.4	1.2-1.4	1.2-1.4
PAQ	15-18	1.5-1.8	1.5-1.8	1.5-1.8	1.5-1.8
mpDA	16-19	1.6-1.9	1.6-1.9	1.6-1.9	1.6-1.9
DCH-99	17-20	1.7-2.0	1.7-2.0	1.7-2.0	1.7-2.0
AEP	18-21	1.8-2.1	1.8-2.1	1.8-2.1	1.8-2.1

Note: Acetone & Water ratio at 80-100, 3-gram circular glass of material

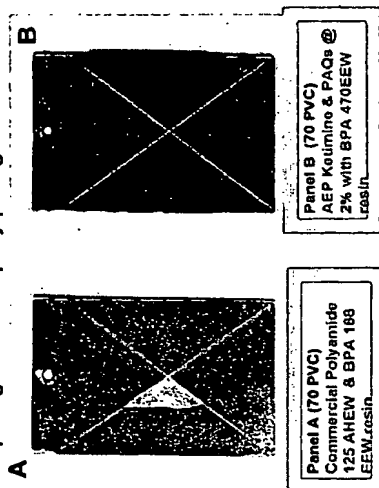
Structure of PAQs

The structures below are general representations of the oligomers GPC data shows 720Mn, 1400Mn, and 29,000Mn Reactions High Mn obtained by heating. FTIR 1640cm-1, and no 3600 hydroxyl



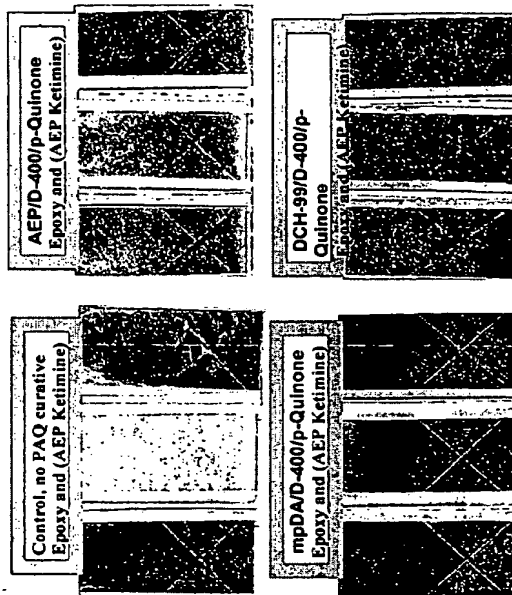
Mg Primer with & w/o PAQ

Panels with 600 hours Prohesion Exposure the commercial polyamide failed the coating has lifted completely underneath with rapid pitting surface rapidly pitting.



Primers @ 1300-hrs w PAQs

Four sets of primer panels below formulated with different PAQs @ 70 PVC. Control failure due to penetration of SO₂ beneath no inhibitor present. AEP/D400 PAQ filled with Brucite while other two PAQs did not. Note scribe lines remained clean.



Summary

Our studies we have established that high PVC magnesium filled epoxy coatings with (PAQ) inhibitors applied to 2024 T-3 aluminum alloys provide some cathodic and inhibitive protection at the surface. At high PVCs, over time, the primer becomes more susceptible to attack by SO₂ as the primer interior fills with Brucite conditions for the growth of Hexahydrate at the primer metal interface are favored leading to rapid failure. The PAQ inhibitor clearly retards the penetration and formation of Hexahydrate and coating failure.

References Cited

1. J. H. Ruddy and S. Erhan, *Electrochimica Acta*, vol. 11, 1967, 1641 (1964)
2. R. N. Adams, *Electrochimica Acta*, vol. 11, 1967, 1641 (1964)
3. J. H. Ruddy and S. Erhan, *Electrochimica Acta*, vol. 11, 1967, 1641 (1964)
4. J. H. Ruddy and S. Erhan, *Electrochimica Acta*, vol. 11, 1967, 1641 (1964)

PART VI

Certain aspects and embodiments of the present invention are described in the following text and figures.

Cathodic Coatings for 2024 T-3 Aluminum

Introduction:

The purpose of this study is to evaluate magnesium metal filled epoxy primers as possible chromate replacement technology for protecting the surface of 2024 T-3 aluminum. The thesis of the study is based upon cathodically protecting the surface of an aluminum alloy with magnesium metal while inhibiting depassivation with an organic partner agent. Micron sized magnesium metal powder at concentrations above CPVC (critical pigment concentration) serves as the sacrificial anode while a PAQ (polyaminoquinone) oligomer serves as the organic inhibitor partner. Initial studies revealed that primers without PAQ inhibitor with PVCs between 55 and 70 quickly delaminated after 500- hours prohesion exposure in dilute Harrison's solution. The failure can be attributed to an excess accumulation of magnesium salts Brucite $Mg(OH)_2$ (within the coating) and Hexahydrite $MgSO_4 \cdot 6H_2O$ (under the coating). Studies with PAQ oligmer in high PVC primers reveal that film delamination as a result Hexahydrite formation beneath the coating does not occur.

Eckart G.m.b.H. 099/99
< 18 micron sized Mg powder



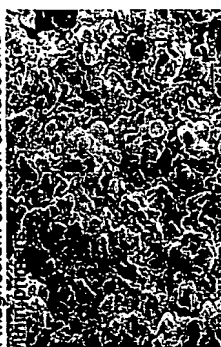
200 x image of 099/99Mg Powder

Magnesium: Is a very active metal it develops a negative galvanic potential when immersed in an electrolyte in seawater at -1.67 volts while that of most aluminum alloys fall between -1.0 to -0.75 volts. When any two metals are coupled together in an electrolyte the one with the more negative or active corrosion potential has the excess activity of electrons which are lost to the more positive alloy. The galvanic potential for 2024 T-3 has been reported at -0.67 volts slightly higher as a result of the 4.4% copper in the alloy leaving a potential difference between 2024 T-3 alloy and magnesium at -1.0 volt.

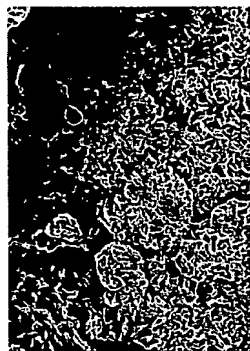
2024 T-3 aluminum (Al-4.4Cu-1.5 Mg-0.6 Mn) is a high strength precipitation hardened grade aluminum alloy used extensively in aerospace applications. It is prone to corrosion due to intermetallic S-phase (Al₃MgCu) particles that set up galvanic cells at high pH's with the Al matrix. The result causes aluminum dealloying as copper is redistributed over its surface, these copper particles then serve as preferential sites for the reduction of oxygen and dissolution of the metal. The dealloying process results in nanoporous Cu-rich remnants that induce metal depletion and pitting about the periphery of the aluminum grain boundaries.

SEMs of Exposed

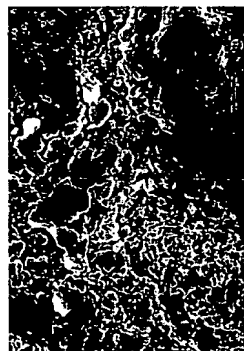
Surface Evolution and residence of Magnesium salts on surface and within primer



600 hr exposure Surface: Dypingite
($Mg_3(CO_3)(OH)_2 \cdot 8H_2O$) & Hydromagnesite ($Mg_3(CO_3)(OH)_2 \cdot 4H_2O$)



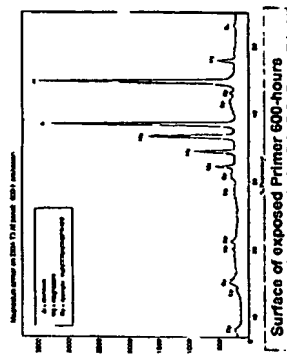
1300 hr exposure Surface & Interior:
Brucite ($Mg(OH)_2$), broad line absorption
corresponds to fine crystalline domains.



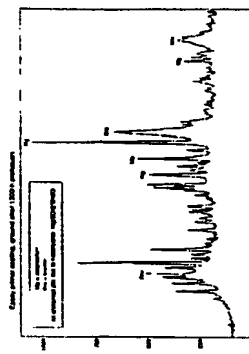
1300 hr exposure lifted underside:
Brucite ($Mg(OH)_2$), rosettes with Hexahydrite
plate emanations

X-Ray Diffraction Patterns

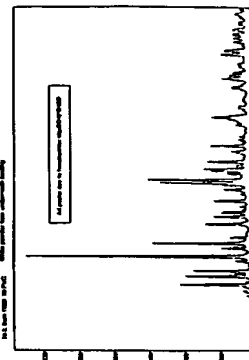
The mechanism of magnesium powder epoxy primer degradation on 2024 T-3 exposed to a dilute Harrison's solution prohesion test can be determined by the crystalline structures of hydroxides and hydrates of magnesium as a function of exposure time.



Surface of exposed Primer: 600-hours



Ground up Primer exposed 1300-hours



Underside of Primer exposed 1300-hours

PART VII

Certain aspects and embodiments of the present invention are described in the following text and figures.

Magnesium Powder Epoxy Primers for 2024 T-3 Al

THE GOOD

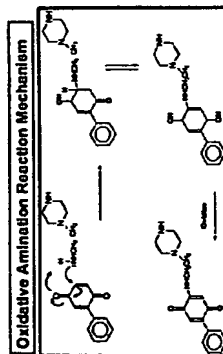
AA2024-T3 Aluminum

AA2024-T3 aluminum is a high strength precipitation hardened grade aluminum alloy used extensively in aerospace applications. The alloy gains its strength from a magnesium rich precipitate that is introduced by the distribution of an intermetallic copper containing homogeneous second phase microstructure. As a consequence of heat treating the alloy becomes more susceptible to corrosion. The corrosion resistance of AA2024-T3 aluminum is provided by its environment. However, it is believed that copper is particularly deleterious to the corrosion resistance of aluminum. The copper rich phases of AA2024-T3 aluminum are located at grain boundaries, intermetallic inclusions and their adjacent depleted regions. These copper rich phases are particularly susceptible to the leaching of copper at its surface. The leaching of copper at its surface leads to the formation of a porous, non-protective layer of copper hydroxide and copper oxide. This layer is higher than that of the passive layer on aluminum. This porous layer is more susceptible to corrosion than the passive layer on aluminum. This porous layer is more susceptible to corrosion than the passive layer on aluminum. This porous layer is more susceptible to corrosion than the passive layer on aluminum.

Introduction:
The purpose of this study was to evaluate the effects of anode sublayer on the corrosion resistance of AA2024-T3 aluminum. The anode sublayer was a magnesium powder filled primer that provided cathodic protection in a salt spray environment. An epoxy primer was used as a base for the anode sublayer. The anode sublayer was applied to the surface of AA2024-T3 aluminum. The anode sublayer was applied to the surface of AA2024-T3 aluminum. The anode sublayer was applied to the surface of AA2024-T3 aluminum.

Phenylquinone amine curatives

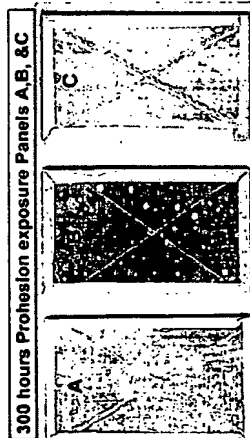
The standard quinone-amine curatives are based on the reaction of a standard hydroquinone derivative, hydroquinone, (a neutral molecule), is oxidized to quinone. The reduction potential for copper is 0.34 volts (vs. SHE) and the reduction potential for copper is 0.34 volts (vs. SHE). The reduction potential for copper is 0.34 volts (vs. SHE). The reduction potential for copper is 0.34 volts (vs. SHE).



THE BAD

Chloride Ion, Cl⁻

Chloride ion is a common contaminant in electrolytes containing chloride ion. Chloride ion is a common contaminant in electrolytes containing chloride ion. Chloride ion is a common contaminant in electrolytes containing chloride ion. Chloride ion is a common contaminant in electrolytes containing chloride ion.

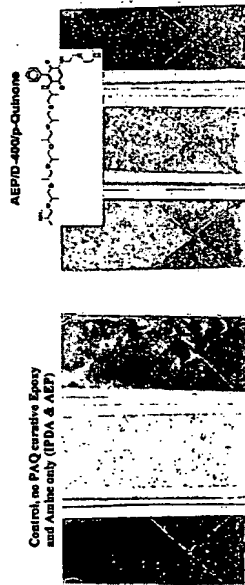


**Control (left): Curative IPDA
Polyamide AHEW: 125
BPA Epoxy: 188 EEW
671PM**

**Center: Curative IPDA
& PAQ/Jeffamine T-
403 Epoxy: DER-
671PM**

**Right: Curative IPDA
Jeffamine T-403 No PAQ
Epoxy: DER 671PM**

Cathodic Protection of Aluminum by Magnesium & phenyl-quinone-amines



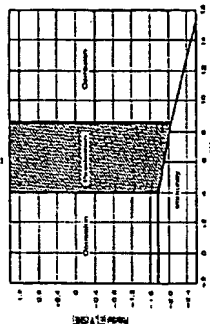
Control, no PAQ curative Epoxy and AHEW curative (IPDA & AHEW)

Control, no PAQ curative Epoxy and AHEW curative (IPDA & AHEW)

THE UGLY

Magnesium metal

Magnesium metal is a highly reactive metal. It is a highly reactive metal. It is a highly reactive metal. It is a highly reactive metal. It is a highly reactive metal. It is a highly reactive metal. It is a highly reactive metal. It is a highly reactive metal.



Pourbaix Diagram for Aluminum

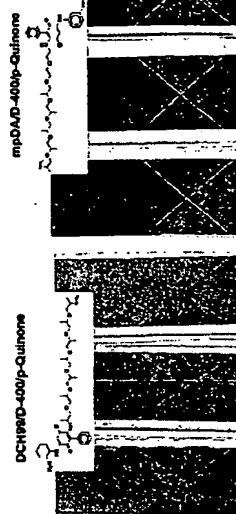
The corrosion resistance of aluminum and its alloys is provided by the presence of a natural oxide passive layer film that protects the metal surface. The corrosion resistance of aluminum and its alloys is provided by the presence of a natural oxide passive layer film that protects the metal surface. The corrosion resistance of aluminum and its alloys is provided by the presence of a natural oxide passive layer film that protects the metal surface.



Magnesium has an HCP crystal structure where upon exposure to air spray in the presence of CO₂ and H₂O, the surface of the metal is rapidly oxidized. The surface of the metal is rapidly oxidized. The surface of the metal is rapidly oxidized. The surface of the metal is rapidly oxidized.

Summary & Conclusion

In our studies we have demonstrated that epoxy coatings applied to 2024 T-3 aluminum alloy perform as well as or better than popular commercial polyamide cathodes. The epoxy coatings applied to 2024 T-3 aluminum alloy perform as well as or better than popular commercial polyamide cathodes.



mpDAD-400p-Quinone

mpDAD-400p-Quinone

1300 hour Salt-spray Prohesion Exposure Magnesium Powder filled PAQ Epoxy Panels, Scribed -X

PART VIII

Certain aspects and embodiments of the present invention are described in the following text and figures.

Magnesium Powder Filled Primer and Extended Lifetime™ Topcoat for Cathodic Protection of 2024 T-3 Aluminum Alloy

Abstract

500 hours direct exposure of 2024 T-3 aluminum panels to Prohesion cycling in Harrison's solution causes rapid corrosion of the alloy to occur. Coating the alloy with an epoxy primer filled with 20 to 200 micron sized magnesium powder, at or above CPVC (critical pigment volume concentration) cathodically protects the alloy for up to 2,000 hours. Cathodic protection of a primed panel appears to occur in two distinct stages, initially, closely packed metal particles connect in the primer to form a conductive path thus circulating charge. Gradually, as the surface of the metal is oxidized porous hydroxides, and possibly conductive, $[MgO, Mg(OH)_2]$ [brucite] domains grow and interconnect providing a conductive path for charge to flow, thus extending the period of protection of that alloy's surface. However, once depleted of brucite structure, and as magnesium sulfate[hexahydrate] salt accumulates at the alloy interface the polymeric coating rapidly fails as aluminum oxide forms and in turn generates the soluble aluminate cation. Primered panels of high pigment volume concentration (PVC) act like a sponge impregnated with electrolyte, magnesium metal, and magnesium hydroxides. As magnesium metal oxidizes both its volume and permeability to electrolyte increase allowing charge to flow both perpendicular and horizontal to the surface of the cathode. Therefore, lines scribed over the primer surface experience a greater more effective and extensive "neighboring" cathodic current contribution. Sealing the surface, with a topcoat, acts to reduce and confine exposed cathode and anode area to the surfaces of the lines scribed through and over the coating. Lacking the porous sponge like structure open to electrolyte passage and neighboring participation, cathodic protection becomes restricted to the local exposed magnesium surface in contact with the alloy substrate. Anode particle-particle contact extending away from the scribe and throughout the body of the primer is believed to contribute to the cathodic protection of the alloy. It is thought that "how fast" the exposed anode in the scribe is consumed is a kinetic parameter that influences the dissolution of magnesium and its hydroxides along the scribes over the panel and is related to topcoat PVC, magnesium particle size and packing.

Introduction

Magnesium powder filled epoxy primers have been formulated above and below CPVC, then subjected to Prohesion cycling in Harrison's solution to emulate acid rain conditions. Upon initial exposure the acidic ($\text{pH} \sim 4.5$) solution quickly attacks magnesium metal yielding hydrogen gas H_2 , the metal oxide MgO , and brucite the metal's hydroxide $\text{Mg}(\text{OH})_2$.⁽¹⁾ Primer PVC (pigment volume concentration) was found to strongly influence integrity of exposed primer coatings.⁽²⁾ High PVC metal content primers contain more surface metal available to serve as sacrificial anode, thus elevating PVC far above CPVC extends galvanic protection to both binder and alloy, however, lower available binder concentration at the metal anode surface caused poor adhesion between primer and interface. Poorly encapsulated magnesium in a sulfate solution quickly forms a high volume of interlaced hydroxide extending over the metal's surface.⁽³⁾ Lower PVC metal load primers develop lower surface hydroxide coverage thus are prone to develop aluminum oxides sooner when alloy surface is damaged or exposed. Formulating primers near CPVC causing particles to pack and connect thereby increasing the coatings effectiveness to serve as a sacrificial anode. Elevating the PVC of a primer above CPVC increases the exposed anode surface area, more anode metal delivers more protection. Primers formulated far above CPVC lack sufficient binder required to effectively encapsulate the metal, as a result connectivity and volume of brucite formed over the surface is greater and more uniform. However, equilibrium eventually favors formation of magnesium sulfate hydrate salts hexahydrate $[(\text{MgSO}_4) \cdot 6 \text{H}_2\text{O}]$, found to precipitate and accumulate at the interface between primer and alloy.⁽³⁾ In turn, accumulation of hexahydrate salt at the alloy interface corresponds to a loss of passivity and evolution of the flakey porous oxide structure corresponding to the oxide observed in figure 1-C at 1,000-hours Prohesion exposure. Once the metal has been depleted by conversion to oxide the remaining binder, at the alloy interface, ruptures and fragments from compressive forces exerted by expanding salt structures. Studies have shown the course of events for the corrosion process of magnesium powder filled epoxy primers follows three distinct events.⁽³⁾

1. EDX spectrum show initial formation of magnesium carbonate hydrates at the liquid/vapor interface, dypingite $[\text{Mg}_5(\text{CO}_3)_4(\text{OH})_2 \cdot 8\text{H}_2\text{O}]$ & hydromagnesite $[\text{Mg}_5(\text{CO}_3)_4(\text{OH})_2 \cdot 4\text{H}_2\text{O}]$ fluffy white carbonate powder formation extends up to the first 500 hours of exposure.
2. Over a more extended period of exposure, magnesium hydroxides formed due to acid oxidation yielding extensive thin crystalline domains of brucite needles $[\text{Mg}(\text{OH})_2]$. Note during this time period the aluminum alloy remains cathodically protected, scribed lines remain clear.

3. Ultimately, failure delamination corresponds to the accumulation of hexahydrate $[(\text{MgSO}_4) \cdot 6 \text{H}_2\text{O}]$ salt at the interface. At which time the interface rapidly covers with aluminum oxide and the coating binder quickly decomposes.

Overall, failure occurs when magnesium has been depleted from the binder matrix and sufficient hexahydrate salts have accumulated at the alloy interface to cause decomposition of the binder. It is believed that during the first two stages of the process the Aluminum alloy substrate is cathodically protected.

Two types of top-coated magnesium powder primers were evaluated, the first topcoat was an impermeable organo-silane film former based upon phenyl-quinone and *n*- β -(aminoethyl)-gamma-aminopropyltrimethoxysilane:

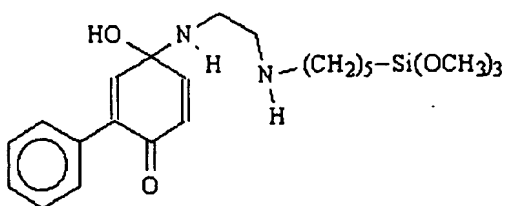


Figure 3-a, reactive intermediate

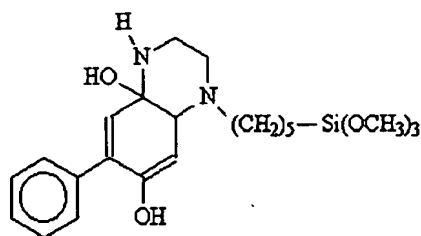


Figure 3-b, stable film former

Figure 3-a, reactive intermediate is applied in a solution of dichloromethane and penetrates into the epoxy primer coating and forms a thin impermeable film which is highly resistant to solvent after 24-hour cure at 30°C. It is believed reactive intermediate 3-a cyclizes and methoxy silane moieties react with surface hydroxyls. The resulting closed pore films restricted migration of electrolyte and prevented hexahydrate from penetrating and precipitating at the alloy interface, figures 4-5 contrast coated and non-coated primers as a function of PVC as a function of Prohesion™ exposure. Water beaded on the surface of the organo-silane treated samples and the white salt residue from water beads atop the treated panels at 500-hours was identified by EDX as hexahydrate. The source of the magnesium salt was due to drainage/condensation from above portion of panel. Panels were stowed with coated portion at the base and the uncoated atop free to drain. The scribes of all panels treated with organo-silane filled with aluminum oxide at 500-hrs exposure irregardless of PVC. However, upon examination panels with lower PVC developed more oxide than those panels near CPVC at 50 to 55 PVC. Panels formulated at PVCs of 60 and 66 suffered disbonding from hexahydrate drainage. It is suspected that a more extensive "local neighboring" effect extends and connects the coating at 50 to 55 PVC range making it slightly more resistant to corrosion. Modification of Harrison's solution with hexahydrate may in turn be the underpinning for a more effective exposure solution for testing aluminum alloys than dilute Harrison's solution alone.

Epoxy Binders

Coatings formulated with magnesium powder for cathodic protection of the aluminum alloy have two distinct disadvantages,

1. Blistering and delamination occurs at alloy interface as hydrogen gas evolves when magnesium metal is oxidized by acid.
2. Adhesion of high metal volume content coating to the alloy surface requires excellent wetting of both magnesium and alloy surfaces.

Ambient temperature cure epoxy/amide systems tend to wet pigments well and as a result yield superior adhesion to aluminum alloys, for example, the combination of Epicure 3115 & Epon 1001-CX ⁽⁵⁾ is often used in epoxy lacquers for high solids primers. Epoxies cured with polyamides have poor acid and chemical resistance, ⁽⁶⁾ and as a result tend to develop blisters and delaminate after brief periods of exposure. Ambient cure polyamines used as epoxy curatives yield improved acid/base and chemical resistance, e.g. DEN-439 & Ancamine 2422 ⁽⁷⁾ but due to development of extensive crosslink density lack flexibility and as a result their adhesion to metal is severely compromised. In addition, polyamines based on primary amines are high surface tension liquids, circa 40–45 dyne-cm making them slightly incompatible with epoxy resins and poor pigment wetting agents limiting their utility to formulations below CPVC. Two-component epoxy coatings formulated with primary amines tend to develop highly cross-link structures and as a result high internal stress accumulate in the coating over time. Development of high internal stresses directly reduces the epoxy binder's adhesion to alloy substrate.

Elastic Modulus (lb/in²) Sward Hardness
ASTM D-2134-93

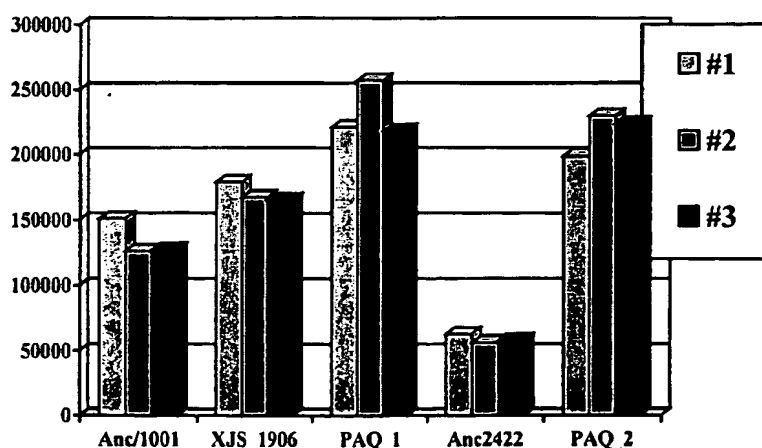


Figure 4, elastic modulus for films from Ancamide 2353(polyamide)/Epon 1001; Dow XUS-19005/DEN-431; phenyl-quinone-amine #1/DEN-431; Ancamine 2422/DEN-431; phenyl-quinone-amine #2/DEN-431.

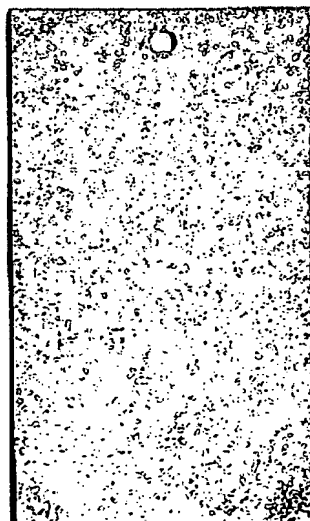
Thus far, no epoxy/amine or amide binder system has performed well enough as a stand alone for magnesium powder cathodic coatings. Overall, ambient cure epoxy binders encapsulate pigments well and form films but lack the versatility required to bind large particle size high metal PVC coatings to an aluminum alloy interface. In sumation, all fall short in adhesion to aluminum alloys at high PVCs.

Bare Aluminum

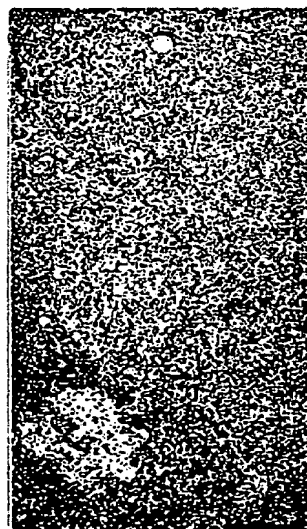
Bare 2024 T-3 aluminum panels were subjected to Prohesion cycling in dilute Harrison's solution for 1000 hours. Six, untreated 2024 T-3 panels were subjected to Prohesion cycling for up to 1000 hours upon which time testing was terminated due to extensive corrosion of the alloy. Initially, and up to 500 hours of exposure the panels were characterized by slow formation of micron sized clusters of oxide and the initiation and growth of pits that filled with a white, passive aluminum oxide Al_2O_3 . This oxide was found to be slightly adherent and in localized clusters, thus characterized by a Pilling-Bedworth ratio of 1.5 for that oxide. ⁽⁸⁾ The Pilling-Bedworth ratio is a ratio of the specific volume of metal oxide developed to specific volume of the metal itself. A P-B ratio of less than one indicates the metal develops a fluffy, penetrable, porous oxide, such as magnesium oxide with a P-B of 0.85. A P-B ratio greater than one yields a higher volume of oxide that is a passive more closely packed compressed structure such as Al_2O_3 . Finally, after 500 hours exposure no remnant of passive Al_2O_3 layer appears to exist the entire surface has been extensively consumed by pitting and replaced by a gray, non-adherent, oxide flake. This non-adherent oxide can be characterized by a Pilling-Bedworth ratio similar to that of iron rust Fe_3O_2 of around three, this very high ratio of oxide to metal in its atomic lattice structure causes high internal compressive forces to develop as the oxide grows. Oxides are characterized as having high compressive and poor tensile strengths thus by nature leaving them prone to flake from the surface as they grow.



5-a Unexposed 2024 T-3



5-b 500-hrs. 2024 T-3



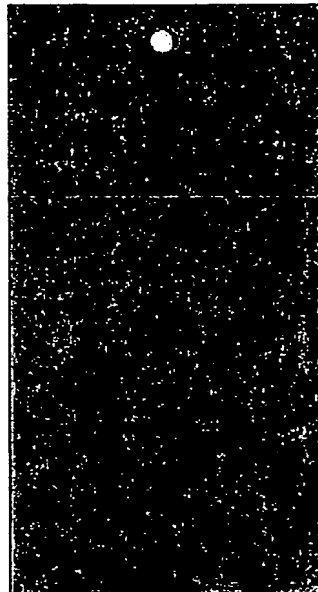
5-c 1000-hrs. 2024 T-3

Organo-Silane Treated 2024 T-3

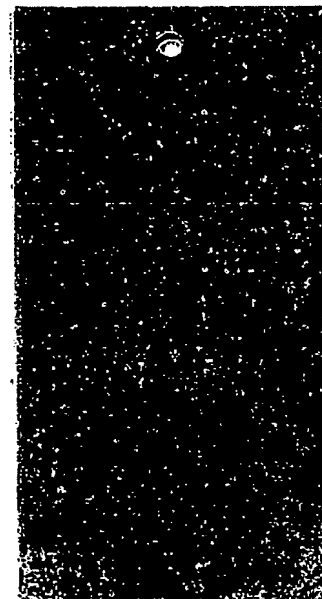
Primers formulated at high PVCs with epoxy binders tend to lack adhesion to 2024 T-3 aluminum surface. An organo-silane adhesion promoter was synthesized and applied to 2024 T-3 and subsequently exposed to Prohesion cycling. Six panels were treated with a 10% solution of a silane modified quinone. The panels were cured 48 hours at 40°C, whereupon a strongly adherent, solvent resistant sub-micron film formed. After 1000 hours exposure white oxide clusters/pits sparsely form over the surface. Surface treated panels arrested the corrosion process by physically blocking dissolution, thereby moderating the corrosion process.



6-a Unexposed, Silane treated 2024 T-3



6-b 500-hrs. Silane treated 2024 T-3

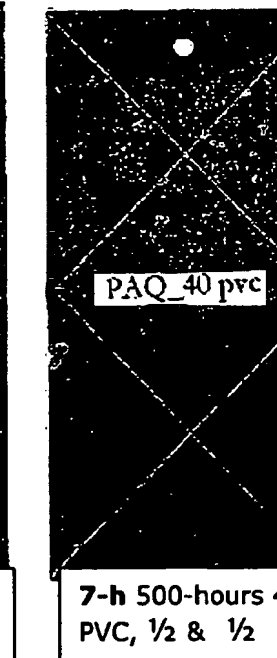
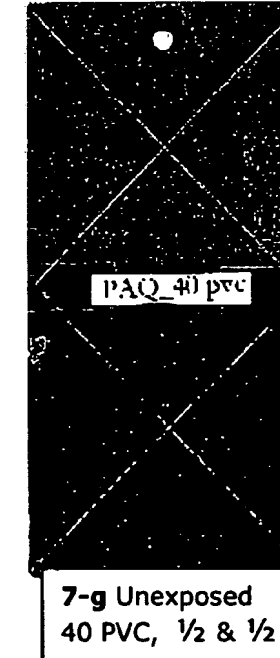
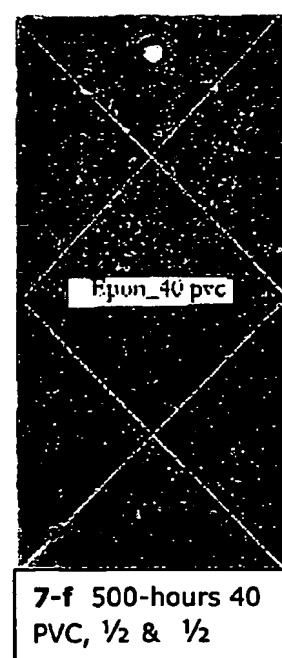
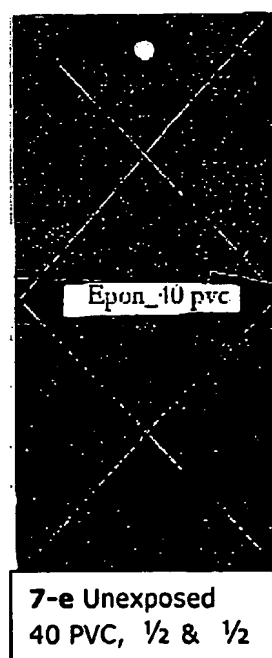
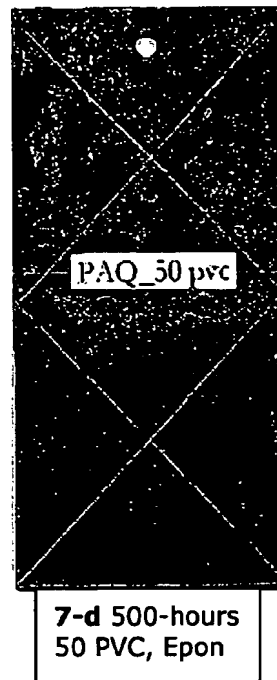
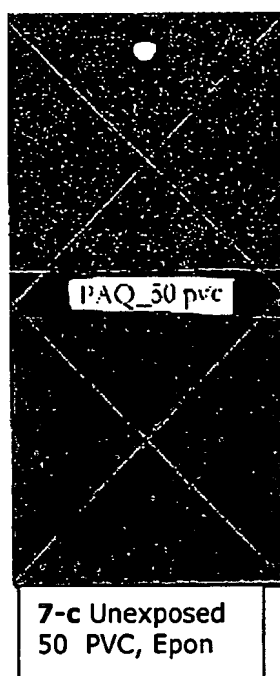
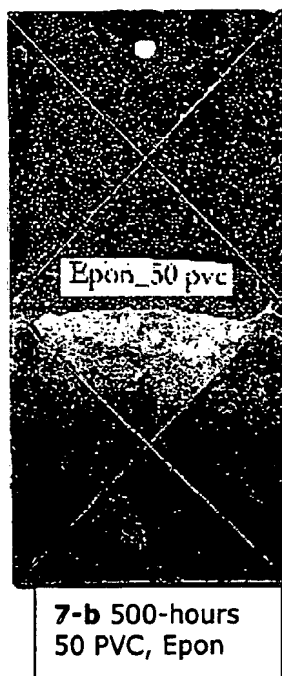
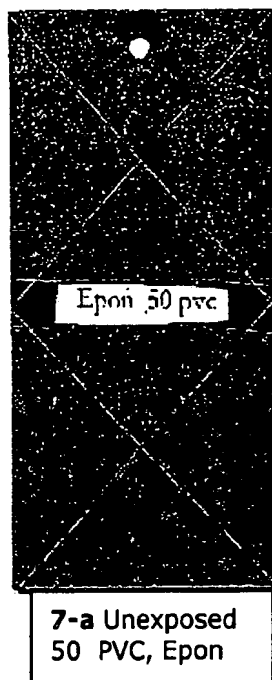


6-c 1000-hrs. Silane treated 2024 T-3

Magnesium Filled Primers

The purpose of the magnesium powder filled primer is to provide cathodic protection to the 2024 T-3 alloy without physically blocking the aluminum surface. Primers formulated above CPVC block less surface than those below CPVC. It has been observed in past studies that those primers formulated above CPVC provide longer periods of protection simply because there is more anode available. Physically blocking the surface occludes cathodic protection when contact between anode and cathode is interrupted. Primers formulated below CPVC, circa 40 PVC are effective at blocking surface and providing limited local cathodic protection so long as the coating itself remains integral and intact. However, once the coating is damaged and the surface exposed cathodic protection becomes limited to the local concentration of magnesium anode at the site of fracture. If the metal is well encapsulated galvanic protection terminates resulting in oxide ingress and lifting about the damaged area. Primers formulated with epoxy binders well above CPVC are prone to lifting and

delamination as adhesion to the surface is poor as a result of epoxy binder preferentially wetting the smaller spherical pigment particles to minimize surface free energy as opposed to wetting a lower energy flat alloy surface. PVC effect illustrated below, series of magnesium primer panels prepared in epoxy binders polyamine (PAQ), and polyamide (EPON), with and without organo-silane surface treatment.



50 PVC Panels

Top row, previous page, two sets of panels before and after 500 hours Prohesion cycling with top section of panels organo-silane treated. Scribed lines of treated section partially filling with aluminum oxide while untreated section scribe lines remained clear. Note presence of white magnesium oxide, Brucite, magnesium hydroxide covering the surface of the untreated. Panels were stowed with silane treated sections set into base of the storage rack allowing drainage from upper untreated portion to accumulate and precipitate on treated portions. The crystalline precipitate covering silane treated panels was identified by x-ray diffraction to be the magnesium sulfate hydrate salt, Hexahydrite. Hexahydrite accumulation was observed to be due to precipitation from liquid drops at liquid/vapor interface.

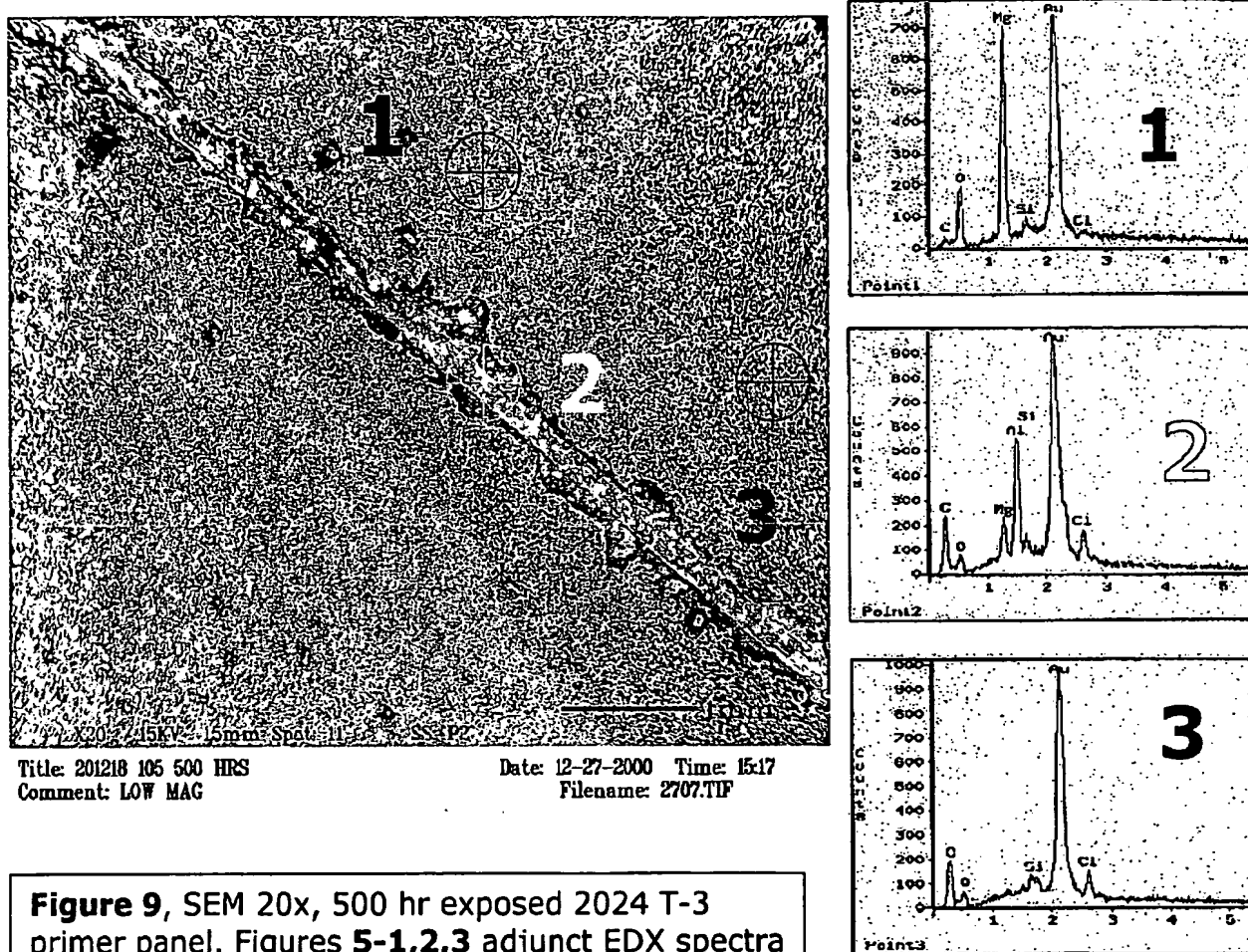
40 PVC Panels

Bottom row, previous page, two sets of panels before and after 500 hours cycling identical treatment as above. Scribed lines of both silane treated portions filled packed solid with aluminum oxide while both sets of untreated panels scribe lines remain clear. Hexahydrite accumulation, darkened areas, over surface of treated portion where untreated panels drained. Brucite white oxide covering surface of untreated portions no lifting under scribes. PVC effect between 40 and 50 samples shows the scribed lines over silane treated portions of the 40 PVC to be packed with aluminum oxide, whereas, for the 50 PVC panels lines contained sparse areas filled with oxide.

Exposed Primer Panel

SEM and corresponding EDX energy disperse x-ray diffraction spectra of three areas of a 50 PVC primer with 20-micron powder at 500 hours exposure revealed different chemical compositions at the panel surface as a function of exposure. SEM and EDX of area one ⁽¹⁾ correspond to white Brucite structure emanating directly from metal in the primer, binder still in tact, fine, needle crystalline structure covering the face of the coating. It is believed that Brucite is an intermediate equilibrium structure formed at the metal surface as a result of magnesium being oxidized by acid. During the first 500 hours of exposure all of the metal available at the surface is oxidized and converted to Brucite, proceeding after 500 hours the structure continues to grow at the expense of the metal anode. SEM and EDX of area three ⁽³⁾ correspond to the epoxy binder matrix depleted of magnesium and Brucite. Distinct demarcation reveals depletion of metal anode starting at the edges of the panel and following an ingression toward the more electrically connected metal rich center. SEM and EDX of area two ⁽²⁾ correspond to the scribed bare 2024 T-3 panel. Higher resolution SEM photomicrographs show the surface to be relatively clear and unblemished by aluminum oxide on a sub-micron scale.

EDX spectra proportional to magnesium carbonate present on surface.



1) White oxide area magnesium hydroxide Brucite over magnesium metal. Note magnesium, oxygen and aluminum. Minimum carbon is detected.

2) Scribed area with no epoxy matrix, nor magnesium metal present. Spectrum shows carbon, oxygen magnesium and aluminum. Possible presence of dypingite, magnesium carbonate structure over aluminum surface.

3) Magnesium depleted epoxy matrix, spectrum shows aluminum, carbon and oxygen in almost equal proportion and intensity to spectrum "2" above.

In summation, it was observed the salts generated during first 1000 hours of exposure did not degrade neither binder nor alloy surface. With reference to the SEM and EDX of area 2, the presence of magnesium carbonate at the surface suggests that it participates in the overall cathodic protection mechanism.

Topcoated Panels

Deft 99 GY-001 Base & Catalyst "Extended Life fluoropolymer Topcoat" was applied to alloy panels formulated with Eckart 200 micron 099/00 magnesium powder. Elevated PVCs require excellent primer adhesion. Primers formulated with 200 micron, (average) particle size magnesium powder above CPVC tend to fare poorly in reverse impact. Poor reverse impact resistance in cathodic coatings has been a good indication of early coating delamination during Prohesion cycling studies. Larger average particle size magnesium powders tend to be coarse and fare poorer in reverse impact than smaller 20 - 200micron size powders. Coarse particles, over 380 micron size, in turn leave the high PVC topcoat prone to failure. Smaller particle sized magnesium powders yield a higher exposed surface area and higher reactivity. The ideal primer will be comprised of a balance of the two at some ideal thickness.

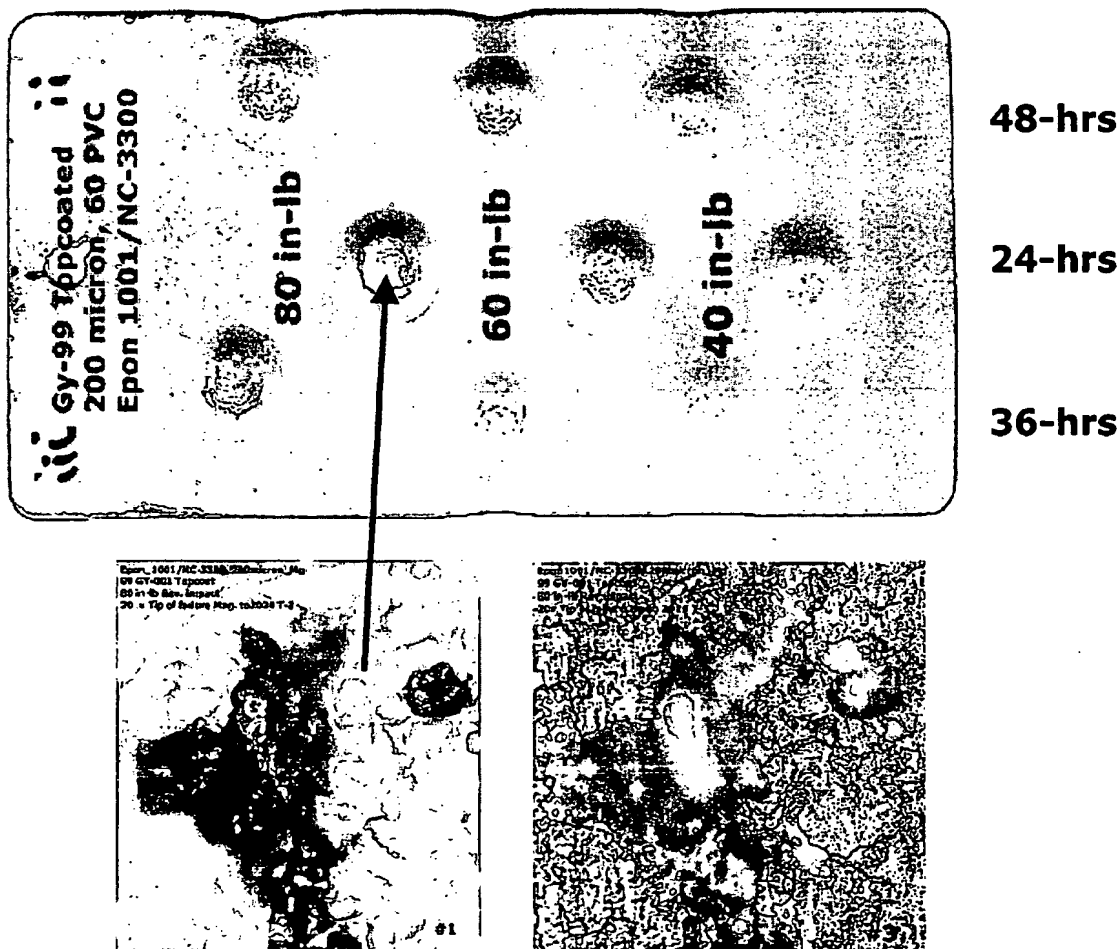
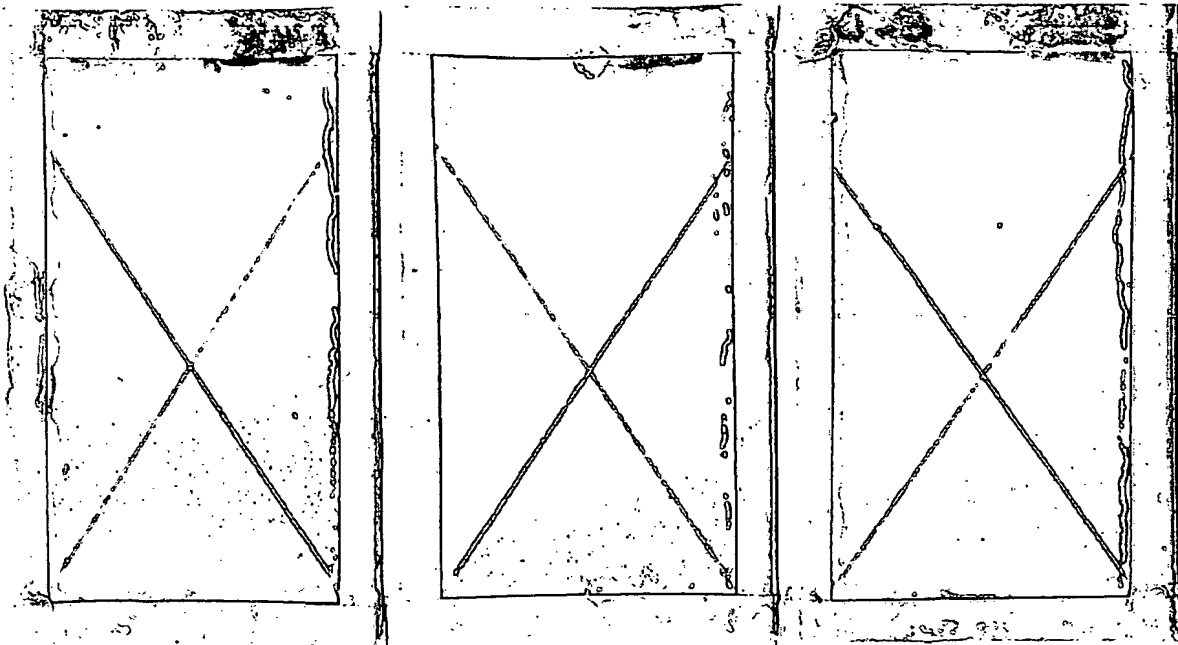


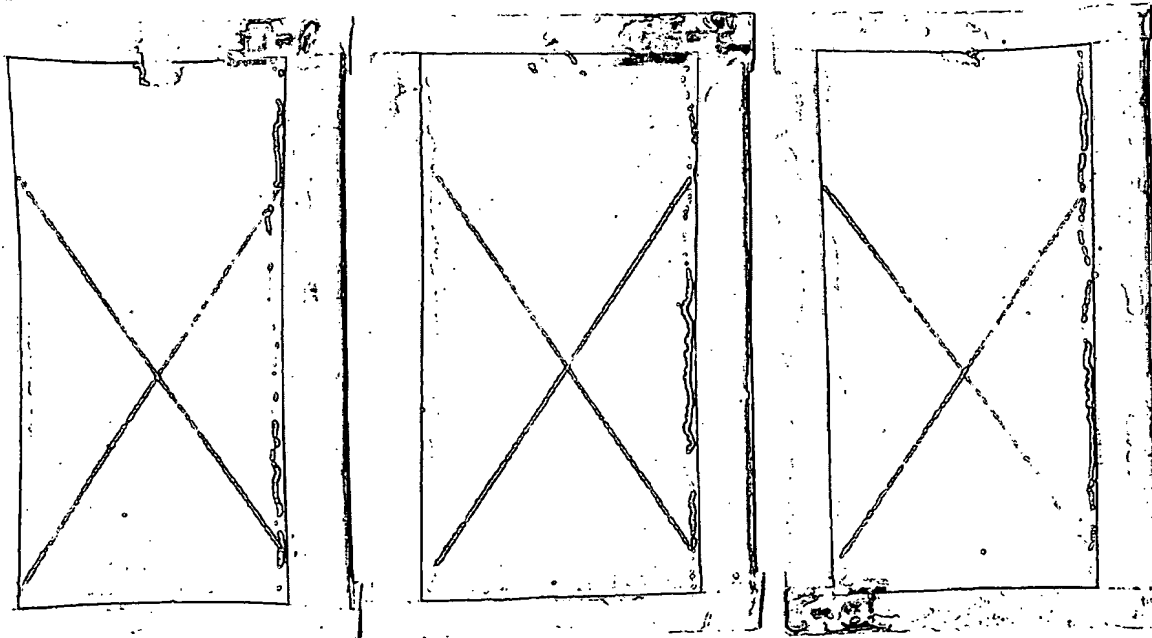
Figure 10; Deft GY-99 70 micron thick film topcoat over 200 micron thick film primer with 200 micron average particle size magnesium powder. Reverse impact results for 24, 36, and 48-hour topcoat cure time.

Topcoat panels Prohesion™ exposure results at 1550 hours for top row of panels
2024 T-3 alloy in triplicate; bottom row 3105 corrosion resistant alloy.

**2024 T-3 alloy with GY-100 Extended Lifetime top-coated magnesium
powder filled primer 1550 hours Prohesion cycling in Harrison's solution**



3105 alloy with GY-100 Extended Lifetime top-coated magnesium powder filled primer 1550 hours Prohesion cycling in Harrison's solution



Polymer binder for primers

High PVC extended lifetime topcoats simply provide surface protection over an extended time period. They must remain integral and not fail or degrade.

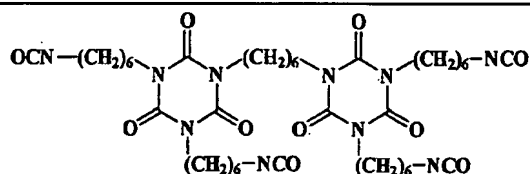
Primers essentially provide the coating's integral guts it connects both surface and substrate and arrests drastically different effects occurring in two separate but interconnected environments. Primers formulated for cathodic protection require a polymer binder that wets metal well, retains flexibility, maintains

solvent and acid resistance, provide, and in addition are not easily hydrolyzed by caustic salts.

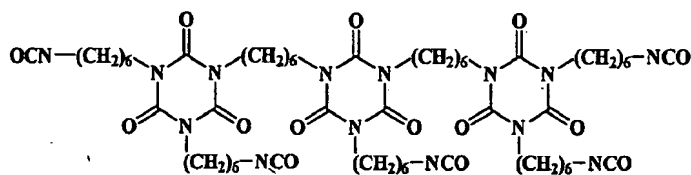
Aromatic moisture cure polyisocyanates are commercially available materials for application to moderately high pH concrete surfaces thus making them suitable as a binder system for magnesium powder filled primers for cathodic protection.

(9) The polyisocyanate binder utilized in these systems forms both urethane and urea linkages at a stoichiometric ratio of 5 to 1. In order of stability to caustic high pH conditions these urethane/urea coatings rank above polyamides and are similar to polyamines. (10)

Polyisocyanurate Oligomers for Moisture Cure High PVC zinc rich primers



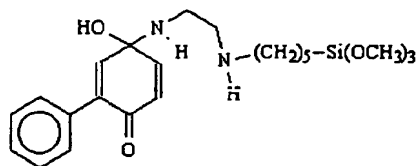
Pentamer



Heptamer

Isocyanate reactivity is greatly enhanced by magnesium metal. Desmodure N-3300 an aliphatic polyisocyanate based on HDI with 20 % labile isocyanate, is categorized as a "slower" polyisocyanate. Initial attempts to incorporate N-3300 polyisocyanates into magnesium powder filled primers yielded gellation.

Polyisocyanate reactivity, in the presence of magnesium is thought to be best controlled by using polyisocyanate pentamers and heptamers with a lower labile isocyanate content along with judicious solvent selection, and metal pigment pretreatment. The binder used for the primer the topcoat study was an epoxy modified polyisocyanate cured the amino-silane substituted phenylquinone.



Solvent swelling 5 to 6 mil film thickness

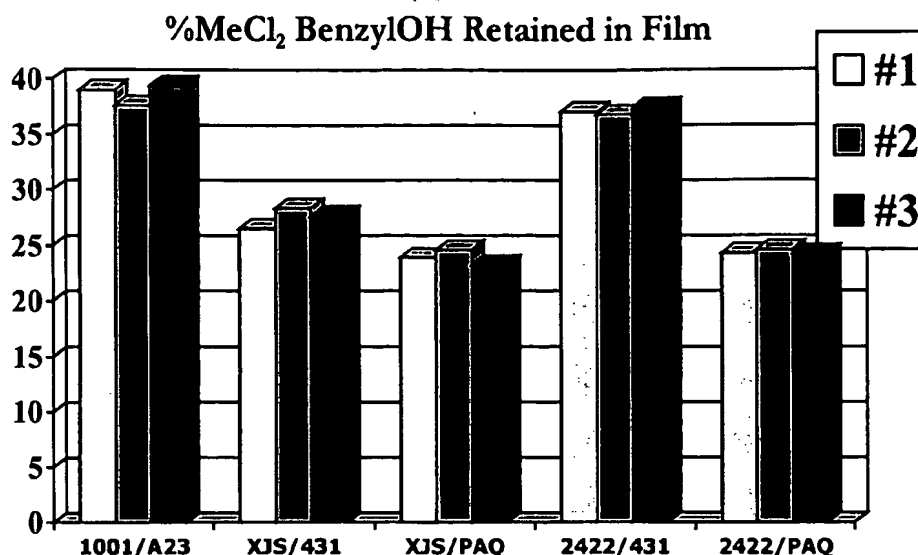


Figure 13; percent solvent retained after 24-hour solvent reflux. 1001/Anc-2353 (polyamide); XJS(polyamine)/DEN-431; XJS(polyamine) & PAQ/DEN-431; Anc-2422 (polyamine)/DEN-431; Anc-2422(polyamine) & PAQ/DEN-431

The above solvent swell graph illustrates the effect adding pheny-quinone PAQ modified polyamines to epoxy binders has on solvent resistance. In addition to solvent resistance pheny-quinone modified amines greatly improve sulfuric acid resistance of epoxy binders. High primary amine content has been found to contribute to reduced adhesion in the PAQ modified poyamine binder systems. A synthesis based upon converting the primary amine to a secondary amine by adding acrylonitrile to the Jeffamine poly(oxypropyleneamines) was carried out by Texaco in the 1970's and now archived by Huntsman Corp. Secondary amines and nucleophiles of similar reactivity are believed to be more suitable for synthesis of phenyl-Quinone Amine curatives used in ambient cure epoxy binder systems.

36 hour Sulfuric Acid Exposure



PAQ_polyamine/EpoxyNovolac



Polyamide/BPA Epoxy

Currently, a moisture cure binder system is being developed that utilizes magnesium powder to catalyze a reaction between an aromatic polyisocyanate and ambient moisture. Reaction kinetics of the polyisocyanate have been observed to be dependent on both polarity of carrier solvent and magnesium powder particle size, where a smaller 20 micron average particle size 099/99 has been found to be far more reactive than the 200 micron average 099/00 powder.

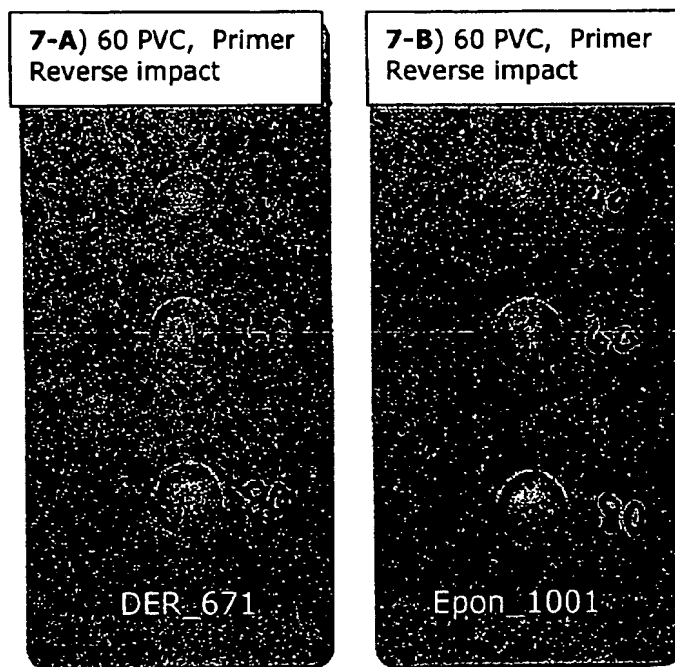


Figure 14-a & b , reverse impact results for primed panels containing Eckart 099/00, 200 micron sized magnesium powder at 60 PVC with current hybrid polyisocyanate/epoxy binder system. Similar results were obtained using two commercially available epoxy resins DER 671PM, panel '7-A' and Epon 1001cx, panel '7-B'. Both resins Taffy process at 450 to 550 EEW. The coating carrier solvent was a xylol /acetone mix, spray applied, single coat approximately 200 micron film thickness. Reverse impact indentations from top to bottom 40, 60, and 80 lb-inch respectively. Overall, the panels with Epon 1001CX had slightly better adhesion possibly a result of better wetting of the non-polar stearate treated magnesium powder surface. Solvent effect may have played a role as the Epon resin was cut in non-polar xylene, while the DER-671PM cut in more polar DOWANOL PM, (propyleneglycol monomethylether). Coating failure at 80 lb-inch from the surface indicates mechanical limits of the polymer binder at that PVC have been greatly exceeded. The 60 lb-in results appear to be the more attainable practical limit for a top-coated panel with a 200 micron sized magnesium powder.

Summary

Aluminum an amphoteric metal corrodes under both acid low pH and alkaline high pH conditions. A Pourbaix diagram gives the thermodynamic relationship between aluminum metal/oxide/hydroxide stability in solution typically over a pH range from 0 to 14. The Pourbaix diagram for pure aluminum shows the metal forms a passive oxide layer over a pH range of 3.5 to 9. However, the presence of coherent copper microstructure in 2024 T-3 alloy renders it more susceptible to corrosion at a slightly higher pH than 3.5. Dilute Harrison solution with a pH~4.5 is acidic and readily oxidizes this aluminum alloy.

In a cathodic coating, magnesium serves as the sacrificial anode and as the anode is consumed, depending on the conditions, oxides and hydroxides are generated that tend to be progressively more alkaline. The alkalinity depends upon the nature and concentration of anion present. Thus far three dominant salts have been observed to occur during exposure carbonate, hydroxide, and sulfate each in turn progressively more alkaline. It is believed that the carbonate and hydroxide salts of magnesium help protect the passive layer of the alloy and participate in the cathodic protection mechanism while highly soluble sulfate salts appear benign to the alloy in the presence of abundant Mg^{2+} . Meaning there is no evidence that magnesium hydroxides (hexahydrate) damages the aluminum passive layer. However, once the primer has been depleted of Mg^{2+} soluble sulfate anion drives the dissolution of aluminum and the alloy corrodes at the rate seen in figures 1-a to 1-3.

Addition of an organo-silane to the surface of the aluminum appeared to physically block the surface and retard migration of electrolyte and dissolution of aluminum. Figures 2-a to 2-c moderated corrosion effect, no soluble organo-silane salts appeared to form in presence of aluminum cation, only small domains of aluminum oxide emanating from surface. Figure 2-c gives a qualitative measure as to size and progression of aluminum oxide on the surface that causes disbonding of adhered silane as the underlying metal is dissolved.

The complete coating system for cathodic protection of 2024 T-3 aluminum with a magnesium powder primer begins at the alloy interface with an organo-silane adhesion promoter that is integral to the binder itself. A moisture cure aromatic isocyanate binder comprises the backbone of the primer polymer adding high chemical and alkaline resistance improved adhesion, flexibility, and wetting of both pigment and alloy surface. Ideal magnesium particle size distribution should range from 10 to 200 microns. As submicron sized magnesium is rapidly consumed and acts to over accelerate cure of primer binder.

References

- 1) D. Elizer and A. Antonyraj, Unusual Behavior of Magnesium an ZM Anodes in Aqueous Electrolytes at High Concentrations, Corrosion, April 2001, Pp. 334-345
- 2) M. Nanna, G.P. Bierwagen, Unpublished work shown at IAB poster session, North Dakota State University, October 1999
- 3) J. Genesca, L. Betancourt, and C. Rodriguez, Electrochemical Behavior of a Magnesium Galvanic Anode Under ASTM Test Method G-97-89 Conditions, Corrosion, July 1996, Pp. 502 - 507
- 4) M. Nanna, G.P. Bierwagen, Unpublished work FSCT Poster session , Chicago, October, 2000, & IAB poster session, North Dakota State University, October 2000
- 5) S. Sumner, Resolution Performance Inc./Epon resins, personal communication, September 1999 & Shell Epon resin formulation guide.
- 6) M. Nanna, Departmental Seminar Presentation, North Dakota State University, April, 2001
- 7) Ancamine 2224 Curing Agent bulletin/guide, Air Products Inc., Hamilton Blvd. Allentown, PA, 1998
- 8) D. R. Asklund, The Science and Engineering of Materials, Alternate Edition, PWS Publishers, 1985, Pp. 510-511
- 9) R.R. Roesler, Bayer Corporation., Personal Communication, NDSU, June 8, 20001
- 10) R.R. Roesler, Polyurethanes for Coatings, Bayer Corporation, June 1999, Pp. 32-36
- 11) Howard Klein, Huntsman Co., Personal Communication, July 2001

PART IX

Certain aspects and embodiments of the present invention are described in the following text and figures.

Magnesium Powder Filled Primer and Extended Lifetime™ Topcoat for Cathodic Protection of 2024 T-3 Aluminum Alloy

Abstract

500 hours direct exposure of 2024 T-3 aluminum panels to Prohesion™ cycling in Harrison's solution causes rapid corrosion of the alloy to occur. Coating the alloy with an epoxy primer filled with 20 to 200 micron sized magnesium powder, at or above CPVC (critical pigment volume concentration) cathodically protects the alloy for up to 2,000 hours. Cathodic protection of a primed panel appears to occur in two distinct stages, initially, closely packed metal particles connect in the primer to form a conductive and sacrificial path thus circulating charge. Gradually, as the surface of the metal is oxidized porous hydroxides, $[MgO, Mg(OH)_2]$ [brucite] domains grow and interconnect providing a conductive path for charge to flow, thus extending the period of protection of that alloy's surface. It is not the surface of the coating that is important but the bulk of the primer. However, once depleted of brucite structure, and as magnesium sulfate[hexahydrate] salt accumulates at the alloy interface the polymeric coating rapidly fails as aluminum oxide forms and in turn generates the soluble aluminate cation in the presence of the high pH due to the oxidized Mg. As magnesium metal oxidizes both its volume and permeability to electrolyte increase allowing charge to flow both perpendicular and horizontal to the surface of the cathode. However, if the Mg metal can be kept in contact with the Al surface, cathodic protection of the alloy remains in effect. Putting on the topcoat slows down the direct acid solution contact with the Mg particles as well as filling the pores in the primer. The cathodic protection still takes place, but the reactive consumption of the Mg slows considerably. Anode particle-particle contact extending away from the scribe and throughout the body of the primer is believed to contribute to the cathodic protection of the alloy. It is thought that "how fast" the exposed anode in the scribe is consumed is a kinetic parameter that influences the dissolution of magnesium and its hydroxides along the scribes over the panel and is related to topcoat PVC, magnesium particle size and packing. Overall, it is believed that using a topcoat at its CPVC, the magnesium powder primer coating systems protection to the 2024 T-3 aluminum both cathodically and passively for up to 3000 hours Prohesion™ exposure before damage to system begins to spread from the scribe.

Introduction

Magnesium powder filled epoxy primers formulated above and near to CPVC, were subjected to Prohesion™ cycling in Harrison's solution to emulate acid rain conditions. Initial exposure in the acidic (pH~4.5) solution quickly attacks magnesium metal yielding hydrogen gas H_2 , the metal oxide MgO , and brucite the metal's hydroxide $Mg(OH)_2$.⁽¹⁾ Primer PVC (pigment volume concentration) was found to strongly influence integrity of exposed primer coatings.⁽²⁾ High PVC metal content primers that contained more surface metal available to serve as sacrificial anode, lasted longer. Thus elevating PVC far above CPVC simply extends galvanic protection to both binder and alloy. However, a highly elevated PVC with less binder at the metal anode surface caused poor adhesion between primer and substrate simply because there was more exposed metal between surfaces. The Mg metal in an acid sulfate solution quickly forms a high volume of interlaced hydroxide extending over the metal's surface.⁽³⁾ Primers formulated near CPVC cause particles to pack densely enough to touch and electrically connect thereby increasing the coatings effectiveness to serve as a sacrificial anode.

Primers formulated far above CPVC lacked sufficient binder to effectively encapsulate the metal, as a result connectivity and volume of brucite formed over the surface is greater and more uniform. However, equilibrium eventually favors formation of magnesium sulfate hydrate salts hexahydrate $[(\text{MgSO}_4) \cdot 6 \text{H}_2\text{O}]$, precipitate and accumulate at the primer and alloy interface.⁽²⁾ In turn, accumulation of hexahydrate salt at the alloy interface corresponds to a loss of passivity and evolution of the flakey porous oxide structure corresponding to the oxide at 1,000-hours Prohesion exposure. Once the metal has been depleted by conversion to oxide the remaining binder, at the alloy interface, ruptures and fragments from compressive forces exerted by expanding salt structures. Studies have shown the course of events for the corrosion process of magnesium powder filled epoxy primers with no topcoat follows three distinct events.⁽²⁾

1. From EDX spectra, one detects formation of magnesium carbonate hydrates at the liquid/vapor interface, dypingite $[\text{Mg}_5(\text{CO}_3)_4(\text{OH})_2 \cdot 8\text{H}_2\text{O}]$ & hydromagnesite $[\text{Mg}_5(\text{CO}_3)_4(\text{OH})_2 \cdot 4\text{H}_2\text{O}]$ extends up to the first 500 hours of exposure.
2. Further exposure yields magnesium hydroxides from acid oxidation which forms extensive thin crystalline brucite needle domains $[\text{Mg}(\text{OH})_2]$, (Note during this time period the aluminum alloy remains cathodically protected, scribed lines remain clear.)
3. Ultimately, film delamination corresponds to the accumulation of hexahydrate $[(\text{MgSO}_4) \cdot 6 \text{H}_2\text{O}]$ salt at the interface. At which time the interface rapidly covers with aluminum oxide and the coating binder quickly decomposes.

Overall, failure occurs when magnesium has been depleted from the binder matrix and sufficient hexahydrate salts have accumulated at the alloy interface to cause decomposition of the binder. However, during the first two stages of the process the alloy surface remains cathodically protected.

Magnesium Filled Primers

The purpose of the magnesium powder filled primer is to provide cathodic protection to the 2024 T-3 alloy. The magnesium powder used in the study was [ECKA Magnesium powder] < 20 μm with particle size ranges from 1 micron to 300 μm ,

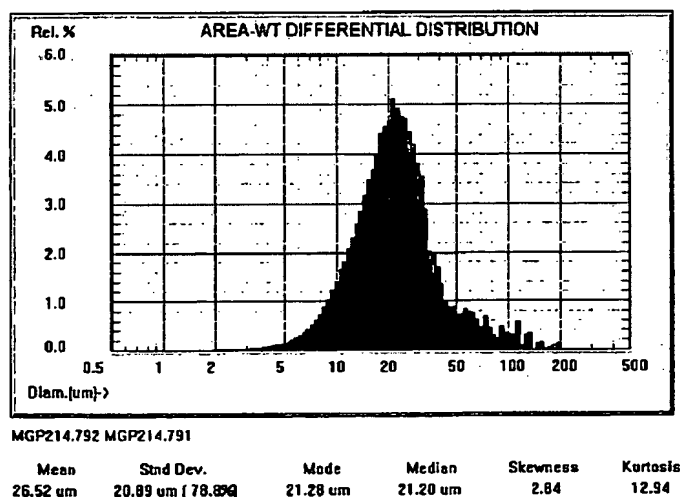


Figure 1 . Area weighted distribution of 20 μm ECKA Mg powder via optical particle counting

Certificate of Origin data sheet identifies the product as magnesium powder, produced from p-magnesium 99.95 % to DIN 17800, the assay data sheet states: Mg (metallic magnesium) content @ 96% and MgO (magnesium oxide) content @ 4%.

Primer open circuit potential measurement

Lopez-Buisan Natta (2001), states the singularity centered at ≈ -1.59 V vs saturated calomel electrode (SCE) in the anodic branch of the Mg polarization curve is a step that systematically appears in different electrolytes and does not correspond to passivation, transpassivation, intergranular corrosion, or impurities. The interpretation is that the anodic oxidation of Mg takes place through two independent mechanisms, starting at different potentials: the monovalent process $\text{Mg} \rightarrow \text{Mg}^+$ at a low potential ≈ -1.59 V_{SCE} and the divalent process $\text{Mg} \rightarrow \text{Mg}^{2+}$ at a higher potential which is closer to the reported -2.78 V_{SCE} . Mg^{2+} is produced nonelectrochemically, as a result of the reaction of Mg^+ with an oxidant or through disproportionation. *"In normal cathodic protection conditions, a Mg anode works in the potential range in which the monovalent process prevails. This process is directly related to its low electrochemical efficiency as a galvanic anode."* ⁽⁴⁾

Figure 2. open circuit potential (OCP) diagram for magnesium powder filled primers, at 50,56, and 60 PVC, in polyamide/epoxy binder exposed to 3% NaCl solution. Initial OCP values for the three sets of panels correspond to a corrosion potential, for Mg metal, $E_{\text{corr}} \approx -1.50$ V to -1.60 V_{SCE} where a monovalent process is assumed to occur. ⁽⁴⁾ Over the preceding 24-hour period the two metals, Mg and the Al alloy, polarize to a mixed potential, E_{mix} , which also corresponds to the corrosion potential, E_{corr} , at which two dissimilar metals being galvanically coupled in solution corrode. ⁽⁵⁾ The observed mixed potential for Mg and Al alloy in this experiment was found to be about $E_{\text{mix}} \approx -0.90$ V to -1.00 V_{SCE} . Figure 2. OCP extending beyond the initial 24 hours period was observed to vary according to primer PVC. Starting with PVC of 60, samples containing the most exposed Mg surface, corresponded to a low anodic (negative) mixed potential, E_{mix} , OCP for the first 5 days of exposure.

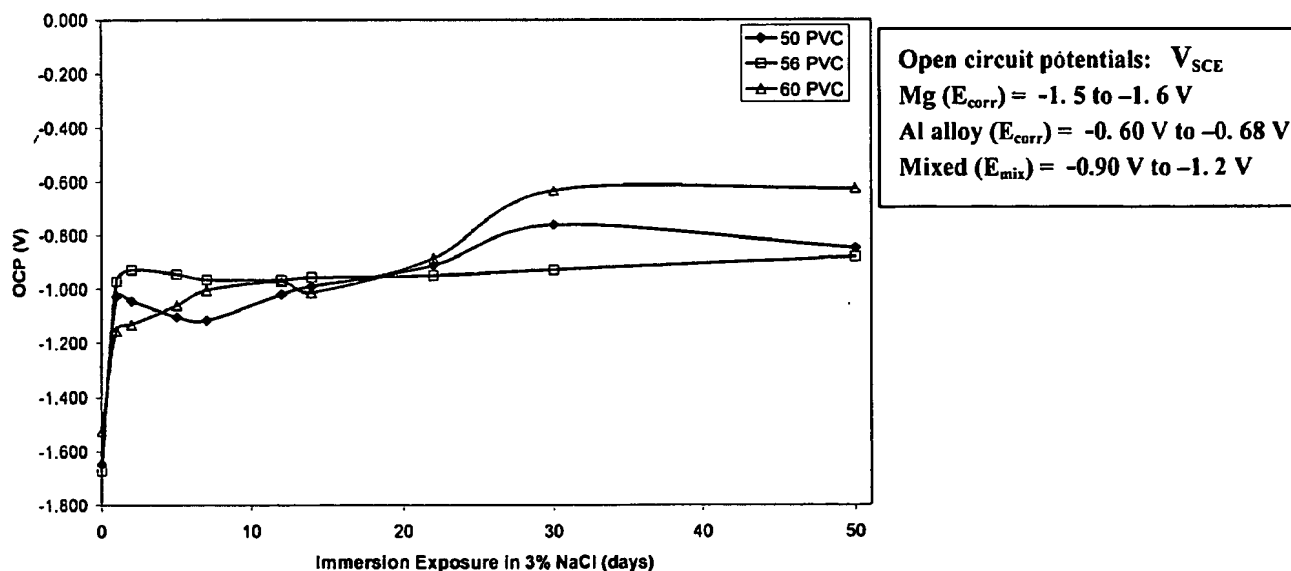
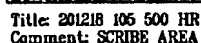


Figure 2. Open circuit potentials vs. SCE of magnesium epoxy-polyamide primers in 3% NaCl immersion conditions ⁽⁶⁾

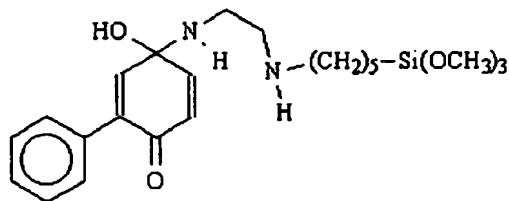
After 8 days of exposure the corrosion potential, E_{corr} , of the 60 PVC samples gradually rises to the open circuit potential of the aluminum alloy ≈ -0.65 V_{SCE} . Thus, signifying corrosion of the Al alloy to be the only electrochemical process occurring. The 56 PVC samples, believed to correspond to the critical pigment volume concentration (CPVC) of the coating yielded the most consistent electrochemical behavior. After 24 hours exposure the 56 PVC samples OCP attained E_{mix} the mixed potential and remained constant thereafter for the duration of the experiment. Thus, suggesting cathodic protection of the Al alloy due to Mg metal occurs most effectively at CPVC.

Figure 3. SEM 50PVC primer with brucite $Mg(OH)_2$ domains emanating from within coating after 500-hours exposure



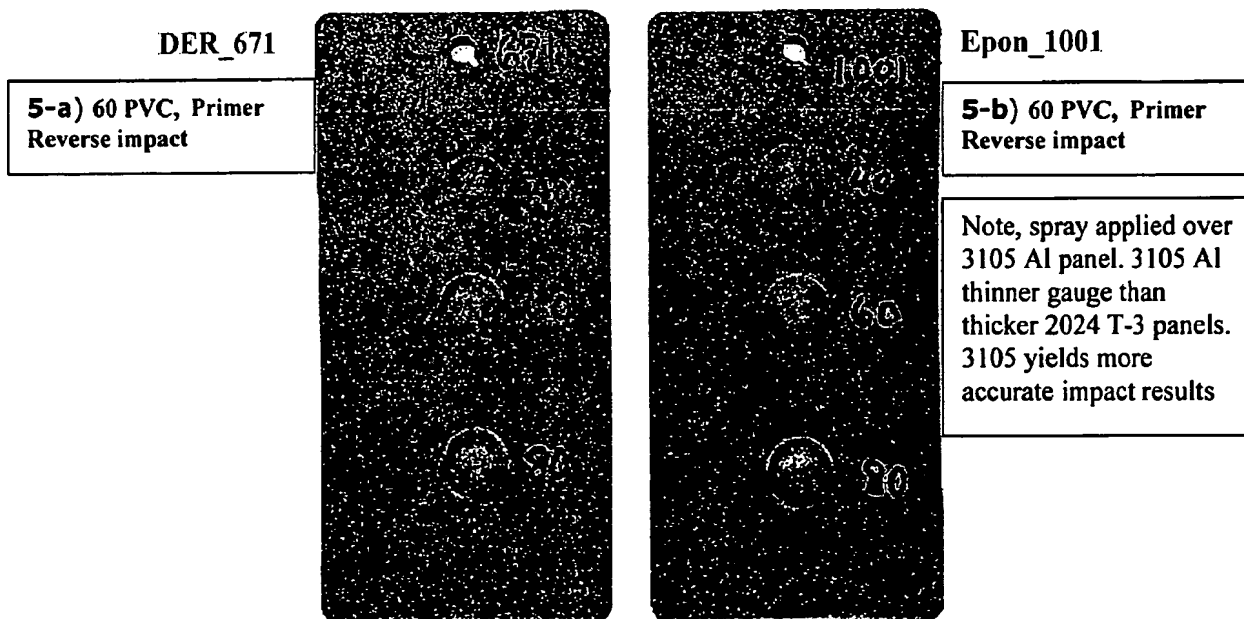
Physically blocking the surface, of the alloy, interrupts cathodic protection when contact between anode and cathode is lost such as when primers are formulated below CPVC, circa 40 PVC limited local cathodic protection occurs if the coating itself remains integral and intact. However, if the coating is damaged and the surface exposed cathodic protection only occurs briefly at the site of fracture. If the metal is well encapsulated galvanic protection terminates resulting in oxide ingression and lifting about the damaged area. In summation, it was observed the salts generated during first 1000 hours of exposure did not degrade neither binder nor alloy surface.

Currently, a hybrid primer binder system uses a reactive intermediate based on phenyl-quinone and N-(aminoethyl)-gamma-aminopropyltrimethoxysilane, figure 4, and magnesium powder to catalyze a reaction between epoxy resin and an aliphatic polyisocyanate that may include ambient moisture. Reaction kinetics of the polyisocyanate are dependent on both polarity of carrier solvent and magnesium powder particle size, where a smaller 20µm average particle size 099/99 was found to be far more reactive than the 200µm Eckart 099/00 powder.



- 91 -

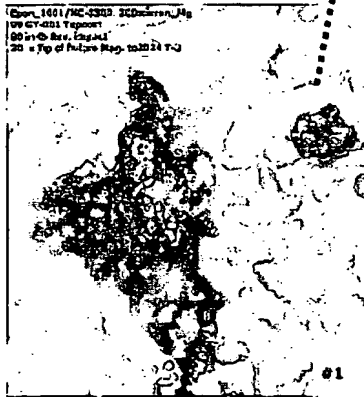
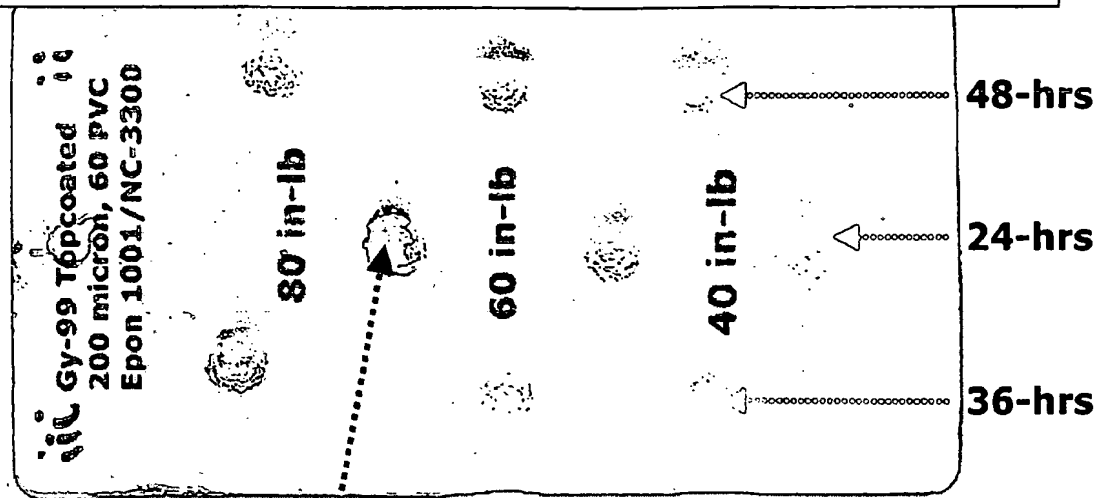
Figures 5a & 5b, primed panels containing Eckart 099/00, 200 micron sized magnesium powder at 60 PVC with current hybrid polyisocyanate/epoxy binder system. Similar impact results were obtained using two commercial epoxy resins DER 671PM, panel '5-a' and Epon 1001CX, panel '5-b'. Both Taffy process resins at 450 to 550 EEW. The coating carrier solvent was a xylol /acetone mix, spray applied, single coat approximately 200µm film thickness. Reverse impact indentations from top to bottom 40, 60, and 80 lb-inch respectively. Overall, the panels with Epon 1001CX had slightly better adhesion possibly a result of better wetting of the magnesium oxide powder surface. Solvent effect may have played a role as Epon resin was cut in non-polar xylene, while the DER-671PM cut in a more polar DOWANOL PM, (propyleneglycol monomethylether). Coating failure at 80 lb-inch from the surface indicates mechanical limits of the polymer binder at that PVC have been greatly exceeded. The 60 lb-in results appear to be the more attainable practical limit for a top-coated panel with a 200µm magnesium powder.



Topcoated Panels

Deft 99 GY-001 Base & Catalyst "Extended Lifetime™" fluoropolymer Topcoat was applied to primed 2024 T-3 and 3105 alloy panels. The primer was formulated with Eckart 200 micron 099/00 magnesium powder. The phenyl-quinone and N-(aminoethyl)-gamma-aminopropyltrimethoxysilane intermediate was cut in 2-methoxyethyl acetate then reacted with Desmodure N-3300, cut in xylene then Epon 1001CX added. The magnesium powder was added only after the binder mixture was diluted sufficiently with xylene yielding a workable potlife for spray application. Primers formulated with 200µm (average) particle size magnesium powder above CPVC tend to fare poorly in reverse impact. Poor reverse impact resistance in cathodic coatings has been a good indication of early coating delamination during Prohesion cycling studies. Larger average particle size magnesium powders tend to be coarse and fare poorer in reverse impact than smaller 20 to 200 µm size powders. Coarse particles, over 380 µm in turn leave the high PVC topcoat prone to failure. Smaller particle sized magnesium powders yield a higher exposed surface area and higher reactivity. The ideal primer will be comprised of a balance of the two at some ideal thickness.

6-a. Top-coated primed panel, 5-b type, reverse impact over 48 hour top coat dry period



6-b @ 20x magnification, profile #1



6-c @ 20x magnification, profile #2

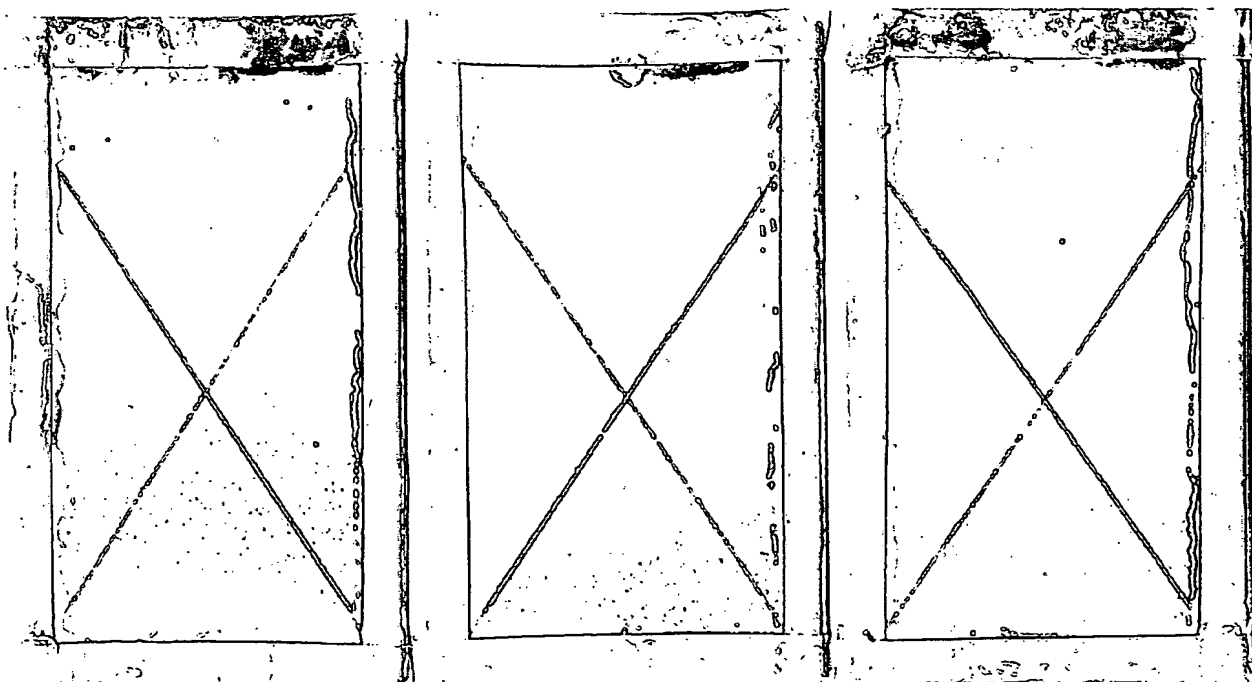
Figures 6b & 6-c impact results for 60 PVC primer top-coated with Deft GY-99, spray applied over 3105 Al panel prepared by wire-brushing

Figure 6a, Deft GY-99, 70 micron thick film topcoat over 200µm thick film primer with 200µm average particle size magnesium powder. Reverse impact results for 24, 36, and 48-hour topcoat cure time. Note 6-b and 6-c, red material is phenylquinone modified epoxy-urethane binder. Black oxide covers large magnesium particles results in poor wetting, binder adsorbs preferentially to panel. However, the silane modified binder appears to hold tenaciously to the panel surface. The black oxide covering the magnesium powder is thought to contain hygroscopically adsorbed water which may reduce adsorption and adhesion of the binder. Improving this surface by lightly milling then applying a suitable organic dryer may act to reduce polyisocyanate reactivity and improve the binder's adhesion.

Top-coat Prohesion™ results

Top-coated primed panels at 1800 hours Prohesion™ exposure, top row of panels figures 7-a, 2024 T-3 alloy topcoated in triplicate top-row. Bottom row 7-b, 3105 corrosion resistant alloy top-coated in triplicate. After 1800 hours Prohesion™ exposure there is no apparent difference between the corrosion resistant grade 3105 alloy and the 2024 T-3 alloy.

Figure 7-a. 2024 T-3 panels, primer from figure 5-a, Deft 99 GY-001 top-coat @ 1800 hrs Prohesion™



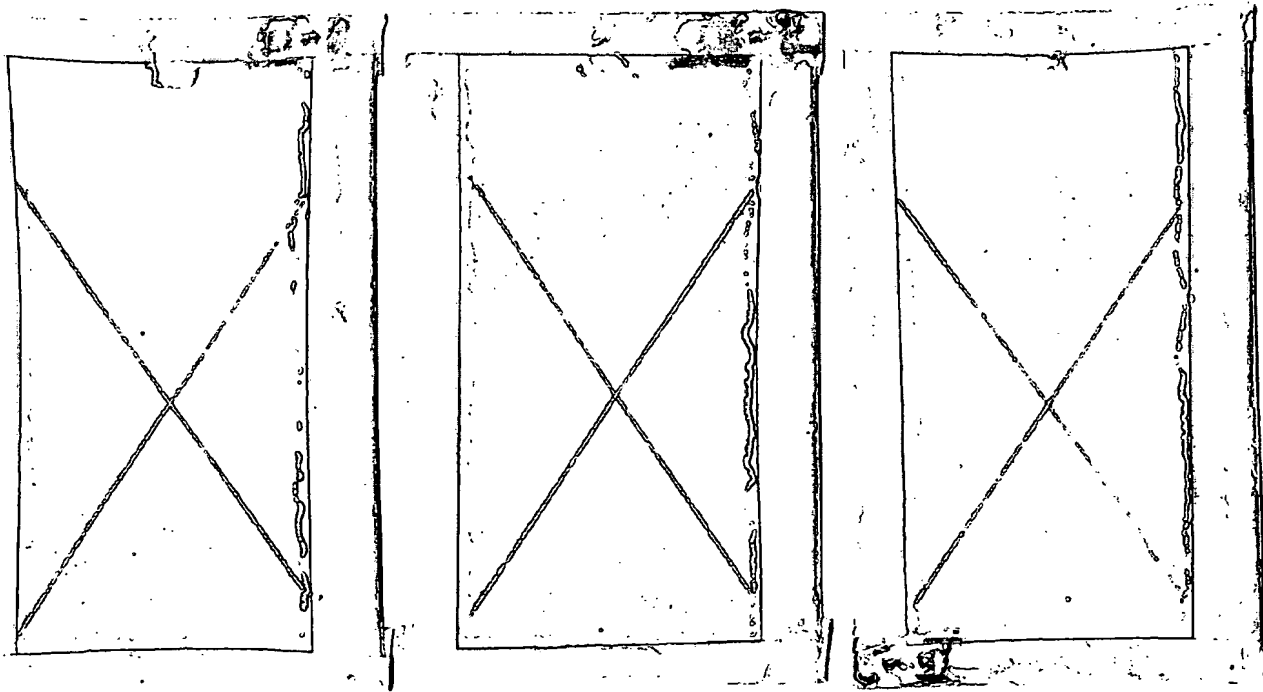


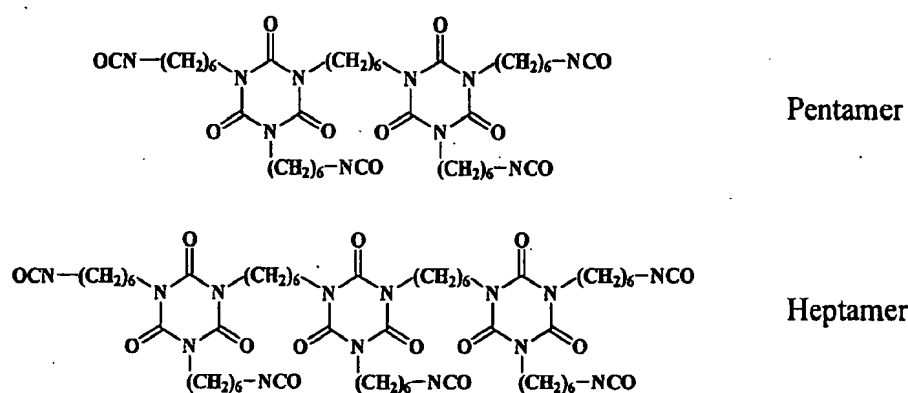
Figure 7-b. 3105 panels, primer from figure 5-a, Deft 99 GY-001 top-coat @ 1800 hrs Prohesion™

Polyisocyanate binder for primers

The high PVC extended lifetime topcoat appears to provide excellent surface protection. By maintaining its high impermeability to moisture the lifetime of the alloy structure is extended because the cathodic primer can effectively serve a longer period of time. The Primer essentially provides the coating's integral guts it connects both surface and substrate and arrests drastically different effects

occurring in two separate but interconnected environments. Primers formulated for cathodic protection require a polymer binder that wets metal, retains flexibility, maintains solvent and acid resistance, and in addition are not easily hydrolyzed by caustic salts. Aromatic moisture cure polyisocyanates are commercially available materials for application to moderately high pH concrete surfaces thus making them suitable as a binder system for magnesium powder filled primers for cathodic protection.⁽⁸⁾ The polyisocyanate binder utilized in these systems forms both urethane and urea linkages at a stoichiometric ratio of 5 to 1. In order of stability to caustic high pH conditions these urethane/urea coatings rank above polyamides and are similar to polyamines.⁽⁸⁾

Figure 7. Polyisocyanurate Oligomers, structural features of pentamer and heptamer⁽⁹⁾



Unfortunately, polyisocyanate reactivity is greatly enhanced in the presence of magnesium metal. Desmodure N-3300 an aliphatic polyisocyanate based on HDI with 20 % labile isocyanate, is categorized as a “slower” polyisocyanate⁽⁹⁾. Initial attempts to incorporate N-3300 polyisocyanates into magnesium powder filled primers yielded gellation. Polyisocyanate reactivity, in the presence of magnesium is thought to be best controlled by using aromatic polyisocyanate pentamers and heptamers with a lower labile isocyanate content along with judicious solvent selection, and metal pigment pretreatment. The binder used for the primer the topcoat study was an epoxy modified polyisocyanate cured with an amino-silane substituted phenylquinone. The main advantage of the aromatic polyisocyanate binder based on pentamers with mol.wt about 2300, is that it is less reactive than the Desmodure N-3300. Therefore, its application properties will be more robust, i.e., potlife, ease of application, kind and amount of solvent(s) used in application, and perhaps the application technique itself.

Summary

The complete coating system for cathodic protection of 2024 T-3 aluminum with a magnesium powder primer begins at the alloy interface with an organo-silane adhesion promoter that is integral to the binder itself. A moisture cure aromatic isocyanate binder comprises the backbone of the primer

polymer adding high chemical and alkaline resistance improved adhesion, flexibility, and wetting of both pigment and alloy surface. Ideal magnesium particle size distribution should range from 10 to 200 microns. As submicron sized magnesium is rapidly consumed and acts to over accelerate cure of primer binder.

Overall, it is believed that with the correct pigment volume relationships, particle size, and polymeric binder, and formulation procedures top-coated magnesium powder primer coating systems are capable of protecting the 2024 T-3 aluminum both cathodically and passively for over 3000 hours Prohesion™ exposure before the onset of damage to the polymer occurs at the scribe.

References

- 1) D. Elizer and A. Antonyraj, Unusual Behavior of Magnesium an ZM Anodes in Aqueous Electrolytes at High Concentrations, Corrosion, April 2001, Pp. 334-345
- 2) M. Nanna, G.P. Bierwagen, Unpublished work shown at student poster session, North Dakota State University, October 1999
- 3) J. Genesca, L. Betancourt, and C. Rodriguez, Electrochemical Behavior of a Magnesium Galvanic Anode Under ASTM Test Method G-97-89 Conditions, Corrosion, July 1996, Pp. 502 – 507
- 4) M.G. Lopez-Buisan Natta, Evidence of Two Anodic Processes in the Polarization Curves of Magnesium in Aqueous Media, Corrosion, August 2001, Pp. 712 - 720
- 5) D.A. Jones, Principles and Prevention of CORROSION, 2nd Ed., (1996), Pp. 444-447
- 6) L. Ellingson, Corrosion Studies for the Protection of Aluminum Alloys and Outdoor Bronze, Masters Thesis, North Dakota State University, June 2001
- 7) M.E. Nanna, G.P. Bierwagen, Unpublished work FSCT Poster session , Chicago, October, 2000, & IAB poster session, North Dakota State University, October 2000
- 8) R.R. Roesler, Bayer Corporation., Personal Communication, NDSU, June 8, 20001
- 9) R.R. Roesler, Polyurethanes for Coatings, Bayer Corporation, June 1999, Pp. 32-36

PART X

Certain aspects and embodiments of the present invention are described in the following text and figures.

Binders Used in Mg-Rich Coatings as Cr-free Primers for Al 2024 T-3

Abstract

Mg-rich coatings with exceptional resistance to corrosion were formulated for cathodic protection of aluminum 2024 T-3 alloy. Top-coating the Mg-rich primers with an Extended Lifetime™ extended protection up to about 3,000 hours. Mg-rich coatings formulated with an epoxy-polyisocyanate-silane 'hybrid' binder and top coated with an Extended Lifetime™ coating protected scribed areas for up to 4,500 hours. In addition, coatings formulated with the hybrid binder were found to be fire retardant at elevated magnesium PVC's (pigment volume concentrations).

Introduction

Polymers binders suitable for Mg-rich coatings applied *in situ* to Al 2024 T-3 structures require high pH stability, excellent adhesion, and ease of handling. Cathodic protection of primed Al 2024 T-3 occurs when closely packed Mg metal particles can be kept in contact with the Al surface. It is not the surface of the coating that is important but the bulk of the primer. Primers formulated near CPVC cause particles to pack densely enough to touch and electrically connect thereby causing the coating to serve as a sacrificial anode. By putting on a topcoat, as the system is actually used in the field, acid dissolution of the Mg metal in the primer is minimized, thereby confining oxidation-reduction processes to an electrically connected coating within the primer layer.

Mg-rich Coating on Al 2024 T-3



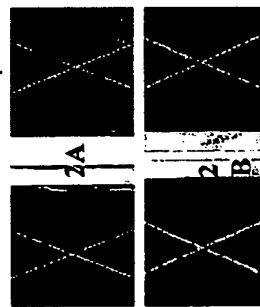
Figure 1. Cathodic protection of top-coated Mg-rich coating over Al 2024 T-3 lengthy exposure to Harrison's solution. Porous mixed oxides of aluminum, copper, and magnesium remaining electrically connected to bulk of primer. So long as the binder is not degraded cathode area remains small relative to a larger electrically connected Mg-rich anode.

Experiment

Three coating polymer systems were evaluated as vehicles for Mg-rich primers, two were commercially available products and an experimental epoxy-urethane-silane hybrid developed in this laboratory. The moisture cure aromatic polyisocyanate, Desmodure™ A-23, utilized is classified as forming both urethane and urea linkages at a stoichiometric ratio of 5 to 1. The ambient cure epoxy/polyamine was liquid BPA Epon™ 828 with an (epoxide equivalent weight) EEW ~ 188 and a Mannich base Epicure™ -3251 polyalkylamines with an AHEW (amine hydrogen equivalent weight) ~ 55.

Prohesion™ Exposure

Q-Panel™ Al 2024 T-3 panels primed with Mg-rich primer at CPVC film thickness of 4 mil and coated with Extended Lifetime™ topcoat at 3mil. Panels were subsequently subjected up to 4,500 hours of Prohesion™ exposure in dilute Harrison's solution at pH=4.0.



Figures 2. A and B: Hybrid epoxy-polyisocyanate at 4-mils on Al 2024 T-3 with Extended Lifetime™ topcoat at 3-mils. Prohesion™ exposure A) 2,500 hrs. and B) 4,500 hrs.

Flammability

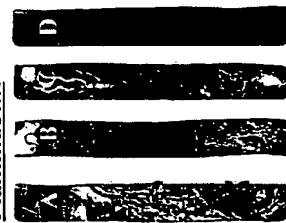


Figure 3. Modified U.L.-94 Flammability test performed on three Mg-rich and one Zn-rich coatings applied to Al 3015 substrate 17 by 67 strips at CPVC - 65 with Delt EL™. A) Mannich base epoxy. B) Zn-rich/epoxy. C) Aromatic polyisocyanate. D) Hybrid polyisocyanate. All were subjected directly to blue cone tip of Bunsen burner flame for 30 seconds.

Electro Impedance spectroscopy

Cylindrical electrode cells with 1.0 cm diameter scribes cut through the coating were filled with the following electrolytes 1) Neutral at 3.0% weight NaCl at pH =6.2; 2) Acidic at 3% weight NaCl adjusted to pH = 2.2 with HCl; 3) Basic at 3% weight NaCl adjusted to pH= 12.75 with NaOH. Measurements were made over an 11-day time period.

Basic 3% NaCl at pH = 2.75

Figures 5, and 6 provide EIS data at 0.01 Hz for |Z| and phase angle for the corrosion behavior of the three samples in figures 4 A, B, and C, in basic conditions at pH = 12.75.

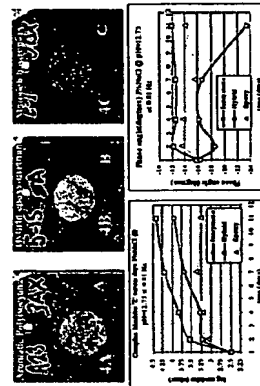


Figure 5. EIS |Z| vs. time

Acidic 3% NaCl at pH = 2.2

Figures 8, and 9 provide EIS data at 0.01 Hz for |Z| and phase angle for the corrosion behavior of the three samples in figure 7 A, B, and C, in acidified conditions at pH = 2.2

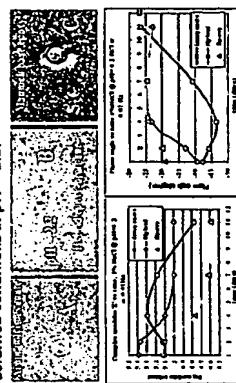


Figure 8. EIS |Z| vs. time

Neutral 3% NaCl at pH = 6.2

Figures 10, and 11 provide EIS data at 0.01 Hz for |Z| and phase angle for the corrosion behavior for similar samples as in figure 7 A, B, and C, in neutral conditions at pH = 6.2.

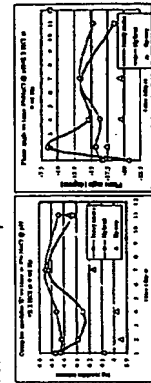


Figure 10. EIS |Z| vs. time

Summary

In summary, protection of Al 2024 T-3 can be achieved by applying a Mg-rich primer formulated at CPVC, with an appropriate organic, or organo-silane modified binder with magnesium powder to be used as the sacrificial anode. Of the presently available aircraft topcoat systems, Delt's Extended Lifetime™ topcoat performed the best in combination with these Mg-rich primers.

PART XI

Certain aspects and embodiments of the present invention are described in the following text and figures.

Binders Used in Mg-Rich Coatings as Cr-free Primers for Al 2024 T-3

Abstract

Mg-rich primer coatings applied to aluminum 2024 T-3 alloy panels were found to have exceptional resistance to corrosion in Prohesion™ exposure when formulated near CPVC. Topcoating the Mg-rich primed coatings with a topcoat yielded extended protection over scribed surface areas for up to about 3,000 hours. Mg-rich coatings were formulated from three polymeric binders: 1) epoxy-polyisocyanate, 2) polyurethane-silane, and 3) epoxy-polyisocyanate-silane 'hybrid' and top coated. Coatings formulated with the hybrid epoxy-polyisocyanate binder resisted flame incineration and in addition yielded cathodic protection of scribed areas for up to 4,500 hours Prohesion™ exposure.

Introduction

Polymeric binders suitable for Mg-rich coatings applied *in situ* to Al 2024 T-3 structures require high pH stability, excellent adhesion, and ease of handling. Cathodic protection of primed Al 2024 T-3 occurs when closely packed Mg metal particles can be kept in contact with the Al surface. It is not the surface of the coating that is important but the bulk of the primer. Primers formulated near CPVC cause particles to pack densely enough to touch and electrically connect thereby causing the coating to serve as a sacrificial anode. By putting on a topcoat, as the system is actually used in the field, acid dissolution of the Mg metal in the primer is minimized, thereby confining oxidation-reduction processes to an electrically connected coating within the primer layer.

Mg-rich Coating on Al 2024 T-3

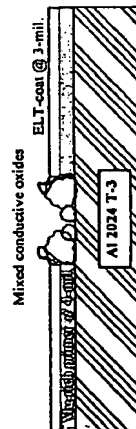


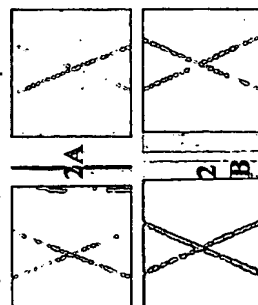
Figure 1. Cathodic protection of top-coated Mg-rich coating over Al 2024 T-3 lengthy exposure to Harrison's solution. Porous mixed oxides of aluminum, copper, and magnesium remaining electrically connected to bulk of primer. So long as the binder is not degraded cathode area remains small relative to a larger electrically connected Mg-rich anode.

Experiment

Three coating polymer systems were evaluated as vehicles for Mg-rich primers, two were commercially available products and an experimental epoxy-urethane-silane hybrid developed in this laboratory. The moisture cure aromatic polyisocyanate, Desmodure™ A-23, utilized is classified as forming both urethane and urea linkages at a stoichiometric ratio of 5 to 1. The ambient cure epoxy/polyamine was liquid BPA Epox™ 828 with an (epoxide equivalent weight) EEW = 188 and a Mannich base Epicure™ -3251 polyalkylamines with an AHEW (amine hydrogen equivalent weight) = 55.

Prohesion™ Exposure

Q-Panel™ Al 2024 T-3 panels primed with Mg-rich primer at CPVC film thickness of 4 mil and coated with Extended Lifetime™ topcoat at 3mil. Panels were subsequently subjected up to 4,500 hours of Prohesion™ exposure in dilute Harrison's solution at pH=4.0.



Figures 2. A and B: Hybrid epoxy-polyisocyanate at 4-mils on Al 2024 T-3 with Extended Lifetime™ topcoat at 3-mils. Prohesion™ exposure A) 2,500 hrs. and B) 4,500 hrs.

Flammability

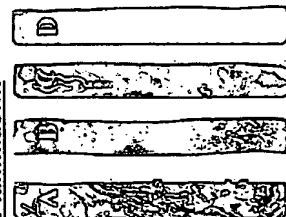


Figure 3. Modified UL-94 Flammability test performed on three Mg-rich and one Zn-rich coatings applied to Al 3015 substrate 17 by 67 strips at CPVC = 65 with Delt ELT™. A) Mannich base epoxy, B) Zn-rich/epoxy, C) Aromatic-polyisocyanate, D) Hybrid were subjected directly to blue cone tip of Bunsen burner flame for 30 seconds.

Electro Impedance Spectroscopy

Cylindrical electrode cells with 1.0 cm diameter scribes cut though the coating were filled with the following electrolytes 1) Neutral at 3.0% weight NaCl at pH =6.2; 2) Acidic at 3% weight NaCl adjusted to pH = 2.2 with HCl; 3) Basic at 3% weight NaCl adjusted to pH= 12.75 with NaOH. Measurements were made over an 11-day time period.

Basic 3% NaCl at pH = 12.75

Figures 5, and 6 provide EIS data at 0.01 Hz for |Z| and phase angle for the corrosion behavior of the three samples in figures 4 A, B, and C, in basic conditions at pH = 12.75.

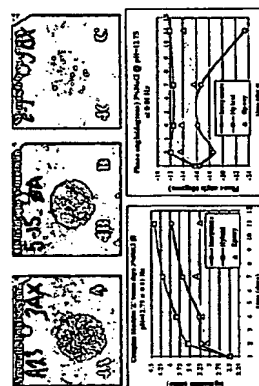


Figure 5. EIS |Z| vs. time

Acidic 3% NaCl at pH = 2.2

Figures 8, and 9 provide EIS data at 0.01 Hz for |Z| and phase angle for the corrosion behavior of the three samples in figure 7 A, B, and C, in acidified conditions at pH = 2.2.

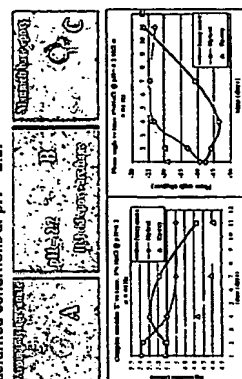


Figure 8. EIS |Z| vs. time

Neutral 3% NaCl at pH = 6.2

Figures 10, and 11 provide EIS data at 0.01 Hz for |Z| and phase angle for the corrosion behavior for similar samples as in figure 7 A, B, and C, in neutral conditions at pH = 6.2.

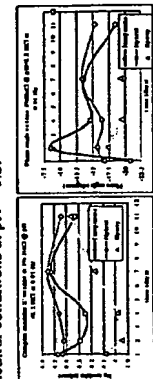


Figure 10. EIS |Z| vs. time

Summary

In summary, protection of Al 2024 T-3 can be achieved by applying a Mg-rich primer formulated at CPVC, with an appropriate organic, or organic-silane modified binder with magnesium powder sacrificial anode. Overall, the success of extending the effective life of this cathodic coating system depends on the fluorinated-polyisocyanate topcoat used in conjunction with the Mg-rich primer.

PART XII

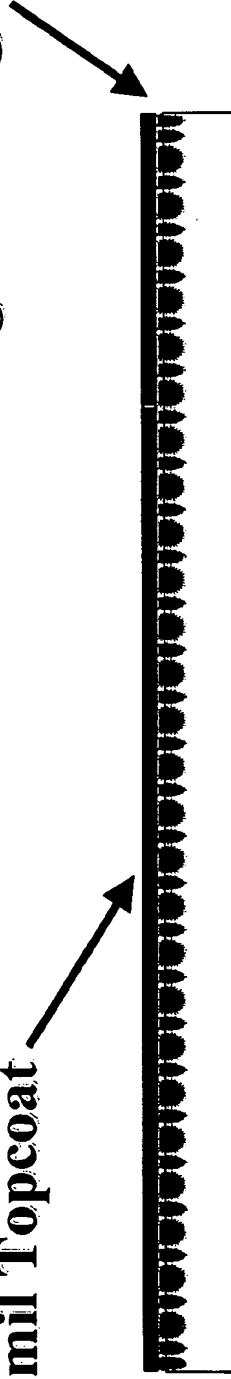
Certain aspects and embodiments of the present invention are described in the following text and figures.

Mg-Rich Coatings for Al 2024 T-3

- * Primer loaded with 20 to 200 micron Magnesium Powder**
- * Formulated near CPVC high Mg (Anode) surface area**
- * Primer Binder Moisture Cure Epoxy-Urethane-Silane**
- * Extended Lifetime™ Top-Coat**
- * 3000 Hours Prohesion™ Protection Scribed Panel**

4-6 mil Mg Primer @ CPVC

3-mil Topcoat



Al 2024 T-3

Mg-Rich Coatings for Al 2024 T-3

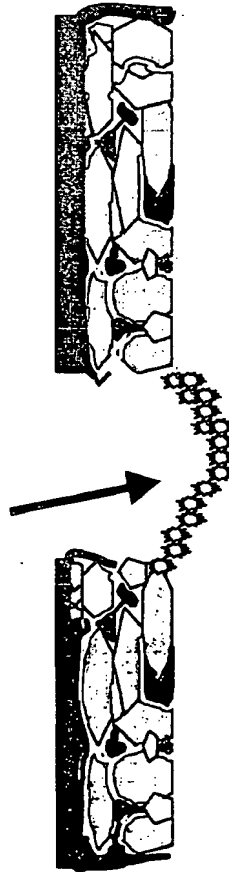
Scribed Panel Exposed to Acid Rain Environment

Electrically Connected Mg-Anode

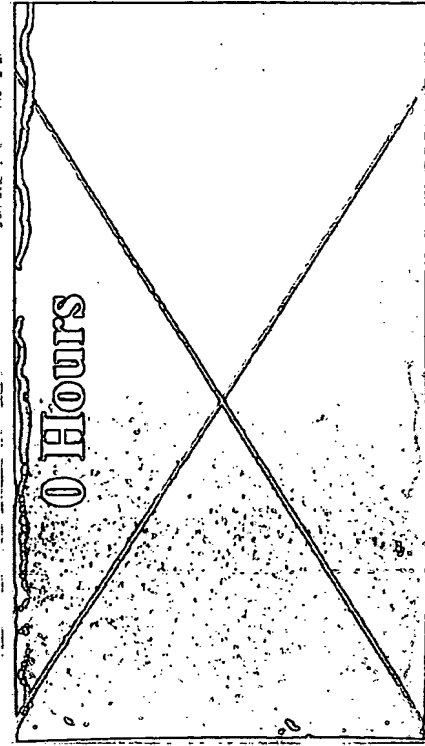


Al 2024 T-3 Cathode

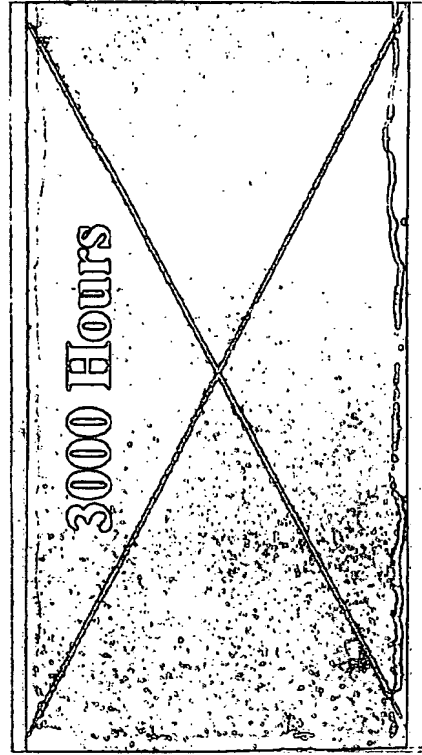
Aluminum Oxide in Scribe



Al 2024 T-3 Cathode



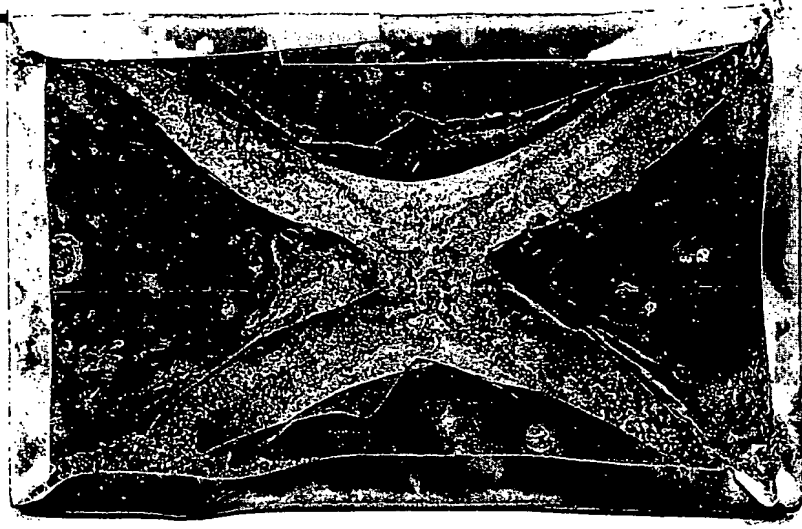
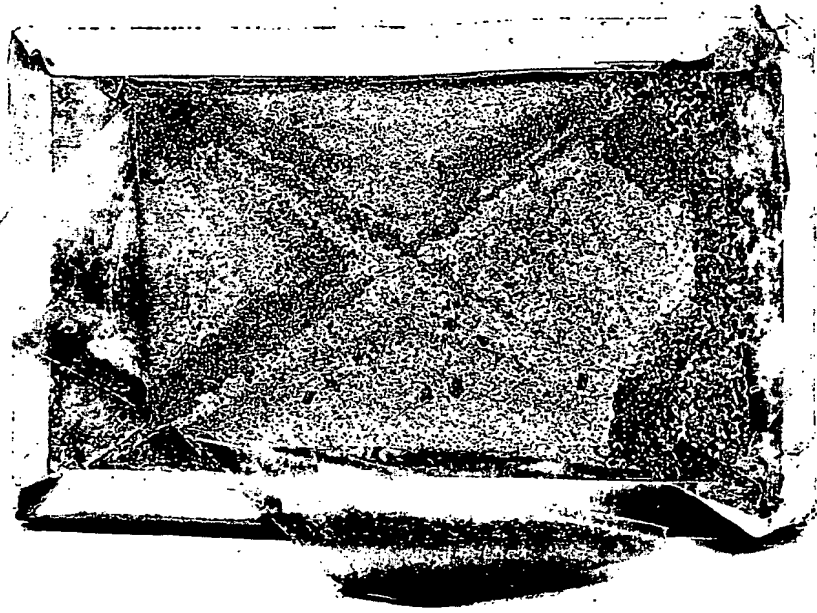
0 Hours



3000 Hours

Mg-Rich Coatings for Al 2024 T-3

Polyamide/BPA Epoxy No Cathodic Protection PAQ/BPA Epoxy



1500 Hours Prohesion Exposure Unpigmented Coatings

Mg-Rich Coatings for Al 2024 T-3

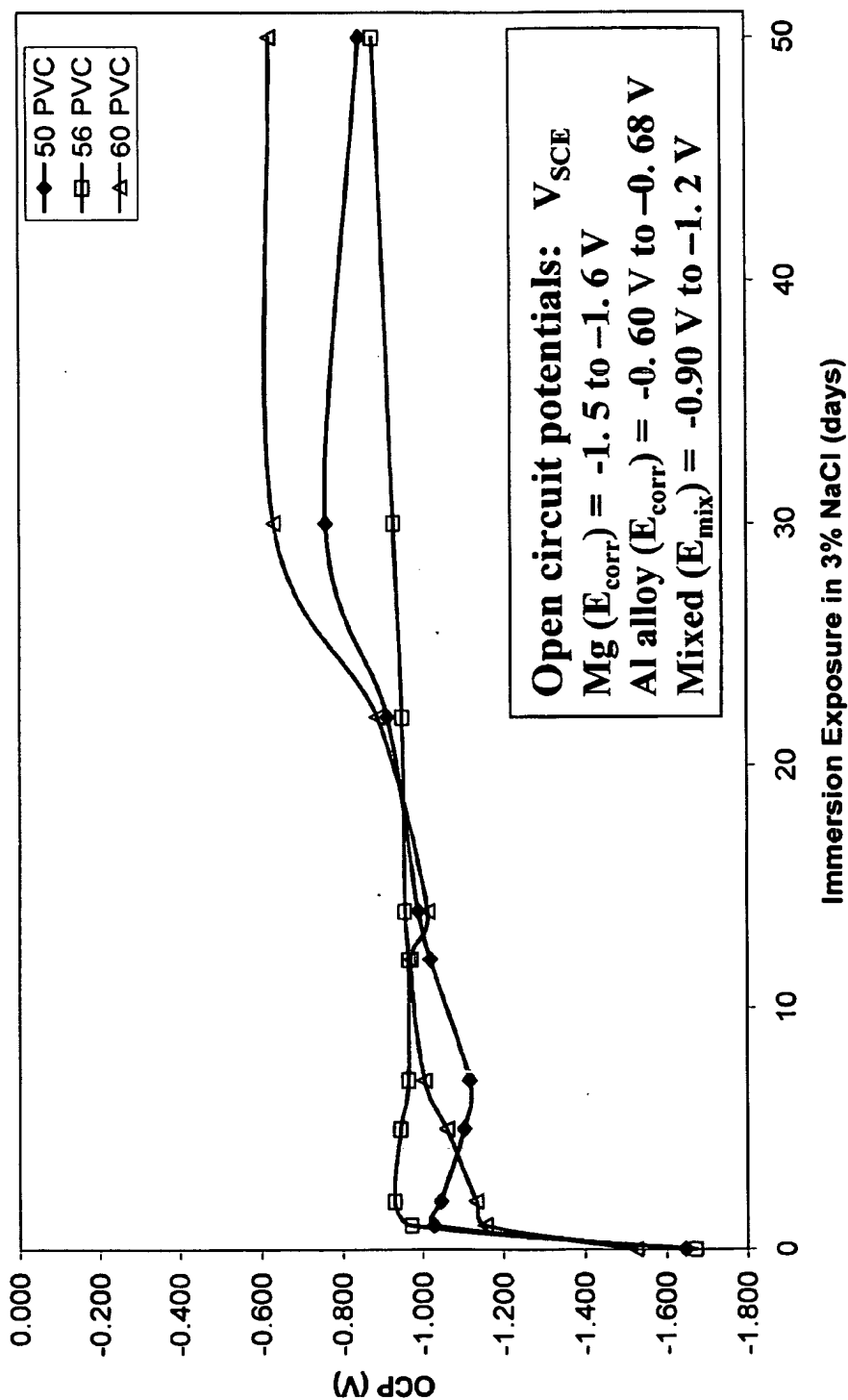
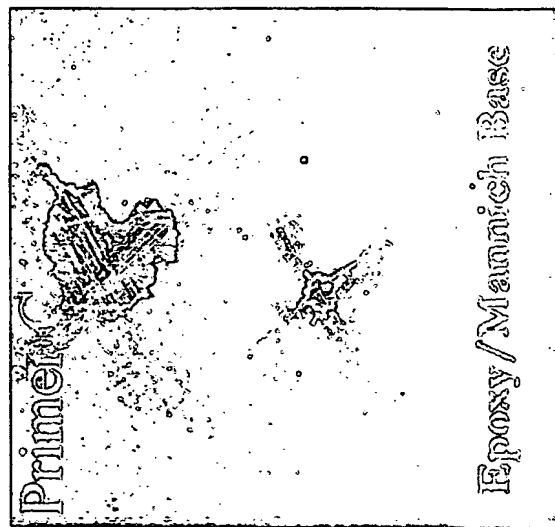
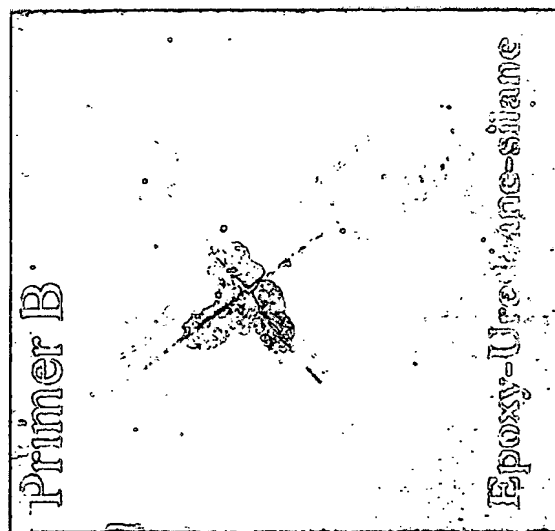
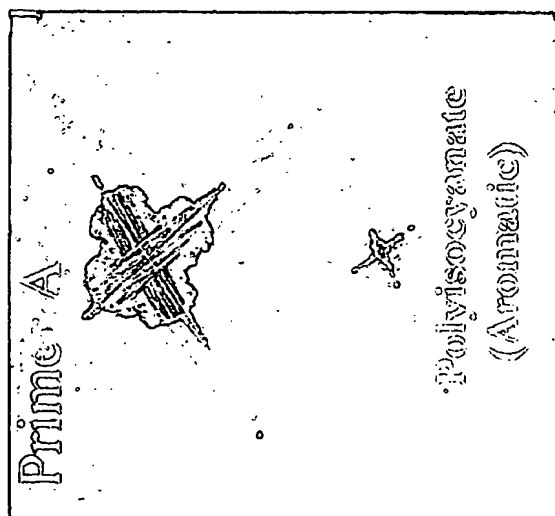


Figure 2. Open circuit potentials vs. SCE of magnesium epoxy-polyamide primers in 3% NaCl immersion conditions ⁽⁶⁾

Mg-Rich Coatings for Al 2024 T-3

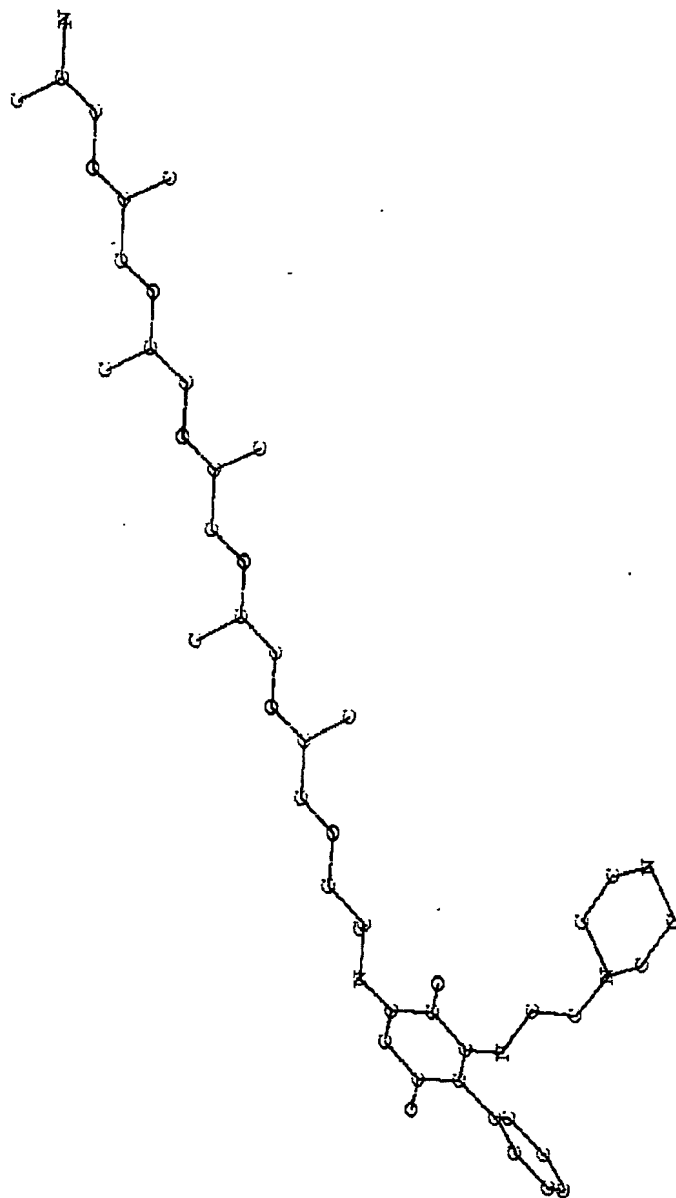


Extended Lifetime™ Top-coated Mg-Rich primers @ CPVC
Coating Solvent Resistance: 1 Hour acetone soak then scraped
Primer Integrity Key to Coating Longevity in Mg-Rich System

PART XIII

Certain aspects and embodiments of the present invention are described in the following text and figures.

Ambient Cure Epoxy Primers with Magnesium Powder for Cathodic Protection



Seminar Introduction & Outline

Main Topic

Development of Magnesium powder filled, ambient cure epoxy primers for application to Aluminum alloys using phenyl-Quinone diamine substituted curatives with Bisphenol-A & F epoxy resins.

- I. Synthesis of Amino-Quinone & Schiff Base Curatives
- II. Corrosion Concepts relevant to Data Analysis
- III. Mixture Experiment Concepts relevant to Data Analysis
- IV. Future Work (evaluation of stress in thin films)

Scientific Hypothesis and Limitations of Study

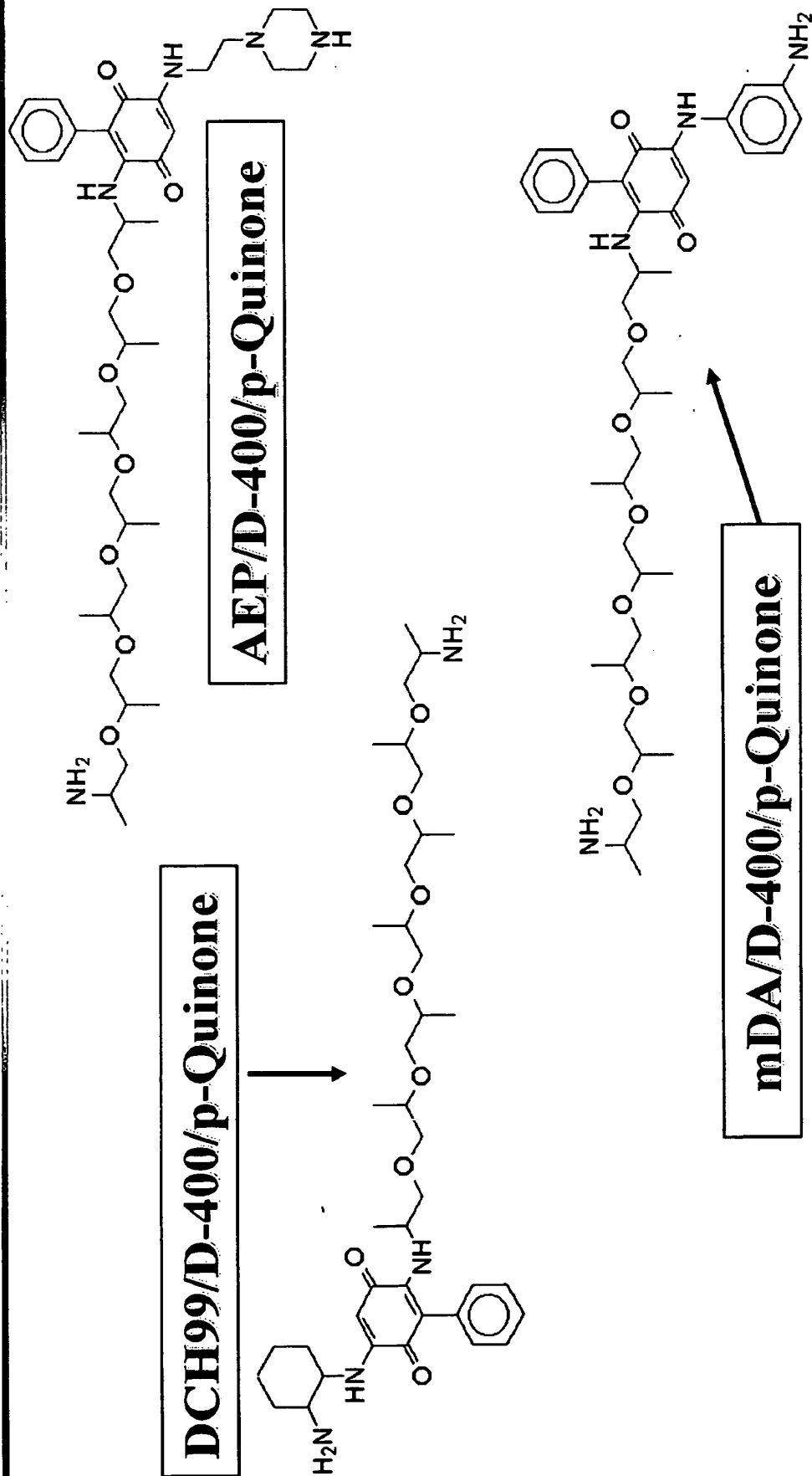
Three model compounds were synthesized formulated into magnesium powder primers and spray applied to 3105 aluminum panels which were subsequently subjected to prohesion exposure.

Null Hypothesis: No difference exists between coatings formulated with amine substituted phenyl quinones subjected to prohesion exposure.

Alternative Hypothesis: There is a significant difference between coatings formulated with amine substituted phenyl quinones subjected to prohesion exposure.

One control was incorporated into the study, and only one single epoxy resin with 5% flexol LOE was used.

Three Model Compound Amine Subst. Phenyl Quinones



Experimental Discussion

- A.** phenyl-Quinones synthesized in dichloromethane, rinsed in water, and fractionally precipitated in acetone & hexanes.
- B.** Moisture Cure Schiff Base Azeotrope with para-toluene sulfonic acid catalyst water removal.
- C.** Magnesium Powder Primer formulated at two PVC's 58 & 65 , PVC's approximated by physical mass calculation.
- D.** Aluminum Panels Sprayed with Epoxy Primer cut in acetone, allowed to cure for 14-days before Prohesion exposure.
- E.** Corrosion parameters for panels exposed to 1300-hrs prohesion evaluated in conjunction with mixture design .

Discussion of Significant Aspects of Work

1. From mixture experiments, it was ascertained that a synergistic relationship occurs for curative combinations in magnesium powder filled epoxy primers. The results lead to improvements in the following coating parameters:

- I. Solvent Resistance and resistance to water penetration**
- II. Cathodic protection of exposed scribed aluminum surface**
- III. Minimum magnesium hydroxide accumulation/
formation on surface**

Inferences drawn from these results imply that suitable formulation has been developed for the second, topcoat, phase of the project.

Characterization & Methodology

Phenyl/Quinone-amine products synthesized

- * FTIR functional groups present**
- * Dilute Solution Viscometry**
- * Differential Scanning Calorimetry**
- * Stoichiometric Ratio to Amine Curative**

Schiff Base Ketimine products synthesized

- * FTIR functional groups present**
- * Differential Scanning Calorimetry**
- * Stoichiometric Ratio to Amine Curative**

Characterization & Methodology

Primer Sprayed on Aluminum Panels (12-mil +/- 3) in triplicate

*Panels 1300-hrs Prohesion in Harrison Solution pH=5.0 +/- 0.2

*Panels evaluated for increase in surface Magnesium Hydroxide with MacBeth Spectrophotomer, relative lightness (L) value measured against FAIL control with highest (L).

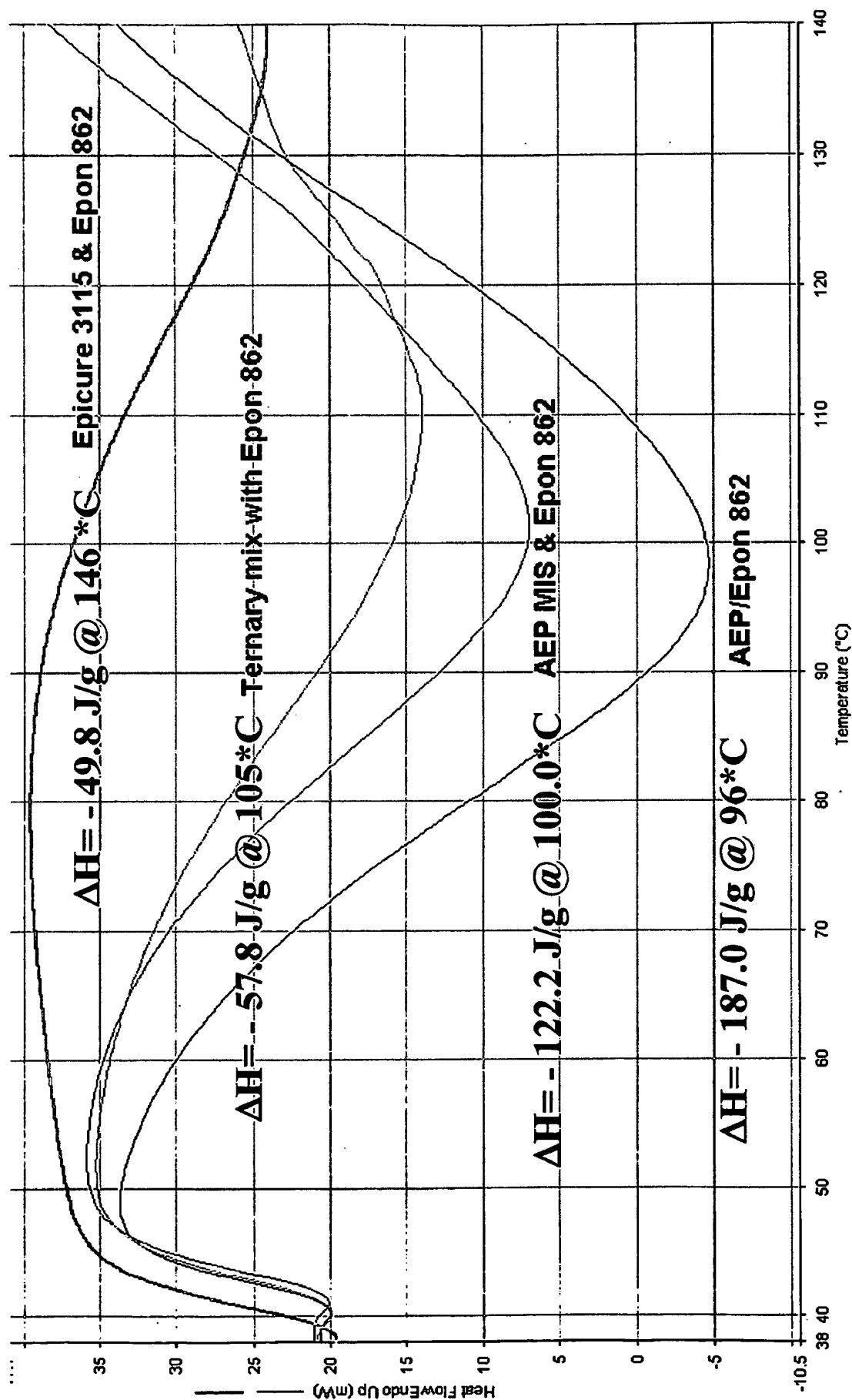
* Average coating delamination under taped area correlated to surface loss of Magnesium(anode) area.

* Solvent swell 6-hr reflux in Acetone weight loss correlated to mixture design three factor interaction

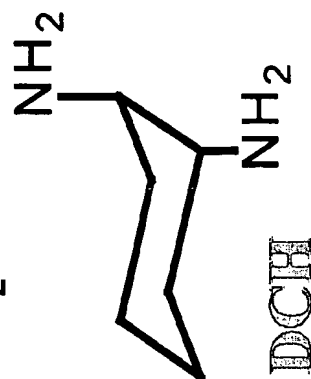
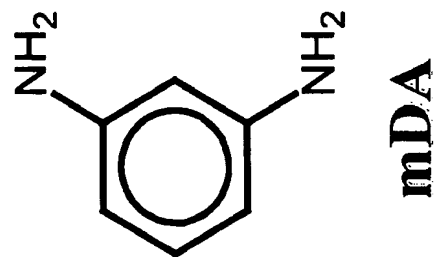
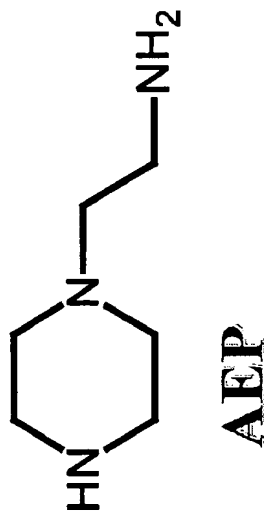
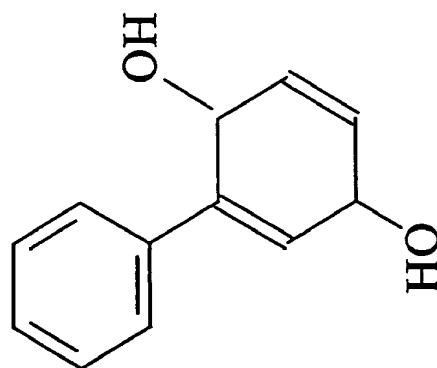
Curative Requirements

- To develop a Phenyl-Quinone Diamine/Jeffamine D-400 curative that cures Bisphenol- A & F epoxy resins at 40°C
- Obtain an ambient cure quinone-amine that reacts preferentially with epoxy resin as opposed to generating Magnesium salts.
- Incorporation of Jeffamine Polyoxypropyleneamines improves physical properties of cured film and promotes cure with epoxy resins.
- Develop a Moisture scavenging curative to moderate the hygroscopic effect of amines which absorb water that can plasticize and add compressive stresses to thin film epoxy coatings.
- Combine synergistic effects of both curatives for high PVC Magnesium primer system.

DSC: Curative Contrast with Epon 862

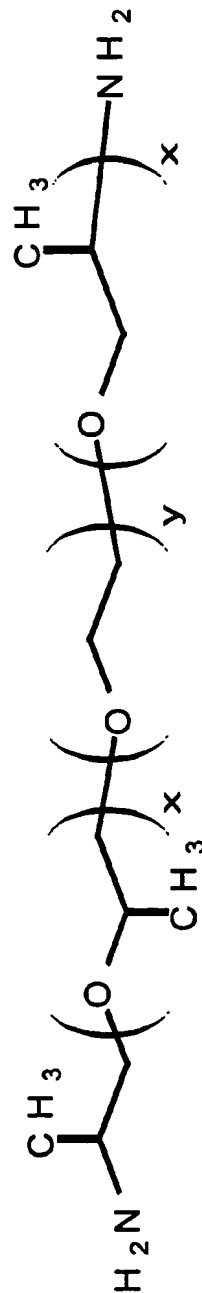


Starting Materials Subst. Phenyl Quinones



Polyoxyalkyleneamines

Polyoxyalkyleneamines (JEFFAMINE® D-230, D-400)

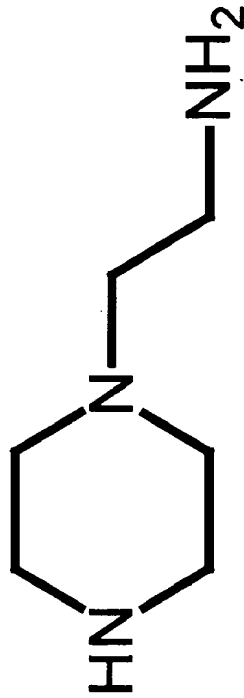


$$\gamma = 33.5 \text{ mN/m}$$

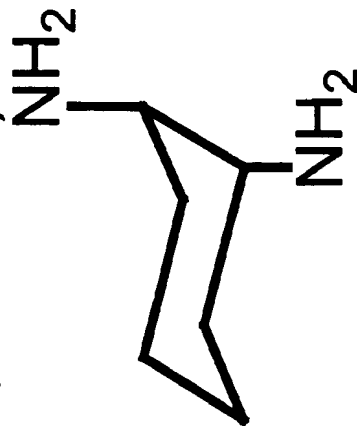
Nitrogen based Curing Agents used

Cycloaliphatic Amines

Aminoethyl Piperazine (AEP) Epi-Cure 3200



1,2-Diaminocyclohexane (DACH or 1, 2-DACH)



Cycloaliphatic Amines

High reactivity

Low viscosity

Low color

Lower yellowing

Nitrogen based Curing Agent used

Aromatic Amines

Highly heat and chemical resistant

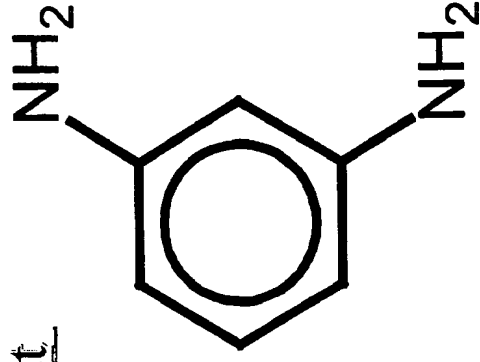
Require heat cure

Excellent balance of physical properties

Have systemic toxicity and are cancer suspect

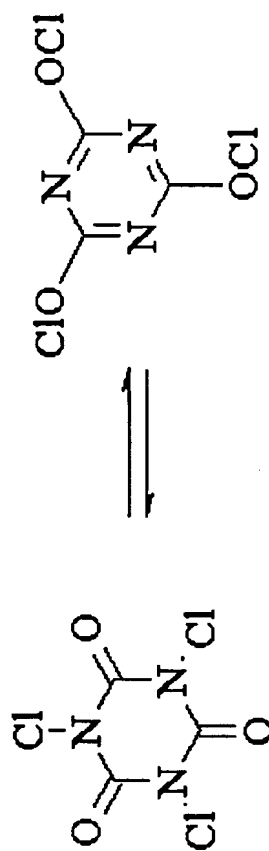
Aromatic Amine

meta-Phenylenediamine (mPDA)

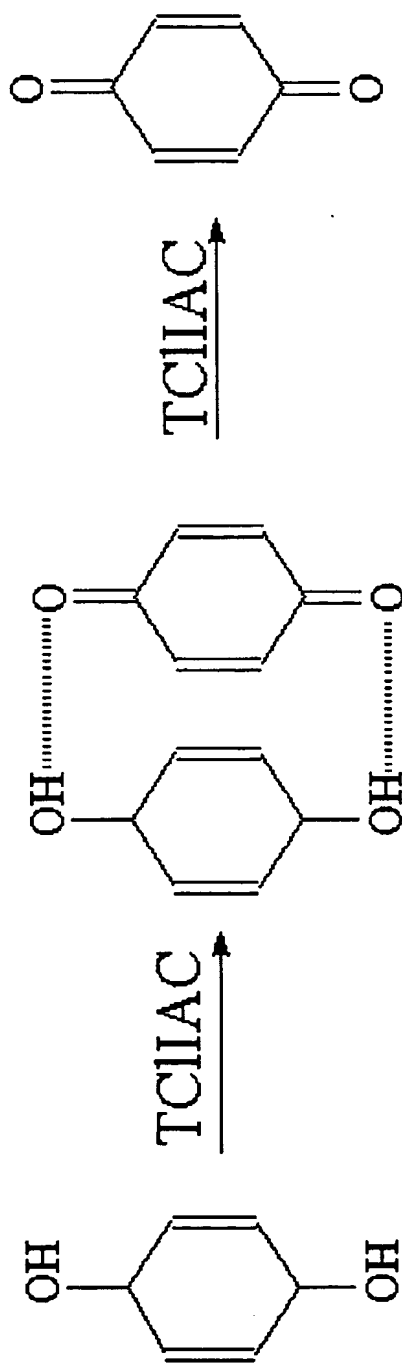


Synthetic Approach to Oxidative amination

Poly(aminoquinones) were prepared by oxidative amination of phenyl hydroquinone in trichloroisocyanuric acid. Primary and secondary alcohols can be distinguished by their rate of oxidation with (TClIAC) primary alcohols react slowly(10-30 minutes) and secondary alcohol take from a few seconds to a minute.



Oxidation Reaction Hydroquinone to Quinone



Hydroquinone

Light Olive

Quinhydrone

Red/vermilion

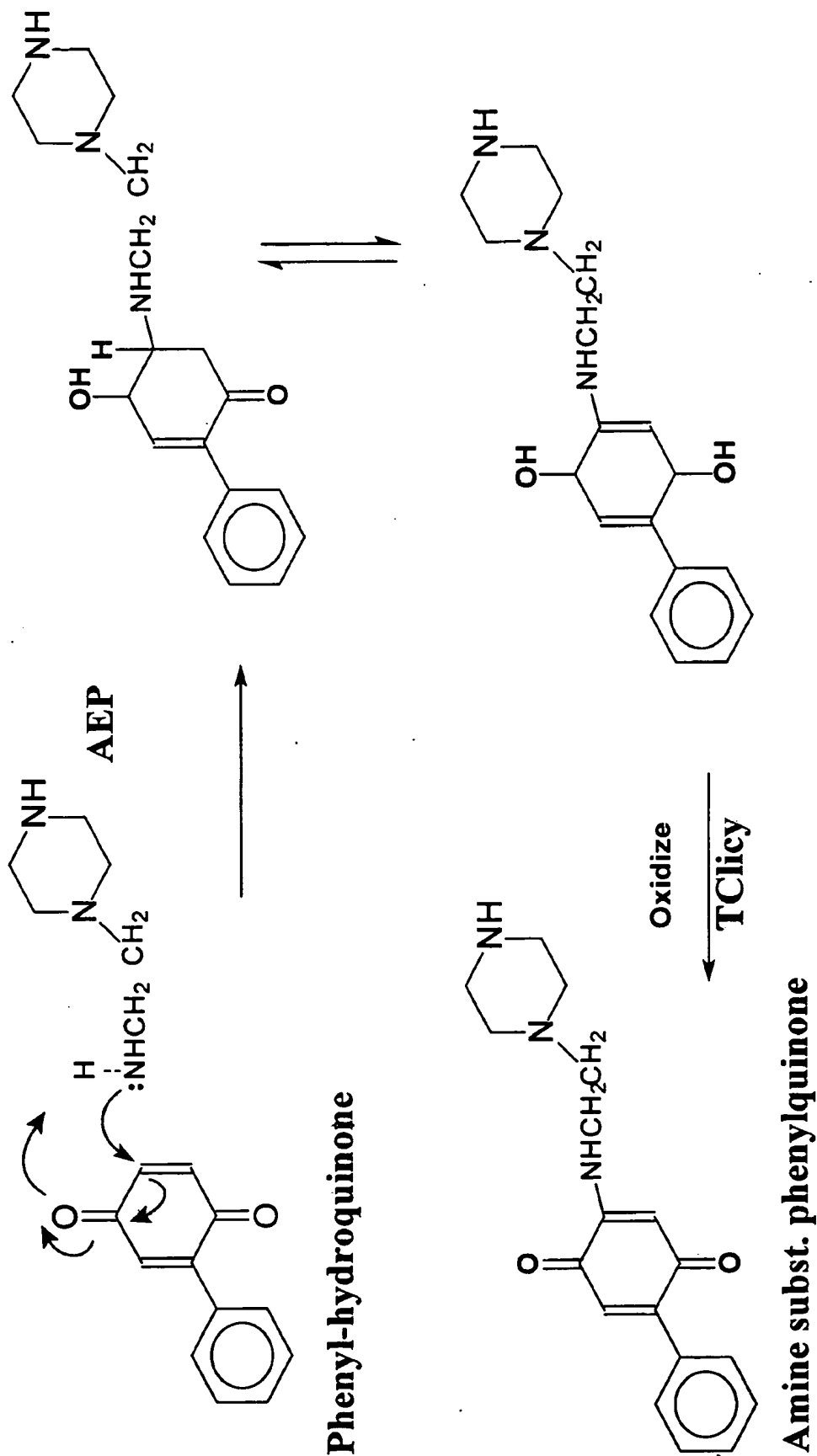
Quinone

Yellow

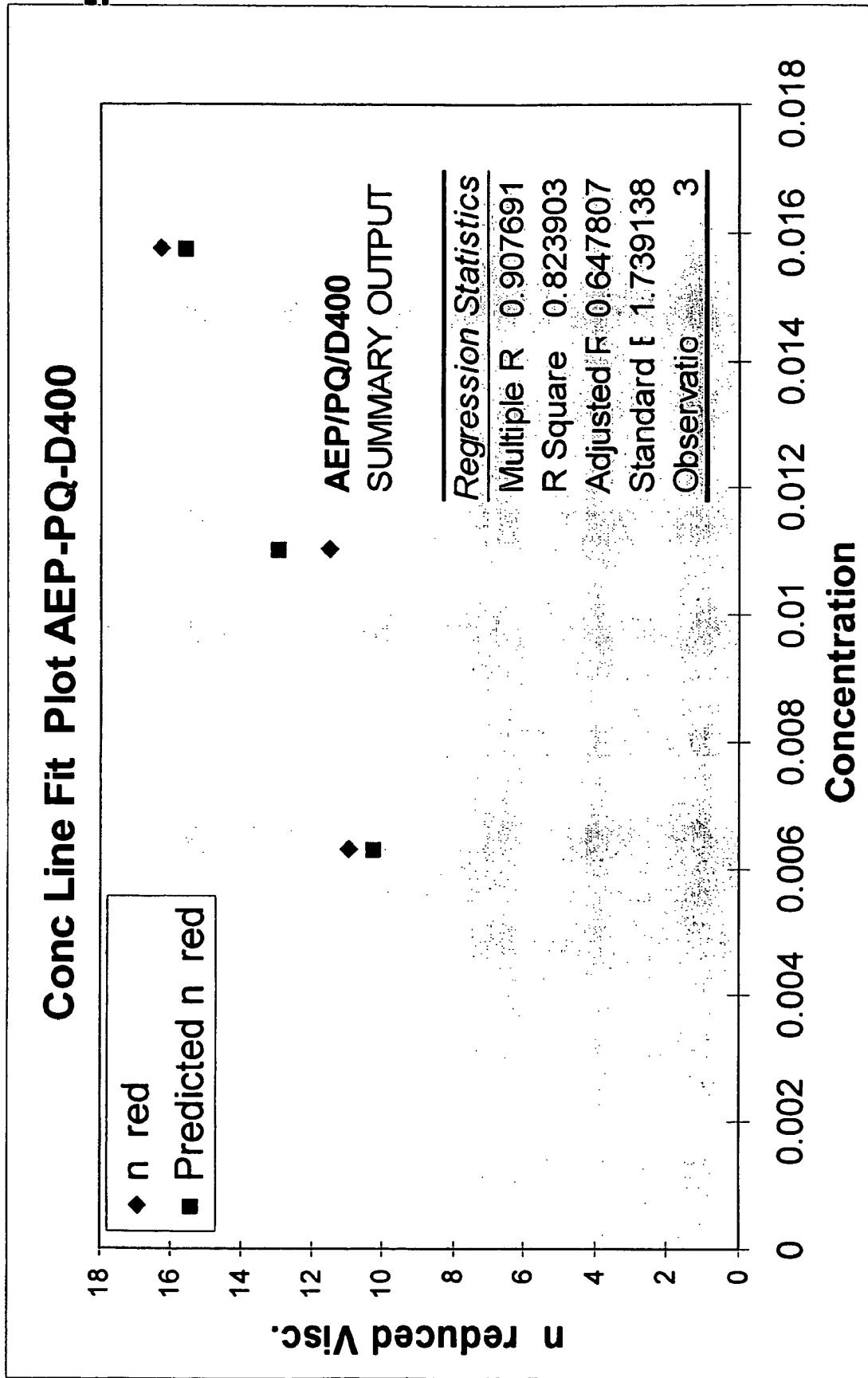
Solutions in dichloromethane

Oxidative Amination Mechanism

Hydroquinone plus Amioethylpiperizine -----> Amine Substituted phenylquinone

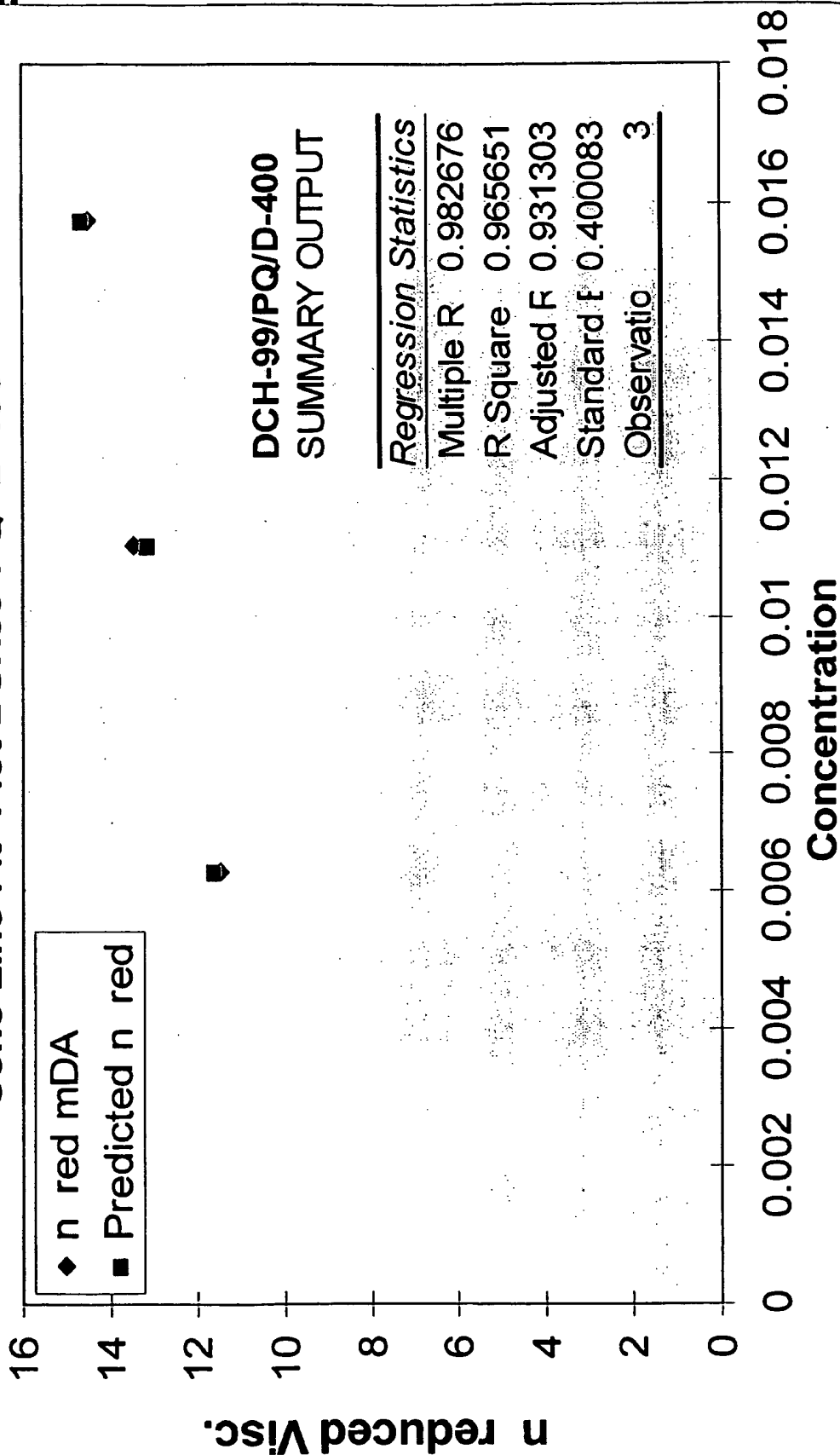


Dilute Solution Viscometry: AEP/D-400

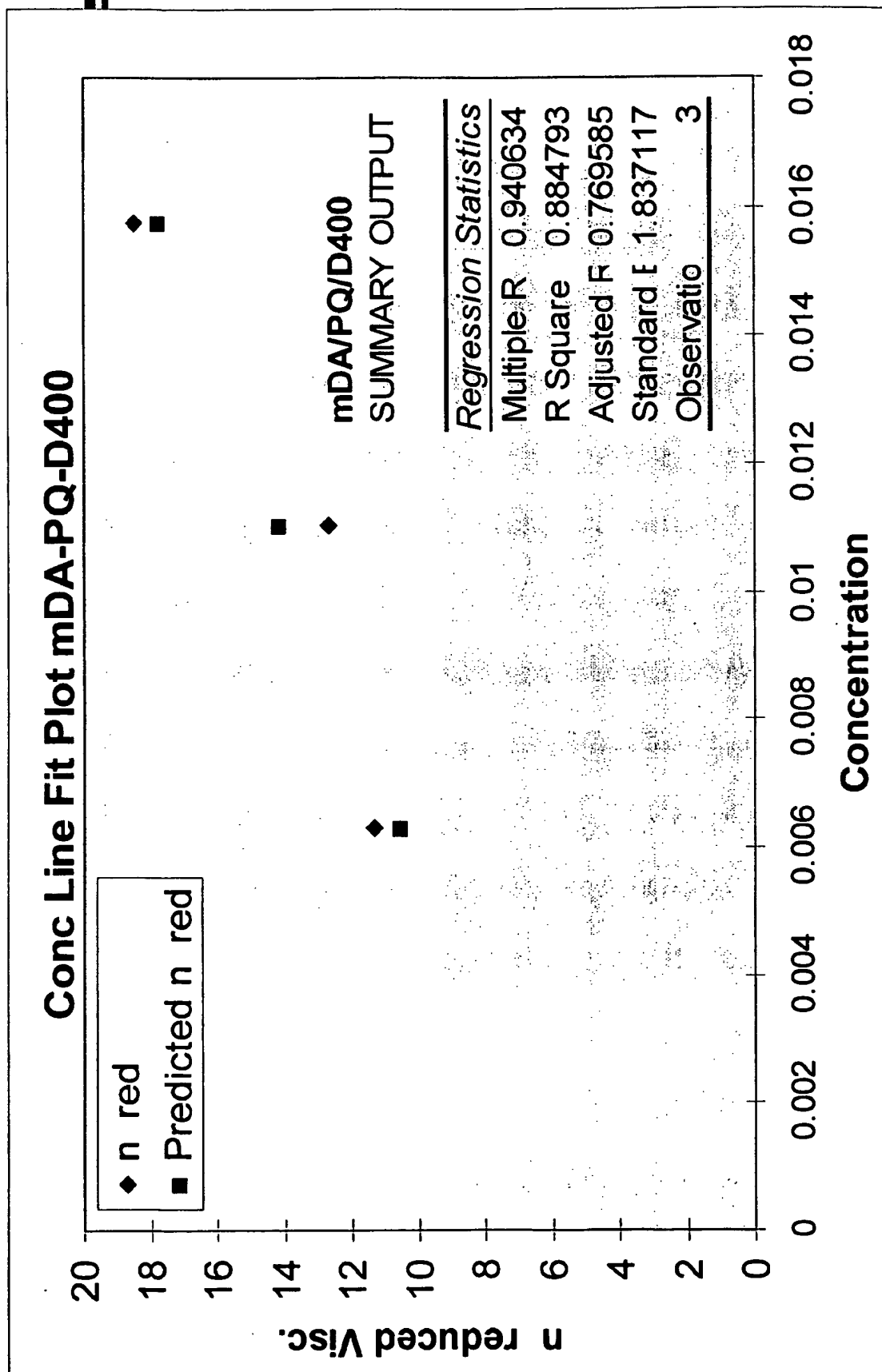


Dilute Solution Viscometry: DCH/D-400

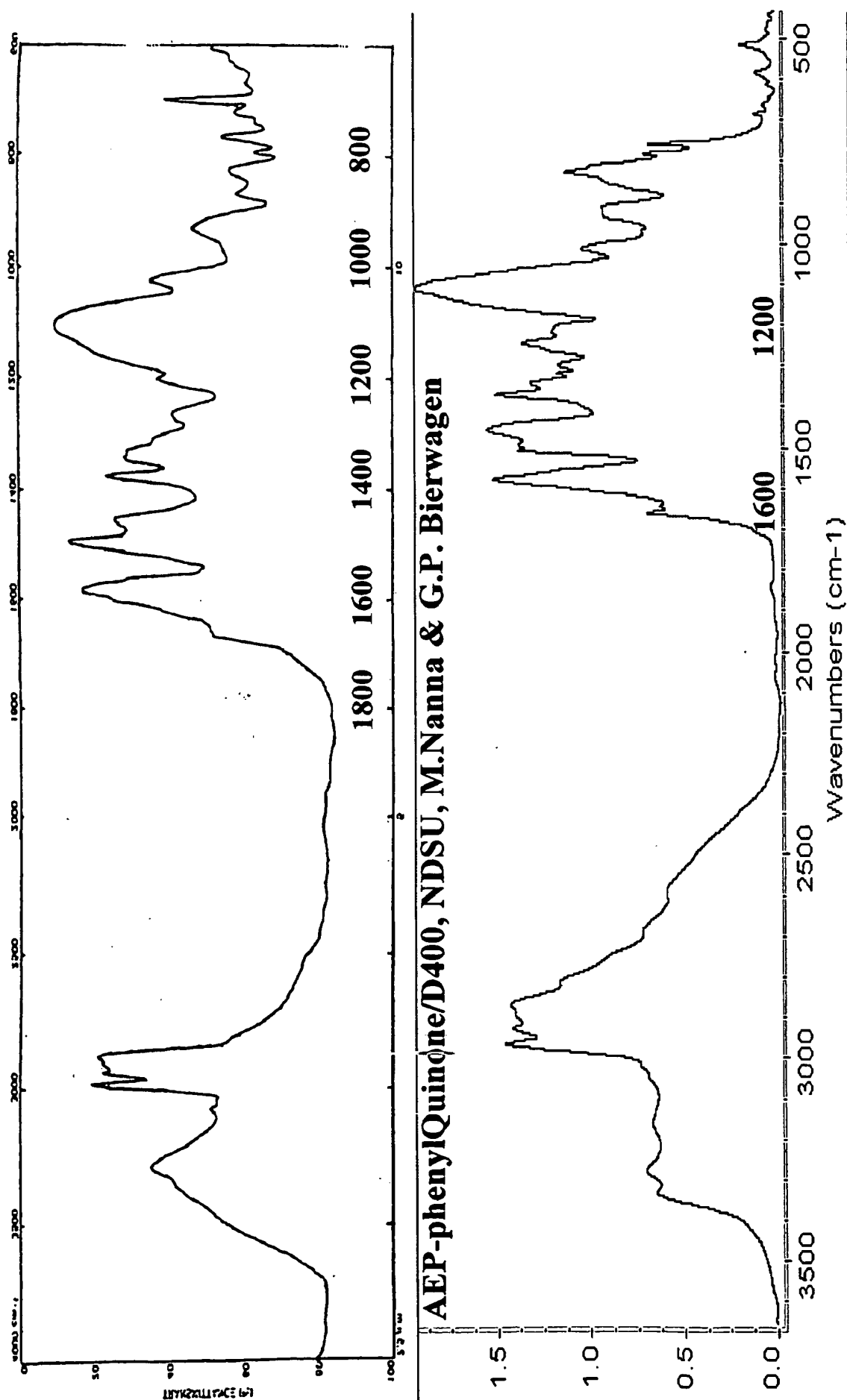
Conc Line Fit Plot DCH99-PQ- D-400



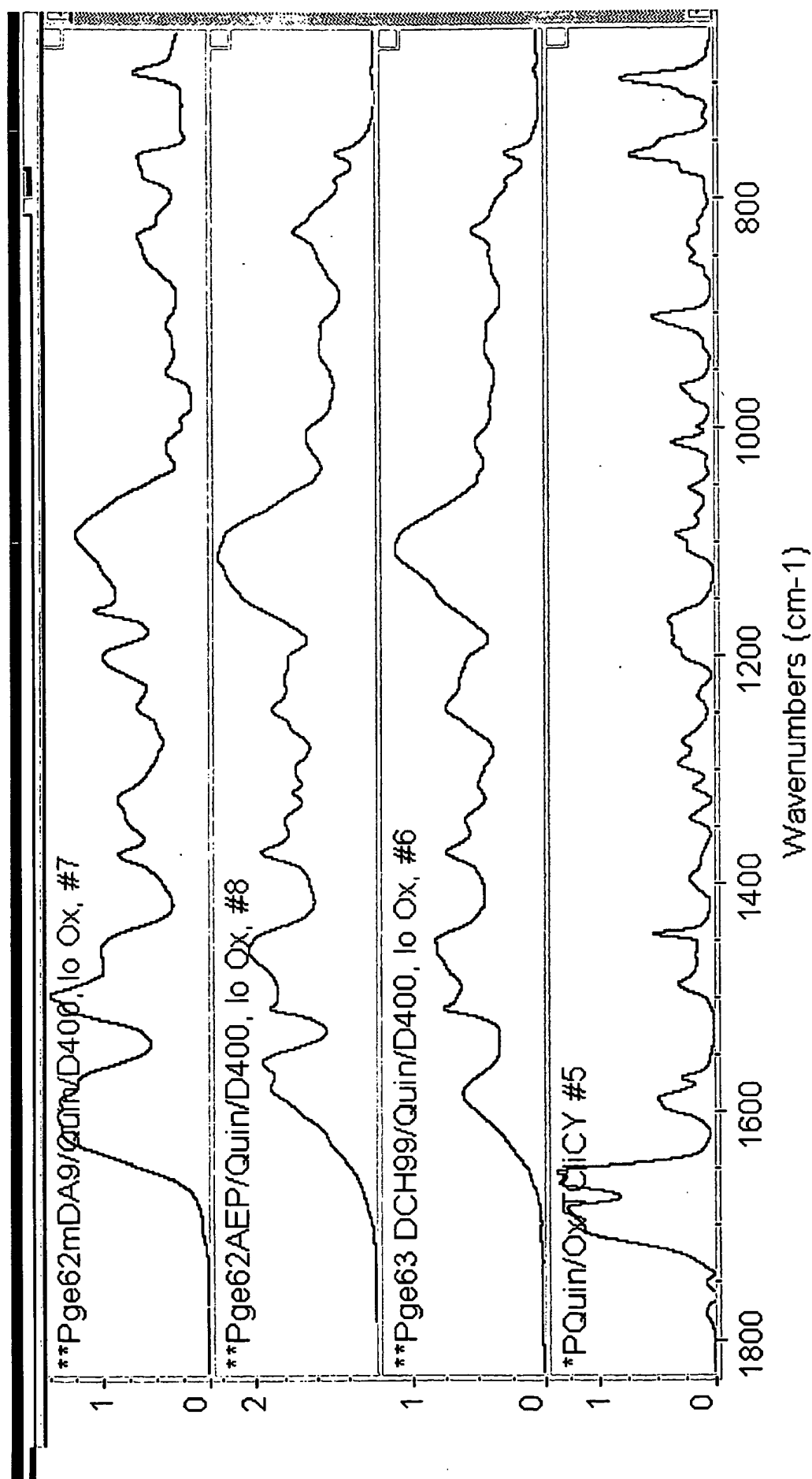
Dilute Solution Viscometry: mDA/D-400



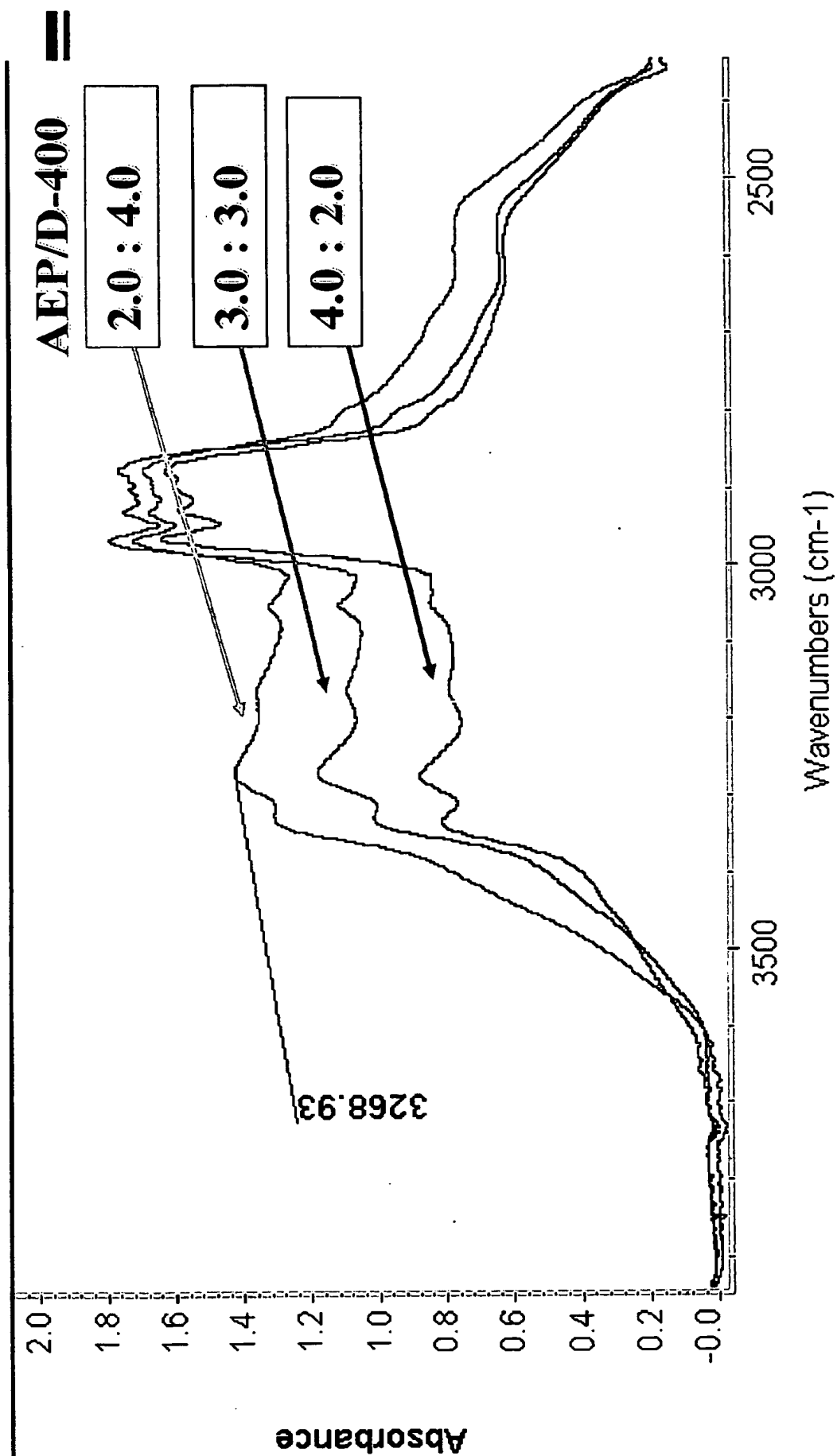
Poly(Amino-phenylQuinone/D-400, IR, T.Ashok & S. Erhan) #3



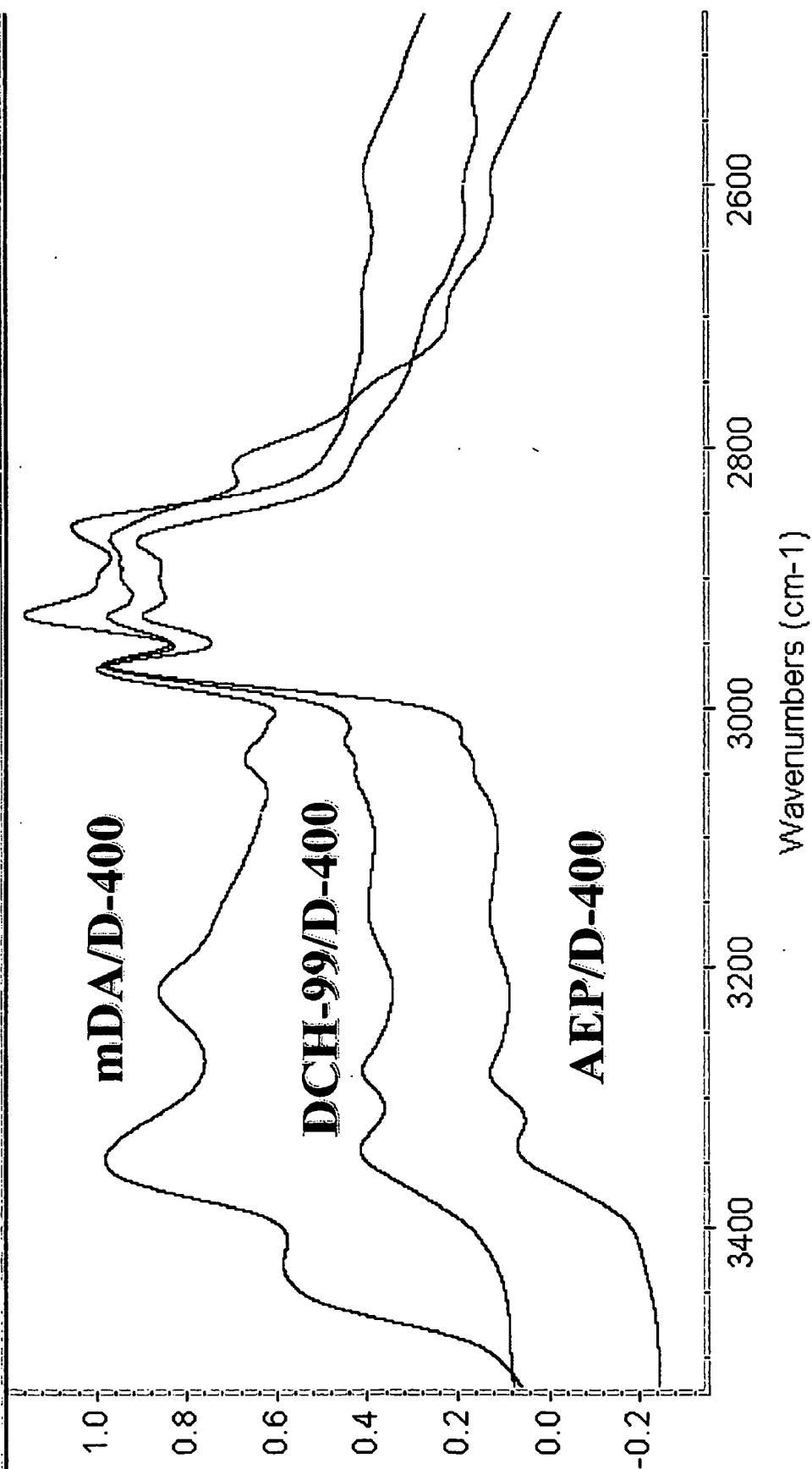
FTIR Quinone vs Quinone/D-400 amines



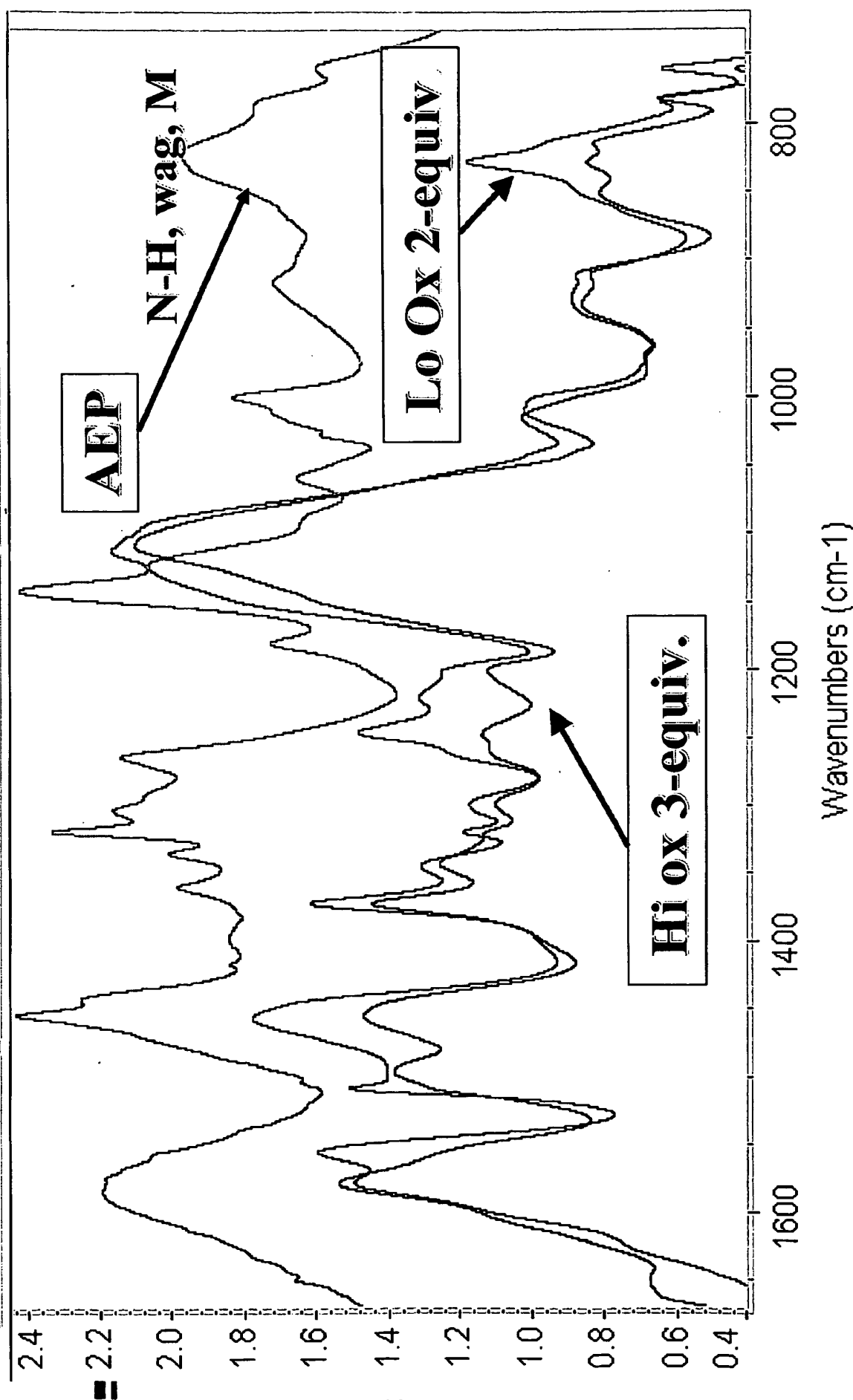
D-400 to AEP ratio affecting Primary Amine



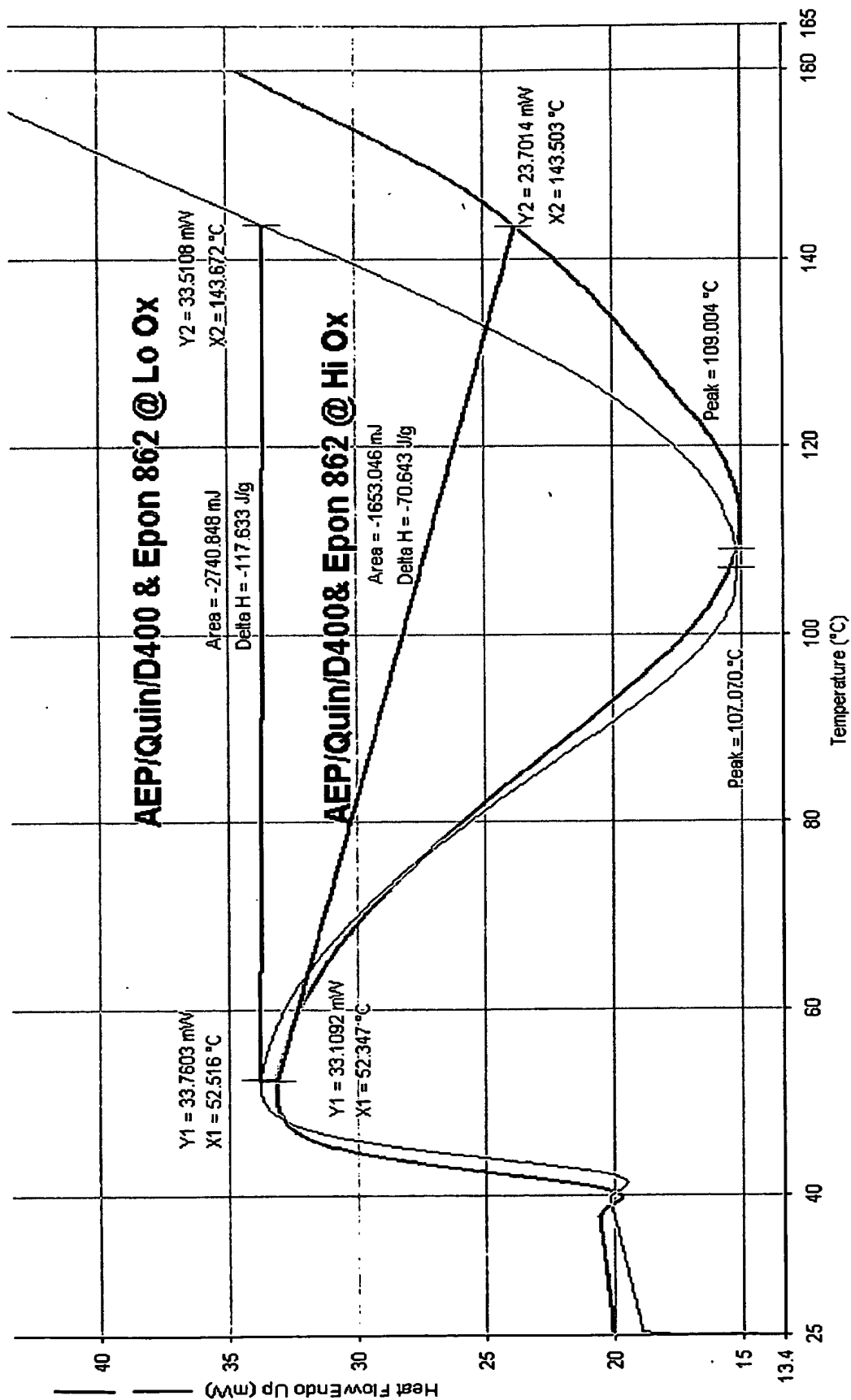
Substituted phenyl|Quinones/Amines/D-400



AEP/D-400/pQuinone at Lo & High Oxidizer Levels

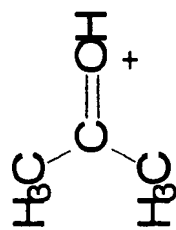


AEP/Quin/D400 HiOx vs. LoOx levels

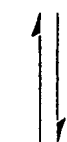


Acetone, AEP/Imine Schiff Base Synthesis

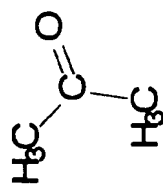
==



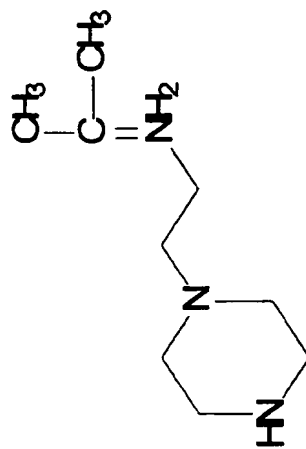
Protonated Acetone



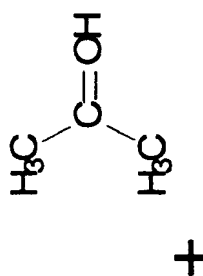
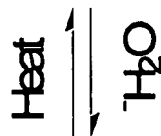
para TolySulfonic Acid



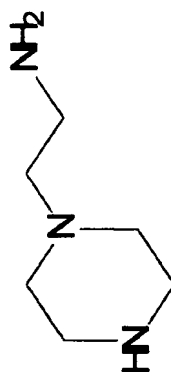
Acetone



Piperizine Ketimine Schiff base

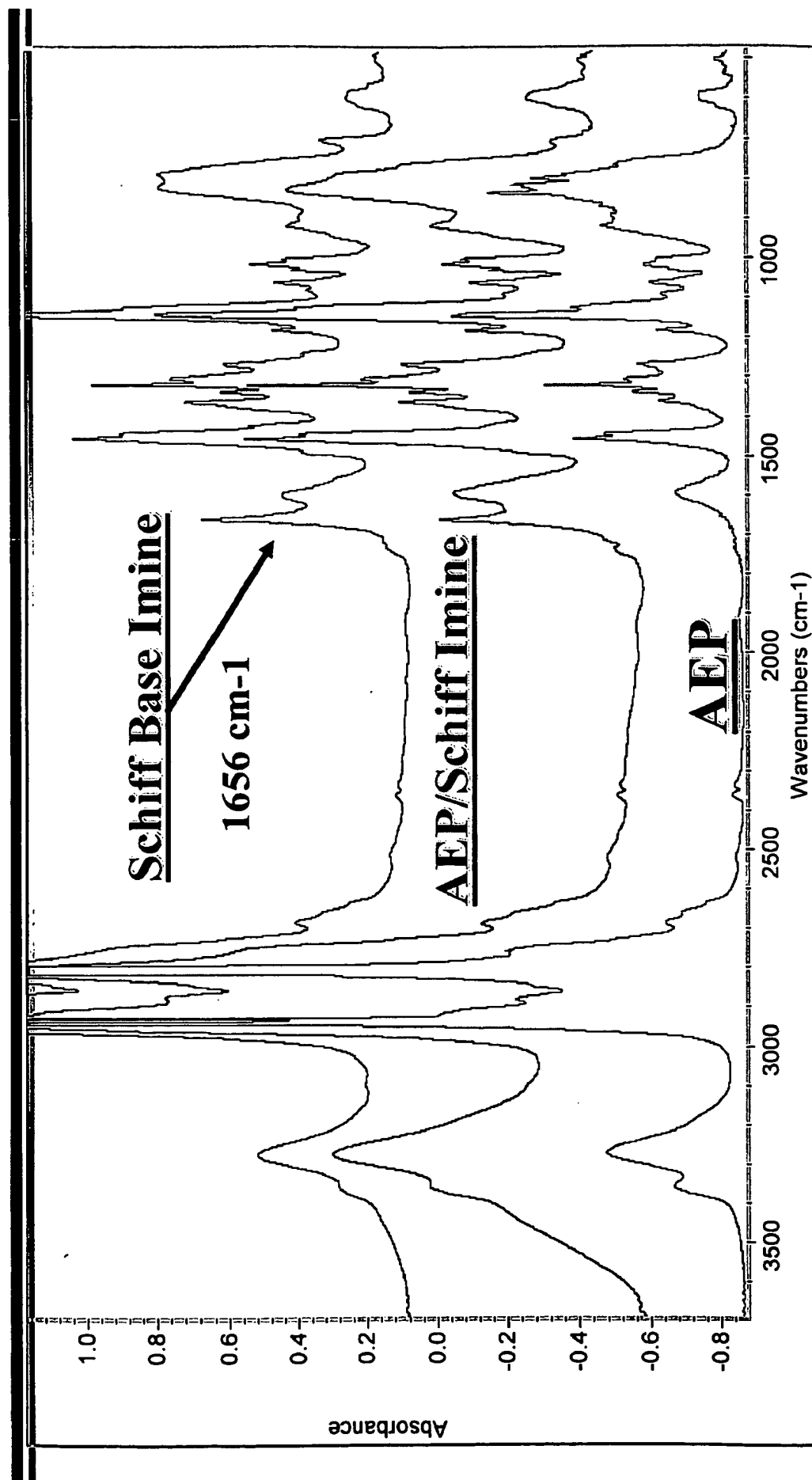


Protonated Acetone



Naminoethylpiperizine

FTIR AEP/ Acetone Schiff Base Progression



Primer Formulation

- **Primers are designed to live in two worlds**
 - ┆ They provide a primary surface over the (Aluminum) substrate
 - ┆ They become the primary surface for the protective topcoat
 - ┆ They contain fillers that Physically block or react with penetrants

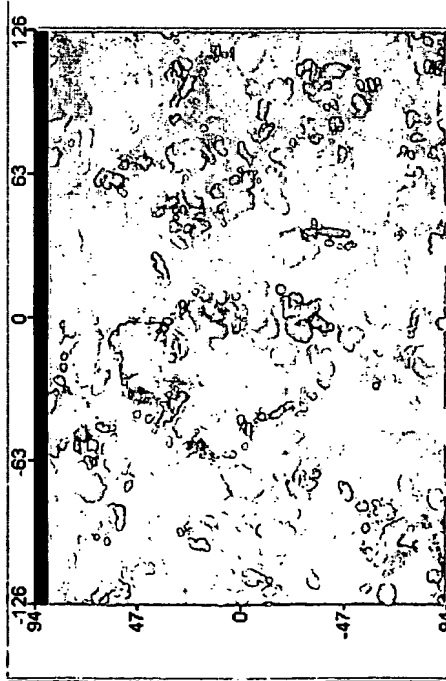
Adhesion is a Main factor for any Primer

- ┆ Resistance to penetration of water and solvents
- ┆ Good mechanical properties, flexibility & Impact resistance
- ┆ Low residual internal stress maximizes adhesion

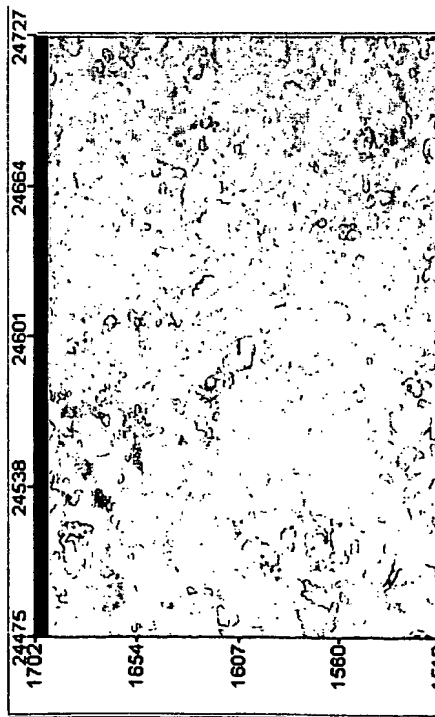
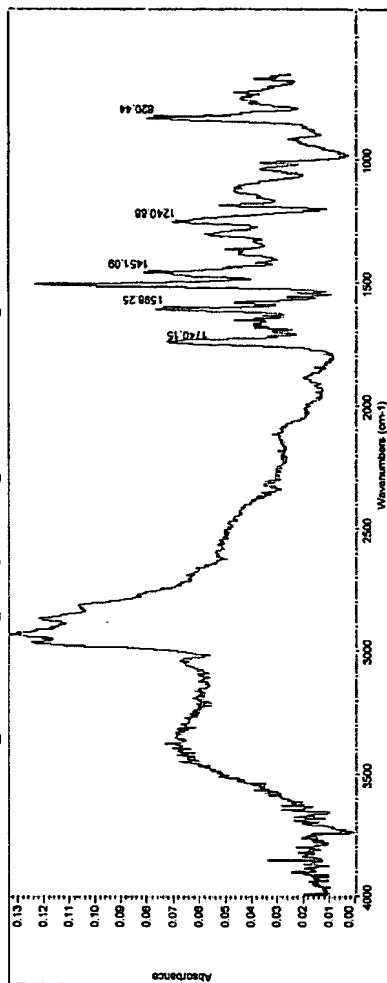
Cathodic protection of Aluminum surface

- ┆ Incorporation of 20 & 200- micron Magnesium Powder into Primer
- ┆ Cathodic protection of Aluminum surface by Magnesium

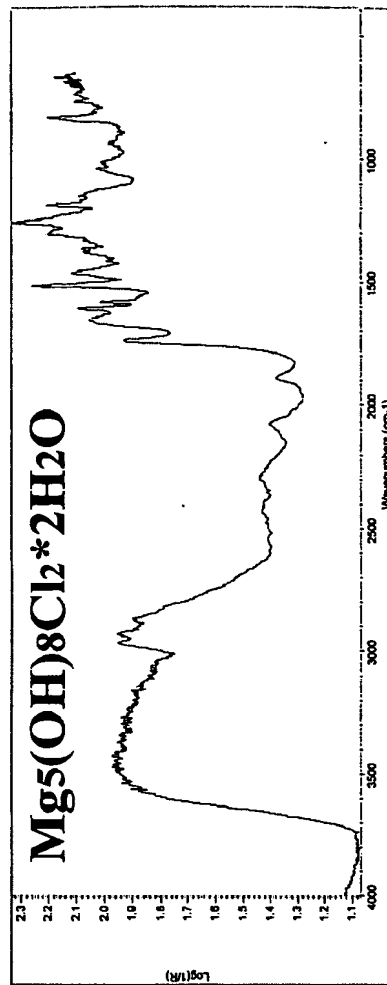
FTIR Microscope: Magnesium Primer Surface with & without Magnesium Hydroxide



75 PVC Unexposed Epoxy Magnesium S spectrum

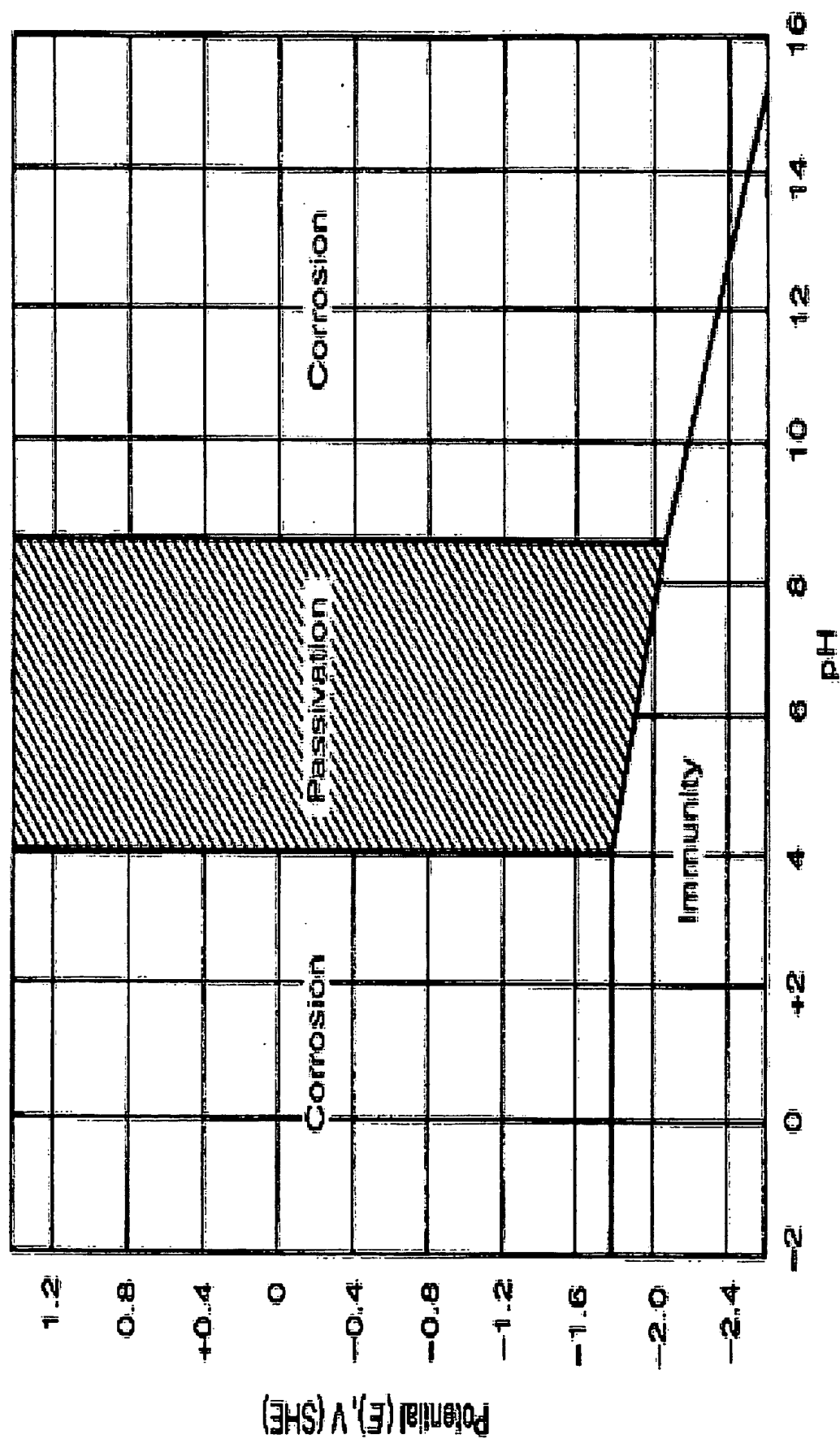


75 PVC Exposed Epoxy Magnesium S spectrum



Pourbaix Diagram

Corrosion, Passivation & Immunity of Aluminum



Effect of pH (Acidity or Alkalinity) on Corrosion Rate

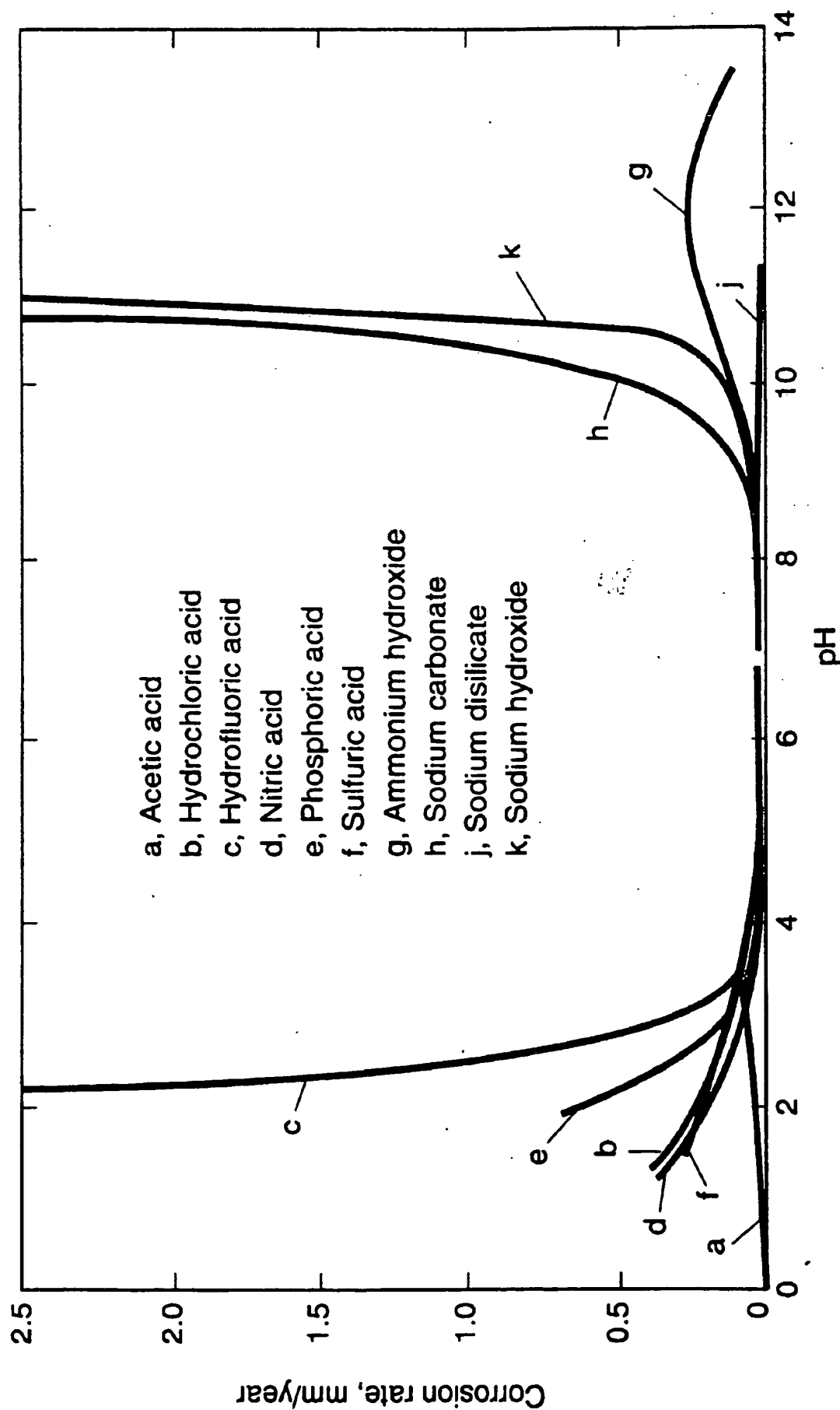
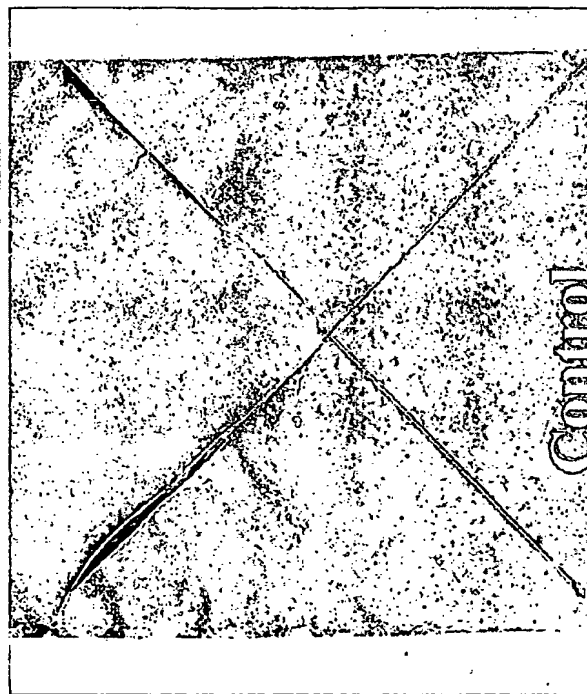
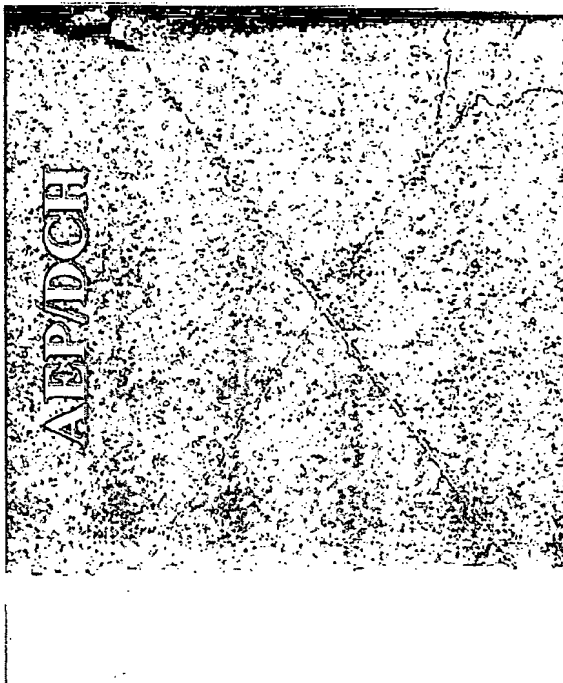
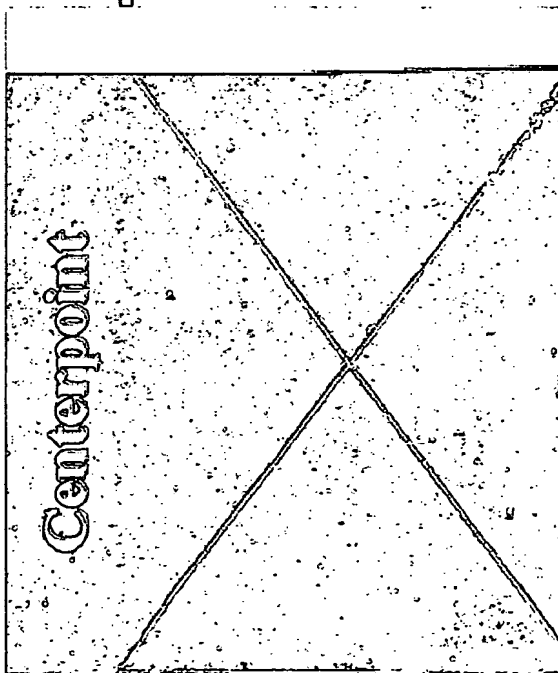
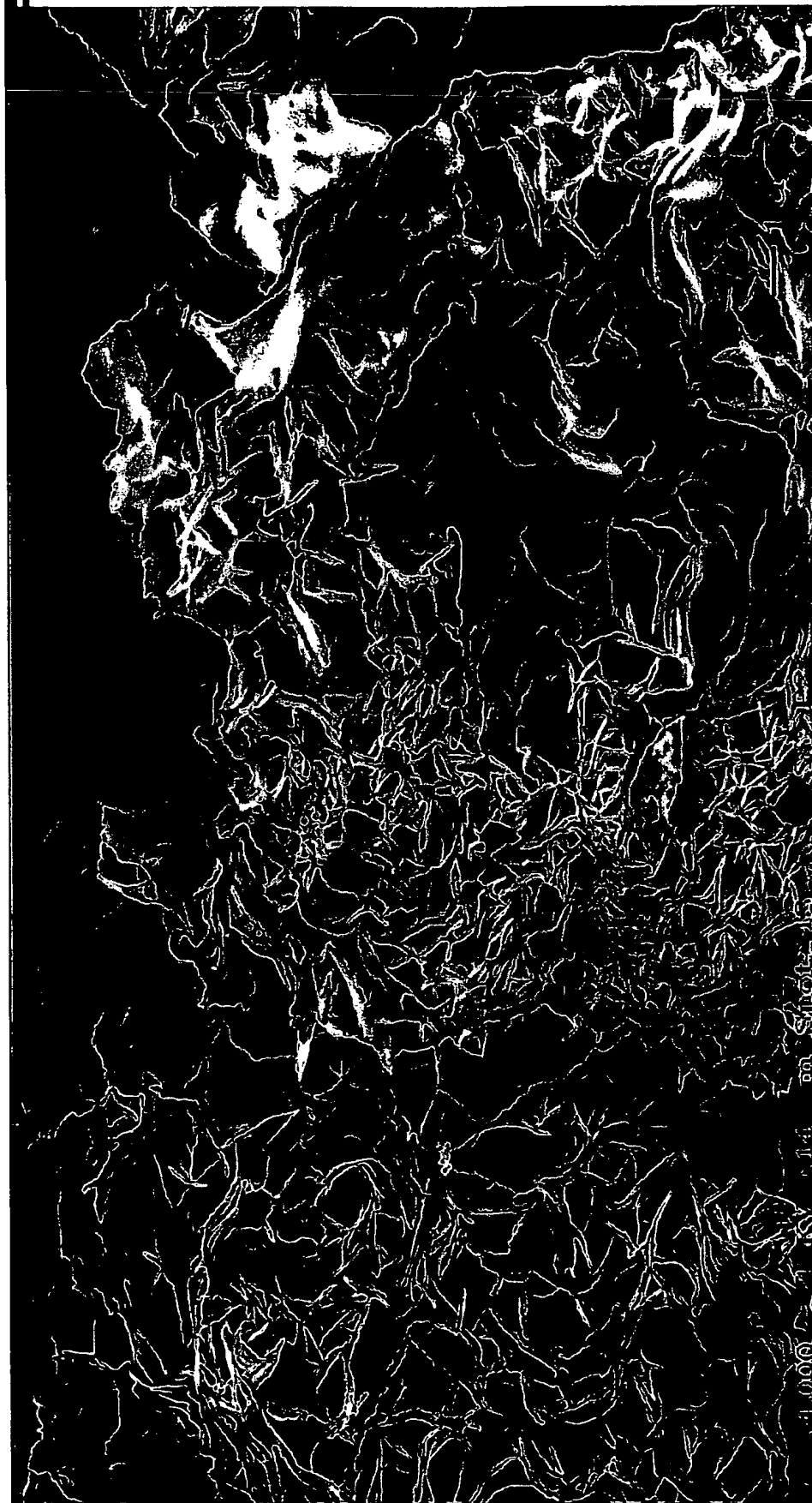


Fig. 9 Effect of pH on corrosion of 1100-H14 alloy by various chemical solutions. Observe the minimal

Primer panels 65 PVC 1300-hrs Prohesion Exposure,



SEM 4000X Surface of Epoxy Magnesium Primer with Magnesium Hydroxide Rosette Emanation from Epoxy Matrix



Title: EPOXY — MG COATING
Comment: SAMPLE 200136 LEAST MG ON AL 2024

SEM 2000X Prohesion Exposed Surface of Epoxy Magnesium Primer with Leached Epoxy Resin Matrix Exposed



Title: EPOXY-MG COATING BROWN AREA
Comment: SAMPLE 200138 HIGHEST MG LEVEL

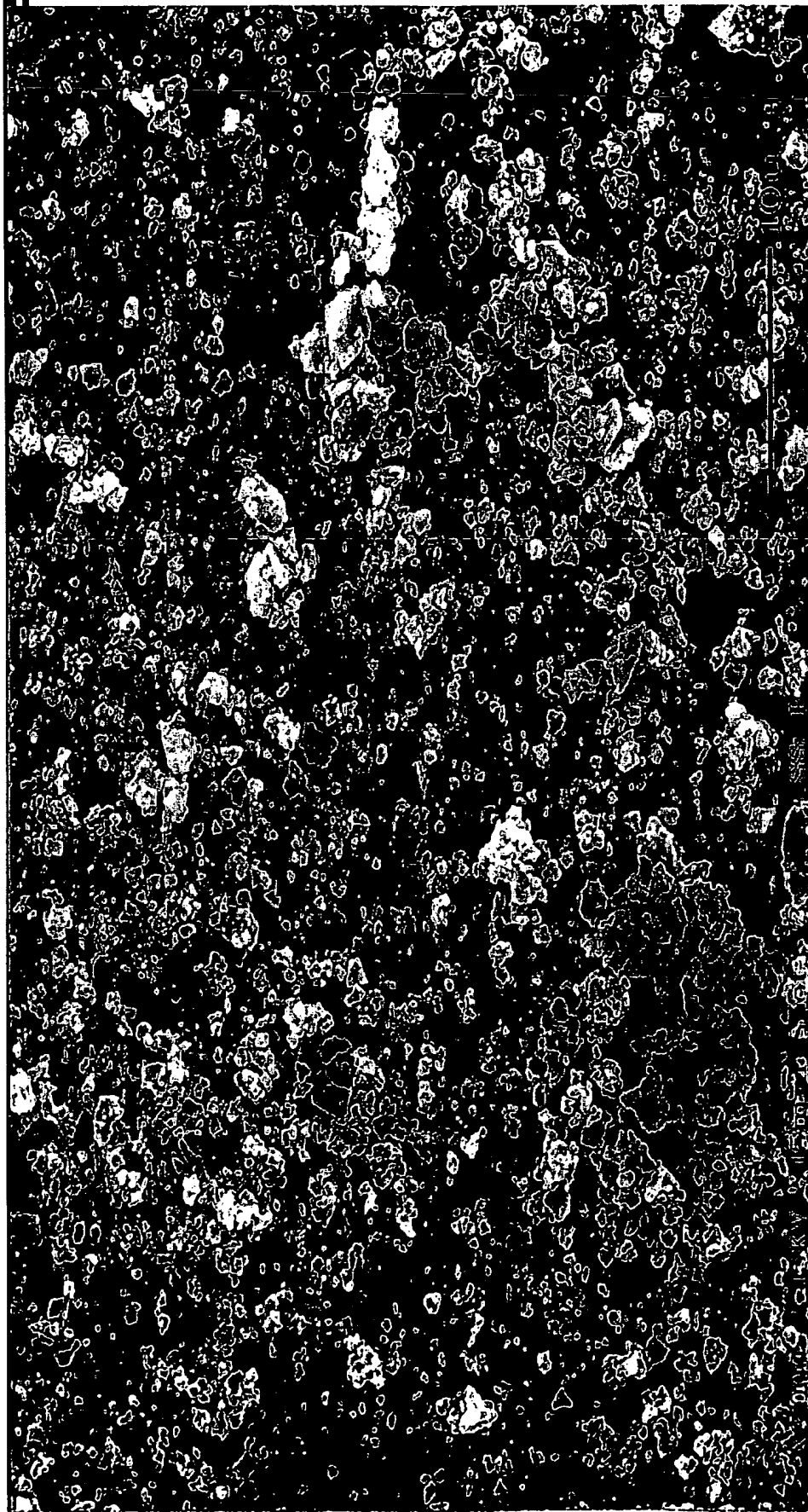
SEM 50X Prohesion Exposed Surface of Epoxy Magnesium Panel Scribed Area with Hydroxide Development on Al Surface



Title: EPOXY-MG COATING

Comment: SAMPLE 200138 AL SUBSTRATE

**SEM 2000X Prohesion Exposed Surface of Epoxy Magnesium
Panel Scribed Area with Hydroxide Development on Al Sufrace**

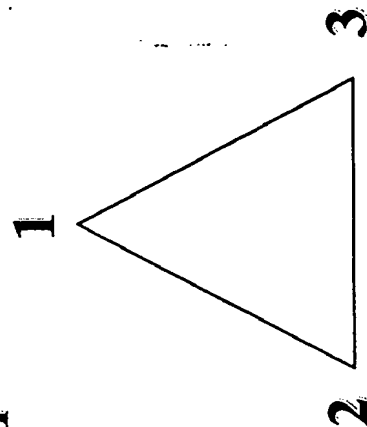


**Title: EPOXY-MG COATING
Comment: SAMPLE 200138**

AL SUBSTRATE

Simplex Lattice Design & Coordinates

Definition: The coordinate system used for the values of the three mixture components 1, 2, and 3 is called a *simplex-coordinate system*.

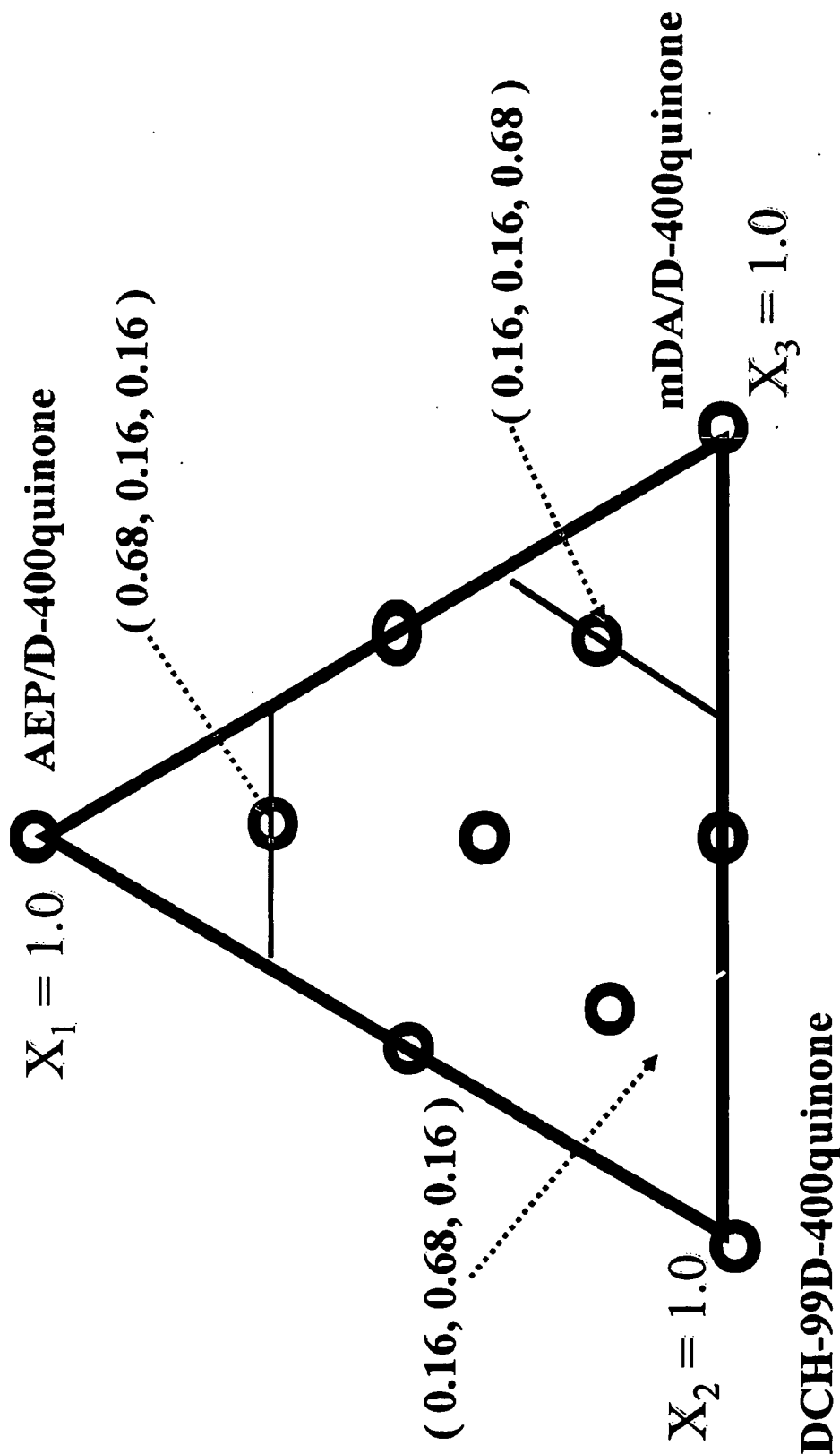


For a $q = 3$ component system where mixture components take on proportions bounded by points within the triangle.

With three components, the coordinates can be plotted on an equilateral triangle where the vertices represent the single-component mixtures. The interior points of the triangle represent the mixtures in which none of the three of the components is absent; the centroid corresponds to the mixture with equal proportions.

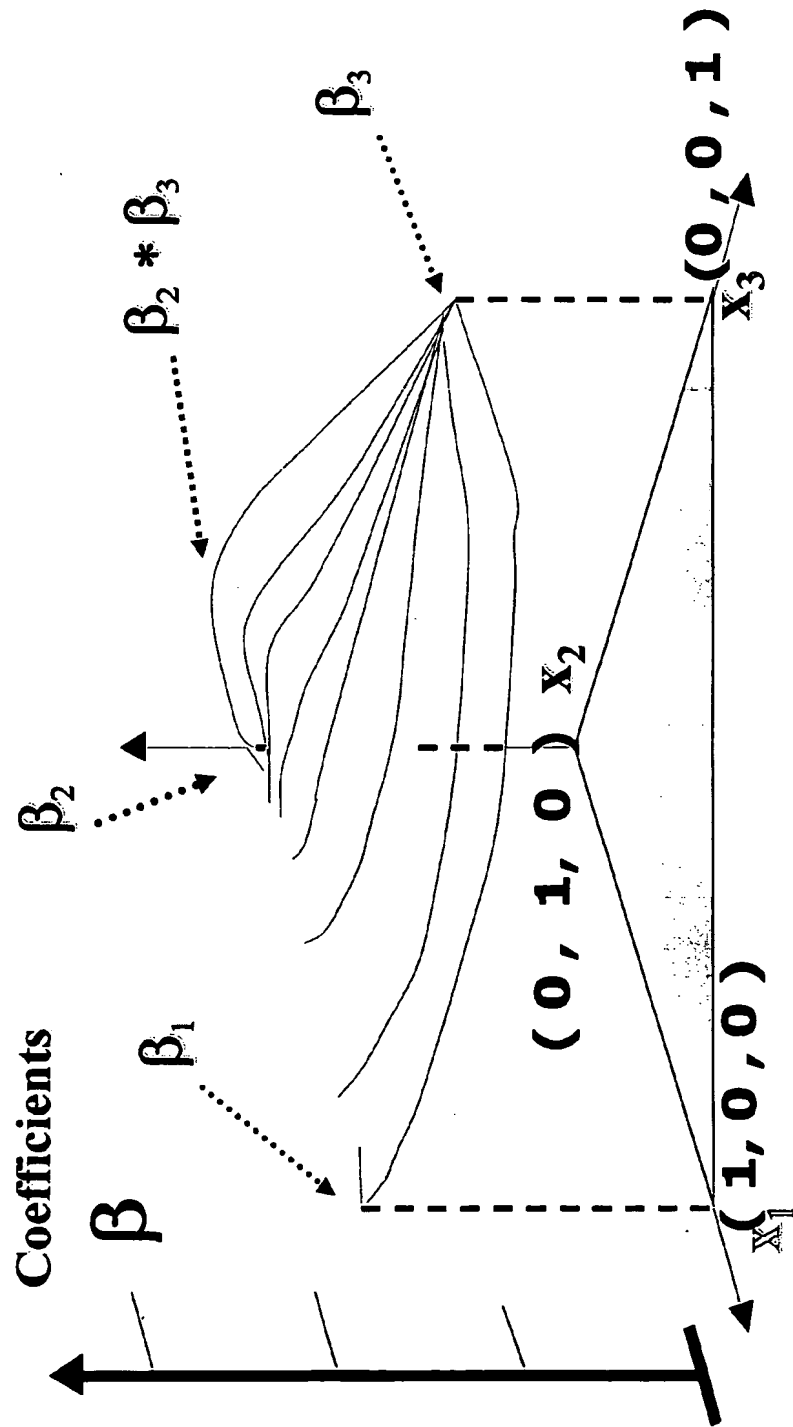
Simplex-Lattice Design, Edgeface

2-D Geometric Plot of Mixture Space



Response Surface Definition: A functional surface, continuous for all measured blend responses whose coordinates are inside of, or on the boundaries of the simplex triangle. The locus of such values for all one, two, or three blends can be visualized as a continuous geometric contour surface above the triangle conforming to the relationship:

$$y_u = \beta_o + \beta_1 x_1 + \beta_2 x_2 + \beta_3 x_3 + \dots + \epsilon_i$$



Model & Hypothesis Testing

$$y = \beta_0 + \beta_1 X_1 + \beta_2 X_2 + \beta_3 X_3 + \beta_4 X_1 X_2 + \beta_4 X_1 X_3 + \beta_5 X_1 X_3 + \beta_6 X_2 X_3 + \varepsilon$$

Null Hypothesis

H_0 : The response does not depend on mixture components

$$H_0: \beta_1 = \beta_2 = \beta_3 \dots \beta_6 = 0 \quad \text{Under } H_0: y = \beta_0$$

$$H_0 \text{ (for plane)} \quad \beta_4 = \beta_5 = \beta_6 = 0$$

If P value Statistic < 0.05 , for each β_j then *reject H_0* for β_j value

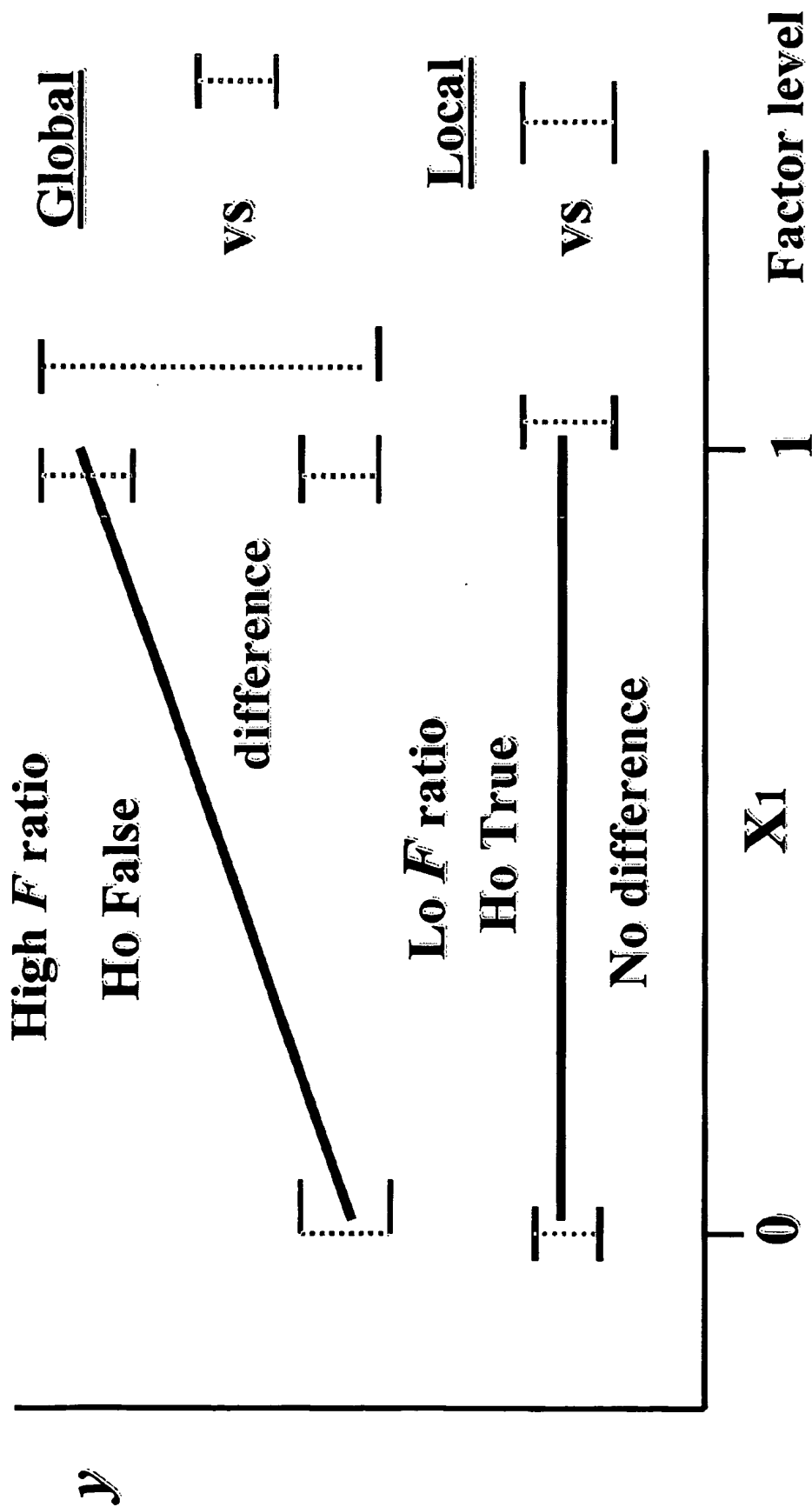
H_A : The response depends on mixture components

$$H_A: \text{not } H_0, \text{ at least one } \beta_j \neq 0$$

$$H_A \text{ (for plane) at least one } \beta_1 = \beta_2 = \beta_3 \neq 0$$

Significance of F ratio Statistic & Mixture Effects

Ratios of variances about the mean of the “y” responses



Summary Statistics for Mixture Response Surface

Whiteness 65PVC

$F(3, 10, 0.05) = 3.71$

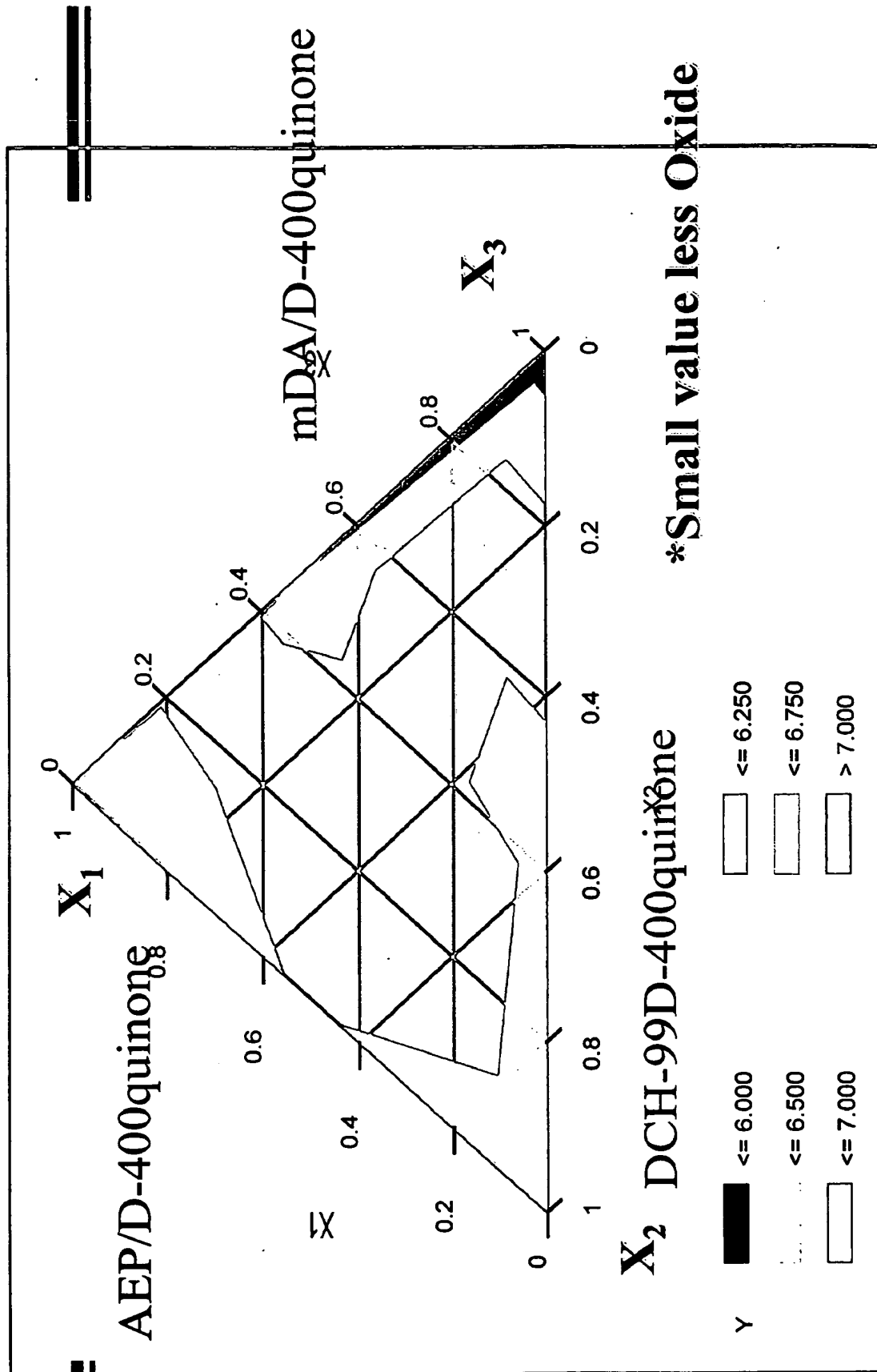
$P \text{ value} < 0.05$

Response:	Y
Summary of Fit	
RSquare	0.991868
RSquare Adj	0.926809
Root Mean Square Error	0.116921
Mean of Response	6.63
Observations (or Sum Wgts)	10

Effect Test	Source	Nparm	DF	Sum of Squares	F Ratio	Prob>F
	X1	1	1	55.932763	854.7596	<.0001
	X2	1	1	53.841388	822.7994	<.0001
	X3	1	1	38.517679	588.6238	<.0001
	X2*X1	1	1	0.193300	2.9540	0.1608
	X3*X1	1	1	0.152586	2.3318	0.2015
	X3*X2	1	1	0.128181	1.9588	0.2342

Contour Plot for 65 PVC Oxide vs Mixture

Contour Plot for Oxide (Whiteness) vs Mixture



Acetone Reflux 6-hrs: Correlation to mixture 58 PVC

Summary Statistics for Mixture Response

Response: Y

Summary of Fit

RSquare	0.986682
RSquare Adj	0.88014
Root Mean Square Error	0.116643
Mean of Response	1.377
Observations (or Sum Wgts)	10

$$F(3, 10, 0.05) = 3.71$$

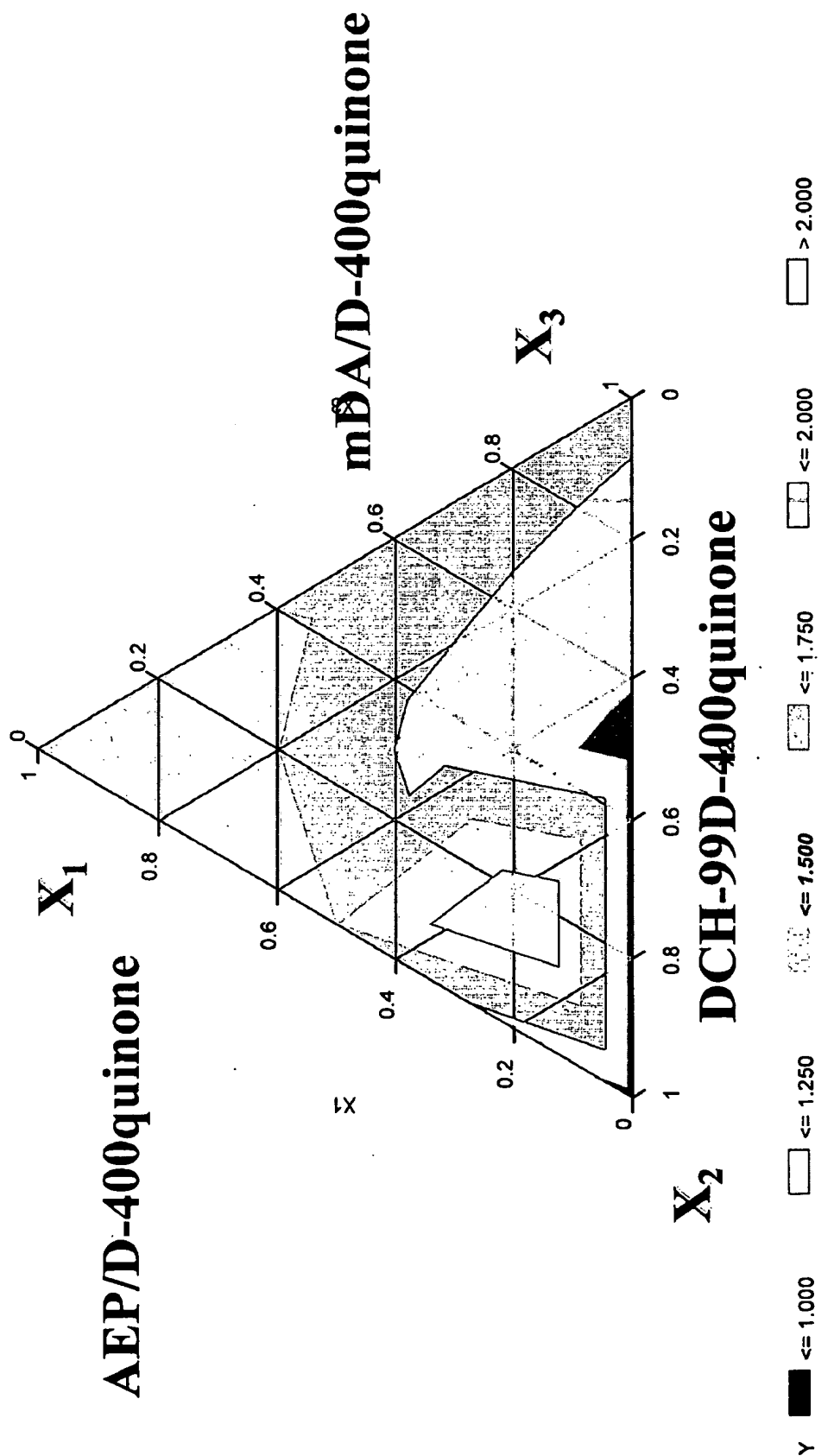
$$P \text{ value} < 0.05$$

Effect Test

Source	Nparm	DF	Sum of Squares	F Ratio	Prob>F
X1	1	1	2.6836846	16.0100	0.0161
X2	1	1	1.3508693	8.0589	0.0469
X3	1	1	1.6748609	9.9917	0.0342
X2*X1	1	1	0.0919022	0.5483	0.5001
X3*X1	1	1	0.0000732	0.0004	0.9843
X3*X2	1	1	0.0050744	0.0303	0.8703

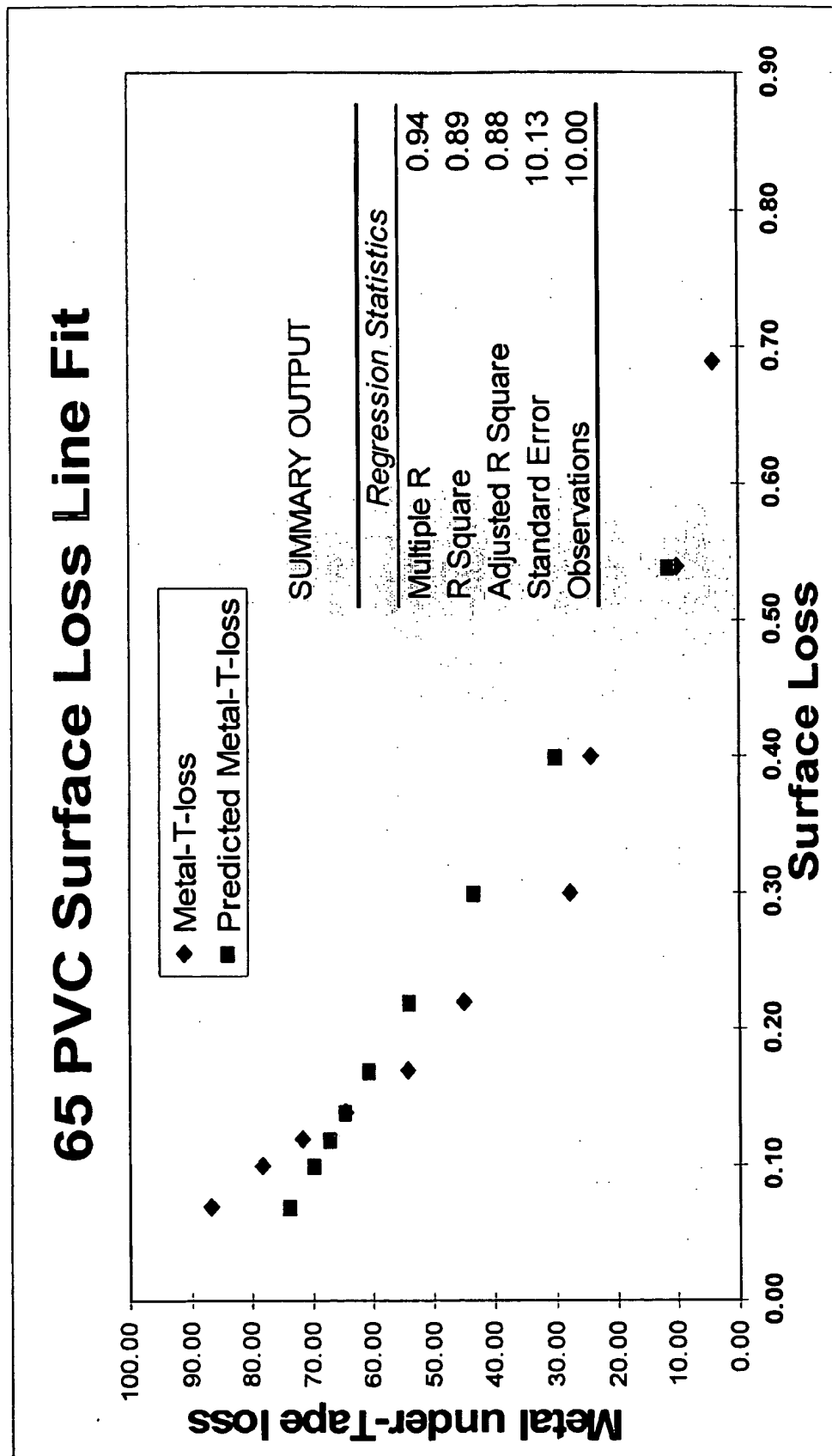
Acetone Reflux 58 PVC Weight loss Contour Plot

Contour Plot for Acetone Reflux Weight Loss 58 PVC



Linear Regression Model with 95% C.I. Limits

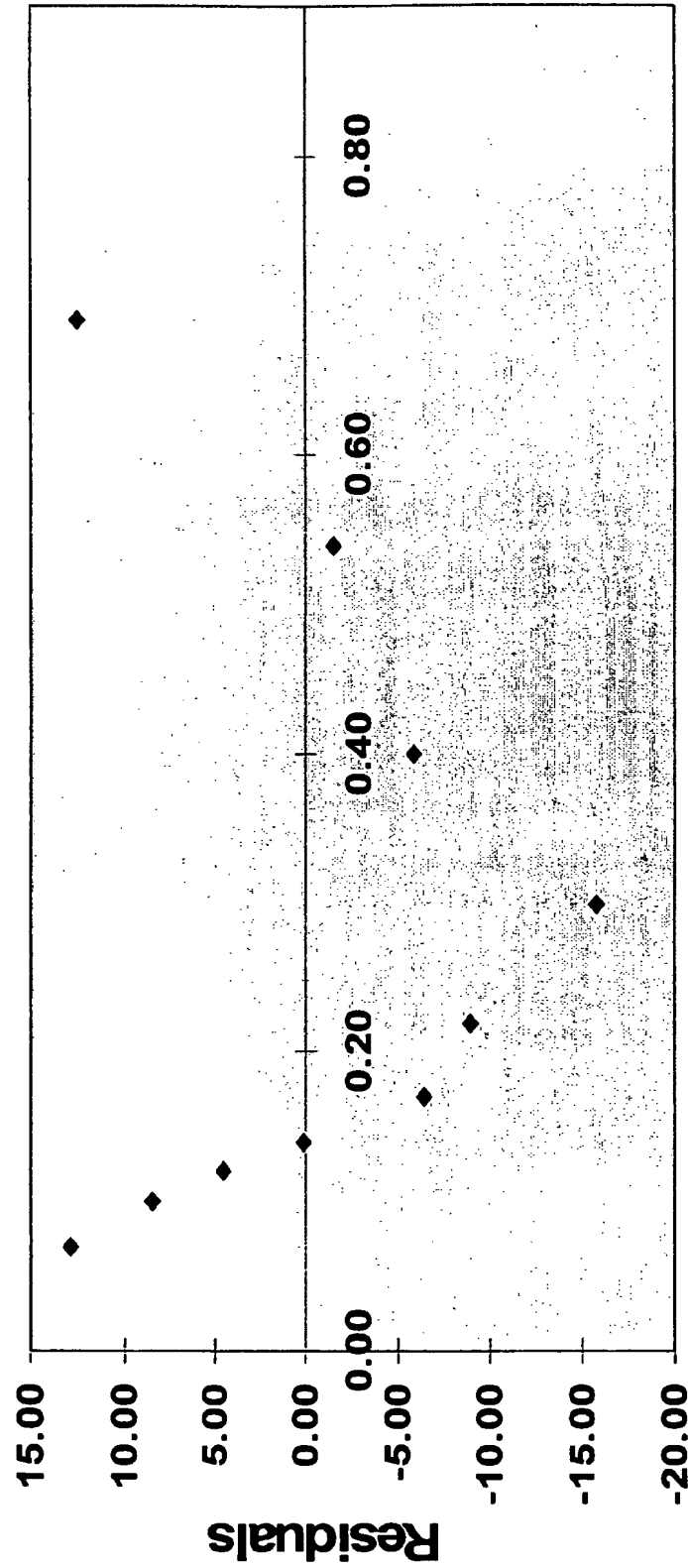
$$\text{Under Tape Loss} = (b) + m (\text{Surface Loss})$$



Residual Analysis for Multiple Linear Regression

Non-homogenous Variance with parabolic trend

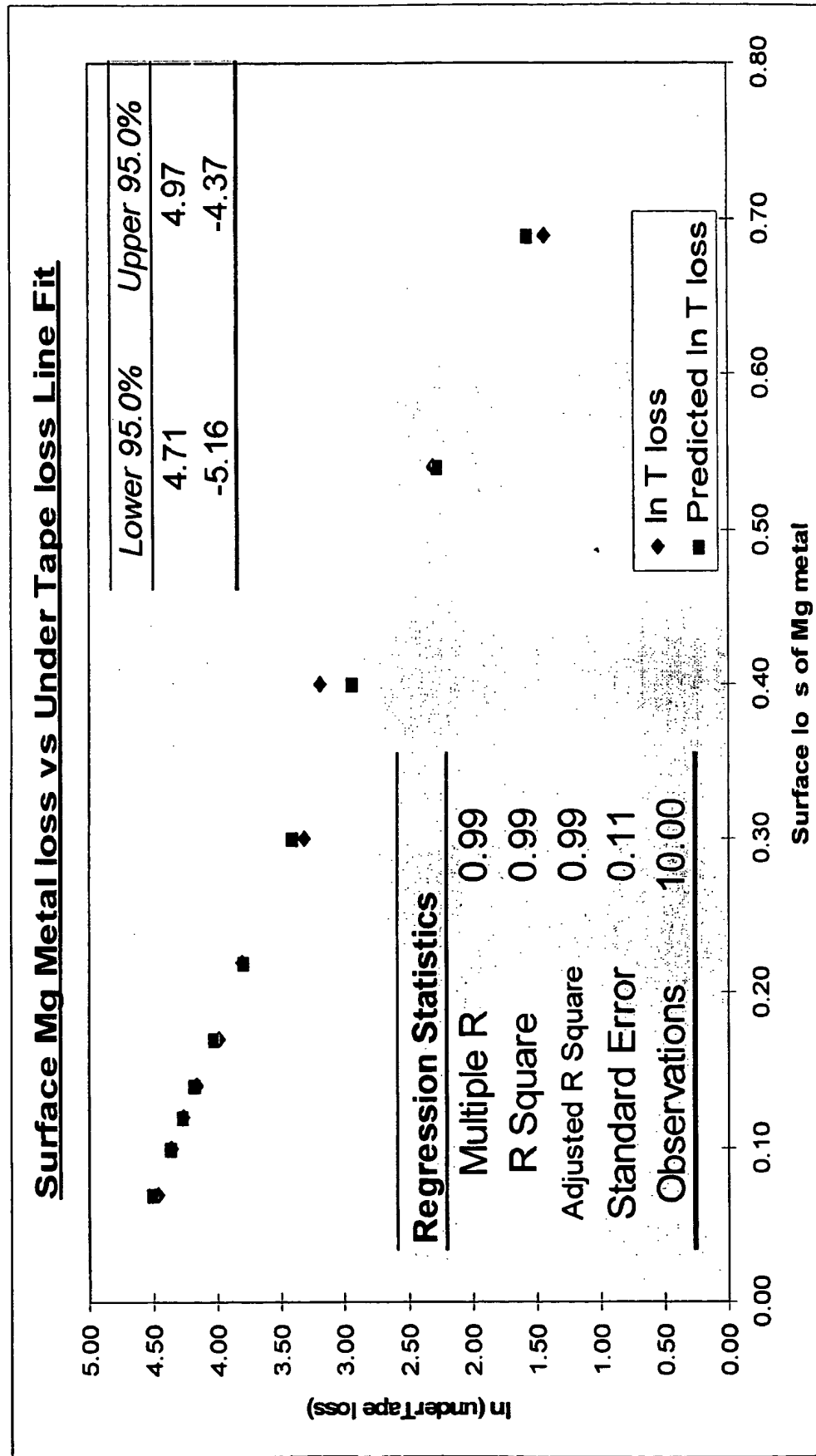
65 PVC Surface Loss Residual Plot



Predicted "Y" from Surface Loss

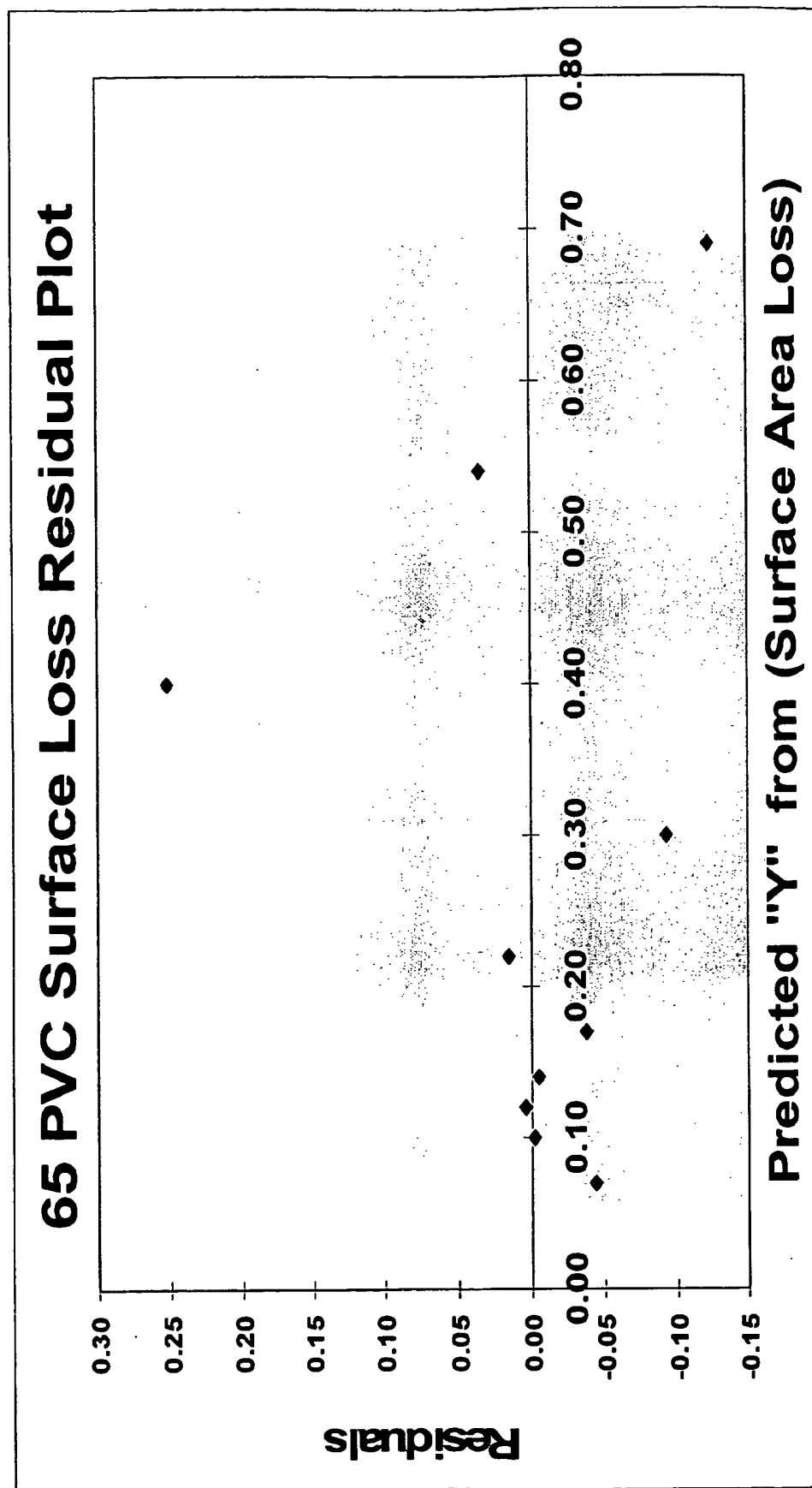
Regression Model with 95% C.I. Limits

$$\ln(\text{metal under Tape}) = \ln(A) + \beta (\text{Surface Loss})$$



Residual Analysis for ln Transformation

Homogenization of Variance



Seminar Summary of Results

- 1. Primer panels formulated with curative mixtures at higher AEP level accumulated higher surface magnesium oxides yielding eventual coating delamination but slower anode consumption. Primer delamination possibly due to the effect of compressive forces building in the film as it fills with magnesium oxides. Primers formulated with higher mDA levels developed less surface oxides, however, had a higher rate of metal loss (anode consumption). Response surface plot indicates higher mDA & DCH-99 yield less accumulated oxide.**
- 2. Coating solvent resistance found to depend on curative mixtures that contained higher proportion of mDA.**
- 3. Correlation of under tape metal loss to surface area loss indicates that primers formulated with a mixture of all three curatives near the simplex centroid yielded moderate oxide levels and cleaner scribe lines after 1300-hrs prohesion exposure in Harrison's solution.**
- 4. Overall, resistance to penetrant is dependent on curative type and mixture ratios in the magnesium powder filled epoxy primer system.**

Future Work & Perspectives

Evaluation of residual & accumulated stresses with respect to thin film amine/epoxy primer formulations.

*** Below 55-microns film thickness water is readily adsorbed by primary amines and swells the film thus adding internal compressive stresses.**

*** Accumulation of corrosion by-products in film matrix (metal oxides, hydroxides, carbonates, & chlorides) yields additional compressive stresses in bulk and at substrate interface.**

Future Work & Evaluation Perspectives

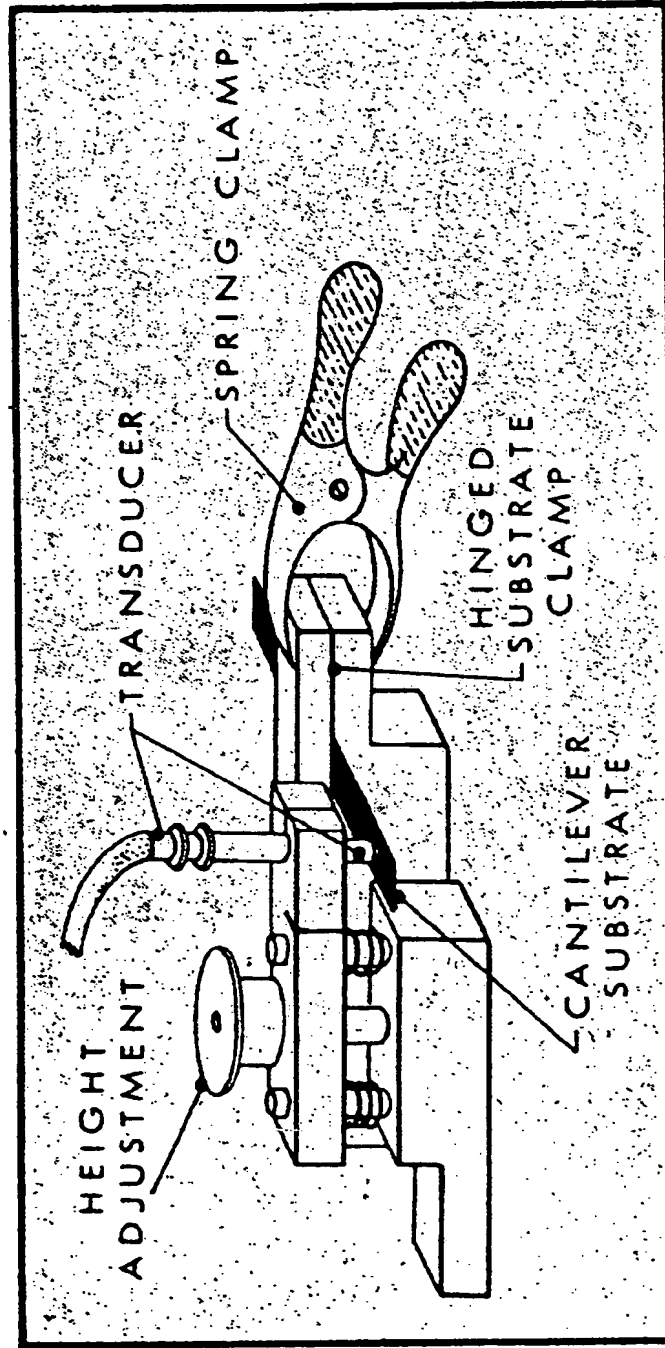


Figure 1—Internal stress measurement apparatus

Internal stress to bending moment per unit width

$$m = \sigma c(t + c)/2$$

m = thickness of metal shim **c** = thickness of coating

σ = stress in coating

Deflection, **d**, at a distance, **ℓ** along the bent cantilever can be expressed in terms of the bending moment : **m**

$$m = d E t^3 / 6 \ell^2 (1 - \nu)$$

where

E = Young's modulus of metal shim

ν = Poisson's ratio of metal shim

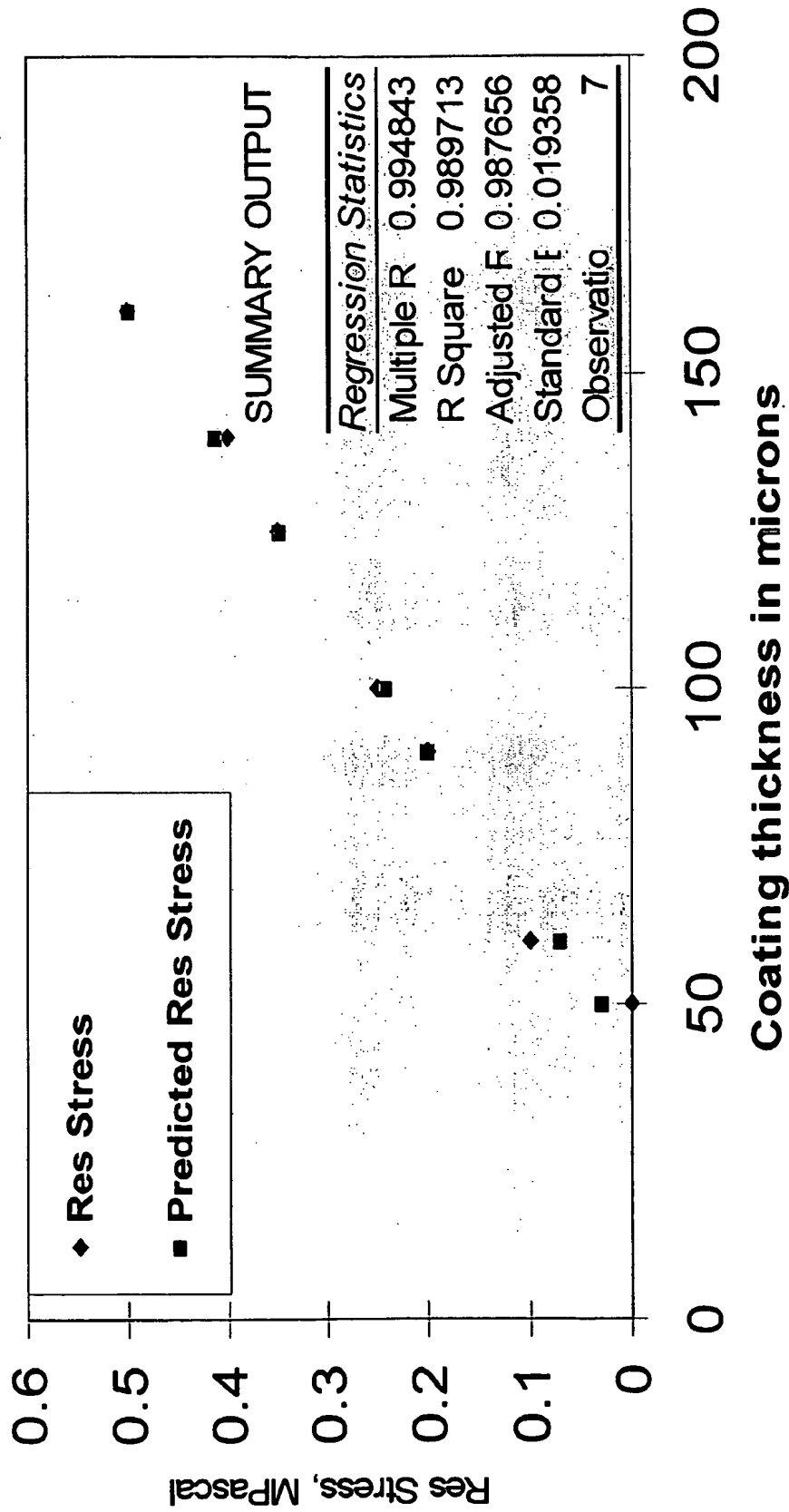
Combining equations. Yields expression for internal stress:

$$\sigma = d E t^3 / 3c \ell^2 (t + c) (1 - \nu)$$

Measured Residual Stress vs Coating Thickness

Epon 828 & DETA ambient cure

Coating thickness/Stress Line Fit Plot



Summary of Stress Development in Solventless Epoxy Coatings

The residual internal stress in solventless amine cured epoxy depends on the thickness of the coating.

- * Below 55 microns about 2-mils, thickness, the stress is small and compressive and almost independent of thickness.**
- * Above this value its tensile increases gradually with coating thickness variation due to two competing processes during cure,
 - 1. Shrinkage due to structural change induced by conversion.**
 - 2. Production of a highly swollen layer due to adsorption of water, from atmosphere, (plasticized water)****

No temperature increase due to exothermic conversion could be detected up to 150 microns, and consequentially internal stress is not thermal in origin and neither will the rate of cure be accelerated by this factor.

References to Seminar

1. T. A. Reddy and S. Erhan, Quinone-Amine Polymers. XII. Synthesis and Characterization of novel Polymers from 2-Phenylbenzoquinone and Aliphatic Diamines, *Progress in Organic Coatings*, 1994
2. T.A. Reddy and S. Erhan, Preparation and Characterization of Reaction Products between 2-Phenylquinone and Several Aliphatic Amines, *International J. Polymeric Matter*, vol.19, pp 109-116, 1993
3. T. A. Reddy and S. Erhan, A Study of Coating Properties of Novel Poly(Amino-Quinone)s Prepared from 2-Methylbenzoquinone and 2-phenylbenzoquinone, J. Applied Polymer Science, Vol 51, 1591-1595, 1994
4. Gene A. Hiegel and Afshin K. Chaharmahal, The TCHAC Tests for Distinguishing Primary from Secondary Alcohols, *J. Chem. Edu. Vol. 74, No. 4 April 1997*

References to Seminar

5. W.P. Jenks Catalysis in Chemistry and Enzymology, Dover Pub. Co, 1987, Pp 183-193
6. N. Kouloumbi, G.M.Tsangaris, S.T. Kyvelidis, Eval. Of Corrosion Behavior of metal Filled Polymeric coatings, J. Coating Technology, Vol. 66. No. 839, 1994
7. J.R. Davis, Corrosion of Aluminum and Aluminum Alloys, American Society for Metals, Materials Information Society, 1999
8. E. Almeida, D. Pereira, & O. Figueri, The Degredation of Zinc Coatings In Salty Aqueous Atmospheres, Progress in Organic Coatings, 17, (1989) 175-174

References to Seminar

9. S.G. Croll, Residual Stress in a Solventless Amine-Cured Epoxy Coating, *J. Coatings Technology*, Vol 51. No.659, Dec. 1979
10. J.W. Holubka & R. A. Dickie, Resin Structure And the Corrosion Resistance Of Organic Coatings, *J. Coating Technology*, Vol. 56, No. 714, 1984
11. John Cornell, How to Run Mixture Experiments for Product Quality, *American Society for Quality Control*, Statistics Division, 1990
12. Shriner, Fuson, Curtin, Morrill, The Systematic Identification of Organic Compounds, 6th Ed. *J. Wiley & Sons, Inc.* 1980, Pp. 122-123

Corrosion Concepts

Galvanic: Spontaneous discharge due to (Red/Ox) reaction

Activity: Charge developed for different metals when put into a salt of their own metals

Electrolyte: Solution that conducts electricity by migration of ions

Resistivity: Something corroding in solution has a low resistivity

Corrosion Concepts

- Galvanic Series Any metal or alloy has an unique corrosion potential E_{corr} when immersed in a corrosive electrolyte.
- Different Alloys Coupled The metal with the more electronegative or active E_{corr} has an excess of electron which are lost to the more positive metal
 - $M \rightarrow M^{n+} + n e^{-}$ (Anode Rxn.)
 - $M^{n+} + n e^{-} \rightarrow M$ (Cathode Rxn.)

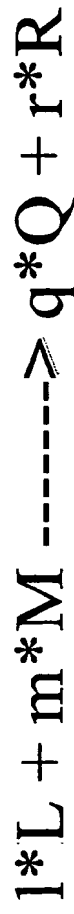
Corrosion Concepts

- Cathodic Protection
- When any two different alloys are coupled together, the metal that serves as the Cathode gains the electrons as it is more positive.
- The metal that loses the electrons is the Anode as it is more negative.
- The more positive metal/Alloy has the rate of its anodic reaction decreased at the expense of the “sacrificial anode” more positive metal.

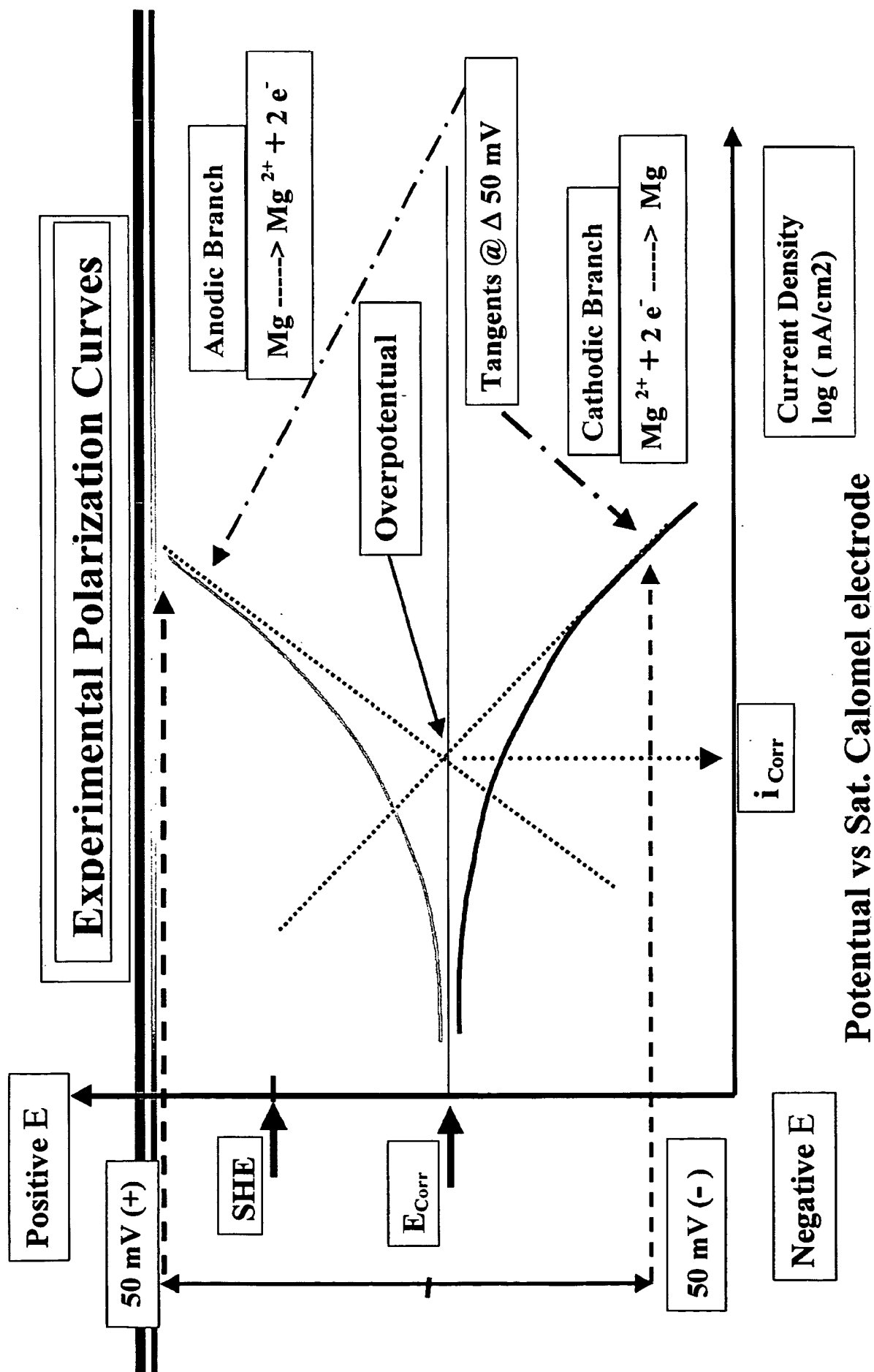
Corrosion Concepts

Kinetics: Employ Nernst Equation:

$$\Delta G = \Delta^* G RT \ln(a^q_O + a^r_R / a^l_L + a^m_M)$$



1. Predict which of several reactions between metals or alloys will occur.
2. Predict the effectiveness of passive film formation, and the effect of environmental impurities, e.g.: sulfides, chlorides.



Polarization Curves for Metal Powder filled Epoxy Primer over Bare Steel, (Typical Corrosion Parameter)

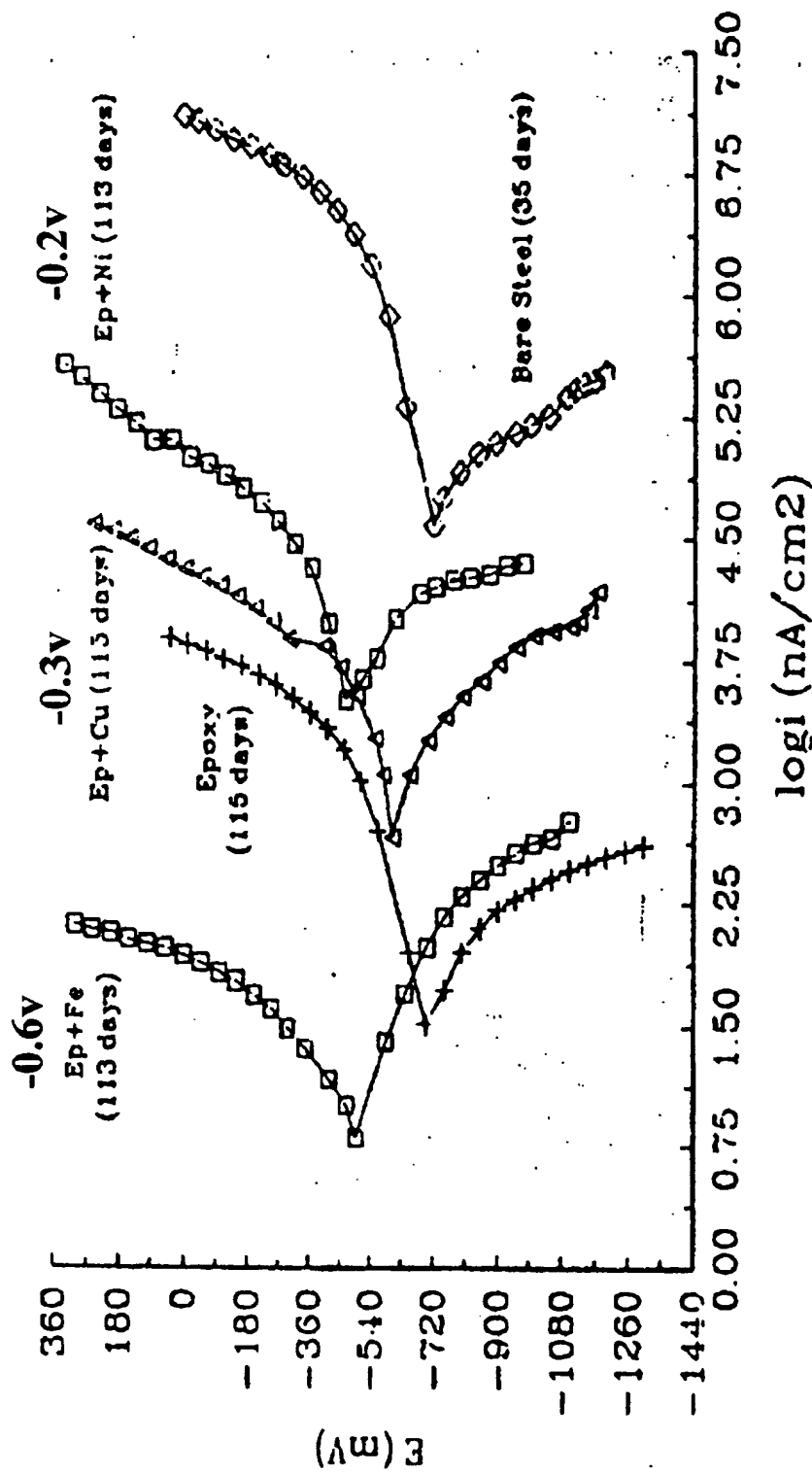
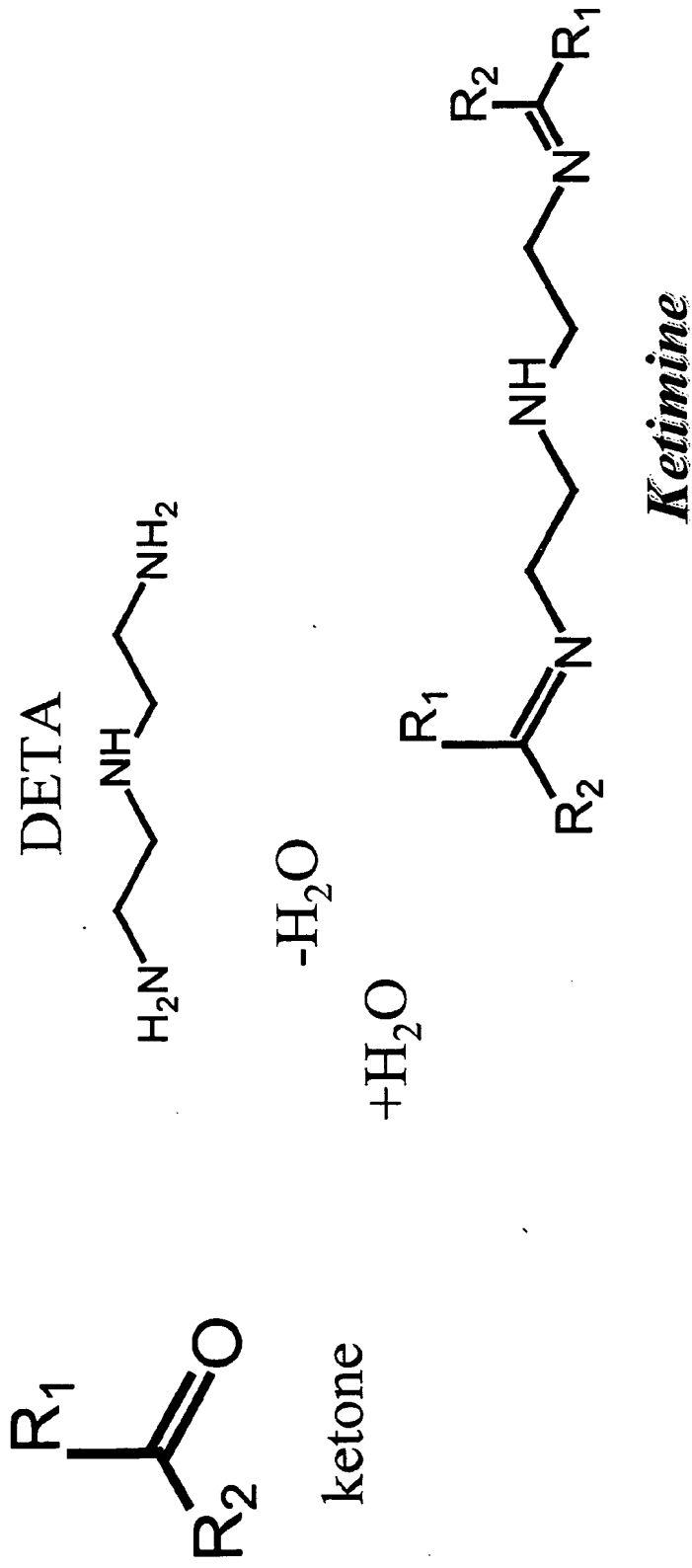


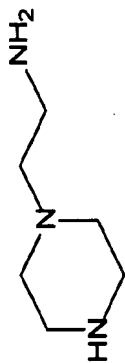
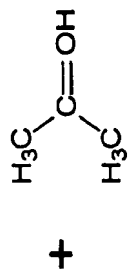
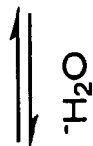
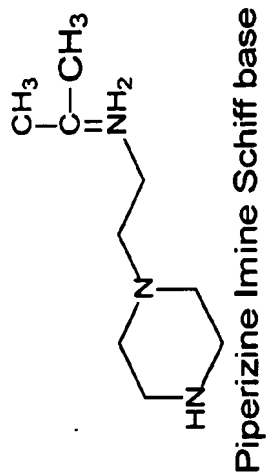
Figure 3—Potentiodynamic polarization plots for uncoated and epoxy coated steel specimens in 3.5% NaCl

Nitrogen based Curing Agents

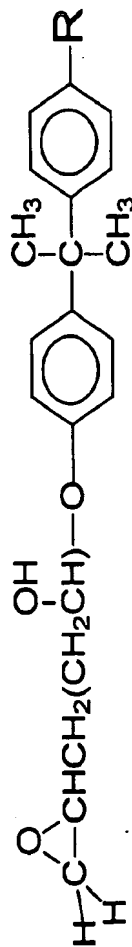
○ Ketimines (blocked amine)



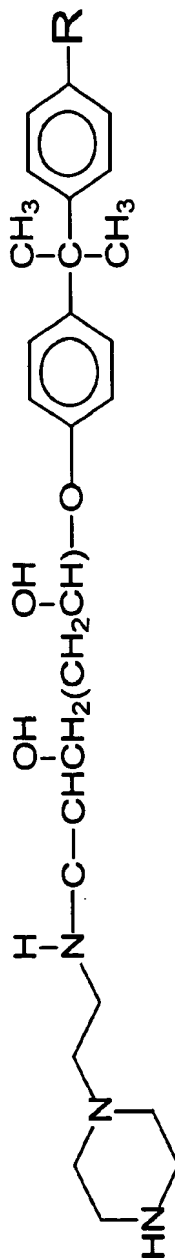
Schiff Base Rxn Scheme with Epoxy Resin



Protonated Acetone



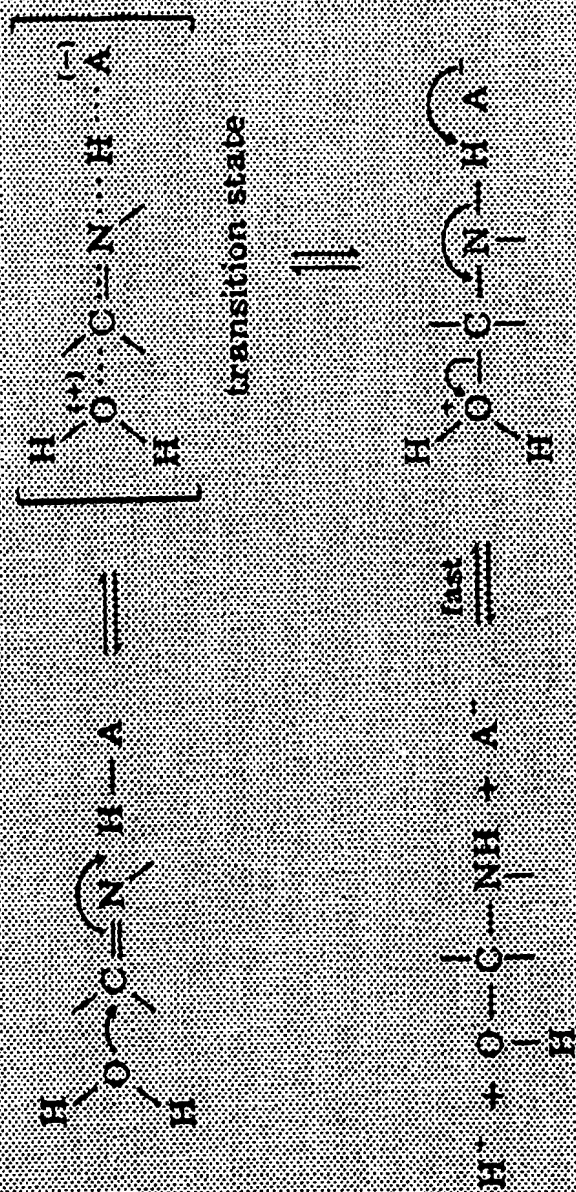
N-aminoethylpiperazine



Water's attack on Schiff Base Imine

C. THE AMBIGUITY OF THE ASSIGNMENT OF THE SITE OF CATALYSIS

Consider the attack of water on an imine, such as a Schiff base or oxime, and the reverse reaction, which is the dehydration of the carbinolamine addition compound. These reactions are subject to general acid catalysis, and the first problem in determining the mechanism of catalysis is to decide at what site the catalyst is acting. As shown in equation 25, it might be acting to donate a



Bronsted Plot for Imine Formation under Basic Conditions

PART I. MECHANISMS FOR CATALYSIS

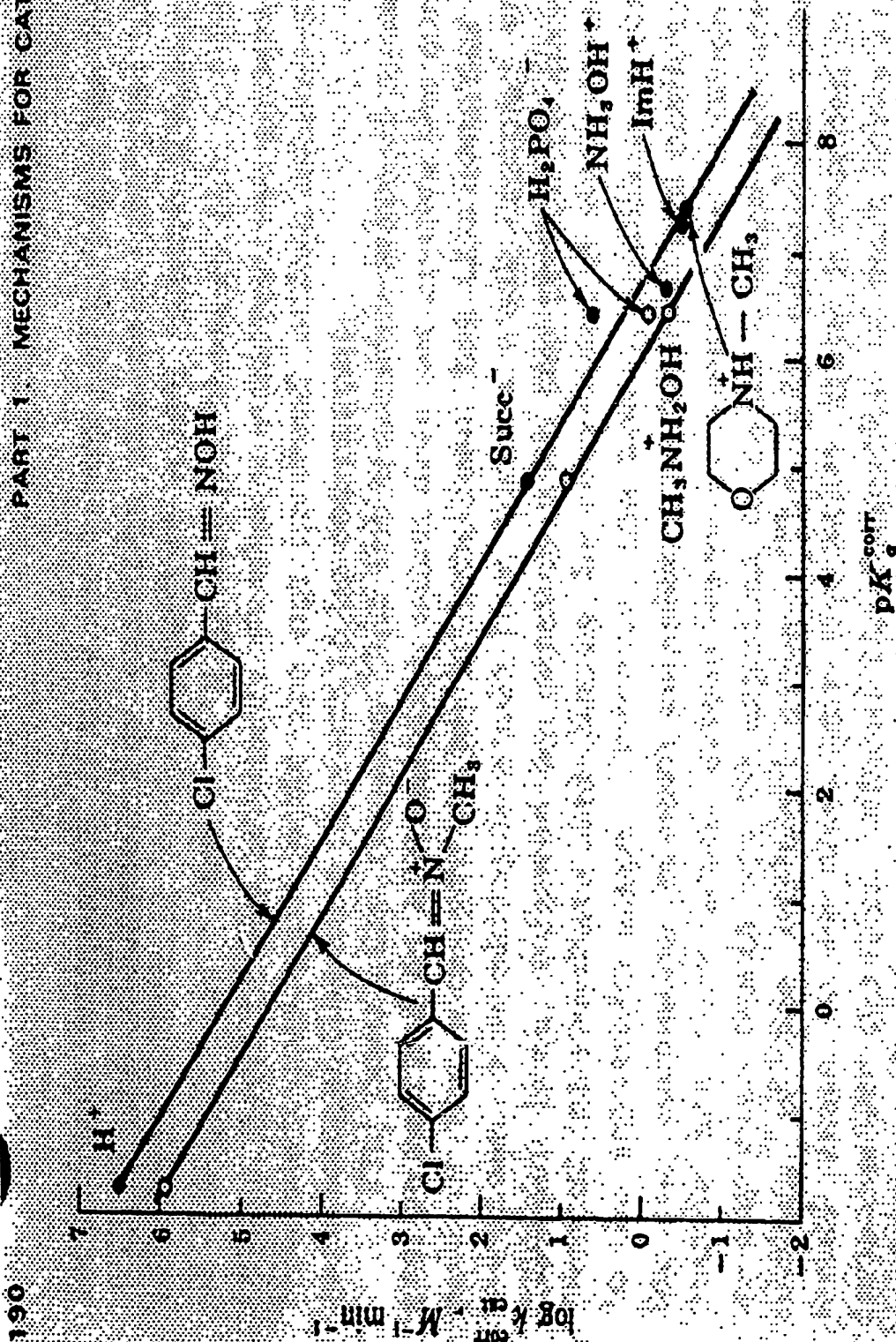
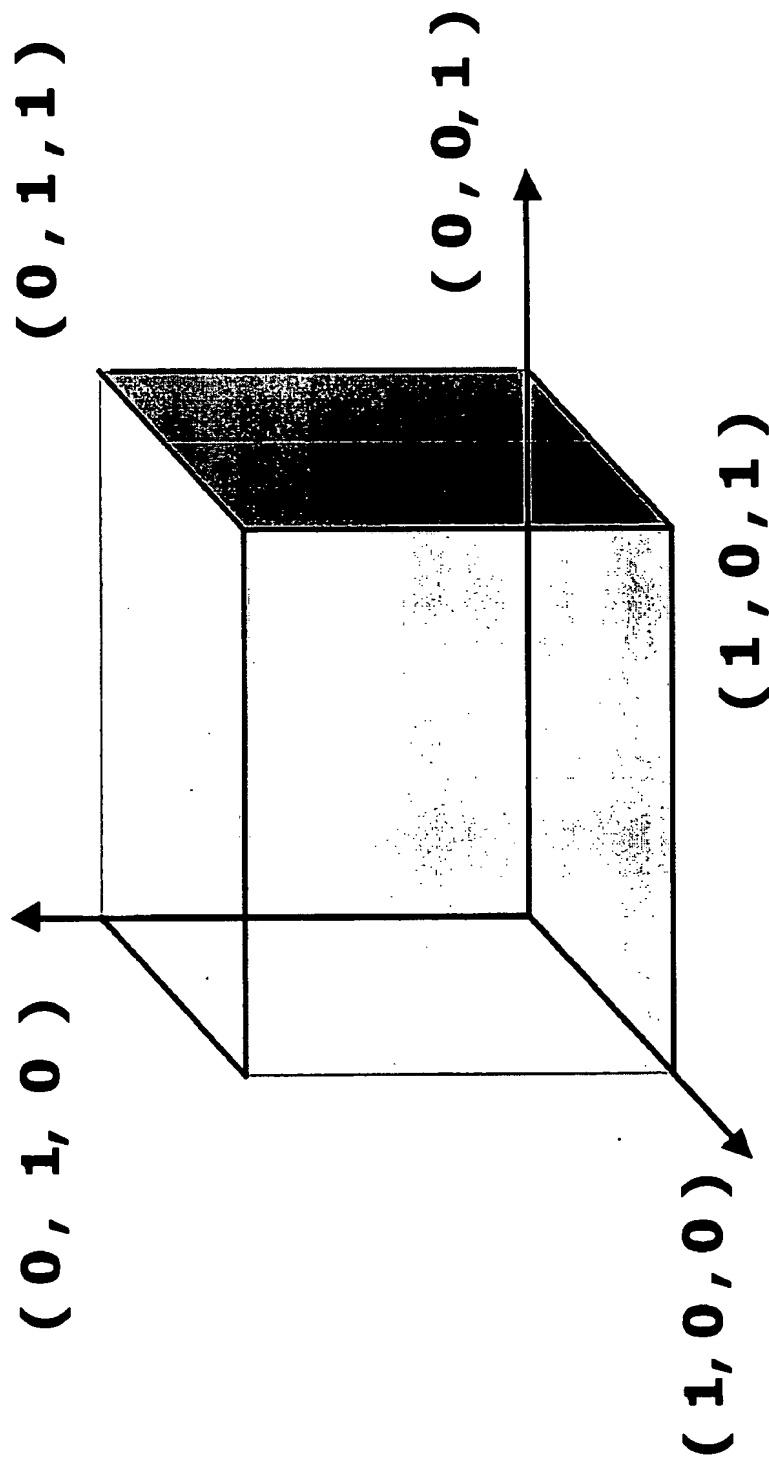


Fig 8. Bronsted plots for general acid catalysis of oxime and nitron formation.

Factorial Experiment: Independent Variables

Definition: An experiment where the response depends upon varying the amount of two or more independent factors over chosen levels. A change in response is measured relative to the change in factor levels while simultaneously holding the levels of other factors constant. Changes in response are called the main effects and the interaction between factors. Factorial studies are best used when variables are independent of each other, classic examples of variables are time, temperature, and pressure.

Three Factor Design Space for Factorial



All three factors in design are not related through any common plane connecting them all simultaneously -INDEPENDENT

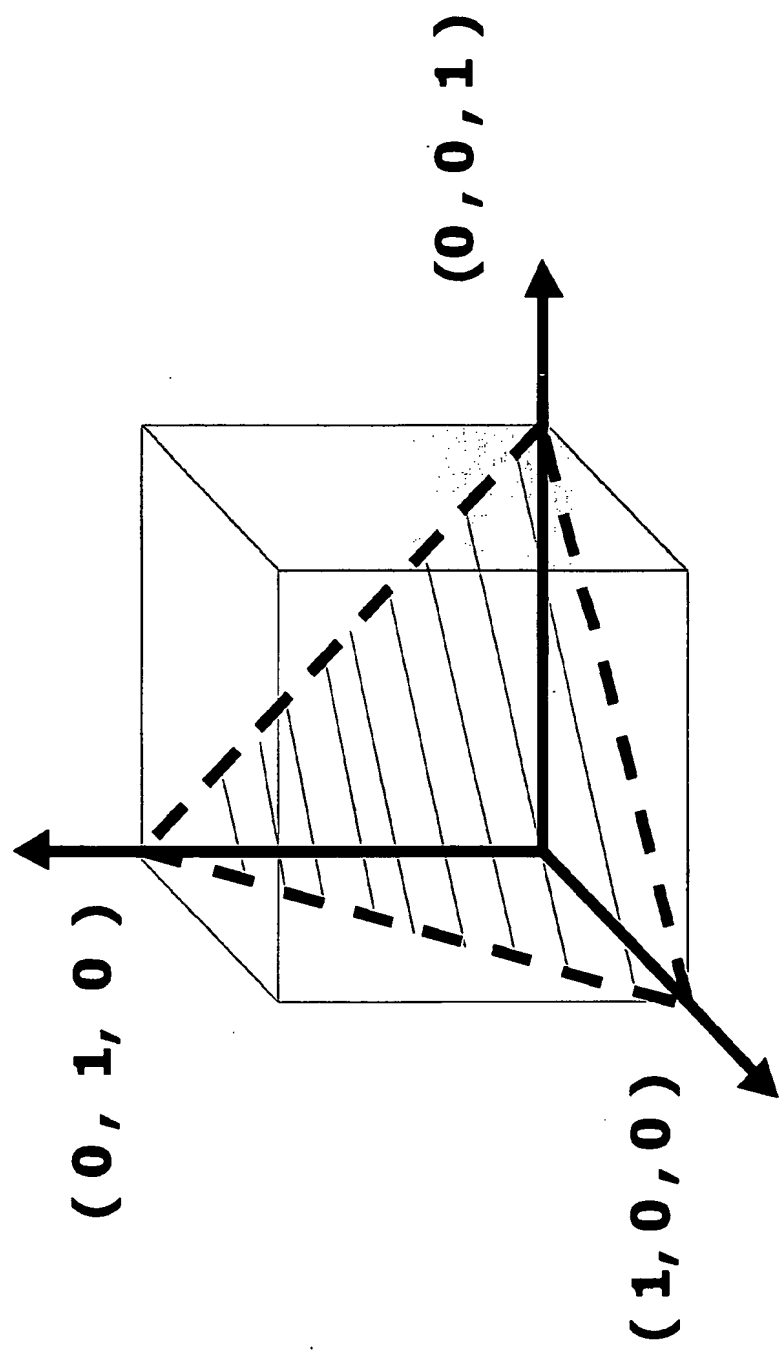
Mixture Experiment dependent Variables

Definition: An experiment where the response depends upon the relative proportions of the ingredients present in the mixture and NOT on the amount of the mixture. In a mixture experiment the total amount of ingredients is held constant. The measure of the response is said to be a measure of the joint blending property of the ingredients of the experiment.

Mixture experiments are best used when variables are dependent upon one another

e.g. polyol A, polyol B, & polyol C

Mixture 3-d Design Space Unit Cube



All three factors in design are related through a common plane connecting them simultaneously making them -Dependent

Response Function from Deterministic Model

For a system containing q components the response function f^t from equation 1-A is expressible as a first or second degree polynomial

$$\eta_i = \beta_o + \sum \beta_i x_i + \varepsilon_i \quad (\text{first degree polynomial})$$

$$\eta_i = \beta_o + \sum \beta_i x_i + \sum_i \sum_j \beta_{ij} x_i x_j + \varepsilon_i \quad (\text{second degree polynomial})$$

In an experimental design consisting of N trials, the observed value of the response is denoted by y_u and it is assumed that y_u in the u^{th} trial varies about a mean η with a common variance of σ^2 for all $u = 1, 2, \dots, N$

After the N observations are collected, the unknown parameters or coefficients in the model are estimated by *method of least squares*, and the coefficients are substituted into the model for use in predicting response values.

Linear Regression Design for Mix Experiment

Assume a functional relationship exists for some property of a coating that can be treated as a random variable η whose distribution depends upon:

I. The proportions of mix variables $u_i = (x_1, x_2, x_3, \dots, x_n)^t$ of real numbers denoting a point in formulation space

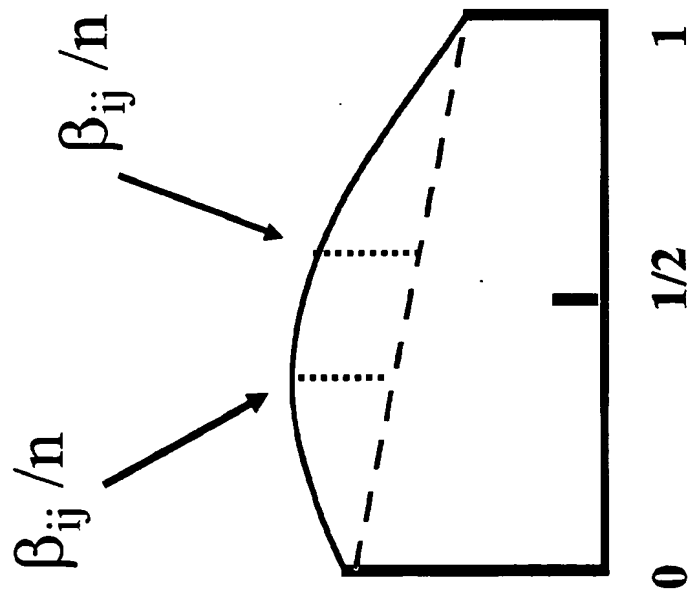
II. A set of "p" parameters $b = (b_1, b_2, b_3, \dots, b_p)^t$ the "p" are unknown to the formulator but are of primary interest because if these parameters are found, the proposed model η is determined.

The deterministic model is ascertained from each of the crucial coating properties and assuming a linear regression model

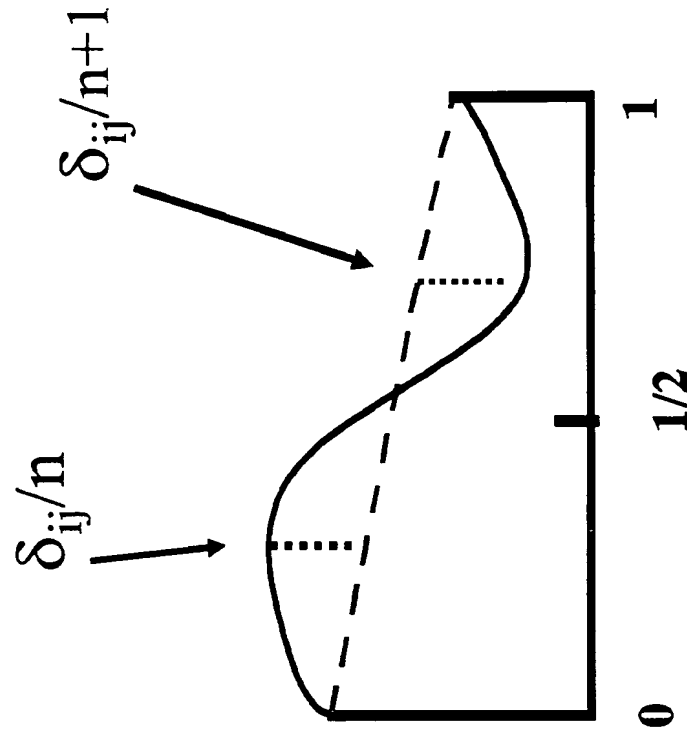
$$\text{equation 1-A} \quad \eta_i = f^t(u_i)b + \varepsilon_i, \quad i = 1, 2, \dots, n$$

where ε_i is the normally independently distributed random error element

Nonlinear Blending of Binary Mixtures



Quadratic Blending $\beta_{ij} > 0$



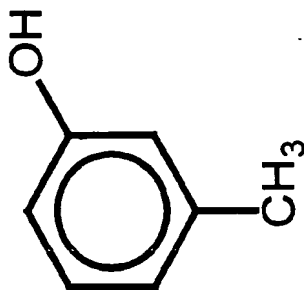
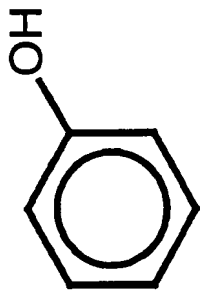
Cubic Blending $\delta_{ij} > 0$

Hydroxylic Accelerators for Most Amines

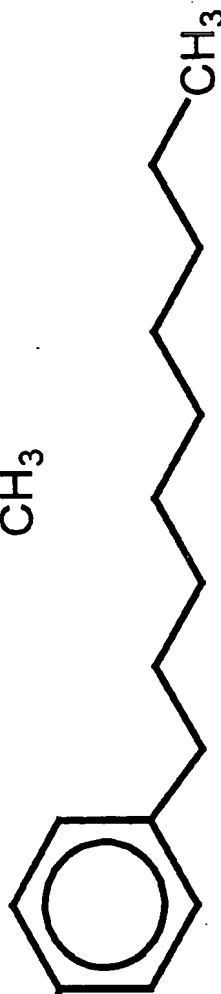
Essentially suck-up and add H₂O to System

Phenols

phenol, cresol

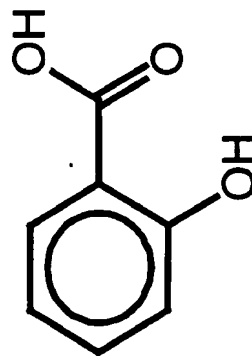


nonylphenol



Acids

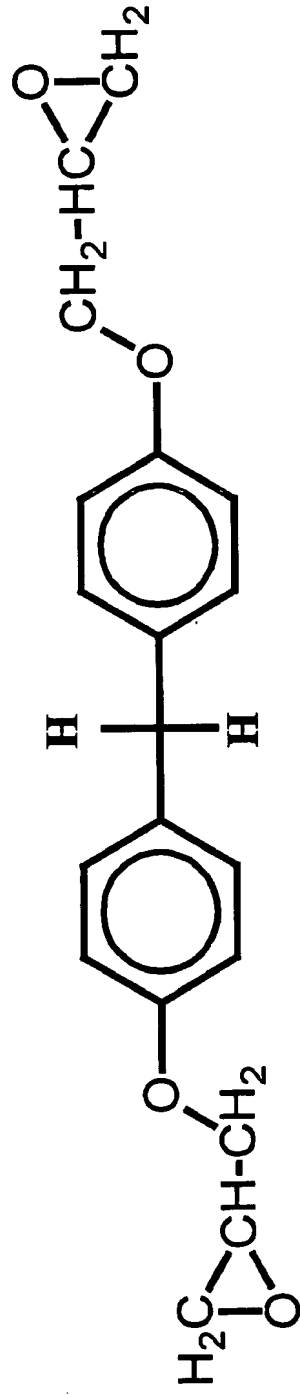
Salicylic acid



Liquid Base Resins Epon 862

- BPF - (Bisphenol of Formaldehyde)
(diphenolmethane)
- Viscous liquids ranging from 2000 to 6000 cP.
EPON Resin 862
Araldite GY 282

$$\gamma = 47.8 \text{ mN/m}$$



Acetone Reflux 6-hrs: Correlation to mixture 58 PVC

Summary Statistics for Mixture Response

Response: Y

Summary of Fit

RSquare	0.885591
RSquare Adj	-0.02968
Root Mean Square Error	0.582625
Mean of Response	2.037
Observations (or Sum Wgts)	10

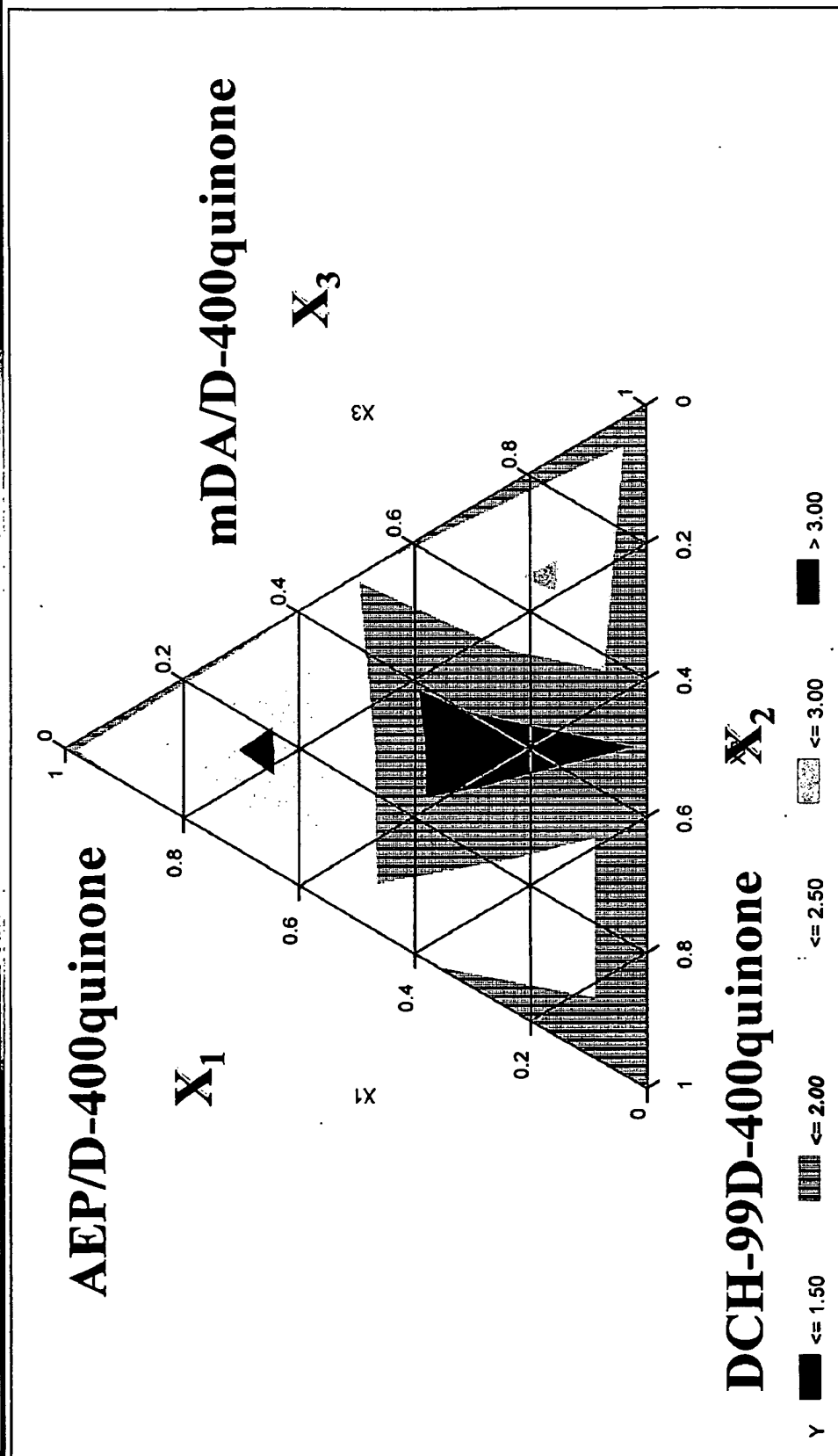
What's Happening Here ?

Effect Test

Source	Nparm	DF	Sum of Squares	F Ratio	Prob>F
X1	1	1	4.7798358	8.4879	0.0435
X2	1	1	2.5874738	4.5947	0.0987
X3	1	1	3.9161290	6.9541	0.0578
X2*X1	1	1	0.2697406	0.4790	0.5270
X3*X1	1	1	0.0489070	0.0868	0.7829
X3*X2	1	1	0.0055717	0.0099	0.9256

Acetone Reflux 65 PVC Weight loss Contour Plot

Contour Plot of Acetone Reflux PVC 65 Weight Loss



58-PVC 6-hr Acetone reflux weight loss

F ratio test results, Test Statistic: $F(3, 10, 0.05) = 3.71$

X_1	X_2	X_3	$X_1 X_2$	$X_1 X_3$	$X_2 X_3$
16.01	8.06	10.00	0.54	0.001	0.03

For X_1, X_2 , & X_3 F ratios are > 3.71 ; The null hypothesis

$H_0: \beta_1 = \beta_2 = \beta_3$ and/or $\beta_{12} = \beta_{13} = \beta_{23} = 0$ is rejected and conclude that *nonplanar binary blending* may be present and the surface may not be planar

For $(X_1 X_2), (X_1 X_3)$, & $(X_2 X_3)$ F ratios are < 3.71 ; Accept : H_A : The response does depend on mixture components; we conclude that response surface is *non-planar* and valid for all two-factor interactions

$$H_A: \beta_1 \neq \beta_2 \neq \beta_3 \text{ \& } \beta_{12} \neq \beta_{13} \neq \beta_{23} \neq 0$$

65 -PVC Oxide Layer development

F ratio test results, Test Statistic: $F(3, 10, 0.05) = 3.71$

X_1	X_2	X_3	$X_1 X_2$	$X_1 X_3$	$X_2 X_3$
854.7	822.8	588.6	2.95	2.33	1.95

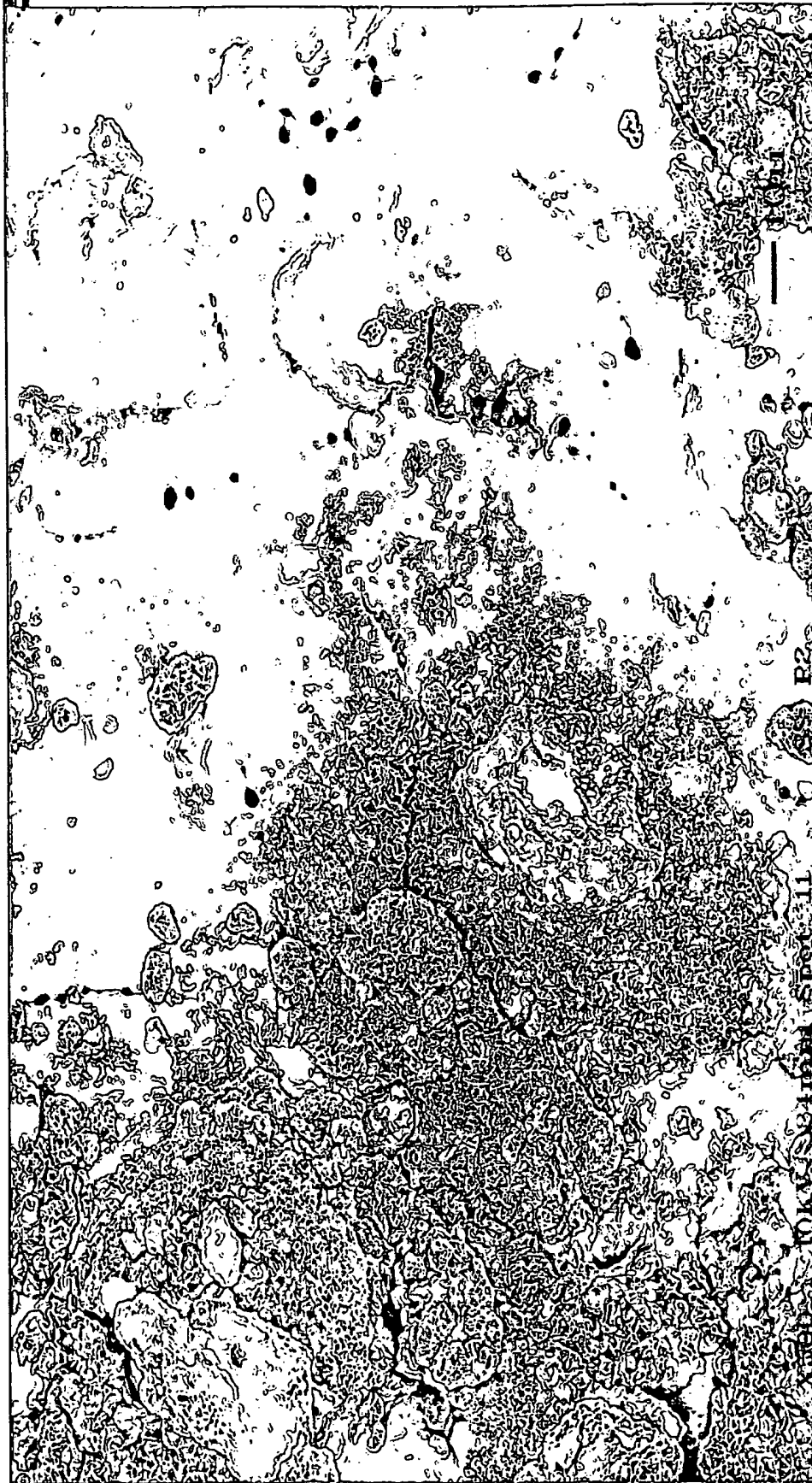
For X_1, X_2 , & X_3 F ratios are $\gg 3.71$; The null hypothesis

$H_0 : \beta_1 = \beta_2 = \beta_3$ and/or $\beta_{12} = \beta_{13} = \beta_{23} = 0$ is rejected and conclude that *nonplanar binary blending* may be present and the surface may not be planar

For $(X_1 X_2), (X_1 X_3)$, & $(X_2 X_3)$ F ratios are < 3.71 ; Accept : H_A : The response does depend on mixture components; we conclude that response surface is *non-planar* and valid for all two-factor interactions

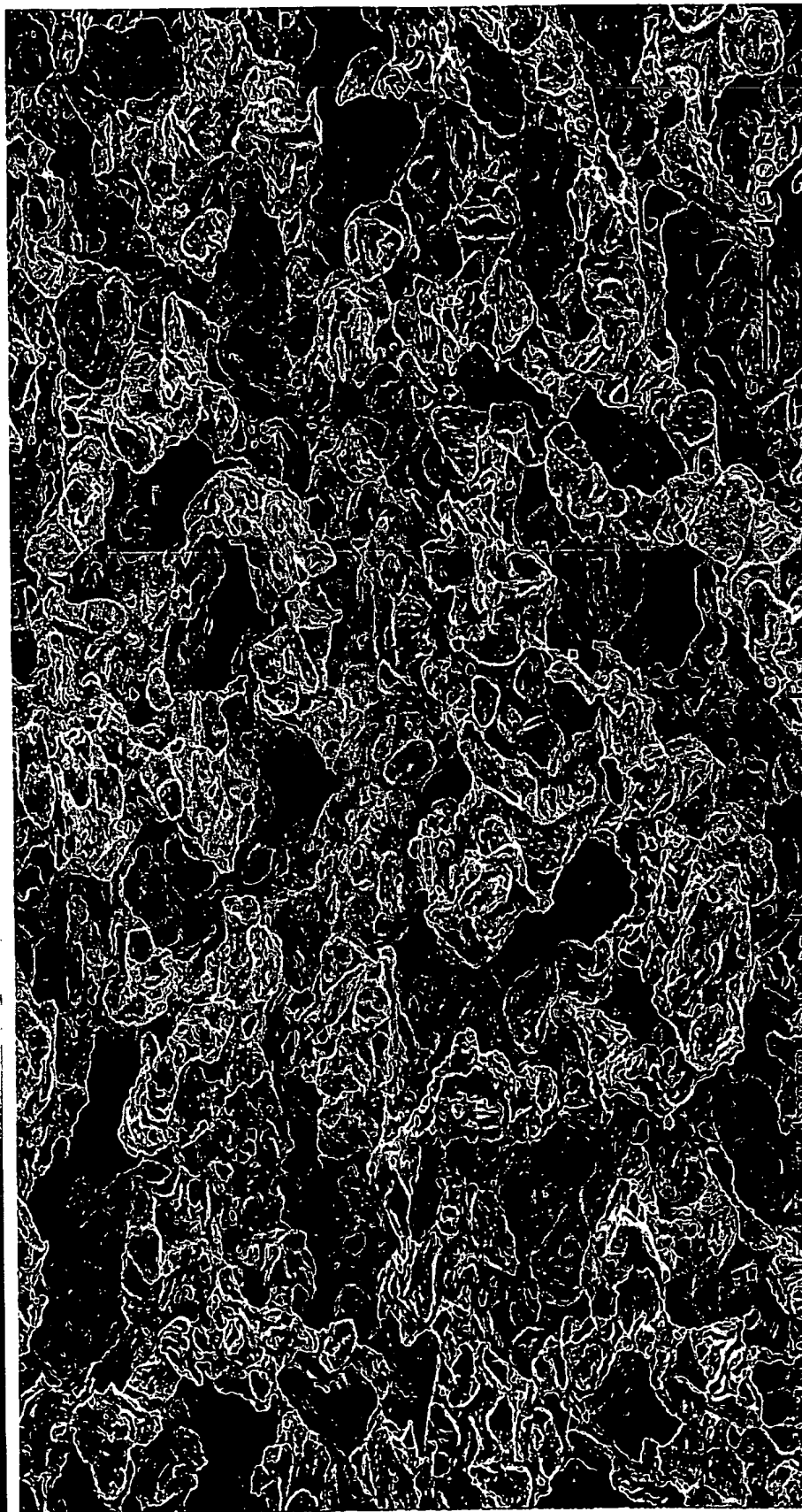
$H_A : \beta_1 \neq \beta_2 \neq \beta_3$ and/or $\beta_{12} \neq \beta_{13} \neq \beta_{23} \neq 0$

SEM 500X Prohesion Exposed Surface of Epoxy Magnesium
Primer with Hydroxide & w/o in bare matrix



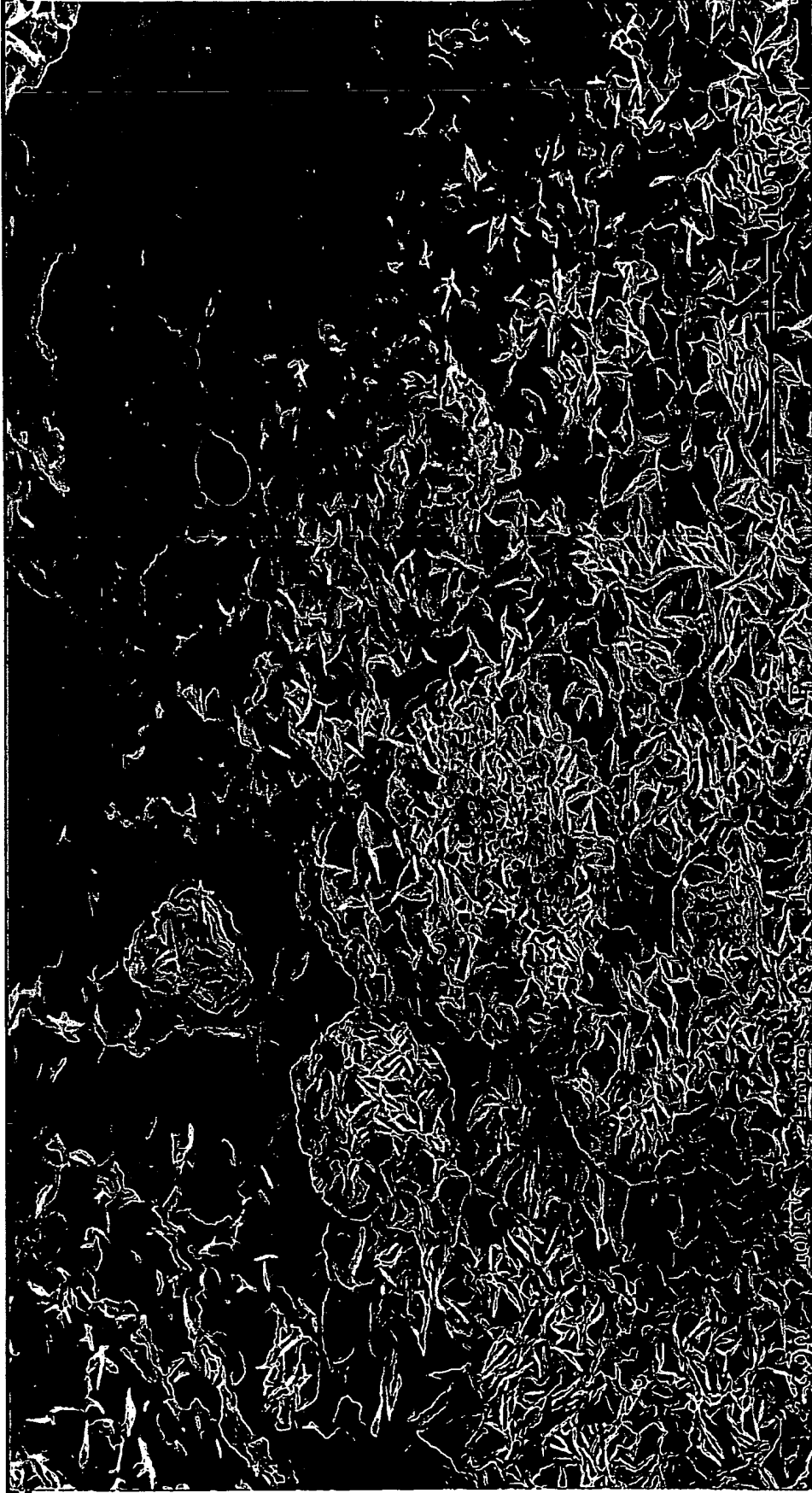
Title: EPOXY - MG COATING
Comment: SAMPLE 200136 LEAST MG ON AL 2024

**SEM 100X Prohesion Exposed Surface of Epoxy Magnesium
Primer with Leached Epoxy Resin Matrix Exposed**



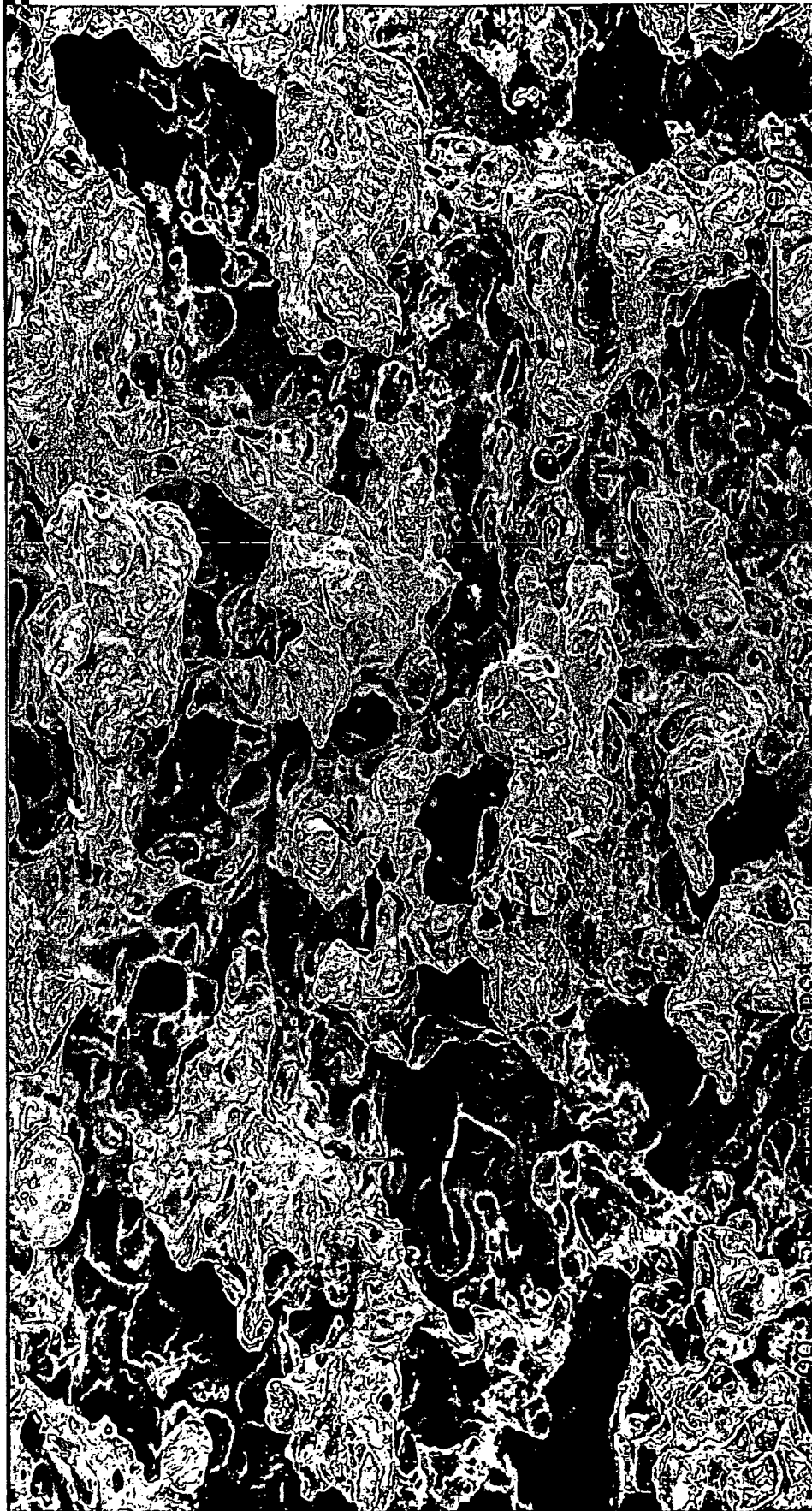
**Title: EPOXY-MG COATING BROWN AREA
Comment: SAMPLE 200138 HIGHEST MG LEVEL**

**SEM 2000X Prohesion Exposed Surface of Epoxy Magnesium
Primer with Hydroxide & w/o in bare matrix**



**Title: EPOXY – MG COATING
Comment: SAMPLE 200136 LEAST MG ON AL 2024**

**SEM 100X Prohesion Exposed Surface of Epoxy Magnesium
Primer with Leached Epoxy Resin Matrix Exposed**

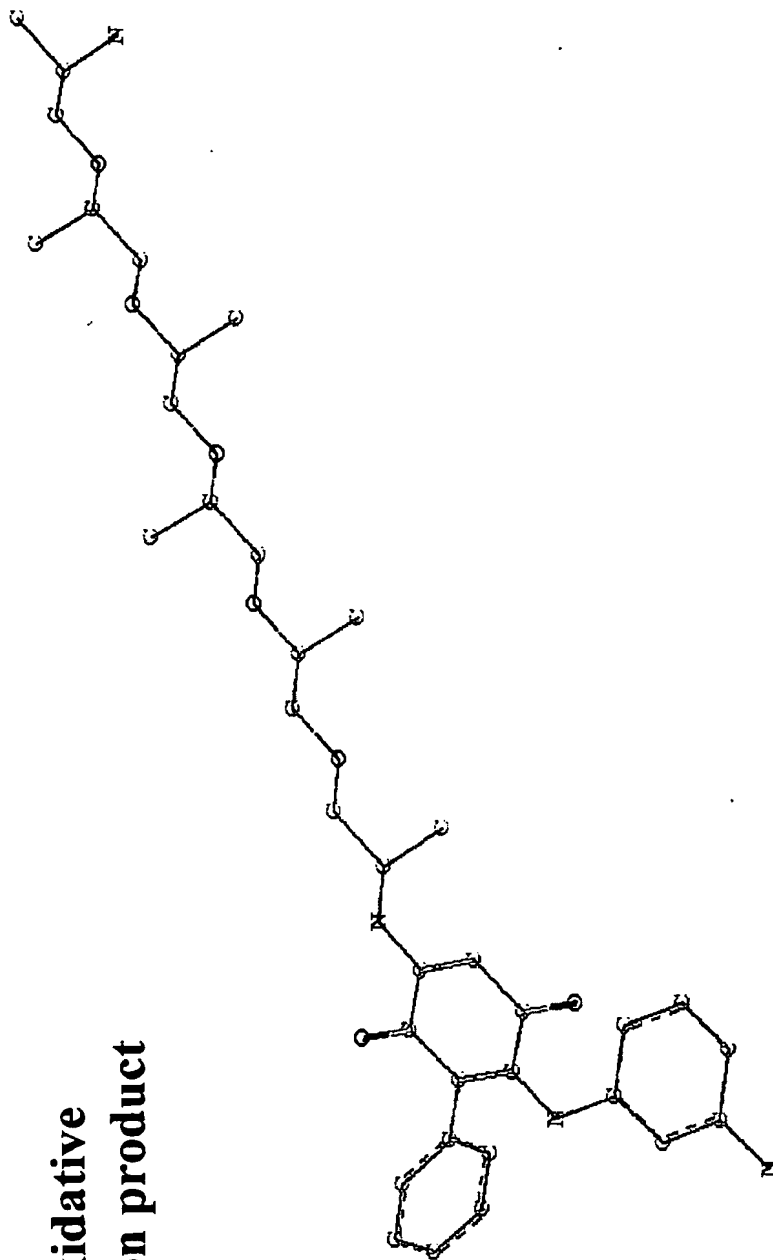


**Title: EPOXY — MG COATING
Comment: SAMPLE 200137 BROWN AREA**

m-Phenylenediamine-phenylquinone/Jeffamine D-400

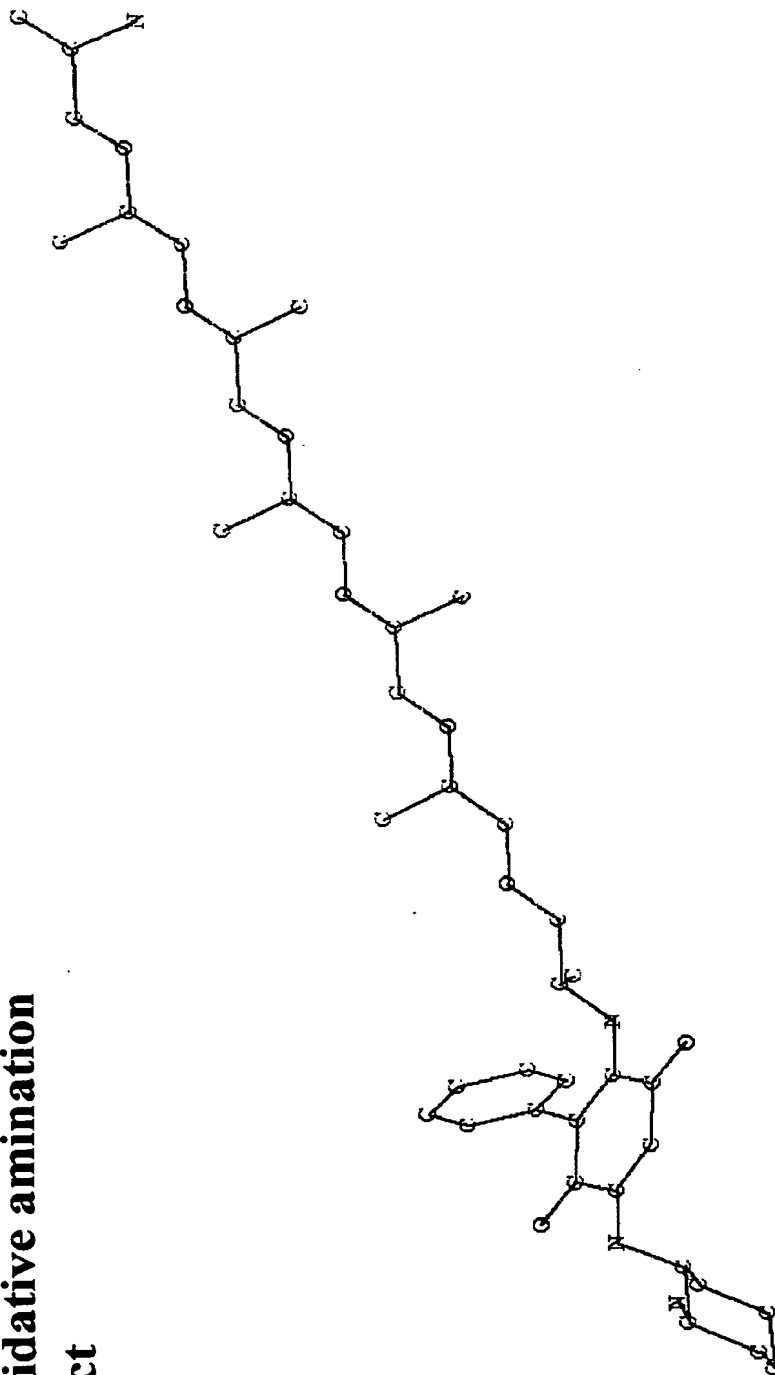
mDA and Jeffamine

D-400 oxidative
amination product



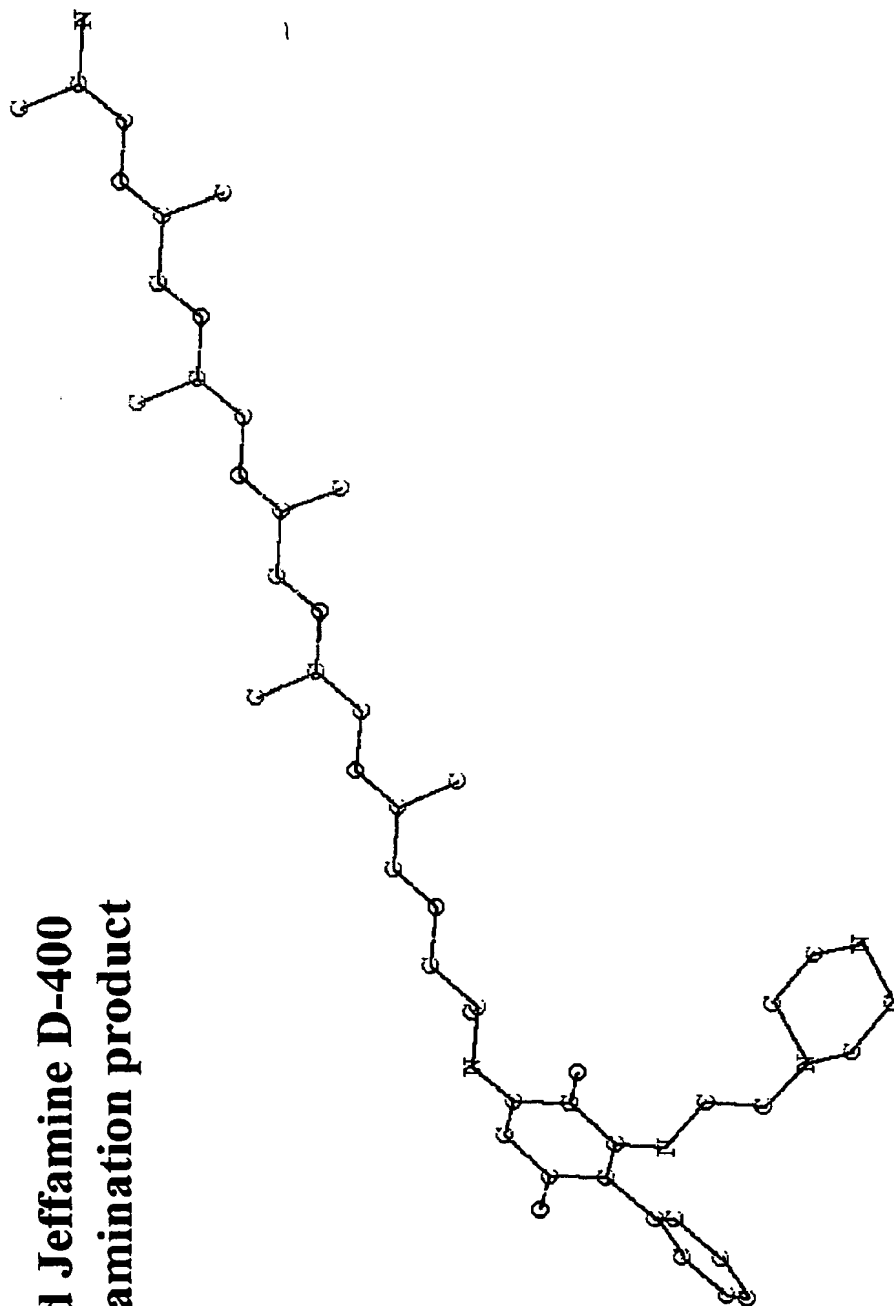
Dicyclohexanediamine-phenylquinone/Jeffamine D-400

DCH-99 and Jeffamine D-400
oxidative amination
product



Amino-ethylPiperazine-phenylquinone/Jeffamine D-400

(AEP) and Jeffamine D-400
oxidative amination product



PART XIV

Certain aspects and embodiments of the present invention are described in the following text.

Binders used in Mg-Rich Coatings as Cr-free Primers for Al 2024 T-3

Polymeric binders suitable for Mg-rich cathodic protective coatings applied *in situ* to Al 2024 T-3 structures require high pH stability, excellent adhesion, and ease of handling and application. Aromatic polyisocyanates based upon 4-4'-Diphenylmethane Diisocyanate and liquid bisphenol-A epoxy cured with polyalkylamine Mannich bases are two binders of choice used in coatings subjected to high pH conditions as well as in zinc-rich cathodic coatings. Work has continued on the use of Mg-rich coatings as substitutes for Cr-free primers for Al 2024 T-3. The primer provides damage protection in scribed areas, and the reaction products of Mg oxidation do not attack the Al substrate. In the current study three binder systems, based upon the above mentioned polyisocyanate and epoxy, plus a silane modified polyisocyanate/epoxy hybrid were formulated into primers at critical pigment volume concentration (CPVC) applied to Q-Panel Al 2024 T-3, then subsequently top-coated with an Extended Lifetime™ coating. Scribed coatings were subjected to Prohesion™ exposure in dilute Harrison's solution with open circuit potential measurements (OCP) made in a 3% sodium chloride solution. Corrosion byproduct generated in scribes during Prohesion™ exposure was measure for pH and analyzed by FTIR and EDX. Overall, it was found that coatings prepared with primers that resisted change in pH along the scribed areas provided a higher level of cathodic protection.

PART XV

Certain aspects and embodiments of the present invention are described in the following text and figures.

Examining Mg-Rich Primers for Al 2024 T-3: Recent Results and Application of Coating System Test Protocol

ABSTRACT

Work begun over two years ago on the use of particulate Mg as a pigment for corrosion protective primers for Al 2024 T-3 has reached the point where several such systems are viable candidates for use in totally Cr-free coatings systems. Using a unique Mg pigment stabilized against air oxidation, initial studies showed that Mg-rich systems gave sacrificial protection of Al without causing corrosion and dissolution of the metal at high pH values caused by Mg oxidation products. Further studies showed that the primer coating by itself and when top-coated exhibited no special fire hazard problems even with the use of the particulate Mg. Initial electrochemical studies showed that the Mg-rich primer developed electrical contact to the Al 2024 T-3 substrate and exhibited mixed-potential behavior directly analogous to the protection of steels by Zn-rich primers. When top-coated with the Extended Life Topcoat (ELT) that is now the topcoat of choice for many AF uses, the initial data indicated that the total coating system provides such excellent protection against corrosion and exterior weathering without any need for Cr-based pretreatments or primer that its performance has exceeded the present coatings system with (ELT + MIL-C-23377 -chromate primer + chromate pretreatment). New results are presented on the reproducibility of these results and the enhancements made to the polymer system used with the Mg-rich pigmentation for improved adhesion and corrosion protection. The results for the test protocol that has been used will be presented for both the best current variants of the Mg-rich primer in comparison to the present system for all parts of the protocol.

INTRODUCTION

Active metal coating systems can be represented in terms of a convenient model that facilitates the design and evaluation of coatings for corrosion control. Zinc-rich systems have been the active metal system of choice for protecting ferrous substrates; however, zinc is not the only active metal used in these systems. Recent reviews of this technology describe this type of coating system.^{1,2} Further, the addition of aluminum flakes and powders to yield mixed metal-rich systems that deliver highly effective cathodic coatings for corrosion control of steels.¹ However, this technology has not been seriously investigated, developed, and applied to an analogous metal rich cathodic coating system for corrosion control of aluminum and its alloys. Traditionally, chromates and chromate treatments have gained the widest acceptance in corrosion control of aluminum and its alloys. In considering a parallel approach to the design of an analogous metal-rich system, for cathodic protection of aluminum there is only one engineering metal more usable than aluminum itself that may be used as a sacrificial anode, namely magnesium. The primary concern associated with designing such an active metal coating system based on a particulate, pigmentary form of magnesium is the issue of the metal's high reactivity and stability in air. Normally powdered Mg represents both a fire potential in manufacture and use of the pigment itself. Fortunately, this concern has been overcome by advanced production technology employed by Eckart GmbH, Velden Germany in their manufacture of pigmentary grades of magnesium. These micron sized powders are commercially available from Eckart GmbH as ECKA™ metallic magnesium powder produced from magnesium 99.95 % and conform to (Deutsches Institut für Normung) DIN 17800 part-7 standards with Mg content @ 96% and MgO (magnesium oxide) content @ 4%. The handling and use hazards are overcome by the formation of a stable oxide layer over the reactive metal greatly reducing the metal powders reactivity. This technology is an extension of the use of controlled Al₂O₃ layers to stabilize Al pigments in water-borne coating systems. The second problem that could be anticipated in the use of Mg in a protection system for Al is the potential formation of a locally high pH environment about the Mg oxidation products which will form in the cathodic protection of Al. The second concern was that the oxidation products of Mg, MgO and its various hydroxides in hydrated form, would create such basic conditions that Al would undergo basic corrosion[†] as is indicated in its Pourbaix diagram.³ It was observed experimentally that the natural Mg oxidation products do not yield a pH high enough to corrode and attack the Al 2024 T-3 alloy, so this concern was also alleviated.

EXPERIMENTAL STUDIES

The mechanism of protection of the alloy by the pigmentary Mg is initially simple, anything with a corrosion potential above the -1.2 V vs SCE of Mg protected from oxidation. This protection potential decreases with time as the Mg is consumed and the E_{corr} drifts positive to the E_{corr} of bare 2024 T-3.⁴ We have seen this in our initial studies of the Mg-rich primers exposed without a topcoat in 3% NaCl solution as well as in later studies of topcoated and scribed Mg-rich primers. Our current electrochemical studies of Mg-rich primers topcoated with the Deft 99 GY-001 ELT™ (Extra Life Topcoat) system without scribing are being performed on systems in both the full exposure protocol^{5,6} (QUV alternating with Prohesion) and in Prohesion only. We are attempting to follow the E_{corr} for the full system during exposure from the EIS experimental potential settings taken prior to each EIS data set.

[†] Eckart GmbH, Kaiserstrasse 30, Furth D-90763, Germany

POLYMER DEVELOPMENT STUDIES

Adhesion is the most important property of an organic coating, when a coating's adhesion fails it becomes worthless. It has been well documented that the best deterrent to adhesion failure in organic coatings lies in developing the right chemical interactions between the binder, pigment, coating layers, and their metallic substrates.⁷ Organo-functional silanes are commonly used as coupling agents and adhesion promoters in epoxide and urethane paints to improve their initial, wet, and recovery of adhesion to aluminum surfaces. Walker^{8,30} describes the reversible breaking of and reformation of stressed bonds between a coupling agent and the substrate and allows stress relaxation without the loss of adhesion when water is present. It is argued that when Si-O-metal bond is broken by intrusion of water, the bond is capable of reforming with some recovery in adhesion. Incorporation of organo-functional silanes requires judicious solvent selection to minimize side reactions that can occur between the organic binder, water and organo-functional silane. The solvent must effectively reduce vehicle viscosity and promote good wetting of the Al alloy substrate. Propylene Carbonate is a high boiling, non-volatile, HAPS compliant, liquid with low toxicity that is completely miscible with many organic solvents such as glycol ethers and is often used as urethane viscosity reducer. In addition, 2-ethyl-3-ethoxypropionate (EEP) is another non-HAPs solvent that has been found effective at retarding isocyanate reactions. Both of these solvents have are suitable in the hybrid epoxy/urea polymer systems as formulated with organo-functional silanes and reactive polyisocyanates. The polymeric materials chosen for the primer was a mixture of epoxy and polyisocyanate (both aromatic MDI and aliphatic HMDI) prepolymers were used. However, what remains to be investigated is the effect of mixtures of aliphatic (HMDI) and aromatic (MDI) prepolymers used in these hybrid systems. The epoxy prepolymer used was Epon 1001X type, as reviewed in *chapter 2.9*, and the polyisocyanates were Desmodure E-23A, a prepolymer of diphenylmethane diisocyanate (MDI), and hexamethylene diisocyanate (HMDI). The moisture cure mechanism involves isocyanate functionality from either HMDI or MDI prepolymers, converted into primary amine, forming both amines and carbon dioxide, that are intermediates in the Hoffmann rearrangement of an isocyanate with water to yield a reactive / reaminated labile amino functionality.⁹ The resulting reaction facilitates the cure of epoxide functionality as well as the remaining isocyanate to yield an epoxy-urea polymeric material. The advantage of such an epoxy-polyurea system lies in 1) the relatively low concentration of amine MEK Schiff base required to cure mixtures of epoxy /polyisocyanate and 2) improved solubility of epoxy 1001X epoxy resin in liquid polyisocyanate. Both effects contribute to improved pigment dispersion in the formulated coating which will be discussed in the following sections.

The simultaneous formation of crosslinking based on two different reactions, as well as materials with different solubilities and mechanical properties sometimes creates what are known as interpenetrating polymer networks (IPN's) as polymer alloys. These consist of two or more distinct crosslinked polymer networks held together by permanent entanglements.¹⁰ Frisch *et al.*¹¹ first reported simultaneous interpenetrating networks (IPNs) composed of a polyurethane (PU) combined with an epoxy polymers. The epoxy backbone promotes toughness and flexibility to cured films while the carbon-carbon and the urethane bonds of the same improve solvent resistance, and adhesion. The epoxy-urethane reaction occurs when the secondary hydroxyl group in the epoxy backbone is reacted with an isocyanate which gives rise to the hybrid structure of such IPNs.¹² 2-ethyl-3-ethoxypropionate (EEP) is primarily used as a retarder in coatings containing polyisocyanates as it possesses slight water solubility, non-toxic, has a low vapor pressure, and is not a skin irritant. In this coating

system EPP has been found to be an effective retarder when used at about 10 percent total solvent. Propylene carbonate (PC) is commonly used as a urethane prepolymer viscosity reducer.²⁴ PC is the primary carrier solvent used in this system, it is used as an isocyanate retarder and wetting agent. Propylene carbonate wets both aluminum and magnesium powder and is an excellent solvent for both the epoxy and polyisocyanate. Both solvents have been found suitable in Mg-rich coatings with organo-functional silanes and polyisocyanates such as hexamethylene diisocyanate (HMDI). On the other hand, moisture-cure polyureas (MCPUR's), such as prepolymers of diphenylmethane diisocyanate (MDI) Desmodur™ E23-A from Bayer Corp., are recommended for use in Zinc-rich coatings applied to steel structures, but the recommended starting formulations and require photo-active aromatic solvents such as xylol that are environmentally unacceptable.¹³

PREPARATION OF SILANE MODIFIED EPOXY-UREA COATINGS

The synthesis of the hybrid polymeric materials was described in this paper. The reactions are carried out in propylene carbonate / 2-ethyl-3-ethoxypropionate (EEP) solvent mix. The crosslinker is thought to react with either the polyisocyanate or epoxy oxirane ring (Epon1001CX) or it may be reacted with an epoxy to form an intermediate that in turn moisture cures with (either polyisocyanate) MDI and HMDI. It is surmised that both hybrid polymeric material systems in this study yield multiple organosilicate (Al-O-Si-R-) crosslinked structures. Table -1, below, lists the materials used in the four coating polymer systems evaluated as primers for Mg-rich coatings: two conventional coatings and two hybrid coatings. The carrier solvent for MC-PUR and the epoxy / polyamide was xylol, an aromatic hydrocarbon solvent mixture, while the carrier for the two hybrid coatings was a 90:10 mix of propylene carbonate (PC) and 3-Ethoxypropionic acid ethyl ester (EEP) both HAPS compliant solvents.

Table 1: Magnesium Rich coating materials

Designation	Material	Supplier
Desmodur® E23-A	MDI polyisocyanate	BAYER
Desmodur ® N3300	HMDI polyisocyanate	BAYER
Bentone® 34	Modified clay	RHEOX
Epon® 1001CX	Bisphenol A epoxy	RESOLUTION
Epon® 828	Bisphenol A epoxy	RESOLUTION
Epicure® 3115	Fatty acid polyamide	RESOLUTION
Eckagranules® PK 31/PK51	Magnesium powder	ECKART
OSi Silwet A 1120	Amino-silane	WITCO
Aerosil R202	Fumed silica	DeGUSSA
Anti Terra U	Wetting agent	BYK Chemie
E LT™	Topcoat	DEFT

The polyisocyanates used in the study were graciously supplied by Bayer Inc[‡], Desmodur™ N3300, 1,6-hexamethylene diisocyanate homopolymer (HMDI) trimer, NCO content at 21%; Desmodur® E-23A a polyisocyanate prepolymer: 4,4'-methylene-diphenylisocyanate (MDI), NCO content at 17%. The epoxy resin and polyamide curative Epicure® 3115 were graciously supplied by Resolution Performance Chemicals[§] diglycidyl ether of bis-phenol A (BPA), 1) Epon™ 1001-X, with epoxide equivalent weight (EEW)~500; 2) Epon™ 828 liquid BPA, EEW~188. The propylene carbonate solvent, (Propasol™ P) was graciously

[‡] Bayer Polymers, 100 Bayer Road, Pittsburgh, PA 15205-9741

[§] Resolution Performance Chemicals, 1600 Smith Street, 24th Floor P.O. Box 4500 Houston, Texas 77210-4500

supplied by Huntsman Performance Chemicals^{**} and the EEP solvent from (Aldrich, Milwaukee, WI). Silquest™ (A-1120) supplied graciously by Witco OSi Specialties^{††}, N-beta-(aminoethyl)-γ-aminopropyltrimethoxysilane all chemicals were used as received.

Table 1: Magnesium Rich coating materials

Designation	Material	Supplier
Desmdodur® E23-A	MDI polyisocyanate	BAYER
Desmudur ® N3300	HMDI polyisocyanate	BAYER
Bentone® 34	Modified clay	RHEOX
Epon® 1001CX	Bisphenol A epoxy	RESOLUTION
Epon® 828	Bisphenol A epoxy	RESOLUTION
Epicure® 3115	Fatty acid polyamide	RESOLUTION
Eckagranules® PK 31/PK51	Magnesium powder	ECKART
OSi Silwet A 1120	Amino-silane	WITCO
Aerosil R202	Fumed silica	DeGUSSA
Anti Terra U	Wetting agent	BYK Chemie ^{‡‡}
E LT™	Topcoat	DEFT

The crosslinker (used in both Epoxy- HMDI and Epoxy- MDI hybrids) was the (7-PQ-6-ol) synthesized in these laboratories, and described in Chapter 4, was added at a ratio of (0.25: 1) equivalent weight (E_w) crosslinker to one E_w of NCO, with the epoxy added at a ratio of 0.75 E_w (esterification value)^{§§} to one E_w of NCO. The epoxy Epon 828 / epicure 3115 (high molecular weight, polyamide, dimerized fatty acid polyamines) was mixed at a stoichiometric ratio as recommended in product bulletin.¹⁴

CRITICAL PIGMENT VOLUME CONCENTRATION ESTIMATES FOR MG-RICH PRIMERS

CPVC is a function of the random dense packing efficiency of the pigment plus adsorbed layer thickness (δ), which must be experimentally determined. This has been discussed extensively in the literature and a recent review considers new developments.¹⁵ In this experiment two magnesium powders, (Eckagranules™ PK 31~30 μ m, and PK-51~70 μ m used as received), with different mean particle size distributions, see Figure 1, below, Aerosil R202™ a hydrophobically modified fumed silica, containing no microcrystalline silica, was used as the rheology control agent due to its effectiveness in epoxy related systems. Due to the nature of the solvents used PC and EEP, both with low vapor pressures, appreciable solvent is not volatilized when atomized via spray application, and as a result, rheology control, via an efficient agent, is necessary to ensure uniform film formation during application. The critical pigment volume concentration (CPVC) of the primers was first approximated by obtaining a resin / powder rub-up value with Aerosil R202™ at 2% vol. on total pigment volume, and the final CPVC was calculated from PSDs of the three pigments, assuming spherical geometry, combined with the experimentally determined resin rub-up values.²⁹ Figure 2 below, shows the calculated CPVCs in a ternary diagram format for the three pigment mixture. The volume fraction coordinates (PK-31 = 0.51, PK-51= 0.47, and R-202 = 0.02) yields a calculated CPVC value in the (yellow region @ PVC =0.475).

^{**} Huntsman Performance Chemicals, 3040 Post Oak Blvd., Houston, TX 77056

^{††} OSi Specialties, A Crompton Corp., One American Lane, Greenwich, CT 06831 2559, USA

^{‡‡} BYK-Chemie USA, 524 South Cherry Street, P.O. Box 5670, Wallingford, CT 06492

^{§§} Product Bulletin: RP:3062-01 / EPON™ Resin 1001F, ©2001 Resolution Performance Products

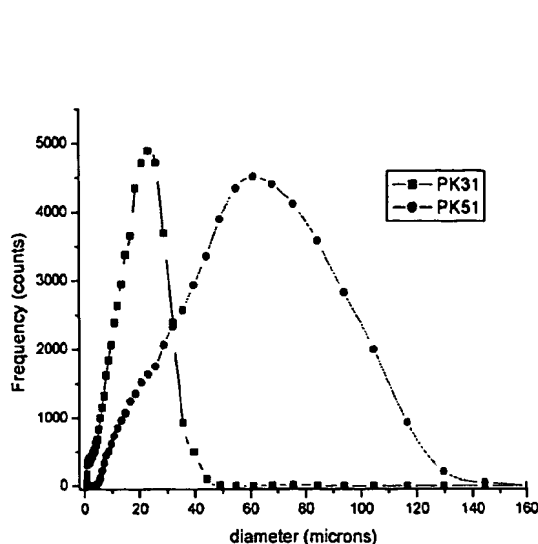


Figure 1- Particle size distributions for Mg powders, Eckagranules™ PK31 and PK51.

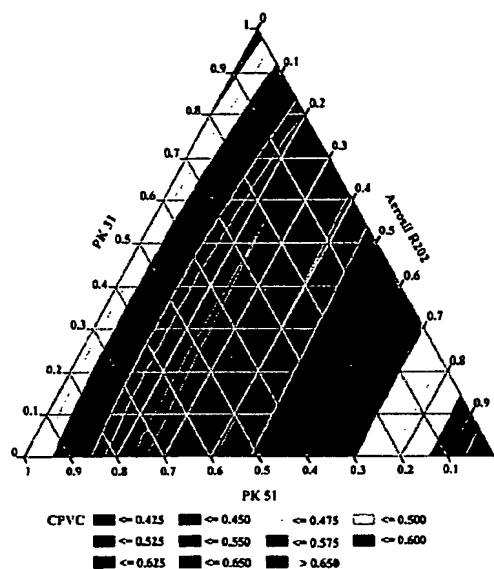


Figure 2- Ternary mixture diagram for PK31, PK-51 and Aerosil™ R202, colored areas correspond to theoretically calculated CPVCs.

Magnesium rich coatings may be viewed analogously to zinc rich systems, in that, as long as there is sufficient electrical contact within the continuous film the interface of the aluminum alloy will remain protected. However, unlike zinc, magnesium metal has a relatively low density of 1.738 g/cm³. This is in sharp contrast to zinc metal with density of 7.133 g/cm³, a denser pigment.

PANEL AND FILM PREPARATION

The primers formulated from materials in Table 1, above, were prepared using conventional techniques. Primers were applied to 6" x 3" Al 2024 T3 Q-panels™, scrubbed with a Scotch Brite™ pad, rinsed and degreased with EEP, then immersed in a 10% phosphoric acid solution for 60 seconds, then rinsed with distilled water. Al panels were surface modified with a 2% mixture of Silwet™ 1120 in acetone / water mix as described in the literature.⁸ The magnesium pigment was mixed slowly into a mixture of epoxy / polyisocyanate solvent with a 1" -diameter propeller blade mixer at 1,000 rpm. The rheology control agent Aerosil™R202 was added slowly to the pigment/binder, resin/ solvent mix after the Mg pigment was added. The resulting paint was applied with a touch-up spray gun, at a pressure setting of 60psi. The coatings were cured at 30° C for 14 days. Primed panels were subsequently top coated with Extended Lifetime™ topcoat. The average film thickness (FT) estimated from EDAX photos reveal primer film thickness to be on the order of ~50 +/- 20 microns with topcoat film thickness at ~ 100 +/- 40 microns.

COATING MORPHOLOGY

The resulting primed and topcoated panels from the four formulations given in Table 2 were observed to develop differing surface textures which are surmised to be related to: 1) pigment dispersion and the polymeric material's ability to wet the magnesium pigment; 2) the solvent evaporation and the type of thixatropes used in the study. Early on it was observed that hydrophobically modified fumed silicas such as Aerosil™R202¹⁶ which has polydimethylsiloxane groups anchored to the surface are not wet by aromatic polyisocyanate resins. According to

Schwindt¹³, the recommended thixatropes for these systems are the organically modified Bentone® clays from Rheox Corp., such as Bentone® 39, which is a hydrophobically modified bentonite clay. The Mg-rich coating systems in this study were comprised of a highly pigmented Mg-rich primer coat followed by a ELT™. The film formation process which is related to the ultimate performance of the coating system is dependent on the coating's morphology as applied to the alloy surface. As discussed previously, the CPVC is related to the maximum packing efficiency of the pigmented material in a coating. Factors leading to pigment agglomeration are known to result in coatings with inefficient particle packing which is related to the coating's CPVC. Generally, when pigment agglomeration occurs the larger the agglomerate the higher the formulated PVC must be to reach a coating's CPVC. Therefore, as a result of poor dispersion or agglomeration, the actual PVC of a poorly dispersed or agglomerated system will be formulated far above the PVC value of a well dispersed system at its CPVC. Thus, this raises the value of lambda (Λ) PVC/CPVC for poorly dispersed systems. Agglomeration of pigments, in such a case, leads to a coating below its CPVC and as a result its performance properties, as a cathodic coating, will not be equal relative to the analogous well dispersed coating system formulated at the same PVC.¹⁵

Micrographs: SEM and EDAX

To examine the sample morphology, SEM and EDAX were used. Samples were assembled on aluminum mounts and coated with gold using a Technics Hummer II sputter coater. Images were obtained using a JEOL JSM-6300 Scanning Electron Microscope. X-ray information was obtained by a ThermoNoran EDX detector using a VANTAGE Digital Acquisition Engine. Figures 5.14 and 5.15, show Al 2024 T-3 substrate, Mg-rich primer, and Deft ELT™ coating contrasted to a 50 micron scale. Figure 3 shows examples of this data.

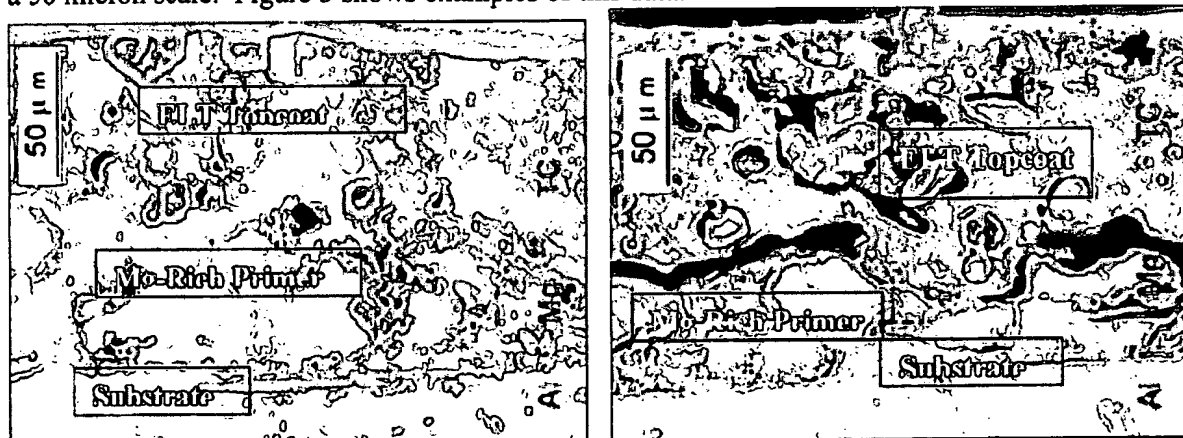


Figure 3 (a) and (b) : SEM lateral profile Mg-rich primers at 50 PVC with ELT™ (a) left silane modified MDI-polyisocyanate / epoxy-urea; (b) right, MC-PUR, MDI polyisocyanate. With (+/-) 70 micron film thickness (FT) ELT™ topcoat. Al 2024 T-3 alloy, (base), Mg powder matrix (middle); ELT™ coating (top).

SEM and EDAX cross sections of the four 50 PVC Mg-rich primers, were acquired from the same samples and are shown in Figures 4 and 5. These latter figures show the pigmentary Mg demonstrating the alignment of Mg powder at the Al interface and its distribution in the polymer matrix which is thought to be related to its dispersion in the coating's polymer matrix and ultimately to its effectiveness as a coating for corrosion control.

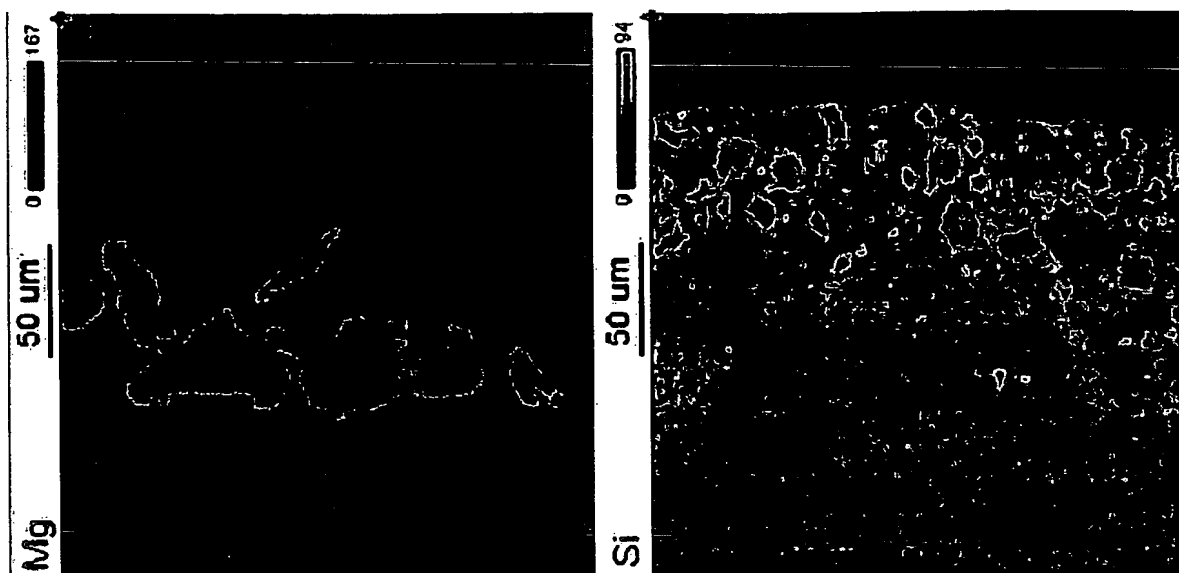


Figure 4. EDAX spectra of lateral profiles of Mg-rich coatings Corresponding to the SEM image in Figure 3 a) with X-ray fluorescence (XRF) counts for magnesium, in red LEFT, and silicone, in blue RIGHT.

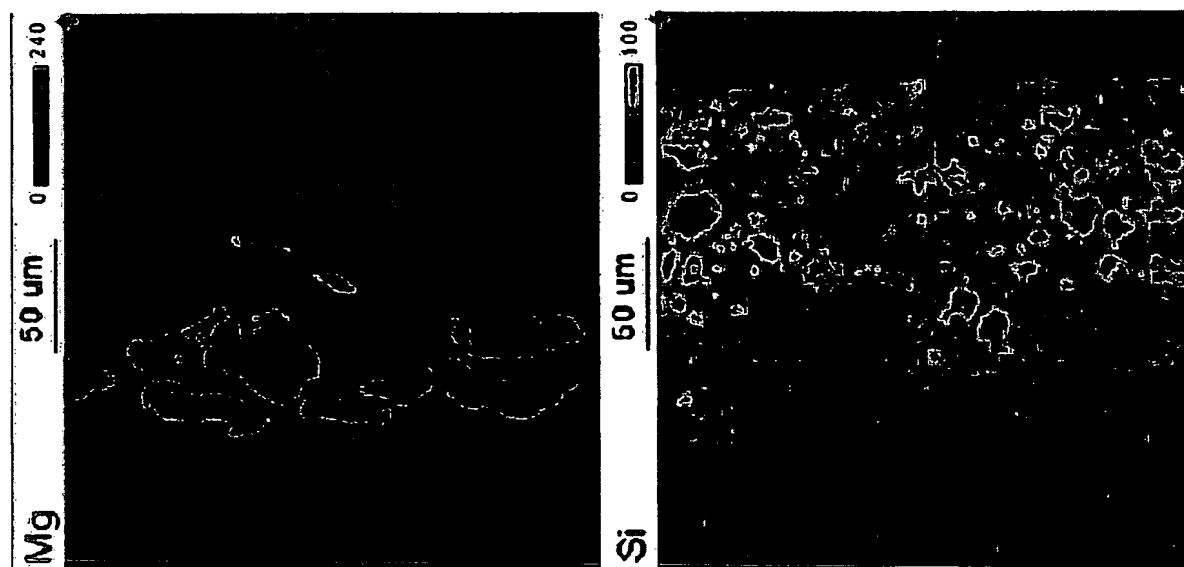


Figure 5. EDAX spectra of lateral profiles of Mg-rich coatings Corresponding to the SEM image in Figure 3 b) with X-ray fluorescence (XRF) counts for magnesium, in red LEFT, and silicone, in blue RIGHT.

The void formation at the interface observed between PUR base primer and ELT™ topcoat was not a local defect but rather a flaw resulting from a wetting problem in adhesion to PUR. It has been observed in other SEM images of identical coating samples analyzed in previous studies.

Our initial assumption regarding these Mg-rich systems was that their CPVC lie somewhere in the 43% to 50% PVC range, and according to theoretical calculations as described above, it was determined to be about 47% PVC. This was also observed in SEM surface analysis of the samples,

but the many SEM figures are not shown. These topographic studies revealed that the effective CPVC of a magnesium rich primer coating is sensitive to agglomeration and may be very formula specific. Considerable variation in the coating's morphology results according to the nature of the polymeric material, solvent system, and thixotrope used.

RECENT ACCELERATED EXPOSURE DATA

In study of the reproducibility of the Mg-rich coatings primers, and to more completely characterized electrochemically the behavior of these primers, a series of primer coatings were made up with all of the polymers used in the original study, and all of these were applied to Al 2024 T-3. An ELT topcoat was then applied to all of these samples, and they were then exposed to both the accelerated test protocol of alternating QUV and Prohesion exposure and also to Prohesion Exposure only. This latter is to cover any concerns that might be expressed by users about exposure requirements related to former Salt Spray Exposure protocols. No one argues any more that Cyclic Salt Spray is less damaging than the ASTM B117 Continuous Salt Spray protocol. We are acquiring a full set of EIS results for these exposure and some ENM data. Examples are given below of the most current exposure results.

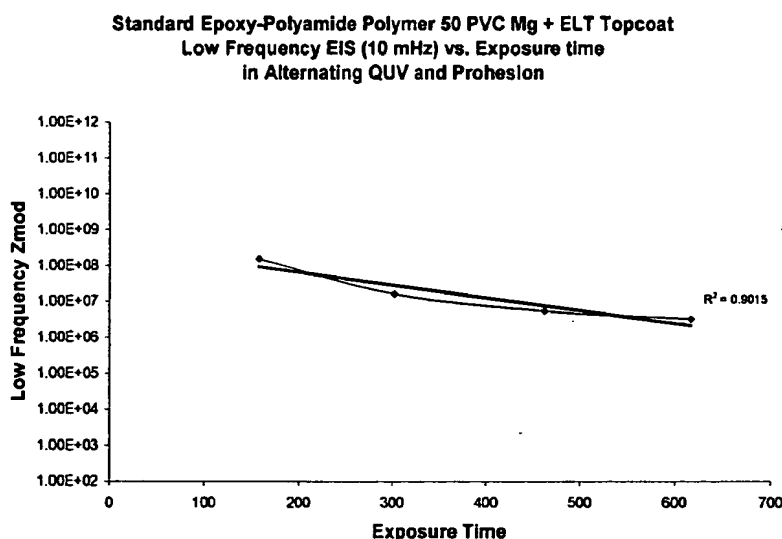


Figure 6. Low frequency EIS vs Exposure Time for Standard Epoxy Polymer Mg-Rich Primer + ELT Topcoat

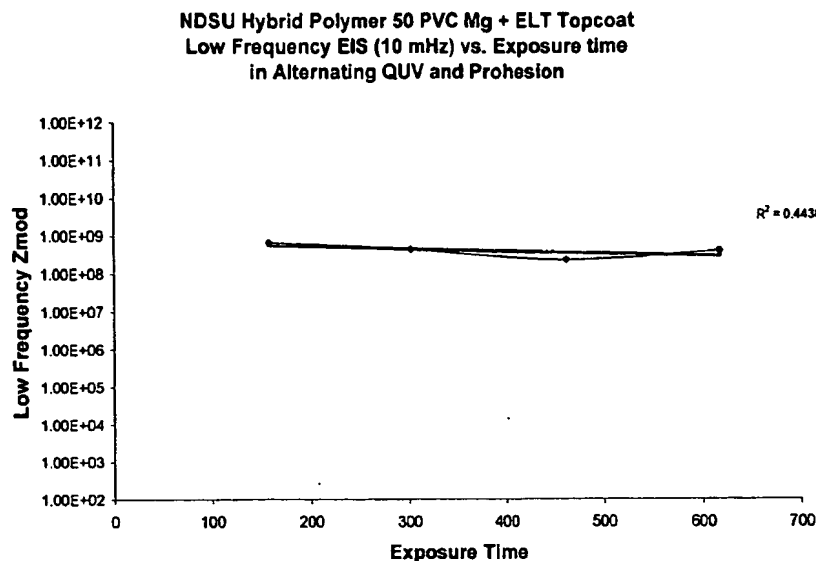


Figure 7. Low frequency EIS vs Exposure Time for NDSU Hybrid Polymer Mg-Rich Primer + ELT Topcoat

In Figures 6, EIS vs. Exposure time results are presented for a standard epoxy-polyamide industrial maintenance polymer based Mg-rich primer with an ELT topcoat and in Figure 7, similar results for one of the improved hybrid polymers developed in this project. The epoxy based version of the primer is showing some decay in performance after 700 hours, but essentially no change has appeared in the hybrid polymer version of the primer. These systems, which are to a large part repeats of some earlier samples, will be monitored carefully to be sure that all the data acquired can be used in qualifying a primer based on this technology for USAF use for the development of a totally Cr-free coating system.

SUMMARY AND CONCLUSIONS

The Mg-rich primer system developed for chrome free protection of Al 2024 T-3 continues to show excellent performance when used with a simple silane pretreatment and the ELT Topcoat. An optimized hybrid primer provides the best performance by a combination of excellent adhesion as well as good durability based in improved crosslinking and film formation plus improved interaction with the Mg pigment.

¹ C. Hare, "Corrosion Control of Steel by Organic Coatings," Ch. 55 in *Uhlig's Corrosion Handbook*, 2nd Edition. R. W. Review, Editor, John Wiley & Sons, New York (2000) pp.1023-1038

² S. Felix, R. Barajas, J.M.Bastidas, M. Morcillo & S. Feliu, "Study of Protections Mechanism of Zinc-Rich paints by Electrochemical Impedance Spectroscopy," in *Electrochemical Impedance Spectroscopy, ASTM STP 1188*, J.R.Scully, D.C.Silverman, & M. Kendig, eds., Amer. Soc. Testing and Materials (ASTM), Philadelphia, PA (1993) pp. 438-449

³ Jones D. A. Jones, *Principles and Prevention of Corrosion*, 2nd Ed., Prentice-Hall, Upper Saddle River, NJ (1996), Ch. 2

⁴ M.E. Nanna, & G.P. Bierwagen, "Mg-Rich Coatings: A new Paradigm for Cr-Free Corrosion Protection of Al Aerospace Alloys," accepted for publication, *J. Coatings Tech.*, April 2004; to be presented in 2003 FSCT Room Award Competition, ICE 2003, Philadelphia, PA, Nov. 14 2003

⁵ Gordon P. Bierwagen and Dennis E. Tallman, "Choice and Measurement of Crucial Aerospace Coating System Properties," *Prog. Organic Coatings*, 41 (2001) 201-217

-
- ⁶ Gordon Bierwagen, Dennis Tallman*, Junping Li and Lingyun He, "EIS Studies of Coated Metals in Accelerated Exposure," *Prog. Organic Coatings*, **46** (2003) 148-157
- ⁷ Funke W., "Problems and Progress in Organic Coatings Science and Technology," *Prog. Organic Coatings*, **31** (1997) 5-9,
- ⁸ Walker, P., "Organo Silanes As Adhesion Promoters for Organic Coatings," *J. Coatings Tech.*, **52**, No. 670 (November 1980) 49-61
- ⁹ Vanderbuilt, B. M., and Clayton, R.E., *Ind. Eng. Chemistry*, No 4 (1965) 18
- ¹⁰ Sperling L.H., *Interpenetrating Polymer Networks and Related Materials*, Plenum, New York, (1981)
- ¹¹ Frisch H.L., Klempner D., *Polymer Engineering Sci.*, **14** (1974)646
- ¹² Hsieh K.H., Han, T.H., *J.Polymer Sci.Part B Polymer Physics*, **28** (1990) 623
- ¹³ Schwindt, J., "Moisture-Cured, Polyurethane-Based, Surface Tolerant Coatings: An Economical Alternative for Corrosion Control," Technical literature from Bayer AG, Leverkusen, Germany, (2000)
- ¹⁴ Product Bulletin, Epi-Cure™ Curing Agent 3115, SC:1714-01, ©2001 Resolution Performance Products
- ¹⁵ G. P.Bierwagen, R.S.Fishman, T. Storsved, and J. Johnson, "Recent Studies of Particle Packing in Organic Coatings," *Prog. Organic Coatings*, **35** (1999) 1-10
- ¹⁶ Degussa, Technical bulletin No. 27, Aerosil® for solvent free-epoxy resins

PART XVI

Certain aspects and embodiments of the present invention are described in the following text and figures.

Mg-Rich Coatings: A new Paradigm for Cr-Free Corrosion Protection of Al Aerospace Alloys

Abstract:

Environmentally acceptable alternative coatings to chromate pigments and pretreatments for corrosion control of Al alloy 2024 T-3, commonly used in aircraft, were designed, formulated and tested as primer coatings to provide protection using particulate Mg-rich pigmentation. The system was designed by analogy to pigmented Zn-rich primer coatings used for the protection of steel. In the current study four coating polymer systems were examined as possible candidates as polymer matrices for Mg-rich cathodic protect coatings. Mg-rich primers were formulated with ~50-micron average particle size magnesium powder, near to the critical pigment volume concentration (CPVC) for this system. Top coated scribed coatings systems have been subjected to Prohesion™ exposure in dilute Harrison's solution for up to 5,000 hours. These coatings are the first non-chromated coatings to satisfy 3,000 hours of such exposure and remain shiny and undamaged in the scribe area, only showing damage at about 4,800 hours. The corrosion byproducts generated in the scribe areas during Prohesion™ exposure were examined by Energy Dispersive X-ray Analysis (EDXA) and the local pH of the coating was determined by the nature of the salt formed as a function of exposure conditions and time.

I. Introduction

A. Initial Motivation

Following by analogy the formulation of Zn-rich primer coatings for the protection of steel, the formulation of Mg-rich primer coatings for protection of aluminum alloys has been examined in this laboratory. The concept was considered when it was realized that a stabilized particulate Mg powder was available which allowed active metal sacrificial protection of Al and its alloys. This work has as its motivation the protection of high strength aircraft Al alloys such as 2024 T-3 and 7075 T-6 without the use of chromate-based pretreatments or chromate pigments. This class of alloys, whose high strength is based on phase separated intermetallic compounds within the bulk alloy, has proved resistant to efforts to develop corrosion protective (pretreatment + coating) systems that do not contain any Cr, a metal whose compounds are notorious for their toxicity and carcinogenicity.¹ Further, any aircraft painting or repainting operation that utilizes Cr-based pretreatments generates large amounts of hazardous waste which can be handled properly only at great cost.²

The basic principles of Zn-rich primer coatings are as follows:^{3,4}

1. Coatings are either organic or inorganic in nature (see *ref. 3* for further discussion).
2. They are pigmented with particulate Zn, in either spherical or flake form.
3. The PVC of the Zn pigment in the coating should exceed the CPVC in order for the coating to properly provide sacrificial/cathodic protection to the underlying steel substrate. Under these conditions, the Zn particles are all in mutual contact as well as in electrical contact with the steel substrate.

4. The mode of protection by these coatings is sacrificial as long as the Zn is electrically connected to the steel, as the Zn is more anodic (reactive) than Fe (major constituent of steel) in the electrochemical series. Then the mixed Zn oxides formed in the sacrificial oxidation fill the damaged areas and also sometimes passivate the steel surface by their basic nature. There is some evidence that the electrical connectivity of the Zn particles carries over from the PVC = CPVC (circa 60-70% by volume) to PVC = Volume Percolation Threshold⁵ for Zn (~30% by volume for spherical particles), so some sacrificial protection occurs over this range even while the Zn is being consumed by sacrificial oxidation. The percolation threshold for flake pigments may be different depending on particle alignment.⁶
5. The organic or inorganic matrix of the coating must be stable under the basic environment created by the zinc oxide, hydroxide, etc, formed from the oxidation of Zn in the presence of electrolyte. It must also adhere well to the steel alloys and be stable in a corroding environment.
6. These primer coatings must be top-coated to function properly and have a long field lifetime. When used properly, these primers provide almost as much protection to steel as galvanizing. With a topcoat, they provide both barrier and damage (sacrificial/cathodic) protection to steel substrates.

As work in this lab and others⁷ has shown that satisfactory corrosion protection was not available for Al 2024 T-3 without the use of chromates, many alternate options for protecting this alloy have been considered by this lab and others, including plasma polymer layers⁸ and conducting polymers^{9, 10}. Because of the availability of particulate Mg appropriate for use as a pigment in coatings,¹¹ it was decided to examine the possibility of designing Mg-rich coatings that would protect Al 2024 T-3 in a manner analogous to Zn protecting iron alloys (steel). There were two confounding features of considering Mg for cathodic protection of Al versus Zn for cathodic protection of Fe. The first was that particulate Mg can be a fire hazard, but this concern was alleviated by the manner in which Mg pigment was delivered by Eckart*. Their particulate Mg has a thin oxide layer that stabilizes it against further oxidation. Eckart GmbH, ECKATM metallic magnesium powder produced from p-magnesium 99.95 % to (Deutsches Institut für Normung) DIN 17800 part-7 standards with Mg content at 96% and MgO (magnesium oxide) content at 4%. The second concern was that the oxidation products of Mg, MgO and its various hydroxides in hydrated form, would create such basic conditions that Al would undergo basic corrosion† as is indicated in its Pourbaix diagram.¹² Fe is mostly passive under basic conditions, so this is not a valid consideration for Zn over steel. As shown below, the natural Mg oxidation products do not yield a pH high enough to corrode and dissolve Al, so this concern was also alleviated.

B. Further Considerations

The primary goal of this Mg-rich technology was the development of a new type of primer for Al alloys and a resultant coating system that is suitable for objects whose structural components are made up of Al 2024 T-3 or other corrosion prone aluminum alloys. The system needed to be easy to apply and repair, be compatible with present aircraft topcoats¹³, and eliminate all use of chromate

* Eckart GmbH, Kaiserstrasse 30, Furth D-90763, Germany

† The primer binder was a 2K epoxy-polyamide: Epon®1001CX and Ancamide® 2353 at stoichiometric ratios

pretreatments and chromate pigments altogether if used as part the total coating system by providing cathodic protection to the alloy. In addition, cyanide and other toxic substances are also used in most methods for chromate pretreatments. The secondary goal in this study has been to chooses or develop coating matrix polymers appropriate for use with Mg and its oxidation products with an environmentally acceptable solvent formulation, so that VOC regulations were met.

II. Proof of Concept: Initial Electrochemical and Exposure Studies

A. Open Circuit Potential and Electrochemical Impedance Spectroscopy EIS Studies

The electrochemical studies of Mg-rich primers (without topcoat) formulated in our laboratory were first carried out on the surface of the primed Al 2024 T-3 alloy immersed in 3% NaCl solution.¹⁴ The corrosion potential, E_{corr} , or open circuit potential (OCP), for the coatings in contact with the alloy was monitored and the (EIS) spectra of three primer sets, as formulated in an epoxy-polyamide polymer matrix, were recorded as a function of time. The OCP is the mixed potential achieved when a corrosion reaction is occurring between the anode and cathode of the reaction system.¹² The data presented below are for three of these primers based on Eckart (Eckagranules™) ~ 50 micron average particle size distribution (PSD) Mg powder at 43, 46 and 50% PVC. These data indicate that the most effective protection from just the primer is about 46% PVC, which was the estimated CPVC for this system.

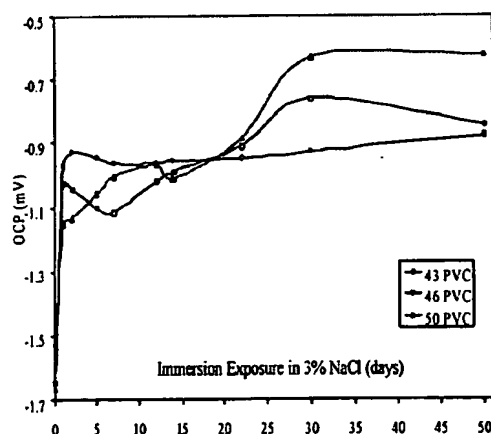


Figure 1. Open circuit potential SCE vs PVC for Mg-rich epoxy/polyamide primers at pH= 6.2 in 3% NaCl⁽¹⁵⁾

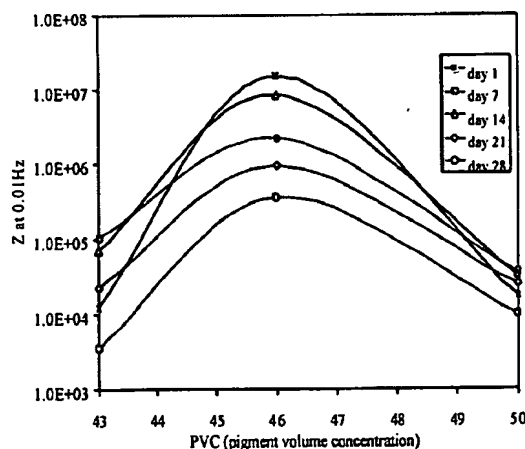


Figure 2. $|Z|$ modulus at 0.01Hz vs PVC for Mg-rich epoxy/polyamide primers at pH= 6.2 in 3% NaCl⁽¹⁵⁾

Figure 1 gives (OCP) vs. exposure time for Mg-rich primers, formulated at 43, 46, and 50% PVC in a polyamide/epoxy coating polymer exposed to 3% NaCl solution at pH ~ 6.2. Interpretation of the events is as follows. Initial OCP values for the three sets correspond to a single electron transfer potential for Mg metal, $E_{Mg} = -1.50$ V to -1.60 V_{SCE}, and the primers appear to be acting like bare Mg¹⁶. Subsequently, over a 24 hour period, Mg and the Al alloy polarize to a mixed potential corresponding to the corrosion potential, E_{corr} , at which the Mg is still sacrificially protecting the Al 2024 whose E_{2024} is -0.68 V vs. saturated calomel electrode (SCE). The observed mixed potential for Mg and Al alloy in 3% NaCl was found to be about $E_{corr} = -0.90$ V to -1.00 V_{SCE}. OCP values

extending beyond the initial 24-hour period varied according to primer PVC. The initial lower mixed potential value, E_{corr} (Figure 1), for the 43% PVC sample is thought to be due to the lower effective active metal area as a result of higher polymer coverage at the Mg/Al alloy interface. Initially, the Mg-anode dominates the OCP. The gradual rise in OCP for the 43% PVC sample toward $E_{2024} = -0.68$ mV_{SCE} is assumed to be due to reactive consumption of the exposed Mg in this system and the disbonding of epoxy coating polymer from the cathode surface. The gradual decrease in OCP of the 43% PVC sample toward $E_{\text{mix}} = -0.90$ V to -1.00 V_{SCE} may be due to resistance polarization by the formation and packing of Mg oxides in the coating. The initial and continuous decrease in OCP of the 50 PVC sample is concluded to be due to a higher void volume in the primer as well as a higher cathode area at the primer alloy interface. The OCP of the 46% PVC sample quickly arrives at the $E_{\text{mix}} = -0.90$ V to -1.00 V_{SCE} value and remains constant for the duration of the test time period. Thus, it is surmised that the 46% PVC primer corresponds to the critical pigment volume concentration (CPVC) for the primer, suggesting that cathodic protection of the Al alloy due to Mg metal occurs most effectively at or near CPVC. Figure 2 shows the impedance modulus $|Z|$ versus exposure time measured in 3% NaCl solution at pH = 6.2 on 43%, 46%, and 50% PVC Mg-rich primers. This figure demonstrates the effect of PVC at CPVC for Mg-rich primers. The Z modulus values for the 46% PVC samples yielded a higher impedance modulus over the 28-day period suggesting proper formulation at or near the critical pigment volume concentration, which is required to ensure close packing of Mg pigment with minimum resistance from the polymer matrix of the system, but with polymer matrix content sufficient enough to ensure good substrate wetting and reasonable physical properties from the primer.

Trends in OCP data suggest three distinct periods that distinguish the evolution and effectiveness of cathodic protection in the Mg-rich primers as a function of exposure time. These are as follows:

Period I. Initial immersion day one, the "activation" period when the value of the corrosion potential shifts to a cathodic value -1.1 V vs SCE, corresponding to the Mg metal / Al-2024 T-3 mixed potential in the electrolyte. Magnesium immediately begins to react with the sodium-chloride solution; it is "activated" leading to better metal-to-metal electrical contact being established between magnesium particles and Al surface.

Period II. Once initially past the "activation" period, the cathodic protection mechanism reaches its peak due to a maximum in the ratio of magnesium-to-aluminum area ratio. This occurs around day 5~7 when the corrosion potential shifts to a more anodic value of about -0.9 V vs SCE; it is where a relative stabilization called the "transition" period occurs.

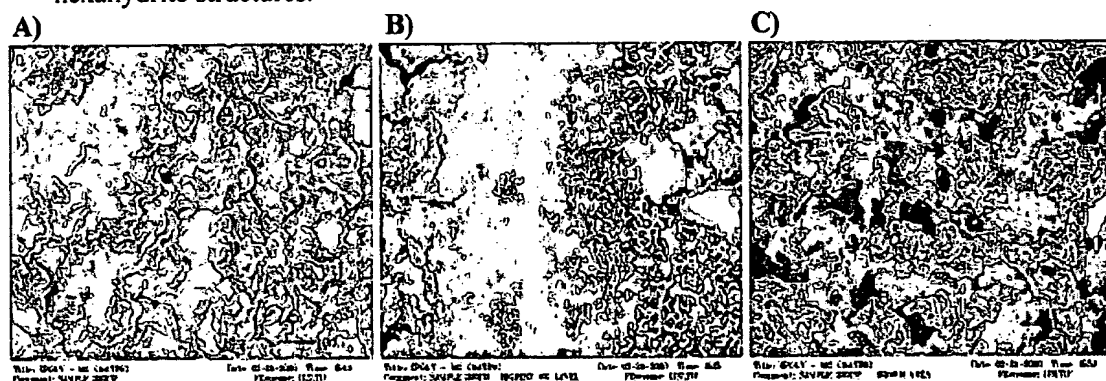
Period III. After the transition period, and up to day 21, the corrosion potential shifts out of the cathodic protection domain, and the potential fluctuates as the film's solution chemistry begins to change. At which time oxygen reduction begins to occur on the upper part of the film causing a local increase in pH that changes the corrosion products from magnesium hydroxychlorides to magnesium hydroxides, the same as at the interface.

B. Initial Accelerated Test

In metal-rich coatings the pigment volume concentration (PVC), is high and close to critical PVC, in the region at which paint properties such as water permeability and cohesive strength change dramatically. Therefore, Prohesion™ cyclic exposure in dilute Harrison's solution with no topcoat allows easy access of acidic electrolyte, atmospheric oxygen, CO₂ and water to the coating's Mg anode. Topcoating the Mg-rich primer insulates or screens it from the primary cyclic effects of

Prohesion™ which in turn prevents observation of the processes that occur when the coating is scratched or chinked when the Al alloy is exposed to an acid rain environment. In order to better observe the occurrence of such processes primed panels were directly exposed to dilute Harrison's solution, without topcoat, and monitored. The pH of dilute Harrison solution is about ~4.5 which corresponds to the pH at which Mg metal readily forms salts with CO_2 , SO_4^{2-} and OH^- . The formation of these salts was observed to occur on the surface and at the interface of the primer over a given time interval that corresponds to three distinct events:

1. EDXA spectra have revealed formation of magnesium carbonate hydrates at the primer liquid/vapor interface, dypingite $[\text{Mg}_5(\text{CO}_3)_4(\text{OH})_2 \cdot 8\text{H}_2\text{O}]$ and hydromagnesite $[\text{Mg}_3(\text{CO}_3)_4(\text{OH})_2 \cdot 4\text{H}_2\text{O}]$. These salts have been observed only to be present up to the first 500 hours of exposure for all non top-coated primed Mg-rich panels tested.
2. For exposure times beyond 500-hours cause brucite $[\text{Mg}(\text{OH})_2]$ domains begin to form and subsequently extend throughout the bulk of the primer. During this time the aluminum alloy remains cathodically protected as scribed lines remain unblemished.
3. For exposure times greater than 1,300 hours, primer failure and film delamination correspond to the accumulation of hexahydrate $[(\text{MgSO}_4) \cdot 6\text{H}_2\text{O}]$ compound at the interface. Failure occurs (Figure 3-B) when Mg-metal and brucite structure have been depleted from the coating polymer matrix and sufficient hexahydrate salts have accumulated at the alloy interface. At which time the coating polymer ruptures and fragments from compressive forces exerted by hexahydrate structures.



Figures 3: A-C. SEM of exposed Mg-rich primer after Prohesion™ exposure: A) Brucite/ $\text{Mg}(\text{OH})_2$ emanating from Mg-rich top of coating (left) at 500-hours; B) Hexahydrate (upper left) and brucite (rosette bottom right) structures, underside of panel at 1,000-hours; C) Vacant epoxy polymeric matrix denuded of Mg and Mg salts (right) after 1,500-hours exposure.

The first 24 hours of exposure to salt fog solution with atmospheric CO_2 , magnesium forms magnesium carbonate compound, at the surface, $\text{Mg}_5(\text{OH})_5 \cdot \text{CO}_3$, which is replaced by a more densely packed magnesium hydroxide $\text{Mg}(\text{OH})_2$ pseudo-hexagonal crystal structure. The rosette structure observed in the magnesium epoxy primer scanning electron microscopy (SEM) images shown in Figure 3-A is consistent with *brucite* magnesium hydroxide $\text{Mg}(\text{OH})_2$ (acicular needle) crystal formed in Prohesion exposure. Further observations were made on the Mg-rich primers exposed to Prohesion™ cyclic salt fog with dilute Harrison's solution:

1. White oxide area magnesium hydroxide (brucite) formed over magnesium metal and energy dispersed X-ray analysis (EDXA) measurements indicated the presence of magnesium, oxygen and aluminum with a minimum amount of carbon detected.
2. In the scribed area with no epoxy matrix or magnesium metal originally present, EDXA spectra show carbon, oxygen, magnesium and aluminum with possible presence of dypingite (magnesium carbonate) structure over the exposed aluminum surface.

In summary, *Table 1* gives the relative pH, the solubility product, and the water solubility for magnesium salts identified in EDXA spectra. It was observed that the salts generated during the first 1,000 hours of exposure increased in local pH according to a stratification scheme from the coating / alloy surface interface toward the external surface of the coating.

Table 1. Magnesium salts solubility pH				
Salt	(designation)	Ksp	H ₂ O g/100ml	pH
Mg(OH) ₂	<i>Brucite</i>	7.1×10^{-12} *	7.8×10^{-4}	9.6 ~ 10.4 **
MgCO ₃ • H ₂ O	<i>Magnesite</i>	3.8×10^{-6} *	0.002 ***	8.0 ~ 8.8 ***
MgSO ₄ • 6 H ₂ O	<i>Hexahydrate</i>	(soluble)	95 ***	6 ~ 9 ***

* CRC Handbook of Chemistry and Physics, 68th Ed., Boca Raton, FL (1987-88)

** Kramer, D., Magnesium, its Alloys and Compounds, US Geological Survey Open-File Report 01-341

*** Seelig, B.D., Salinity and Sodidity in North Dakota Soils, EB-57, North Dakota Extension Service, May 2000

The degradation process of Mg-rich coatings exposed to an acidic environment may be described as follows. The more acidic salt (i.e., hexahydrate) was identified at the alloy interface where local pH conditions are lower due to anodic polarization conditions that drive cationic species, such as Al³⁺ from solution towards the Al interface.¹⁷ The carbonate salt was found to develop on the top of the coating along with Mg(OH)₂, and both are identified as species that form at higher pH. In addition, the damaged / scribed areas did not degrade neither the coating polymer nor the alloy surface until after the depletion of Mg(OH)₂ and as the accumulation of hexahydrate salts occurred. According to Kramer¹⁸ aqueous magnesium hydroxide acts a pH buffer that does not exceed a pH=10.5 even in the presence of excess Mg(OH)₂.

C. Conclusions of Preliminary Feasibility Studies

These very encouraging results were obtained from a simple Mg-rich coating based on an off-the-shelf (OTS) polymer system with no optimization efforts. They showed that the oxidation products of the Mg pigment in an exposure environment, fairly typical of what an actual system might see in field exposure, did not cause basic corrosion of the Al 2024 T-3 alloy. Further, the Mg-rich system did provide cathodic protection to the Al 2024 T-3, giving the system significant corrosion protection properties in a completely Cr-free system with no chromates in pretreatment nor chromate pigments in primer. The research studies now proceeded to improve of the coating polymer system and additional formulation studies.

III. Formulation Improvement by Coating Polymer Design and Preparation

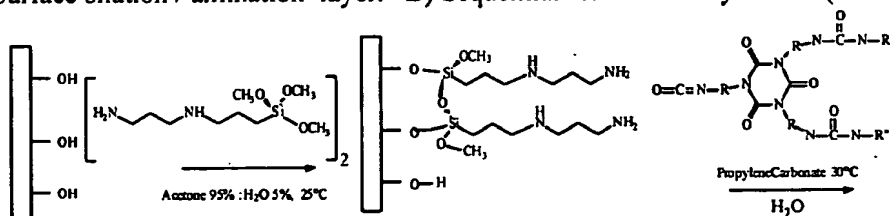
A. Coating Polymer Selection

Traditionally, two-pack zinc epoxy/polyamide polymer materials have been used for cathodic protection of steel as they result in crosslinked matrices with a good adhesion and resistance against alkalis, so that any alkaline reaction involving zinc does not affect the binder itself.¹⁹ More recently, epoxy siloxane "hybrid" coatings have been reported²⁰ to represent a significant advancement compared to epoxy, epoxy acrylic and polyurethane coatings. Hybrid polymeric matrices, for high performance primers, are designed as polymer composites or alloys that contain a polymer backbone with at least two types of reactive groups that can take part in crosslinking and network formation under at least two different mechanisms.

B. Silane Modified Multi-Layer/IPN Polymer Matrix

The design of an improved polymeric matrix for Mg-rich coatings involves an easy to prepare multi-layer scheme that requires minimum preparation of the Al alloy surface and is derived from existing sol-gel technology. The reaction scheme entails initial application of an organo-silane (N-β-(aminoethyl)-γ-aminopropyltrimethoxysilane) with subsequent grafting of organic layers from the surface into the bulk by utilizing a novel silane modified crosslinker.²¹ The coating scheme is akin to the "sol-gel" process, but involves a multilayer approach that utilizes an organo-silane substrate treatment from which a moisture-cure polyisocyanate is applied which has been reported²² to involve an initial reaction with water to form an unstable carbamic acid intermediate that spontaneously decarboxylates into an amine and carbon dioxide, as shown in Figures 4A-C. To complete the scheme, further bulk crosslinking reactions between epoxy, silanol, and isocyanate are proposed to occur with from an aminated surface into the bulk by employing a bulk / surface crosslinker. In brief, the prepared organo-silane modified surface was subsequently sprayed with a 20 percent solution of polyisocyanate in propylene carbonate, with one of two poly isocyanate prepolymers, 1) 1,6-hexamethylene diisocyanate homopolymer (HMDI) trimer, as depicted in *Figures 4 A-C* below, and 2) 4,4'-methylenediphenylisocyanate (MDI) prepolymer similar scheme. Uniform coverage of the wet surface was approximated at ~ 2 mils / 50 microns using a wet film thickness gauge.

A) Surface silation / amination layer. B) Sequential reaction of layer with (HMDI) or (MDI).



C) Below: Further polymerization is surmised to take place from the surface layer and extend into the bulk.²³ It is the hydrolysis of the isocyanate to form carbamic acid²⁴ (forming both amines and carbon dioxide, that are intermediates in the Hoffmann rearrangement²⁵ of an isocyanate with water) to yield the reactive / reaminated second layer.²⁶

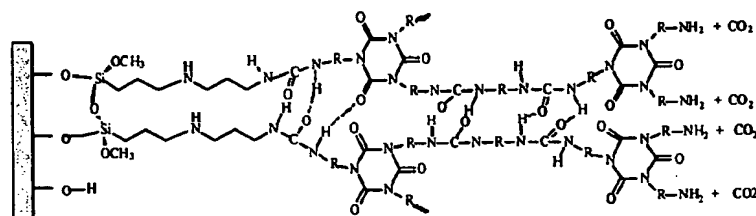


Figure 4. Development of multi-layer covalent structure: **A)** to **B)** amino-silane layer at the Al surface. **B)** to **C)** isocyanate-functionalized monomers and hydrolysis, with atmospheric water to yield covalent structure with hydrogen bonded parallel multi layers.

The bulk reaction, extending from the surface, occurs between 1) the polyisocyanate, in the primer formulation and the aminated surface (*Figure 4C*); 2) the isocyanate and 7-phenyl-1-[4-(trimethyl-silyl)-butyl]-1,2,3,4-tetra-hydro-quinoxalin-6-ol crosslinker (*Figure 5*) which is surmised upon further hydrolysis to form both polyurea and polysiloxane IPN structure. The silane modified epoxy (HMDI or MDI) hybrids results from a polymeric material consisting of polyurea, polyurethane (from polyisocyanate prepolymer), epoxy-amine, and organo-silane linkages.

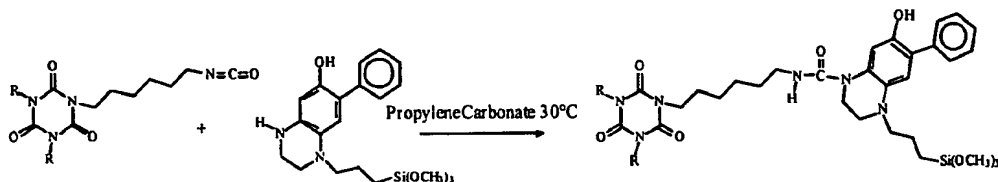


Figure 5. Isocyanate monomers, and crosslinker: 7-phenyl-1-[4-(trimethyl-silyl)-butyl]-1,2,3,4-tetra-hydro-quinoxalin-6-ol depicting bulk epoxy/ isocyanate IPN growth throughout the bulk phase.

C. Coating Formulations

The materials used in this study are summarized in *Table 2*.

Formulation	Materials
(A) Hyb-E23A	Desmodur™ E23-A, Aerosil R202, Eckagranules™ PK51/31, Epon™ 1001CX, Propylene Carbonate/EEP
(B) MC-PUR ²⁷	Desmodur™ E23-A, Bentone® 34, Eckagranules™ PK51/31 Anti Terra®U, Aromatic solvent Xylol
(C) Hyb-N3300	Desmodur™ NC-3300, Aerosil™ R202, Eckagranules™ PK51/31, Epon™ 1001CX, Propylene Carbonate/EEP
(D) Epoxy-Polyamide	Epon™ 828, Epicure® 3115, Aerosil™ R202, Eckagranules™ PK51/31, Anti Terra™U, Aromatic solvent Xylol,

IV. Mg-rich Coatings Formulation and Characterization Studies

A. Critical Pigment Volume Concentration Estimates for Mg-rich Primers

CPVC is a function of the random dense packing efficiency of the pigment plus adsorbed layer thickness (δ), which must be experimentally determined. This has been discussed extensively in the literature and a recent review considers new developments.²⁸ The procedure for obtaining CPVCs for these Mg-rich systems is described as follows. Two Magnesium powders Eckagranules™ PK 31 with a mean particle size distribution (PSD) of 30 μ m, and PK-51 with a mean PSD of 70 μ m, were used as received, (see Figure 6) and mixed at a 52%-PK31: 48%-PK51 volume. A 52:48 volume mix of the two powders was found to yield a higher bulk density value than that of either powder alone. The critical pigment volume concentration (CPVC) of the primers was first approximated by obtaining a resin /powder rub-up value with Aerosil®R202 at 2% vol. on total pigment, and the final CPVC was calculated from PSDs, provided by Eckart GmbH, for the three pigments, assuming spherical geometry, combined with the experimentally determined resin rub-up values. Figure 7 shows calculated CPVCs from the ternary diagram for the three-pigment mixture. The volume fraction coordinates (Pk-31 = 0.51, Pk-51= 0.47, and R-202 = 0.02) yields a theoretic CPVC value in the yellow region (@ PVC = 0.475), which corroborates the experimentally surmised CPVC, ascertained from the EIS data in Figures 1 and 2, above.

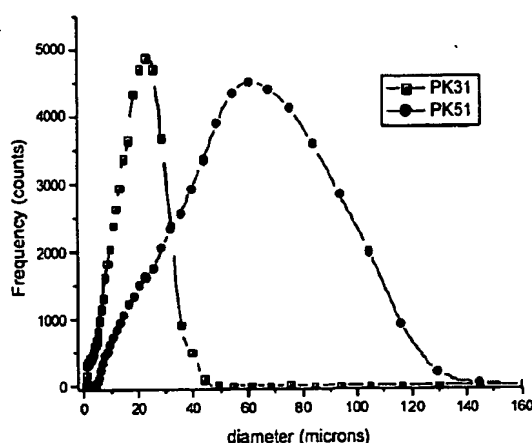


Figure 6. Particle size distributions for Mg powders, Eckagranules™ PK31 and PK51 courtesy of Eckart GmbH, Germany. CPVCs.

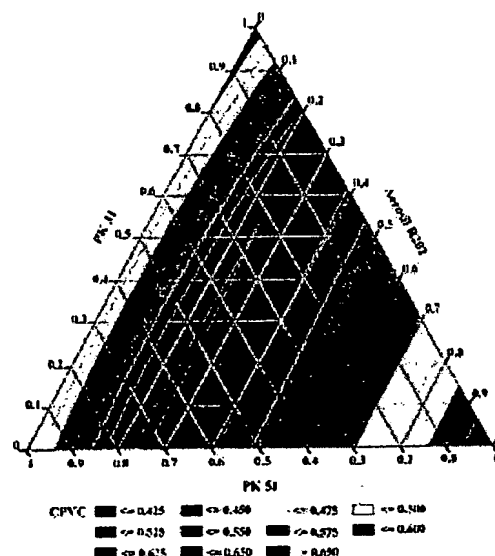


Figure 7. Ternary mixture diagram for Pk31, Pk-51 and Aerosil® R202, colored areas corresponding to theoretically calculated

B. Characterization of Mg-rich Coatings Properties

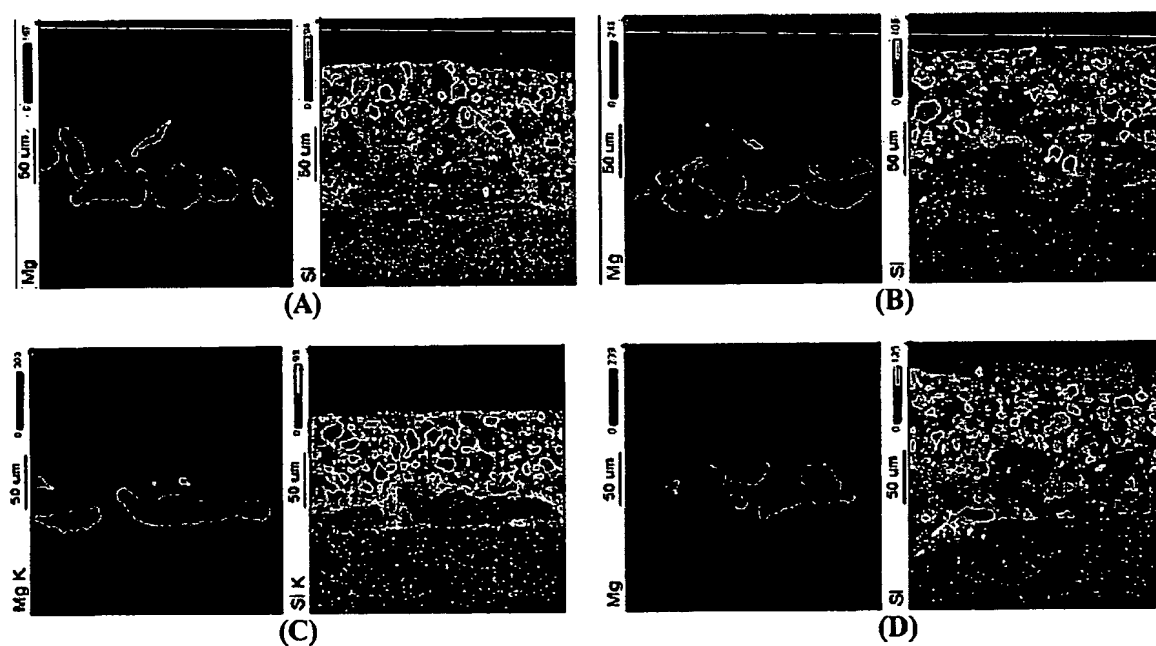
1. Panel and Film Preparation

The primers from materials in Table 2 were applied to 6"x 3" Al 2024 T3 Q-panels™, scrubbed with a Scotch Brite™ pad, rinsed and degreased with EEP, then immersed in a 10% phosphoric acid solution for 60 seconds and rinsed with distilled water. Al panels were surface modified according to

methodology described in literature.²⁹ Mg-rich coatings were applied with a touch-up spray gun, the coatings cured at 35° C for 14 days. Primed panels were subsequently top coated with Extended Lifetime™ Topcoat. The average film thickness (FT) ascertained from SEM and EDAX images reveal primer film thickness to be estimated at about 50 +/- 20 microns with topcoat film thickness estimated at about 100 +/- 40 microns, see SEM and EDAX images Figures 8 A-D.

2. Micrographs SEM and EDAX

Coated samples were assembled on aluminum mounts and coated with gold using a Technics Hummer II sputter coater. SEM and EDAX Images were obtained using a JEOL JSM-6300 Scanning Electron Microscope. X-ray information was obtained by a ThermoNoran EDX detector using a VANTAGE Digital Acquisition Engine. *Figures 8 A-D*, show EDAX cross sections of the four 50 PVC Mg-rich primers, with pigmentary Mg X-ray fluorescence (XRF) counts in red, and Silicon XRF counts, in blue, demonstrating the general alignment of Mg powder at the Al interface and pigment distribution in the polymer matrix which is thought to be related to its dispersion in the coating's polymer matrix and ultimately to its effectiveness as a coating for corrosion control.



Figures 8: A-D. EDAX images, lateral profiles of Mg-rich coatings at 50 %PVC over Al 2024 T-3 substrate with primer FT~50µm and ELT™ topcoat FT ~ 70 µm. Magnesium XRF counts in red and silicon XRF counts in blue. For (A) Epoxy-MDI hybrid; (B) Moisture Cure Polyurea (MC-PUR); (C) Epoxy-HMDI hybrid; (D) Epoxy / polyamide.

C. Testing of Mg-rich Coatings

1. Mechanical Properties of Mg-Rich Coatings

Tensile properties were measured according to (ASTM D 2370-82) using an Instron™ model 5542 with Merlin (2) software. DMTA measurements were made with a Rheometrics model 3-E dynamic mechanical analyzer.

BEST AVAILABLE COPY

2. Flammability Testing of Mg-Rich Coatings

Six-inch strips were cut from top-coated Mg-rich Al panels and subjected to a modified flammability test, referenced in document IPC-SM840B (International Printed Circuit). Also refer to test method 2.3.10.1 and the U.L.-94 flammability specification using a Bunsen burner, with a tube length of 4 inches, I.D. 0.37 inches with methane gas at equivalent 1000 BTU/Ft³. A propane torch with flame temperature 1120°C (or 2048°F)³⁰ was applied for thirty seconds to the backside of the aluminum panel covered with coatings. This test was further modified by scribing an X over the face of each panel to directly expose magnesium metal in the coating to air / oxygen.

3. Exposure Testing

Prohesion™ exposure was performed according to ASTM D5894-96. Top-coated Mg-rich panels were prepared by covering panel backside and edges with 3M electroplater's tape and edges were then sealed with a 2-K industrial epoxy from Aldrich. Topcoated panels were scribed through the surface of the coating with a carbide tip glass scribe where an X pattern was formed thus exposing the Al surface.

4. Electrochemical Impedance Spectroscopy (EIS)

The corrosion protection properties of primed panels were evaluated by (EIS). The experimental set-up consisted of a three-electrode cell containing 40 ml of 3.0 wt% NaCl aqueous solution, open to air, held at room temperature ~22°C / 72°F. A saturated calomel electrode (SCE) was used as the reference electrode and a stainless steel plate served as the counter-electrode. All measurements were performed at the open circuit potential of the system. EIS measurements were performed with a Gamry PC-4 / 300TM electrochemical measurement system with potentiostat-galvanostat. Impedance spectra were recorded with a frequency sweep from 0.01Hz to 10kHz, the amplitude of the signal perturbation was 10mV (rms), and Gamry 3.1 Framework™ software was used to analyze the data in Bode plot form. These results are presented below.

V. Test Results

A. Viscoelastic Properties of Coating Polymers

Table 3 gives the measured viscoelastic properties for five polymer systems: T_g , elastic storage modulus E' (minimum), and calculated crosslink density. The significant differences in reported glass transition temperatures are assumed to be related to the individual coatings chemical properties at full cure. Crosslink density was calculated from (E'): ($T = T_g + 50^\circ\text{C}$) at which the material is in the rubbery state; where ν_e is the elastically effective crosslink density³¹: $\nu_e = 3 E' / RT (T + T_g)$.

Table 3. Viscoelastic properties of polymer films

Polymer film	T_g (°C)	Crosslink density (mol/cm ³)	E' (Pa) minimum
N3300 (MC-PUR)	122	3.4×10^{-3}	2.6×10^7
E23A MC-PUR	159	5.8×10^{-4}	6.6×10^5
Epoxy-polyamide	65	2.1×10^{-3}	2.0×10^7
Hyb-N3300	96	1.3×10^{-3}	1.3×10^7
Hyb-E23-A	100	6.9×10^{-4}	6.9×10^6

The results in Table 3 also suggest the difference in the chemical composition of crosslinks formed may lead to observed differences in T_g s. According to Hale and Macosko,³² changes in T_g arise both from disappearance of chain ends and the formation of chemical crosslinks that yield elastically effective chain density at higher levels of branching.

B. Mechanical Properties of Mg-rich Coatings

Table 4 gives the measured tensile properties of coating polymer films. Tensile tests were conducted on coating polymer film strips with no visible voids. Mechanical properties in (Table-4) show an improvement in both of the hybrid system's tensile strength and tensile modulus properties over their parent materials. The tensile modulus is known to be a better indication of a film's mechanical properties, as its measurement is less defect dependent than the film's tensile strength. A high tensile modulus also suggests that the material is more elastic which implies higher degree of cure or conversion.

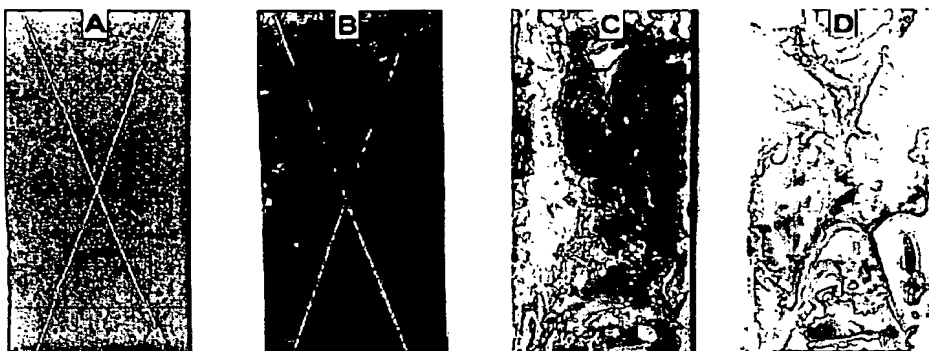
Table 4. Mechanical properties of polymer films

Polymer Film	Elongation at-break (%)	Tensile strength (MPa)	Tensile modulus (Mpa)
N3300 (MC-PUR)	8.0 ± 0.1	45 ± 7	1250 ± 90
E23A (MC-PUR)	5.0 ± 0.3	25 ± 6	825 ± 110
Epoxy-polyamide	18.0 ± 0.1	5 ± 0.9	150 ± 50
Hyb-N3300	6.0 ± 0.3	56 ± 9	1800 ± 50
Hyb-E23-A	5.5 ± 0.2	50 ± 5	1500 ± 50

Both of the hybrid silane modified epoxy-urea/urethane analogs show lower T_g s than the parent materials with no significant difference in crosslink density, suggesting the presence of (–N–R–Si–O–Si–R–N–) bonds throughout the IPN matrix.

C. Flammability

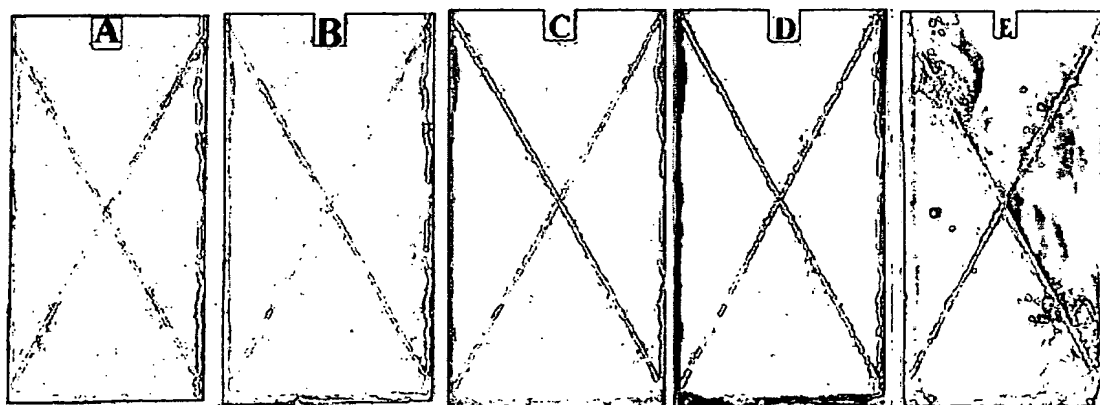
Flame retardant (FR) coatings describe coatings that delay ignition and hinder flame spread. The common test method for evaluating flammability is the Limiting Oxygen Index (LOI) test (ASTM D 2863), a material is normally considered as flammable if the LOI is less than 26.³³ These coatings were all coated with a fluorinated ELTTM topcoat that may have contributed in some measure to the coatings non-flammability (Figure 9 A-D). The most often reported parameter associated with coating flammability is the material's limiting oxygen index (LOI) value. Epoxy / polyamine systems, vary from a low of 24 to a high of 32 for silane modified ceramer epoxies³⁴ while fluorinated polyurethanes are rated up to 50. Another contributing factor to improved non-flammability is the presence of the isocyanurate linkage. HMDI has been reported³⁵ to possess an inherently higher thermal stability than that of other urethane linkages, such as MDI, as the latter is reported to dissociate at about 200°C. In general, flammability decreases as the proportion of isocyanurate trizine ring increases.^{36, 37, 38}



Figures 9: A, B, C, and D. Results from modified UL-94 flammability test. From least affected A) 50 %PVC Hybrid epoxy/urea/urethaneN3300; B) 50 %PVC Hybrid E23A to most affected C) 50% PVC MC- PUR; D) 50% PVC Epoxy-polyamide.

D. Accelerated Exposure

Prohesion™ exposure in dilute Harrison solution, (NH₄SO₄) acid rain conditions, resulted in Mg-rich coatings with conventional binders maintaining clean scribes up to ~ 1,000 hours, in contrast with those coatings formulated with hybrid binders that realized clean scribes up to 3,000 hours and showed signs of failure at 5,000 hours. The integrity of the primer vehicle appears to be the main issue associated with improved corrosion control in these systems. All samples of Mg-rich primer coatings gave better performance in this exposure than the standard chromate based system with similar topcoat, and as seen in *Figure 10*, the best performing of these Mg-rich systems after 4,800 hours visibly performed better than a non-pigmented primer/ELT™ system (*Figure10-E*) after 1,800 hours exposure.



Figures 10: A, B, C, D and E. Prohesion™ (ASTM D5894-96) results for Al 2024 T-3 panels from formulation (C) *Table-2*, Mg-Rich primer Hybrid N3300 at 50% PVC with ELT™ topcoat at A) 0-hrs.; B) 1,200 hrs.; C) 3,000-hrs.; D) 4,800-hrs. and contrasted with E) an epoxy Epon™828/Ancamide™ 2353 polyamide (non Mg pigmented primer) with ELT™ topcoat at 1,800-hrs.

VI. Proof of Concept: Extended Electrochemical Study

A. Electrochemical Studies of Mg-Rich coatings

EIS studies of the Mg-rich primer at 50%PVC (above CPVC) with topcoat, under conditions of high, neutral, and low pH were performed. An EIS test method was used that involved subjecting circularly scribed Mg-rich coatings to immersion varying the pH conditions in 3% NaCl solutions. This method was utilized to help differentiate among the various primer formulations developed in this work. Subjecting the system to acid (pH=2.8), neutral and basic (pH= 2.0) 3% NaCl immersion under scribed conditions allowed comparison of the formulations in a wide range of exposure conditions. The Mg-rich Al 2024 T-3 panels were topcoated with (Deft 99 GY-001 ELT™), a very chemically resistant coating, scribed, and then subjected to continuous immersion. Three coating systems were evaluated as Mg-rich coatings, two commercially available OTS products and one hybrid silane modified epoxy-urea developed in this laboratory.²¹

1. Moisture cure (MC-PUR) aromatic polyisocyanate, Desmodur™ E23A, polyurea.³⁹
2. Epoxy/polyamine consisting of Epon™ 828 with a Mannich base polyalkylamine curative Epicure™ 3251.
3. Hybrid silane modified epoxy-urea consisting of Epon 1001 and Desmodur™ N3300 aliphatic polyisocyanate, the silane was Silquest™ A-1120 (N-β-(aminoethyl)-γ-aminopropyl trimethoxysilane) see Table 2 formulation C.

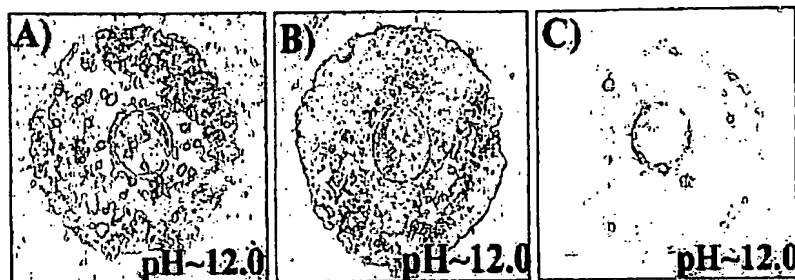
B. Experimental Setup

Cylindrical electrode cells were mounted over samples with 1.0 cm diameter circular scribes cut through the coating exposing Al 2024 T-3 surface. Cylinders were filled with electrolytes of the following compositions: 1) Basic at 3% weight NaCl adjusted to pH= 12.0 with NaOH; 2) Acidic at 3% weight NaCl adjusted* to pH=2.8 with HCl; 3) Neutral at 3.0% weight NaCl at pH=6.2. Impedance measurements were carried out over an 11-day time period pH adjusted at each test interval, (see section IV-C-4 for testing methodology). Unscribed topcoated films were also examined electrochemically to try to determine what is happening in undamaged coatings due to immersion in neutral 3% NaCl solution.

C. Results

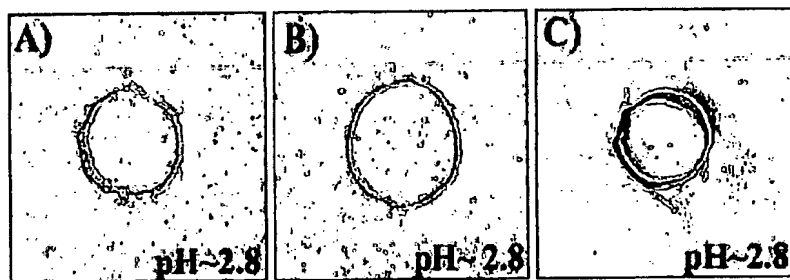
The visual results from the scribed exposure tests (Figures 11-12 below) indicated that under conditions of high and low pH the Mg-rich coating formulated with traditional coating polymers, i.e., MC-PUR and the epoxy/Schiff base have weakness at these pH extremes. At high pH =12 samples (A) and (C) blistered after immersion exposure. At low pH =2.8, immersion exposure caused the film to disbond and lift from the substrate. The amino-silane modified hybrid polymer matrix provides a much more pH resistant system in an Mg-rich coating in adhesion and reactivity than the more traditional polymers. As Zhu and van Ooij⁴⁰ have noted that protonated amine ($-NH_3^+$) from γ-APS (γ-aminopropyltriethoxysilane) in films on Al 2024 T-3 promotes the ingress of corrosive chloride ions into the film. No visible difference in scribed samples after 11-days testing suggests conditions at pH=6.2 yield higher stability at the primer coating/interface.

Basic conditions: pH=12.0, (Al most prone to dissolve)



Figures 11: A) E23A, MC-PUR; B) Hybrid Epoxy-urea; C) Epoxy-Mannich base. Scribed samples after 11-days immersion and EIS testing at pH=12.0.

Acidic conditions: pH=2.8, (Mg most prone to dissolve)



Figures 12: A) E23, AMC-PUR; B) Hybrid Epoxy-urea; C) Epoxy-Mannich base. Scribed samples after 11-days immersion and EIS testing at pH=2.8.

D. Electrochemical Studies

The literature on metal-rich paints as studied by EIS provides good insight into the metal-rich coatings that have not been topcoated, but are exposed directly to the immersion electrolyte.^{41,42} Essentially, what these authors have seen is the lifetime of the reactive metal in the coatings and the transition of cathodic protection behavior when sufficient metal is present to protect the substrate, to a more barrier-like system as metal oxides formed in the originally porous metal rich primer and reduced the porosity to give a higher resistance film. Our examinations of scribed systems gave similar results, and are shown in *Figures 13-15*, below. Our results just show the low frequency impedance modulus, $|Z|_0$ vs. time as this tracks the resistance of the coating system vs. time quite well.⁴³ Impedance data from damaged/scribed systems is notoriously difficult to interpret, as the damaged area of the coating dominates the electrochemical behavior of the system when its surface area is large. The impedance measurement in this case is averaging over the entire surface area under study.⁴⁴ The low $|Z|$ modulus values seen in *Figures 13-16* indicate conductive pathways are dominating the measurements in scribed areas. Comparison to the $|Z|_0$ data from undamaged neutral systems as shown in *Figure 16* demonstrates this further. In this case, all of the coatings are in excess of $10^6 \Omega$, some as high as $10^{10} \Omega$, while all of the scribed systems exhibit $|Z|_0$ values below $10^5 \Omega$, some as low as $\sim 150 \Omega$.

Basic conditions: pH=12.0, (Al most prone to dissolve)

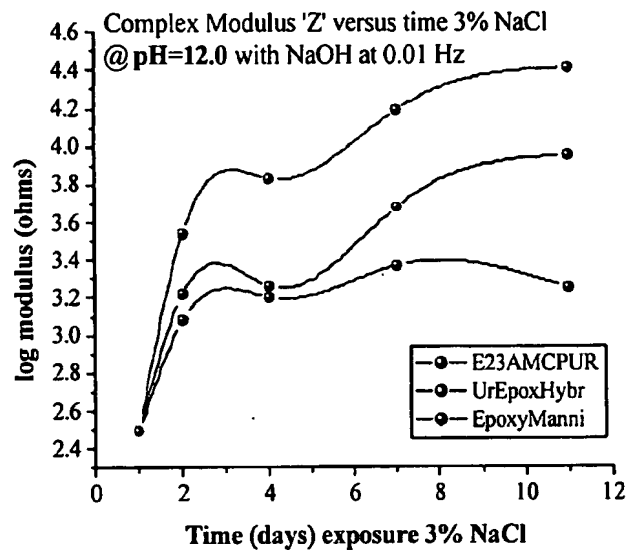


Figure 13. Log modulus vs time plot for circular scribe sample in basic immersion conditions at pH =12.0 .

Acidic conditions: pH=2.8, (Mg most prone to dissolve)

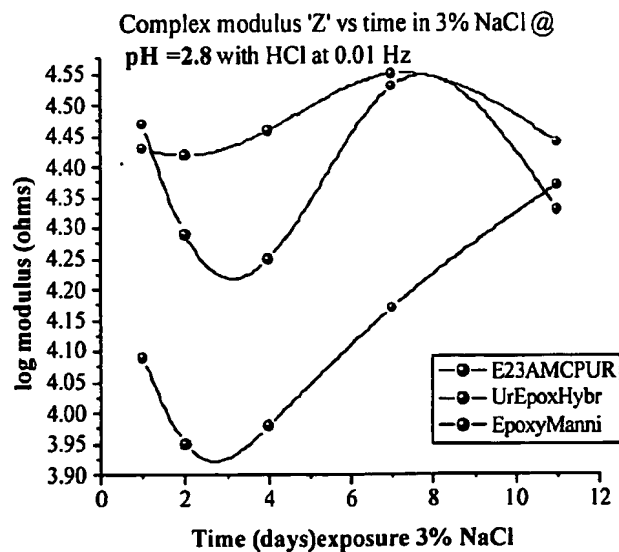


Figure 14. Log modulus vs time plot for circular scribed sample in acid immersion conditions at pH= 2.8.

Neutral conditions: pH=6.2, (Al stable, Mg meta-stable)

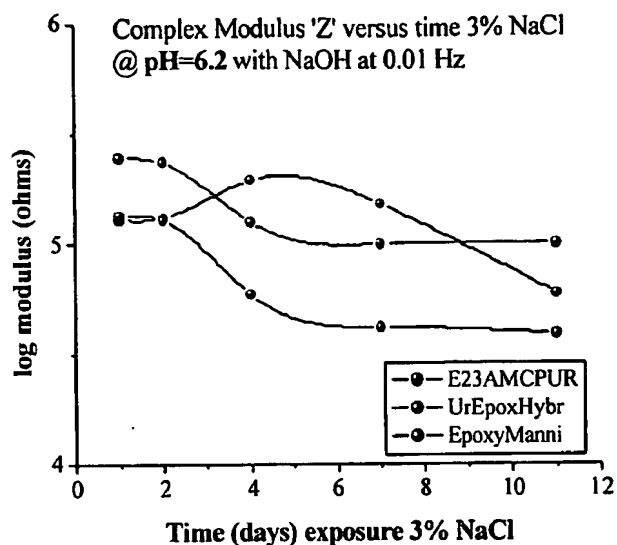


Figure 15. Log modulus vs time plot for circular scribed sample in 3% NaCl, neutral immersion conditions at pH=6.2.

E. Electrochemical Impedance Spectroscopy (EIS) of Non-Scribed Mg-rich Coatings

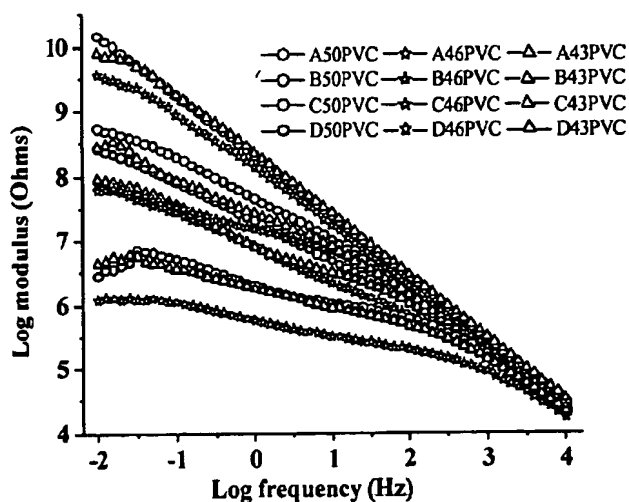


Figure 16. Bode plot of the four topcoated Mg-rich systems after 3 weeks continuous immersion in 3% NaCl solution: A) Epoxy-MDI hybrid; B) Polyurea (MC-PUR); C) Epoxy-HMDI hybrid; D) Epoxy / polyamide. Primers formulated at 43, 46, and 50 PVC.

Generally, it is reported⁴⁵ that low frequency impedance values less than 10^7 ohms/cm² result in coatings with a short service lifetime, and coatings with low frequency impedances greater than 10^7 ohms/cm² result in longer lifetimes. Much more data analysis on the electrochemical data for these Mg-rich systems must be performed, including estimates of diffusion effects from the Warburg tails of the data gathered from the damaged/scribed system, as well as estimates of water up-take from system capacitance calculations. This will be presented in a later paper from this laboratory and in the NDSU PhD. Thesis of M. Nanna, now in preparation.

All of the electrochemical data, especially that of *Figure 16*, corroborated that the coating system with the Mg-rich primer based on the hybrid polymers system performed the best

VII. Discussion of Results

A. Dynamic and Mechanical Property Results

Viscoelastic DMTA measurements of polymer films revealed that hybrid silane modified Epoxy-urea/urethanes displayed lower T_gs at equal crosslink densities to those of the parent materials suggesting the formation of bulk (-N-R-Si-O-Si-R-N-) bonds throughout the IPN matrix. In addition, the tensile properties of the silane modified epoxy-urea hybrids were better than their parent materials.

B. Flammability Results

There was no observed difference in flammability with respect to PVC for any of the four systems tested. The two conventional coatings, Polyurea (MC-PUR) and (Epoxy / polyamide) disbonded, liquefied, and incinerated with subsequent rapid magnesium incineration. The Hybrid-E23A, MDI, did not liquefy nor disbond, but formed a limited amount of char, without incineration of the magnesium metal. The Hybrid N3300, aliphatic, containing N-alkylisocyanurate⁴⁶ did not char nor did the Mg incinerate. It may be surmised that this Mg-rich coating was more covalently bonded to the Al substrate through the (-Al-O-Si-) linkages that may have exerted a positive influence on decreasing the coating's flammability.

C. Prohesion® Exposure Results

Results of (ASTM D5894-96) performed on the four coating systems with varying pigmentary Mg content from 43, 46, and 50% PVC, showed no clear trend in PVC as a function of exposure in dilute Harrison's solution. However, the 50% PVC samples in the hybrid formulations did perform slightly better. The silane modified Epoxy-MDI hybrid system performed best reaching about 5,000 hours before failure, while the aliphatic silane modified Epoxy-HMDI hybrid coatings failed over a range of 3,000~3,400 hours. The two other conventional Mg-rich coating systems: Polyurea (MC-PUR) and (Epoxy / polyamide), failed over a time period between 2,000 to 2,600 hours with no clear difference between the two conventional OTS coating systems.

D. Electrochemical Impedance Spectroscopy (EIS) Results

The EIS data for the damaged/scribed systems in *Figures 13-15* seem to indicate that the Mg-rich primers are providing active, cathode protection of Al 2024 T-3, and that the mode of protection of these systems is similar to Zn-rich primers for steel.

The undamaged coatings (see *Figure 16*) yield EIS data in Bode format after three weeks of 3%NaCl immersion for Mg-rich primers plus topcoat that shows no clear trend in PVC of Mg in the systems. The performance of the hybrid polymers system exceeds the other samples among the four coating systems studied and maintained the highest $|Z|_0$ throughout the study. Further, the behavior of this coating system was almost purely capacitive with only one time constant throughout this exposure, indicating an excellent coating system. However, the low frequency impedance $[Z]$ modulus in the (0.01 to 0.1Hz) range for the MC-PUR coatings is observed in the range of 10^6 ohms/cm² which is two orders of magnitude below the average for the other systems. This behavior is thought to be due to poor wetting of the primer by the ELT™ topcoat as revealed in SEM profiles, similar to *Figure 8*, in which numerous air channels and voids were observed to have formed at the primer/topcoat interface. Aside from this discrepancy the other coating systems displayed impedances that correspond to long lifetimes.

VIII. Conclusion

This study has shown that these pigmentary Mg systems provide sacrificial cathodic protection of Al aerospace alloys in a mode analogous to that of zinc-rich systems. It was also found that coatings formulated with conventional binders and conventional HAP solvents performed poorly in contrast with a hybrid silane modified epoxy-urea IPNs derived from non-HAP solvent systems. Thus it is crucial that this new paradigm for corrosion protection of Al by Mg-rich pigmentation be obtained in a coating polymer system that provides proper film properties for use as an aerospace primer coating.

References and Literature Cited

- ¹ J. Janata, D.Baer, G.P.Bierwagen, H.Birbaum, R. Buchheit, A. Davenport, H.Isaacs, F.Hedberg, M.Kendig, F.Mansfeld, B.Miller, A.Wieckowski, & J.Wilkes, "Issues Related to Chromium Replacement," presented at 187th Meeting of The Electrochemical Society, May 21-26, 1995, Reno, Nevada
- ² R.L.Twite, G.P.Bierwagen, "Review of Alternatives to Chromate for Corrosion Protection of Aluminum Aerospace Alloys," *Prog. Org. Coatings*, 33 (1998) 91-100
- ³ C. Hare, "Corrosion Control of Steel by Organic Coatings," Ch. 55 in *Uhlig's Corrosion Handbook*, 2nd Edition. R. W. Review, Editor, John Wiley & Sons, New York (2000) pp.1023-1038
- ⁴ S. Felix, R. Barajas, J.M.Bastidas, M. Morcillo & S. Feliu, "Study of Protections Mechanism of Zinc-Rich paints by Electrochemical Impedance Spectroscopy," in *Electrochemical Impedance Spectroscopy, ASTM STP 1188*, J.R.Scully, D.C.Silverman, & M. Kendig, eds., Amer. Soc. Testing and Materials (ASTM), Philadelphia, PA (1993) pp. 438-449
- ⁵ S. Böhm, R.J. Holness, H.N. McMurray and D.A. Worsley, "Charge percolation and sacrificial protection in zinc-rich organic coatings," Eurocorr 2000, Queen Mary and Westfield College, London, 10th-14th September 2000
- ⁶ Kalendová, A., Kuckáčová, A., *Macromol. Symp.*, 187 (2002) 377-386
- ⁷ Joseph H. Osborne, Kay Y. Blohowiak, S. Ray Taylor, Chad Hunter, Gordon P. Bierwagen, Brenden Carlson, Dan Bernard, and Michael S. Donley, "Testing and Evalation of Non-Chromated Coating Systems for Aerospace Applications," *Prog. Organic Coatings*, 41 (2001) 217-225
- ⁸ H.K.Yasuda, C.M.Reddy, Q.S.Yu, J. Deffeyes, G.P.Bierwagen & L.He, "Effect of Scribing on Corrosion Test Results," *Corrosion*, 57 (2001) 29-34
- ⁹ He, J., Johnston Gelling, V., Tallman, D.E., Bierwagen, G. P. and Wallace, G.G., "Conducting Polymers and Corrosion III: A Scanning Vibrating Electrode Study of Poly(3-Octyl Pyrrole) on Steel and Aluminum," *J. Electrochem. Soc.*, 147 (2000) 3667-3672
- ¹⁰ D.E.Tallman, Y. Pae, & G.P.Bierwagen, "Conducting Polymers and Corrosion 2: Polyaniline on Aluminum Alloys," *Corrosion*, 56 (2000) 401-410
- ¹¹ Information from Eckart GmbH, Kaiserstrasse 30, Fürth D-90763, Germany and technical references therein
- ¹² Jones D. A. Jones, *Principles and Prevention of Corrosion*, 2nd Ed., Prentice-Hall, Upper Saddle River, NJ (1996), Ch. 2

- ¹³ Gordon P. Bierwagen and Dennis E. Tallman, "Choice and Measurement of Crucial Aerospace Coating System Properties," *Prog. Organic Coatings*, **41** (2001) 201-217
- ¹⁴ Vsevolod N. Balbyshev, Gordon P. Bierwagen & R.L. Berg "Electrochemical Studies of Vinyl Ester Coatings for Fuel Tanks," Ch. 23 in American Chemical Society, ACS Symposium Series 689, *Organic Coatings for Corrosion Control*, G.P. Bierwagen, ed., 1998, p.292
- ¹⁵ Ellingson, L., "Corrosion Studies for the Protection of Aluminum Alloys and Outdoor Bronze," Masters Thesis, North Dakota State University, June (2001)
- ¹⁶ Song G., Atrens A., StJohn D., Nairin J., Li Y., "The Electrical Corrosion of Pure Magnesium in 1N NaCl," *Corrosion Science*, **39** (1997) 855-875
- ¹⁷ Bunker, B.C., Nelson, G.C., Zavaldil, K.R., Barbor, J.C., Wall, F.D., Sullivan, J.P., Windlisch, C.F. Jr., Englehart, M.H., and Baer, D.R., *J. Phys. Chem. B*, Vol. **106**, pp. 4705 – 4713 (2002)
- ¹⁸ Kramer, D., *Magnesium, its Alloys and Compounds*, US Geological Survey Open-File Report 01-341
- ¹⁹ Van Vliet, C.H., *Prog. Organic Coatings*, **34** (1998) 220-226
- ²⁰ Keijman, J.M. - High Solids Coatings: Experience in Europe and USA - Paper 40, Proceedings PCE Conference, The Hague, The Netherlands "Protecting industrial and marine structures with coatings", March 1997
- ²¹ Nanna, M.E., Ph.D. Dissertation, *Mg-Rich Coating Systems for AA 2024-T3 with Silane Modified Epoxy-Urea Primers*, North Dakota State University, Polymers and Coatings Department, (in preparation -2003)
- ²² Ni, H., Nash, H.A., Worden, J.G., Soucek, M.D., *J. Polymer Sci.: Part A: Polymer Chem.*, **40** (2002) 1677-1688
- ²³ Kohli, P., and Blanchard, G.J., *Langmuir*, **16** (2000) 4655-4661
- ²⁴ Vien, D. L.; Colthup, N. B.; Fateley, W. G.; Grasselli, J. G. *The Handbook of Infrared and Raman Characteristic Frequencies of Organic Molecules*; Academic Press: London, (1991)
- ²⁵ Ege, S. N. *Organic Chemistry*; Heath, D. C. and Co.: Lexington, (1989)
- ²⁶ Aresta, M.; Quaranta, E. *Tetrahedron*, **48** (1992) 1515
- ²⁷ Adapted from: Bayer Desmodure™ E-23A Moisture Cure Urethane, Zinc Rich Primer, Formulation # 294-35
- ²⁸ G.P.Bierwagen, R.S.Fishman, T. Storsved, & J. Johnson, "Recent Studies of Particle Packing in Organic Coatings," *Prog. Organic Coatings*, **35** (1999) 1-10
- ²⁹ Walker, P., "Organo Silanes As Adhesion Promoters for Organic Coatings," *Journal of Coatings Technology*, Vol. **52**, No. 670, November, pp. 49-61 (1980)
- ³⁰ Bhargava, A., and Griffin, G.J., *J. Fire Sciences*, **17**, (May/June 1999) 188-208
- ³¹ Hill, L.W., *Prog. Organic Coatings*, **31** (1997) 235-243
- ³² A. Hale, C. W. Macosko and H. E. Bair, *Macromolecules*, **24** (1991) 2610
- ³³ Tewarson, A. and Pion, R. F., *Combust. Flame*, **26** (1976) 85-103
- ³⁴ Chiang, C-L., Wang, F-Y., Ma, C-C., M., and Chang, H-R., *Polym. Degrad. Stab.*, **77** (2002) 273-278
- ³⁵ Reymore HE, Lockwood RJ, Ulrich H., *J. Cell. Plast.*, **14** (1979) 332
- ³⁶ Dick C, Dominguez-Rosado E, Eling B, Liggat JJ, Lindsay CI, Martin SC, *Polymer*, **42** (2001) 913-23
- ³⁷ Fabris, H.J., "Thermal and oxidative stability of urethanes," *Advances in Urethane Science and Technology*, Vol. 4, pp. 891-911 (1976)
- ³⁸ Singh, LW, and Mollica, J.C., *Rubber Age*, **98** (1966) 12
- ³⁹ Schwindt, J. Moisture-Cured, Polyurethane-Based Surface Tolerant Coatings: An Economical Alternative for Corrosion Control, Leverkusen, Germany, Bayer Co., Formulation # 294-35 (2001)
- ⁴⁰ Zhu, V., and van Ooij, W.J., *J. Adhesion Sci. Tech.*, Vol. **19** (2002) 1235-1260
- ⁴¹ J.R. Vilche, E.C.Bucharsky & C.A.Guidice, "Application of EIS and SEM to evaluate the influence of pigment shape and content in ZRP formulations on the corrosion prevention of naval steel," *Corr. Sci.* , **44** (2002) 1287-1309
- ⁴² C.M. Abreu, M. Izquierdo, M Keddad, X.R.Novoa, and H. Takenouti, " Electrochemical Behaviour of An-rich Epoxy paints in 3% NaCl Solution," *Electrochim. Acta*, **41** (1996) 2405-2415
- ⁴³ Gordon Bierwagen, Dennis Tallman*, Junping Li and Lingyun He, "EIS Studies of Coated Metals in Accelerated Exposure," *Prog. Organic Coatings*, **46** (2003) 148-157
- ⁴⁴ L.V.S.Phillippe, G. Walter and S.B.Lyon, "Invesigating Local Degradation of Organic Coatings," *J. Electrochem. Soc.*, **150** (2003) in press
- ⁴⁵ Bierwagen, G.P., Jeffcoat, C.S., Li, J., Balbyshev, S., Tallman, D.E., and Mills, D.J., *Prog. Organic Coatings*, **29** (1996) 21-20
- ⁴⁶ Levchek, L.V., Levcheck, G.F., Balabanovich, I.A., Gambino, G., and Coasta, L., *Polym. Degr. and Stab.*, **54** (1996) 217-222

PART XVII

Certain aspects and embodiments of the present invention are described in the following text and figures.

Environmentally Acceptable Coatings for Aerospace Alloys

Abstract

An environmentally acceptable coating system has been developed and tested for use on aluminum alloy structures. The coating system is based on magnesium-rich technology which is analogous to zinc-rich technology that has been traditionally used for protecting steel structures. The system is easily manufactured as paint and can be applied with conventional spray equipment. Performance tests have demonstrated excellent corrosion resistance, durability, and flame retardant properties.

Why do we need something different?

Chromate compounds in aqueous solutions are well known to improve the corrosion resistance of many metals and alloys. However, health and environmental hazards associated with hexavalent chromium have been increasingly recognized, and as a consequence much research has been initiated world-wide to find more environmentally-friendly alternatives to chromate. Chromium is a Resource Conservation and Recovery Act (RCRA) listed characteristic waste (D007), and certain anodizing waste streams can be listed as nonspecific source hazardous wastes (F006), by the EPA. No suitable replacement is yet identified at present, because the mechanism of chromate inhibition still remains unclear and thus no methodology to develop new alternatives is established.

Innovation

Development of a magnesium-rich coating system for aerospace aluminum alloys that is an environmentally benign replacement of chromate-based technologies.

What's the cost of Mg-Rich Coatings?

Production costs (Estimate)		
-	Given 3-lbs per gallon Mg Powder ~ 65-PVC cost~ \$500.00	
-	figure Mfctr. cost \$800/gallon ~ 300 ft2/gal (primer) [Very Liberal]	
-	& (\$100/gallon ELT)~200 ft2/gal (primer)	
-	Total cost for Primer and Topcoat at~ \$1,000 per /gallon:	
-		
-	<u>Mg-Rich System</u>	<u>Chromated System</u>
-	Paint	\$14.50/ft2
-		
-	Application cost	< \$11.20/ ft2

- **Plus:**
- *Reduced HAZMAT disposal costs * Greatly reduced hazardous materials *
- Reductions in medical claims * All non HAPs listed Solvents* Landfill disposable *
- Reduction of paint facilities * Shirt environment * No HAZMAT protective gear.
- (Note: cost of Mg powder~ 80mm may eventually approach cost of atomized Mg powder less than 5 mm @ \$13.00 per pound)

Accomplishments

A magnesium powder primer/ coating system that does not contain chemicals or materials that are hazardous, toxic, or give rise to health and safety concerns.

Successful demonstration of protection for greater than 3,000 hours during salt fog exposure, according to MIL-C-81706, for aerospace aluminum alloys, such as 2024T-3.

The Mg-Rich coating can be applied by dipping, painting, or spraying, with short treatment times at low temperatures, and is compatible with existing cleaning and pretreatment procedures.

Only commercially available chemicals and materials are used, which do not require special storage provisions and can be easily adapted into existing application methods.

I. Silane Modified Multi-Layer / IPNs

The growth of covalent silane-functional multilayer assemblies, for coatings used in corrosion control, can be derived from multi-layer isocyanate / amine, polyurea chemistry that involves surface-bound terminal amines reacting with isocyanates and water to produce an aminated surface that can subsequently react with solution phase isocyanates.[1] Kohli, P., and Blanchard, G.J., *Langmuir*, Vol. 16, pp. 4655- 4661 (2000)40

I. Silane Modified Multi-Layer / IPNs

The growth of covalent silane-functional multilayer assemblies, for coatings used in corrosion control, can be derived from multi-layer isocyanate / amine, polyurea chemistry that involves surface-bound terminal amines reacting with isocyanates and water to produce an aminated surface that can subsequently react with solution phase isocyanates.[1] Kohli, P., and Blanchard, G.J., *Langmuir*, Vol. 16, pp. 4655- 4661 (2000)40

Surface reactions:

The polymerization reactions in this experiment were initiated at the Al surface from lateral M–O–S–R–NH₂ bonds, (where M~Al, and R–NH₂ ~ organic moiety) parallel to the substrate and extending into the bulk:

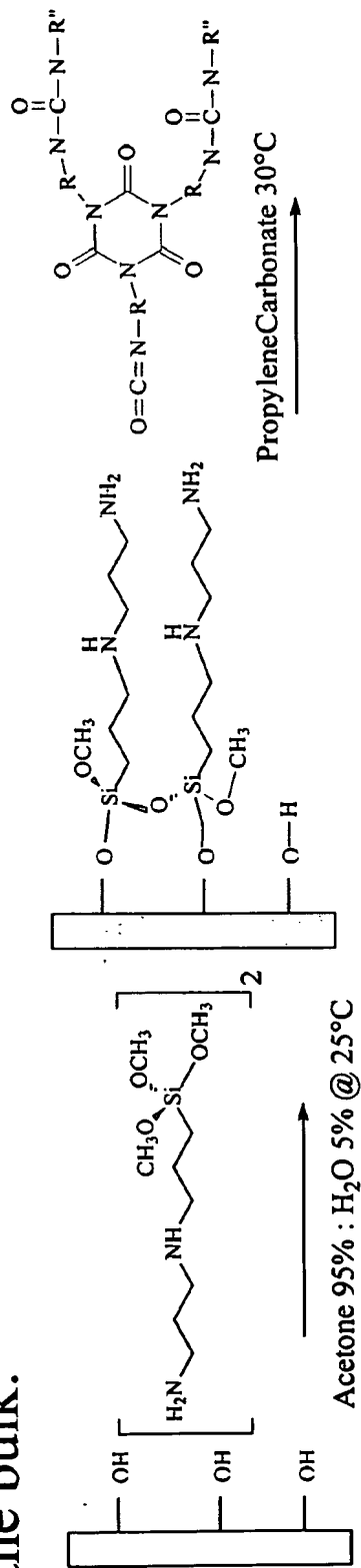


Figure -1 initial sol reaction with surface hydroxyls and β -(aminoethyl)- γ -aminopropyltrimethoxysilane

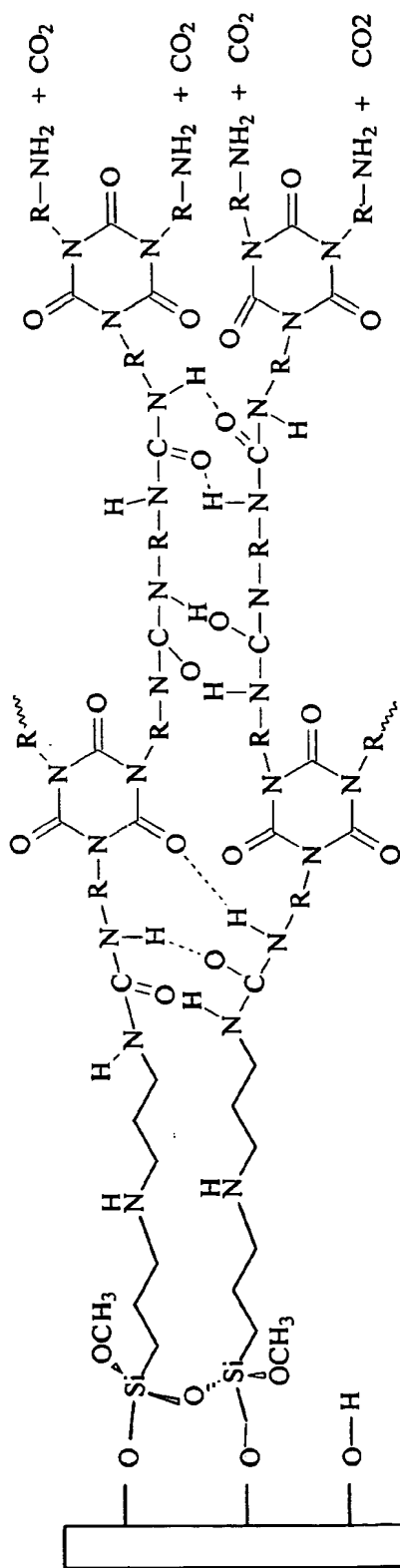


Figure -2 terminal surface amines reacting with isocyanates in solution phase (HMDI or MDI prepolymers) (forming both amines and carbon dioxide, that are intermediates in the Hoffmann rearrangement of an isocyanate with water) to yield a reactive / reaminated second layer.

Bulk reactions with crosslinker

The crosslinker (used in both Epoxy- HMDI and Epoxy- MDI hybrids) : 7-phenyl-1-[4-(trimethyl-silyl)-butyl]-1,2,3,4-tetra-hydro- quinoxalin-6-ol (figure 3, center) synthesized in these laboratories, was added to promote bulk polymerization throughout the IPN matrix.

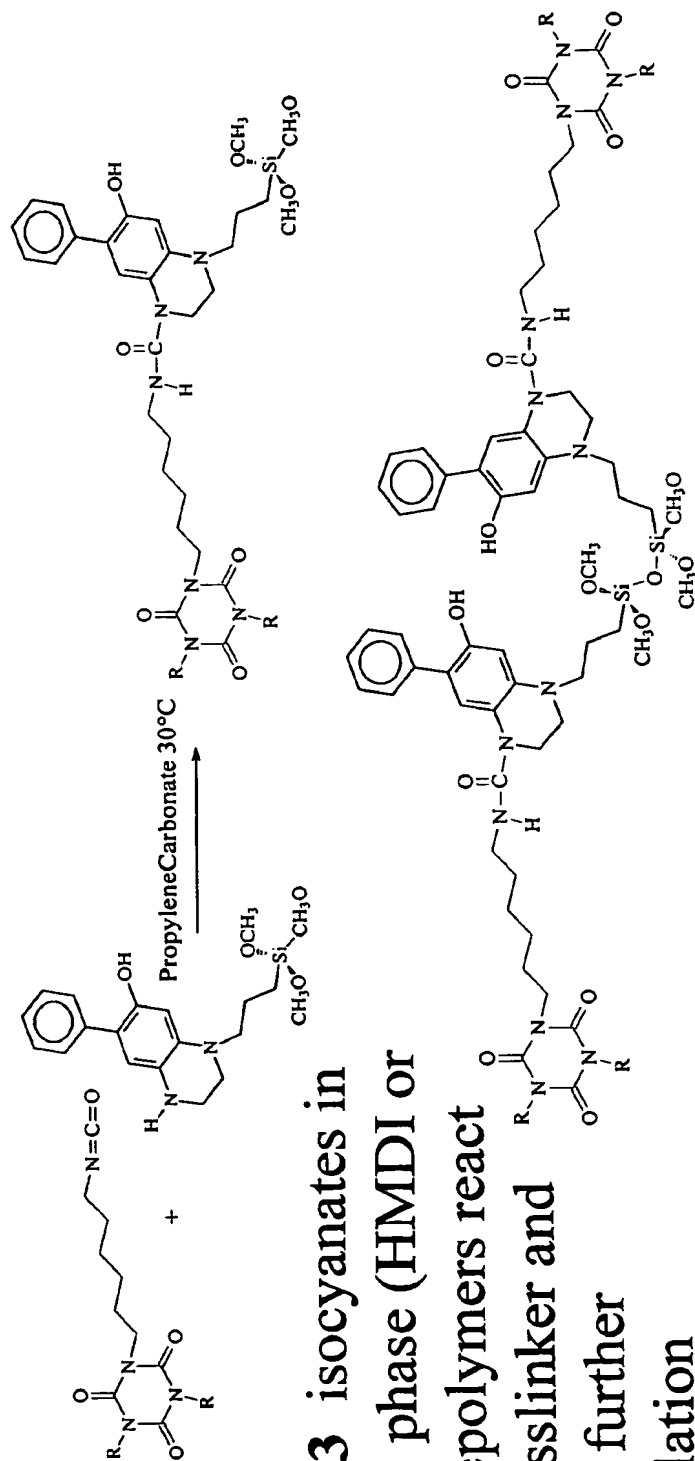


Figure -3 isocyanates in solution phase (HMDI or MDI prepolymers react with crosslinker and undergo further hydrosylation

Mechanical Properties of Polymers

Tables 1 & 2- give mechanical properties of polymeric films from hybrid polymers and select resin systems:

Table 1 Viscoelastic properties of binder films			
Binder	Tg (°C)	Crosslink density (mol/cm ³)	E' (Pa) minimum
N3300 (MC-PUR)	122	3.4 x 10 ⁻³	2.6 x 10 ⁷
E23A MC-PUR	159	5.8 x 10 ⁻⁴	6.6 x 10 ⁵
Epoxy-polyamide	65	2.1 x 10 ⁻³	2.0 x 10 ⁷
Hyb-N3300	96	1.3 x 10 ⁻³	1.3 x 10 ⁷
Hyb-E23-A	100	6.9 x 10 ⁻⁴	6.9 x 10 ⁶

Table 2 Mechanical properties of coating polymer films			
Polymer Film	Elongation at-break (%)	Tensile strength (MPa)	Tensile modulus (Mpa)
N3300 (MC-PUR)	8.0 ± 0.1	45 ± 7	1250 ± 90
E23A (MC-PUR)	5.0 ± 0.3	25 ± 6	825 ± 110
Epoxy-polyamide	18.0 ± 0.1	5 ± 0.9	150 ± 50
Hyb-N3300	6.0 ± 0.3	56 ± 9	1800 ± 50
Hyb-E23-A	5.5 ± 0.2	50 ± 5	1500 ± 50

III. Magnesium-Rich Primers

- The primers were prepared using conventional techniques. The magnesium powder was a 50:50 volume mix, of (Eckagranules™ PK 31 ~ 30µm, and PK-51 ~ 70µm) provided by Eckart Inc. and was used as received. A 50:50 volume mix of the two powders yielded a higher bulk density value than that of either powder alone, and 60PVC was selected as the upper limit to the approximated CPVCs for each system, see figure 7.

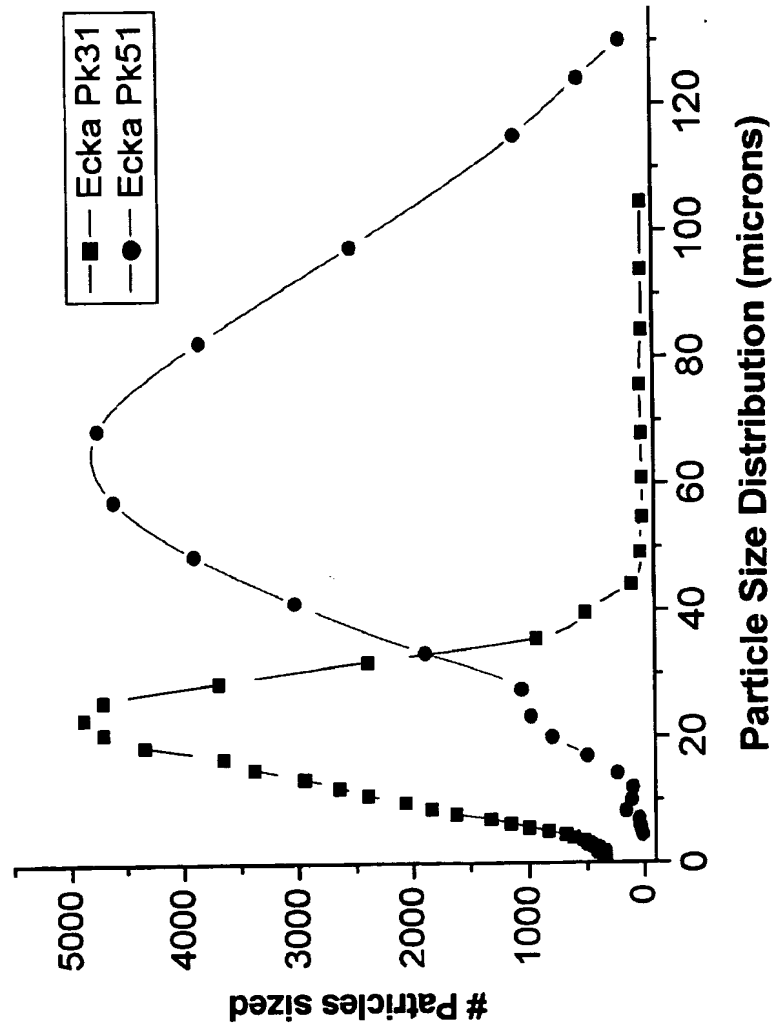


Figure 4- Particle size distribution (PSDs) For magnesium powders, Eckart Pk31 ~ 30 μ m & Pk51~70 μ m Eckart granuels® used at a 50:50 mix

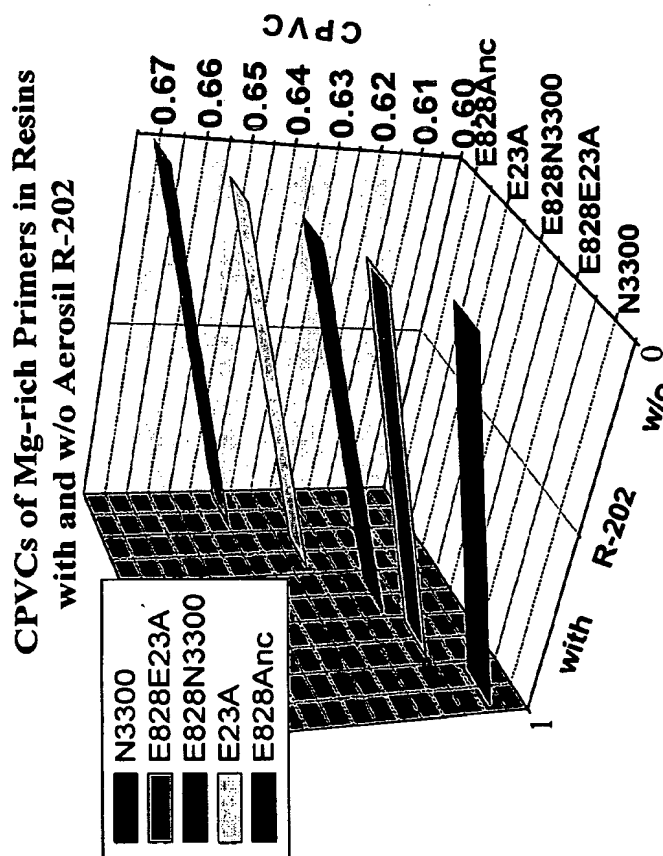


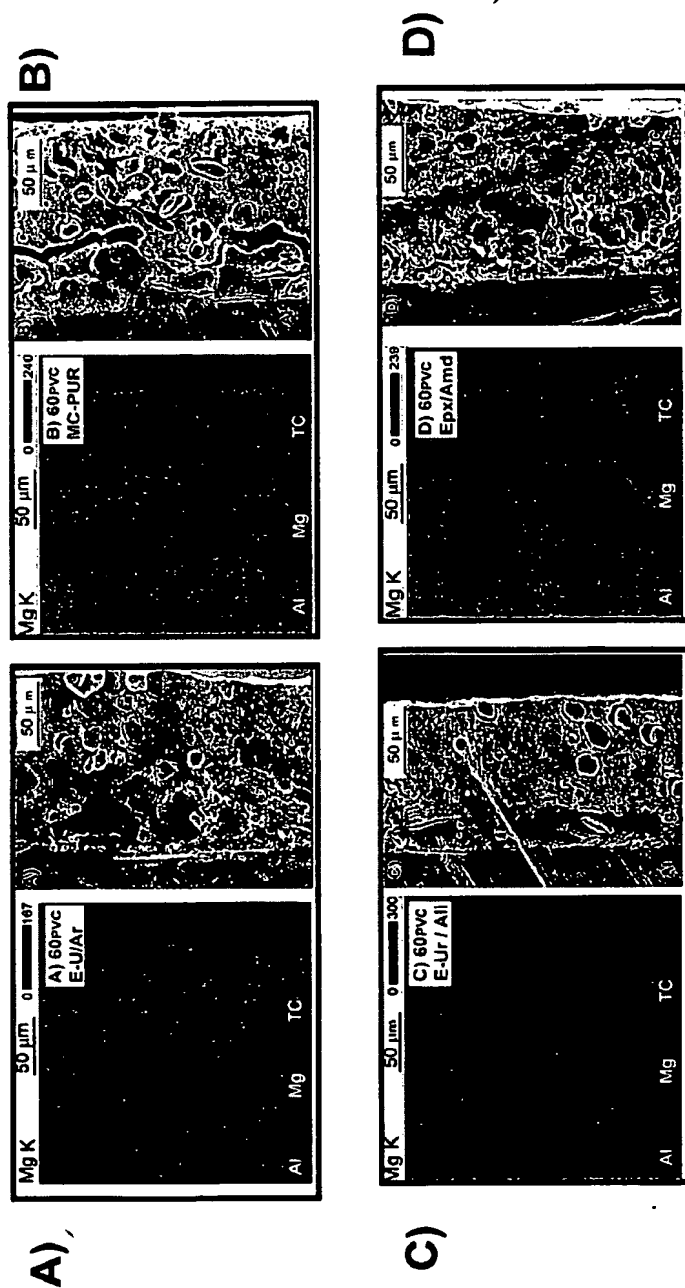
Figure 5- Effect of resin type and filler on critical pigment volume concentration (CPVC) oil absorption (OA) of magnesium powders with and without Aerosil™ R2O2 silica

Magnesium rich Primers & Topcoat

Table 2- Magnesium rich primer materials / formulations

Formulation	Materials
A) Hyb-E23A	Desmdodure® E23-A, Aerosil® R202, Eckagranules® PK51/31, Epon® 1001CX, Propylene Carbonate/EEP
B) MC-PUR	Desmdodure®E23-A, Bentone® 34, Eckagranules® PK51/31, Anti Terra®U, Aromatic solvent Xylol
C) Hyb-N3300	Desmdodure® NC-3300, Aerosil® R202, Eckagranules® PK51/31, Epon® 1001CX, Propylene Carbonate/EEP
D) Epoxy-Polyamide	Epon® 828, Epicure® 3115 [†] , Aerosil® R202, Eckagranules® PK51/31, Anti Terra®U, Aromatic solvent Xylol,

Figures 6 A, B, C, and D are EDAX & SEM cross section profiles of **A)** 60 PVC Epoxy-MDI hybrid; **B)** 60 PVC Moisture cure Polyurea (MC-PUR); **C)** 60 PVC Epoxy-HMDI hybrid; **D)** Epoxy / polyamide. Al 2024 T-3 substrate with ~50 micron FT Mg-rich primer, topcoated with ~70 micron film thickness ELT™ topcoat.



Flammability and Mg-rich coatings

The two conventional coatings, (figure -7) disbonded when heated, liquefied, and incinerated with subsequent magnesium incineration; both followed the path (figure-8) of combustion products and char-2 ~ C2. The Hybrid-E23A, from MDI, did not liquefy or disbond, but formed a limited amount of char-1 ~ C1, without incinerating the magnesium metal. Finally, the HybridN-3300, from (HMDI) aliphatic, evolved non-flammable gas and did not char. It may be surmised that coatings covalently bonded to the Al substrate through -Si-O-Si- linkages acts to increase the effective limiting oxygen index(LOI).

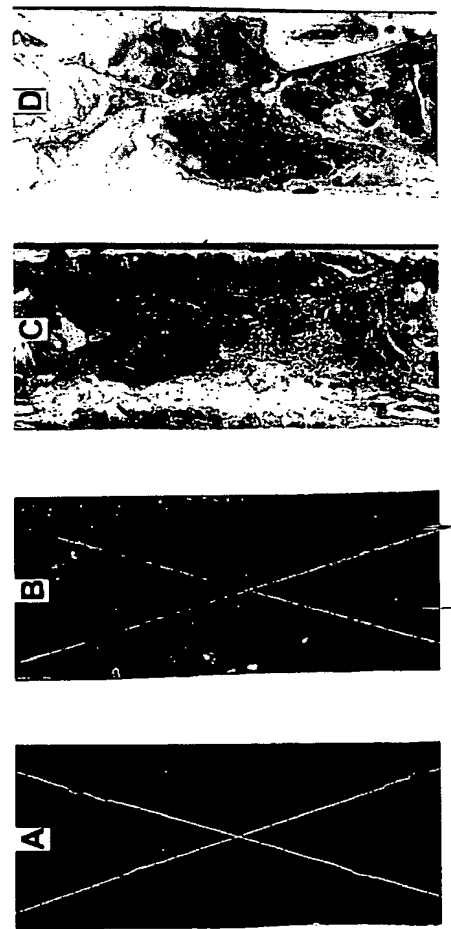


Figure 7- A, B, C, and D—results from modified UL-94 flammability test 1120°C (2048°F) was applied for 30 seconds. From least affected Hybrid N3300; B) HybridE23A to most affected C) MC-PUR; D) Epoxy-polyamide.

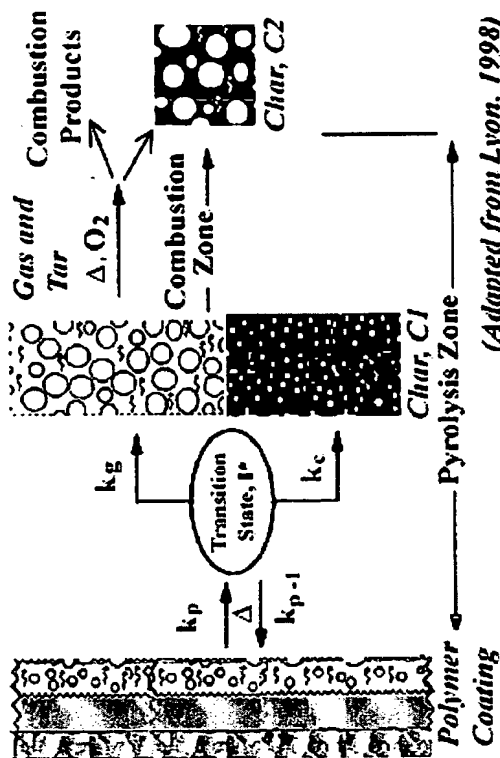
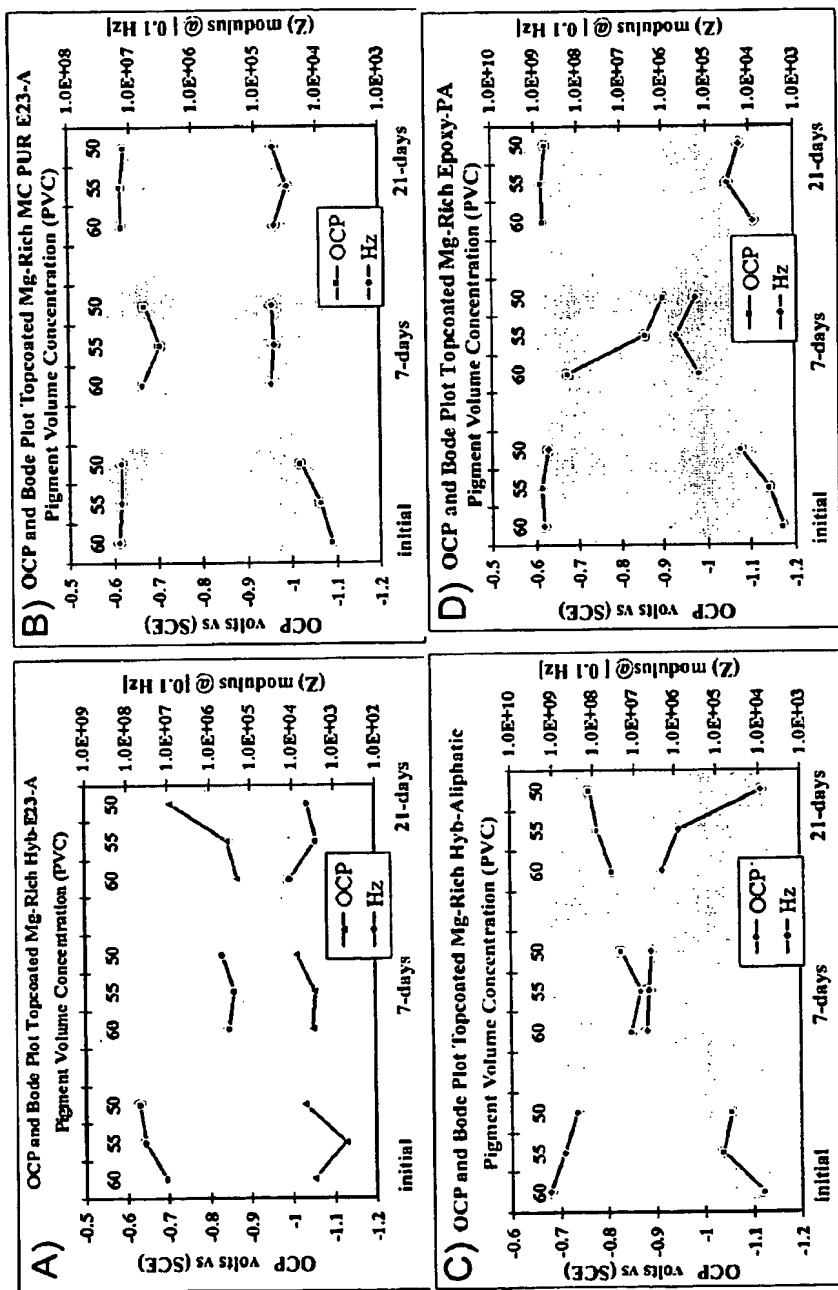


Figure 8- kinetic flammability model adapted from Lyon (1998).
Lyon, R.E., Polymer Degradation and Stability, Vol. 61, pp. 201-210 (1998)

VI. Electrochemical Testing



Figures 9 A, B, C, & D – Effect of exposure in 3% NaCl solution on open circuit / Ecorr / low frequency impedance \sim (0.1 Hz) for topcoated Mg-rich primers at 50, 55, and 60 PVC for the four coating systems: A) Hybrid E23A; B) MC-PUR; C) Hybrid N3300; D) Epoxy-polyamide.

EIS) and E_{corr} Open circuit Potential (OCP)

- From (figures 9 A-D) OCP and EIS data, collected on topcoated Mg-rich panels show three distinct periods that clearly distinguish the evolution and effectiveness of cathodic protection in the Mg-rich coatings as a function of exposure time in 3% NaCl.
- **Period I.** Initial immersion day one, the “activation” period when the value of the corrosion potential shifts to a cathodic value 1.1V vs SCE, corresponding to the Mg metal / Al-2024 T-3 mixed potential in the electrolyte. Magnesium immediately begins to react with the NaCl solution, it is “activated” leading to better metal-to-metal electrical contact being established between magnesium particles and Al surface.
- **Period II.** Once past the “activation” period, the cathodic protection mechanism reaches its peak due to a maximum in the ratio of magnesium-to-aluminum area ratio. This occurs around day 5~7 when the corrosion potential shifts to a more anodic value of about -0.9V vs SCE; it is where a relative stabilization called the “transition” period occurs.
- **Period III.** After the transition period, and up to day 21, the corrosion potential shifts out of the cathodic protection domain, and the potential fluctuates as the film’s solution chemistry begins to change. At which time oxygen reduction begins to occur on the upper part of the film causing a local increase in pH that changes the corrosion products from magnesium hydroxides to magnesium hydroxides, the same as at the interface.
- Overall, figures 9-A-D show that the hybrid coatings maintained slightly more negative E_{corr} values at 21 days exposure suggesting less change in the magnesium-to-aluminum area ratio as a result of better coating adhesion to the substrate.

Conclusion

Coatings formulated with conventional binders and HAP solvents (epoxy/polyamide & MC-PUR) performed poorly in contrast with the hybrid silane modified epoxy-urea-urethanes with non-HAP solvents. This study serves as a reference and starting point for the development of coatings based on Mg-rich pigmentation with inorganic / organic hybrid polymeric matrices used for corrosion control of aerospace alloys.

PART XVIII

Certain aspects and embodiments of the present invention are described in the following text.

Enhancing the Performance and Efficiency of Mg-rich Primers for Aluminum and its alloys

Concept #1

Instead of the present high electrical resistance, low dielectric constant, polymer matrix used in the Mg-rich coatings under development at NDSU, use a matrix that consists of:

- a. an inherently conducting polymer such as doped polyaniline or doped polypyrrole
 - b. a polymer matrix modified to increase its conductivity by the presence of a very small particle size conductive pigment such as C-black
 - or, c. a polymer doped with pigmentary form of an inherently conducting polymer.
- Such a formulation of an Mg-rich primer would extend the lifetime of effectiveness of such a primer beyond its present electrical connectivity to Mg limitations of the percolation threshold limitation (circa 30% volume fraction Mg) to almost 100% electrical connectivity to Mg through a conductive polymer matrix. This would make almost all of the Mg pigment useful in the cathodic protection of the Al or Al alloy substrate.

Concept #2

Develop a Mg-rich coating with an inherently conducting polymer (ICP) as its polymer matrix which has the ICP doped with organic or inorganic dopants that are corrosion inhibitors for Al and its alloys. This would extend the corrosion protective lifetime of such a primer beyond the limits imposed by the amount of Mg pigment present.

PART XIX

Certain aspects and embodiments of the present invention are described in the following text and figures.

MG-RICH COATINGS FOR Al 2024 -T3 FROM SILANE MODIFIED HYBRID EPOXY-POLYUREA POLYMERIC MATERIALS

ABSTRACT

This study has shown that pigmentary magnesium-rich coating systems can be devised to provide sacrificial cathodic protection to Al 2024 T-3 / aerospace alloys in a mode analogous to that of zinc-rich systems for steel. It was also found that conventional coatings formulated with traditional polymeric materials and "hazardous air pollutant" (*HAP*) solvents performed poorly in these Mg-rich systems in contrast with the novel silane modified hybrid epoxy-urea polymeric materials containing non-HAP solvents. Moreover, through exploring siloxane chemistry, similar to those *sol-gel* systems, a hybrid epoxy-urea polymeric material was custom tailored and applied in a multi-layer fashion to an Al 2024 T-3 substrate for corrosion control that yielded performance properties surpassing those delivered by conventional technology. Thus a new paradigm for corrosion protection of Al by Mg-rich pigmentation was obtained in a coating polymer system that provides proper film properties for use as an aerospace primer coating. By the combination of the inorganic polymeric structure of the polysiloxanes with the organic epoxy binder system, the coating allows the replacement of traditional anti-corrosive systems with three or four coats by a two coat system, i.e., Mg-rich primer plus topcoat. The final implication of all

of these studies lies in the overall convenience these systems can deliver as they are applied and cure at room temperature with minimum surface preparation requirements. The coating system is spray applied which underscores another convenient feature that it delivers to those who chose to employ it. However, it may also be surmised that at this stage of development that these coating systems may not be appropriate for providing corrosion control to all structural aluminum alloy systems. However, for the sake of environmental acceptance, effectiveness of corrosion control, and ease of application this system has demonstrated great potential as a corrosion coating for aerospace aluminum alloys such as Al 2024 T-3.

Chapter 1. Coatings for Structural Aluminum Alloys

Introduction

As an environmentally allowable alternative to chromate pigments and pretreatments commonly used in corrosion control coatings for Al alloy 2024 T-3 (widely used in aircraft), primer coatings as part of an integral coating system, based on particulate magnesium pigmentation, analogous to Zn-rich primer coatings used to protect steel structures, were investigated for the purpose of providing protection to this Al alloy. In addition, the nature of a suitable polymeric material for use as a binder matrix in these Mg-rich cathodic protective coatings applied to AA 2024 T-3 structures was investigated as well. Such polymer matrices were synthesized, formulated and tested. The results showed that all Mg-rich primers afforded some element of cathodic protection to the Al 2024 T-3 substrate, but the discerning factor in these studies was the primer's ability or inability to sustain stability in high pH conditions, yield excellent adhesion, be easy to apply, and most important provide wet adhesion in the presence of an aggressive environment.

Purpose of this study

The major objective of this investigation is the development of a non-chromated and environmentally benign coating system that can be easily applied to aluminum alloys to better service and protect a wider range of structural applications. For example, the coating system conforms to high structural engineering standards required by aerospace technologies. The first step lies in identifying and efficient, low cost, environmentally acceptable, corrosion inhibitor that may be incorporated into a viable coating system. Next, the major scientific issues pertaining to the development of such a system will be

identified, such as material synthesis, characterization, test protocol, and performance testing. The coating system will be evaluated in terms of ease of processing and application, efficiency, performance, price, reproducibility, safety, stability, service life, and toxicity.

Coating systems for structural aluminum alloys have become more complex as the list of integral selection factors grows to include even more performance characteristics such as, efficiency in cost and application, environmental impact, future maintenance and eventual disposal of removed coatings. Since the 1960's, strontium chromate based primers in combination with high solids epoxy coatings and polyurethane topcoats applied to structural aircraft have been state of the art in corrosion protection and weathering resistance. As formulated, these high solids, high build chromated epoxy coatings exhibit excellent corrosion protection and performance in addition to their compliance with the low VOC regulations. Originally these high solids coating systems, specifically the high solids, high build epoxy coatings, were developed as high performance primers, for use in conjunction with a chromate surface preparation. The tolerance for aluminum surfaces by these systems was obtained by integrating low molecular weight low viscosity epoxy and synthetic resin blends combined with selected curing agent mixtures and a chromate conversion coat.

Present coating systems rely heavily on use of organic polymers in conjunction with chromate pigments and / or chromate surface treatments such as chromate conversion coating (CCC) systems. As an alternative to these (CCC) systems, silicon based inorganic coatings using silicates and silicones as binders have been used to use to protect a wide array of steel structures in a variety of environments. The chemistry of these silane

modified systems involves a process called hydrolytic polycondensation and has lead to a particularly successful approach to formulating high solids coating with organic binder systems, such as epoxy siloxane hybrid coatings. The chemical combination of aliphatic / aromatic epoxies with polysiloxanes results in a polymer with higher performance characteristics than those obtained by the physical combination of both polymers.

These epoxy siloxane hybrid coatings are “high solids” vehicles that attain volume solids contents of up to 90 percent and can be achieved by combining organic binders with siloxane polymers, in this way the properties of the traditional resins have been selectively and significantly upgraded. The versatility of the siloxane chemistry enables the construction of polysiloxane hybrids with epoxies, vinyls, acrylates, fluorinated and phenol resins. Overall, coating systems based on the combination of the inorganic polymeric structure of the polysiloxanes with the organic epoxy binder system, have lead to coatings that combine the corrosion resistance of high build epoxy polymers and the weatherability of the best aliphatic polyurethane finish coats.

Another key property of siloxane modified compositions is their inherent compatibility with reactive metals such as zinc. As a result, considerable improvement in durability and corrosion resistance has been achieved by the introduction of siloxane modified zinc-rich epoxy primers with epoxy siloxane topcoats. Results from a series of exposure and performance tests -by various independent laboratories -such as, Norsok spec. standard M-CR-501, ACQPA, ISO 12944, U.S. Navy testing, showed that silane modified coatings demonstrated improved performance and concluded that coating systems consisting of a zinc based primer with the epoxy siloxane topcoat performed better than any other coating system tested. ¹

Background

Since the mid-1970's, the coatings industry has been widely affected by government regulatory agencies instituting a myriad of preventative measures to protect or improve the environment and change the perceived maligned practices of the coatings industry. It all came to pass when the California Air Resources Board (CARB) identified the solvents in coatings as a contributor to air pollution via photoactive reactions that may occur with nitrogen oxides in the presence of sunlight and heat to generate lower atmospheric ozone. The term applied to these solvents and contributors of air pollution was volatile organic compounds (VOCs), as they have since been classified as the solvents in coatings and paints that evaporate during application, drying and curing.² Through out the 1990's, a time of maximum regulatory impact, difficult and challenging chores faced the industry and forced it to face the paradigm of modern coating systems design.

During this period of proposed change the drive towards environmentally acceptable coatings industry's response was initially to reformulation for compliance and to take a more scientific approach to solving the coatings paradigm. The most commonly accepted definition of a scientific approach is that it is an organized body of knowledge dealing with the physical and chemical information of materials commonly used in products. To realize results from this new organizational effort, the coatings industry investigated new procedures called "test protocol" where for any specific kind of coating a set of testing procedures could be applied that related directly to the kind of testing the paint system required to simulate and evaluate its performance in a logical manner. Establishing this new testing protocol required deviation from traditional methodology that had failed to keep pace with the mandates of newly imposed changes.

Spurning these changes in the governmental arena were the sweeping acts and orders such as those derived from the following:

- **Pollution Prevention Act Of 1990**
 - Source reduction
 - Recycled in an environmentally safe manner
 - Treated in an environmentally safe manner
 - Disposal or other release into the environment should be deployed only as a last resort
- **Executive Order 12856**
 - “...The federal government should become a leader in the field of pollution prevention through the management of its facilities, its acquisition practices, and in supporting the development of innovative pollution prevention programs and technologies”
- Coatings systems must comply with most stringent regulation
 - Must determine which regulations may apply to a coating/solvent
 - Paint by Paint
 - Formulation by Formulation
- Goal: HAP-Free Solvents and De-painters
 - Reduce/ Eliminate need for Record-keeping
 - Eliminates need for detailed material composition
- HAP-Free others where practical
 - Certain High-Performance applications may still require High HAPs
Wherever possible, eliminate HAPs, increasing Solids/HAPs ratio.

“The Department of Defense must improve its environmental performance by actively implementing policies that embrace pollution prevention in all phases of the acquisition process, the procurement of goods and services and in the life-cycle management of our installations.”

Secretary of Defense William Perry
11 August 1994

In addition to these broad changes, it was also decided that military aircraft in the aging Air force fleet have now been required to serve far in excess of their anticipated service lifetimes.³ Starting from a study of 1991 statistics, revealed that 31 percent of the

entire U.S. aircraft fleet exceeded performance and design goals and it was projected that by the year 2000 about 60 percent of the worldwide fleet of U.S. manufactured aircraft would be 20 years old.⁴ For example, see Figures 1-A and 1-B, below. Many of the Air Force's workhorse aging aircraft such as the Fairchild A-10 Thunderbolt II attack plane that first flew in May 1972 and Boeing's B-52 Stratofortress bomber that first flew in 1952 are still in service in year 2003 with plans to retain them for yet another 20 years. Figure 1-A, below, gives a time progression account of aircraft in US Air Force inventory with relative portion of new aircraft groups to be subsequently added to old, and Figure 1-B, below, gives supplemental cost projections for avionics maintenance.^{5,6,7,8}

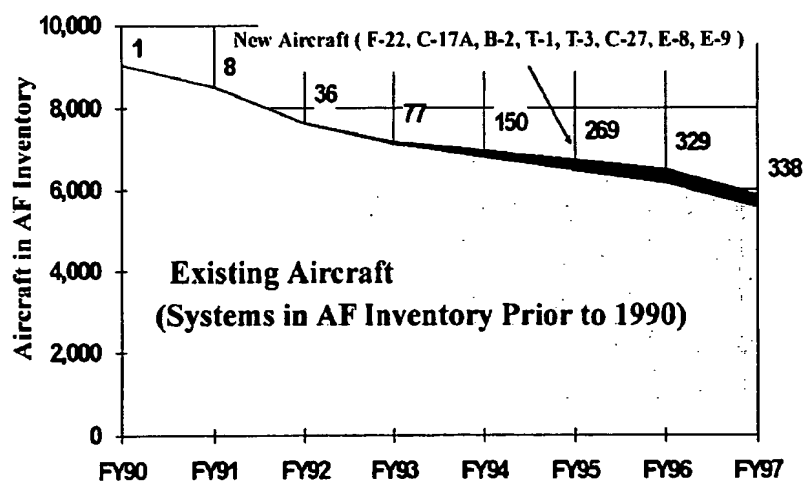


Figure 1-A. US Air Force aircraft inventory and projected supplement schedule.⁹

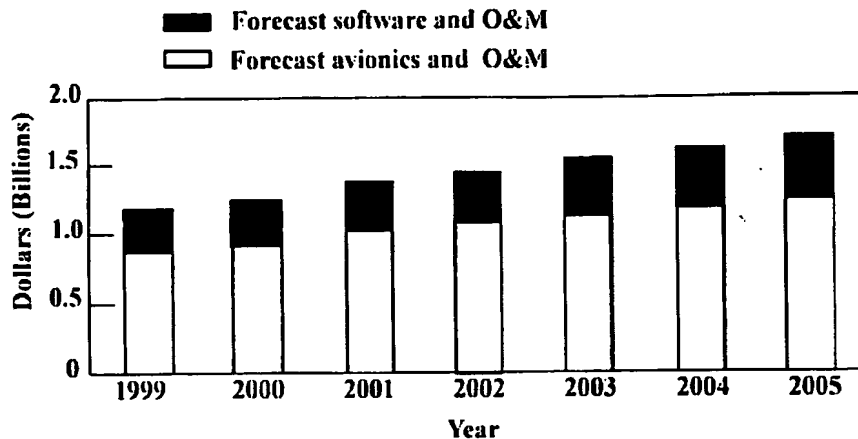


Figure 1-B. US Air Force forecast for projected cost (in dollars) for supplemental software and avionics overhead & maintenance (O&M).⁹

In light of such forecast statistics the USAF Office of Scientific Research responded by reaching out to qualified universities and funding numerous projects on Al corrosion inhibition and protection through the Defense Advanced Research Projects. These grants came in the form of University Research Initiative (URI) programs, one of which was established at North Dakota State University in the Polymers & Coatings department in 1996. As a result of such an association the Polymers and Coatings department at NDSU has greatly furthered the advancement of such multi-parameter methods / techniques that have been successfully applied to the evaluation and testing of structural coatings used to protect military aircraft fabricated with high strength aluminum alloys for the U.S. Air Force (USAF).^{10, 11}

Therefore, the emphasis of this thesis will focus on a combination of traditional formulation protocol augmented with fast and reliable testing procedures to establish a methodology for developing hybrid coating systems that may advance corrosion control in modern aircraft systems. The nature of this work also involves the investigation of basic

corrosion phenomenon associated with aluminum alloys such as 2xxx (Al-Cu), commonly used in the manufacture of aircraft structural components.

Traditionally, precipitation grade hardened high strength Al alloys, containing heterogeneous microstructures formed from intermetallic compounds (IMC) of Cu, Mg, Fe and Mn, are used with protective coating systems containing Cr^{IV} , chromates, and dichromates that are especially effective at inhibiting Al alloy corrosion¹². These corrosion resistant aircraft coating systems for aluminum substrates typically consist of a conversion coating layer, a primer layer, and a topcoat. In practice, chromate conversion coatings (CCC) can either be deposited on the Al surface anodically by an applied anodic current¹³, or developed chemically by the reaction of a tri- and hexavalent chromium salt solution (i.e., Alodine™)¹⁴ with the Al metal.¹⁵ In spite of the widespread success and use of CCC systems in protecting Al aircraft structures, as well as Cr-pigmentation, the use of chromates is being curtailed as they have been found to be carcinogenic, expensive to handle, and on an annual basis are the source of one of the highest maintenance costs incurred by the Air Force¹⁶.

Generally, corrosion processes describe the oxidation of a metal at its surface which acts to weaken and / or disfigure it. Most metals are active enough to be converted to their oxides, and it is generally accepted that corrosion occurs by an electrochemical action involving the creation of small galvanic cells on the surface of the metal.¹⁷ It has been observed that the bulk of structural corrosion damage to aging aircraft emanates from components involved in the joining process to the airframe itself such as rivets, fasteners, lap splices, joints, and spot welding. All of these joining methods are associated with metallurgical and environmentally induced factors that affect the alloying elements in the

metal, and once changed the exterior and interior surfaces of the aircraft become more susceptible to corrosion.¹⁸ For example, in the C/KC 135 fleet, crevice corrosion occurring in the spot welded lap joint/doubler and environmentally induced corrosion around steel fasteners on the upper wing skins have been observed and addressed as major corrosion issues.¹⁹

Categorically, there are three broad factors associated with corrosion processes in aluminum alloys: 1) metallurgical; 2) mechanical, and 3) environmental. Metallurgically induced factors include heat treatment, chemical composition of the alloying elements, material discontinuities, for example the presence of voids, precipitates, grain boundaries/orientation, and / or copper concentration in second-phase (S-phase).²⁰ Mechanical factors include cycle-dependent fatigue, and fatigue crack initiation. Further, environmental factors contributing to corrosion include temperature, moisture content, pH, electrolyte, type of salt present, and frequency and duration of exposure.²¹

The most widely accepted factors contributing to corrosion processes in military aluminum aircraft structures^{22, 23} are direct chemical attack (i.e. aggressive phosphate ester hydraulic fluid leaks), galvanic corrosion (when metals of different electrochemical potential are in contact in a corrosive medium), crevice corrosion (i.e. when a corrosive liquid gains access to crevices in or between components), pitting corrosion (i.e., a localized attack that leads to the formation of deep and narrow cavities), and stress corrosion (i.e., when tensile stress or a critical environment conditions cause a dealloying to occur at grain boundaries which results in the formation of anodic precipitate areas). Overall, among all of these corrosion types, material thinning by pitting at particle sites is the most basic corrosion mechanism affecting Al 2024 T-3 fuselage skin material.²⁴

Generally, Al-2024 T-3 is used for the exterior fuselage, wing skins and flight control surfaces where pits are observed to form in exposed grain structure when subjected to environmental conditions that favor pitting. Pitting corrosion in Al 2024 T-3 occurs when cathodic particles (Al, Cu, Fe and Mn) dissolve in the alloy matrix while anodic particles (Al, and Mg) also dissolve leading to intergranular corrosion.²⁵ It has been approximated that there are roughly three times more anodic particles than cathodic particles in Al 2024 T-3, therefore it is most prone to intergranular corrosion induced by pitting.²⁶ The downside and oversight and failure to address airframe corrosion damage due to shallow pitting, or damage related to fatigue and cracking has been reported to lead to catastrophic consequences such as in the mid 1950's when two Comet airplanes failed in high altitude flight²⁷ and the Aloha Airlines incident of 1988.^{28,29}

Moreover, what appears to have gained wider acceptance is the application of systematic procedures / methods for predicting aircraft coating damage tolerance using probabilistic models.³⁰ NDI eddy current technology such as the MAUS IV eddy current system currently selected by the Air Force as the NDI tool for detecting / assessing hidden corrosion induced damage of fuselage components during programmed depot maintenance (PDM).³¹ Overall, the administration of such new NDI techniques and data mining procedures into planned maintenance programs for aging aircraft is a clear cut example of how effective instituted programs such as (URIs) can be at providing scientific analysis and solutions to reduce the high maintenance costs associated with an aging aircraft fleet. Until only recently, the detection and arrest of minor damage to airframes was based upon a wait until the plane was scheduled for its major overhaul procedure, at which time only then was it completely stripped and any major corrosion problems were identified and fixed.

1.1 Aluminum Alloy 2024 T-3

Given the practical significance of this alloy, and many other closely related structural aluminum alloys, the aerospace industry has devoted significant resource to characterizing the properties associated with its elemental composition in hopes to gain a clear insight to its corrosion behavior. Figure 1.1-3 illustrates the chronological progression of structural aluminum alloy development, as a function of yield strength, in the aerospace industry. According to figure 1.1-3, modern airframes are composed of higher strength, corrosion resistant aluminum alloys that supercede the AA 2024 T-3 grade. The main advantage to modern aluminum alloys is that they possess higher strengths and do not contain significant copper levels that contribute to problematic corrosion of the alloy. See Appendix 1.1 for more detailed discussion of Al 2024 T-3.

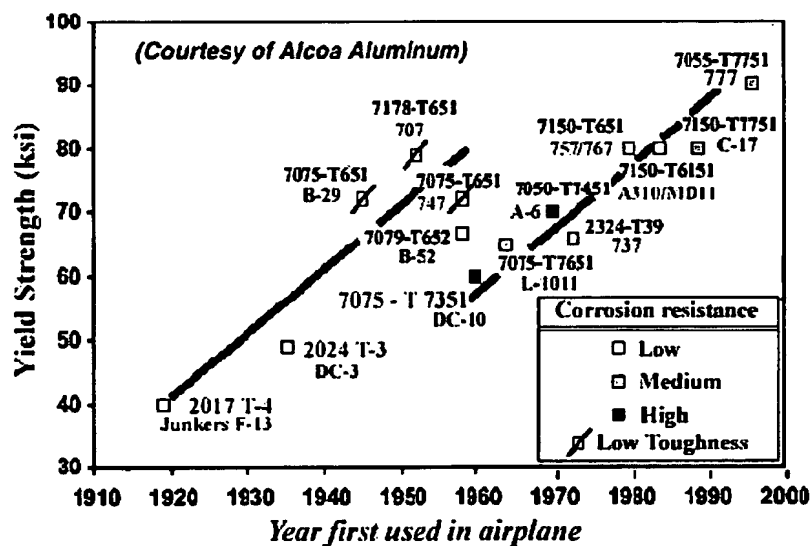


Figure 1.1-1: Chronological yield strength increase for aerospace Al-alloys.

1.2 Traditional Coatings for Corrosion Control

It is widely agreed upon that the major cause of coating failure on metallic substrates can be contributed to the development of oxidation or corrosion at the metal / coating interface.^{32,33} Generally, for many older polymeric coatings, it has been demonstrated that the rate of moisture induced adhesion corrosion failure can be correlated to the ease of polymer linkage hydrolysis within the polymer matrix.³⁴ Corrosion induced intra-matrix polymer degradation due to surface hydroxides has often been correlated to the presence of easily hydrolyzable functionality such as the presence of saponifiable moieties within the polymeric binder matrix. A good coating binder is one that imparts the ability to maintain its transport resistance properties that retard and thwart water induced adhesion loss and the rapid lateral spread of corrosion.³⁵

Over the last 100 years evolutionary changes have been shaped primarily by the development of new polymeric binder materials. Such changes made to polymeric binder systems often spring from the synthesis of new classes of chemical functionality that can be applied to generating macromolecules *in situ*. These developmental changes are driven by performance requirements established to best suit a particular set of conditions present, e.g., the substrate, painting conditions, desired coating finish, and the environment to be withstood by the coating. In comparison with other coatings technologies as depicted in Figure 1.2-1, below, organic polymeric binders, as vehicles for paints, have undergone some of the most dramatic changes in the field of coatings technology.

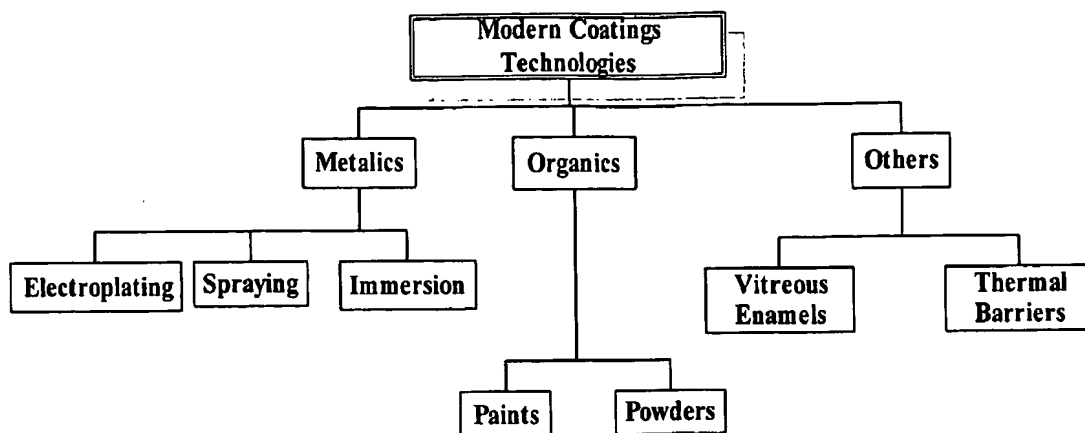


Figure 1.2-1 Schematic for process and methods used to develop modern coatings systems.

Zinc-rich paints incorporate zinc flakes or dust/ powder into a coating to cathodically protect a more galvanically noble ferrous substrate from corrosion. These paints are usually applied as primers with a loading of zinc sufficient to allow continuous electrical contact throughout the coating so that an exchange current can flow between anodic areas, where the sacrificial zinc metal is corroded, to the ferrous cathodic area to be protected.³⁶ In various formulations of zinc-rich coatings the pigment (zinc dust) is usually loaded to around 92 percent by weight yielding a PVC of approximately 79 percent for silicate vehicles and 70 percent for organic vehicles, hence the term “*zinc-rich*” is applied to both inorganic and organic binders.^{37, 38}

Organic zinc-rich paints, have been formulated with a wide variety of binder systems that include chlorinated rubber, polyurethanes, polyureas, polystyrene, acrylics, vinyls, and various epoxy epoxy resins such as epoxy esters, polyamide cured and high molecular weight lacquers that need no curing agent.³⁹ They are typically used as exterior undercoats or primers on marine structures, highway bridges, and exterior structures that require protection from water immersion, salt, humidity, and mild chemicals. Zinc-rich

coatings work well in environments whose pH lies between (4 -to-10), but in both inorganic and organic zinc-rich coatings, the duration of cathodic activity is finite, and the effects of zinc polarization, pushing down the potential (-1 to -1.2 vs Cu/CuSO_4), gradually decreases and the galvanic protection mechanism changes to that of a barrier mechanism.⁴⁰ This transition to barrier mechanism occurs as the accumulation of corrosion by-products consisting of zinc oxides and carbonates block and fill porous sites within the binder matrix.^{41, 42}

1.3 Mg-rich Polymeric Binder Development

What had been anticipated early on in these studies was that the integrity of conventional polymeric binder systems such as those used in zinc-rich systems may not suffice when used in an analogous Mg-rich system. Figure 1.3-1, below, gives the schematic for the approach taken in the development of the polymeric materials used as candidate Mg-rich coatings.

Initially, the assumption made was that a 2K epoxy consisting of a diglycidal ether of bisphenol A (DGEBA), either in liquid or solid resin form, with a heterocyclic polyamine curative would suffice. However, such coating systems based upon heterocyclic primary amines acted to: 1) turn the polymeric binder material green (due to the presence of Mg metal), and 2) resulted in brittle films with no adhesion to the Al-2024 T-3 substrate. On the other hand, Mg-rich coatings derived from epoxy / polyamidoamines, Figure 1.3-1 (candidate #1), yielded improved adhesion and flexibility and provided a polymeric binder material with suitable resistance to alkali corrosion byproducts. As a result, this system was the first system to be investigated using electrochemical testing techniques, as presented in chapter 3, "*Proof of initial concept*". The polyurea system, Figure 1.3-1 (candidate #2),

based upon isocyanate prepolymers of MDI, originally designed for concrete coatings, showed improved performance over the epoxy/polyaminoamide systems.

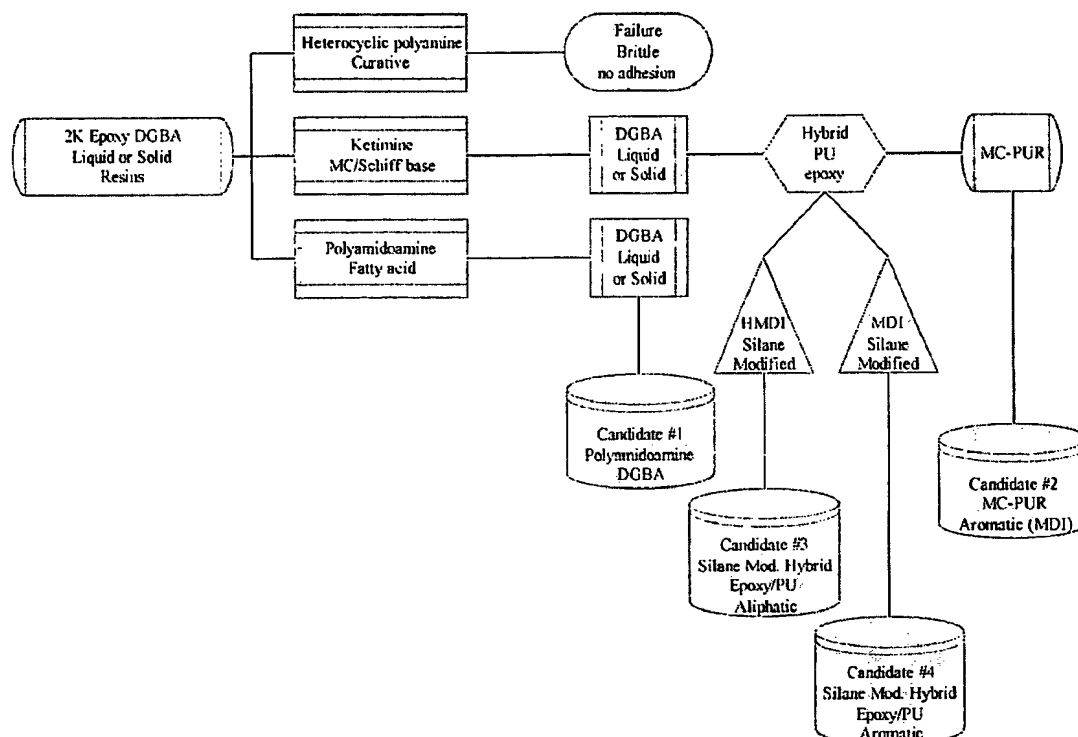


Figure 1.3-1 Schematic flow diagram of polymeric binder development for Mg-rich coating systems.

The development of the hybrid systems, Figure 1.3-1 (candidates #3 and #4), stems from initial studies with moisture cure Schiff base imine curatives, such as those discussed in Chapter 3. The main feature of these systems is the absence of the primary amino group that was observed to contribute to side reactions with magnesium metal. It is surmised that the presence of the imino group (sans labile hydrogen) allows these systems to be used as an adjunct curative in an “epoxy-polyurea” hybrid polymeric system, as described in Chapter 3. In addition, these “hybrid” epox-polyurea systems yielded improved adhesion and performance when modified with a bulk silane crosslinker.

1.4 Concluding Remarks

The simplest way to prevent aluminum from corrosion is to cover the structure with paint and isolate it from water. Unfortunately, most paints come off quickly and the structure needs to be frequently repainted, thus resulting in a high maintenance cost. Since it is almost impossible to ensure the complete integrity of a coating in practice, it is highly desirable to have a protective coating that stays effective even if it is scratched. Cathodic protection can be achieved by using a sacrificial anode metal for protection. For example, when iron is placed in electrical contact to a metal with a higher tendency to oxidize such as magnesium and zinc, the more reactive metal will then oxidize in place of iron. Since oxidation is accompanied by the giving up of electrons, a supply of electrons to the steel member will only stop it from corroding.

Based upon the underlying principles that apply to protecting steel with zinc-rich coatings the question arises can aluminum alloys be protected analogously by using magnesium-rich coatings? If so, what investigations and methodology related to the chemistry, physics and metallurgy of Mg-rich systems can be applied directly from analogous Zn-rich coating systems? Can the same polymeric binder matrices used in zinc-rich systems be interchanged, or do fundamental differences in the physio-chemical corrosion processes required altogether new or "hybrid" binder systems to be developed. Can the resulting coating systems even be considered as effective, and if so how can they be evaluated? Essentially, the first step to answering any of these questions lies in investigating the existing body of scientific knowledge surrounding established Zn-rich system *vis-à-vis* a literature search, then from which proceed to formulate, test, establish mechanisms and methodology, and evaluate candidate coating systems accordingly.

References / Bibliography

- ¹ Keijman, J.M., Properties and Use of Inorganic Polysiloxane Hybrid Coatings for The Protective Coatings Industry, J. Corrosion and Protective Materials, Lisbon, November, (2000) available online at http://www.psx700.com/pdf/lecture_portugal_22_11_00.PDF
- ² Censullo, A., C., D. R. Jones, and M. T. Wills (2002): "Investigation of Low Reactivity Solvents," Final Report for California Air Resources Board Contract 98-310, May 10.
- ³ Mahadevan, S., and Pan, S., Corrosion Fatigue Reliability of Aging Aircraft Structures, *Prog. Struct. Engng Mater*, Vol 3, pp 188-197, (2001)
- ⁴ Pitts S. and Jones R., Multiple –site and widespread fatigue damage in aging aircraft, *Engineering Failure Analysis*, Vol 4 (4), pp 237-257, (1997)
- ⁵ USAF Blue Ribbon Advisory Panel Report on Aircraft Coatings Materials Directorate, Wright-Patterson Laboratory, (1995)
- ⁶ Twite, R.L., and Bierwagen, G.P., Review of Alternatives to Chromate Replacement for Corrosion Protection of Aerospace Alloys, *Progress in Organic Coatings*, Vol. 33, pp 91-100, (1998)
- ⁷ Aging U.S. Aircraft, Final Report, Committee on Aging of U.S. Air Force Aircraft, National Materials Advisory Board, National Academy Press, Washington DC, (1997)
- ⁸ Agarwala, VS, Corrosion and Aging Aircraft. *Canadian Aeronautics and Space Journal*, Vol. 42, (2) pp 68-71 (1996)
- ⁹ Aging Avionics in Military Aircraft, www.nap.edu/openbook/0309074495/html/16.html
- ¹⁰ Department of the Air Force, Air Craft Structural Integrity Program, Airplane Requirements, MIL-STD-1530A, (1975)
- ¹¹ Negaad, G.R., *The History of the Aircraft Structural Integrity Program*, Aerospace Structures Information Analysis Center (ASIAC), Report No 680.IB, (1980)
- ¹² Alternatives to Chromium for Metal Finishing, National Center for Manufacturing Sciences, Ann Arbor (1995)
- ¹³ MIL_A_8625 Type I or Type II anodizing
- ¹⁴ Henkel Surface Technologies, Madison Heights, MI

- ¹⁵ Primer coatings; epoxy, water-borne, MIL-PRF-85285; Primer coatings: epoxy, high solids, MIL-PRF-23377 chemical and solvent resistant finish, BMS-11 Type I, The Boeing Company, Seattle, WA
- ¹⁶ Report of the Ad Hoc Committee on Life Extension and Mission Enhancement for Air Force Aircraft, Vol 1, Executive Summary, US Air Force Scientific Advisory Board Report No. SAB-TR-94-01, Washington, DC, (1994)
- ¹⁷ Rebbapragada, S., Palakal M.J., and Pidaparti R.M., Corrosion Detection and Quantification Using Image Processing for Aging Aircraft Panels, The Third Joint FAA/DoD/NASA Conference on Aging Aircraft, Albuquerque NM, 20-23 September (1999)
- ¹⁸ Metals Handbook –Ninth Edition, Corrosion, Vol 13, Publ: American Society for Metals (ASM), Metals Park, OH (1987)
- ¹⁹ Groner, D.J., U.S. Air Force Aging Aircraft Corrosion, Current Awareness Bulletin, Structures Division, Wright Laboratory, Spring (1997)
- ²⁰ Bucheit, R.G., Grant, R.P., Hlava, P.F., McKenzie, B., and Zender, G.L., Local Dissolution Phenomena Associated with S Phase (Al_2CuMg) Particles in Aluminum Alloy 2024-T3, *J. Electrochem. Soc.*, Vol. 144, No. 8, pp 2621 – 2628, August (1997)
- ²¹ Wallace and Hoeppner, Aircraft Corrosion Causes and Case Histories, AGARD Corrosion Handbook, Vol 1, AGARD-AG-278-Vol. 1, (1985)
- ²² Collins, J. A., Failure of Materials in Mechanical Design, New York, Wiley (1993)
- ²³ Jones, D. A., Principles and Prevention of Corrosion, Macmillan Publishing Co., 1st Ed., pp 260-261, (1992)
- ²⁴ Hoeppner, D.W., Chandrasekaran V., and Taylor, A.M., Review of Pitting Corrosion Fatigue Models, International Committee on Aeronautical Fatigue, July (1999)
- ²⁵ Chen, C-S., Gao, M., and Wei, R.P., Micro-Constituent Induced Pigment Corrosion in a 2024 T-3 Aluminum Alloy, *Corrosion*, Vol. 52, pp. 8-15, (1996)
- ²⁶ Jones, D. A., Principles and Prevention of Corrosion, Macmillan Publishing Co., 1st Ed., pp 4, (1992)
- ²⁷ Bates, P.R., Technical Considerations for Managing Aging Rotorcraft, In: Chang, C.I., and Sun, C.T., Structural Integrity in Aging Aircraft, AD Vol. 47, pp 21-34, ASME, New York, (1995)

- ²⁸ Hendricks W.R., The Aloha-airlines accident –a new era for aging airplanes. In: Atluri, S.N., Sampath, S.G., and Tong, P., Structural Integrity of Aging Airplanes, Berlin, Heidelberg, Springer, pp 153-165 (1991)
- ²⁹ Howard, M.A., Mitchel, G.O., and Tietz, H., Development of Procedures for Using Nondestructive Inspection Equipment to Detect Hidden Corrosion on U.S. A.F. Aircraft Page 3-35, Annapolis MD, ARINC, Contract Report F41608-93-D0649, (1995)
- ³⁰ Harlow, D.G., and Wei, R.P., A Probability Model for the Growth of Corrosion Pits in Aluminum Alloys induced by constituent Particles, Engineering Fracture Mechanics, Vol. 59 (3), pp 357 –377, (1998)
- ³¹ Nieser, D.E., Effects of Corrosion on C/KC135 Structural Life and Flight Safety to 2024, Proceedings of the Fourth Joint DoD/FAA/NASA Conference on Aging Aircraft, St Louis, MO, pp 15-18, May (2000)
- ³² Liedheiser, H., Corrosion-NASE, Vol. 38, No. 7, pp. 374 (1982)
- ³³ Dickie, R.A., in “*Adhesion Aspects of Polymeric Coatings*” K.L. Mittal, Ed., Plenum, New York, NY, pp. 389 (1983)
- ³⁴ Holubka, J.W., Hammond, J.S., DeVires, J.E., and Dickie, R.A., *Journal of Coatings Technology*, Vol. 52, No. 670, pp. 63 (1981)
- ³⁵ Hammond, J.S., Holubka, J.W., DeVires, J.E., and Dickie, R.A., *Corrosion Sci.*, Vol. 21, pp. 239 (1981)
- ³⁶ Zinc Coatings, Microstructures of Various Zinc Coatings, American Galvanizers Assoc., Englewood CO, Copyright (2000) available on-line at <http://www.galvenizeit.org>
- ³⁷ Smith, L.M., ed., Generic Coating Types, An Introduction To Industrial maintenance Coating Materials, SSPC-95-08, Mudd, R., Organic Zinc-Rich, Chtr.9, Technology Publishing Co., Pittsburgh, PA, pp. 149 – 163 (1996)
- ³⁸ Jones, D.E., Principles and Prevention of Corrosion, Macmillan Publishing Company, New York, NY, pp 480-482, (1992)
- ³⁹ Tator, K.B., *Metals Handbook*, Vol. 13, Corrosion, 9th ed., ASM International, Metals Park, OH, pp 399 (1987)
- ⁴⁰ Mitchell, M.J., Zinc Silicate or Zinc Epoxy as The Preferred High Performance Primer, International Protective Coatings, Akzo Nobel, (1998), available online at http://www.international-pc.com/pc/technical/tech_papers/SAfrica_99.PDF

⁴¹ Munger, C.G., "*Corrosion Resistant Zinc Coatings*," Chtr. 6, in Corrosion Control by protective Coatings, pp 129, NACE International, Houston, TX (1984)

⁴² Hare, C.H., Corrosion Control of Steel by Organic Coatings, J. Protective Coatings Linings, Vol. 15, No. 7, pp 17 (1998)

Chapter 2 Literature Review

2.1-1 Introduction to Metal Rich Coatings

The purpose of this section is to provide clear insight to the mechanisms involved in corrosion control of Al 2024 T-3 by both conventional means and by developing a Mg-rich coating system which may also be analogous to modeling existing Zn-rich coating systems. Essentially, coatings are simple inventions used to keep corrosive agents and electrolytes separated from metal surfaces. It is widely recognized that failure of a coating at the metal interface leads to increased water and oxygen permeation and as a result the accelerated corrosion of the metal.⁴³ However, oxygen and water transmission alone may not be the sole factors involved with the corrosion of metals. Moreover, the presence of ionic salts that can accumulate in a localized electrolyte solution may act to promote corrosion reactions to a far greater extent than oxygen or water alone. Therefore, by simply filtering out such ionic species and preventing them from reaching an interface corrosion control of the metal may be achieved.

Thus far corrosion resistant coatings for aluminum have been devised to provide good adhesion at the metal-polymer interface which protects surface oxides (native oxide films) in the presence of water and aggressive anions such as chloride. But the downfall of the typical barrier coating is that it possesses no preventative mechanism to arrest electrolyte transport through the film and the eventual accumulation of salts at the interface that promote loss of adhesion and corrosion once the barrier has been ruptured. In the absence of some additional chemical agent or inhibitor, organic polymeric materials alone are not cost effective alternatives to providing suitable corrosion protection to aluminum metal.

Aside from inhibitive chromate technology, sacrificial / metal-rich systems used in conjunction with organic coatings such as zinc powder in zinc-rich systems have greatly extended the range of protection afforded to ferrous structures exposed to extreme environmental conditions. Metal rich coating systems have been designed to be relatively easy to apply, convenient, non-toxic, and greatly extend the life expectancy of the structure they service. Based upon the simplicity and effectiveness of such systems, a similar extension of this technology into protective coatings for aluminum structures is proposed as it may well evolve into a highly effective, low cost, environmentally acceptable, means by which to protect aluminum and its alloys for years to come.

Consequently, before addressing any approach to designing reactive metal coating systems for Al alloys such factors engendering polymeric matrix compatibility with active metal components must first be clearly investigated and established. Only thereafter, can the reactive metal component be subsequently applied and evaluated as a viable coating system. Therefore the direction and emphasis of this literature review will start from the base substrate material and proceed toward the specific design relative to a polymeric material.

2.1-2 Corrosion Control by Coatings

Corrosion of a metal is an electrochemical process and protection of a metal is usually achieved in one of three ways: 1) providing an impenetrable barrier; 2) addition of an inhibitive component to prevent oxidation, or 3) by cathodic protection, either by imposing a negative potential with a DC source connected to a sacrificial anode, or by adding a reactive metal pigment that galvanically protects the surface. Generally, arresting corrosion, starts with stopping current flow at the metal surface by directly controlling or

altering the fundamental thermodynamic processes that occur at the metal surface / interface.

Corrosion control investigations into this phenomenon are typically concerned with the chemistry, physics and metallurgy of the metallic substrates and the means by which compounds on the surface / interface might influence the course of an oxidation process. Generally, this is accomplished by using potential–pH diagrams known as *Pourbaix diagrams* for Al, Fe, and Zinc to identify solution equilibrium conditions where stability or instability can be expected. Essentially, Pourbaix⁴⁴ diagrams allow one to interpret the effects of pH and potential difference as well as the effect of oxygen concentration at a metal interface.

Also, of crucial importance and closely related to these thermodynamic parameters are the more subjective kinetic factors that allow one to relate the stability of passive oxide layers in a given environment to be appraised and permit estimation of the corrosion rate of a metal by measuring its corrosion current. In addition, kinetic and thermodynamic data can be put to further use by plotting / correlating the movements of anodic and cathodic areas beneath a coating's interface to further assess the effects of corrosion in a given environment.

As an example, the treatment of aluminum alloys with chromate pretreatments to arrest corrosion under coatings has been thoroughly investigated by using thermodynamic and kinetic parameters to assess both chemical and electrical modes of action. The most successful investigations of this phenomenon have involved predicting the inhibiting actions of ions such as CrO_4^{2-} and PO_4^{2-} on the metal's surface oxides and its underlying surface structure. Most of these studies correlate changes at the metal's surface as a

function of exposure duration to changes in metal oxide morphology or metal loss. Barrier properties of protective coatings are classified according to the degree to which they exclude oxygen and water vapor transmission to the metal interface thereby determining the course of the underlying corrosion processes. In addition, they act to arrest current from flowing between anodic and cathodic site. It has been well documented that water vapor acts to displace polymers from substrates on which they are adhered or adsorbed, and it is known that some organic films can function as weak ion exchangers and therefore when subjected to a corrosion current source become susceptible to dielectric breakdown that in turn increases permeability of ionic species to the surface.

Covering a reactive metal's surface with a coating has long been a way of introducing one or more surface properties. Replacing an air-metal interface with a coating-metal interface serves to greatly reduce corrosion and preserve the metal's mechanical properties.⁴⁵ It has been noted by Funke⁴⁶ that the most important property of a coating, its adhesion to a substrate, is the primary factor associated with corrosion mechanisms (coating failure) and that the adsorption of binder molecules on a molecular scale plays the decisive role in determining the adhesion of a coating to a substrate.

In recognition of this action, much work has been devoted to the development of polymeric coatings that prevent moisture adsorption at the metal-polymer interface thus greatly reducing the rate of metal corrosion.^{47, 48, 49} It is commonly accepted that corrosion control by coatings can be implemented by using one or a combination of three primary mechanisms.^{50, 51, 52}

- 1) By acting as a physical barrier to isolate the substrate from the environment.⁵³

- 2) By inhibition action of reactive materials, usually a soluble pigment, that reacts with some component of the vehicle to form a compound that forms a passive film that further inhibits corrosion.⁵⁴
- 3) By action of an inhibiting pigment, or by cathodic protection from either a metal- rich sacrificial anode incorporated into the vehicle of the coating making it an electrically contiguous, by an imposed external current system used in conjunction with a sacrificial anode electron source material.⁵⁵

2.1-3 Barrier coatings

Figure 2.1-4, below, rely on the parallel alignment of lamellar particles or flakes in a coating to present a physical barrier that minimizes electrolyte ingress toward the metal substrate. In barrier coatings, pigments reduce the permeability of the coating if they have a lamellar structure that increases the diffusion path length in the coating.

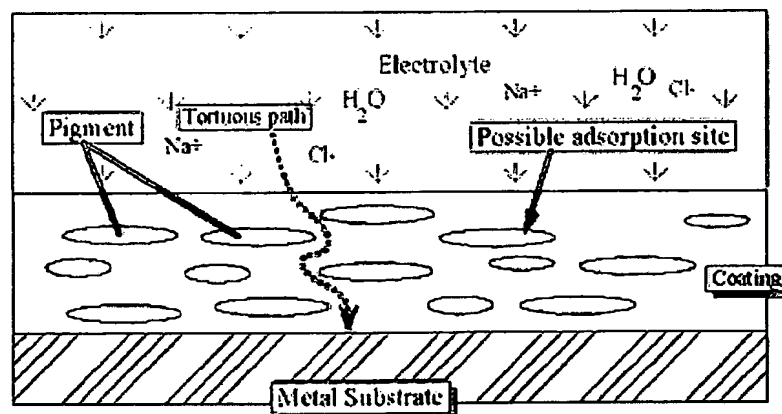


Figure 2.1-4, Corrosion control of metal by barrier addition of filler.

Pigments such as, graphite, mica, micaceous iron oxides, and aluminum, among others act as barriers to ion transport. The relationship between the volume of pigment and

binder (pigment volume concentration, %PVC) is another factor of the greatest importance in these types of paints.^{56,57} Corrosion control by the barrier effect has been described by Hare⁵⁸ as the limitation of corrosion current to anodic areas by the control of two coating parameters:

1. An impermeable organic binder that maximizes coating electrical resistance.
2. Inclusion of insoluble pigmentation whose geometric orientation acts to minimize access of electrolyte to cathodic surface by imposing a tortuous path.

Hare⁵⁵ reported on the change in barrier properties of coatings as a function of exposure to aqueous NaCl solutions using direct current (DC) resistance measurements. Typical resistance values reported for protective coatings are on the order of 10^{10} ohms·cm² initially, and with further exposure the resistance falls to about 10^8 ohms·cm² once an aqueous pathway to the film has been established.

Mayne⁵⁹ disputed the concept of barrier coatings functioning by exclusion of water and oxygen from the metal surface and proposed that coating films could prevent current flow between anodic and cathodic areas by providing high electrical resistance at / or above the interface, and cited the high ionic impermeability of well prepared coating films. In addition, Mayne⁵⁹ cited oxygen permeability, Table 2.1-1, below, as a mechanism for barrier protection and measured oxygen and water permeation through 4-mil (100-micrometer) paint films and found that oxygen and water levels were far in excess required to sustain an average rate of corrosion on unprotected steel. From which, Mayne proposed that even though water and oxygen were free to diffuse to the interface, soluble electrolyte was effectively blocked, and that the water reaching the interface was not conductive enough to carry appreciable corrosion current.

Table 2.1-1, below, shows levels of water and oxygen transmitted through a coated steel interface and levels of water and oxygen at a bare steel surface required to sustain an “average” corrosion rate reported in milligrams Fe / cm² / year. Morcillo *et al.*⁶⁰ concluded that under conditions of (high salt levels at the interface and a water permeable film), oxygen permeability was correlated to the degree of underfilm corrosion at the interface. Funke⁷⁴ states that the establishment of an electrochemical cell beneath the coating can only occur in the presence of a continuous aqueous phase, and that water permeability may not be the underlying rate-determining step in underfilm corrosion.

Water and Oxygen Levels at Surface of Coated & Uncoated Steel				
Author / (Reference) Corrosion Rate	Coated (H ₂ O) (mg / cm ² / year)	Bare (H ₂ O) (mg / cm ² / year)	Coated (O ₂) (mg / cm ² / year)	Bare (O ₂) (mg / cm ² / year)
J.O.E. Mayne ⁵⁹ @ 70 mg Fe / cm ² / year	200 – 1,100	11	4 - 53	30
Bauman* (Funke & Haggen) ⁶¹ @ 40 mg Fe / cm ² / year	N/A	1.1 – 2.2	N/A	2.9 - 54

2.1-4 Inhibitive Coatings

Figure 2.1-3, below, commonly rely on a reactive material and some component of the vehicle to form a compound which supports a passive film that further acts to impede or inhibit corrosion by affecting either anodic (dissolution) or cathodic (*polarization*)

* Bauman quoted by Haagen and Funke

reactions⁶². One generally accepted mechanistic scheme of anodic inhibition is that a soluble inhibitor breaks down anodic (dissolution) processes that serve to displace the potential of the underlying metal by 0.2 - 0.6V in a positive direction⁶³. Frenkel, *et al.*⁶⁴ report on how inhibition action of chromates on aluminum alloys depends upon chromate storage and release of Cr^{IV} species to inhibit cathodic reactions such as oxygen reduction at active sites.

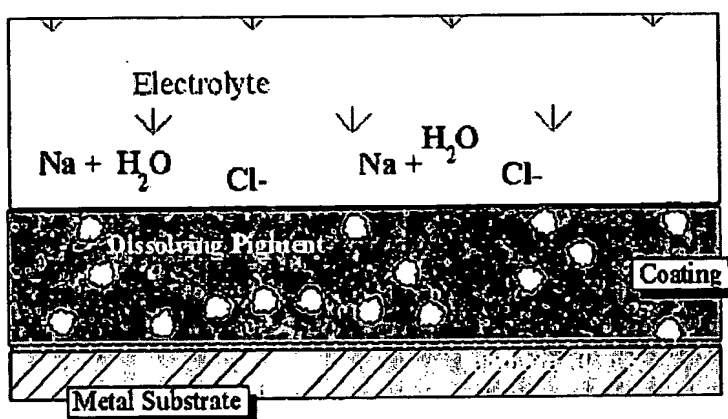


Figure 2.1-5: Corrosion control of a metal by inhibition pigment.

Generally, inhibitive additives liberate some ionic species into the coating causing an inhibitive layer to form that protects the surface. Inhibitors such as chromates which reduce the anodic corrosion reaction are termed anodic inhibitors, whereas those (e.g. polyphosphates) reducing cathodic corrosion reaction are termed cathodic inhibitors. If anodic inhibitors are used in an insufficient amount, they tend to increase pitting. Cathodic inhibitors are safer in this respect. Mixed anodic and cathodic inhibitor systems are also used. Chromate and dichromate coatings have been used to protect aluminum alloys for over 50 years. According to currently accepted views, chromate conversion coatings are a mixture of hydrated amorphous Cr (III)-Cr (IV) oxide, and hydrated aluminum oxide, and

small quantities of minor added ingredients.⁶⁵ Their widespread use has been primarily due to their combination of self-healing action and the ability to act as binders that form an adherent coating at the alloy surface.⁶⁶

2.1-5 Cathodic Protection

Figure 2.1-6, below, cathodic inhibition relies on the galvanic action of a reactive metal or sacrificial anode in the form of zinc and aluminum flake or particles, with some sort of surface treatment to facilitate a controlled dissolution of sacrificial metal that promotes electron transport through the coating and to the surface of the metal that is to be protected. However, once the sacrificial metal has been consumed the galvanic protection mechanism is finished. Thermodynamically, the anodic corrosion of Al can be retarded by pushing down its potential (-1 to -1.2 *versus* Cu / CuSO₄) into its immunity region.^{Error!}

Bookmark not defined., 67

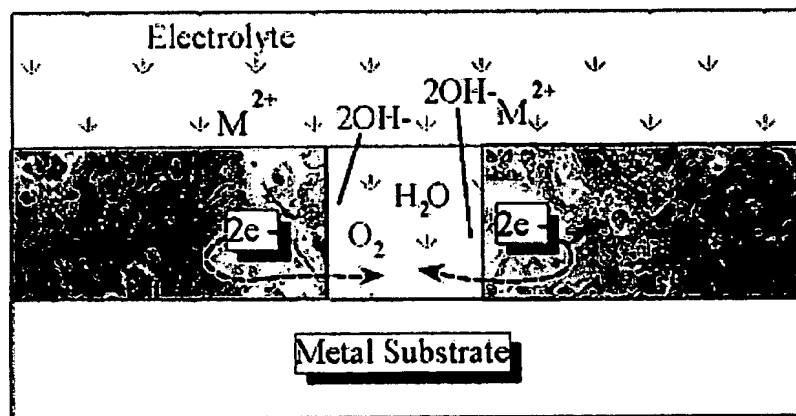


Figure 2.1-6: Corrosion control of metal by metal-rich coating, depicting electron transfer process between (sacrificial anode in the coating) and H₂O and O₂ in the electrolyte.

The current necessary to obtain this potential decrease may be supplied by a sacrificial anode such as zinc or magnesium, or by some aluminum alloys (seawater only) or by an impressed current source (electrolysis cell using an inert anode such as graphite or titanium). The magnitude of the current depends upon the (*overpotential*)⁶⁸ and resistance characteristics of the system to be protected.⁶⁹

2.1-6 Corrosion Control by Metal-rich Coatings

The most generally accepted inhibitive mechanism for these coatings, Figure 2.1-6, involves an active "*sacrificial*" metal pigment (more active than the metal substrate it is to protect), incorporated into a vehicle at sufficiently high volume concentration to make it electrically congruent so that it may facilitate electron transport through the coating allowing the sacrificial anode to corrode as opposed to the metal substrate cathode.^{70, 71}

There are two essential components to these reactive metal coatings:

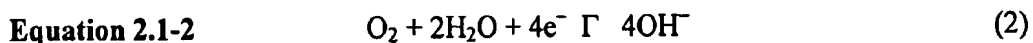
1. A sacrificial anode or galvanically negative electrode, where excess electrons accumulate due to the release of positively charged ions into an electrolyte.
2. A cathode or galvanically positive electrode where electrons are consumed by discharge of ions into an electrolyte.

Common practice in commercially available inhibitive metal containing coating systems has been to formulate active metal pigment with binder systems that synergistically moderate the dissolution of the pigment to yield voluminous metal oxides or carbonates that in turn block further corrosion attack.⁷²

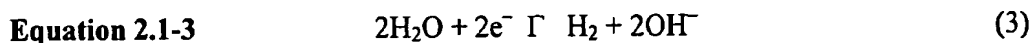
2.1-7 Aluminum Pigments

Aluminum pigments have been used in engineered paints and protective coatings for many years. Such aluminum pigments occur in the shape of flakes of varying sizes, for example those used in corrosion control coatings are about 20 - 40 μm wide and 1 μm thick. It is thought that pigment geometry and metallic nature is responsible for most of the observed properties in protective paints.

Generally, it has been shown⁷³ aluminum pigments improve the barrier properties of protective paints.⁷⁴ The mechanism attributed to their corrosion protection is related to their ability to impede the transport of water and oxygen through the coating; thus insulating the substrate surface from cathodic reactions involving oxygen. These pigments are said to be impermeable to water and oxygen as the relative diffusion path of an intrusive species becomes longer as it is forced to go around the particles all of which decreases the permeability through the paint.⁷³ Structures in seawater protected by zinc or aluminum anodes are polarized to between -800 and -1100 mV SCE. At these potentials the cathodic reaction can be both reduction of oxygen and hydrogen evolution:



(Reduction of Oxygen)



(Hydrogen evolution)

Leidheiser *et al.*⁷⁵ showed that above -1000 mV SCE the oxygen reduction reaction dominates, while below this potential the hydrogen evolution dominates. However, in the cathodic areas under the coating the potential is probably well above -1000 mV SCE, due to the high resistance between the anode and the cathode. According to Leidheiser *et*

*al.*⁷⁵ the oxygen reduction reaction is the predominant reaction occurring under the coating.⁴⁸ Since most paint films are permeable to both oxygen and water⁷⁵ it can be assumed that these reactants are transported through the film to the interface. Leidheiser *et al.* have also shown this experimentally⁴⁹ that the transport of cations occurs laterally from the holiday under the disbonded area of the coating.⁷⁶ The disbonded area is usually found to increase proportionally with time, i.e. the disbonded distance from the holiday in the coating is proportional with the square root of time.^{77,78} According to Skar⁷⁹ the transport of cations was rate limiting. Leidheiser^{80,81} and Parks *et al.*⁸² have also corroborated claims that cations are transported through the coating when the specimen is under cathodic polarization.

2.1-8 Corrosion of Al and Inhibition by Mg Powder

The Pourbaix diagram⁴⁴ for aluminum / water system shown in Figure 2.1-7, below, predicts that aluminum corrodes at pH values greater than about ~ 9. The oxide on the surface dissolves in high pH environment and can not protect the metal.

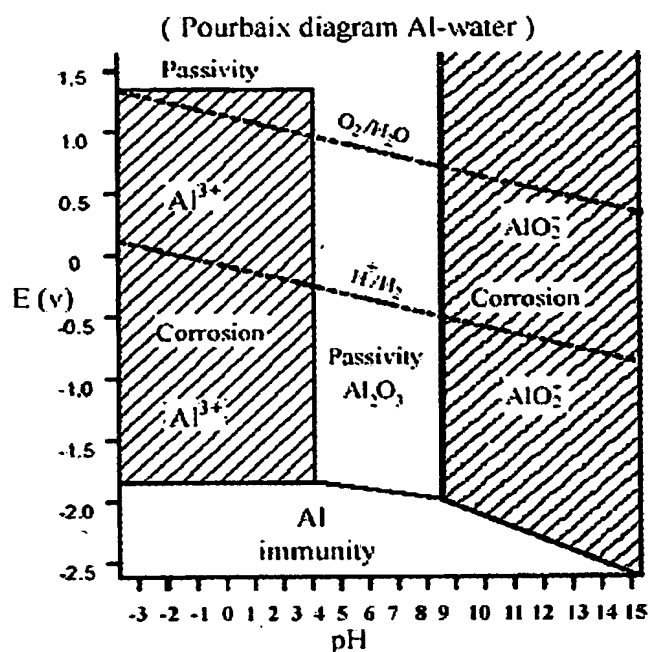


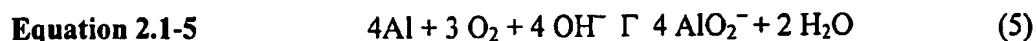
Figure 2.1-7: Pourbaix diagram for Al/ Al₂O₃ / AlO₂⁻ / H₂O, E(V) vs pH.

At high pH, the corrosion reaction at the surface of Al removes hydroxide from the electrolyte, which may reduce the pH at the Al / coating interface according to Equ. 2.1-4:



(High pH oxide dissolution)

Generally, cathodic disbonding has been attributed to the build up of hydroxide at the Al coating interface, this reaction may therefore decrease the rate of disbonding. According to Equ. 2.1-5, below, the possibility of Al powder as an oxygen scavenger. The corrosion of the aluminum pigments may consume the oxygen before it reaches the Al surface. Since the Al is not passive, due to the high pH, the corrosion of the pigments (5) is not inhibited:



(High pH reaction of Al with O₂)

Leidheiser *et al.*⁸³ suggest that corrosion of Al pigments / metal can also involve another mechanism where the oxide on the surface of the pigment / metal may act as a buffer. However, according to J.O.E. Mayne⁵⁹, Table 2.1-1, the concentration of oxygen O₂ permeating a coating was estimated at between 4 – 53 mg / cm² / year, while the water permeation rates through a coated metal are shown, Table 2.1-1, to be on the order of 200 – 1,100 mg / cm² / year. Clearly, by virtue of roughly two orders of magnitude, those reactions involving Al and water will be favored over “possible” reactions involving O₂ diffusion.

As previously noted, Funke⁷⁴ states that the establishment of an electrochemical cell beneath the coating can only occur in the presence of a continuous aqueous phase, and that water permeability may not be the underlying rate-determining step in underfilm corrosion. Moreover, according to Leidheiser *et al.*⁷⁵ in the cathodic areas under the coating, where the potential is probably well above -1000 mV SCE, due to the high resistance between the anode and the cathode, the oxygen reduction reaction, Equ. 2.2-1 is the predominant reaction occurring under the coating.⁸³

According to Lunder *et al.*⁸⁴ corrosion attack on magnesium, in aqueous environments, usually involves micro-galvanic coupling between the cathodic and anodic areas. It is well known that magnesium metal dissolves in aqueous environments according to an electrochemical reaction with water to produce magnesium hydroxide and hydrogen gas.⁸⁵ It is also usually reported that magnesium corrosion is relatively insensitive to the oxygen concentration^{86, 87, 88} even though oxygen is an important factor in atmospheric corrosion of the metal.⁸⁹ (See appendix 2.1)

2.1-9 Recent Developments

Recent developments in coatings for corrosion control of metals are essentially non-chromate hybrid systems whose modes of action overlap both barrier and inhibitive mechanisms. They have been described as passivating additive/films or compounds because the mechanisms responsible for their performance are not well understood.⁹⁰ Poly(phenylene oxide) (PPO), has been described and used as a thin primer or wash coat treatment for aluminum.⁹¹ Spellane⁹² claims that the action of PPO films on a metal substrate involves an electrochemical or redox reaction with the metal and its oxide, suggesting that the coating exhibits a passivating characteristic, or synergism of the binder itself with the metal. Yet another variation involves polyaniline (PANI) intrinsically conductive polymer based coatings known as "Ligno-PANI" patented by *Geer et al.* and adopted by the National Aeronautical Space Administration⁹³ a lignosulfonic acid doped polyaniline additive. It is claimed that they provide a barrier to corrosion attack and when filled with an aluminum flake react preferentially to the metal substrate in a corrosive environment.⁹⁴ Conducting polymers, sometimes referred to as organic metals, such as doped polyaniline and phenylenediamine can be modified to increase their conductivity, stability, effective red-ox range and corrosion resistance of both iron and aluminum.^{95, 96}

2.1-10 Summary

Protective coatings for aluminum aircraft structures usually consist of a primer and topcoat paint applied either by dipping, brushing, or spraying.⁹⁷ The standard aircraft primer coat specified under Class N in MIL-PRF-23377 or MIL-PRF-85582 consists of an epoxy-polyamide binder with an anti-corrosive agent, which serves to protect the substrate and provide superior adhesion.⁹⁸ Modern high performance topcoats, conforming to MIL-

PRF-85825 "coating" polyurethane, are applied directly to military aircraft in order to ensure desired durability and optical properties for protection in diverse operational environments.

Essentially, the role of the polymeric binder is to provide a liquid vehicle that wets and covers the reactive metal surface and upon curing forms the protective solid matrix without compromising the physical characteristics of the metal at its interface. Both primer and topcoat systems have been designed especially for this purpose and are applied as low molecular weight reactive oligomers. They have been designed as either inorganic or organic polymeric vehicles, or a hybrid combination of the two. Generally, the chemical reactions leading to high molecular weight polymeric matrices occur between two reactive species in the coating for example between an epoxy and an amide, or it might react with moisture in the air such as the formation of polyurea linkages by a polyisocyanate and water. It is the low molecular weight polymeric binder component that determines both the application and physical properties of the coating.

Currently, coating systems for corrosion control of aluminum alloys are evaluated by ease of processing and application, efficiency, performance, price, reproducibility, safety, stability, service life, and toxicity. The effectiveness of any organic coating depends primarily on the interfacial adhesion strength between the metal and polymer and thus far the state of the art coating systems for corrosion control of Al 2024 T-3 aluminum alloy are based upon a chromate- conversion-coating system. The efficiency of these systems can be evaluated in terms of processing which starts with a total system application approach. Starting from the beginning the whole process must be simple and easy to apply, with minimum surface preparation and treatment involved. The coating is spray applied by

application of organic primer (epoxy), followed by a final (polyurethane) topcoat, highly pigmented with chromate and corrosion inhibitors.

Reproducibility of corrosion control has been consistent when strontium chromate (SrCrO_4) inhibitors are added to both the surface treatment and primer, promoting a porous oxide that retains chromate, and provides surface for adhesion. Stability of the coating has been derived from the integral primer, topcoat, surface treatment corrosion protection mechanism of these current coatings. It should be noted that such a system possess negligible barrier properties; however, ($\text{EIS} - |\text{Z}|_{\text{mod}} = 10^6 \Omega \cdot \text{cm}^2$) it functions by maintaining a protective electrolyte environment at the coating-metal interface whereby the protective mechanism is activated when water penetrates and is transported throughout the porous coating. The extended service life of the coating depends upon environmental factors such as the triggering of the coating's defense mechanism whereupon when a defect or breach of the surface occurs the *in-situ* solubilization, dissociation, hydrolysis, and diffusion processes act to mobilize the corrosion inhibitors and repassivate the affected area.⁹⁹ Unfortunately, chromate toxicity and safety concerns combined with their associated disposal costs are the two overwhelming factors acting to curtail any extended use of these coating systems in the foreseeable future.

An alternative approach that will be further investigated for corrosion control of Al 2024 T-3 is the incorporation of pigmentary Mg particles into a coating where it is suspected that they may act as a sacrificial inhibitory pigment that preferentially reacts with water and solution hydroxyl from the reduction of O_2 as a result of gradual cathodic polarization conditions occurring at the coating / interface. Overall, the general effect of adding pigmentary Mg metal to a coating is that preferential dissolution of Mg metal as

opposed to the Al metals protective oxide layer would occur at high pH conditions thus preventing cathodic disbonding of the coating from the Al surface.

References / Bibliography

- ⁴³ Negle, O., and Funke, W., *Progress in Organic Coatings*, Vol. 28, pp. 285-289 (1996)
- ⁴⁴ Pourbaix, M., *Atlas of Electrochemical Equilibrium in Aqueous Solutions*, Pergamon Press, London, (1966)
- ⁴⁵ Bierwagen, G.P., *Handouts from Course "Corrosion and Its Control by Coatings"*, North Dakota State University, Fargo, Summer (2000)
- ⁴⁶ Funke W., Problems and Progress in Organic Science and Technology, *Progress in Organic Coatings*, Vol. 31, pp 5-9, (1997)
- ⁴⁷ Nithianandam V.S., Chertok F., and Erhan S., Quinone-Amine Polymers, VIII: Curing Studies on Jeffamine® D-400-p-Benzoquinone Polymer, *Journal of Coatings Technology*, Vol. 63, No. 796, pp 47-54, May (1991)
- ⁴⁸ Han M., Bie H., Warren G., Nikles D., Amine-Quinone Polyimides that Protect Iron Against Corrosion, *Mat. Res. Soc. Symp.*, Materials Research Society, Vol 629, (2000)
- ⁴⁹ Hu Y., Nikles D., Preparation of Sulfur-Quinone Polyurethanes and Their Use to Inhibit Corrosion of Iron Particles, *J. Polymer Science: Part A: Polymer Chemistry*, Vol. 38, pp 3278-3283 (2000)
- ⁵⁰ Funke, W., Thin-layer Technology in Organic Coatings, *Progress in Organic Coatings*, Vol. 28, pp 3-7, (1996)
- ⁵¹ Bierwagen, G.P., Reflection on Corrosion Control by Organic Coatings, *Progress in Organic Coatings*, Vol. 28, pp 43-48, (1996)
- ⁵² Hare, C. H., Barrier Coatings, *Journal of Protective Coatings and Linings*, Vol. 15, pp 17, (1998)
- ⁵³ Bierwagen, G.P., Jeffcoat C.S., Li, J., Balbyshev, S., Tallman, D. E., Mills, D.E., Use of Electrochemical Noise Methods (ENM) to Study Thick High Impedance Coatings, *Progress in Organic Coatings*, Vol. 29, pp 19-29, (1996)
- ⁵⁴ Frankel, G.S., and McCreery, R.L., Inhibition of Al Alloy Corrosion by Chromates, *The Electrochemical Society, Interface*, pp 34-38, Winter (2001)

- ⁵⁵ Hare, C.H., Wright, S.J., Anti-Corrosive Primers Based on Zinc Flake, *Journal of Coatings Technology*, Vol. 54, No. 693, pp 65-76, October (1982)
- ⁵⁶ Gowri, S., and Balakrishnan, K., The Effect of the PVC/CPVC Ratio on The Corrosion Resistance Properties of Organic Coatings, *Progress in Organic Coatings*, Vol. 23, pp 363-377 (1994)
- ⁵⁷ Bierwagen, G.P., Fishman, R., Storsved, T., Johnson, J., Recent Studies of Particle Packing in Organic Coatings, *Progress in Organic Coatings*, Vol. 35, pp 1-9 (1999)
- ⁵⁸ Hare, C., "Protective Coatings: Fundamentals of Chemistry and Composition," Chap. 24, Item SSPC 94-17, Technology Publishing Co., Pittsburgh; (1994)
- ⁵⁹ Mayne, J.E.O., Mills D.J.J., *J. J Oil Color Chem. Assoc.* Vol. 58, pp 155 (1975)
- ⁶⁰ Morcillo, M.; Barajas, R.; Feliu, S.; Bastidas, J.M., SEM Study on the Galvanic Protection of Zinc-rich Paints, *Journal of Materials Science*, Vol. 25, Issue 5, pp 2441-2446 (1990)
- ⁶¹ Funke, W.J., and Haggen H., *Ind. Eng. Chem. Prod. Res. Dev.* Vol. 17, pp 50 (1978)
- ⁶² Drisko, R., et al., (Eds.), "Corrosion and Coatings: An Introduction to Corrosion for Coatings Personnel," Chapter 3, Item 98-0, *Soc. Prev.Coat*, Pittsburgh (1998)
- ⁶³ Miksic, B.A., Inhibited Polymeric Coatings Basic Principles and Future Perspectives, NACE Publication, Houston, TX, pp 1-8, (1976) published online www.cortecvci.com/Publications/Papers/ VCI Fundamentals/CTP-9.pdf
- ⁶⁴ Frenkle, G.S., and McCreery, R.L., Inhibition of Al Alloy Corrosion by Chromates, *The Electrochemical Society, Interface*, Winter, pp34-38, (2001)
- ⁶⁵ Xia, L., McCreery, J., *J. Electrochem. Soc.* (1999)
- ⁶⁶ Listed on the National Standards and Specifications Web Site <http://www.nssn.org>
- ⁶⁷ Jones, D.E., "Principles and Prevention of Corrosion", Macmillan Publishing Company, New York, NY, pp 80-83, 121-127 (1992)
- ⁶⁸ [Http://jchemed.chem.wisc.edu/JCESoft/CCA/CCA3/MAIN/VOLTAGE/PAGE1.HTM](http://jchemed.chem.wisc.edu/JCESoft/CCA/CCA3/MAIN/VOLTAGE/PAGE1.HTM) (1999 Division of Chemical Education, Inc., American Chemical Society)
- ⁶⁹ Hollingsworth, E.H., Hunsicker, H.Y. and Schweitzer, P.A.: Corrosion and Corrosion Protection Handbook, Pt. Aluminium Alloys, pp.153-186, Marcel Dekker Inc., New York and Basel, (1989)
- ⁷⁰ Muller, B., *Journal of Coatings Technology*, Vol 68, No. 863, pp 51 (1996)

⁷¹ Revie, R.W., (Ed.) "Uhlig's Corrosion Handbook," Second Ed., Wiley & Sons Inc., New York, NY, Parts II and III, (2000)

⁷² Pfeifer, A., "Dacromet and Geomet Environmentally Compliant Cadmium Replacement Coatings," U.S. Navy & Industry Corrosion Technology Information Exchange, Louisville; July 19-22, (1999)

⁷³ Hare, C. H., "Protective Coatings - Fundamentals of Chemistry and Composition", Technology Publishing Company, Pittsburgh (1994)

⁷⁴ Funke, W., *J. Coatings Technology*, Vol. 55, No: 705, pp. 31-38 (1983)

⁷⁵ Leidheiser, H. Jr., *Corrosion*, Vol. 38, No: 7, pp. 374-383 (1982)

⁷⁶ Stratmann, M., Feser, R., and Leng, A., *Electrochimica Acta*, Vol. 39, No: 8/9, pp. 1207 (1994)

⁷⁷ Jin, X. H., Tsay, K. C., Elbasir, A., and Scantlebury, J. D., In: D. Scantlebury and M. Kendig (ed), *Advances in Corrosion Protection by Organic Coatings*, The Electrochemical Society, Pennington, NJ, 37-47 (1987)

⁷⁸ Kendig, M., Adisson, R., and Jeanjackuet, S., In: Scantlebury D., and Kendig, M. (ed), *Advances in Corrosion Protection by Organic Coatings*, The Electrochemical Society, Pennington, NJ, 2-4 (1989)

⁷⁹ Skar, J. I., "Cathodic Disbonding of and Transport of Charge through Paint Films", Norwegian Institute of Technology, Trondheim (1990)

⁸⁰ Leidheiser, H. Jr., Mills, D. J., and Bilder, W., "Permeability of a polybutadiene coating to ions, water and oxygen", In: M. W. Kendig and H. Leidheiser (ed), *Corrosion Protection by Organic Coatings*, The Electrochemical Society, Pennington, 23-36 (1987)

⁸¹ Leidheiser, H., Jr., *J. Adhes. Sci. Tech.*, Vol: 1, No: 1, pp. 79 (1987)

⁸² Parks, J., and Leidheiser, H. Jr, "Ionic Migration Through Organic Coatings and Its Consequences to Corrosion", *Ind. Eng. Chem. Prod. Res. Dev.*, Vol: 25, No: 1, pp. 1-6 (1986)

⁸³ Leidheiser, H., Wang, W. and Igetoft, L., *Progress in Organic Coatings*, Vol. 11, pp. 19-40 (1983)

⁸⁴ Lunder, O., Nisancioglu, K.R., Hansen, S., *Corrosion of Die Cast Magnesium-Aluminum Alloys*, SAE Technical Paper Series #930 755, Detroit, (1993)

- ⁸⁵ Emley, E.F., *Principles of Magnesium Technology*, Pergamon Press, New York, NY, (1966)
- ⁸⁶ Makar, G. L., Kruger, K., *Int. Mater. Rev.*, Vol., **38**, issue (3), pp. 138 (1993)
- ⁸⁷ Makar, G. L., Kruger, K., *J. Electrochem. Soc.*, Vol. **137**, issue (2), pp. 414, (1990)
- ⁸⁸ Uhlig, H. H., Revie, R. W., Uhlig's "The Corrosion Handbook", Ch. 20, Wiley, New York, NY (1985)
- ⁸⁹ Loose, W.L., in H.H. Uhlig's "The Corrosion Handbook", John Wiley and Son, New York, NY, pp.218 (1966)
- ⁹⁰ Brooman, E. W., Modifying Organic Coatings to provide Corrosion resistance –Part III: Organic Additives and Conducting Polymers, Metal Finishing, Pp. 104-110, June (2002)
- ⁹¹ Pompili, M., (Ed.), "Metal Corrosion Protection: One Electroactive Approach," News & Analysis at Surface finishing.com; posted April 18, (2000) at <http://www.surfacefinishing.com>
- ⁹² Spellane, P., and Via, F., U.S. Patent 6,004,628; December 21, (1999)
- ⁹³ Anon., S., "Water-Based Electroactive/Conducting Polymers," NASA Success Story No. 2025, NASA TechTracS; September 3 (1999)
- ⁹⁴ Doukenbroad, M., "Double the Rust Relief with Inherently Conductive Polymers," News & Analysis at Paintand coatings.com; October 13, (2000), posted at <http://www.catize.com>
- ⁹⁵ Meneguzzi, A., *et al.*, *J. Electrochem. Soc.*, Vol. 148, No 4, B121, (2001)
- ⁹⁶ Gelling, V.J., Wiest, M.M., Tallman, D.E., Bierwagen, G.P., and Wallace, G.G., Electroactive-conducting polymers for corrosion control: 4. Studies of poly(3-octyl pyrrole) and poly(3-octadecyl pyrrole) on aluminum 2024-T3 alloy, *Progress in Organic Coatings*, Volume 43, Issues 1-3, November 2001, Pages 149-157
- ⁹⁷ Osborne J.H., Blohowiak K.Y., Taylor R.S., Hunter, C., Bierwagen G.P., Carlson B., Bernard D., Donely M.S., Testing and Evaluation of Nonchromated Coating Systems for Aerospace Applications, *Progress in Organic Coatings*, Vol. 41, pp 217-225, (2001)
- ⁹⁸ Moore D., Protective Finishing Systems for Navy Aircraft. (Environment-Friendly Protective Coatings), *Adv. Materials Process*, Vol. 155, Issue 4, pp 31-34, April (1999)

⁹⁹ Donely, M., Evaluation of Corrosion Protection Performance of Sol-Gel Surface Treatments on AA2024 T-3, Partners in Environmental Technology Workshop, November (2001) Available online at [http:// www.serdp.org/symposiums/2001/ presentations/3C-Donley.pdf](http://www.serdp.org/symposiums/2001/presentations/3C-Donley.pdf)

Chapter 2.2 Metal Polymer Interface

2.2-1 Polymers on Metal Surfaces

The purpose of this section is to establish the status of the substrate and the necessary conditions required to promote film formation. In contrast to metals, organic polymers have low surface energies and consequently usually don't readily wet out over a surfaces very well.¹⁰⁰ Generally, it is observed that both classes of material may possess cohesively weak surface layers, and polymeric materials with such layers, usually results from migration of additives or of low molecular weight polymer fractions to the polymer / metal interface.¹⁰¹ A wide range of treatment applications have been reported¹⁰² for enhancing adhesion of polymers, some involve aggressive chemical treatment in strong oxidizing solutions, such as chromic acid or permanganate and have been employed with hydrocarbon polymers. Another reported alternative pretreatments to 'wet' chemical treatment are surface flaming and the action of gas plasma or reactive ion etching.^{103,104}

Defects in organic coatings originating from aluminum surface contaminants are known to adversely affect corrosion resistance at the coating / metal interface.¹⁰⁵ The application of a polymeric material / coating to a metal surface creates an interfacial layer where the two surfaces contact each other.¹⁰⁰ Adhesion between a polymer-metal interface can be improved by removing weakly adherent inconsistent surface oxide layers from the

metal, by increasing the substrate surface porosity, and by improving the energy dissipative mechanism(s) at the interface. (See appendix 2.2)

2.2-2 Mechanical Adhesion

By definition, mechanical adhesion is the gripping force of the coating onto the surface that results from interlocking of microscopic asperities over a surface / contact area.¹⁰⁶ These interactions are proportional to the force needed to resist the movement of the coating from its position in the absence of other adhesion components. The most common way of increasing the mechanical adhesion is to increase the area of contact between the coating and the substrate. One way to accomplish this is by increasing the number of surface peaks or roughness of the surface to render a depth of the profile. It has been observed that by changing the round shape of the profile to an angular profile, a considerable increase in the adhesive strength results.¹⁰⁷

2.2-3 Chemical Adhesion

Polar-polar adhesion, which is a form of chemical adhesion, is associated with the force of attraction between the positive and negative poles of the substrate and the coating. It is the combined total of all hydrogen bonding between the coating and the metal. According to Meyers¹⁰⁷, the approximate energy associated with hydrogen bonding at an interface can be anywhere from 10-to-40 kcal/mol. Polar-polar adhesion is greatly enhanced by increasing the proportion of polar functionality in a coating. This is usually accomplished by select resin systems, curing agents, and other constituents that have polar groups. An enhancement of polar-polar adhesion can also be achieved by increasing the application temperature. Usually, it is reported¹⁰⁸ that the application of higher

temperatures act to increase the cross-link density of most coating system, allowing more interactions between the dipoles, thus enhancing the polar-polar chemical adhesion component.¹⁰⁹

2.2-4 Organic Coatings on Metallic Substrates

According to Funke¹¹⁰, the film thickness of industrial organic coatings varies from millimeters for protecting metals against heavily corrosive environments up to a few microns in case of wash-primers or can coatings. In addition, the properties of organic films differ between the surface and the bulk of the same material which implies a structural difference in the way macromolecules conform and arrange themselves on the surface of a material as opposed to in the bulk. It has also been reported that significant improvements in wet adhesion of coatings to aluminum or steel substrates can be obtained by prior pretreatment with very dilute binder solutions, before after drying a subsequent layer of normal film thickness was applied.^{111,112}

Funke¹¹³ 1985, showed that adhesion under humid or wet conditions is more meaningful for assessing a coatings corrosion control protection than under dry adhesion, and that “wet adhesion”, (wet adhesion is the ability of coating to resist the interfering penetrating action of water molecules at interfacial or adhesion bonds), should also be considered as a factor controlling the barrier properties of organic coatings. As previously discussed regarding adhesion, above, besides mechanical interlocking, polar interactions, acid-base interactions especially, and hydrogen bonding are all responsible for adhesion; however, these bonds are themselves susceptible to the disrupting action of water.

Funke¹¹⁰, described two possible ways to counteract bond rupture in coatings by ingress of water molecules: 1) forcing the bonds to cooperate with each other and

choosing application conditions which, by a suitable chain conformation of the binder molecules; 2) allow a maximum number of bonding groups per molecule to interact with the metal substrate. The role of such cooperative and conformational effects for improving wet adhesion is indicated schematically in Figure 2.2-1, below, together with the possibility of reorientation and prearrangement of macromolecules Figure 2.2- 2, below.

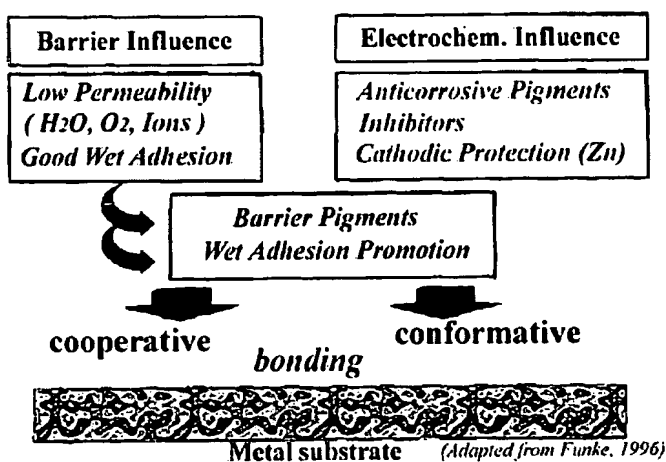


Figure 2.2-1: Protective coating mechanisms, as described by cooperative, *left*, and conformative, *right*, from Funke.

The cooperative mechanism, describes a dynamic equilibrium situation where acid-base interactions and hydrogen bonds augment adhesion due to their degree of dissociation and water solubility of the carboxylate in solution. These dynamic interactions must be stabilized to improve wet adhesion. Stabilization is possible by attaching bonding groups to rigid polymer backbone chains, which force neighboring bonds to cooperate Figure 2.2-2, below. It should be noted that chain rigidity should be introduced after, and not before, the adsorption process, because stiff macromolecules cannot insert themselves into loops, or sufficiently adapt themselves to micro-contours over the metal surface. The “conformative” mechanism¹¹⁰, the one pertinent to metal-rich coating systems, describes a system where

the concentration of a polymeric binder in a paint, which is usually larger in magnitude compared to those concentrations used in adsorption experiments, results in coatings possessing high concentration of polymeric binder molecules, which after application tend to adsorb at the surface of the metal substrate.

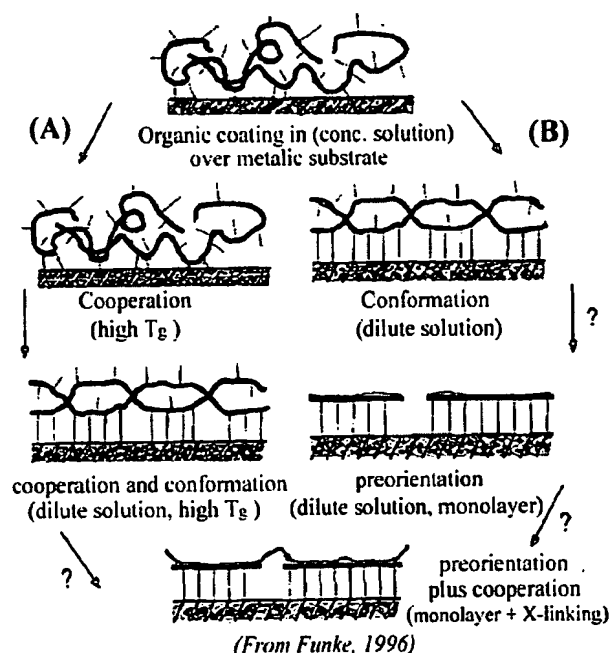


Figure 2.2-2: Structure and bonding of polymer layers on metallic substrates, (from Funke, 1996.)

The problem can be further defined in that numerous macromolecules must compete with their neighbors for adsorption sites. As a consequence of this competition for adsorption sites, only a small fraction of the adhesive groups of the macromolecule end-up interacting with the metal surface. This is in stark contrast to the mechanism describing excessive dilution, where the macromolecules at the metal surface have enough sites available for adsorption, which means coverage of the metal surface is insufficient. Therefore, what is sought is some optimum concentration where a maximum number of adhesive groups per macromolecule wet and adsorb onto the interface of the metal

substrate. Another aspect related to interfacial wet adhesion is the chemical nature of the adhesive groups. Assuming, near neutral conditions, the surface of most metals, such as steel or aluminum, are hydrophilic as a due to the presence of thin oxide layers. Figure 2.2-3, below, depicts the effect of cooperative functional groups at promoting good interactions between polymeric material and areas surrounding a flawed metallic surface.

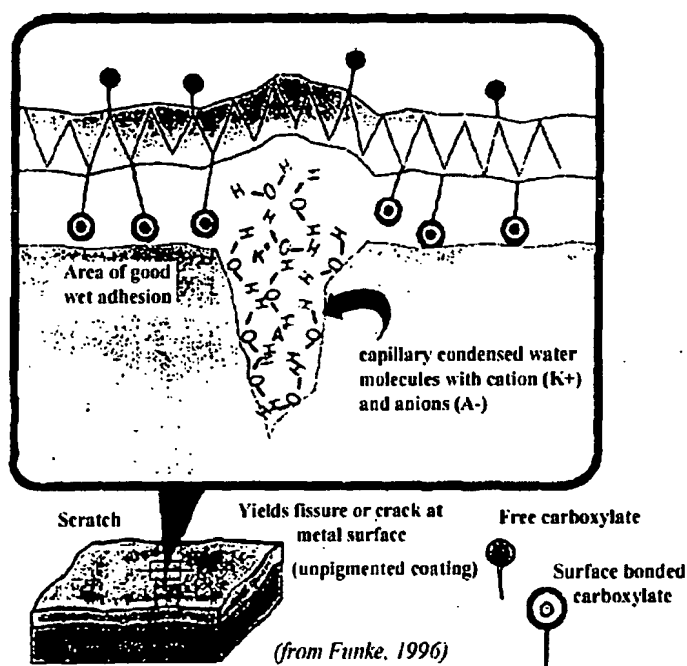


Figure 2.2-3: Corrosion of coated metal with good wet adhesion, but developing undercut corrosion in flaw, (from Funke, 1996.)

Therefore, polymeric macromolecules will have good interactions with these metal surfaces when polar groups are incorporated as structural elements of the polymeric binder molecules. On the other hand, even though such “cooperative” functional groups may promote good wet adhesion to the metal substrate, the presence of such molecules associated with the polymeric binder material may not also be beneficial to the properties of the bulk of the coating film. Therefore, to maximize the effectiveness of adsorption, in

either case conformation or cooperative, the metallic surface must be made relatively smooth on a micron scale to prevent corrosion from initiating at flawed sites that may contain impurities such as dissolved salts and water.

2.2-5 Summary

The application of organic coatings to metal surfaces has been described in a general terms associated with mechanisms of adhesion of polymers and forces acting at the coating / substrate interface that tend promote or detract from macromolecule / polymer adhesion. One assumption has been that the properties of polymers/ macromolecules adsorbing at a metal surface are different than those of the polymer in bulk. Based upon this assumption, a conformation approach, involving pretreatment with a dilute polymeric material, was suggested by Funke¹¹⁰, as a means by which to improve the adhesive properties of a coating. In addition, two other methods¹¹⁰ have been suggested as well: 1) use of reactive molecules of low molecular weight, which after physical or chemical adsorption can be connected by crosslinking or improving the molecular adaptation to the metal surface structure; 2) by incorporating small reactive, mobile binder molecules, which may which may be crosslinked after adsorption. Overall, it may be surmised that the most effective approach to be taken in the development of Mg-rich coatings for corrosion control of aluminum alloys would be to follow the “conformative” approach and prepare a micro-smooth, high energy surface with a dilute solution of low molecular weight oligomer containing reactive or crosslinkable functional groups that can be crosslinked to a bulk applied metal-rich primer later.

References / Bibliography

- ¹⁰⁰ Bierwagen, G.P., "Surface Defects and Surface Flows in Coatings," *Progress in Organic Coatings*, Vol. 19, pp. 59 – 68 (1991)
- ¹⁰¹ Reeves, L.A., Kiroski, D., and Packham, D.E., *Surf. Interf. Anal.* Vol. 23, pp. 299 (1995)
- ¹⁰² Reiter, H. in *Handbook of Adhesion* (D.E. Packham, ed.) pp. 192, Longman, (1992)
- ¹⁰³ Ryntz, R.A, *Prog. Organic Coatings*, Vol. 25, pp.73 (1994)
- ¹⁰⁴ Brewis, D.M. (Ed.) *Surface Analysis and Pretreatment of Plastics and Metals*, Applied Science, London, (1982)
- ¹⁰⁵ Mayne, J.E.O., *J. Oil Color Chem. Assoc.*, Vol. 58, pp. 155 (1975)
- ¹⁰⁶ Bikerman, J.J., *The Science of Adhesive Joints*. " Academic Press: New York, (1965)
- ¹⁰⁷ Meyers, D., *Surfaces, Interfaces, and Colloids, Principles and Applications*, VCH Publishers, pp. 405-414 (1991)
- ¹⁰⁸ Hollenhead, J.B. and Wightman, J.P., *J. Adhesion*, Vol. 37, pp. 121 (1992)
- ¹⁰⁹ Mills, G. D., in *Proposal of the Theoretical Mechanisms of Foam Formation, Adhesion, and Cathodic Disbondment of Fusion Bonded Epoxy Coatings.*, *Corrosion* Vol. 86, paper #313. Houston, TX, March 17-21, (1986)
- ¹¹⁰ Funke, W., *Progress in Organic Coatings*, Vol.28, pp. 3-7 (1996)
- ¹¹¹ Arslanov, V.V., and Funke, W., *Progress in Organic Coatings*, Vol. 15, pp. 365 (1988)
- ¹¹² Funke, W., *Farbe und Lack*, Vol. 93, pp. 721 (1987)
- ¹¹³ Funke, W., *J. Oil Colour Chem. Assoc.*, pp. 229 (1985)

Chapter 2.3 Surface Treatments for Aluminum

2.3-1 Surface Treatment Methodologies

The purpose of this section is to describe the methodologies and importance of surface treatment in the preparation of an Al alloy surface for improved adhesion and corrosion control. Usually, aluminum alloys must be protected against corrosion in by application of a coating or some surface treatment or surface modification (i.e., metal finishing, anodizing, chromate conversion coatings, metallic cladding with Alclad®, corrosion protection compounds, and solution phase inhibitors). For the purpose of this discussion, the specific objective relevant to any of these techniques is to be able to modify the metal's surface within an environmentally compliant context that supports addition of a multi-functional coating for corrosion control of Al alloys. Generally, the desired attributes of any surface treatment, or inhibitor (whether stored in a metal / polymer coating), are that the surface remains somewhat impervious to change, or through action of a coating it promotes a high capacity to resist change, some solubility in the aqueous phase over the coating when released, and delivers a high inhibiting efficiency.

Aluminum and aluminum alloy materials are widely used for aircraft construction. Unfortunately, aluminum is a very active metal and appears high in the electrochemical series of elements and corrodes very easily. On the other hand, aluminum is generally corrosion resistant due to the formation of a tightly-adhering oxide film that provides corrosion control under most corrosive conditions. Another important aspect of aluminum is that most metals, more noble, that come into contact with it form galvanic couples that

cause Al to corrode. In some cases the corrosion products of the “other” metal in contact with aluminum causes the aluminum to corrode as well. In addition, to galvanic corrosion most aluminum alloys are highly prone to various forms of pitting, intergranular corrosion and intergranular stress corrosion cracking.

Treatments commonly used to protect aluminum and aluminum alloys range from simply inducing coverage of the surface of the alloy with its own oxide, to preparation of a *sol-gel* silicate surface that can undergo further organic-inorganic modification, to the treatment of the surface with rare-earth compounds to promote “*self-healing*” when the metal is scratched or damaged:

Anodizing: Electrochemically thickening an oxide layer, increased barrier protection.

Sol-gels: Protection afforded via barrier of covalent Si-O-Al bonds, inability to “self-heal”.

Rare earth metals: cerium, molybdenum, lanthanum, and yttrium “self-heal” properties Mansfeld¹¹⁴ cerium research (nano-particle ceria) Mechanism → blocking of the copper rich / intermetallic precipitates (cathodic regions) due to the deposit of Ce-rich precipitates suppressing the formation of local cathodes.

2.3-2 Improving the Surface

Usually, when considering bonding at the Al adherend-adhesive interface, the Al adherend surface can be enhanced by some method of pretreatment prior to adhesive bonding. It is generally accepted¹¹⁵ that surface pretreatments can result in dramatic improvements in some or all of the following adherend surface characteristics:

- 1) Increase in surface wettability, important in maintaining “wet adhesion”.
- 2) Removal of unwanted weak boundary layers that promote poor adhesion.
- 3) Increase in macro- and microroughness on a uniform scale to enhance wetting.

- 4) Increase in chemical and mechanical stability of surface oxides.
- 5) Increase in chemical interaction between adhesive and adherend.

Chemical adhesion can also be increased by chemical pre-treatments of the surface. Chemical pre-treatments directly modify the surface to provide more reactive sites for coating to chemically bond with the substrate. Several studies^{116,117,118} have demonstrated the importance of the surface properties (chemistry) of adherends in adhesion mechanisms. Typically the adherend (metal) surface is physically and / or chemically treated to enhance the bond strength and durability.^{119,120,121} Weak boundary layers such as weak oxide layers, release agents, and low molecular weight species can be effectively removed from the adherend surface by suitable surface pretreatments.¹²² (See Appendix 2.3_X for surface treatment methodologies)

2.3-3 Phosphoric Acid Anodizing (PAA)

Polymer-metal mechanical interlocking occurs when a coating penetrates into porous geometric areas of an adherend surface^{123, 124}. Adhesion by interlocking requires penetration of a liquid into a pore to be effective, increased surface roughness alone has been observed to lead to decreased adhesive strengths¹²⁵. Therefore, in order to maximize adhesion between both surfaces either one or both of the surfaces may be chemically altered to enhance or promote bonding within a modified interfacial area. It is common practice during either the manufacture or maintenance of an airframe to etch it in phosphoric acid to provide a clean corrosion free surface for bonding to occur. Therefore, phosphoric acid anodizing is often chosen over other anodizing electrolytes because the hydration rate of the oxide during formation is relatively slow which makes the oxide more

stable.¹²⁶ Figure 2.3-1, below, depicts the phosphoric acid anodic oxide (PAA) on aluminum emanating perpendicular to the surface and consisting of an array of porous cylindrical hexagonal cells aligned in a columnar structure¹²⁷. It has been reported by Clearfield, *et al.*¹²⁸, that the resulting structure of the anodic phosphoric acid oxide surface film consists of a mixture of bayerite and boehmite.

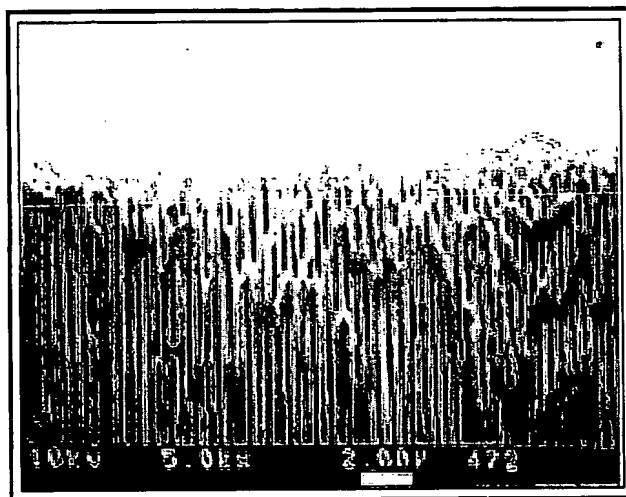


Figure 2.3-1: Phosphoric acid anodic oxide on aluminum from Clearfield *et al.*¹²⁸

It was reported that when Al is anodized in an acid (usually sulfuric (H_2SO_4), oxalic ($\text{H}_2\text{C}_2\text{O}_4$), or phosphoric (H_3PO_4) acids), deep pores can form, with diameters varying that have been found to range between 5 and 100 nm and with lengths up to several microns in depth. The bottom of each pore also consists of a thin “barrier layer” (10-100 nm thick) over the metallic Al surface; the pore diameter depends on pH, anodization voltage, and choice of acid. This porous structure has been called “pore-type film” (PTF) or “alumite”.¹²⁹

Thompson, *et al.*¹³⁰, reported a model for anodic oxide film growth consisting of two parts: 1) pure alumina in the cell boundary, and 2) a layer of phosphate

microcrystallites extending from the cell to wards the pore. A schematic representation of the PAA oxide is depicted in Figure 2.3-2, below. The adherend surface roughness, of the order of tens of nanometers, yields bond durability by improving the energy dissipative mechanism(s) at the interface. However, according to Suzuki¹³¹, phosphate coatings are not as good as chromate conversion coatings due to the formation of both cathodic sites and small randomly spaced uncoated pinholes or anodic sites on the metal surface. The resulting pinholes leave the phosphate coatings prone to degradation under corrosive conditions such as when exposed to salt water. The widely used phosphoric acid anodization is commonly preceded by a phosphoric acid / chromate-containing (FPL-etch™) Forest Products Laboratory.

In 1977 Russell¹³², published results which suggested that an etch designated 'P' etch might be able to replace the FPL process, both as a treatment in its own right and as a preliminary to phosphoric acid anodizing. The 'P' etch consisted of sodium sulphate and ferric sulphate dissolved in a sulphuric acid – nitric acid mixture. This etching / anodization leads to a particular type of coating is known as a conversion coating as it involves converting the surface of a metal substrate into an adherent, porous, passive, inorganic oxide film via an anodization process.

In a recent experiment to determine the adhesive durability of bonds formed on PA surfaces, Pike¹³³ formed PA amorphous aluminum oxide coatings on 2024 T-3 by solvent casting aluminum alkoxides in toluene and determined that the joints with inorganic primers had wet dry lap shear and T-peel strengths equivalent to those joints containing standard organic primers.

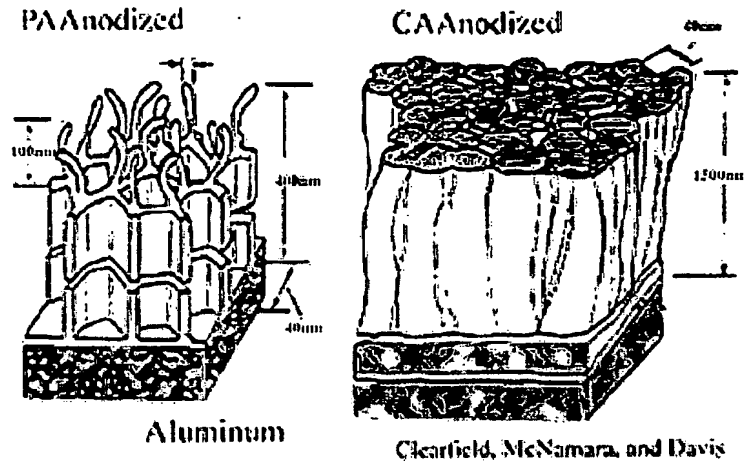


Figure 2.3-2: PA anodized *versus* CAA anodized oxide structures.

As a result, Pike concluded that the mechanism of mechanical interlocking does not play a significant role in adhesive durability of bonds formed with inorganic primed surfaces. Pike's hypothesis was that some type of chemical interaction was responsible for the improved adhesion, or that the morphological features of the primed surface minimized the formation of weak boundary layers in the interphase. In a more recent study, Pike and DeCrescente¹³⁴, showed that water-based inorganic primers adherends prepared from aminosilane modified alumina system resulted in a more versatile primer system when used in conjunction with various epoxy adhesive formulations.

2.3-4 Chromic Acid Anodizing

(CAA) is the most common anodization pretreatment for aluminum alloys, CAA etching leaves a microscopically rough oxide morphology on the aluminum alloy surface, that enhances bond durability. Chromate-based passivation or chromic acid anodizing (CAA) has been applied to metals and/or metallic coatings for over 60 years, and the treatment, a protective film forms on the surface, comprised of trivalent and hexavalent chromium compounds.¹³⁵ The process occurs in a stepwise sequence consisting of a

chromic-sulfuric acid etch, followed by chromic acid anodizing under a constant potential with a gradually increase in voltage.¹³⁶ The morphology of CAA films depicted in Figure 2.3-2 is reported to be process dependent with variations occurring in film development according to the etching process and rate of voltage application.¹²⁷ Compared to the PAA films, CAA films are more densely packed and have less electrolyte anion incorporated into their structure and consist primarily of alumina.¹³⁷

2.3-5 Chemical Conversion Coatings

(CCC) are by far the most commonly used surface treatment for aluminum. CCC produces, by means of dissolution of aluminum metal, and through reaction with a passivating solution of soluble hexavalent chromium salts and chromic acid, a precipitate of insoluble compounds that passivate the metal surface enabling it to resist chemical attack by O_2 , Cl^- , H_2O species, and e^- transport.¹³⁸ In common terminology, “Alodine™” is the generic term referring to chromate conversion coatings that are derived from the Henkel Surface Technologies “Alodine™ process”.¹³⁹ Conversion coatings are the first in a tier of coatings applied to an aluminum substrate they are usually followed with a primer and topcoat Figure 2.3.3, below.

Overall, the advantage of conversion coatings lies in their ability to: 1) inhibit corrosion, if the paint film is ruptured the corrosion will not spread underneath the paint film; 2) they provide two types of adhesion: a) mechanical adhesion due to penetration of a liquid film into porous crystalline cavities (mechanical interlocking); b) they provide adhesion via intermolecular forces (electronic forces). The two most popular processes for obtaining conversion coatings are based upon *in situ* development of an inorganic primer over the alloy’s surface. The process involves formation of amorphous aluminum oxides

over the alloy surface by treatment with either phosphoric acid or a chromic acid anodizing processes.^{140, 141}

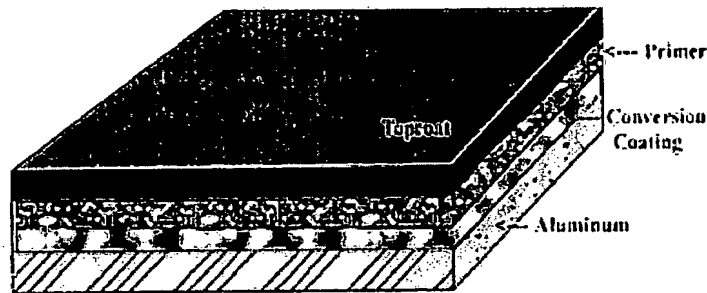


Figure 2.3-3: Schematic of AA 2024 T-3 coating system with conversion coat and topcoat.

The advantage of anodic oxidation of aluminum in solutions of chromic or phosphoric acid over anodization is that it requires a shorter treatment time and can be done with relatively inexpensive chemical solutions. The big disadvantage is the presence of Cr(IV) and F⁻ ions that present health and waste disposal problems. Generally, all of the methods: phosphate, or chromate-phosphate, and chromate conversion coating treatments yield good corrosion inhibition. However, the above methods are reported to yield lower bond strengths between coating and substrate compared to plain anodized aluminum.¹⁴¹ Overall, the improved corrosion resistance of CCC is said to be due to the hydration of aluminum and that this hydration-inhibition property can be attributed to the presence of the more hydrolytically stable surface films of hydrated chromium (III) phosphate and chromium (III) oxide.¹³⁷

2.3-6 Hydration of Thin Oxide Films

Aluminum's native oxide layer is a dynamic structure formed at the Al_2O_3 interface in the presence of water whereby Al-O-Al bonds are hydrated and undergo reversible reactions to form Al-OH species. According to Bunker *et al.*¹⁴², for hydrolysis under anodic polarization conditions, for each water molecule consumed, one Al-O-Al linkage is broken and two aluminum trihydroxide $\text{Al}(\text{OH})_3$ species are formed. The resulting native oxide is a dynamic structure in which Al-O-Al bonds are constantly being broken and reformed by reversible hydrolysis that adds or subtracts hydroxide ion from the lattice. Where it is suggested¹⁴³ that extensive hydration eventually produces oxyhydroxide or hydroxide phases such as AlOOH and $\text{Al}(\text{OH})_3$ that are thermodynamically more stable than Al_2O_3 at room temperature up to 100°C .^{144,145} Generally, the passive films that form act as diffusion barriers and their thickness is dependent on the extent of film hydration.¹⁴³

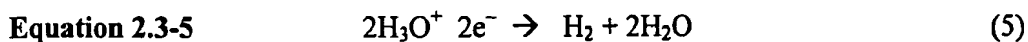
The nature of oxide films that develop over the surface of aluminum are reported¹⁴⁶ to be different from that of the bulk and possess different morphologies which tend to stratify from the surface up. Oxide films observed to develop over aluminum metal at normal atmospheric conditions are composed of two layers: 1) an inner amorphous oxide, *bayerite* layer [$\beta\text{-Al}_2\text{O}_3 \cdot 3\text{H}_2\text{O}$]; 2) an external thicker more permeable hydrated aluminum trihydroxide $\text{Al}(\text{OH})_3$ layer. Still another form of hydrated aluminum oxide *gibbsite* [$\alpha\text{-Al}_2\text{O}_3 \cdot 3\text{H}_2\text{O}$] and its trihydroxide *hydrogillite* $\text{Al}(\text{OH})_3$ can be formed as a result of corrosion processes occurring in an amorphous film.¹⁴⁶ (See appendix 2.3)

2.3-7 Acid-Base Effects on Polymer-Metal Adhesion

Acid-Base effects strongly influence coating adsorption as under ambient conditions metal oxide surfaces generally terminate with an outer most layer of hydroxyl groups, and in the presence of a metal cation the surface hydroxyl groups can either be acidic or basic in nature.^{147,148} In the case of an amphoteric metal such as aluminum the polymer / metal system can exhibit an amphoteric behavior as well. Yamabe¹⁴⁹, reported that the stability of polymer-metal interface was dependent on acid-base interactions between the polymer and metal surface itself, and that the metal surface's isoelectric point (IEP) and the polarity or pK_A of the polymer determined an *ionic interaction* parameter that predicted the stability of hydrogen bonds formed at the polymer-metal interface. (See Appendix 2.3-2.)

2.3-8 Corrosion Inhibition by Cerium

Corrosion inhibition of copper-containing aluminum alloys by rare earth metal salts (REMS) has been investigated by Mansfeld *et al.*^{150,151} where it was reported that the formation and precipitation of cerium oxides or hydroxides occurred over cathodic sites on the Al alloy surface. From these studies it was determined that such precipitates can be associated with a blocking effect and local increase in alkalinity at the copper cathodic sites that acts to decrease the rate of the reduction reaction (the hydrogen evolution reaction), Equ. 2.3-5, which has been implicated as the major reduction reaction occurring in such an alkaline environment.¹⁵²



In a recent study by Mansfeld *et al.*^{Error! Bookmark not defined.}, the corrosion protection of cerium conversion coatings formed on pure magnesium and a magnesium alloy, WE43, was studied by D.C. polarization and A.C. impedance techniques. REMS coatings were observed to show reduced dissolution of magnesium in a pH 8.5 buffer solution. This was ascribed to the formation of protective magnesium hydroxy corrosion products and mixed rare earth/magnesium oxide/ hydroxides. It was observed that protection continued until REMS coatings were consumed by the formation of magnesium corrosion products.

Overall, it was reported¹ and surmised that as these rare earth/magnesium oxide/ reactions proceed, local areas of alkalinity form from which subsequent precipitation of rare earth oxides/hydroxides occurs. The rare earth oxides/hydroxides appeared to nucleate on pure magnesium and the magnesium alloy, with the presence of the alloying additions in the magnesium alloy having little effect. These conclusions were also corroborated with other studies by Goldie and McCarroll.¹⁵³

In a more recent study by Yu and Cao¹⁵⁴, cerium sealing of anodized LY12 (2024) alloy was accomplished by immersion of samples into a $\text{Ce}(\text{NO}_3)_3$ solution, see Figure 2.3-6, below. The resulting corrosion resistance of the Ce films was investigated by electrochemical impedance spectroscopy (EIS) after immersion in NaCl solution for up to 60 days. The results of the study showed that inner Ce sealing of the anodized film was not corroded until about 60 days of immersion. Thus, it was determined that by sealing the anodized layer with Ce the corrosion-resistance-of-the LY12 alloy was greatly enhanced.

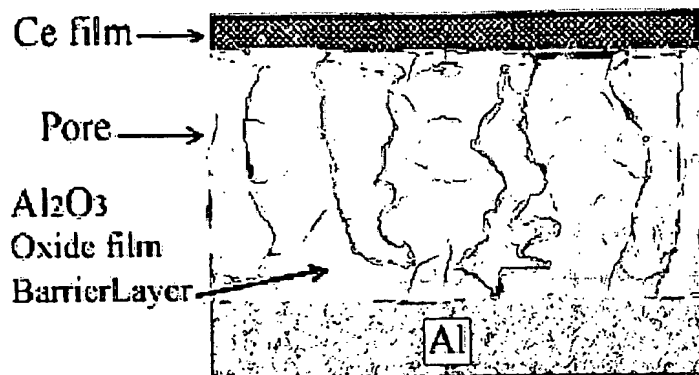


Figure 2.3-6: Schematic model for sealing of Ce anodized LY12 alloy, adapted from Yu and Cao, (2003).¹⁵⁴

2.3-9Summary

In summary, the means by which to prepare and protect an aluminum alloy surface, for corrosion control, have all have involved some means of chemical modification of the aluminum surface via inducing different chemical compositions or structures to grow and emanate from metal into a passive oxide layer. These well established chemical processing techniques have been shown to be capable of producing, relatively smooth, thick, porous, (anodic) oxides structures at the Al /Al₂O₃ interface depending on the particular process chosen. In addition, the process of preferential absorption of polymeric material onto a prepared Al metal oxide surface was shown to be strongly influenced by the resulting pH of the metal oxide surface itself and the acidic / basic property of the polymeric material. Spectroscopically, such interactions were observed from simple FTIR experiments between a given class of polymer / functional group and metal oxide surface. Such observations based upon differences in absorption energies are relatively small but the methodology has shown merit.

Central to the discussion of surface preparation for use with a metal-rich cathodic coating is the fact that aluminum readily forms $\gamma\text{-Al}_2\text{O}_3(\text{s})$ / γ -alumina which occurs spontaneously with a measured $\Delta G_{298^\circ\text{K}} \sim -1564.2 \text{ kJ/mol}$, as well as the hydration product bayerite $\beta\text{-Al}(\text{OH})_3(\text{s})$ $\Delta G_{298^\circ\text{K}} \sim -1149.8 \text{ kJ/mol}$. Figure 2.3-6, below, depicts the nature of the oxide surface which is essentially a magnet for various salts.

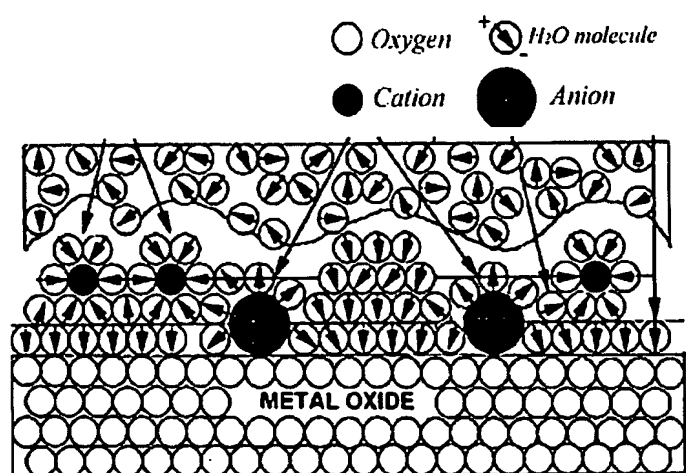


Figure 2.3-6: Depiction of hydrated Al metal oxide surface that has been exposed to water and electrolyte.

Moreover, most discussions regarding corrosion control of Al metal via chemical means involve promotion of oxide stability various means. However, since the metal is covered with oxide and the cations and anions of other metal salts which are always present, true metal to metal contact between metal-rich coating and substrate is impossible. Therefore, any means involving cathodic protection of an aluminum alloy must address retarding the dissolution of γ -alumina and bayerite structures through an electrochemical means.

The essential features required for promoting good adhesion between polymer and metal substrate are that the Al metal surface be prepared smooth on a micro-scale with a chemically treated oxide that promotes interactions, such as those between acid-base functionally of surface and polymer. Overall, since the energetics of oxide formation are favorable at the metal / γ -alumina interface while the weak-link lies in the energetics at the β -Al(OH)₃ bayerite / γ -AlOOH(s) boehmite interface, attempts should be focused on promoting reaction with organo-silanes that yield stable hydrophobic organo-silicate that aid in preserving the passive metal oxide matrix. Cerium, when incorporated at the interface as a film or coating, has been shown to inhibit the primary reduction reaction occurring on the surface of Al alloys containing copper at pH's circa ~ 8.5, (which is at the upper stability limit for Al according to Pourbaix diagrams previous section 2.1), by precipitation of rare earth hydroxides/oxides. All of which is central to the preservation of the β -Al(OH)₃ bayerite / γ -AlOOH(s) boehmite interface in the presence of copper cathodic sites is the application of REMS such as cerium.

In addition, when used in conjunction with magnesium, they showed a similar activity by the precipitation of rare earth hydroxides/oxides at the surface of magnesium thus inhibiting corrosion of the magnesium metal by preferentially forming oxides/hydrides. Finally, the solution treatment of anodized aluminum with Ce(NO₃)₃ has been shown to be an effective means by which to protect a hydrated Al metal oxide surface. Therefore, the current means by which to prepare an Al 2024 T-3 surface for subsequent deposition of a Sol-Gel or metal-rich coating have been reviewed and elucidated.

References / Bibliography

- ¹¹⁴ Rudd, A.L., Breslin, C., B., and Mansfeld, F., *Corrosion Science*, Vol. 42, pp. 275-288 (2000)
- ¹¹⁵ Kaelble, D.H., "Physical Chemistry of Adhesion." Wiley-Interscience: New York, NY, (1971)
- ¹¹⁶ Wood, G.C., and O'Sullivan, J.P., *Acta Electrochimica*, Vol. 15, pp. 1865 (1970)
- ¹¹⁷ Digby, R.P., and Packham, D.E., *Intl. J. Adhesion Adhesives*, Vol. 15, pp. 61 (1995)
- ¹¹⁸ Arrowsmith, D.J., and Clifford, A.W., *Intl. J. Adhesion Adhesives*, Vol. 5, pp. 40 (1985)
- ¹¹⁹ Wake, W.C., *Adhesion and the Formulation of Adhesives*, pp. 65-71, Applied Science, London, (1976)
- ¹²⁰ Clearfield, H.M., Shaffer, D.K., Vandoren, S.L. and Ahearn, J.S., *J. Adhesion*, Vol. 29, pp. 81 (1989)
- ¹²¹ Pike, R.A., V.H., Patarini, Zatoski, R. and Lamm, F.P., *Intl. J. Adhesion Adhesives*, Vol. 12, pp. 227 (1992)
- ¹²² Morris, A.E.P. and Shanahan, M.E.R., *Intl. J. Adhesion Adhesives*, Vol. 14, pp. 145 (1994)
- ¹²³ Arrowsmith, D.J., and Moth, D.A., *Trans. Inst. Met. Finish.*, Vol. 64, pp. 163 (1986)
- ¹²⁴ Ko, C.U., Balcells, E., Ward, T.C., and Wightman, J.P., *J. Adhesion.*, Vol. 28, pp 247 (1989)
- ¹²⁵ Allen, K.W., *Int. J. Adhes. Adhes.*, Vol. 13, pp 67 (1993)
- ¹²⁶ Sun, T.S., Chen, J.M., Venables, J.D., *Appl. Surface Sci.*, Vol. 1, pp 2002 (1978)
- ¹²⁷ Venables, J.D., McNamara, D.K., Chen, J.M., Sun, T.S., and Hopping, R.L., *Appl. Surf. Sci.*, Vol. 3, pp 88 (1979)
- ¹²⁸ Clearfield, H. M., McNamara, D. K. and Davis, G. D. "Surface Preparation of Metals", in *Engineered Materials Handbook*, Vol. 3, Adhesives and Sealants, H. F. Brinson, ed., ASM International, Materials Park, OH, pp. 259 (1990)
- ¹²⁹ Thompson, G. E.; Wood, G. C., Anodic Films on Aluminium. In *Treatise on Materials Science and Technology*, Vol. 23: *Corrosion: Aqueous Process and Passive Films*; Scully, J. C., Ed.; Academic Press Inc., New York, Chapter 5, pp. 205-329 (1983)

- ¹³⁰ Thompson, G.E., Furneaux, R.C., Wood, G.C., Richardson, J.A., and Goode, J.S., *Nature, (London)*, Vol. 272, pp 433 (1978)
- ¹³¹ Suzuki, I., *Corrosion-Resistant Coatings Technology*, Marcel Dekker, New York, (1989)
- ¹³² Russell, W.J., *J. Appl. Polym. Sci.*, Appl. Polym. Symp. No. 32, pp. 105 (1977)
- ¹³³ Pike, R.A., *Int. J. Adhes. Adhes.*, Vol. 5, pp. 3, (1985)
- ¹³⁴ Pike, R.A., and DeCrescente, M.A., *Int. J. Adhes.*, Vol. 11, pp.154, (1991)
- ¹³⁵ Almeida, E., Diamantino, T. C.; Figueiredo, M. O.; Sa', C. *Surf. Coat. Technol.*, Vol. 106, pp. 8 (1998)
- ¹³⁶ Bijlmer, P.F.A., Jr., in "Adhesives Bonding of Aluminum Alloys," Thrall, E.W., and Shannon, R.W., ed., Marcel Dekker, Inc., New York, NY, pp. 21 (1985)
- ¹³⁷ Wernick, S., Pinner, R., and Sheasby, P.G., "*The Surface Treatment and Finishing of Aluminum and its Alloys, Fifth Ed.*," Redwood Burn Limited, Trowbridge, UK, (1987)
- ¹³⁸ Zhao, J., Frankel, G., McCreery, R.L., *J. Electrochem. Soc.* Vol. 45, pp. 2258 (1998)
- ¹³⁹ Lytle, F.W., Gregor, R.B., Bibbins, G.L., Blohowiak, K.Y., Smith, R.E., Tuss, G.D., *Corrosion Sci.* Vol. 37, pp. 349-369 (1995)
- ¹⁴⁰ Pike, R.A., *Int. J. Adhes. Adhes.*, Vol. 5, pp 3 (1985)
- ¹⁴¹ Minford, J.D., "*Handbook of Aluminum Bonding Technology and Data*," Marcel Dekker Inc., New York, NY, pp 1-10 (1993)
- ¹⁴² Bunker, B.C., Nelson, G.C., Zavadil, K.R., Barbour, J.C., Wall, F.D., and Sullivan J.P., Hydration of passive Oxide Films on Aluminum, *J. Phys Chem. B*, Vol. 106 pp. 4705 – 4713 (2002)
- ¹⁴³ Alwitt, R. S. The Aluminum-Water System. In *Oxides and Oxide Films*; Diggle, J. W., Vijh, A. K., Eds., Marcel Dekker: New York, Chapter 3, (1976)
- ¹⁴⁴ Wefers, K., and Bell, G. M. Oxides and Hydroxides of Aluminum, *Technical Paper No. 19*; Alcoa Research Laboratories, (1972)
- ¹⁴⁵ Wefers, K., and Misra, C., "Oxides and Hydroxides of Aluminum," *Tec. Pap. Alcoa Res. Lab.*, pp 19 (1987)

- ¹⁴⁶ Ruberto, C., Bulk and Surface Structures of κ Alumina, *Licentiate Thesis*, Applied Physics Report 98-37 Chalmers University of Technology and Göteborg, Sweden, (1998)
- ¹⁴⁷ Bolger, J.C., in “*Adhesion Aspects of Polymer Coatings*,” Mittal, K.L. (Ed.), pp 3, Plenum Press, New York, NY (1983)
- ¹⁴⁸ Fowkes, F.W., *J. Adhesion Sci. Technol.*, Vol. 1, pp 7-27 (1987)
- ¹⁴⁹ Yamabe, H., Stabilization of the Polymer-Metal Interface, *Progress in Organic Coatings*, Vol. 28, pp. 9-5 (1996)
- ¹⁵⁰ Mansfeld, F. and Wang, Y. *Br. Corros. J.*, Vol. 29 Pp. 194 (1994)
- ¹⁵¹ Mansfeld, F. and Wang, Y., Shih, H., *J. Electrochem. Soc.*, Vol. 138, Pp. 74 (1991)
- ¹⁵² Emley, E.F., *Principles of Magnesium Technology*, Pergamon Press, Oxford, (1966)
- ¹⁵³ Goldie, B.P.F., and McCarroll, J.J., Australian Patent, AU-32947/84, (1984)
- ¹⁵⁴ Yu, X., and Cao, C., *Thin Solid Films*, Vol. 423 Pp. 252–256 (2003)

Chapter 2.4 Silane Coupling Agents for Al 2024T-3

2.4-1 Silane Adhesion Promoters

The purpose of this section is to review the application of organo-silane coupling agents to aluminum metal / metal hydroxide surfaces, the chemistry of organo-silicate formation, and coating system derived from organo-silane coupling agents used as surface modifiers or adhesion promoters for improved corrosion control as well. Overall, the emphasis will be placed on the development of a coating interface between the metal's oxide and an applied coating layer.

Generally, the most commonly reported approach involved in designing coating systems derived from such materials from the metal oxide surface and extending into an organic coating has been the sol-gel approach. In brief, such coatings can be applied to Al 2024 T-3 by simply covering a prepared Al alloy surface with dense silanol layer, followed by the application of an organo-silane to promote gel structure throughout an organic matrix, Figure 2.4-1, below. However, the unresolved question regarding most sol-gel derived coatings is their brittleness.

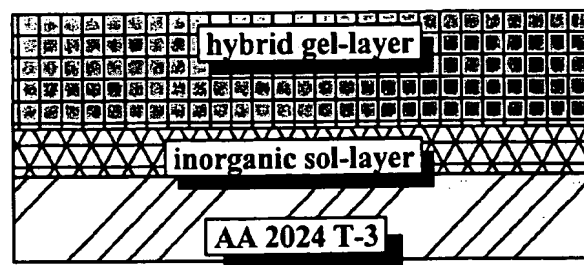


Figure 2.4-1: Generalized schematic of sol-gel coating over Al metal substrate.

The principle behind silane modified polymeric matrices, for corrosion control of coatings is that they must be designed as polymer composites or alloy that consists of chemical bonding in different or intermediate phases of a “hybrid” organic -inorganic matrix that results in covalent structure and modified interfacial properties of the resulting polymeric material. Such organic-inorganic modification is critical in terms of resulting film properties and compatibility between the organic and inorganic moieties. For example, if the level of organic modification is too low, the resulting films can be glasslike with good durability but with poor overall coating performance properties. As a result of such imbalances further progress is sought in the development and synthesis of hybrid polymeric materials for these systems that possess enhanced flexibility and better resistance to acid and solvents.

Adhesion of coatings to aluminum surfaces is often poor, especially when the polymeric matrix has no chemical affinity to bond to the substrate surface. Often moisture, and acid or base interactions are what promote corrosion induced adhesive failure. A common chromate replacement strategy used in preparing aluminum alloy surfaces has been to use organo-silane coupling agents to improve the adhesion of polymeric binders to substrates such as glass, silica, alumina or active metals. The action of silane coupling has been described in such terms as that of surface treatments that interpose a layer of intermediate modulus, lowering the stress concentrations and enabling larger volumes of material to be involved in energy dissipating viscoelastic or plastic deformation. The effect of an interfacial 'composite' region¹⁵⁵ where substrate and adhesive merge over a distance of nanometres or micrometres will similarly smooth out a sharp modulus change between the two phases.

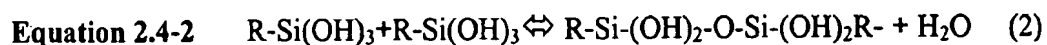
Silanes used to enhance adhesion of polymers are known as coupling agents. Organosilane coupling agents function by forming covalent bonds between an inorganic metal oxide and an organic molecule / polymer through an intermediate silane Al–O–Si–C bond. Most silane coupling agents introduce organic functionality at the γ carbon where the effect of the functional group on the alkoxy group is minimized, Table 2.4-1, below, commonly used coupling agents.^{156,157} The adhesion of coatings containing silane materials involves complex relationships between polymer-substrate interphases. However, practically all common organic polymers can be bonded to a mineral surface by one of the coupling agents listed in Table 2.4-1, below.

Table 2.4-1: Representative commercial silanes

<i>Abbreviation</i>	<i>Chemical formula and name</i>
γ -APS	$\text{H}_2\text{NCH}_2\text{CH}_2\text{CH}_2\text{Si}(\text{OCH}_2\text{CH}_3)_3$ [gamma-aminopropyltriethoxysilane]
CPS	$\text{ClCH}_2\text{CH}_2\text{CH}_2\text{Si}(\text{OCH}_3)_3$ [chloropropyl-trimethoxysilane]
EPS	$\text{CH}_2\text{OCH}_2\text{CH}_2(\text{OCH}_3)_3\text{Si}(\text{OCH}_3)_3$ [3-glycidoxypropyltrimethoxysilane]
γ -UPS	$\text{NH}_2\text{C}(=\text{O})\text{NH}_2\text{CH}_2\text{CH}_2\text{CH}_2\text{Si}(\text{OCH}_3)_x\text{O}(\text{C}_2\text{H}_5)_{3-x}$ [gamma-ureidopropyltrialkoxysilane]
γ -MCPS	$\text{HSCH}_2\text{CH}_2\text{CH}_2\text{Si}(\text{OCH}_3)_3$ [gamma-mercaptopropyltrimethoxysilane]
VS	$\text{CH}_2=\text{CHSi}(\text{OCH}_3)_3$ [vinyltrimethoxysilane]
γ -GPS	$\text{CH}_2\text{OCHCH}_2\text{O}-(\text{CH}_2)_3-\text{Si}(\text{OCH}_3)_3$ [gamma-glycidoxypropyltrimethoxysilane]

Treatment of inorganic surfaces with reactive silanes as coupling agents has been studied extensively by Plueddemann^{158,159} who established that silane coupling agents form covalent oxane bonds (Al–O–Si) with mineral surfaces where M= Si, Ti, Mg, Al, Fe, etc. by an equilibrium reaction Equ. 2.4-1, below, with true bond breaking and formation in the presence of water with an activation energy of 98.7 kJ/mol. According to Boerio¹⁶⁰, effective silane coupling only occurs when two steps: 1) hydrolysis, and 2) condensation are favored. Hydrolysis is a stepwise reaction that requires water so the alkoxy groups of

the silane can be converted into silanol groups with the formation of an alcohol as a byproduct. After hydrolysis, the condensation process transforms the silanol groups into polysiloxanes / silsesquioxane networks according to Equ.(s) 2.4-1 and 2.4-2:



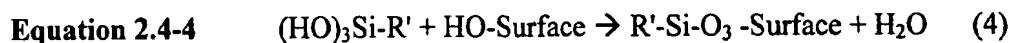
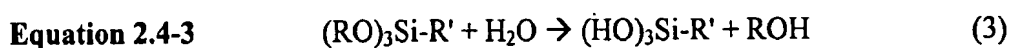
Siloxane bond hydrolysis can be catalyzed by benzoic acid or potassium hydroxide and has an activation energy of around 25 kJ/mol which is on the order of hydrogen bonding. Since acid or base catalysts lower the activation energy of the condensation reaction the resulting siloxane structure may become more prone to hydrolysis. Plueddemann¹⁶¹ postulated three preparation conditions for ensuring bonding in the presence of water:

1. Maximum conversion of M-O-Si bonds, shifting the mass action equilibrium in Equ. 2.4-2, above, to favor the right side of the equation.
2. Exclusion of water from the surface, minimize water penetration to the interface (use hydrophobic spacer groups on the silane.)
3. Develop silanol-polymer structure at the interface (use a trialkoxy / trifunctional silanes.)

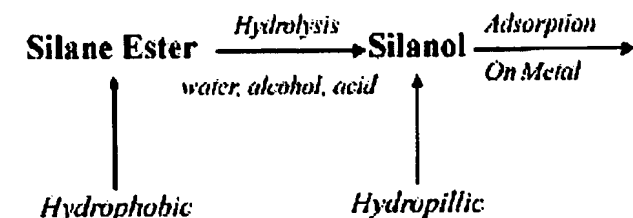
Silanes are commonly used to treat surfaces of inorganic substrates such as aluminum trihydrate¹⁶², alumina¹⁶³, and silica¹⁶⁴ by condensation with surface hydroxyl groups, in addition they can be incorporated directly into a polymer matrix for subsequent bonding to an inorganic substrate.¹⁶⁵ The most common type of silane coupling agents are trialkoxysilanes and in theory the silane hydrolyzes to form a silanol that chemically reacts

with hydroxyl groups from an inorganic substrate and with organic functional groups of an oligomer / polymer forming a polymerized poly(siloxane) bond between the polymer and the inorganic oxide surface.^{166, 167}

The generic reaction is hydrolysis for substituted silanes (alkoxides) and reaction of the product with the adherend surface according to Equ.(s) 2.4-3 and 2.4-4:



where R = alkoxy such as methoxy, or ethoxy and R' = can be any organic polymer with functional group: amine, sulfide, epoxy, etc. and the coupling reaction is depicted in Figure 2.4-2, below, involves silanol hydrolysis and the formation of silsesquioxane networks that can blend into the polymer-matrix at the interface.¹⁶⁸



Mechanism of silane formation on metal surface
(Adapted from van Ooij, 1998)

Figure 2.4-2: Mechanism of silane formation on metallic surface.

According to Arkles *et al.*¹⁶⁹, the three most commonly used classes of silanes are *chloro*, *methoxy* and *ethoxy* silanes. Chlorosilanes are most reactive but evolve corrosive hydrogen chloride on hydrolysis. Methoxy silanes are of intermediate reactivity and evolve toxic methanol. Ethoxy silanes are least reactive but evolve non toxic ethanol. Generally

the reactivity differences between methoxy and ethoxy silanes are only minor, and at typical hydrolysis pH (acidic ~5, basic ~9), both versions hydrolyze in under 15 minutes at 2% silane concentrations. Coupling agents are normally added in the range of about 0.5 to 2% of the weight of the polymeric binder material.¹⁷⁰ According to Plueddemann¹⁷¹, silanes whether used as a primer or additive, must concentrate in and remain at the interface region between the coating and metal surface where they may crosslink with the polymer (if thermoset) or form a rigid silsesquioxane network, as depicted in Figure 2.4-3, below.

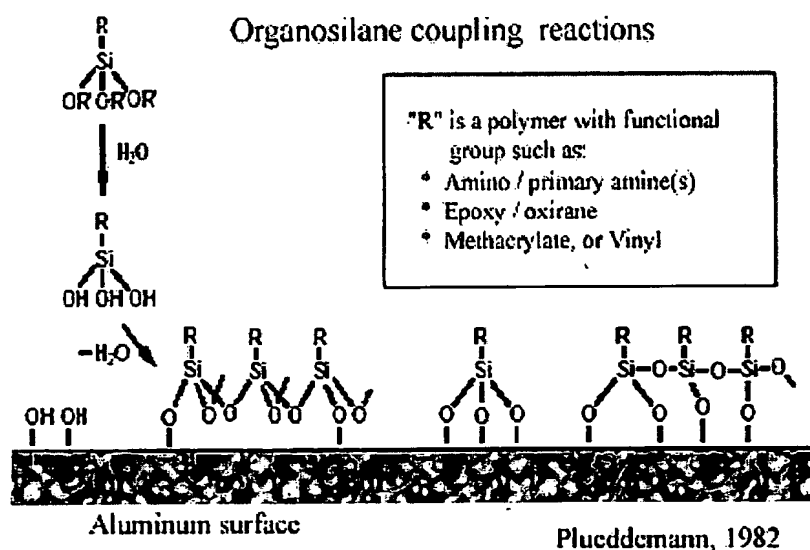


Figure 2.4-3: Organosilane coupling reactions to metal surface, adapted from Plueddemann¹⁵⁸ (1982).

Development of silane structure at the inorganic interface, as depicted in Figure 2.4-3, previous, has been described to occur and be controlled by the following parameters: solution concentration, temperature, pH; solvent, electrolyte, length of exposure, type of treatment according to the following:

1. *Aqueous solutions.* Walker¹⁷⁹ describes preparation of dilute solutions of organosilanes in water and acetone solutions. This layer often results in multi-layered structures that can be tailored or removed with solvents.
2. *Organic solutions.* Are prepared from dry organic solvents such as ethanol / toluene mixtures that tend to form monolayer like structures.¹⁷²
3. *Particulate Blend.* Fillers such as ceramic or pigments are modified with a silane coupling agents before they are blended into a polymeric resin.¹⁷²
4. *Vapor Phase Deposition.* Silanes can be volatilized and allowed to condense on an inorganic surface to yield a perfect monolayer structure.¹⁷³

Generally, uniform monolayer surface structure is reported to promote more specific bonding interactions. Monolayers can be generated from monochloro or or alkoxy silanes. Conversely, trichloro or trialkoxy silanes can form network or "multilayer" structures at the surface from crosslinking of the silanetriols produced during hydrolysis. According to Plueddemann¹⁵⁸ at a 0.5 – 2 percent silane concentration in aqueous alcohol typically 3-8 molecular layers are produced.

Arkles *et al.*¹⁵⁷, report a general method for preparing silylated surfaces on metal oxides from depositions of aqueous alcohol solutions according to the following procedure: a 95% ethanol-5% water solution is adjusted to pH~ 4.5 - 5.5 with acetic acid. The silane is added with stirring to yield a 2-percent final concentration and allowed to equilibrate for five minutes to facilitate hydrolysis and silanol formation. Once the surface has been treated, it must be rinsed free of excess materials by dipping briefly in ethanol. Final cure of the silane layer is for 5-10 minutes at 110°C or for 24 hours at room temperature (<60% relative humidity). For aminofunctional silanes the above procedure can be modified by

omitting the additional acetic acid. Generally, a 2% starting point concentration of trialkoxysilane yields a deposition of a film 3-8 molecular layers in thickness.¹⁵⁷

According to Arkles¹⁵⁷, monoalkoxysilanes are always deposited in monolayers or incomplete monolayers. Unfortunately, monolayers suffer from one severe disadvantage. Cleavage of the bond is readily accomplished in high or low pH, resulting in adhesive failure. While the multilayer structure is inherently less uniform, it possesses dramatically improved hydrolytic stability at the polymer/ silane /substrate interface. The crosslinked network is not dissolved if one bond is broken, unlike the situation for monolayers, where a broken bond results in adhesive failure at that area of the surface. The bulky isopropyl groups sterically block attack by acidic or basic nucleophiles. Figure 2.4-4, below, gives equilibrium effect of high or low pH on the rate of silanol oligomerization:

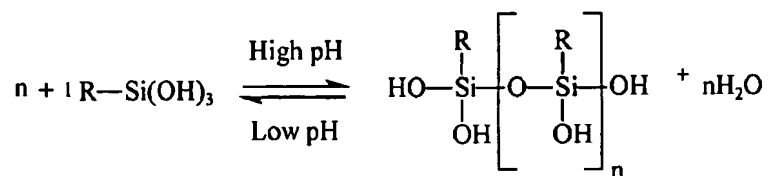


Figure 2.4-4: Silanol oligomerization, pH dependence.

Rapid rates of oligomerization eventually result in gelation, as evidenced by turbidity or precipitated solids. Such solutions are ineffective as coupling reagents. The factors contributing to stability of silanols have been reviewed by Arkles *et al.*¹⁵⁷, and silanols are reported to be stabilized by the following methods:

1. Neutral conditions
2. Limited condensation (high dilution)
3. Presence of hydroxylic species (alcohols are stabilizers)

4. Silanes forming stable zwitterions. Amino silanes form such species and are among the most stable water borne species. They readily dissolve in water on stirring and are most stable at pH~ 10-11.

Based on recent studies^{174, 175}, all silanes suitable for corrosion protection are divided into two major categories, (i.e. *mono*-silylfunctional silanes '*mono* silanes' and *bis*-silylfunctional silanes *bis*- silanes). *Mono silanes*, are silane coupling agents of the type $R-(CH_2)_3Si(OR')_3$ (where R- is an organofunctional group, and O-R' is the (hydrolyzable alkoxy group), and typical examples are γ -aminopropyltriethoxysilane (γ -APS) and (γ -ureidopropyltriethoxysilane (γ -UPS). According to Rider *et al.*¹⁷⁶, a silane coupling agent will improve environmental durability at the polymer-Al interface by: 1) increasing the density of strong bonds between the oxide and the adhesive; 2) improving the hydrolytic stability of the aluminum oxide, and that the formation of a weak hydrated layer on the aluminum surface is significantly hindered by the formation of a cross-linked multilayer (i.e., silane hydrolysis / condensation). The presence of a silane monolayer on Al decreases water adsorption on the surface, and inhibits hydration of the metal oxides.¹⁶¹

One of the most common silane surface treatments for aluminum alloys described in the literature^{177, 178, 179} involves application of an surface-interfacial primer¹⁵⁹ by using a dilute aqueous solutions of γ -aminopropyltriethoxysilane (γ -APS). Plueddemann¹⁵⁸ found that when the organic functional group was a primary amine, such as (γ -APS), no external acid or base catalyst was required for hydrolysis as the amine and water alone would catalyze autocondensation. Arkles¹⁵⁷, reports that aminoalkylalkoxy silanes such as (γ -APS) hydrolyze immediately upon contact with water and condense slowly to form oligomers, and silsesquioxane networks such as depicted in Figure 2.4-4, above. The rate

of silane hydrolysis is dependent upon the basicity of the organofunctional group and on internal chelation of the amine functional group with the silanolate.

It has been well documented¹⁸⁰ that the best deterrent to adhesion failure in organic coatings lies in developing the right chemical interactions between the coating polymer, pigment, coating layers, and their metallic substrates.¹⁸⁰ The most effective strategy, thus far, has been to develop coatings whose polymer matrix hydrophilicity decreases during cure as the polymer matrix coating undergoes film formation and solidifies.¹⁸⁰

Organofunctional silanes are commonly used as coupling agents and adhesion promoters in epoxide and urethane paints to improve their initial, wet, and recovery adhesion to aluminum surfaces. The “Reversible Hydrolytic Bond Mechanism Theory”, discussed by Walker¹⁸¹, proposes the reversible breaking and reformation of stressed bonds between a coupling agent and the substrate, which allows stress relaxation without the loss of adhesion when water is present. It is argued that when Si-O-metal bond is broken by intrusion of water, the bond will be capable of reforming with some recovery in adhesion.¹⁸²

2.4-2 Sol-Gel Coating Chemistries

These coatings have been reported as one of the most promising protection systems for metals.^{183, 184} The sol-gel process and its applications have been studied for several decades and there is a growing body of literature available.^{185,186,187,188,189,190,191,192}

Essentially, sol-gel systems are organically modified ceramic coatings comprised of a ceramic portion of the coating that provides adhesion, and hardness, while the organic matrix provides film flexibility and durability. (See Appendix 2.4-3)

2.4-3 Interface Treatment Summary

Even though much work has been done to elucidate the formation of chemical bonds between the coating and metal oxide as the primary means by which adhesion of systems primed with silanes may be enhanced. Good adhesion of a silane primed epoxy to aluminum has been described and attributed to the corrosion protection offered by a cured polysiloxane film on the aluminum oxide^{193, 194} which acts to minimize diffusion of water to the aluminum oxide and thereby inhibiting hydration of the oxide. Plueddemann¹⁹⁵, incorporated a hydrophobic silane into polysiloxane films and observed that diffusion of water to the aluminum oxide interface was reduced, thus hydration and weakening of the interface due to bond failure did not readily occur. The utility of aminosilanes in surface treatments for corrosion control has been called into question by van Ooij^{Error! Bookmark not defined.} and Petrunin, *et al.*¹⁹⁶, who assert that “a positively charged layer, such as γ -APS, tends to activate local metal corrosion in chloride containing media by promoting the adsorption of chloride ions on the metal surface.” (See Appendix 2.4-4)

2.4-4 Amino-Silanes and Metal Hydroxides

Aminoalkylfunctional silicones have a broad array of applications as a result of their chemical reactivity, their ability to form hydrogen bonds and, particularly in the case of diamines, their chelating ability. Additional reactivity can be built into aminoalkyl groups in the form of alkoxy groups. Aminoalkylsiloxanes are available in the three classes of structures typical for silicone polymers: 1) terminated; 2) pendant group, and 3) T-structure. Aminopropyl terminated polydimethylsiloxanes react to form a variety of polymers including polyimides, polyureas and polyurethanes. Silanes are often used as

adhesion promoters to metal hydroxide surfaces to generate a covalent bond between the $\text{Al}(\text{OH})_3$ surface and some reactive component of the coating.¹⁹⁷ The proposed reaction scheme for the treatment of an $\text{Al}(\text{OH})_3$ pseudobohmite surface with an amino functional silane, as shown in

Figure to 2.4-15, below.

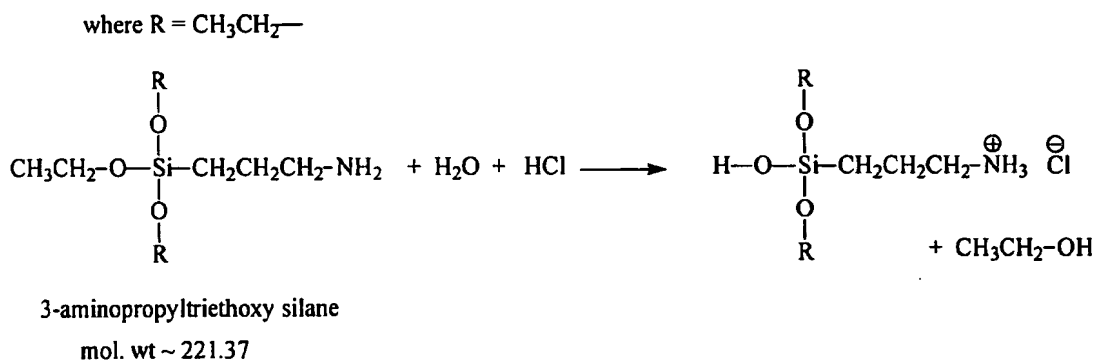


Figure 2.4-11: Activation of 3-aminopropyltriethoxysilane with dilute HCl.

Acidifying the silane with HCl converts it to a water soluble salt where it can be applied in the form of an aqueous solution, as discussed by Walker¹⁸¹, to a prepared metal oxide surface consisting of pseudobohmite or bayerite, see Figure 2.4-12, below.

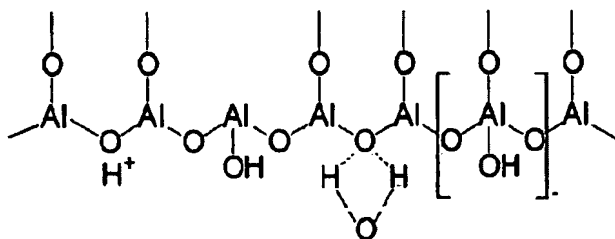


Figure 2.4-12: Aluminum oxide / hydroxide structure, with hydroxyl, acid and base structures.

The solution of water soluble amino-silane can then be applied to the Al metal oxide surface where an aluminino-silicate bond is formed, Figure 2.4-13, below. In

addition, dimerization side reactions of the silane through the hydroxyl groups¹⁵⁸ are a by product as well.

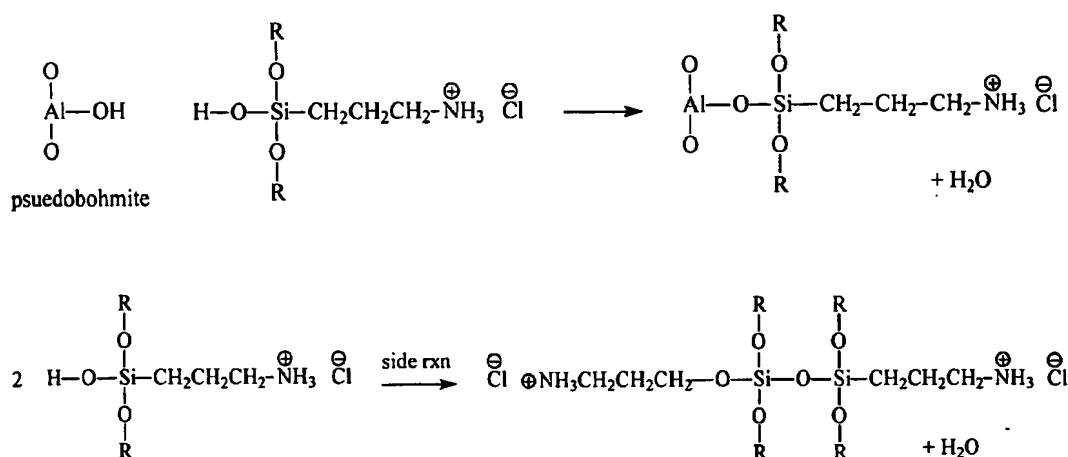


Figure 2.4-13: Reaction of activated 3-aminopropyl dimethylethoxysilane with Si-OH surface, *above*, and dimerization side reaction, *below*.

After the above reaction, an organic functional group has been covalently attached to the metal oxide surface yielding an amine functionalized metal hydroxide surface now capable of reacting with an isocyanate as shown in *Error! Reference source not found.* below, covalently bonding it into the matrix as well.

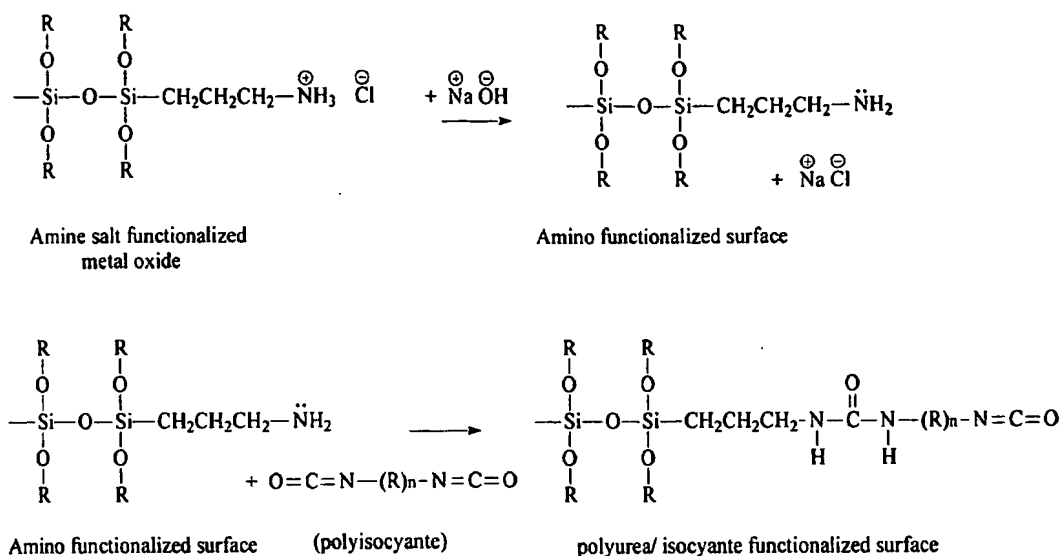


Figure 2.4-14: Neutralization of the tertiary amine salt with NaOH and Reaction of an amino-silane treated silica pigment surface with a polyisocyanate.

2.4-5 Integrated Coating System

According to Bierwagen¹⁹⁸, “the goals of the Sol-gel process are to generate a chemically bonded structure that undergoes a controllable gradient in chemical properties from inorganic metal oxide at the surface through mixed inorganic / organic structure to the purely organic of a primer coating”, according to Figure 2.14-5, below.

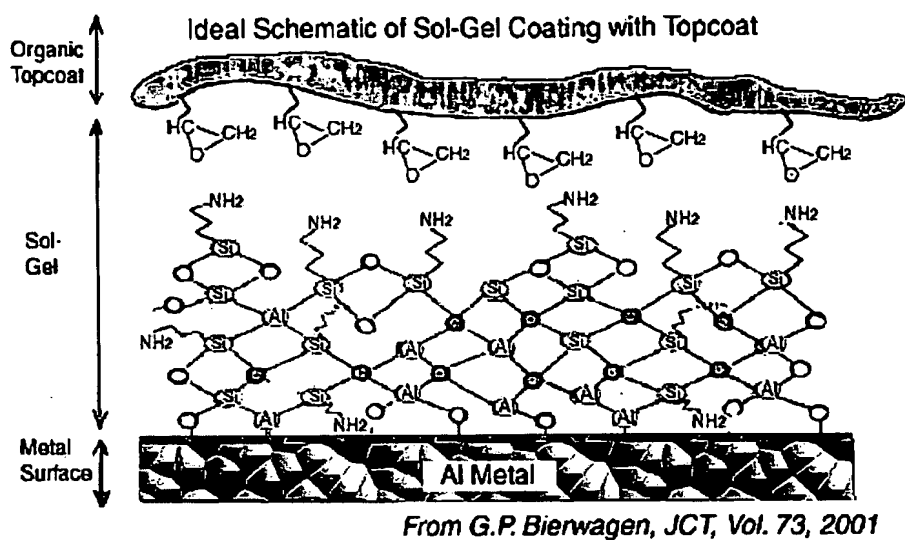


Figure 2.4-15: Schematic showing integrated coating system, from Bierwagen, (2001).¹⁹⁸

2.4-6 Assembled Multi-layer Coatings

The specific chemical systems based upon sol-gel / ormosil chemistries involving covalent interlayer linkages of the organo-silane moiety to metal oxides have been well reviewed in previous section. However, the keystone to the growth of robust, covalent silane-functional multilayer assemblies, that may be of practical use in coatings for corrosion control, have their roots in the development of multi-layer isocyanate / amine, polyurea chemistry that involves a surface-bound terminal amines reacting with isocyanates and water to produce an aminated surface that can subsequently react with solution phase isocyanates to generate surface layer polyureas.^{199,200,201,202,203,204}

In a recent publication, Blanchard and Kohli²⁰⁵, proposed a novel route for facilitating “layer-by-layer and spontaneous growth of covalently bound multilayers” on a specially prepared gold and silicon substrates. According to Banchard *et al.*⁷⁰, conversion of the surface was carried out by sol reaction of (3-aminopropyl) dimethylethoxysilane (APDES) with labile hydroxyls and the polymerization was described to take place both on

the surface and in the bulk. Initially, an isocyanate such as 4,4'-methylene diphenyl isocyanate(MDI) was reacted with surface amines, as depicted in Figure 2.4-16, in the solution phase at the surface, while the alternating copolymerization of 4,4'-methylenedianiline (MDA) isocyanate/amines, as depicted in Figure 2.4-16 , below, was subsequently carried out with surface bound and bulk isocyanates. According to Blanchard and Kohli⁷⁰, irregardless of which reaction pathway dominates, the overall effect is a statistical layer growth for each cycle.

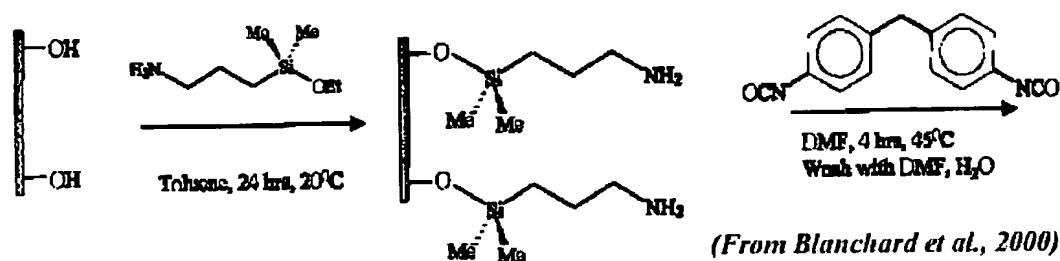


Figure 2.4-16: Sol reaction of (3-aminopropyl) dimethylethoxysilane (APDES) with labile surface hydroxyls, and primary amine solution / surface reaction with (MDI). ,*(from Balnchard and Kohli, 2000).*

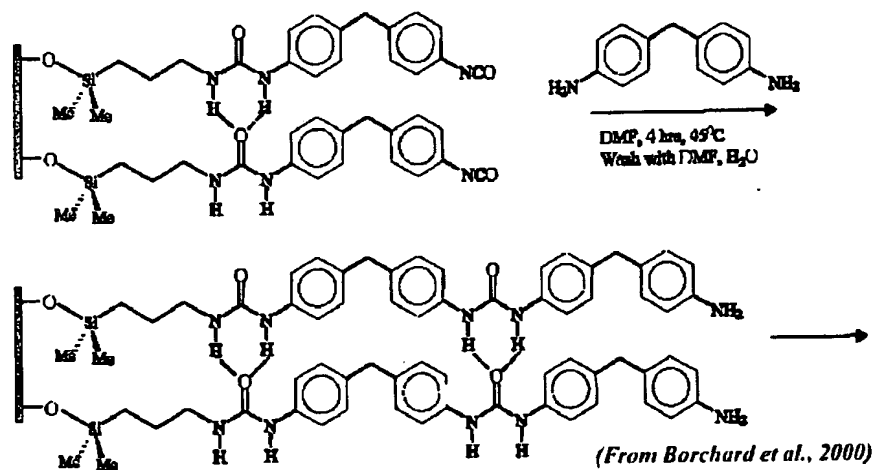


Figure 2.4-17: The alternating copolymerization of 4,4'-methylenedianiline (MDA) isocyanate/amine, *(from Balnchard and Kohli, 2000).*

Blanchard and Kohli's⁷⁰ studies describe two routes to producing polyurea multilayers by alternate exposure of a metal's surface to diisocyanates and diamines to produces a multilayer structure with discrete control over layer growth. The polymerization was carried out using only the isocyanate monomer, at 45°C, in the presence of a small amount of water resulted in the growth of spontaneous but consistent multilayer growth. The authors²⁰⁵ found that the structural properties of the urea multilayer assemblies grown using two similar but different schemes were the same despite the difference in extent of control that was exerted applying the two methods. They contribute this consistency to the presence of layers that are hydrogen bonded laterally through the urea functionalities.

2.4-7 Summary

The objective of this section was to review the preparation and application of surface treatments to Al metal surfaces to which a hybrid (organic/inorganic) coating system might be conveniently applied. The term *sol-gel* chemistry applies to surface preparation via reactive silanes with sequential film forming processes over such Al metal oxide surfaces. Existing sol-gel technology has demonstrated that organic coatings can be bonded covalently to such Al metal oxides and that such coatings are capable of providing a high level of corrosion control under relevant pH conditions. Moreover, the most significant technological application to emerge from this *sol-gel* technology has been through the grafting of polyisocyanates to an aminated metal oxide surface, as described by Blanchard and Kohli. Of the reactive organo-silanes, the amino silanes are the easiest to prepare and apply due to autocatalysis or complexing which promotes these reactions at the metal oxide surface. However, the presence of primary or secondary amine has been noted

to have a detrimental effect at promoting dissolution of copper from the Al 2024 T-3's S-phases. Therefore, complete conversion of the aminated surface the Hoffman reaction with a polyisocyanate is necessary to minimize such effects.

In light of these findings it can be surmised that a method whereby naturally occurring or induced metal oxide structure formed over the Al surface can be greatly preserved or protected by conversion of its labile hydroxyls into alumino-silicate structures containing an hydrophobic organic polymeric material that in turn acts to retard dissolution of the metal oxide and corrosion of the metal. In terms of devising and designing a sacrificial metal-rich coating system comprised of pigmentary magnesium, this surface preparation modification technique may also be valid and serve as a corrosion control utility tool when applied directly to the surface of the magnesium metal itself. Such a surface consisting of MgO and Mg(OH)₂ may constitute a suitably reactive surface and as a first line of defense in arresting the ingress and migration of both Cu²⁺ and Cl⁻, which have been implicated in the destruction of the Al₂O₃/Al(OH)₃ protective oxide layer.

References / Bibliography

¹⁵⁵ Davies, R.J. and Ritchie, M.D., *J. Adhesion*, Vol. 38, pp. 243 (1992)

¹⁵⁶ Arkles, B., Tailoring Surfaces with Silanes, Gelest, Inc., *Chemtech*, Vol. 7, pp36-49, December (1977)

¹⁵⁷ Arkles, B., Commercial Hybrid Organic-Inorganic Polymers, Gelest, Inc., *Organosilicon Chemistry IV: From Molecules to Materials* eds. N. Auner, J. Weis, Wiley-VCH, pp. 592-612 (2000)

¹⁵⁸ Plueddemann, E.P., "*Silane Coupling agents*," Plenum Press, New York, NY, (1982)

- ¹⁵⁹ Plueddemann, E.P., Present Status and Research in Silane Coupling, Interfaces in Polymer, Ceramic and Metal Matrix Composites, Elsevier Science Publications Co., pp 17-33 (1988)
- ¹⁶⁰ Bertelsen, C.M., and Boerio, F.J., Linking Mechanical Properties of Silanes to their Chemical Structure, *Progress in Organic Coatings*, Vol. 41, pp 239 -246 (2001)
- ¹⁶¹ Plueddemann, E.P., Silane Coupling Agents, Plenum Press, New York, NY (1982)
- ¹⁶² Horne, W.E., Balaba, W.M., and Parker, A.A., United States Patent No. 5,543,173 (1996)
- ¹⁶³ Parker, A.A., Tsai, M., Biresaw, G., Stanzione, T.T., Armstrong, G.H., and Marcinko, J.J., *Mater. Res. Soc. Symp.Proc.*, Vol. 249, pp 273-278 (1992)
- ¹⁶⁴ Fowkes, F.M., Dwight, D.W., and Cole, D.A., *J. Non-Crystalline Solids*, Vol. 120, pp 47-60 (1990)
- ¹⁶⁵ Mittal, K. L. (Ed.), *Silanes and Other Coupling Agents*, VSP, Zeist, The Netherlands (1992)
- ¹⁶⁶ Abela, M-L., Watts, J. F. and Digbyb, R. P., The Adsorption of Alkoxysilanes on Oxidized Aluminium Substrates, *Int. J. Adhes., Adhes.*, Vol. 18, Issue 3, pp 179-192 (1998)
- ¹⁶⁷ Chadhury, M.K., Gentle, T.M., and Plueddemann, E.P., *J. Adhesion Sci. Technol.*, Vol. 1, pp 29 (1987)
- ¹⁶⁸ Pohl, E.R., and Osterholtz, F.D., in: *Molecular Characterization of Composite Interfaces*, Ishida, H., and Kumar, G., (Eds.), pp 157-170. Plenum Press, New York, NY (1985)
- ¹⁶⁹ B. Arkles, J.R. Steinmetz, J Zazyczny and P. Mehta "Factors Contributing to the Stability of Alkoxysilanes in Aqueous Solution", *Silicon Compounds Registry and Review*, 5th Edition (1991). Article available from *United Chemical Technologies*.
- ¹⁷⁰ Driver, W.E., *Plastics Chemistry and Technology*, Van Nostrand Reinhold, New York, NY, pp 117 (1970)
- ¹⁷¹ Plueddemann, E.P., *Progress in Organic Coatings*, Vol. 11, pp. 297 (1983)
- ¹⁷² Parker, A.A., The Effect of Silane Hydrolysis on Aluminum Oxide Dispersion Stability in Ceramics Processing, *J. Adhes. Sci. Technol.* Vol.16, pp679-701 (2002)

- ¹⁷³ Atul, P., Russell, T.W.F., Huff, M.C., Hot-Wire Chemical Vapor Deposition of Silicon from Silane: Effect of Process Conditions, *Department of Chemical Engineering*, University of Delaware, Newark DE, (2002) available on line at <http://www.udel.edu/iec/pubs/RWBpubs/RWB107.pdf>
- ¹⁷⁴ Arnott, D. R., Wilson, A. R., Rider, A. N., Lambriandis, L. T. and Farr, N. G., *Appl. Surface Sci.* Vol. 70/71, pp. 109– 113 (1993)
- ¹⁷⁵ D. Zhu, and van Ooij, W.J., *J. Adhesion Sci. Technol.*, Vol. 16, No. 9, pp.1235 – 1260 (2002)
- ¹⁷⁶ Rider, A. N. and Arnott, D. R., *Su. Interface Anal.*, Vol. 24, pp. 583–590 (1995)
- ¹⁷⁷ Comyn, J., Kinloch, A.J., Horley, C.C., Mallik, R.R., Oxely, D.P., Pritchard, R.G., Reynolds, S., and Werrett, C.W., *Int. J. Adhes. Adhes.*, Vol. 5 pp. 59 (1985)
- ¹⁷⁸ Ondrus, D.J., Boerio, F.J., and Grannen, K.J., *J. Adhes.*, Vol. 29, pp. 27 (1985)
- ¹⁷⁹ Walker, P., Organo Silanes As Adhesion Promoters For Organic Coatings, *J. Coatings Technology*, Vol. 52, No. 670, pp. 49-61 (1980)
- ¹⁸⁰ Funke, W., "Problems and Progress in Organic Coatings Science and Technology," *Progress in Organic Coatings*, Vo. 31, pp. 5–9 (1997)
- ¹⁸¹ Walker, P., "Organo Silanes As Adhesion Promoters for Organic Coatings," *Journal of Coatings Technology*, Vol. 52, No. 670, November, pp. 49-61 (1980)
- ¹⁸² Rosen M.R., "From Treating Solution to Filler Surface and Beyond The Life History of a Silane Coupling Agent," *J. Coatings Technology*, Vol. 50 (No.644) 70 – 82 (1978)
- ¹⁸³ Guglielmi, M., *Sol-Gel Sci. Technology*, Vol. 25, pp. 443-449 (1997)
- ¹⁸⁴ Chou, T.P., Chandrasekaran, C., Cao, and G.Z, *J. Sol-Gel Science and Technology*, Vol. 26, pp. 321–327, (2003)
- ¹⁸⁵ Mager, M., Mechtel, M., and Kirchmeyer, S., in: Conference Papers, *Silicones in Coatings II*, Paint Research Association, Florida, (1998)
- ¹⁸⁶ Hofacker, S., Mechtel, M., Manger, M., Kraus, H., *Progress in Organic Coatings*, Vol. 45, pp. 159–164 (2002)
- ¹⁸⁷ Osborne, J.H., *Progress in Organic Coatings*, Vol. 41, pp. 280–286 (2001)

- ¹⁸⁸ Metroke, T.L., Parkhill, R.L., Knobbe, E.T., *Progress in Organic Coatings*, Vol. 41, pp. 233-238 (2001)
- ¹⁸⁹ Mager, M., Schmalsteig, L., Mechtel, M., and Kraus, H., *Macromol. Mater. Eng.* Vol. 286, No. 11, pp. 682-684 (2001)
- ¹⁹⁰ Parkhill, R.L., Knobbe, E.T., and Donley, M.S., *Progress in Organic Coatings*, Vol. 41, pp. 261-265 (2001)
- ¹⁹¹ Ni, H., Johnson, A., Soucek, M., Grant, J., and Vreugdenhil, A., *Macromol. Mater. Eng.* Vol. 287, No. 7, pp. 470-479 (2002)
- ¹⁹² Du, J.Y., Damron, M., Tang, G., Zheng, H., Chu, C.-J., and Osborne, J.H., *Progress in Organic Coatings*, Vol. 41, pp. 226-232 (2001)
- ¹⁹³ Boerio, F.J., and Ho, C.H., *J. Adhes.*, Vol. 21, pp 25 (1987)
- ¹⁹⁴ Abel, M-L, Rattana, A., and Watts, J. F., Interaction of Epoxy Analogue Molecules with Organosilane-Treated Aluminum: A Study by XPS and TOF-SIMS, *Langmuir*, Vol. 16, pp 6510-6518 (2000)
- ¹⁹⁵ Plueddmann, E.P., and Pape, P.G., *Mod. Plast.*, Vol. 62, pp 78, July (1985)
- ¹⁹⁶ Petrunin, M. A., Nazarov, A. P., and Mikhailovski, Yu. N., *J. Electrochem. Soc.* Vol. 143, pp. 251 (1996)
- ¹⁹⁷ Wicks, Z. W.; Jones, F. N.; Pappas, S. P. *Organic Coatings: Science and Technology*; Wiley: New York, (1992)
- ¹⁹⁸ Bierwagen, G.P., *J. Coatings Technology*, Vol. 73, No. 915, pp. 45-52 (2001)
- ¹⁹⁹ Etter, M. C., and Panunto, T. W. *J. Am. Chem. Soc.*, Vol. 110, pp. 5896. (1988)
- ²⁰⁰ Etter, M. C.; Urbanczyk-Lipkowska, Z.; Zia-Ebrahimi, M.; Panunto, T. W., *J. Am. Chem. Soc.*, Vol. 112, pp. 8415 (1990)
- ²⁰¹ Zhao, X., Chang, Y.-L., Fowler, F. L., and Lauher, J. W., *J. Am. Chem. Soc.*, Vol. 112, pp. 6627 (1990)
- ²⁰² Kane, J. J., Liao, R.-F.; Lauher, J. W., and Fowler, F. W., *J. Am. Chem. Soc.*, Vol. 117, pp. 12003 (1995)
- ²⁰³ Schauer, C. L., Matwey, E., Fowler, F. W., and Lauher, J. W., *J. Am. Chem. Soc.*, Vol. 119, pp. 10245 (1997)

²⁰⁴ Hollingsworth, M. D.; Brown, M. E.; Santarsiero, B. D.; Huffman, J. C., and Goss, C. R., *Chem. Mater.* Vol. 6, pp. 1227 (1994)

²⁰⁵ Kohli, P., and Blanchard, G.J., *Langmuir*, Vol. 16, pp. 4655- 4661 (2000)

Chapter 2.5 Active Metal Systems (Zinc-rich) Mechanistic

2.5-1 Metal-rich Coating Model

The purpose of this section is to identify the key electrochemical features of a cathodic corrosion coating system, such as a zinc-rich primer, and illustrate the accepted protection mechanism and measurement techniques used to classify it. This section addresses mechanistic aspects of zinc rich coatings (ZRC) and gives a generic description of the electrochemical processes involved in a zinc-rich / active metal cathodic protect anti-corrosive coating systems designed to protect a steel substrate. It is thought that these same principles could be applied to an analogous Mg-rich system for the cathodic protection of aluminum alloys.

The earliest reports of zinc-rich coatings originate from work done by Evans²⁰⁶ and Mayne²⁰⁷ in England and Nightingall^{208,209} in Australia and since then zinc rich coatings have developed into the surest method of corrosion inhibition yet devised by the coatings industry. Generally, they are composed of particulate dispersions of metallic zinc in an inorganic (silicate based) or organic (polymer based) binder have undergone a number of manifestations in terms of binder, fillers, and curing technology resulting in the most popular anti-corrosion primers on steel structures to date.²¹⁰ The galvanic protection

mechanism, that is central to zinc-rich coatings, is based on the electrochemical principle that zinc is less noble than steel and when electrical contact between the steel and the zinc metal is established, the latter will provide electrons to the steel making it inert to corrosion. This galvanic protection is based on the fact that zinc is less noble than steel and when electrical contact between the steel and the zinc metal is established, the latter will provide electrons to the steel making it inert to corrosion. When polymeric materials are used, the binder vehicle itself becomes the dielectric binding the pigment particles into a matrix to ensure electrical contact between the zinc particles and the steel to be protected. Since then ZRCs have been widely used for the protection of steel surfaces in marine and industrial environments for well over sixty years, and the number of mechanisms by which they protect a steel substrate has been studied extensively.^{211,212,213,214,215,216,217,218,219,220,221} The performance properties and corrosion resistance of solvent-based ZRCs strongly depend on pigment volume concentration (PVC), shape and size of zinc dust.²²² (See Appendix 2.5-1)

2.5-2 Zinc-rich Coating Systems

The classical zinc-rich coating system, as described by Hare and Kurnas²²³, consists of spherical zinc-dust powder in a polyamide-epoxy polymeric material matrix, Figure 2.5-2; with adjunct performance properties listed in Tables 2.5-1 and 2.5-2, below. Cathodic coatings or cathodic protection is realized by coatings whose PVC falls into the “Formulating window” range. (See Appendix 2.5-2)

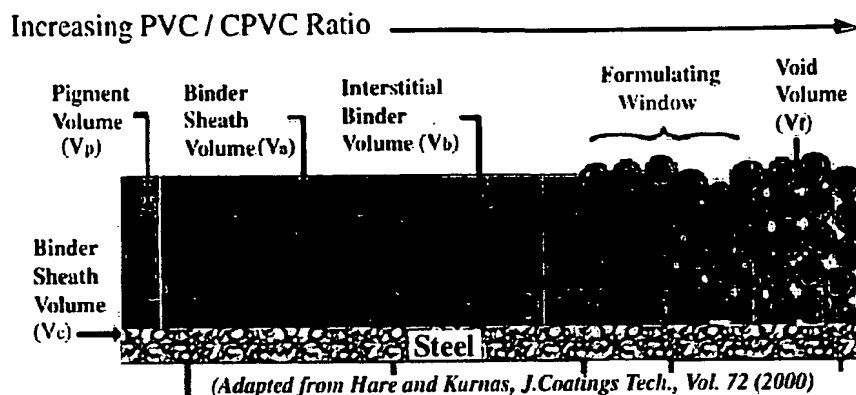


Figure 2.5-2: Schematic of zinc-rich coating (paint / primer) over steel substrate with zinc-powder with respect to PVC/CPVC ratio (Λ).

2.5-3 Corrosion Potential –the Electrochemical Parameter

The surface potential of a corroding metal E_{corr} is an indicator of the thermodynamic corrosion status, and by definition, corrosion potentials refer to an open circuit (no current flow) measurement. Corrosion potentials can provide an indication of the active or passive behavior in certain systems, unfortunately, on its own; the potential value does not provide information on the rate of corrosion (*kinetics*), see Appendix 2.5-3.

As an example, in a recent study Molnar and Liszi²²⁴ demonstrated the effect of percent zinc content by mass, also related to volume fraction (ϕ), in (ZRP) zinc rich paints on time-dependent open circuit potential (OCP) for painted steel electrodes immersed in a 3% or 0.1 M sodium-chloride solution. With reference to Figure 2.5-4, below, OCP were measured on four ZRPs, see Table 2.5-4 below, after 2, 8, 24, 48, 96 and 168 hours of exposure figure the period of sacrificial protection afforded by a ZRP is approximately proportional to percent (mass/mass) zinc present.

Table 2.5.4: (ϕ) data for ZRP, Molnar & Liszi		
<i>Code</i>	<i>Binder</i>	<i>Zinc content (% m/m)</i>
A	epoxy	85.2
B	epoxy	87.9
C	epoxy	89.0
D	no information	57.0

According to Marchebois *et al.*²²⁵, zinc-rich powder paints are often formulated in solvent-based ZRC epoxy systems with a complex mixture of zinc pigments, but the zinc concentration is generally reported to be well below 90% by weight. From Figure 2.5-4, below, the OCP values for the ZRPs decrease linearly with time as immediately after immersion all four samples attain OCP values of $\sim -0.86\text{V/SCE}$, or $\sim -1.1\text{ V/SHE}$ which is the value considered to represent the threshold of cathodic protection for iron.^{226, 227} However, after less than 24 hours the OCP of sample D increases to a value of $\sim 0.65\text{ V/SHE}$, signifying at the 57% zinc level the ZRC yields a decrease in sacrificial protection as zinc dissolution proceeds. This finding is consistent with the absence of effective charge percolation between zinc particles, despite possible conductivity arising from electrolyte ingress into pores within the coating.

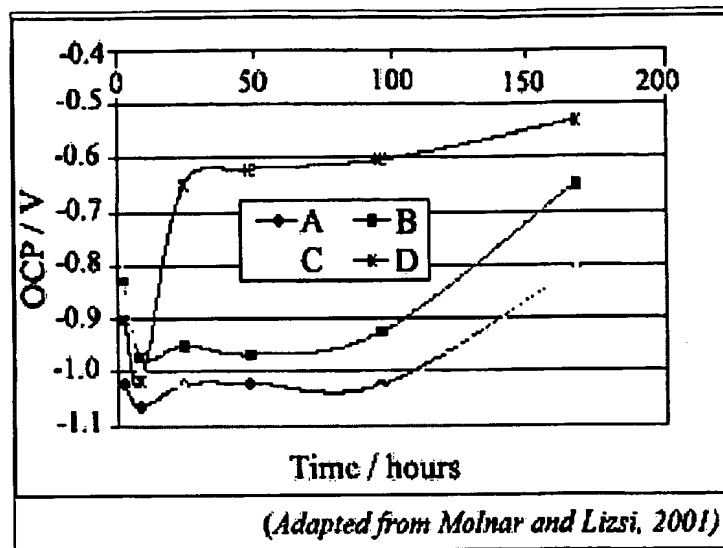


Figure 2.5-4: Shows that for (%) = 57, 85, 87 and 89 the ZRPs initially provide sacrificial protection, with OCP remaining below -1.0 vs. SHE. However, based upon sustained sacrificial protection only those ZRPs with (%) by weight) $\geq 70\%$ remained effective.

2.5-4 Electrochemical impedance spectroscopy (EIS)

Sacrificial protection has typically been investigated using time-dependent free corrosion potential (fcp) or OCP measurements.²²⁸ Electrochemical impedance spectroscopy (EIS) of (A.C. impedance) is a popular technique used to determine the electrical impedance of a metal electrolyte interface at various A.C. excitation frequencies over a range of about 10^{-3} to 10^5 Hz.^{229, 230, 231, 232} EIS is a popular technique that can be used to predict corrosion rates and evaluate the performance of chemical corrosion inhibitors and the moisture content of a coating prior to corrosion. In addition, it can also be used to predict the effectiveness of a coating over time and to quantify the actual effectiveness of the coating at various times.^{233, 234, 235, 236, 237, 238} (See Appendix 2.5-4)

2.5-6 The EIS and OCP Zinc-rich Model Study

Abreu *et al.*²²¹, used electrochemical techniques to interpret and develop a model accounting for zinc particle to particle contact that gave physical meaning to the mechanisms involved in cathodic protection of a zinc-rich epoxy paint on steel in a 3% sodium-chloride solution. According to Abreu *et al.*²²¹, the observed evolution and fluctuations in electrochemical measurements through out the experiment can be explained by variations in the zinc-to-steel area ratio that occur as a function of exposure time in the corrosive electrolyte medium. A galvanic couple between the zinc particles in the film and the steel substrate was described as the distinct spatial separation between the anodic and cathodic processes occurring in the system. (See Appendix 2.5-6)

2.5-7 Summary

Electrochemical methodology has been shown to be essential to identifying the basic parameters associated with ZRP for cathodic corrosion control. Through the use of such electrochemical testing methodology zinc-rich primers can be quickly evaluated for effectiveness by monitoring the length of time a zinc-rich coating maintains an active corrosion potential as a function of exposure to an electrolyte solution. In addition, through application of appropriate circuit analysis techniques, information regarding other electron transfer processes can be evaluated to better understand the corrosion processes occurring as the coating makes its transition from being cathodic in nature to that of a simple barrier system which occurs after the active metal has been consumed.

It may be surmised that a similar testing protocol might be effective at examining similar aspects of magnesium-rich coatings formulated for corrosion control of Al alloy. In the first place, a galvanic couple between the two metals must yield a significant mixed

potential difference, OCP value, between that of the Al-2024-T-3 and the magnesium metal. For example zinc-rich systems yield a potential difference of about (- 1.0 volt) vs SCE, and in order for a Mg-rich system to be effective it must develop a potential difference, OCP, of the same magnitude. Secondly, the corrosion of magnesium metal should be similar to that zinc metal in that the zinc hydroxide corrosion byproducts, produced as a result of exposure to NaCl solution, serve to influence the electron transfer processes in the coating as it fills with corrosion byproducts. Finally, it would also be assumed that such electrochemical measurement processes might reveal whether corrosion byproducts contributed by the magnesium anode are excessively corrosive and damage polymeric materials used as the coating matrix.

References / Bibliography

- ²⁰⁶ Evans, U.R., *Metals and Alloys*, Vol. 2, No. 2, pp. 62-64 (1931)
- ²⁰⁷ Mayne, J. E. O., and Evans, U. R., *Soc. Chem., Ind. Rev.* Vol. 12, pp. 109 (1944)
- ²⁰⁸ Nightingall, V.C.J., *J. Inst. Eng.*, Vol. 14, pp. 253-258 (1942)
- ²⁰⁹ Nightingall, V.C.J., British Patent #505,710, May, 16 (1939)
- ²¹⁰ Mayne, J. E. O., *Soc. Chem., Ind. Rev.* Vol. 66, pp. 93 (1947)
- ²¹¹ Ross, T. K. and Linghard, J., *Trans. Inst. Metal Finishing* Vol. 40, pp.186 (1963)
- ²¹² Newton, D. S. and Sampson, F. G., *J.O.C.C.A.*, Vol. 48, pp. 382 (1965)
- ²¹³ Theiler, F., *Corros. Sci.*, Vol. 14, pp. 405 (1974)
- ²¹⁴ Ross, T. K. and Wolstenholme, J., *Corros. Sci.* Vol. 17, pp. 341 (1977)
- ²¹⁵ Szauer, T. and Brawt, A., *J.O.C.C.A.* Vol. 67, pp. 13 (1984)
- ²¹⁶ Lindquist, S. A., Mesaros, L., and Stevenson, L., *J.O.C.C.A.*, Vol. 68, pp. 10 (1985)

- ²¹⁷ Feliu, S., Barajas, R., Bastidas, J. M. and Morcillo, M., *J. Coatings Technol.* Vol. **61**, pp. 63 (1989)
- ²¹⁸ Feliu, S., Barajas, R., Bastidas, J. M. and Morcillo, M., "Study of Protection Mechanisms of Zinc Rich Paints by EIS", in *Electrochemical Impedance: Analysis and Interpretation*, ASTM STP1188 (Edited by J. R. Scully, D. C. Silverman and M. W. Kendig), ASTM, Philadelphia, pp. 438 (1993)
- ²¹⁹ Pereira, D., Scantlebury, J. D., Ferriera, M. G. S. and Almeida, M. E., *Corros. Sci.*, Vol. **30**, pp. 1135 (1990)
- ²²⁰ Faidi, S. E., Scantlebury, J. D., Bullivant, P., Whittle, N. T. and Savin, R., *Corros. Sci.*, Vol. **35**, pp. 1319 (1993)
- ²²¹ Abreu, C. M., Izquierdo, M., Keddah, M., Nóvoa, X. R. and Takenouti, H., *Electrochim. Acta*, Vol. **41**, pp. 2405 (1996)
- ²²² Vilche, J.R., Bucharsky, E.C., and Giudice, C.A., *Corros. Sci.*, Vol. **44**, pp. 1287 (2002)
- ²²³ Hare, C.H., and Kurnas, J.S., *J. Coatings Technology*, Vol. **72** pp. 21-27 (2000)
- ²²⁴ Molnar F., and Liszi, J., Protective Properties of Zinc-rich Paints, (University of Veszprem) 2001 Joint International Meeting - the 200th Meeting of *The Electrochemical Society, Inc.* and the 52nd Annual Meeting of the *International Society of Electrochemistry*, San Francisco, California, September 2-7 (2001)
- ²²⁵ Marchebois, H., Touzain, S., Joiret, S., Bernard, J. and Savall C., *Progress in Organic Coatings*, Vol. **45**, pp. 415-421 (2002)
- ²²⁶ NACE, RP-01-69, RP-05-75, RP-06-75, RP-01-76, USA.
- ²²⁷ British Standard CP 1021:73.
- ²²⁸ Ashworth, V., "The Theory of Cathodic Protection and Its Relation to the Electrochemical Theory of Corrosion", in *Cathodic Protection*, Ellis Horwood, Chichester (U.K.), (1986)
- ²²⁹ Gileadi, E., *Electrode Kinetics for Chemists, Chemical Engineers, and Materials Scientists*, VCH Publisher, Inc., New York, NY (1993)
- ²³⁰ Mansfeld, F., "Electrochemical Impedance Spectroscopy (EIS) as a New Tool for Investigation Methods of Corrosion Protection", *Electrochimica Acta*, Vol. **35** (10), pp. 1533-1544 (1990)

- ²³¹ Walter, G.W., "A Review of Impedance Plot Methods Used for Corrosion Performance Analysis of Painted Metals", *Corrosion Sci.*, Vol. **26** (9), pp. 681-703, (1986)
- ²³² Kendig, M., Scully, J., "Basic Aspects of Electrochemical Impedance Application for the Life Prediction of Organic Coatings on Metals", *Corrosion*, (1), pp. 22 (1990)
- ²³³ Jeffcoate, C. S., Bierwagen, G. P., "Electrochemical Comparison of Coating Performance in Flowing vs. Stationary Electrolyte" ACS Symposium Series 689, Organic Coatings for Corrosion Control, G.P. Bierwagen, ed., pp. 151 (1998)
- ²³⁴ Balbyshev, V. N., Bierwagen G. P., and Berg, R.L., "Electrochemical Studies of Vinyl Ester Coatings for Fuel Tanks," ACS Symposium Series 689, Organic Coatings for Corrosion Control, G.P. Bierwagen, ed., pp. 292 (1998)
- ²³⁵ Conners, K.D., Van Ooij, W.J., Mills, D.J., Bierwagen, G.P., *British Corrosion J.*, Vol. **35**, pp. 141-144. (2000)
- ²³⁶ Bierwagen, G.P., Li, J., He, L., and Tallman, D., "Fundamentals of the Measurement of Corrosion Protection and the Prediction of Its Lifetime in Coatings," accepted for publication in Proceedings of the 2nd International Symposium on Service Life Prediction Methodology and Metrologies, Monterey, CA, Nov. 14-17, 1999, J. Martin and D. Bauer, ed., ACS Books, Washington, DC (est. Fall 2001)
- ²³⁷ Mills, D. J., Bierwagen, G. P., Tallman, D.E., and Skerry, B.S., "Characterization of Corrosion under Marine Coatings by Electrochemical Noise Methods," Proc. 12th International Corrosion Congress, Vol. 1, pp. 182-193, (paper 486), Houston, TX (1993)
- ²³⁸ Yasuda, H.K., Reddy, C.M., Yu, Q.S., Deffeyes, J., Bierwagen G.P. and He, L., "Effect of Scribing on Corrosion Test Results," *Corrosion*, Vol. **57**, pp. 29-34 (2001)

Chapter 2.6 Pigment Binder Relationships

2.6-1 Coatings Pigmented by Volume

The purpose of this section is to illustrate the volume relationships involved with pigmented coating systems and how they can be used to establish parameters that lead to optimization of a metal rich coating system's corrosion control potential. This section also addresses the topic of pigmented coating systems as a mass of particles consolidated to various degrees in a given polymeric vehicle. Its focus is on pigmentation in metal-rich coatings systems, such as the popular zinc-rich systems. It should be noted that many of the generic principles apply to non-metal rich systems as well. However, for the purpose of this review those concepts central to the function and performance of these metal-rich coating systems will be emphasized. (See Appendix 2.6-1)

2.6-2 Critical Pigment Volume Concentration (CPVC)

The packing fraction (PF) describes the maximum fractional volume of pigment or particulate matter, binder, in a tightly packed mass where all of the particles are wetted and dispersed (separated) by the matrix and there is just enough matrix to fill the spaces between particles to produce a continuous, void-free system that corresponds to the point at which the composition is at its maximum rigidity (modulus).²³⁹ Analogously, in paint and coatings industry the packing fraction is called the pigment volume concentration commonly abbreviated CPVC where it has been widely recognized as an established relationship to a pigmented coating or film's performance properties and its physical characteristics.²⁴⁰ A pigmented coating's physical and performance properties were shown to be related to its volume indices, packing density, continuity, and porosity as depicted in Figure 2.6-1.

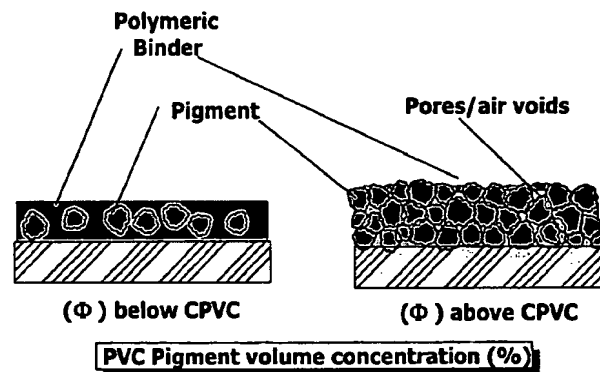


Figure 2.6-1: Primer coating depicting pigment volume / vehicle relationship below CPVC (left); and above CPVC (right)

These results were first elucidated by H. Wolff (1929)²⁴¹ and they describe an “all-purpose transition point” of performance and physical properties common to all pigmented

coatings. In Wolff's interpretation, "...The optimum protective effect of paint films produced from mixed pigments is actually identified with the highest degree of packing of pigment particles." Wolff further defines the packing density as "...the volume content of pigment in a unit volume of paint, or the pigment content of the paint in percent volume." Wolff's identification of a "critical oil absorption point" corresponded to a simultaneous transition in such properties such as resistance to blistering, rusting, heat, tensile strength, and exterior weathering.^{242, 243} In this first interpretation of CPVC it suggests that a basic pigment characteristic may influence film properties in a predictable way, but does not necessarily require that they perform in concert. It is simply the volume concentration of pigment at the end-point of the spatula rub-out oil-adsorption test (ASTM D-281).

A second interpretation of CPVC was proposed by Asbeck and Van Loo (1949)²⁴⁴ in their article "Critical Pigment Volume Relationships" they describe a graph that indicates "breaks in the permeability, rusting, blistering, and gloss curves occur at a more or less definite point..." The authors use the words "breaks" and "points" to describe a transition over a range of PVC's. It is a formulator-determined pigment / vehicle relationship that implies for any pigmented coating or paint system there is a PVC, called the "CPVC" at which a considerable number of measurable dry-film characteristics pass through a transition from good-to-poor, poor-to-good, high-to-low, or low-to-high, etc. It should be noted that it was the choice in gloss scale that resulted in an apparent transition anywhere in the general vicinity of the identified "point". (See Appendix 2.6-2)

2.6-3 Pigment Packing Factor (ϕ)

The pigment packing factor, (ϕ), pigment packing factor is defined as the ratio of the volume of the pigment to the total volume of the coating, including voids, equation 2.6-

pf. Essentially, the difference between PVC and pigment packing factor (ϕ) is that PVC is based on the solids content of the coating, while the pigment packing factor is based upon solids content plus any air voids (interstitial air spaces).

Equation 2.6-3

$$\phi = \left\{ \frac{V_p}{V_p + V_b + V_a} \right\}, \quad (3)$$

where V_p is the pigment volume, V_b the binder volume and V_a is the volume of air (pore volume) in the coating. V_p and V_b are calculated from the weights and densities of pigment and binder. Error! Bookmark not defined. According to figure Figure 2.6-3, since void air space below CPVC is absent, in the region denoted by ($PVC < CPVC$) and following the pigment packing factor line, the values of PVC and (ϕ) are the same. However, above CPVC, the PVC and (ϕ) diverge. For the region ($PVC > CPVC$), (ϕ) remains constant, whereas PVC increases to an end point value of 1.0 (100% pigment).

2.6-4 Particle Shape

Particle shape, with respect to pigmented zinc-rich coatings, is a major consideration in pigment selection. In a typical ZRP, zinc is usually introduced as spherical pigments known as zinc dust that consists of chemically pure metallic zinc, in the form of near spherical particles of selected sizes and size distribution.²⁴⁵ In general, most of the spherical zinc dust produced in the USA is a relatively coarse dust, whose diameter averages from 6 to 8 μm .²⁴⁶ Finer zinc dusts used in other countries are denoted as: 1) fine zinc dust with an average particle size of about 4–5 μm ; and 2) super fine zinc dust, which exhibits particle sizes in the order 2–3 μm .²⁴⁶

If the pigment is to supplement the mechanical properties of a coating film, stress that usually results due to stretching or bending must be transferred from the polymeric

film to the strong and stiff pigment. Stress transfer is more efficient if the mineral particles are smaller, because for a given concentration greater mineral surface is exposed to intercept the stress. Effective stress transfer also requires a certain minimum aspect ratio. With the trend following an increased aspect ratio, once this ratio is exceeded, the efficiency of stress transfer increases as well. Platy and acicular particles are therefore preferred. While small particle size and large surface area promote the durability of a coating film, they also promote high vehicle demand, which lowers critical pigment volume concentration (CPVC) and limits loading levels.

2.6-5 Oil-Absorption (OA)

The oil absorption of a pigment reflects a composite effect of the following factors - particle shape, particle size distribution and surface area, effect of pigment PVC on CPVC, and pigment-matrix interaction. Oil absorption values are therefore a useful guide to the coatings formulator's selection of the optimum combination of pigments and extender pigments required to adjust the zinc to vehicle ratio required in the formulation of a ZRP coating. Error! Bookmark not defined.

The spatula rub-out oil absorption test (ASTM D 281) gives an indication of binder demand by determining the amount of linseed oil that is just sufficient to coat the pigment particles and fill the inter-particle interstices. The two components of oil absorption warrant separate consideration. The first is the amount of oil required to wet and coat the pigment particles, and this depends on the pigment's surface area, which is in turn affected by its particle size distribution, hydrophilicity, and its porosity, which is a result of its lattice structure. Secondly, after the particles are coated with linseed oil, the other

component of oil absorption is the additional oil that fills the interstices. In effect, this test gives a measure of relative surface area of the pigment-linseed oil composite and has some value in indicating the pigment's CPVC in a coating.²⁴⁴

According to Hare²⁴⁷ the following equation is often cited to relate oil absorption to CPVC, equation (2.6-4):

$$\text{Equation 2.6-4} \quad \text{CPVC} = \left\{ \frac{1}{1 + \text{OA}\rho / 93.5} \right\} \quad (4)$$

where OA is the oil absorption and ρ is the specific gravity of the pigment.

The OA has value has been generally considered a good predictor of CPVC in solvent paints. However, there are two critical assumptions that must be met; first, it assumes that 100 percent zinc pigment at its tightest packing configuration occurs, where $(1 - \text{CPVC})$ is the volume of the vehicle making up the film. Secondly, according to Bierwagen²⁴⁸, that all the pigment particles act individually in a "random packing array" and are consistently connected to neighboring particles as opposed to being flocculated prior to film formation. Generally, this equation considers the effect of a pigment's specific gravity, or weight per gallon, on CPVC, and that for a given oil absorption, a higher specific gravity results in a lower CPVC.²⁴⁸

However, Hare *et al.*²⁴⁹, point out that zinc dust is not composed of a uniform particle size and therefore smaller zinc particles tend to fill in some of the interstitial volume between the larger particles. A typical zinc dust varies in particle size distribution from smallest 0.5 μm to largest 60 μm , with the average particle size in the 5 μm to 7 μm range. Consequently, the result of this disparity results in a depression in the void volume below the 36.1 percent for uniform spheres. According to Patton^{Error! Bookmark not defined.}, the

packing factor of such arrays fall between 69 and 73 percent zinc volume, thus indicating a 27 to 31 percent interstitial void volume. According to Hare *et al.*²⁴⁹, the following correction applies:

From equation (2.6-4):

$$\text{Equation 2.6-4} \quad \text{CPVC} = \left\{ \frac{1}{1 + \text{OAP} / 93.5} \right\} \quad (4)$$

yielding: $V_v = (1 - \text{CPVC})$ the volume of the vehicle making up the film. This value will be larger than the void volume of the corresponding dry (vehicle free) matrix $(1 - \phi)$ because of the adsorbed layers V_a and V_c on the surface of both pigment (a) and steel substrate(c), where (ϕ) is the packing factor assigned to the zinc particle size distribution and $(1 - \phi)$ is the "interstitial volume of the dry matrix" as depicted in top of Figure 2.6-4, below.

Therefore, the physical significance of these parameters as shown in Figure 2.6-4, leads one from Equ. 2.6-4 to Equ. 2.6-5:

$$\text{Equation 2.6-5} \quad \text{CPVC} - V_b = V_a + V_c \quad (5)$$

where V_b or V_n (the interstitial volume at the CPVC) may be assumed to be equal to $(1 - \phi)$ the interstitial volume of the dry matrix.

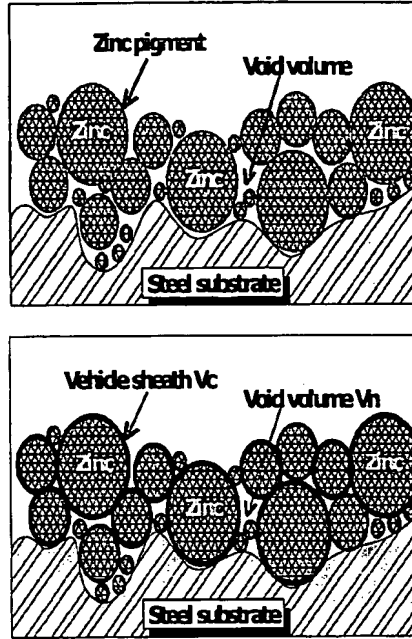


Figure 2.6-4: Relationship between vehicle volume at the CPVC [top] and void volume at the tightest packing [bottom]. Vehicle volume at CPVC [bottom] with vehicle sheath V_c larger than the corresponding dry vehicle free matrix [top], while void volume $V_b = V_n$ [bottom] is diminished because of volumes V_a and V_c .²⁴⁷

Essentially, this approximation, according to Equ. 2.6-5, becomes more valid as the particle size increases and the distribution tends toward uniform “mono-sized” particles.

This is achieved by substituting ($V_b = 1 - \phi$) into Equ. 2.6-5 leads to:

$(\phi - \text{CPVC}) = V_a + V_b$ and rearranging leads to Equ. 2.6-6:

$$\text{Equation 2.6-6} \quad (V_a + V_b) = \phi - \text{CPVC} \quad (6)$$

which corresponds to the minimum value of vehicle that can be incorporated into the primer to form a cohesive film. This relationship holds for smooth surfaces, sandblasted surfaces are considered to be coarse and as a result require supplemental vehicle to offset the decrease in CPVC that occurs on sandblasted steel as opposed to those values

ascertained on smooth ceramic surfaces. As a means to compensate for such surface effects, Hare *et al.*²⁴⁹, proposed the use of a roughness factor M that is related to both the mill profile and the absorbancy of various sand blasted surfaces. This factor can be used to modify standard oil absorptions in the CPVC, from Equ. 2.6-7 as follows:

Equation 2.6-7
$$CPVC = \left\{ \frac{1}{1 + M OA \rho / 93.5} \right\} \quad (7)$$

Overall, the substrate vehicle demand can be a subjective parameter and vary according to condition for example, the degree of pitting before sandblasting blasting. In addition, the volume solids of the primer is a more relevant measure or estimate of possible downward or declining shifts in CPVC and a consequent increase in (Δ) when a primer is being applied over a surface with considerable roughness. In addition, Hare *et al.*^{Error!}
 Bookmark not defined., assert that the magnitude of the effect tends to decrease with increasing film thickness and as the quantity $\left\{ \frac{V_c}{V_a + V_b + V_c} \right\}$ is decreased the film at the surface is increased.

2.6-6 Intuitive CPVC in a Nutshell

The CPVC calculation can be approached intuitively in terms of the relationship between two associated components: 1) the oil absorption (OA) value, and 2) the configuration / packing factor of the pigment(s). Generally, it is the largest pigment in the particle size distribution that exerts the largest effect on the CPVC of the coating. As an intuitive example of what the CPVC calculation means an example of a hypothetical coating system consisting of polymeric binder and one pigment, a 100% solids system will be examined. It will be assumed that this hypothetical coating will consist of a polymer and

pigment properly dispersed at the coating's CPVC. From which an OA value was ascertained, given in grams oil to 100 grams pigment; this yields a volume of oil which is a surrogate for the polymeric binder. The next component is the pigment's packing factor, which gives its configuration and the associated maximum volume at its packed configuration. Putting two plus two together the volume of oil adsorbed (from OA determination is associated with the volume of pigment at its maximum packing configuration which results in the CPVC when indexed according to Equ. 2.6-8, below.

Generally, the confusion associated with CPVC calculations often arises due to the fact that it involves a maximum packing configuration, such as that for simple spheres, as opposed to just the maximum pigment volume at the OA rub-up end-point. The previous sections have demonstrated the mechanics and parameters associated with the critical pigment volume concentration (CPVC). Essentially, the difference between PVC and CPVC is that PVC can be measured, according to the equation below; while CPVC can not be measured it must be determined.

- a) PVC is the pigment *volume* content of a coating that contains a binder and at least one pigment. The PVC serves as a *volume* index for the ratio of pigment(s) to binder in a coating.

Equation 2.6-8

$$PVC = \frac{\sum_{i=1}^n \text{Pigments}_i}{\sum_{i=1}^n \text{Pigments}_i + \sum_{i=1}^n \text{Binder}} \times 100 \quad (8)$$

- b) CPVC is the *coatings* critical pigment volume concentration which refers to the transition point above or below which substantial differences in the appearance and behavior of a paint film will be encountered. Overall, it is the most pigment you can

put into a cured film without air voids forming due to an insufficiency of the continuous phase polymer matrix. Moreover, many coatings properties catastrophically change at the CPVC.

2.6-7 CPVC and Zn-rich Formulation with Thixotropes

In practical applications, zinc-rich organic formulations require addition of certain types of thixotropes / rheology agents, anti-gassing agents, or desiccants, and as a result the pigmentation is never 100 percent zinc metal. Almost all of these additives possess higher oil adsorption and lower specific gravities than zinc. Even at low levels these materials tend to depress CPVC; when (Λ) is kept constant the PVC is also depressed. Often such additive induced depressions in PVC directly alter CPVC significantly. For example, pyrogenic silicas are used as thixotropes. If the pyrogenic silica has a specific gravity of 2.2 and an oil absorption of 300 g/g, and it is added to a system with a CPVC estimated at 65.6 % based on 100 percent zinc metal pigmentation, the following reasoning applies to the CPVC estimation according to Equ.(s) 2.6-9 and 2.6-10:²⁵⁰

$$\text{Equation 2.6-9} \quad \text{CPVC} = \frac{1}{1 + \frac{0.98 \text{ OApZinc} + 0.022 \text{ OApSilica}}{93.5}} \quad (9)$$

$$\text{Equation 2.6-10} \quad \text{CPVC} = \frac{1}{1 + \frac{48 + 13.2}{93.5}} = 0.604 \text{ or about } \sim 60.4 \% \quad (10)$$

The above calculated CPVC for the pigmentary mix at 60.4 % PVC differs by 5% for the 100 percent Zn-metal system at 65.6% PVC. The physical significance of the decrease in calculated CPVC is that vehicle is displaced from volume that the added modifying pigment occupies. Therefore, since CPVC is a function of the random dense

packing efficiency of the pigment plus adsorbed layer thickness (δ), which must be experimentally determined.

Thus, at the CPVC of the modified pigmentary mix, both pigments possess an adsorbed layer (δ) volume which differs from that vehicle layer volume adsorbed on the 100 % Zn metal surface at its CPVC. Overall, the difference lies in the volume of Zn metal displaced by the added modifying pigment, and in this case the pigment with dramatically higher oil absorption value has a more pronounced effect at depressing the CPVC of the primer.

In reality the actual oil absorption values of the pigment mix (zinc + modifying pigment) can vary considerably from calculated values, especially when the modifying pigment's particles distribution differs significantly from that of the zinc metal. In many instances, this is due to the filling of interstitial volume between the larger particles, by smaller modifying pigment, that otherwise would fill with vehicle volume. The end result is a somewhat lower practical oil adsorption value than those calculated from individual pigments making up the pigmentary mix. The corollary to the above analysis is that unless the effects of pigment modification are considered and compensated for, the altering of PVC by addition of modifying pigments can significantly alter the zinc-rich primer (Λ) value leading to greater porosity or reduced galvanic activity, depending upon the direction and magnitude of the change in CPVC. (See Appendix 2.6-4 CPVC Error and measurement)

2.6-10 Efficiency in Zinc-rich Coating Systems

Thus far it has been shown how zinc particle morphology and related electrochemical mechanisms involving physico-chemical aspects of zinc powder are

closely tied to corrosion-inhibition efficiency of ZRCs used in cathodic protection systems.²⁵¹ Formulation of efficient ZRCs has recently been studied by Kalendová *et al.*²⁵² who examined the effect of select parameters such as zinc pigment particle size and shape, PVC, and polymeric binder matrix on the performance of zinc-metal coatings used to provide sacrificial protection for corrosion control.

Kalendová *et al.*²⁵², described the difference between the two types of zinc particles, lamellar vs spherical, to act as an effective barrier to arrest water vapor transmission. They measured water vapor diffusion resistance values for pigmented coatings at a constant 50 % PVC for both types of pigment particles and concluded that “lamellar pigmented zinc coatings create a more efficient barrier to water vapor transmission than isometric spherical zinc particles”, Figure 2.6-10 below.

The results of the study were also analyzed in terms of the “barrier effect” as described by Leclercq²⁵¹ and specific effects observed by Kalendová *et al.*²⁵² “where the action of zinc metal in coating films allows the capacity to neutralize the acid corrosive medium penetrating through the film... with the capacity to effectively restrict the diffusion of acidic components from the coating-film surface towards the substrate metal.”

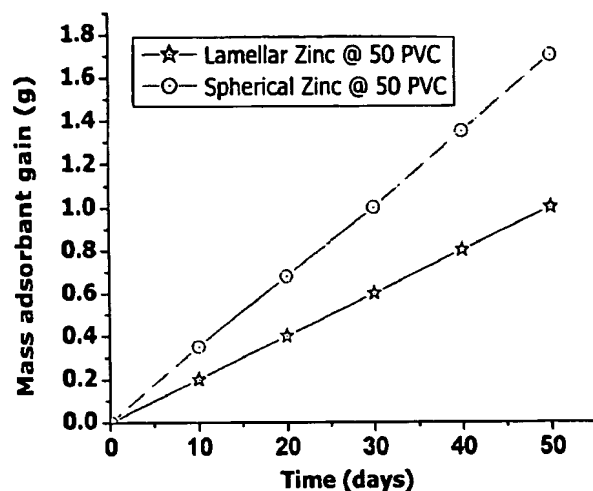
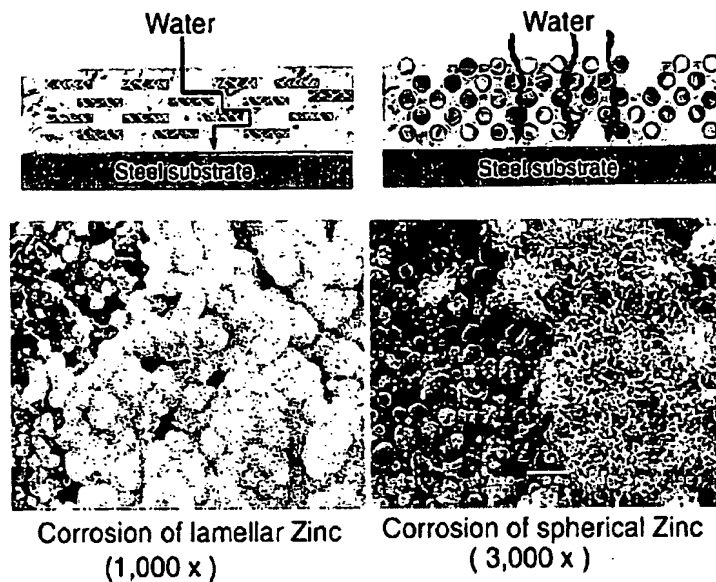


Figure 2.6-10: Time dependence of mass adsorbent gain in grams vs time for coatings pigmented at 50 %PVC with (.) spherical zinc: (ζ) lamellar zinc,(from Kalendová *et al*).

As can be seen in Figure 2.6-11, SEM images, a significant amount of information regarding the evolution and nature of the morphology of corrosion products emanating from ZRCs with different particle shapes is apparent. SEM results from Figure 2.6-11 , below, show the evolution of dense spherical clusters at the surface of lamellar zinc (1,000%), contrasted to (lower-right) a less dense, acicular sparse clustering of corrosion product, at a higher magnification (3,000%), that appear to emanate more from the interior of the coating as opposed to a clustered formation at the surface.



(Adapted from Kalendová et al., 2002)

Figure 2.6-11: Illustrative scheme of water vapor transmission / Penetration through coatings composed of different particle shapes: lamellar zinc (top-left); spherical zinc (top-right). SEM results of corrosion products coatings after 800-hr exposure to salt chamber conditions. (Adapted from Kalendová et al., 2002).

Finally, the effect of PVC and type of polymeric binder matrix, as shown in Figure 2.6-12 below, is discussed by Kalendová et al.²⁵² which shows the “anticorrosion efficiency” which was defined as results from salt spray test (ISO 7250) at 1000 hours exposure. The essential features of Figure 2.6-12, below, are the effects of coating PCV in the polymer matrix, which appears to be independent of polymeric binder system used in each, as each coating system rises and falls in an analogous fashion. The effect of the polymeric binder itself which appears to have a pronounced effect where coatings formulated with epoxy-ester binder systems are more efficient than either polyurethane or 2K epoxy. However, the authors offered no explanation as to the observed difference in performance between the vehicle / polymeric material systems tested.

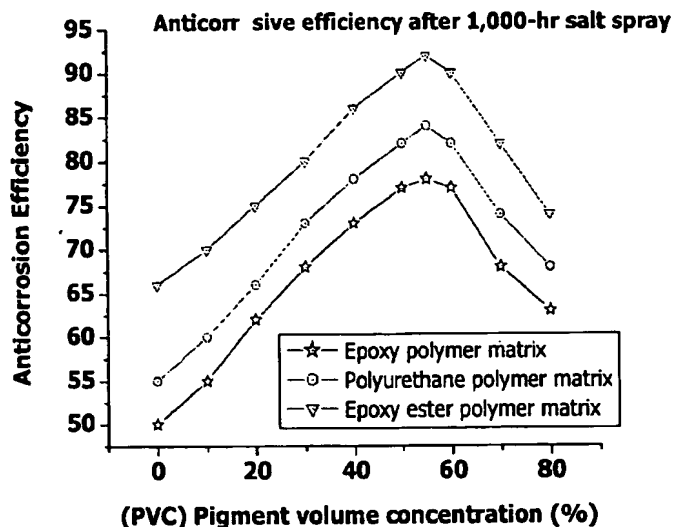


Figure 2.6-12: Anticorrosive efficiency of the zinc coatings dependence on amount of zinc pigment (spherical $\sim 2.9\mu\text{m}$ average, at 1,000-hour exposure salt spray); and 2) polymeric binder matrix (ζ)Epoxy 2-K; (\circ) Polyurethane binder; (Δ) Epoxy-ester binder, (Adapted from Kalendová et al., 2002).

2.6-11 Conclusion

The fundamental properties of zinc-rich coatings can best be described in terms of volume relationships which are more meaningful than those described by density. In general this holds true for other pigmented coating systems as pigment density values can range anywhere between 2.12 g/cm^3 for most fumed silicas to 4.2 g/cm^3 for common grades of rutile TiO_2 . In addition, were one to contrast pigmented metal-rich coatings formulated with zinc versus magnesium one might immediately recognize that the large difference in densities between these two metals. Volume relationships are much more convenient to use as in any pigmented coating system they can be normalized in terms of the PVC/CPVC ratio (Λ). Such an index allows one to compare metal-rich systems formulated from zinc or magnesium on a common scale, and classify/ascribe such corrosion related

phenomenon to a measured number that can be associated with a similar relative error distribution.

Pigment volume concentrations (PVCs) are important due to their ability to predict and relate corrosion related phenomenon such as blistering, rusting, and permeability to actual coating formulation. As best stated by Dickie, 1985²⁵³, "at low PVC the pigment is fully wet by resins. At high PVC there remain untitled interstices between pigment particles. Moisture exclusion, adsorption, and permeation are strongly affected by pigment/binder and pigment/water interaction. Strong pigment/binder interaction tends to result in restricted molecular mobility, reduced swelling, and reduced water transmission through pigmented film. Strong pigment/water interaction tends to result in increased water uptake by the film and increased film permeability, especially at high PVC."

Refences / Bibliography

- ²³⁹ Hay, T.K., *Journal of Paint Technology*, Vol.46, pp. 44-50, (April, 1974)
- ²⁴⁰ Bierwagen, G. P., Hay, T. K., *Progress in Organic Coatings*, Vol. 3, pp. 281 (1975)
- ²⁴¹ Wolff, H., *Farben-Ztg.* Vol. 34, (52) pp. 2940 (1929)
- ²⁴² Wolff, H., Zeider G., *Kolloid-Zeitschrift*, pp. 74, (1) 97, (1936)
- ²⁴³ Wolff, H., Zeider G., *Paint Varnish Prod. Mgr.* Vol. 16, (6) 7 (1937)
- ²⁴⁴ Asbeck, W.K.; Van Loo, M. *Ind. Eng. Chem.* Vol. 41 (7) pp.1470, (1949)
- ²⁴⁵ Munger, C.G., *Corrosion Prevention by Protective Coatings*, Third ed., NACE, Houston, TX, (1986)
- ²⁴⁶ Kafka, A.S., Chap. V 'Zinc pigment', in: Patton, T.C. (Ed.), *Pigment Handbook*, Vol. I, pp. 819-832. (1973)
- ²⁴⁷ Hare, Clive H., *Protective Coatings*, Technology Publishing Co., Pittsburgh, (1994)
- ²⁴⁸ Bierwagen, G.P., *Journal of Coatings technology*, Vol. 64, No. 806, pp. 71-75 (1992)
- ²⁴⁹ Hare, C.H., O'Leary, M.J., and Wright, S.J., *Modern Paint and Coatings*, pp. 30-36, June (1983)
- ²⁵⁰ Patton, T.C., *Paint Flow and Pigement Dispersion*, 2nd Ed. pp. 187, Wiley (1979)
- ²⁵¹ Leclerq, M., *Eur. Coat. J.*, No.3, pp.106 (1991)
- ²⁵² Kalendová, A., Kuckačová, A., *Macromol. Symp.*, Vol. 187, pp. 377-386 (2002)
- ²⁵³ Dickie, J.S., *ACS Syrup. Set, Applied Polymer Sci.*, pp. 285 (1985)

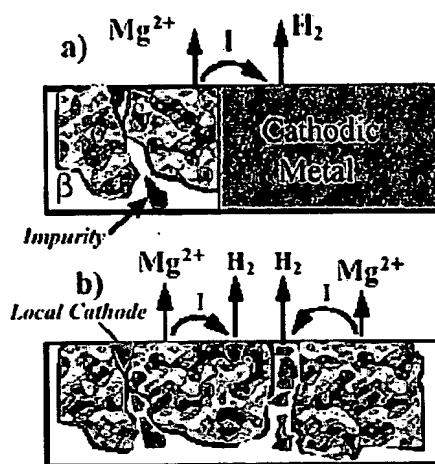
Chapter 2.7 Magnesium Metal Corrosion

2.7-1 Magnesium Metal

The purpose of this section is to illustrate the electrochemical behavior of magnesium metal and relate its physio-chemical properties to a cathodic protect Mg-rich coating for corrosion control of aluminum alloys. Magnesium is the eighth most abundant element and constitutes about 2% of the earth's crust while in the ocean it is the third most plentiful metal dissolved in sea water with an average concentration of 0.13 percent.²⁵⁴ It is one of lightest structural metals available and possesses high strength / weight ratio, non-toxicity, non-magnetic, high thermal and moderate electrical conductivity with a density of 1.7 g/cm^3 compared to aluminum at 2.70 g/cm^3 ; as a result it is an extremely attractive engineering material.²⁵⁵ Magnesium and its alloys are of particular interest to in the aerospace and transportation industries. As an example, Volkswagen used magnesium alloy components in an engine.²⁵⁶ However, the lack of widespread use of magnesium and its alloys is primarily due to their poor corrosion resistance properties. Such corrosion resistance is especially poor when a magnesium alloy contains specific metallic impurities such as iron or copper, or when the magnesium alloy is exposed to aggressive electrolyte species such as Cl^- , SO_4^{2-} , or ClO_4^- ions.^{257,258,259} (See Appendix 2.7-1, reactivity of MG metal).

Generally, magnesium and magnesium alloys are known to be particularly susceptible to galvanic corrosion, which is usually observed as heavy localized corrosion when magnesium is place in direct contact with a more cathodic metal. Such cathodes can either be internal, as in the case of secondary impurities or external as in the case when it is

in direct contact with another metal.²⁶⁰ Magnesium metals and alloys essentially undergo two kinds of galvanic corrosion, external and internal, are illustrated in Figure 2.7-1 below. For example, cathodes can be external as other metals in contact with magnesium, or may be present as internal or secondary impurity phases.



(Adapted from Song & Aitrens, 1999)

Figure 2.7-1: (a) external galvanic corrosion;
(b) Internal galvanic corrosion.

Comprehensive studies²⁶⁰ have shown that differences in electrode potential and galvanic series, between two metals, alone can not be used to determine the effectiveness of cathodic protection that a metal, such as magnesium, might provide when coupled to another metal. The effectiveness of a galvanic couple depends on the nature of the two metals being coupled, as metal surfaces that promote the reduction of H^+ to H_2 are said to possess a low "overvoltage" or "overpotential" for such a reaction. For example, according to Table 2.7-1, below, standard reduction potentials, indicate that copper and platinum should not reduce H^+ to H_2 . Although the E^0 's for the reduction of Ni^{2+} and Pb^{2+} to the metals are slightly negative (-0.257 and -0.125 V NHE), while experience demonstrates

that the reduction potential must be less than -0.6 V before reduction of H^+ will take place. Only zinc (E_{red}^0 of $Zn^{2+} = -0.762$ V) meets this standard. Reduction of hydrogen ions at the metal surface is most favored when metal-hydrogen bonds are of intermediate strength so that the hydrogen will be weakly bound to the metal during electron transfer, but not so strongly bound as to prevent the formation and escape of H_2 gas²⁶¹, Figure 2.7-2, below.

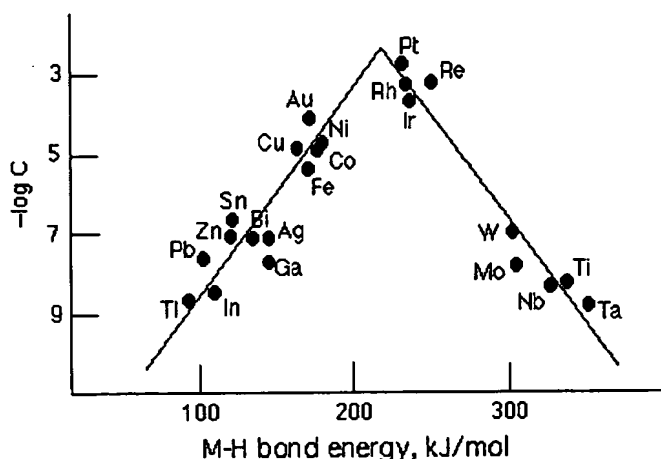


Figure 2.7-2: This is a plot of the negative logarithm of the exchange current (C) versus M-H bond energy. Hydrogen gas is evolved most rapidly for metals at the top of the peak²⁶¹.

Metals with low hydrogen overvoltage, such as Ni, Fe, and Cu, constitute efficient cathodes for magnesium, and will cause severe galvanic corrosion. Metals that combine an active corrosion potential with high hydrogen overpotential, such as Al, Zn, Cd, and Sn, are much less damaging.^{Error! Bookmark not defined.} According to Jones²⁶², the galvanic corrosion rate is increased by the following factors: high conductivity of the medium, large potential difference between anode and cathode, low polarizability of anode and cathode, large area ratio of cathode to anode, and small distance from anode to cathode.²⁶³ (See Appendix 2.7-2 to 2.7-3 for Electrochemical description of Mg corrosion)

2.7-6 Pourbaix Diagrams and Aqueous Equilibria

The most traveled road to arresting corrosion on metal surfaces with organic coatings has been to directly control the thermodynamic conditions in a given corrosive environment. One of the most popular methods for predicting such relationships has been through the use of potential-pH diagrams known as Pourbaix diagrams.²⁶⁴ The utility of Pourbaix diagrams lies in their ability to provide information on the effects of pH and potential in addition to the effects of oxygen concentration on a metal in an aqueous environment.²⁶⁵

The primary assumption regarding Pourbaix diagrams is that equilibrium conditions must apply to such a metal in an aqueous environment, and that there is an electrochemical relationship between the aqueous solubility of such metals and pH. In other words, for any given chemical process, Pourbaix diagrams can not reflect any chemical species or intermediates if they do not participate in an aqueous electrochemical equilibrium process. For example, Figure 2.7-11, below, depicts the Pourbaix-pH diagram for aluminum in water, with lines and areas depicting the relative stabilities and instabilities oxygen and hydrogen. The aqueous aluminum species are shown as a function of applied potential and pH.

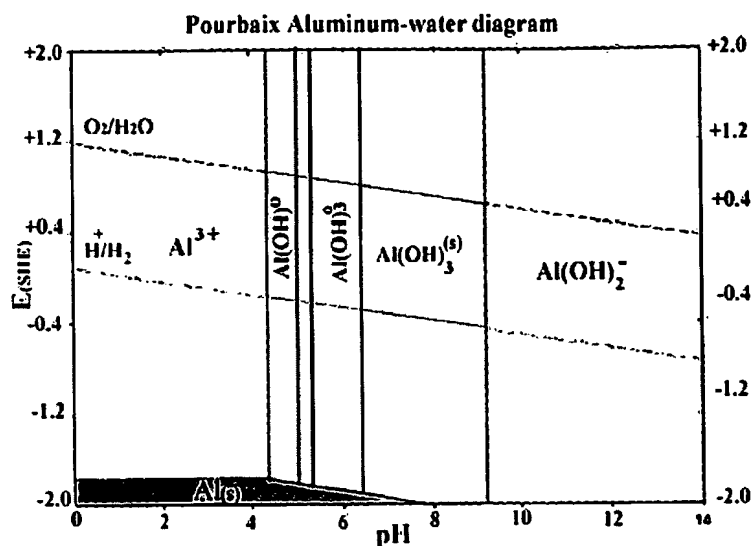


Figure 2.7-11: Pourbaix diagram for aluminum in water. The diagram depicts areas of relative thermodynamic stability for aqueous aluminum species.²⁶⁵

The diagram clearly shows areas where Al metal stability can be ascertained from the areas of the diagram in which no Al anions or Al cations are in aqueous equilibrium. It should be noted that water can act as an oxidizing agent and if a chemical species is to be stable in aqueous solution, it must not react with water through a red-ox process. In other words, the oxidation and reduction potentials of the species must be such that it is thermodynamically unfavorable for the species to be either oxidized or reduced by water.

These diagrams are a practical tool and have been used to develop corrosion resistant organic coatings and to predict corrosion as a function of oxygen penetration into such coatings. In addition, they are used as a guide to determine favorable pH conditions for the addition of buffering agents into coatings as well as the addition of zinc powder into zinc-rich paints that provide cathodic protection by bringing the substrates surface into the immune region; or used to predict stability, where, by using some other metal, the potential can be shifted to form an anodic protective film so pitting does not occur.

Perrault^{Error! Bookmark not defined.} used thermodynamic data not available to Pourbaix to develop a potential–pH diagram shown in Figures 2.7-12-(a) and 2.7-12-(b) and Figure 2.7-13. Perrault stated that the Pourbaix diagram must include the thermodynamic data for magnesium hydrides and the monovalent magnesium ion.⁶⁰ After considering the significance of MgH_2 and Mg^+ , Perrault concluded that a thermodynamic equilibrium did not exist for such a magnesium electrode in contact with an aqueous solution. He asserted that, on a magnesium surface, different reactions might be simultaneously involved, depending on the surface state of the magnesium.

Song *et al.*²¹ studied cathodic hydrogen evolution rates of pure magnesium in HCl and H_2SO_4 acidic solutions and found that for the film-free surface, the data supported the involvement of the Mg^+ intermediate in the metal dissolution process. However, this mechanism only occurred on a film-free surface and that for the magnesium samples with surface film, i.e., magnesium in 1 N NaOH, there was no evidence to support the univalent Mg^+ intermediate in the reaction mechanism.

Figures 2.7-12(a) and 2.7-12(b), Perrault-Pourbaix diagrams, consist of a modified Pourbaix diagram that depicts equilibria in the $\text{Mg-H}_2\text{O}$ system including the Mg-hydride species; noting Figure 2.7-12(a) where at potentials below 2.37 V(SCE) Perrault's concept of $\text{Mg-H}_2\text{O}$ involved the magnesium hydride species at the aqueous-metal interface.

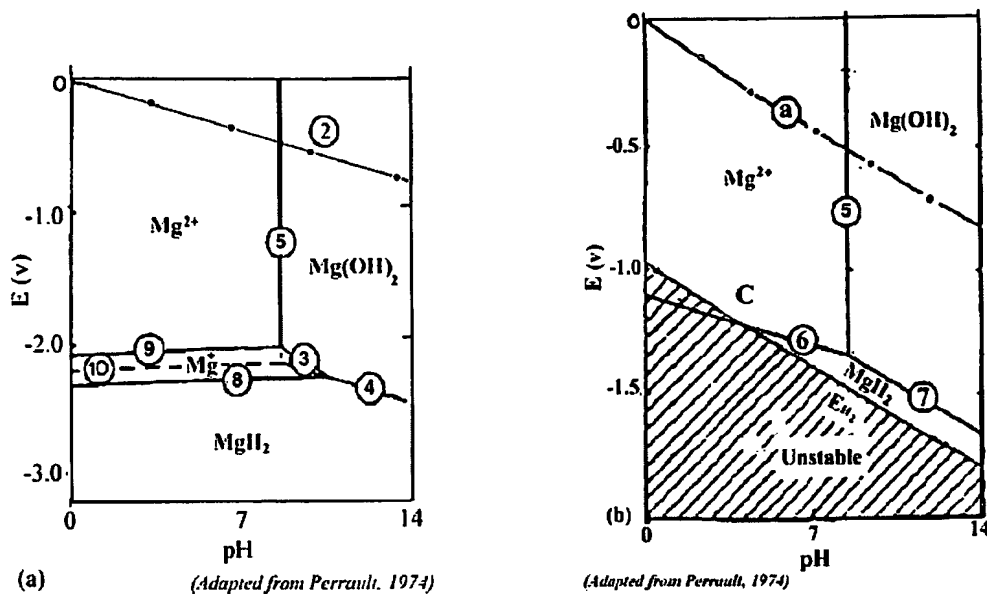
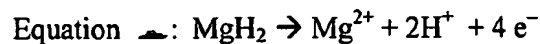
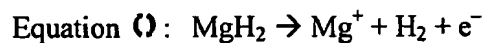
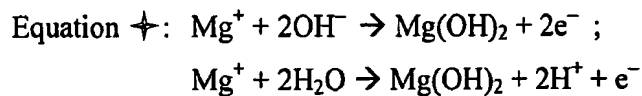
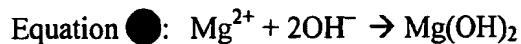
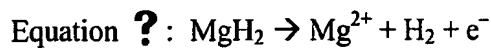


Figure 2.7-12: Perrault-Porbaix diagrams for equilibria in the Mg- H_2O system in the presence of H_2 molecules; 2.7-12 b) stability domains of Mg compounds in aqueous solutions with an hydrogen overpotential of ~1 volt.

Ringed numbers denote the equilibrium reactions that separate different regions of the diagrams according to:



A more comprehensive overview of the overall magnesium-H₂O corrosion process has been described by Eleizer *et al.*²⁶⁶, in terms of potentiodynamic polarization studies of magnesium metal in aqueous solutions. (See appendix 2.7-5 for further details)

2.7-7 Magnesium Anodic Dissolution Behavior

More recently, López-Buisán Natta²⁶⁷, studied the behavior of anodic branch of Mg polarization curves for electrodes of differing Mg composition, (i.e., 99.999 wt% Mg; 99.98 wt% Mg alloyed with Mn) in different electrolytes, (i.e., 0.3% wt NaCl; 3.0 wt% NaCl; 0.05 N HCl) and found evidence of two anodic processes at two different electrode potentials corresponding to two different Mg anodic dissolution processes / mechanisms. According to López-Buisán Natta²⁶⁷, the three classical unexplained electrochemical facts related to magnesium (NDE) in aqueous media are:

- 1) The paradox called “anodic reduction” of hydrogen.
- 2) The very low practical current carrying capacity (PCC)
- 3) The reducing power of equimolar mixtures of Mg with halides.

The theoretical current capacity (TCC) of a Mg anode, based upon valency of 2⁺, is given to be circa 0.252 A-year / kg. However, its practical current capacity (PCC) has been observed over the interval of 0.1 A/m² to 1.0 A/m², to be about 0.126 A-year / kg , (which is about ~50% of its TCC). The significance of these numbers lies in the proportion that applies to cathodic “efficiency” of a sacrificial anode, where for higher current densities Mg efficiency can reach ~ 55 percent while zinc anodes attain values higher than 95 percent. The observed discrepancy by a factor of ~2 between TCC and PCC values

suggests that a valency of +1 should be used to calculate the electrochemical equivalent of magnesium.

All of which leads to the preponderance of the NDE if magnesium dissolves as Mg^+ , as proposed by Greenblatt²⁶⁸, a PCC > 50% of the TCC can not be expected to occur nor be explained. Therefore, the following paradox: if the dissolution of Mg is a divalent process, then the reduction of hydrogen cannot be explained in terms of the observed current densities. However, if the process takes place through a monovalent species then the observed efficiencies >50 percent can not be explained. Therefore, according to López-Buisán Natta²⁶⁷, anodic Mg dissolution takes place through two different mechanisms, that depend on applied potential. The experimental observations for anodic dissolution of magnesium are as follows:

1) The monovalent process $Mg \rightarrow Mg^+$ at low potential (LP), with $E_1 = -1.56$ V(SCE), with Taffel slope 0.239 V/decade.

2) The divalent process $Mg \rightarrow Mg^{2+}$ at higher potential (HP) with $E_2 = -2.78$ V (SCE) with Taffel slope 0.102 V/decade.

At LP, Mg^+ electrochemical production starts. Mg^{2+} is produced non-electrochemically as a result of the reaction of Mg^+ with an oxidant or through disproportionation. At HP, the electrochemical production of Mg^{2+} starts, in parallel with the mechanism of LP. The Taffel slope of the monovalent process was observed at 0.239 V/decade which corresponds to charge-transfer-controlled kinetics involving one electron, with an anodic transfer coefficient of 0.25 for Mg^+ . Likewise, for the divalent process, with an observed Taffel slope of 0.102 V/decade, this also corresponds to charge-transfer kinetics with an anodic transfer coefficient of ~0.29. In each case the low anodic transfer coefficients signified an

electrical asymmetry between the metal / oxide and metal / electrolyte junctions.²⁶⁹ This may be observed in contrast to measurements made in an acid medium (0.05 N HCl), that yielded values for the anodic Taffel slope at 0.775 V/decade, indicative of diffusive controlled kinetics through the surface film.¹⁴

With respect to the reducing power of equimolar mixtures of Mg with halides, according to the author²⁶⁷ the effect of some anions, such as halides on the anomalous anodic dissolution is similar to the effect of complexing action of halogens on Al^{+} .²⁷⁰ The negative effect of chloride ions on the efficiency of Mg anodes has been described by Peabody.²⁷¹ The solution reaction of the stabilized Mg^{+} diffuses away from the metallic / oxide substrate where it eventually decays to Mg^{2+} through a reaction with an oxidant or through disproportionation, the second 3s electron does not return to the metal. Instead it becomes involved in the production of H_2 (the anodic reduction of hydrogen).^{Error! Bookmark not defined.}

2.7-8 Summary

Principally, due to its high galvanic activity, magnesium metal must be carefully designed and engineered for use in structural objects and particular attention must be given to exclude it from chloride containing environments. The efficiency of magnesium as a sacrificial anode has been discussed in terms of the negative difference effect (NDE), overpotential, and the dissolution of Mg through two different mechanisms, that depend on applied potential. All of which imply that: 1) according to NDE Mg is an effective anode in the reduction of hydrogen; 2) the overpotential between Mg and Al is relatively high indicating that excessive galvanic corrosion does not quickly generate a burned-out anode; 3) In the presence of chloride salt / solutions the efficiency of Mg as a sacrificial anode

depends on the monovalent process that corresponds to charge-transfer-controlled kinetics involving one electron.

The Perrault-Pourbaix diagram for Mg-H₂O shows conditions for stability of Mg²⁺ / MgO / Mg(OH)₂ in H₂O; however it was noted that that thermodynamic equilibrium of Mg might not occur due to so many different reactions simultaneously involved on the magnesium surface, depending on the surface state of the magnesium. Generally, for most Mg-H₂O systems it has been observed that above pH~7 Mg(OH)₂ forms preferentially as brucite. Moreover, according to Kramer²⁷², aqueous magnesium hydroxide acts a pH buffer that does not exceed a pH~10.5 even in the presence of excess Mg(OH)₂.

In summary, the preponderance of designing a Mg-rich coating for corrosion control of Al alloys. Mg metal is attractive from the point of view that 1) the Mg metal itself constitutes an effective sacrificial anode when coupled to Al and 2) the general corrosion byproduct Mg(OH)₂ also serves as a corrosion inhibitor and is available in several commercial grades such as, MHT 60 S Magnesium Hydroxide Premium Grade and MHT 100 Magnesium Hydroxide Technical Grade Powder Dow Chemicals, which are sold as filler additives used in coatings for corrosion control, as Mg(OH)₂ is noted for its effectiveness at neutralizing acids and acts as a buffer system in the coating.

References / Bibliography

- ²⁵⁴ Kramer, D.A., Magnesium, its Alloys and Compounds, U.S. Geological Survey Open-File Report 01-341
- ²⁵⁵ Emley, E.F., *Principles of Magnesium Technology*, Pergamon Press, New York, NY, (1966)
- ²⁵⁶ Hawke, D., Corrosion and Wear Resistance of Magnesium Die Castings, SYCE 8th International Die casting Exposition and Congress, Detroit, Paper No. G-T75-114 (1975)
- ²⁵⁷ Makar, G.I., Kruger, J., and Joshi, A., in *Advances in Magnesium Alloys and Composites*, (Eds: H.G. Paris, W.H. Hunt,), International Magnesium Association and Non-Ferrous Metals Committee, TMS, Phoenix, AZ, January 26, pp. 105-121 (1988)
- ²⁵⁸ Linder, O., Lein, J.E., Aune, K., Nisancioglu, K., *Corrosion*, Vol. 45, (9), pp. 741 (1989)
- ²⁵⁹ Nisancioglu, K., Lunder, O., Aune, T.K., Corrosion mechanism of AZ91 Magnesium Alloy, Proc. Of 47th World Magnesium Association, Mcleen, Virginia, pp. 43-50 (1990)
- ²⁶⁰ Shreir, L. L., *Corrosion*, Vol. 1, Metal/Environment Reactions, Newnes-Butterworths, Ch. 4, pp. 86-100, (1965)
- ²⁶¹ Available on line at:
[Http://jchemed.chem.wisc.edu/JCESoft/CCA/CCA3/MAIN/VOLTAGE/PAGE1.HTM](http://jchemed.chem.wisc.edu/JCESoft/CCA/CCA3/MAIN/VOLTAGE/PAGE1.HTM)
(1999 Division of Chemical Education, Inc., American Chemical Society)
- ²⁶² Jones, D.A., *Principles and Prevention of Corrosion*, Macmillan Publishing Co., New York, NY, pp. 170-180, (1992)
- ²⁶³ Loose, W. S., in *Corrosion and Protection of Magnesium* (Eds: L. M. Pidgeon, J. C. Mathes, N. E. Woldmen), ASM Int., Materials Park, OH 1946, pp. 173- 260. DGM Informationsgesellschaft, Oberursel, Germany, pp. 201 (1992)
- ²⁶⁴ Pourbaix, M., *Atlas of Electrochemical Equilibrium in Aqueous Solutions*, Pergamon Press, London, (1966)
- ²⁶⁵ Jones, D.E, *Principles and Prevention of Corrosion*, 1st Ed., pp. 49-63, Macmillan Publishing Co., New York, NY (1992)
- ²⁶⁶ Eliezer, D., and Antonyraj, A., *Corrosion*, NACE Int., Vol. 57, No. 4, pp. 334 – 345
- ²⁶⁷ López-Buisán Natta, M.G., *Corrosion*, NACE International, Vol. 57, No8., pp. 712-720 (2001)

²⁶⁸ Greenblatt, J.H., *J. Electrochem Soc.*, Vol.103, No. 10, pp. 539 (1956)

²⁶⁹ J.O'M. Bockris, Reddy, A.K.N., *Modern Electrochemistry*, pp. 939 -950, Vol. I
Plenum Press, New York, (1970)

²⁷⁰ Garreau, M, Bonora, P.L., *J. Appl. Electrochem.*, Vol. 7, pp.197 (1977)

²⁷¹ Peabody, A.W., *Control of Pipeline Corrosion*, NACE: Houston, TX, pp.118 (1967)

²⁷² Kramer, D., *Magnesium , its Alloys and Compounds*, US Geological Survey Open-File
Report 01-341

Chapter 2.8 Benzoquinone Reactivity and Oxidation of 1,4-

Benzoquinone

2.8-1 Introduction to Quinones in Coatings

Polymeric materials derived from amino-quinones have recently been developed^{273,274,275} into coatings for corrosion control of iron and are the focus of ongoing research.²⁷⁶ Typically, what has been reported is that high molecular weight amino-quinone polymers protect the surface of metal by virtue of their hydrophobicity and their ability to coordinate to the surface of the metal through a proposed coordination complex mechanism.²⁷⁷ However, most of these accounts involve high molecular weight polymeric materials that are very insoluble and require high VOC, hazardous air pollutant solvents (*HAPS*) to solubilize the material for use in a coating. Although, attempts have been made to synthesize various oligmeric species of amino-quinones, derived from various diamines and 1,4-benzoquinone starting materials, for example, such as epoxy curatives²⁷⁸ in high solids coatings formulations with environmentally acceptable solvent systems. Unfortunately, aside from the afore mentioned reports and published works by Nikles *et al.*²⁷⁹, on amino-quinones for polyisocyanates, little has surfaced in the literature regarding development of curatives for epoxy or other hybrid polymeric material systems.

The purpose of this literature review section is: 1) examine the general chemical features of quinones; 2) review the general reaction mechanism(s) that apply to nucleophilic substitutions involving amino-quinones, i.e, 1,4-benzoquinone and 2-phenyl-

1,4-phenylquinone with various nucleophiles; 3) examine the aqueous red-ox equilibrium of the hydroquinone-quinone moiety, and 4) examine the general properties of *N*-chloroamines, such as cyanuric acid, the synthesis of trichloroisocyanuric acid (TCCA), and the utility of TCCA as an inexpensive but efficient oxidizing agent for the oxidation of hydroquinone / phenylhydroquinone to their associated quinonoidal structures.

2.8-2 Quinones

Quinones, comprise a group of compounds in which two hydrogen atoms of a benzene nucleus are replaced by two oxygen atoms. This replacement may take place either in the *ortho* or *para* positions, giving rise to orthoquinones or to paraquinones. The *para* or “true quinones” are obtained by the oxidation of hydrocarbons with chromic acid or of various *para* di-derivatives of benzene with chromic acid mixture. The paraquinones are generally crystalline solids of a yellowish color, having a characteristic sharp odor and being volatile in steam.²⁸⁰ The reaction of *p*-1,4-benzoquinone with unoccupied ring positions or those (quinonoids) with occupied, but displaceable moieties are subject to facile adduction by activated amino, hydroxyl, and thiol groups occurs via the classic Michael addition, Figure 2.8-1.^{281,282}

Quinones as Michael Acceptors

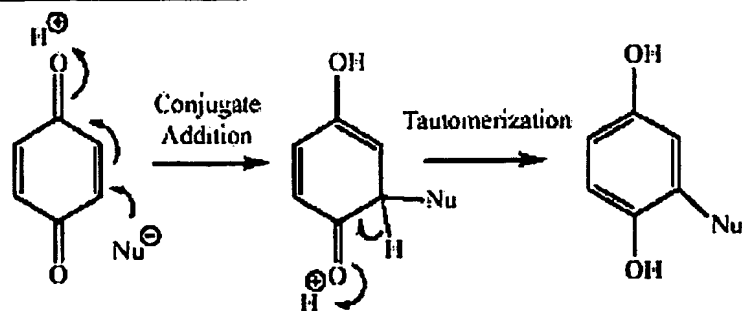
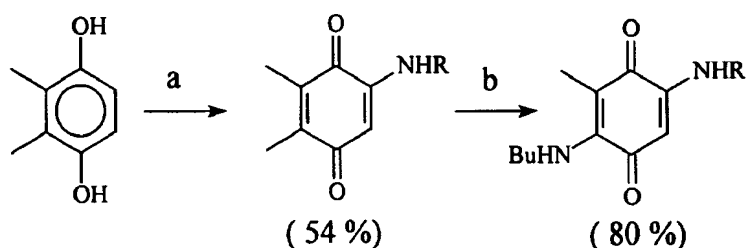


Figure 2.8-1: Reaction 1,4-benzoquinone with nucleophile with tautomerization to substituted hydroquinone.²⁸¹

These quinonoid reactions are classified as highly exothermic, facile aldol condensations that exhibit low activation energies and readily occur at 37°C. Further, these reactions are classified as thermodynamically controlled, which implies that their rate determining step is a nucleophilic Michael addition which forms anionic intermediates with all subsequent steps being faster than the first. Nitrogen addition to quinonoid compounds can occur in one of two ways: 1) nuclear amination²⁸³ of a quinonoid ring by substitution of hydrogen, alkyl groups, or halides by an amine moiety; 2) side chain substitution or amination by the replacement of hydrogen from an alkyl group on the quinonoid ring by an amine as shown in Figure 2.8-2, below.^{281, 283}

Scheme 1



a: 5 eq. RNH₂, EtOH, 1 day, R.T., air, R = (CH₂)₁₇CH₃

b: excess. BuNH₂, reflux 1.5 hour, air

Figure 2.8-2: scheme 1 (from Chakraborty et al. 1998)²⁸⁴ diamination using two different amines in the reaction of (a) 2,3-dimethylhydroquinone with octadecylamine yielded product 2-octadecylamino-5,6-dimethylquinone (54%); (b) excess BuNH₂ yielded the diheteroaminated product 2-octadecylamino-5-(n-butyl-amino)-6-methylquinone (80%).

According to Cameron²⁸⁵, side-chain substitution or amination²⁸⁶ takes place by replacement of hydrogen from an alkyl group on the quinonoid ring by an amine. Both primary and secondary amines are known to yield nuclear and side-chain amination. Further, according to Cameron *et al.*^{285, 285}, nuclear amination Figure 2.8-2, usually occurs

with primary amines while side-chain amination usually occurs with secondary amines with bulky side groups. The reaction of 1,4-benzoquinone with amines occurs spontaneously, even below ambient temperature, yielding a mono-substituted hydroquinone. If the resulting substituted hydroquinone is further oxidized to a mono-substituted benzoquinone, it can in turn react with another amine moiety to yield a 2,5-disubstituted hydroquinone, as shown in Figure 2.8-3.²⁸⁷

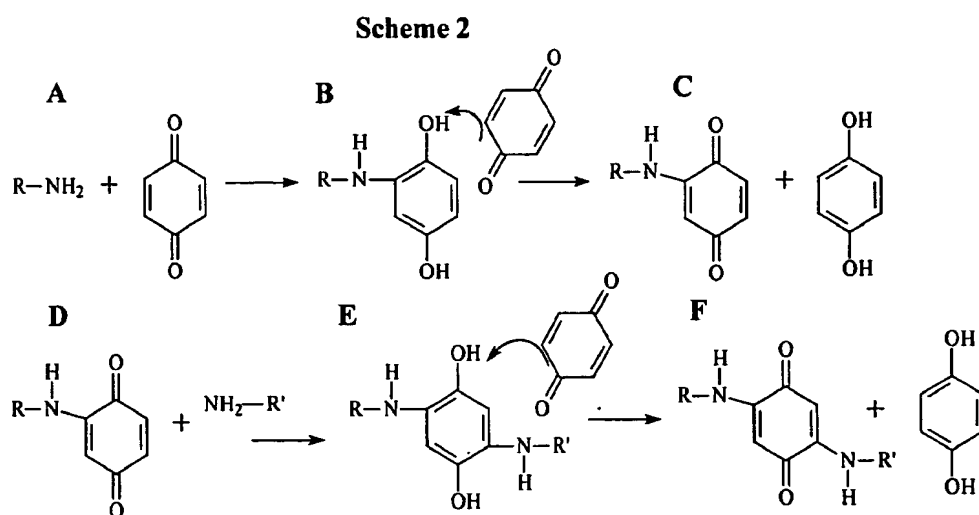


Figure 2.8-3: Scheme 2 (from Erhan *et al.*²⁹⁰ 1991), nuclear amination.

When the reaction is carried out in the presence of excess *p*-benzoquinone, free benzoquinone can function as an oxidizing agent to further oxidize the substituted hydroquinoneamine, as the presence of electron donating amino substituents lowers the oxidation potential of the quinone moiety.²⁸⁸ For example, a measure of the ability of a substance to accept electrons is its reduction potential E^0 , Figure 2.8-4, below.

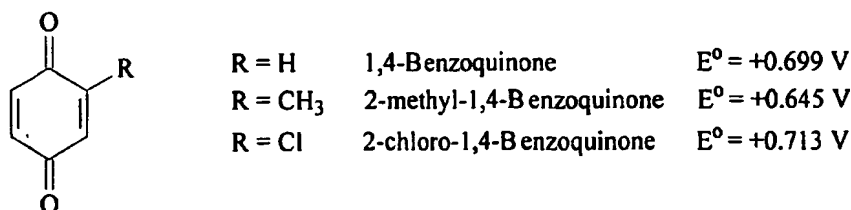


Figure 2.8-4: Electron acceptance in substituted quinonoidal ring.

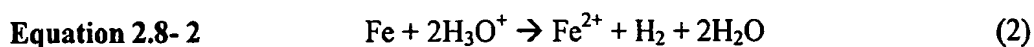
It should be noted that a more positive E° indicates a greater thermodynamic preference to accept electrons (to be reduced) according to this E° data.²⁸⁹ A (2-R-benzoquinone) with a more electron-withdrawing group, or more resonance contributors for the reduced form, should be more easily reduced, while presence of an electron donating group lowers the oxidation potential and hence acts to enhance oxidation.²⁸⁹

The stoichiometry in (Scheme 2), Figure 2.8-3, above, must account for the actual number of quinone molecules required to oxidize the disubstituted hydroquinones. However, when *p*-benzoquinone is used as an oxidizer a non-stoichiometric ratio of oxidizer must be employed. According to Erhan *et al.*²⁹⁰ an average of four equivalents of *p*-benzoquinone are required to facilitate one 2,5-quinone-diamine moiety. All of which wastes *p*-benzoquinone and leaves free hydroquinone in solution which in turn interferes with any process that involves precipitating and recovering any amino-substituted benzoquinone product in water. (See Appendix 2.8-1 for reactivity of Quinonoidal ring)

2.8-5 Aqueous Equilibrium of Quinone / Hydroquinone

Nikles *et al.*²⁷⁹, hypothesized that the 2,5-diamino-1,4-benzoquinone moiety, from amine-quinone polymers, strongly adsorbs on to the surface of iron, preventing moisture adsorption. By blocking moisture adsorption, the amine-quinone polymer would inhibit corrosion. However, Nikles *et al.*²⁷⁶, also state that the mode of chemisorption, in this case, is not understood and is one of their research objectives. The amine-quinone functional group could make a coordinate bond to a surface site through the amine, as proposed by

Phani *et al.*²⁹¹, amine-quinone polymers adsorb on the metal surface through the imine moiety of the polymer chain. FTIR spectra of the polymer film grown on mild steel showed a shift from wave number values of 1650 to 1690 cm⁻¹ in the characteristic band of the imine quinone moiety. This shift was cited as evidence of donor-acceptor interactions between the *p*-electrons of the polymer and the vacant d-orbitals of the iron surface atoms. Unfortunately, Nikles *et al.*, only present data collected for samples exposed to a pH ~2 buffered solution at zero potential difference:



Where it was reported by Nikles²⁷⁹ that under such test conditions the Fe²⁺ species is allowed to remain soluble in the buffer solution through out the duration of the experiment. However, Nikles²⁷⁹ data does not show conditions for quinone-amine polymers tested at higher pH as the corrosion of Fe⁰ favors increased pH conditions. In addition, based upon the red-ox aqueous equilibrium of quinone / Fe, Fe⁰ is a possible reductant of quinone / hydroquinone under most pH conditions. (See Appendix 2.8-2)

2.8-7 Oxidation of para-benzoquinones

Techniques describing the oxidation of phenols and hydroquinone date back to the late 1800's.²⁹² The red-ox equilibria between dihydroxybenzenes hydroquinone and their quinone oxidation states are so facile that milder oxidants other than chromate (K₂Cr₂O₇/H₂SO₄ Jones reagent) typically used for oxidizing alcohols, can be used.²⁹³

Scheme HQ/Q-2
Oxidation of hydroquinone with Fremy's Salt
 (a milder oxidant than chromate)

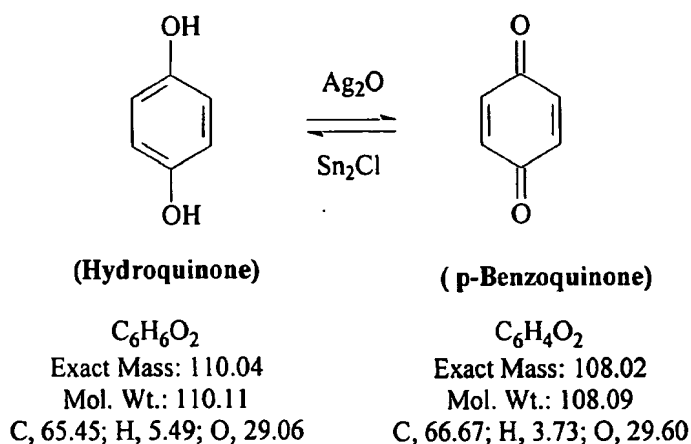
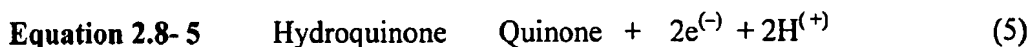


Figure 2.8-10: Oxidation of hydroquinone with Fremy's salt.²⁹⁴



One such oxidant is Fremy's salt, Figure 2.8-3, (Scheme HQ/Q-2) and Equ. 2.8-5. Although chromic acid oxidation of phenols having an unsubstituted *para*-position gives some *p*-quinone product, the reaction is complex and is not synthetically useful.²⁸¹ Hydroquinone or *para*-dihydroxy-benzene is readily oxidized to the corresponding 1,4-Benzoquinone (*para*) or ordinary quinone, $\text{C}_6\text{H}_4\text{O}_2$, and sublimes as golden yellow needles, a bright yellow crystalline solid, M.P.: 115 °C and darkens when exposed to light.²⁸⁰

Consequently, since the later 1800's many techniques have been devised to oxidize hydroquinone to quinone: hydroquinone using CrO_3 ²⁹⁵; quinones from phenols or hydroquinone H_2O_2 (60%) (10 ml, 0.22 mol)²⁹⁶; from hydroquinone with $\text{V}_2\text{O}_5/\text{NaClO}_3$ (another variation)²⁹⁷; from hydroquinone using hydrogen peroxide²⁹⁸; from hydroquinone

using sodium dichromate²⁹⁹; from hydroquinone using Nitrogen oxide^{300, 301}; hydroquinone from diphenyl diselenide catalyzed H_2O_2 ³⁰²; hydroquinone from HI and H_2O_2 ³⁰³; by catalytic oxidation of hydroquinones using NaNO_2/HCl ³⁰¹; oxidation of hydroquinone using $(\text{NH}_4)_2\text{Ce}(\text{NO}_3)_6$ (CAN) and $(\text{NH}_4)_2\text{Cr}_2\text{O}_7$ on SiO_2 ³⁰⁴; hydroquinone from thallium nitrate.³⁰⁵

Erhan²⁷⁴ employed oxidizing schemes such as inorganic chromates, permanganates, hypochlorites such as calcium hypochlorite in THF to obtain quinone-amine polymers in low yield. Nikles *et al.*³⁰⁶, used O_2/EtOH in copper (II) chloride hydrate in THF to yield quinone-amine polymers in high yield. Morey and Saá³⁰⁷, used KBrO_3 as a cooxidant used in conjunction with cerium (IV) species, ceric ammonium nitrate (CAN)³⁰⁸, but only resulted in the oxidation of quinones on a small millimolar scale. Most recently, Krohn *et al.*³⁰⁹ have used CAN in TBHP (*tert*-butyl hydroperoxide) as the oxidizing reagent for such transformations involving phenols and hydroquinone mono and dimethyl ethers are converted to their corresponding quinones. For further reviews on CAN / cerium IV oxidations see references.^{310,311,312}

Recently, such oxidation schemes involving nuclear amination reactions have been used to form quinonamine polymers for coatings on metal surfaces.^{290,306,313,314,315,316,317, 318,319, 320}

However, it should be noted that all of the preceding schemes forming quinone-amine polymers involve Michael addition to 1,4-benzoquinone with unoccupied ring positions, as depicted in (Scheme 2) Figure 2.8-3. Consequently, clear but subtle differences in quinone structure lead to differences in the substitution mechanism and reactivity of the molecule

with a nucleophile. For example, Figure 2.8-2, above, reaction (a) and reaction (b), in (Scheme 1) lies the two addition mechanisms; where as shown in scheme (a) involves nuclear amination of a long chain alkylamine; where as (b) in (Scheme 2) Figure 2.8-3, involves a side-chain amination where an alkyl group is displaced as a result of the second amine bonding in the position *para* to the first group even at the expense of the alkyl group.

Another example, of how a substituted quiononoid structure can influence the reaction mechanism is when a condensation reaction, at the carbonyl carbon, is desired over the thermodynamically favored the Michael addition. Typically, 2, 6-dimethylbenzoquinone is used which effectively blocks the Michael addition. In this case a quinone-imine is formed under acidic conditions as described by Hall *et al.*³²¹ who has used the Lewis acid TiCl_4 / DABCO (1,4-diaza bicyclo(2,2,2)octane) in o-dichloro-benzene to prepare such poly(benzoquinone imines) by the condensation process.

2.8-8 Properties of Cyanuric / Isocyanuric Acid

Cyanuric acid has been known for over 200 years, but achieved commercial importance only in the mid-1950s primarily via its derivatives. The chemistry of cyanuric acid is diversified because of multiple reaction sites. *N*-Chlorination of cyanuric acid produces chloroisocyanurates that are widely used as disinfectants, sanitizers, and bleaches. The *triallyl*- and *tris*(2-hydroxyethyl) derivatives are employed as cross-linking and curing agents, and *tris*(2,3-epoxypropyl)isocyanurate is used in weather-resistant powder coatings. Melamine cyanurate finds significant use as a fire retardant in plastics. Considerable interest has developed in the use of cyanuric acid for reduction of nitrogen oxides in exhaust gases from combustion of oil, gas, and coal.

Nomenclature is based on the *keto-enol* tautomers. The trihydroxy form is variously designated cyanuric acid, s-triazine-2,4,6-triol or 2,4,6-trihydroxy-s-triazine. The *trioxo* structure, or s-triazine-2,4,6(1H,3H,5H)-trione is the basis for the isocyanuric acid nomenclature. The triazine-based system is preferred in the scientific literature and is used by government regulatory agencies; however, the less cumbersome (iso)cyanurate designations persist in commerce. The keto form normally predominates in cases of *keto-enol* tautomerism. In alkaline solution, the anion formed is that of the hydroxy tautomer. (See appendix 2.8-4 for properties of *N*-chloroamines)

2.8-10 Trichloroisocyanuric acid, (TCCA)

Trichloroisocyanuric acid, 1,3,5-trichloro-1,3,5-2,4,6,-(1H,3H,5H)-trione (TCCA, (Scheme 1) with the commonly used trade names, Symclosene, ACL-85, or Chloreal, was first reported in 1902 by Chattaway and Wadmore.³²² The authors describe that trichloriminocyanuric acid is obtained in a quantitative yield from the reaction of the potassium salt of cyanuric acid (2) with chlorine gas³²³ Figure 2.8-11, (Scheme TCCA-22). Later Birckenbach and Linhard described the synthesis of TCCA through cyclization of *N*"-carbonyl-*N,N*-dichlorourea.³²⁴

As shown in the structure, Figure 2.8-12, TCCA belongs to the large group of *N*-chloroimides and amides which is a subgroup of the more general *N*-chloroamines. *N*-chloroamines are inorganic or organic nitrogen compounds with at least one chlorine atom attached to nitrogen. The oldest example is monochloroamine NH_2Cl known since the beginning of the 19th century. The solvent-free material, isolated at $-70\text{ }^\circ\text{C}$, disproportionates violently at $-50\text{ }^\circ\text{C}$ to ammonium chloride and the explosive nitrogen

trichloride.³²⁵ Thereafter, the widespread use of TCCA and its monosodium salt DCCA became industrially important.³²⁶ In 1952 Monsanto obtained a patent on the synthesis of TCCA.³²⁷ In 1960 W.R. Grace obtained a second patent on the synthesis of TCCA.³²⁸ Purex obtained in 1958 a patent on a method for the purification of TCCA through dissolution in concentrated H_2SO_4 and dilution with ice water.³²⁹

Scheme TCCA-2
Synthesis of Trichloroisocyanuric acid (TCCA)

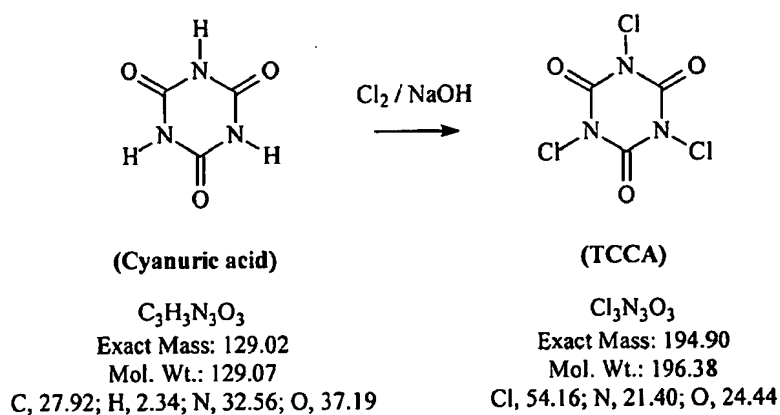


Figure 2.8- 12: Scheme TCCA-2, depicting common synthesis of TCCA.

2.8-11 Trichloroisocyanuric acid, Oxidizing Agent

A well documented aqueous reaction^{330,331,332,333} involving TCCA involves the oxidation of hydrazine by the reaction of water with TCCA to produce hypochlorous acid according to *Figure 2.8-13*:

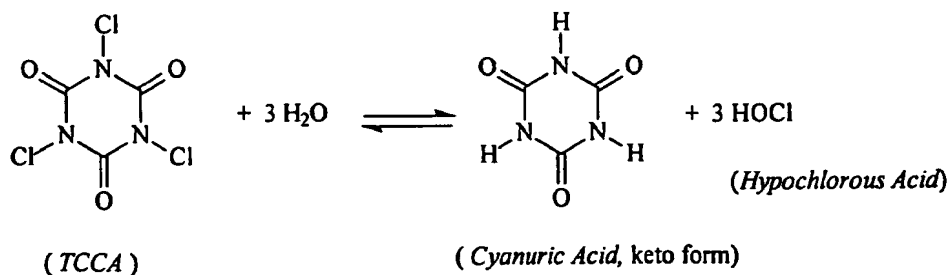
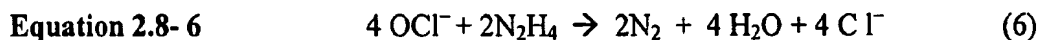


Figure 2.8- 13: Aqueous reaction with water, formation of HOCl by TCCA.

The reaction with hydrazine and hypochlorous acid occurs in alkaline medium according to Equ. 2.8-6:



Hypochlorite has been found to be a strong but effective oxidizer, and it was originally used by Erhan *et al.*²⁷³, who reported its use in much of their work involving the oxidation of hydroquinone to quinone. However, due to its affinity to react with atmospheric moisture the authors abandoned it as a reagent due to inconsistencies in reactivity of the slightly exposed reagent.²⁷⁷

TCCA has a high solubility in most organic solvents, for example, in acetone (350 g/L); ethyl acetate (385 g/l); and Toluene (70 g/L). In 1957 the first use of TCCA for the oxidation of alcohols was reported³³⁴ for the oxidation of steroid and terpene alcohols, and in 1992 Hiegel and Nalbandy³³⁵ reported oxidation of secondary alcohols in acetone with TCCA and pyridine as a base to scavenge the released HCl. In a more recent paper Giampaolo *et al.*³³⁶, report on a safe but mild technique for the general oxidation of alcohols to carbinols to corresponding carbonyl compounds with TCCA. What has been proposed in this thesis is the oxidation of hydroquinone / phenylhydroquinone, which is relatively easy to oxidize, to quinone / phenylquinone using TCCA in dichloromethane solvent.

2.8-12 Summary

The general chemical features of quinones and the pertinent reaction mechanism (s) that applies to the development of oligomeric polymeric materials have been reviewed.

Two such reactions were reviewed; the first nuclear amination and the second side chain substitution. The nuclear amination reaction has been described as the favored mechanism for Michael addition of primary amines to 1,4-benzoquinones which pertains directly to the synthesis of those amino-quinone polymers reported in the literature. The most important topic of this review was the mechanism of conjugate addition to quinones. Generally, the reaction at the C5- position was shown to be the preferred center for nucleophilic attack, by strong nucleophiles, due to the higher electrophilicity of position C5- for unprotonated quinones.

Contrary to claims regarding the hydrophobicity of amino-quinone polymers, it is assumed that such oligomeric materials, as described by Nikles *et al.*²⁷⁶ possess limited water solubility and therefore the quinone moieties of these polymeric materials are subject to aqueous red-ox equilibrium. In considering the general red-ox equilibrium of the quinone / hydroquinone species it is clear that under pH conditions greater than six ~6 and a potential difference more negative than 0.V the dominant form of the quinone / hydroquinone species is the monophenolate ion. Likewise, for pH conditions more acidic than pH< four ~4, under the same potential difference conditions, the equilibrium species favors the reduced form of the quinone / hydroquinone species. Therefore, the claims of enhanced adhesion performance may require modification to include effects of a hydrophobic monophenolate ion under relevant pH and potential conditions.

Finally, a class of reactive materials *N*-chloroamines, such as cyanuric acid, was described as the parent material for the synthesis of trichloroisocyanuric acid, TCCA. TCCA has been described as an inexpensive, mild but efficient oxidant, and in the context

of this thesis has been selected as the preferred oxidant for the oxidation of 2-phenylhydroquinone to 2-phenyl-1,4-benzoquinone.

References / Bibliography

- ²⁷³ Reddy, T.A., Macaione, D., and Erhan, S., *J. Polymer Sci., Part A: Polymer Chemistry*, Vol. **32**, Issue: 10, pp. 1977-1982 (1994)
- ²⁷⁴ Reddy, T.A., and Erhan, S., *J. Polymer Sci., Part A: Polymer Chemistry*, Vol. **32**, Issue: 3, pp. 557-565 (1994)
- ²⁷⁵ Reddy, T.A., and Erhan, S., *J. Polymer Sci., Part A: Polymer Chemistry*, Vol. **51**, Issue: 9, pp. 1591-1595 (1994)
- ²⁷⁶ Nikles, D.E., Liang, J.-L., Cain, J.L., Chacko, A.P., Webb, R.I., and Belmore, K., *J. Polymer Sci., Part A: Polymer Chemistry*, Vol. **33**, Issue: 17, pp. 2881-2886 (1995)
- ²⁷⁷ Kaleem, K., Chertok, F., Erhan, S., *J. Polymer Sci., Part A: Polymer Chemistry*, Vol. **27**, Issue: 3, pp. 865-872 (1989)
- ²⁷⁸ Rushing, R.A., Thompson, C., and Cassidy, P.E., *J. Applied Polymer Science*, Vol. **53**, Issue: 9, pp. 1211-1219 (1994)
- ²⁷⁹ Nikles, D.E., Chacko, A.P., Liang, J.L., Webb, R.I., *J. Polym. Sci., Part A: Polym. Chem.*, Vol. **37**, pp. 2339-2345 (1999)
- ²⁸⁰ Beilstein Handbook (4th Ed.) Vol. B7 (*Isocyclic Compounds*), No. 3764
- ²⁸¹ Finely, K.T., *The Chemistry of Quinonoid Compounds*, Patai, S., Ed.; John Wiley & Sons: New York, NY, pp. 900-1101 (1974)
- ²⁸² Crosby, A.H., and Lutz, R.E., *J. Am. Chem. Soc.*, Vol. **78**, pp.1233 (1956)
- ²⁸³ Cameron, D.W., Giles R.G.F., and Titman, R.B., *J. Chem. Soc., C*, pp. 1245 (1969)
- ²⁸⁴ Chakraborty, M., McConville, D.B., Niu, Y., Tessier, C.A., and Youngs, W.J., *J. Org. Chem.*, Vol. **63**, pp. 7563-7567 (1998)
- ²⁸⁵ Cameron, D.W., Scott, P.M., and Todd, L., *J. Chem. Soc.*, pp. 42 (1964)
- ²⁸⁶ Cameron, D.W., Cromartie, R.I.T., Hameid, Y.K., Scott, P.M., and Todd, L., *J. Chem. Soc.*, pp. 62 (1964)

- ²⁸⁷ Nithianandam, V.S., Chertok, F., and Erhan, S., *J. Coatings Technology*, Vol. **63**, No. 796, pp. 51-54 (1991)
- ²⁸⁸ Carey, F.A., and Sundberg, J., 'Advanced Organic Chemistry, 3rd Ed., Part A: Structure and Mechanisms, pp. 539 – 556, Plenum Press, New York, NY (1990)
- ²⁸⁹ Brown W.H. and Foote C.S., *Organic Chemistry*, 2nd Ed., Saunders College Publ., sections 20.5, 20.6 and 21.3 (1998)
- ²⁹⁰ Nithianandam, V.S., and Erhan, S., *Polymer*, Vo. **32**, pp. 1146 (1991)
- ²⁹¹ Phani, K. L. N., Pitchumani, S., Muralidharan, S., Ravichandran, S., and Iyer, S. V. K. , *J. Electroanalytical Chemistry*, Vol. **353**, Issues 1-2, pp. 315-322 (1993)
- ²⁹² Bayrac (Bull. soc. chim., **1894** (3) II, p. 1129)
- ²⁹³ Wade L.G., JR., *Organic Chemistry*, Prentice Hall, New Jersey, pp. 449 (1986)
- ²⁹⁴ Teuber, H.; Rau, W. *Chem. Ber.* **1953**, Vol. **86**, pp. 1036 and Zimmer, H.; Lanken, D. C.; Morgan, S. W. *Chem. Rev.*, Vol. **71**, pp. 229 (1971)
- ²⁹⁵ A. I. Vogel, *Practical Organic Chemistry*, 5th Ed, pp.1025 (1989)
- ²⁹⁶ *J. Org. Chem.* Vol. **54**, pp. 728-731 (1989)
- ²⁹⁷ *JACS*, Vol. **58**, pp. 646-647 (1936)
- ²⁹⁸ Spiceboy, US Pat 4,973,720
- ²⁹⁹ J. B. Hedrickson et al, *Organic chemistry*, 3rd edition, McGraw-Hill, New York, (1970)
- ³⁰⁰ *J. Org. Chem.* Vol. **59**, pp. 2529-2536 (1994)
- ³⁰¹ *Tet. Lett.* Vol. **35**, (9) pp. 1335-1338 (1994)
- ³⁰² Pratt D.V., Ruan F., Hopkins P. B, *J. Org. Chem.*, Vol. **52**, pp. 5053 (1987)
- ³⁰³ Correale, M., *J. Org. Chem.*, Vol. **54**, pp. 728-731 (1989)
- ³⁰⁴ *Synthesis* pp. 641 (1985)
- ³⁰⁵ McKillop, A.; Perry, D. M.; Edwards, M.; Autus, S.; Farkas, L.; Nogrady, N.; Taylor, E. C. *J. Org. Chem.* Vol. **41**, pp. 282 (1976) and reference therein.

- ³⁰⁶ Han, M., Bie, H., Nikles, D.E., and Warren, G.W., *J. Polym. Sci.: Part A: Polymer Chem.*, Vol. **38**, pp. 2893-2899 (2000)
- ³⁰⁷ Morey, J., and Saá, J.M., *Tetrahedron*, Vol. **49**, pp. 105 (1993)
- ³⁰⁸ Jacob, P. III, Callery, P.S., Shulgin, A.T., and Castagnoli, J., JR., *Org. Chem.*, Vol. **41**, pp. 3627 (1976)
- ³⁰⁹ Krohn, K., and Vitz, J., *J. Prakt. Chem., Procedures / Data*, Vol. **342**, No.8, pp. 825 – 827 (2000)
- ³¹⁰ Syper, L., Kloc, K., and Mlochowski, J., *Synthesis*, pp. 571 (1979)
- ³¹¹ Molander, G.A., *Chem. Rev.*, Vo. **92**, pp. 29 (1992)
- ³¹² Ho, T.L., *Synthesis*, pp. 347 (1973)
- ³¹³ Kaleem, K., Chertok, F., and Erhan, S., *J. Polym. Sci., Part A: Polym. Chem.*, Vol. **27**, pp. 865 (1989)
- ³¹⁴ Nithianandam, V.S., and Erhan, S., *J. Appl. Polym. Sci.*, Vol. **42**, pp. 2385 (1991)
- ³¹⁵ Nithianandam, V.S., Chertok, F., and Erhan, S., *J. Coatings Technology*, Vol. **63**, No. 796, pp. 47-49 (1991)
- ³¹⁶ Reddy, T.A., and Erhan, S., *Intern. Polymeric Matter.*, Vol. **19**, pp. 109-116 (1992)
- ³¹⁷ Colletti, R.F., Stewart, M.J., Taylor, A.E., McNeill, N.J., and Mathias, L.J., *J. Polym. Sci., Part A: Polymer Chem.*, Vol. **29**, pp. 1633 – 1638 (1991)
- ³¹⁸ Nikles, D.E., Chacko, A.P., Liang, J.L., Webb, R.I., *J. Polym. Sci., Part A: Polym. Chem.*, Vol. **37**, pp. 2339-2345 (1999)
- ³¹⁹ Vaideeswaran, K., Bell, J.P., and Nikles, D.E., *J. Appl. Polym. Sci.*, Vol. **76**, pp. 1338-1350 (2000)
- ³²⁰ Han, M., Bie, H., Nikles, D.E., and Warren, G.W., *J. Polym. Sci.: Part A: Polymer Chem.*, Vol. **38**, pp. 2893-2899 (2000)
- ³²¹ Boone, H.W., Bryce, J., Lindgreen, T., Padias, A.B., and Hall, H.K., JR, *Macromolecules, Communications to the Editor*, Vol. **30**, pp. 2797-2799 (1997)
- ³²² Chattaway, F. D.; Wadmore, J. M., *J. Chem. Soc.*, Vol. **81**, pp. 191 (1902)

- ³²³ Ura, Y.; Sakata, G. *Ullmann's Encyclopedia of Industrial Chemistry*, 6th ed.; Wiley-VCH: Weinheim, 2001. (b) *Merck Index*; Merck & Co.: Whitehouse Station, NJ, (1996)
- ³²⁴ Birckenbach, L. *Chem. Ber.*, Vol. 63, pp. 2528 (1930)
- ³²⁵ Bretherick, L. *Handbook of Reactive Chemical Hazards*, 5th ed.; Butterworth-Heinemann Ltd.: London, Vol. 1, Entry 3857, pp. 1259 (1995)
- ³²⁶ Hands, W. J. *Soc. Chem. Ind.*, Vol. 67, pp. 66 (1948)
- ³²⁷ Hardy, U.S. Patent 2,607,738, (1952)
- ³²⁸ Christian, U.S. Patent 2,956,056, (1960)
- ³²⁹ Lorenz, U.S. Patent 2,828,308, (1958)
- ³³⁰ Faizullah, A.T., and Townshend, A., *Anal. Proc.* Vol. 22, pp. 15 (1985)
- ³³¹ Collins, G.E., Lattuner, S., and Rose-Pehrsson, S.L., *Talanta*, Vol. 42, pp. 543 (1995)
- ³³² Safavi, A., and Baezzat, M.R., *Anal. Chim. Acta.*, Vol. 358, pp. 121 (1998)
- ³³³ Halvatzis, S.A., Timotheou-Potamia, M.M., and Calokerinos, A.C., *Analyst*, Vol. 115, pp. 1229 (1990)
- ³³⁴ Mukawa, F., *Nippon Kagaku Zasshi*, Vol. 78, pp. 450 (1960) and *Chem. Abstr.* Vol. 53, pp. 5338 (1960)
- ³³⁵ Hiegel, G.A., and Nalbandy, M., *Synth Commun.* Vol.22, pp. 1589 (1992)
- ³³⁶ De Luca, L., Giampaolo, G., and Porcheddu, A., *Organic Letters*, Vol. 3, pp. 3041 – 3043 (2001)

Chapter 2.9 Epoxy, Urethane / Urea, and Hybrid Epoxy-Urea Materials

2.9-1 Epoxy Polymeric Materials

The purpose of this section is to illustrate the chemical nature of the epoxy-amine and polyisocyanate coating systems and the definition and development of so called “hybrid” polymeric coatings from these materials. Epoxy polymers originate from the work of Castan (1936)³³⁷ who reacted glycidyl ether of bis-phenol A with phthalic anhydride for plastics used in dentistry, and Greenlee, Devoe, and Renolds (1939) who were experimenting with caustic susceptible ester links in coating films. Epoxies are defined as molecules containing one or more oxiranylmethyl ethers or esters, in a terminal position, usually called glycidyl ethers or esters. Epoxies were the first two component (2-K) convertible vehicles to be used for both elevated temperature (50° to 150° C) bake and room temperature cure systems. Most epoxy resins or liquid resins can be blended with hardeners to produce air-drying coatings / films with toughness and resistance that approaches many baked films³³⁸. Metal primers formulated from epoxies are the most commonly used vehicles for protecting structural applications. (See Appendix 2.9-1 for discussion of epoxy resins and 2K curatives).

2.9-2 Extent of cure Epoxies

The extent of cure of a polymeric material is directly proportional to its corrosion control properties as a coating or a film. Unreacted oligomeric materials can be easily hydrolyzed under relatively mild exposure conditions, especially when combined with other coating additives such as solvents, fillers, TiO₂, rheology modifiers, etc. Therefore, it is important to ensure that conditions of full cure can be achieved for a given polymeric material under a given set of cure conditions.

The mechanism and extent of cure, of an epoxy amine system, can be used to model the influence of an amine curative's kinetic behavior on the development of network morphology in resulting polymer matrices.³³⁹ In a recent study by Paz-Abuin *et al.*³⁴⁰ the autoacceleration³⁴¹ effect observed in epoxy-diamine systems, such as [diglycidyl ether of bisphenol A (DGEBA)/*m*-xylene diamine (mXDA)] was investigated and found to be related to free volume developed in the polymer matrix as a function of temperature and tertiary amine accumulation. This dependence was found to be kinetically tied to the overall cure mechanism as depicted in Figure 2-9-5, below, and described in three steps: 1) initiation up to 20-to-25% of conversion; 2) autoacceleration, and 3) inhibition.^{342,343,344,345} proceeds via a chemical / physical balance where the free volume exerts an influence according to tertiary amine concentration, Figure 2.5-6, below.

Depending on the cure temperature and the free volume, the reaction can be autoaccelerated or inhibited. When the developing matrix contains larger spaces the local concentration of monomer remains relatively higher than bulk concentration, and the reaction rate shows a sharp increase. Conversely, after gelation the free volume exerts a strong influence on the termination rate constant that is related to the autoacceleration from tertiary amine observed in the propagation step. Thus when the available free volume space

in the matrix begins to decrease, free monomer movement becomes retarded and the polymerization reaction “starved” or physically-controlled.

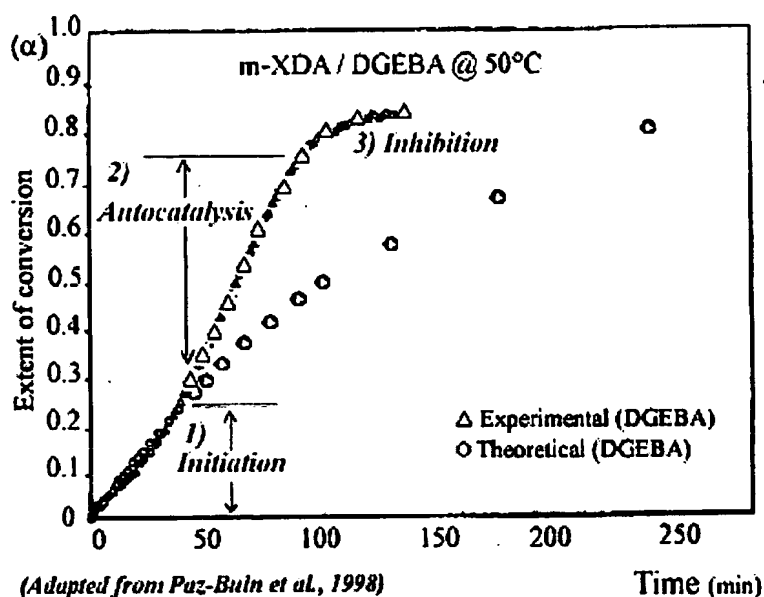


Figure 2-9.5: Extent of conversion for m-XDA / DGEBA system depicting three stages of cure, and autocatalytic / tertiary amine effect on conversion (α) as shown in difference between theoretical cure (—) and Experimental (Δ) conversion. According to Paz-Abuin *et al.*³⁴⁰ for epoxy conversions above 25% reaction control.

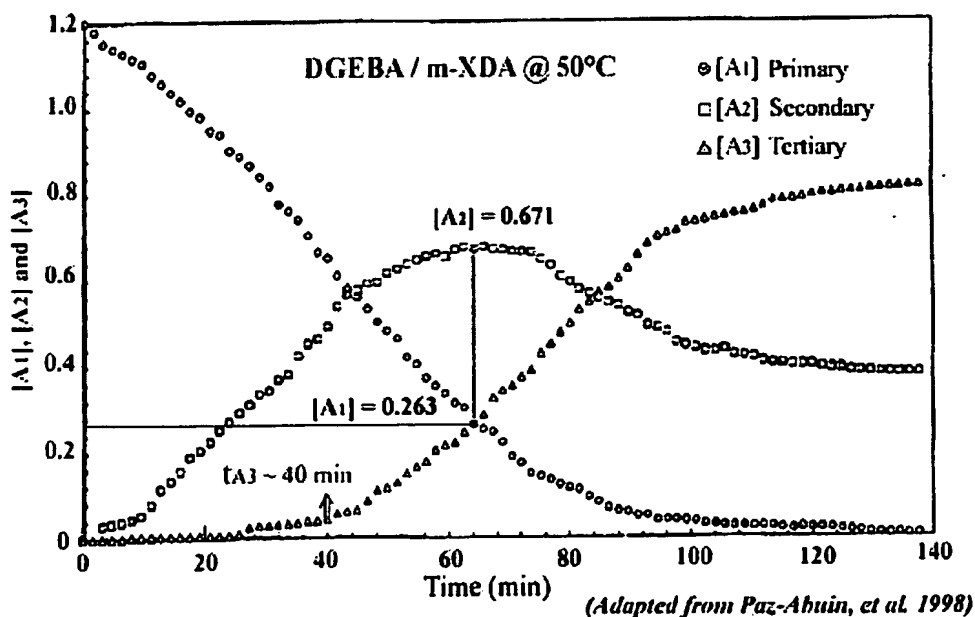


Figure 2.5-6: Effect of tertiary amine accumulation on autocatalysis kinetics, courtesy of Paz-Abuin, *et al.*³⁴⁰ At $t = 40$ minutes autocatalytic effect begins, in reference to system in figure 2.5-5, gelation starts between 25 and 30 % conversion and kinetics of system change to diffusion control after ~ 67% conversion. ^{Error!}

Bookmark not defined.

2.9-3 Solvent Effect Epoxies

Solvents are known to affect the curing rate and solidification of epoxy-amine systems as the curing process is delayed due to solvent to evaporation, and during which time the system remains more mobile than without solvent present. According to May and Tanaka ^{Error! Bookmark not defined.}, both proton- and electron-donor solvents can greatly effect reaction kinetics of epoxide-amine systems. According to Rozenberg ^{Error! Bookmark not defined.}, proton donors act to decrease the reaction induction period, as well as increases the reaction rate, which relates to a more pronounced effect the higher the solvent acidity. While the opposite effect is true with respect to electron donor solvents that act to decrease both the initial induction and post-induction reaction rate, and this inhibition effect has been observed to follow increasing conversion of epoxide group. ^{Error! Bookmark not defined.} According to Fiala *et al.*³⁴⁶, the inhibition effect of the electron-donor solvents is due to the decreased concentration of proton donors in the reaction system as a result of their bonding to electron-donor molecules of the solvent, initially to amines and then to hydroxyl groups. Generally, the use of protic solvents or other proton-donor paint components, in epoxy-amine systems, contributes to accelerating the cure reaction, thus yielding higher degrees of conversion and increased cross-link density. (See Appendix 2.9-2 for resulting microstructure description of epoxy / amine).

2.9-8 Polyurethane / Polyurea Systems

Polyurethanes originate from the work of Bunsen (1848) and Hofmann (1871). The earliest polyurethanes were developed by Otto Bayer and coworkers at I. G. Farbenindustrie, Germany in 1937^{347, 348, 349 350, 351, 352} formed by reacting toluene diisocyanate with a polyhydroxol compound.³⁵³ The first polyurethanes were commercially an aliphatic isocyanate was reacted with a diamine to form polyureas that were infusible, but very hydrophilic. Further research, in that era, was carried out when an aliphatic isocyanate was reacted with a glycol that yielded a unique new class of polyurethanes with elastic qualities, and shortly thereafter the industrial scale production of polyurethane began in 1940.^{354, 355, 356} In 1952, the first polyisocyanate, toluene diisocyanate (TDI), became commercially available, and by the early 1960s, B.F. Goodrich³⁵⁷ produced Estane, Mobay marketed Texin, and Upjohn who marketed Pellethane in the United States, and while in Europe Bayer and Elastgran marketed Desmopan and Elastollan, respectively. (See Appendix 2.9-5)

2.9-14 Polyurea Systems

The reactions between isocyanates and primary amines have been characterized as very fast with low activation energy, usually several kilocalories per mol, and the half-life of the reaction of aliphatic amines with aromatic isocyanates is on the order of milliseconds.³⁵⁸ Moisture-cured polyureas, consisting of isocyanates can react with the hydroxyl group in water (H-OH) to form a unique class of coatings known as moisture-cured ureas. Single package moisture-cured polyureas are derived from isocyanate prepolymers that, when applied, react with the humidity in the air to form a tough, hard resinous film.³⁵⁹ According to the Hoffmann rearrangement, the carbamic acid should

hydrolyze to the corresponding amine in basic solution with the evolution of CO₂ Figure 2.9-15, below.

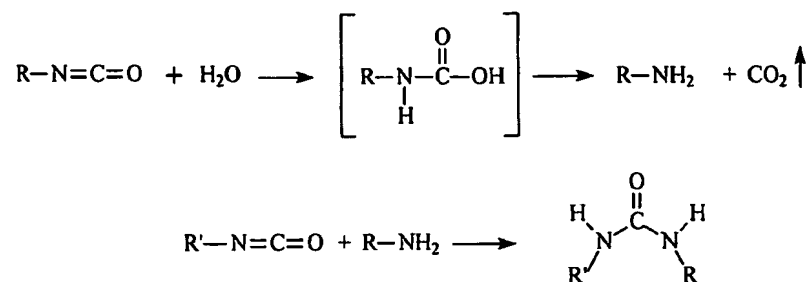


Figure 2.9-15: Urea formation from water and isocyanates, Hoffman rearrangement. Error! Bookmark not defined.

Because of their rapid rate of reaction, aromatic isocyanates are used almost exclusively in moisture-cured polyurea MC-PURs. The isocyanate component is typically in the form of a prepolymer or quasi- prepolymer with %NCO values in the range of 10-20% with room temperature viscosities of less than 2000 cps.³⁶⁰ Most of the polyisocyanate prepolymers are based on aromatic MDI derivatives, such as the 2,4'- and 4,4'- isomers. Generally, the amine component(s) used in the formation of true polyurea formulations are aliphatic in nature and possess hindered amine groups.³⁶¹ Since it is necessary to reduce the system's reactivity relative to primary amine analogs, secondary amines have become widely employed because they slow the reaction profile of polyurea system.³⁶²

The catalysis of urea groups was observed and explained in terms of a mechanism that proposed hydrogen bonding property between the urea carbonyl groups and the hydroxyl groups. The presence both of basic tertiary nitrogen and of acidic hydrogen atom in one urea group makes it theoretically possible for them to function as either acid or base

catalysts.³⁶³ Baker and Bailey³⁶⁴ suggested an acid-catalyzed mechanism for the urea product catalyzed reaction, Figure 2.6-16, below, as follows:

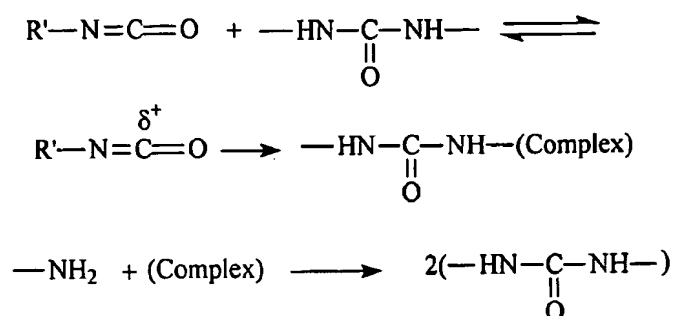


Figure 2.9-16: Acid catalyzed urea mechanism proposed by Baker and Bailey.

According to Baker and Bailey³⁶⁴ the reaction was facilitated by association (complex), Figure 2.9-17, below, of the acidic hydrogen in urea group with the carbonyl-oxygen atom in isocyanate group, and thus the requisite polarization of the carbonyl group in isocyanate group toward nucleophilic attack by the reactant amine:

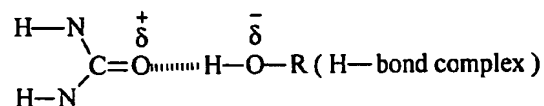


Figure 2.9-17: Catalysis of urea group through hydrogen bonding.

Figure 2.9-18, below, suggests that the catalysis of urea groups occurs by way of hydrogen bonding according to the following mechanism:

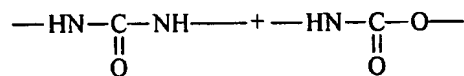
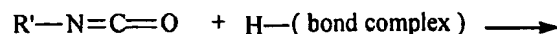
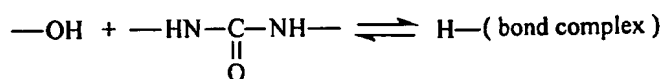


Figure 2.9-18: promotion of nucleophilic reactivity of isocyanate groups through formation of hydrogen bonding complex. (from Baker and Bailey³⁶⁴)

Hydrogen bonding promotes nucleophilic enhancement due to hydroxyl-oxygen influence on isocyanate groups, and thereby increasing the rate of isocyanate-hydroxyl association and complex formation. In this mechanism, the urea group acts like a base instead of an acid. The catalysis of urea groups is thought to occur in terms of a possible mechanism that promotes a hydrogen bonding effect between the urea carbonyl groups and the hydroxyl groups.³⁶⁵ (See Appendix 2.9-4 for solvent effects on isocyanates).

2.9-16 Hybrid Epoxy-Urethane/Urea IPNs

Coatings applied to structural applications are often distinguished according to the modulus of the materials to which they are applied. The structural material either possesses a high or low modulus of elasticity. For example, metals are materials that possess a high modulus, whereas low modulus materials are elastomers. The properties of such materials are determined from the components they are manufactured from as well as by the adhesion strength between the material and coating. Therefore, primer coatings for metal surfaces require polymeric matrices that can be designed with intermediate properties that can bridge the gap between materials of high modulus and those of lower modulus. For example, epoxy matrices, commonly used in primer formulations, are known to provide

high T_g , high modulus protective matrices with good adhesion to metal surfaces. However, they are generally deficient in the basic elastomeric qualities needed to promote adhesion, strength, and toughness at an interface. In addition, “hybrid” polymeric matrices, for high performance primers, must be designed as polymer composites or alloys that contain a polymer backbone with at least two types of reactive groups that can take part in crosslinking and network formation under two different mechanisms. It is the creation of chemical bonding in different or intermediate phases of the “hybrid” matrix that contributes to the enhanced structure and interfacial properties of the resulting polymeric matrix.

Epoxy resins (ERs) are widely used as the matrices of high-performance composite materials because of their stiffness, chemical resistance, and high temperature stability. However, they are rigid, inherently brittle, and have poor crack resistance^{366,367,368} when cured with stoichiometric amounts of common curing agents such as aliphatic or aromatic polyamides, dicarboxylic acids, anhydrides, boron trifluoride, and tertiary amines. In addition, their low impact resistance greatly limits the use of these polymeric resins in structural applications. Even though epoxies display excellent adhesion to metals with good chemical resistance there are several disadvantages to epoxies in general: 1) epoxies generally do not display good elongation which can cause cracking that leads to coating failure and / or water intrusion; 2) some epoxies contain solvents or additives that can leach out of the coating and cause undesirable side reactions at interfaces.

Polyurethanes are known to display good elongation and resistance to cracking due to their elastomeric nature, but their relative low thermal resistance and strength limit their applications. Therefore, several researchers have proposed^{369, 370, 371, 372, 373} IPN combinations to improve properties of PUs and ERs. Even though much work has been

done on the synthesis and properties of PU/ER IPNs^{374,375,376,377} most of it has focused on improving the brittleness of ERs.^{378, 379, 380, 381} (See Appendix 2.9-5 for further discussion).

2.9-20 Summary

The purpose of this review has been to demonstrate the general reactions associated with the primary classes of polymeric materials commonly used in metal rich coatings. This review has focused on ambient cure coating systems, i.e., systems capable of achieving full cure over a temperature range of 30°C to 40°C and the general catalysis mechanism associated with each. Generally, epoxy amine reactions can be catalyzed by tertiary amines and phenolic compounds such as nonylphenol or benzyl alcohol. The autocatalysis mechanism, described by Rosenberg^{Error! Bookmark not defined.}, involves the participation of the amino-alcohol moiety generated by addition of a primary amine to epoxide.

Most isocyanate reactions have been reported to be catalyzed by acidic hydrogens from polyhydric alcohols that are transformed into carbamates or urethanes, in addition, polyurethanes can be catalyzed by combinations of tertiary amines and tin catalysts; however type and configuration of both the isocyanate and polyol materials and temperature determine the extent of the reaction. Generally, polyurethane formation from isocyanates is far more complex and usually involves a reaction mechanisms that is dependent on the nature of the catalyst added. For example different rate-laws and structural-reactivity relationships have been observed³⁸² to occur upon addition of differing acid-base (HX) catalysts. According to Schwetlick *et al.*³⁸², the three general cases have been described as: 1) moderate acidity, such as a phenol or alcohol, that promotes a single

step concerted mechanism; 2) strong bases as catalyst; 3) Less acidic but stronger nucleophilic HX such as aromatic amines.

Polyurea systems from polyisocyanates and primary or secondary amines are generally catalyzed by water as true polyureas are not hybrid systems but rely on the water promoted autocatalysis mechanism to achieve high conversion and higher molecular weight. The hybrid epoxy-urethane systems have been characterized as systems that involve an elastomeric polyisocyanate and labile hydroxyls from diglycidyl ethers of bisphenol-A. Currently, there have been no autocatalysis mechanism ascribed to facilitating these reactions; however, these reactions are believed to be promoted by the presence of PU elastomer. What remains to be determined is the influence of each of these mechanisms on the cure of "hybrid" polymeric systems comprised of two or more of these functional groups and whether the "hybrid" system can achieve near or full conversion as compared to that of either of the parent materials.

References / Bibliography

- ³³⁷ Wicks, Z. W., Jones, F. N., Pappas, S. P., *Organic Coatings: Science and Technology*, Vol. 1: Film Formation, and Appearance, Wiley-Interscience, pp 162 – 166, (1992)
- ³³⁸ DOW, Technical Bulletin, Epoxy Resins, High-Performance Epoxy Resins, Dow Plastics, Dow Chemical Co., Copyright (1998)
- ³³⁹ Swier, S., and Van Mele, B., *J. Polym. Sci.*, : Part B: Polymer Physics, Vol. **41**, 594–608 (2003)
- ³⁴⁰ Paz-Abuin, S., Lopez-Quintela, A., Pellin, M.P., Varela, M., and Prendes, P., *J. Polym. Sci.*, Part:A: Polym. Chemis., Vol. **36**, pp. 1001-1016 (1998)
- ³⁴¹ Cardenas, J. N and O'Driscoll, K. J, *J. Polym. Sci. Polym. Chem. Ed.*, Vol. **14**, pp. 883 (1976)
- ³⁴² Arai, K. and Saito, S. J., *J. Chem. Eng. Japan*, Vol. **9**, pp. 302 (1976)
- ³⁴³ Marten, F. L., and Hanielec, A. E., *Am. Chem. Soc. Symp. Ser.*, Vol. **43**, pp. 104 (1978)
- ³⁴⁴ Chern, C. S. and Poehlein, G. W., *Polymer Eng. Sci.*, Vol. **27**, pp. 788 (1987)
- ³⁴⁵ Cole, K. C., Hechler, J. J., and Noel, D., *Macromolecules*, Vol. **24**, pp. 3098 (1991)
- ³⁴⁶ Fiala, V., and Lidařik, M., *Makromol. Chem.*, Vol. **154**, pp.81 (1972)
- ³⁴⁷ O. Bayer, *The diisocyanate polyaddition process (polyurethanes). Description of a new principle for building up high-molecular compounds*, *Angew. Chem.*, **A59**, pp. 257 (1947)

- ³⁴⁸ I. G. Farben, DE-PS 728.981, (1937)
- ³⁴⁹ Farbenfabriken Bayer, DE-PS 913.474, (1941)
- ³⁵⁰ DRP 728981 (1937), invs.: O. Bayer, H. Rinke, W. Siefken, L. Orthner, H. Schild.
- ³⁵¹ Ital. Pat. 3667704 (1938), inv.: O. Bayer.
- ³⁵² O. Bayer, *Angew. Chem.*, Vol. 59, pp. 257 (1947)
- ³⁵³ Bayer, O., et al., German patent 728,981, November 12, (1942)
- ³⁵⁴ A. E. Christ, W. E. Hanford (to du Pont), U.S. Patent 233639, (1940)
- ³⁵⁵ Brit. Pat 580 524, 1940 (to ICI), Brit. Pat. 574 134, (1942)
- ³⁵⁶ P. Pinten (to A. G. Dynamit), *Ger. Pat.* 932 633, (1943)
- ³⁵⁷ C. S. Schollenberger, (to B.F.Goodrich), U.S. Patent 2871218, (1955)
- ³⁵⁸ Pannone, M. C.; Macosko, C. W., *J. Appl. Polym. Sci.*, Vol. 34, pp. 2409 (1987)
- ³⁵⁹ Wicks, Z. W., Jones, F. N., Pappas, S. P., *Organic Coatings: Science and Technology*, Vol. 2: Film Formation, and Appearance, Wiley-Interscience, pp. 201, (1992)
- ³⁶⁰ House, D.W. and R.V. Scott, Jr. "The Use of a New Class of Light-Stable Aliphatic diamines for Polyurea and Polyurethane Coatings". *Proceedings of the SPI 35th Annual Polyurethanes Technical/Marketing Conference*, pp. 74-87 (1994)
- ³⁶¹ Perez, A., Jr., Hillman, K., Secondary Aliphatic Diamine Chain Extenders in Aliphatic Polyurea Spray Applications, *Huntsman Corporation*, available on line.
- ³⁶² House, D.W., D. Ilijevski, and R.V. Scott, Jr. "A Novel Coating System Utilizing Stripped TDI-Based Prepolymers." *Conference Proceedings of the Polyurethanes Expo '99*, Alliance for the Polyurethanes Industry, pp. 53-61 (1999)
- ³⁶³ Willoughby, B.G., "PU Catalysts – Unravelling the Mystery," presented at the *Polyurethane Manufacturers Association Spring Meeting*, (1998)
- ³⁶⁴ Baker, J. W. and Bailey, D. N., *J. Amer. Chem. Soc.*, Vol. 79, pp. 4652 (1957)
- ³⁶⁵ Luo, N., Wang, D-N, and Ying, S-K, *J. Appl. Polym. Sci.*, Vol. 61, pp. 367 -370 (1996)

- ³⁶⁶ May, C. A., Ed., *Epoxy Resin Chemistry and Tech-* 29. H. Lee and K. Neville, *Handbook of Epoxy Resins, Technology*, Marcel Dekker, New York, (1988)
- ³⁶⁷ Le May, J.D., and Kelly, F.N., in *Structure and Ultimate Properties of Epoxy Resins*: Dušek, K., Ed.: Springer-Verlag: New York, NY, Vol. 78, pp.115 (1986)
- ³⁶⁸ Ng, H., Manas-Zloczower, I., *Polym. Eng. Sci.*, Vol. 33, pp. 211 (1993)
- ³⁶⁹ Frisch, K. C., Klempner, D., and Mukherjee, S. K. *J. Appl. Polym. Sci.*, Vol. 18, pp. 689 (1974)
- ³⁷⁰ Cassidy, E. F., Xiao, H. X., Frisch, K. C., and Frisch, H. L. *J. Polym. Sci. Polym. Chem. Ed.*, Vol. 22, pp. 2667 (1984)
- ³⁷¹ Cassidy, E. F., Xiao, H. X. Frisch, K. C. and Frisch, H. L., *J. Polym. Sci. Polym. Chem. Ed.*, Vol. 22, pp. 1839 (1984)
- ³⁷² Hsieh, K. H. and Han, J. L., *J. Polym. Sci. B.*, Vol. 28, pp. 623 (1990)
- ³⁷³ Hsieh K. H. and Han, J. L., *J. Polym. Sci. B.*, Vol. 28, pp. 783 (1990)
- ³⁷⁴ Pernice, R., Frisch, K. C. and Navare, R., *J. Cell. Plast.*, Vol. 18, pp. 121 (1982)
- ³⁷⁵ Klempner, D., Berkowski, L., Frisch, K. C., Hsieh, K. H., and Ting, R., *Rubber World*, Vol. 192, pp. 16 (1985)
- ³⁷⁶ Klempner, D., Muni, B., Okoroafor, M., and Frisch, K. C., *Advances in Interpenetrating Polymer works*, Vol. II, Technomic Publishing, pp. 1 (1990)
- ³⁷⁷ Lee, Y., Ku, W., Tsou, J., Wei, K. and Sung, P., *J. Polym. Sci.: Part A: Polym. Chem.*, Vol. 29, pp. 1083 (1991)
- ³⁷⁸ Hsieh, K. H., Chiang, Y. C., Chern, Y. C., Chiu, W. Y. and Ma, C. C. M., *Angew. Makromol. Chem.*, Vol. 193, pp. 89 (1991)
- ³⁷⁹ K. H. Hsieh, Y. C. Chiang, Y. C. Chern, W. Y. Chiu, C. C. M. Ma, *Angew. Makromol. Chem.*, Vol. 194, pp. 15 (1992)
- ³⁸⁰ Chern, Y. C., Hsieh, K. H., Ma, C. C. M. and Gong, Y. G., *J. Mater. Sci.*, Vol. 29, pp. 5435 (1994)
- ³⁸¹ Prakash, N. A., Liu, Y. M. , Jang, B. Z. and Weng, J. B., *Polym. Comp.*, Vol. 15, pp. 479 (1994)

³⁸² Schwetlick, K., Noack, R., and Stebner, F., *J. Chem. Soc., Perkins Trans.*, 2, pp. 599-608 (1994)

Chapter 2.10 Thermal Stability of Polymeric Coatings

2.10-1 Fire Retardant Coatings

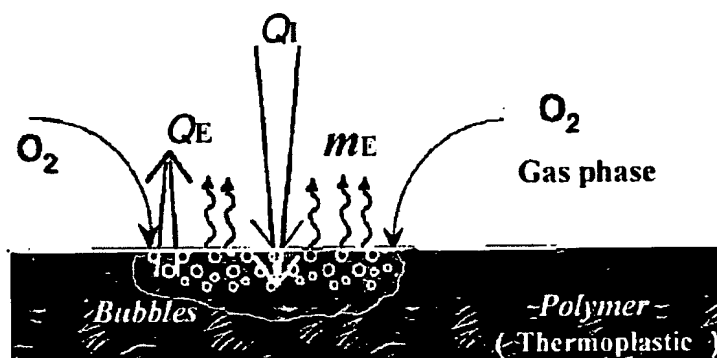
The purpose of this section is to illustrate the definition of fire retardant coatings and review the generic model and mechanism relative to coating combustion. This section addresses and provides rationale for the combustion behavior of some common polymeric materials used in coatings when subject to established testing protocol. The emphasis is placed on defining the pertinent mechanism ascribed to flame retardant polymeric materials used in coatings and how those materials may be further modified or enhanced for use in a coating system containing a reactive metal such as pigmentary magnesium.

Generally, most polymeric binders are based on hydrocarbons where the polymer is composed of C-C bonds, and as a result they tend to be high-molecular weight, relatively low-density, that cross-link and condense after evaporation of a solvent carrier. Most

coatings are designed as thick films, but thin enough to allow full solvent evaporation without entrapment. In most cases, film attachment to the metal substrate is principally through mechanical interactions with a few covalent bonds between OH groups in the case of metal oxides attached to active organic groups in the polymer.³⁸³ (See Appendix 2.10-1 for discussion of Flame-retardant coatings)

2.10-2 Polymer Combustion Cycle

Combustion of polymeric materials, Figure 2.10-1, below, is usually characterized by a coupling between condensed and gas phase phenomena involving a complex coupling of free radical chemical reactions with heat and mass transfer processes. In order to burn a polymeric material thermal energy must be added to the material to raise its temperature sufficiently to initiate degradation.



(Adapted from Kashiwagi, 1994)

Figure 2.10-1: Generation and transport of bubbles containing small molecules From the interior of the polymer melt where: Q_E is the average heat release rate per unit area, (radiant flux in W/cm^2); Q_I is the average flame heat flux in W/cm^2 , and mE is the mass of volatile degradation products boiling out of the coating.

The required thermal energy needed to incinerate a coating can be supplied from either an external source, in the case of an ignition event, or from an adjacent flame as energy feedback, in the case of flame spread and burning. Thermal radiation is a primary

mode of energy transfer from the flame to the polymer surface except for small samples (roughly less than 10-cm diameter).^{384,385,386} (See Appendix 2.10-2 for further discussion)

As a corollary to the polymer pyrolysis process, only when the polymer combustion cycle is interrupted at some point can an element of fire resistance be achieved. Generally, there are at least two approaches that have been considered: The first of these, solid phase inhibition, focuses on the modifying the polymer substrate to: 1) improve the thermal stability of the polymer which normally require more heat to decompose; 2) promote highly crosslinked char formation, which means that a concurrent decrease in the volatile product and the carbonaceous char can reduce the heat transfer from the flame and cut off diffusion of new fuel into the gas phase, and 3) generate water to cool the surface of the polymer and increase the amount of heat needed to maintain the flame.

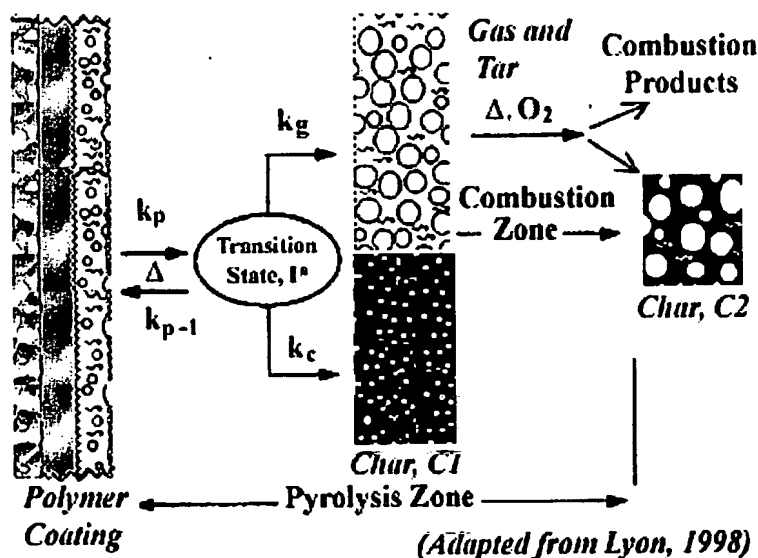


Figure 2.10-4: Kinetic model for polymer / coating flaming combustion.³⁸⁷

2.10-3 Magnesium Pyrolysis

The burning of many metals, notably magnesium, is a vapor-phase reaction and depends upon metal purity, metallurgical conditions, temperature, gas composition, and type of oxide film.³⁸⁸ These reactions have been noted to occur at some distance from the surface, and in the case of magnesium production of Mg vapor is a fairly simple task due to the fact that magnesium has a relatively low boiling point (1110°C). The ignition of a solid, e.g., a metal, will occur when the heating effect of the exothermal oxidation reaction overcomes the cooling of the solid by conduction, convection, and radiation. Some of the basic principles of spontaneous ignition of a metallic surface oxidizing at high temperature have been discussed by Hill, *et.al.*³⁸⁹

The pyrolysis of Mg metal is a red-ox reaction in addition to a combination and combustion reaction. Solid Mg metal begins as oxidation number 0, Mg^0 , and upon oxidation, both magnesium oxide and magnesium nitride the oxidation number of magnesium is 2^+ , Mg^{2+} ; magnesium has lost electrons therefore has been oxidized. Two types of energy are produced in this reaction heat energy 1) $\Delta H_f^{MgO} = -601.83 \text{ kJ/mole}$ (kiloJoules per mole) the 'heat of formation' for MgO the negative sign indicates the formation is exothermic; 2) light energy approximately 10% of the energy of combustion occurs as light in this reaction, more light than any other known reaction.³⁹⁰

The ignition temperature of magnesium and magnesium alloys in oxygen from 0.166 to 10 atmospheres pressure was studied by Fassell, *et.al.*³⁹¹ Ignition temperature was defined as the "explosion temperature", that is, the temperature at which the rate of oxidation suddenly becomes extremely rapid and a "flame" appears. They found that ignition temperature values were reproducible for any given alloy. Their experimental results indicated that the ignition temperature of magnesium was independent of the

nonprotective oxide film thickness which was not in agreement with the theory of Eyring and Zwolinski³⁹² which indicates that the ignition temperature is dependent on the oxide film thickness.

2.10-4 Metal Peroxide Formation

The pyrolysis of magnesium metal does not proceed through formation of magnesium peroxides, and on the contrary, magnesium 2^+ cations (Mg^{2+}) act as peroxide scavengers when heated due to their intrinsic charge density. From the preceding section, the general thermal decomposition process of non-halogen containing polymers involve production and propagation of reactive intermediates that participate in free radical pyrolysis in the presence of O_2^{2-} peroxides. The general feature regarding Beryllium, magnesium and calcium is that they don't form peroxides when heated in oxygen, but strontium and barium do. The reason being there is an increase in the tendency to form the peroxide as you go down the group as opposed to an increasing tendency to form the metal's oxide and oxygen from a peroxide (O_2^{2-}) as you go up the group. The general reaction of such a metal as the magnesium cation (2^+) with peroxide ion, O_2^{2-} occurs as depicted in Figure 2.10-5:

The covalent bond between the two oxygen atoms is relatively weak and if a small metal cation M^{2+} ion is brought into close proximity of the peroxide ion electrons in the peroxide ion will be strongly attracted towards the positive ion. As a result, the metal oxide ion as depicted in Figure 2.10-5, below, simply breaks off.

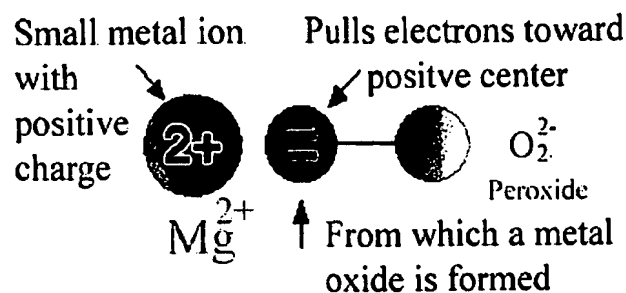


Figure 2.10-5: Metal cation (Mg^{2+}) / peroxide (O_2^{2-}) metal oxide forming reaction as opposed to pyrolysis.

It is said that the positive ion polarizes the negative ion which is more favorable if the positive ion is small and highly charged - if it has a high charge density. Therefore, ions of the metals at the top of the Group have such a high charge density (because they are so small) that any peroxide ion that comes near them falls to pieces to give an oxide and oxygen. However, as you go down the Group and the positive ions get bigger, by virtue of reduced charge density, they don't exert as much effect on the peroxide ion. Barium peroxide can form because the barium ion is so large that it doesn't exert such a devastating effect on the peroxide ions as the metals further up the Group. (See Appendix 2.10-4 for Fire retardant additives)

2.10-8 Testing Methods for Fire Retardant Coatings

Generally, flammability can not be measured by a single parameter because of the complex nature of the combustion process.³⁹³ For example, a structural house fire is likely to have different characteristics than an airplane fire, and therefore the resulting test methods developed to characterize different aspects of a material's combustion behavior must take into account such differences. Some parameters used to describe the combustion

of a polymer include ease of ignition, flame spread, ease of extinction, smoke obscuration, smoke toxicity, and heat release rate.^{Error! Bookmark not defined.,394,395}

A material's ease of ignition is an important parameter used to evaluate the fire resistance of a polymeric material because if the material can withstand exposure to a heat source without ignition, then combustion is prevented. This parameter can be measured by subjecting a sample of the material to an ignition source for a specific amount of time. The ignition source may either be a specific temperature or heat flux and the material is considered to have failed if it ignites under those conditions.³⁹⁶ The variables of interest in this test are: 1) the angle at which the sample is exposed to the ignition source, and 2) the heat flux of the source. From which the nature of flame propagation can be ascertained by varying the test angle of the specimen which results in a large differences the material's ignitability.

As a result of these conditions, significant differences in horizontal *versus* vertical tests are always observed. Materials with lower melting or softening points will always melt and flow away from the ignition source. Such effects are desirable in terms of fire resistance because if the melting or softening point of the material is lower than the ignition temperature, the material will simply flow away from the ignition source and avoid ignition. Generally, ignition resistance is usually accompanied by an increase in smoke emission and toxic gases, such as carbon monoxide.³⁹⁵ Once the material has ignited, the next important characteristic of the flame is how fast it spreads. This is parameter is especially important for materials that are used in construction and transportation applications.³⁹⁷

Different test methods have been developed for this purpose.³⁹⁸ For example, the test method FAR 25.853, developed by US Department of Transportation Federal Aviation Administration (FAA)³⁹⁹ is extensively utilized in the global aircraft industry. In this test, the specimen is oriented vertically, horizontally, or at a 45 degree angle and exposed to a specified Bunsen burner ignition source. Test criteria consist of burn distance, the occurrence of dripping behavior, and whether the material continue to burn once the ignition source is removed. In general, if a material ignites easily, then its flame will spread rapidly because the flame propagation front advances the ignition process.

Generally, flame spread depends on ignition temperature, orientation, thermal properties of the polymer, and flame heat flux. The orientation of the sample is an important variable in the flame spreading test. For example, a flame will spread up to one order of magnitude faster up a vertically orientated sample ignited at the bottom than has that same sample been ignited at the top. The reason being is that heat is transferred more efficiently ahead of the burning zone if flame propagation proceeds in an upward direction.⁴⁰⁰

A material's heat release rate is another factor⁴⁰¹ that is used to characterize the flammability of a polymeric material. Many experts in this area currently regard it as the most important variable in flammability testing.^{Error! Bookmark not defined.} Heat release rate is usually measured⁴⁰² by cone calorimetry, which is based on the oxygen consumption principle. A cone calorimeter is usually used to apply a specific heat flux to a material. The heat flux can be varied from 0 to 100 kW/m² to a sample that is either a horizontally or vertically mounted. It gives a measure of the ignitability, heat release rate, and toxic gases emitted from the sample.⁴⁰³

The material's ignitability is another parameter that is usually measured according to the time period over which a sample can withstand exposure to a specific heat flux before ignition occurs. Once the specimen has ignited, the heat release rate is measured as a function of time using the oxygen compensation method which is a measurement of the amount of oxygen consumed from an air stream. This test assumes that for each Joule of combustion heat generated, there is a proportional quantity of oxygen molecules depleted from the exhaust stream. However, in practice, the test measures flow rate and oxygen concentration levels.^{Error! Bookmark not defined.} Finally, from the heat release rate, the combustion process of a given material can be monitored and measured from start to finish.

Another important and well-established test methodology for evaluating flammability involves subjecting the material to a Limiting Oxygen Index (LOI) Test. The oxygen index test (ASTM D 2863), measures the minimum concentration of oxygen in a flowing mixture of oxygen and nitrogen that just supports flaming combustion of a sample that burns downward in a candle-like configuration (width 6.5 mm % length 70-150 mm % thickness 3 mm). Problems caused by melting and the results depending on the sample thickness and geometrical configuration were reported for this test.⁴⁰⁴ The relevance of this test to real fires has been questioned (the test measures the trend of an extinction limit of a material only under the specific conditions tested), but many chemists have long been using this test since the required equipment is inexpensive and only a small sample size is required.⁴⁰⁵

In the LOI test, a bar specimen is placed vertically in an up-stream atmosphere of oxygen and nitrogen and is ignited at the top. The composition of the atmosphere is

measured at the point at which self-sustained combustion occurs after ignition, and the LOI is calculated by the mole fraction of oxygen in the mixture according to Equ. 2.10-1:

Equation 2.10-1
$$LOI = \frac{[O_2]}{[O_2] + [N_2]} \times 100 \quad (1)$$

The advantage of the LOI method is its reproducibility and ranking of materials by a large number scale. This allows one to study the effect of chemical structure on the combustion behavior of a material. For example, a material with LOI >21, which is the mole fraction of oxygen in air, should not sustain combustion, see Table 2.10-1, below. However, because actual fire conditions are likely to be different from test fire conditions, a material is normally considered as flammable if the LOI is smaller than 26.⁴³²

Table 2.10-1: Limiting oxygen index (LOI) values of polymeric materials

Polymeric material	Limiting Oxygen Index (LOI)
Polyethylene	16 -17
Polystyrene	18-19
Epoxy-amine	21-25* **
Epoxy-amine-silane (modified)	32**
Polyamide (Nylon (6) – (6, 6)	24-29
Wool	26
Polysulfone	29-30
Phenol-formaldehyde	34-35
Poly(vinyl chloride)	45-49
Polytetrafluoroethylene	94-95

*(From VanKrevlen., 1975); (From X. Li et al. 2002)*⁴⁰⁶ (From C.LChaing et al. 2002)*

More modern test protocol / techniques can measure the flammability characteristics of ignition, heat release rate, and combustion products are the Cone Calorimeter Test (ASTM E 1354) and Factory Mutual Research Corporation's

Flammability Apparatus.^{407,408} These tests determine transient heat release rate by measuring transient oxygen consumption rate in the exhaust gases. Since the heat release from the unit mass of oxygen consumed during combustion is and LIFT or equivalent tests.^{409,410,411}

2.10-9 Thermal Degradation of Polyurethanes

Polyurethanes are a class of polymers that are susceptible to thermal, photo, chemical, and hydrolytic degradation. According to Wood *et al.*⁴¹², isocyanate-polyol stoichiometry is an important factor in revealing the structure and thermal properties of urethane-modified polyisocyanurates simply because polymer degradation is dependent on the relative amounts of urethane and isocyanurate linkages present.⁴¹³ The principle factor is the amount of isocyanate used, usually expressed as the isocyanate index which is a measure of the amount of isocyanate used relative to the theoretical stoichiometric amount.

What is often reported⁴¹⁴ is that a considerable excess of isocyanate, with a large proportion of the trimeric cyclic isocyanurate structure is what imparts significant thermal stability to the polymer.⁴¹⁵ The isocyanurate linkage has been reported to possess an inherently higher thermal stability than that of the urethane linkage, the latter dissociates easily at about 200°C⁴¹⁶ and that in general, flammability decreases as the proportion of isocyanurate increases.^{417,418,419} The degradation mechanisms of simple polyurethanes derived from poly(ethylene glycol) (PEG) and 4,4'-diisocyanato diphenylmethane (MDI) were studied in detail by Grassie and co-workers.^{420,421,422} Who suggested that polyurethanes break down by a combination of three independent pathways: (1) dissociation to the original polyol and isocyanate; (2) formation of a primary amine, an

alkene, and a carbon dioxide in a concerted reaction involving a six-membered cyclic transition state, and (3) formation of a secondary amine and carbon dioxide through a four-membered ring transition state, as shown Figure 2.10-6, below.^{423,424,425}

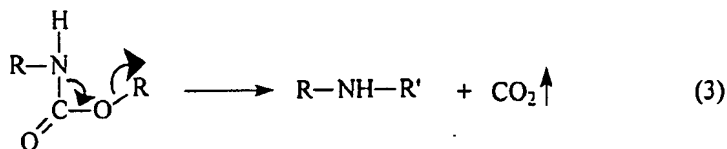
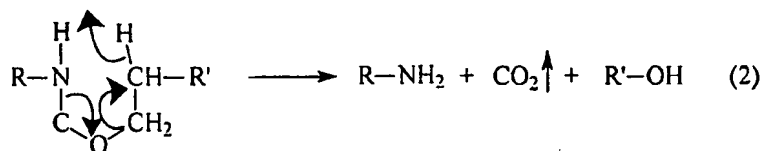
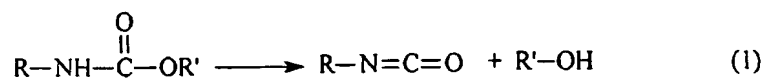


Figure 2.10-6: Scheme for thermal decomposition of polyurethane.

Where equation (1) which becomes significant at 150-160°C, was believed to be the predominant mechanism contributing to the primary degradation products, e.g. diisocyanate and diol, that have been identified through FTIR.⁴²⁶ These primary degradation

products can also give secondary decomposition products, such as carbondiimides, and according to Figure 2.10-7, below.^{427,428,429}

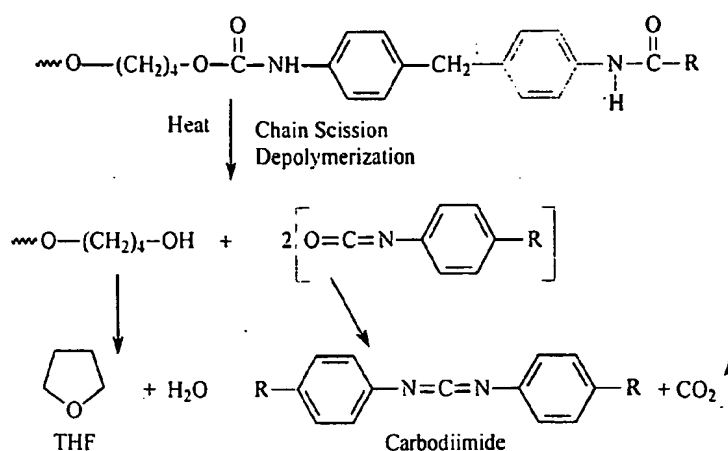


Figure 2.10-7: Pyrolysis of urthane linkage to yield carbodiimide.

In another example, Cunningham *et al.*⁴³⁰ undertook a study on the flame resistance of a series of polyisocyanurates and found that at a fixed isocyanate mass fraction the limiting oxygen index (LOI) increases with the increasing molecular mass of the polypropylene glycol (PPG) used in the formulation. Over a range of isocyanate mass fractions, they found the LOI of foam based on PPG of molecular mass 200 to be consistently lower than that of a comprised of PPG of molar mass. In a similar study Levcik *et al.*⁴¹⁵ examined the effect of melamine and its derivatives as fire retardants for nylon (6) and (6, 6) and found that melamine and melamine cyanurate provoke melt dripping and extinction of the flame without the formation of combustible drops. According to Williams⁴³¹ nylons show inherent fire retardancy, since they contain nitrogen in the structure. In contrast to aliphatic polyesters with an oxygen index (OI ~21), nylons have a higher (OI ~25) which is due solely to the presence of nitrogen between the isostructural units, Figure 2.10-8, below.

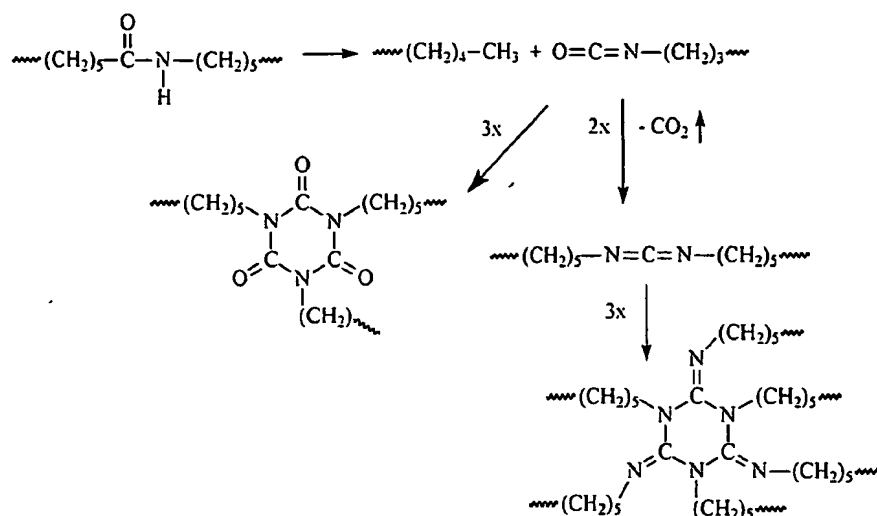


Figure 2.10-8: Thermal decomposition of nylon-6, formation of N-alkylisocyanurate.

According to Levčík *et al.*⁴¹⁵, the thermal decomposition of nylon-6 undergoes chain scission yielding carbodiimide functionalities where the resulting isocyanurate chain ends undergo dimerization to carbodiimide or trimerization to N-alkylisocyanurate. In addition, the carbodiimide can also trimerize to N-alkylisotriazine. These secondary reactions increase the thermal stability of the solid residue and increase the yield of the char.

2.10-11 Silane (Ceramers) Modified Epoxy Coatings

Van Krevelen⁴³², found that a linear relationship between LOI and the amount of char residue formed by halogen-free polymers existed and that a high char yield was correlated to an increase the flame retardance of the material. According to Pearce *et al.*⁴³³ an increase in formed char limits the amount of volatile carbon containing gases released, which decreases the extent of the pyrolysis reactions, as well as decreasing the thermal conductivity of the surface of the burning material.

The reported limiting oxygen indices (LOI) values for epoxy systems, see Table 2.10-1, vary from a low of 24 for typical pure epoxy amine / amide systems, to a high of 32 for silane modified ceramer epoxy.⁴³⁴ In a recent study Chang *et al.*⁴³⁴, prepared an epoxy containing silicon and phosphorous hybrid (modified epoxy ceramer) and compared its thermal degradation and flame retardance to that of a "pure epoxy". Based on kinetic studies from thermogravimetric data (TGA) they concluded that the thermal stability of a ceramer modified epoxy hybrid was no better than that of the pure epoxy. However, the ceramer modified epoxy possessed better flame retardance due to the higher percentage of char formed from high temperature pyrolysis. The reported char yield of the pure epoxy was reported at 14.8 wt. % and that of the modified epoxy hybrid was 31 wt. % at 800°C.

The corollary to Chiang *et al.*'s.⁴³⁴ experimental findings lie in the significance of activation energy results obtained from thermal degradation kinetic studies on the two polymer materials under nitrogen atmosphere conditions. Values of E_a (activation energy) for the modified epoxy hybrid were approximated at $E_a \sim 116$ kJ/mol while the pure epoxy was approximated at $E_a \sim 282$ kJ/mol. The smaller E_a lower activation energy value of the epoxy hybrid was attributed to the presence of the phosphorous-carbon bonding (P-C) which was hypothesized to be susceptible to chain scission during thermal degradation.⁴³⁵

⁴³⁶ Reported bond energies of P-C, C-C, C-O, and C-H are 260, 347, 284, and 368 kJ/mol respectively appear to corroborate the weakest-link-in-the chain effect.⁴³⁷

2.10-12 Summary

The most significant aspect of the following review is that it demonstrates the pyrolytic nature of both polymeric materials and magnesium metal. Most important is the fact that by virtue of its charge density Mg metal does not form highly combustible metal peroxides upon heating in oxygen which implies that combustion control of this metal can be achieved by other means associated with cooling of the solid by conduction, convection, and radiation. Another important aspect of the following review is that it demonstrates essential principles involved with the development of flame retardant polymeric materials used in coatings for two general classes of polymeric materials: 1) polymers synthesized via chain reaction or step-growth, and 2) polymeric materials via sol-gel or ceramer modified hybrids. These studies serve also to highlight the fact that not all polymeric materials are created equal and that polymer structure relation principles relate directly to a coating's flame resistance. In addition, it outlines some established measurement protocols for quantitatively determining the flammability parameters associated with a given polymeric material.

Finally, it addresses specific flammability studies of polyisocyanates / polyureas, revealing the essential reasons for the more inherent flame resistant qualities imparted to one class of polyurethanes over others. In addition, it provides further insight into how ceramer systems, for example, those derived from a ceramer modified epoxy polymeric material compare to the parent epoxy material. All of these studies are intended to supply a general background for further insight into developing cathodic protect coatings with pigemntary magnesium which is a significant part the material brought forth and developed in this thesis.

Refernces / Bibliography

- ³⁸³ Anon. "Handbook of fire retardant coatings and fire testing services" Technomic Publishing Co., Lancaster, Pa, 265 pp. (1994)
- ³⁸⁴ Vandersall, H.L., "Intumescent coating systems, their development and chemistry,, J. Fire Flamm., Vol. 2, pp. 97- 140 (1971)
- ³⁸⁵ Kay, M., Price A.F., and Lavery I., "A review of intumescent materials, with emphasis on melamine formulations" *J. Fire Retard. Chem.*, Vol. 6, pp. 69-79 (1979)
- ³⁸⁶ Finlayson, E. U., Aung, W., and Kashiwagi, T., "Theoretical Models for Combined Radiation-Conduction in Polymeric Solids Heated by External Radiative Fluz," *Proceedings of 1987 ASMEJSME Thermal Engineering Conference*, Vol. 1, ASME, New York, (1987)
- ³⁸⁷ Lyon, R.E., *Polymer Degredation and Stability*, Vol. 61, pp. 201-210 (1998)
- ³⁸⁸ *Pyrophoric Materials Handbook: Flammable Metals and Materials*, by Charles R. Schmitt, P.E., C.H.C.M.; Edited By Jeff Schmitt, Chapter 5
- ³⁸⁹ Hill, P. R. *et.al.*, "High Temperature Oxidation and Ignition of Metals," Report NACA RML 55L 23b, National Advisory Committee for Aeronautics, Langley Aeronautical Laboratory, Langley Field, VA (March 26, 1956)
- ³⁹⁰ Reynolds, W. C., "Investigation of Ignition Temperature of Solid Metals," Report No. NASA-TN-D182, National Aeronautics and Space Administration, Washington, D.C., (October, 1959)
- ³⁹¹ Fassell, W. M. Jr., *et.al.*, *Jour. of Metals*, Vol. 3, pp. 522-528 (1951)
- ³⁹² Eyring H., and Zwolinski, B. J., "The Critical Temperature for Combustion of Metals and Their Alloys," *Record of Chemical Progress*, Wayne University (July-October 1947)
- ³⁹³ National Research Council Publication NMAB-4772, *Improved Fire-and Smoke-Resistant Materials for Commercial Aircraft Interiors*, National Academy Press, Washington, D.C., (1995)
- ³⁹⁴ Fabris, H. J. and Sommer, J. G., *Rubber Chem. and Technol.*, Vol. 5, No.3, pp. 522 (1977)
- ³⁹⁵ National Research Council Publication NMAB-4772, *Improved Fire-and Smoke-Resistant Materials for Commercial Aircraft Interiors*, National Academy Press, Washington D.C., (1995)
- ³⁹⁶ Federal Motor Vehicle Safety Standard (FMVSS) 302-*Test Procedure and*

Specimen Preparation, Docket 3-3 Notice 6: Fed. Reg. 38 Nr. 95, May 17, (1973)

³⁹⁷ Babauskas, V. and Peacock, R. D., *Fire Safety Journal*, Vol. 18, pp. 255 (1992)

³⁹⁸ ISO R 3795, *Road Vehicles-Determination of burning behavior of interior materials for motor vehicles*

³⁹⁹ FAR 25.853 Appendix F, *Federal Rep.* Vol. 53, No. 165 25. Aug. (1988)

⁴⁰⁰ Li, B. and Wang, J., *J. Fire Sciences*, Vol. 15, No. 5, pp. 341-357 (1997)

⁴⁰¹ Babauskas, V., in *Flame Retardants '90*, Edit by The British Plastics Federation, Elsevier Applied Science, New York, (1990)

⁴⁰² Kaplan, H.L., Grand, A. F. and Hartzell, G. E., *Combustion Toxicology*, Technomic Publishing, Lancaster, PA, (1983)

⁴⁰³ *Fire Safety Aspects of Polymeric Materials Volume 1*, Technomic Publishing Co. Inc., Connecticut, (1977)

⁴⁰⁴ Van Krevelen, D. W., *Properties of Polymers*, Elsevier/North-Holland, New York, (1975)

⁴⁰⁵ Stuetz, D. E., Diedward, A. H., Zitomer, F. and Barnes, B. P., *Polym. Sci., Polym. Chem, Ed*, Vol. 18, pp. 967-985 (1980)

⁴⁰⁶ Li, X., Ou, Y., and Shi, Y., *Polymer Degradation and Stability*, Vol. 77, pp. 383-390 (2002)

⁴⁰⁷ Barbrauskas, V., *Fire Mater.* Vol. 8, pp. 81-95 (1984)

⁴⁰⁸ Tewarson, A. and Pion, R. F., *Combust, Flame*, Vol. 26, pp. 85-103 (1976)

⁴⁰⁹ Mitler, H. E., *Twenty-Third Symposium (Interaationrd) on Combustion*, The Combustion Institute, Pittsburgh, pp. 1715-1721. (1990)

⁴¹⁰ Cleary, T. G., and Quintiere, J. G., *Fire Safety Science Proceedings of the Third International Symposium*, Elsevier, London, pp. 647-656 (1991)

⁴¹¹ Karlsson, B., and Magmrsson, S. E., *Fire Safety Science—Proceedings of the Third International Symposium*, Elsevier, London, pp. 667-78 (1991)

⁴¹² Wood G, editor. *The ICI Polyurethanes Book 2*. Chichester: ICI/ Wiley, (1990)

⁴¹³ Duff, D.W., Maciel G.E., *Macromolecules*, Vol. 24., pp. 651, (1991)

- ⁴¹⁴ Duquesne, S., Le Bras, M., Bourbigot, S., *et al.*, *Polym. Degrad. Stab.*, Vol. 74, No. 3, pp. 493-499 (2001)
- ⁴¹⁵ Levchek, L.V., Levcheck, G.F., Balabanovich, I.A., Gambino, G., and Coasta, L., *Polym. Degrad. and Stab.*, Vol. 54, pp. 217-222 (1996)
- ⁴¹⁶ Reymore HE, Lockwood RJ, Ulrich H., *J. Cell. Plast.*, Vol. 14, pp. 332 (1979)
- ⁴¹⁷ Dick C, Dominguez-Rosado E, Eling B, Liggat JJ, Lindsay CI, Martin SC, *Polymer*, Vol. 42 pp. 913-23 (2001)
- ⁴¹⁸ Fabris, H.J., Thermal and oxidative stability of urethanes. *Advances in Urethane Science and Technology*, Vol. 4, pp. 891-911, (1976)
- ⁴¹⁹ Singh, LW, and Mollica, J.C., *Rubber Age*, Vol. 98, pp.12 (1966)
- ⁴²⁰ Grassie, N., and Scott, G., *Polymer Degradation and Stabilization*, Cambridge University Press, Cambridge, (1985)
- ⁴²¹ Grassie N, Zulfikar M., *J. Polym. Sci, Polym Chem Ed.* Vol.16, pp.1563 (1978)
- ⁴²² Grassie, N, and Perdomo-Mendoza, G.A., *Polym. Degrad. Stab.*, Vol. 10, pp. 267 (1985)
- ⁴²³ Jen, A.K., Wong, K.Y., Rao, V., Drost, K., and Mininni, R.M., *Mat. Res. Symp. Proc.*, Vol. 247, pp. 59 (1992)
- ⁴²⁴ Prasad, P.N. and Reinhardt B.A., *Chem. Mater.* Vol. 2, pp. 660 (1990)
- ⁴²⁵ Hampsch, H.L., Yang, J., Wong, G.K. and Torkelson, J.M., *Polym. Commun.*, Vol. 30, pp. 40 (1989)
- ⁴²⁶ Chao, D. Y., Kuo, W. J., Wang, N. H., Lee, C. L., and Yang, K. H., *J. Appl. Polym. Sci.*, Vol. 67, pp. 19-26 (1998)
- ⁴²⁷ Goodson, T. III, Gong, S. S. and Wang, C.H., *Macromolecules*, Vol. 27, pp. 4278 (1994)
- ⁴²⁸ Sullivan, L.A. and Lackritz, H.S., *Mat. Res. Soc. Symp. Proc.* Vol. 392, pp. 69 (1995)
- ⁴²⁹ Hampsch, H.L., Yang, J., Wong, G.K. and Torkelson, J.M., *Macromolecules*, Vol. 23, pp. 3648 (1990)
- ⁴³⁰ Cunningham A, Eling, B, Sparrow, DJ., *Cell Poly.*, Vol. 6 pp. 42-60 (1987)

- ⁴³¹ Williams, I.G., *Plastics Rubber Process. Application*, Vol. 4, pp.239 (1984)
- ⁴³² Van Krevelen, D.W., *Polymer*, Vol. 16, pp. 615 (1975)
- ⁴³³ Pearce, E.M.,and Liepins, R., *Environ. Health Perspect.*, Vol. 11, pp. 69 (1975)
- ⁴³⁴ Chiang, C-L., Wang, F-Y., Ma, C-C., M., and Chang, H-R., *Polym. Degrad. Stab.*, Vol. 77, pp. 273-278 (2002)
- ⁴³⁵ Corbridge, D.E.C., *Phosphorous*, Elsevier Co., (1990)
- ⁴³⁶ Montaudo, G., Puglisi, S., Scamporrino, C.E., and Vitalini, D. *Macromolecules*, Vol. 17, pp. 1605 (1984)
- ⁴³⁷ Shankwalkar, S.G., Crutz, C., *Ind. Eng. Chem. Res.*, Vol. 33, pp. 740 (1994)

Chapter 3 Initial Magnesium Rich Coatings Studies

3.1 Introduction

Environmentally allowable alternative coatings to chromate pigments and pretreatments for corrosion control of Al alloy 2024 T-3, commonly used in aircraft, have been designed, formulated and tested as primer coatings that provide protection using particulate Mg-rich pigmentation. The system was designed by analogy to pigmented Zn-rich primer coatings used for the protection of steel. Their anti-corrosive properties are based on two different mechanisms: 1) they serve as a barrier and; 2) they act as a cathodic protector. In the current study four coating polymer systems were examined as possible candidates as polymer matrices for Mg-rich cathodic protect coatings. Mg-rich primers were formulated with ~50-micron average particle size magnesium powder, near to the critical pigment volume concentration (CPVC) for this system. Scribed coatings systems in the initial study were subjected to Prohesion™ exposure in dilute Harrison's solution (NH_4SO_4) for up to 1,500 hours. The corrosion byproducts generated in the scribe areas during Prohesion™ exposure were examined by scanning electron microscopy (SEM) and the local pH of the coating was determined by the nature of the salt formed as a function of exposure conditions and time.

3.2 Overview of the Coating System

Following by analogy the formulation of Zn-rich primer coatings for the protection of steel, the formulation of Mg-rich primer coatings for protection of aluminum alloys has been examined in this laboratory. This work has as its motivation the protection of high strength aircraft Al alloys such as 2024 T-3 and 7075 T-6 without the use of chromate-

based pretreatments or chromate pigments. This class of alloys, whose high strength is based on phase separated intermetallic compounds within the bulk alloy, have proved resistant to efforts to develop corrosion protective (pretreatment + coating) systems that do not contain any Cr, a metal whose compounds are notorious for their toxicity and carcinogenicity.⁴³⁸ Further, any aircraft painting or repainting operation that utilizes Cr-based pretreatments generates large amounts of hazardous waste which can be handled properly only at great cost.⁴³⁹

The basic principles of Zn-rich primer coatings are as follows:⁴⁴⁰

1. Coatings are either organic or inorganic in nature.⁴⁴¹
2. They are pigmented with particulate Zn, in either spherical or flake form.
3. The PVC of the Zn pigment in the coating should exceed the CPVC in order for the coating to properly provide sacrificial / cathodic protection to the underlying steel substrate. Under these conditions, the Zn particles are all in mutual contact as well as in electrical contact with the steel substrate.
4. The mode of protection by these coatings is first sacrificial as long as the Zn is electrically connected to the steel as the Zn is more anodic (reactive) than Fe (major constituent of steel) in the electrochemical series, and then the mixed Zn oxides formed in the sacrificial oxidation fill damaged areas and also sometimes passivate the steel surface by their basic nature. There is some evidence that the electrical connectivity of the Zn particles carries over from the $PVC = CPVC$ (circa 60-70% by volume) to $PVC = \text{Volume Percolation Threshold for Zn}$ (~30% by volume for spherical particles), so some sacrificial protection occurs over this range even while

the Zn is being consumed by sacrificial oxidation.⁴⁴² The percolation threshold for flake pigments may be different depending on particle alignment.

5. The organic or inorganic matrix of the coating must be stable under the basic environment created by the zinc oxide, hydroxide, etc, formed from the oxidation of Zn in the presence of electrolyte. It must also adhere well to the steel alloys and be stable in a corroding environment.

6. These primer coatings must be top-coated to function properly and have a long field lifetime. When used properly, these primers provide almost as much protection to steel as galvanizing. With a topcoat, they provide both barrier and damage (sacrificial / cathodic) protection to steel substrates.

7. Zinc-rich films function sacrificially in the presence of a conductive electrolyte to protect the steel by discharging the corrosion current within the film and producing oxidized zinc.

Currently, satisfactory corrosion protection is not available for Al 2024 T-3 without the use of chromates, although many alternate options for protecting this alloy have been considered by this lab and others, including plasma polymer layers⁴⁴³ and conducting polymers.^{444,445} When the availability of particulate Mg for use as a pigment in coatings,⁴⁴⁶ became known in this lab it was decided to examine the possibility of designing Mg-rich coatings that would protect 2024 T-3 in a manner analogous to Zn protecting iron alloys (steel). There were two confounding features of considering Mg for cathodic protection of Al versus Zn for cathodic protection of Fe. The first was that particulate Mg can be a fire hazard, but this concern was alleviated by the manner in which

Mg pigment was delivered by Eckart*. Their particulate Mg has a thin oxide layer that stabilizes it against further oxidation. The second concern was that the oxidation products of Mg, MgO and its various hydroxides in hydrated form, would create such basic conditions that Al would undergo basic corrosion as is indicated in its Pourbaix diagram⁴⁴⁷ Figure 1-A, below. Fe is mostly passive under basic conditions, so this is not a valid consideration for Zn over steel. As shown below, the natural Mg oxidation products do not give a high enough pH to corrode and dissolve Al, so this concern was also alleviated.

The Pourbaix potential-pH diagram for aluminum, Figure 3.1-A, below, is based solely on thermodynamic parameters and does not provide information on the metal's corrosion rate. However, the diagrams can be used to predict relative oxide stability and resistance to general dissolution in the pH range of 4 to 9. As a rule, the protective oxide film on aluminum is stable in aqueous solutions over the pH range from 4.0 to 9.0. With regard to magnesium Perrault⁴⁴⁸ used thermodynamic data not available to Pourbaix to develop a potential-pH diagram shown in Figure 1-B, below, for magnesium. After considering the significance of MgH_2 and Mg^+ , Perrault concluded that a thermodynamic equilibrium did not exist for such a magnesium electrode in contact with an aqueous solution. He asserted that, on a magnesium surface, different reactions might be simultaneously involved, depending on the surface state of the magnesium. According to Krammer,⁴⁴⁹ aqueous magnesium hydroxide acts a pH buffer that does not exceed a pH~9.5 even in the presence of excess $\text{Mg}(\text{OH})_2$. Therefore, in the absence of an external acidic environment, pH conditions at the Al_2O_3 / $\text{Mg}(\text{OH})_2$ interface may not significantly exceed the pH~9 thermodynamic stability limit for aluminum.

* Eckart GmbH, Kaiserstrasse 30, Furth D-90763, Germany

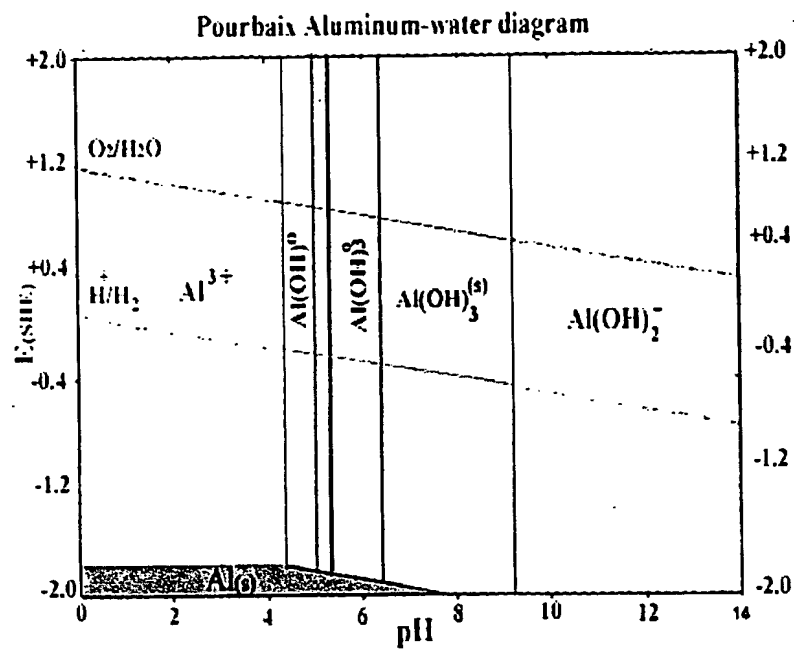
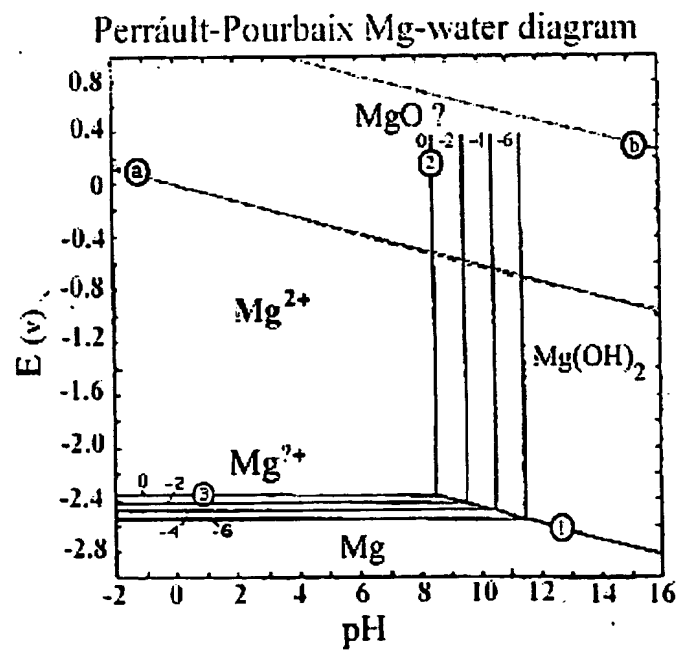


Figure 3.1-A: Pourbaix diagram for aluminum in water.⁴⁴⁷



3.1-B: Perrault-Pourbaix diagram⁴⁵⁰ for magnesium in water.

Usually, the oxide film is soluble in strong acids and alkalis. However, the corrosion of aluminum alloys cannot always be determined solely on the basis of pH alone, as the nature of and identity of the individual ions present in solution, such as Cl^- or Cu^{2+} , exert a significant influence on corrosion rate as well.

3.3 Further Considerations

The principle reason for undertaking this research is to develop a practical and suitable coating system for objects whose structural components are made up of aluminum alloys that require effective protection by an environmentally benign coating system. An example of a “real-use” situation of this technology would be to spray apply the magnesium powder primers to an aircraft exterior then follow-up with some kind of suitable top-coat. Once in service, *in situ* repair to damaged areas could be easily accommodated by simply sanding and reapplying both primer and top-coat. The complete coating system for cathodic protection of Al 2024 T-3 begins at the alloy interface with the polymeric binder vehicle itself. The ideal magnesium particle size distribution for this application should range from 10 to 200 microns. As submicron sized magnesium is rapidly consumed during the course of electrolyte exposure and macro sized Mg powder is highly prone to incineration. Overall, it is believed that with the correct pigment volume relationships, particle size, and polymeric binder system the top-coated Mg-rich primer systems would be capable of protecting Al 2024 T-3 over a wide variety of application conditions.

Moreover, another objective of the foregoing study has been to examine magnesium pigments as a potential raw material for use in anticorrosive Mg-rich primers and to determine the underlying relationships between primer coating polymer, magnesium PVC,

and corrosion by-products formed. It also aims at establishing how and if they may detrimentally affect the aluminum alloy during service. The significance of all these findings is that a more extensive knowledge base has been developed and tested on materials, formulation techniques, and application of coatings formulated with magnesium powders for cathodic protection of aluminum alloys. These results can now be compared and contrasted to coatings that both parallel and differ from existing zinc-rich coating systems, which have been used extensively to provide cathodic protection to steel structures. In summary, while the full optimization of this technology is yet to be realized, a wide range of possibilities and variations in coating polymer components exist, making this a most interesting and valuable raw material for use in achieving corrosion control with environmentally benign coating systems.

Finally, the system has been designed to be easy to apply and repair with any and all chromate pretreatments and chromate pigments eliminated altogether if used as the primer layer of a total coating system. In addition, the primer's polymeric matrix was developed with an environmentally acceptable solvent film carrier, propylene carbonate, which brought the coating material into compliance with more stringent VOC regulations that are now rigorously enforced.⁴⁵¹

3.4 Pigmented Metal-rich Coating Systems

Generally, organic binders used in cathodic primer systems have densities ranging from 1.0 g/cm³ for polyisocyanates to 1.16 g/cm³ for typical polyamide / BPA-epoxies, and when dissolved in a suitable solvent the density of the vehicle is far less than the bulk density of zinc. As a result of its higher density zinc powders tend to settle in all zinc-rich coatings which can cause considerable heterogeneities in many film applications.⁷ In zinc-

rich systems with organic vehicles, the outer surface of zinc oxide has been characterized as forming a dielectric vehicle sheath, (Hare and Wright, 1982)⁴⁵², composed of zinc oxide and organic binder. Zinc-rich coatings require that the pigmentary zinc be in close contact proximity in order to establish electrical conductivity. The fact is that metal-to-metal contact is never really possible in systems containing cohesive organic films. Only when (PVC/CPVC) is unity or above ($\Lambda = 1$) and the zinc/vehicle matrix achieves its closest packing array can the dielectric be reduced to a minimum level and electrical conductivity maximized.

3.5 Metals in the Coating Systems

Another important consideration in developing Mg-rich primers has been to accurately contrast the similarities and differences between the two analogous systems, Mg-rich vs Zn-rich, especially, in regard to the electrochemical behavior of the zinc-rich system immersed in an aqueous electrolyte. For example, Abreu *et al.*⁴⁵³, demonstrated that at the beginning of an experiment, when a zinc-rich paint (ZRP) is immersed into an electrolyte, the zinc-oxide covering the zinc particles immediately begins to react with the sodium-chloride solution, leading to better metal-to-metal electrical contact being established between zinc particles and the steel plate substrate. This initial immersion or "activation" period when the value of the corrosion potential shifts to a cathodic value corresponding to the zinc plate in the electrolyte has been explained in terms of the different times it takes to "activate" zinc particle as the thickness of the zinc oxide is different for different sized particles throughout the film. In addition, the physical effect of adsorbed polymer on the pigment surface causes it to behave as a dielectric which tends to retard the initial metal activation process as well. The first postulate ascribed to organic

zinc-rich systems is that in order for the organic Zn-rich primer to provide cathodic protection to a substrate the Zn particles must be packed close enough to touch each other and the steel substrate and conduct current generated by the zinc / steel galvanic cell. Generally, the principle difference between zinc pigmentation and magnesium is that zinc is a good metallic conductor, even when formulated below its CPVC. On the other hand, pigimentary magnesium is a relatively poor conductor for a metal but still a much better conductor than any coating polymer. However, as long as it supplies electrons and the potential is large enough to move them through the metal it is a valid conductor.

3.6 The Magnesium Metal Anode

Magnesium rich primer coatings may be viewed analogously to zinc rich systems, in that, as long as there is sufficient electrical conduction within the continuous film at the interface the aluminum alloy must remain protected so long as magnesium is available for corrosion. However, unlike zinc, magnesium metal has a density of 1.738 g / cm^3 and its micron sized powders, physically less dense, have bulk densities ranging from 0.87 to 0.58 g / cm^3 . In sharp contrast to zinc metal that has a density of 7.133 g / cm^3 , and even as a pigment has bulk densities in the range 4.56 to 5.20 g / cm^3 , depending on the polydispersity or particle size distribution (PSD) of the zinc spheres. Eckart GmbH, ECKA™ metallic magnesium powder produced from p-magnesium 99.95 % to (Deutsches Institut für Normung) DIN 17800 part-7 standards with Mg content @ 96% and MgO (magnesium oxide) content @ 4%.

Bulk density measurements were taken of the Mg powders, as received from Eckart, by filling and refilling a 50-ml graduated cylinder with powder and then weighing the powder after sonicating the cylinder at 400-Watts for 45 minutes to help disperse the

powder. The bulk density calculation for each sample involved a measured weight, in grams, of the final 50 ml volume of Mg-powder. Generally, the particle mixture values obtained of the sub-micron / micron powders, with mean particle size distributions (PSD)s in the range of 20 to 50 micron had bulk densities values of 0.68-to-0.79 g/ cm³; while larger mean PSD Mg-powders circa 200 micron yielded bulk density values in the range of 0.58-to-0.61 g/ cm³.

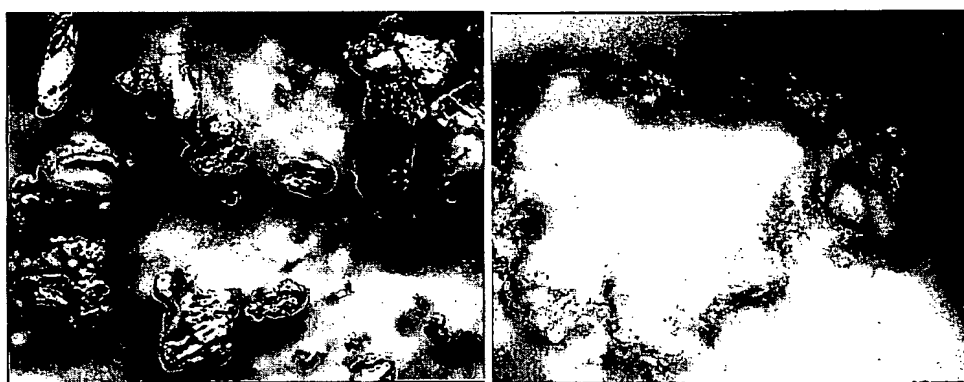
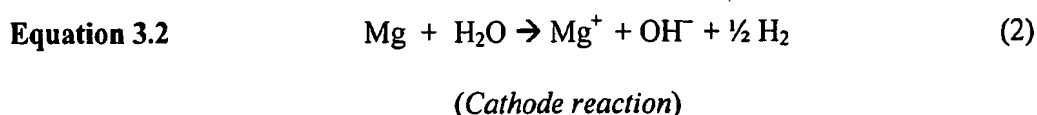
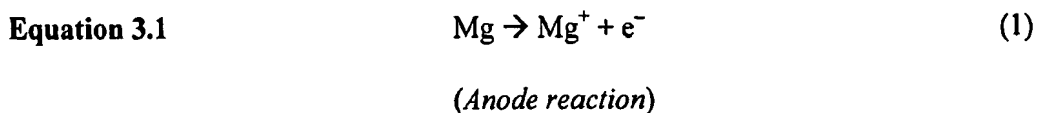


Figure 3.2: 50 micron average particle size Mg-powder, *left* optical microscope image at 20-% and *right* Raman microscope image at 50-% magnification.

In a recent publication, Song and Atrens⁴⁵⁴ describe magnesium cathodes based upon the hydrogen overvoltage⁴⁵⁵ developed between the two metals in the galvanic couple. Their assessment was that metals, such as (Al, Zn, Cd, and Sn) that combined an active corrosion potential with a high hydrogen overpotential constituted better cathodes for magnesium than those with low hydrogen overpotentials, such as (Fe, Ni, and Cu) as the later are highly efficient and can cause severe galvanic corrosion to occur. In the same study, Song and Atrens⁴⁵⁴ describe and propose a unified model for magnesium's anomalous electrochemical behavior known as the negative difference effect (NDE) discussed in section *chapter 2.8* literature review. The NDE effect was first described by Petty, *et al.*⁴⁵⁶; followed by Tunold *et al.*⁴⁵⁷; Rausch *et al.*⁴⁵⁸; Kokoulina *et. al.*⁴⁵⁹; James *et*

al.⁴⁶⁰ as a relationship between the anodic current density and an excess corrosion rate at low current densities. According to the model the anodic dissolution of magnesium only involves one electron, Equ. 3.1 and 3.2, below.



Half of the electrons are consumed, which means that at the same current density, more magnesium is dissolved than expected.⁴⁶¹ Magnesium is first oxidized to the intermediate Mg^+ ion and then chemically reacts with water to produce hydrogen and Mg^{2+} . In contrast with aluminum that forms a stable surface film that prevents the NDE from occurring, magnesium suffers high corrosion rates in aqueous solutions in the presence of anions as (Cl^- , SO_4^{2-} , or OH^-) due to this phenomenon.⁴⁵⁴

The efficiency of magnesium as a sacrificial anode has been discussed in terms of the negative difference effect (NDE), overpotential, and the dissolution of Mg through two different mechanisms, that depend on applied potential. All of which imply that 1) according to NDE Mg is an effective anode in the reduction of hydrogen; 2) the overpotential between Mg and Al is relatively high indicating that excessive galvanic corrosion does not quickly generate a burned-out anode; 3) In the presence of chloride salt / solutions the efficiency of Mg as a sacrificial anode depends on the monovalent process that corresponds to charge-transfer-controlled kinetics involving one electron process. Therefore, according to López-Buisán Natta⁴⁶¹ anodic Mg dissolution takes place through

two different mechanisms that depend on applied potential. The experimental observations for anodic dissolution of magnesium are as follows:

1) The monovalent process $\text{Mg} \rightarrow \text{Mg}^+$ at low potential (LP), with $E_1 = -1.56 \text{ V(SCE)}$, with Taffel slope 0.239 V/decade involving charge transfer kinetics with anodic transfer coefficient of 0.25.

2) The divalent process $\text{Mg} \rightarrow \text{Mg}^{2+}$ at higher potential (HP) with $E_2 = -2.78 \text{ V (SCE)}$ with Taffel slope 0.102 V/decade with charge transfer involving two electrons with anodic transfer coefficient of 0.29.

At LP, Mg^+ electrochemical production starts. Mg^{2+} is produced non-electrochemically as a result of the reaction of Mg^+ with an oxidant or through disproportionation. At HP, the electrochemical production of Mg^{2+} starts, in parallel with the mechanism of LP. The primary effect of the NDE in evaluating Mg-rich coatings is its relevance to the monovalent single electron transfer process observed in the initial OCP value as tested in NaCl solutions.²⁴

3.7 Proof of Concept: Initial Prohesion™ Exposure

Some general observations regarding initial epoxy binder matrices for Mg-rich primers show that ambient temperature cure epoxy/amide systems appear to wet the Mg pigments well and as a result yielded good adhesion to the aluminum alloy. For example, the combination of Epicure™ 3115 (fatty acid polyamide) and Epon™ 1001CX (solid DGEBA resin, (EEW~450), epoxide equivalent weight (EEW) as discussed in literature review section Chapter 2.9, is often used in epoxy coatings that function as high solids primers. The combination of this kind of epoxy / polyamide system is widely used in

reactive metals zinc-rich systems, but when used as a primer vehicle for Al 2024-T3, this polymer is always augmented with a strontium chromate surface pretreatment. Work done in this laboratory has shown that polyamide cured DGEBA-epoxy systems do not possess acid stability below pH~3.

In contrast to the polyamide-cured epoxy systems, ambient, 2K systems formulated with polyamines such as Ancamine™ 2422 (AHEW~49, adducted-polyamine)⁴⁶² amine hydrogen equivalent weight (AHEW) as discussed in literature review section Chapter 2.9, such epoxy curatives utilizing DER™-331 or Epon™ 828 (Liquid DGEBA resin, EEW~188) can yield improved acid / base and chemical resistance, but overall lacked flexibility and as a result their adhesion to metal was severely compromised. In addition, such polyamines based on primary amines are high surface tension liquids, [circa 40–45 dyne-cm making them slightly incompatible with epoxy resins circa ~30 dyne-cm] causing them to yield poor pigment wetting and thus limiting their utility to formulations below CPVC.

The initial studies performed with two-component epoxies formulated with primary amines, such as Ancamine™ 2422, yielded coatings that were hard and brittle with poor adhesion to the AA 20420T-3 substrate. Moreover, the first Mg-rich coatings formulated with high functionality polyamines, turned from colorless to green, probably as a result of a reaction involving the curative's primary amines with Cu^0 in the magnesium metal and atmospheric moisture. Overall, it was observed that the performance of the off-the-shelf (OTS) systems, polyamine, and polyamide was not satisfactory enough for them to be used as a robust polymer matrix for Mg-rich coatings. Of the two classes of curatives tested the ambient cure polyamides were observed to better wet the Mg pigment and form uniform

films at both high and low PVCs. This was determined by comparing unpigmented 2-mil film thickness films cast on 5" x 3" x .025" Q-Panel Al 3115, and subjecting them to 1) ASTM D2794-93 Reverse Impact and; 2) D522-93a(2001) Standard Test Methods for Mandrel Bend Test of Attached Organic Coatings, 1/8" mandrel. Generally, the polyamide systems were found to possess better adhesion to the Al 22420 T-3 substrate than the polyamines. In addition, these polyamine / epoxy coatings were observed to delaminate and crack when flexed or stressed while the polyamide cured coatings were observed to possess on average better than + 60 lb-inch reverse impact ASTM D 3363. The three stand out problems associated with these 2K epoxy systems tested as a primer vehicle for Mg-rich primers was that:

1. Blistering and delamination occurred at alloy interface (probably due to evolution of hydrogen gas) as a result of magnesium metal being oxidized by acid.
2. Adhesion of high metal volume content coating to the Al alloy surface appears to require a polymeric binder with excellent wetting of the alloy surface.
3. The polymeric matrix must develop good solvent resistance with a minimal development of internal stress.

The polymeric binder matrix chosen for the first Mg-rich primer study was a moisture cure epoxy system. The curative was based upon a ketimine (Schiff base) derived from aminoethylpiperazine (AEP) and methyl ethyl ketone (MEK) synthesized in this laboratory. It was added to EPON 1001CX-75, EEW-450 (solid DEGEBA cut in MEK and xylene). The reasoning for choosing a curative based on an AEP / MEK Schiff base was based on early observations that modified primary amines yielded green epoxy coatings when mixed with magnesium powder. This is thought to be due to the amine

solubilizing and complexing with Cu^{2+} in the presence of atmospheric moisture. Primary amines are hygroscopic while ketimines may be more hydrophobic and not readily solubilize the Cu^0 . Therefore, it was reasoned that by controlling the concentration of primary amine released in the coating, the discoloration effect could be minimized or eliminated. In the end, results from the (AEP/ MEK Schiff-base) cured epoxy primers proved successful as the discoloration of the Mg-rich primers did not occur.

A brief description of the procedure involved with the synthesis of an AEP / MEK ketimine involves an azeotropic distillation⁴⁶³ of aminoethylpiperazine (AEP) and methyl ethyl ketone (MEK) and in toluene at 126°C for three hours. The Schiff base ketimine was separated from the toluene liquor by evaporation with a rotavap apparatus. The product was characterized by Fourier transform infrared (FTIR) spectroscopy, Figure-3.3, spectra.

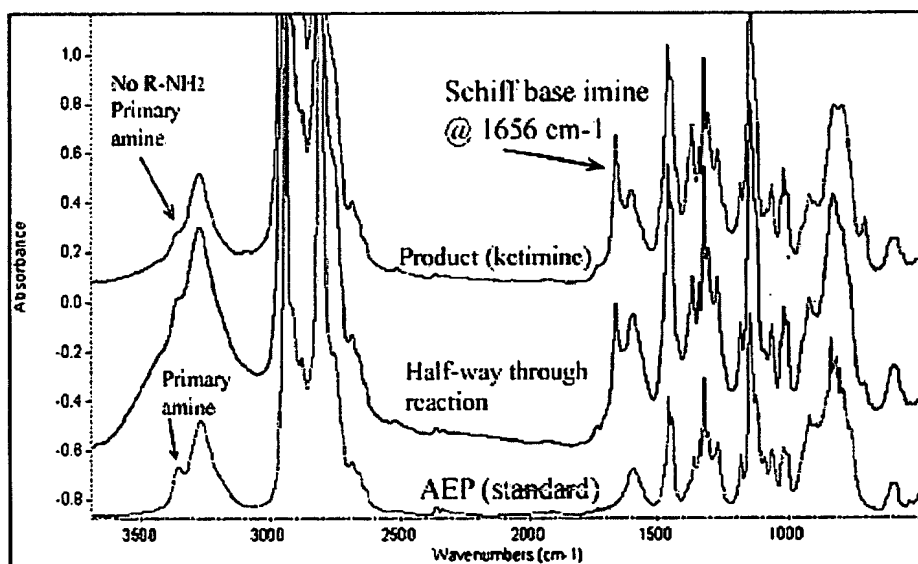
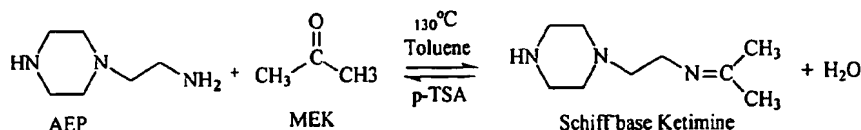


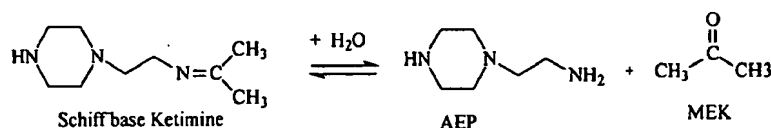
Figure-3.3: FTIR spectra of aminoethyl piperazine (AEP) Epi-Cure 3200 (standard) IR frequencies: 762 cm^{-1} : NH_2 deformation of primary amine; 829 cm^{-1} : secondary amino, end of piperazine ring N-H wag; 1013 cm^{-1} : aliphatic amine; 1247 cm^{-1} : secondary amine end of piperazine ring; 1590 cm^{-1} to 1610 cm^{-1} : primary and secondary amino NH deformation, primary higher than secondary; 3347 cm^{-1} ; 3285 cm^{-1} : amines N-H stretch.

The formation of the Schiff base reaction Figure 3.4-1, below, occurs under general acid catalysis, such as para-toluene sulfonic acid. Figure 3.4 -2, water's attack of on the Schiff base imine and the reverse reaction, which is the dehydration of the carbinolamine addition compound. The product ketimine Figure 3.4-3, below, the starting material upon dehydration yielded a primary amine with a low amine hydrogen equivalent weight (AHEW) and when combined with an epoxy possessing a relatively high epoxide equivalent weight (EEW) yielded reaction Figure 3.4, below.

1)



2)



3)

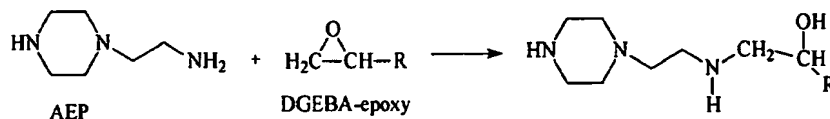


Figure-3.4: Reaction schemes 1-3, for 1) the synthesis of the aminoethylpiperazine / MEK ketimine (Schiff-base); 2) carbinolamine reaction with water to regenerate primary amine 3) Epoxy-amine reaction, primary amine AEP with DGEBA oxirane to yield alkinolamine.

The principle reasoning for formulating (with a lower AHEW polyamine) was that by combining a low (AHEW) ketimine curative with a high (EEW) less amine, by mass, would be required to cure the epoxy. Based upon the fact that polyamines have varying to limited solubility in DGBA epoxy resins, as reviewed in Chapter 2.9. What is observed is that that polyamines form domains at the interface that influence the microstructure of the

polymeric matrix formed. As reviewed in Chapter 2.9, excess amine limits the coatings performance properties. Therefore, the result of a lower AHEW species would be that the amine would be more solubilized by the epoxy resin and not and not partition and that the ketimine would not separate and partition as readily at an interface as would a primary polyamine.⁴⁶⁴ In addition, it is surmised that a moisture cure polyamine avoids the effect of rapid crosslink formation that can lead to high internal stresses developing in the coating film.

A another reason for choosing AEP is the presence of its heterocyclic ring, which is known to catalyze epoxide reactions, thus obviating the need to add nonylphenol catalysts, which in turn leads to water sensitivity issues. As a result, the negative effects of the amine were minimized, and the green salts did not form in the presence of the Mg-powder and atmospheric water. Simple performance tests used to screen the 2K systems showed that the 2K (AEP/ MEK Schiff base) DGEBA epoxy yielded acceptable results. Reverse impact was better than 60 inch-lb, and mandrel cone bend was 180° over a 1/8" mandrel. Solvent resistance was estimated at (+) 200 MEK double-rubs.

3.8 Panel and Film Preparation

The primers from materials in (Table 2) were prepared using conventional techniques. Primers were applied to 6" x 3" Al 2024 T3 Q-panels™, scrubbed with a Scotch Brite™ pad, rinsed and degreased with methyl ethyl ketone (MEK), then rinsed with distilled water. The first Mg-rich coatings were applied with a touch-up spray gun, the coatings cured at 35° C for 14 days, and the resulting film thicknesses measured with an Elcometer© film thickness device. The average film thickness was 3.0 +/- 0.5 mils.

3.9 Initial Exposure Studies Using the Prohesion™ Cycle

Prohesion™ exposure was performed according to ASTM D5894-96. The Mg-rich panels were prepared by covering panel backside and edges with 3M electroplater's tape and edges were then sealed with a 2K industrial epoxy from Aldrich. The panels were scribed through the entire coating with a carbide tip glass scribe, forming an X pattern, thus exposing the Al surface. Prohesion™ cyclic exposure in dilute Harrison's solution with no topcoat follows three distinct events:

1. EDXA spectra have revealed formation of magnesium carbonate hydrates at the primer liquid/vapor interface, dypingite $[\text{Mg}_5(\text{CO}_3)_4(\text{OH})_2 \cdot 8\text{H}_2\text{O}]$ and hydromagnesite $[\text{Mg}_5(\text{CO}_3)_4(\text{OH})_2 \cdot 4\text{H}_2\text{O}]$. These salts have been observed only to be present up to the first 500 hours of exposure for all non top-coated primed Mg-rich panels tested.
2. For exposure times beyond 500-hours cause brucite $[\text{Mg}(\text{OH})_2]$ domains to form and subsequently extend throughout the bulk of the primer. During this time the aluminum alloy remains cathodically protected as scribed lines remain unblemished.
3. For exposure times greater than 1300 hours, primer failure and film delamination corresponds to the accumulation of hexahydrite $[(\text{MgSO}_4) \cdot 6\text{H}_2\text{O}]$ compound at the interface.

Failure occurs see Figure 3.8, below, when Mg-metal and brucite structure have been depleted from the coating polymer matrix and sufficient hexahydrite salts have accumulated at the alloy interface. At which time the coating polymer ruptures and fragments from compressive forces exerted by hexahydrite structures.

In the first 24 hours of exposure to salt fog solution with atmospheric CO_2 , magnesium forms magnesium carbonate, $\text{Mg}_5(\text{OH})_5 \cdot \text{CO}_3$, which is replaced by a more densely packed

magnesium hydroxide $\text{Mg}(\text{OH})_2$ pseudo-hexagonal crystal structure. The rosette structure observed in the magnesium epoxy primer scanning electron microscopy (SEM) images shown in Figure 3.5, below, is consistent with *brucite* magnesium hydroxide $\text{Mg}(\text{OH})_2$ (acicular needle) crystal formed in Prohesion exposure. Further observations were made from results of Mg-rich primers exposed to Prohesion cyclic salt fog with dilute Harrison's solution see Figure(s) 3.5 –to- 3.8, below:

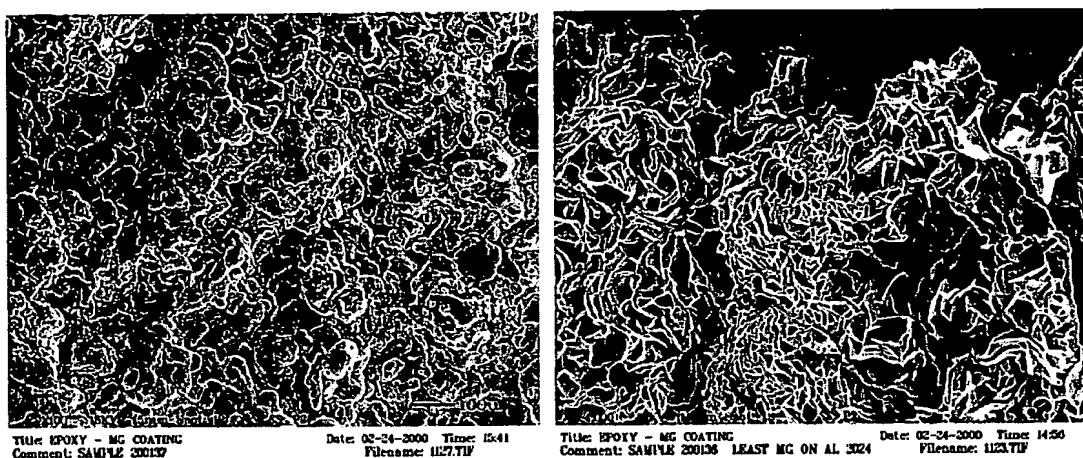


Figure-3.5: SEM image, exposed Mg rich panel, with brucite rosette structure at 1,300 hrs Prohesion™ exposure at *left* 100-% magnification and *right* 4,000-% magnification.

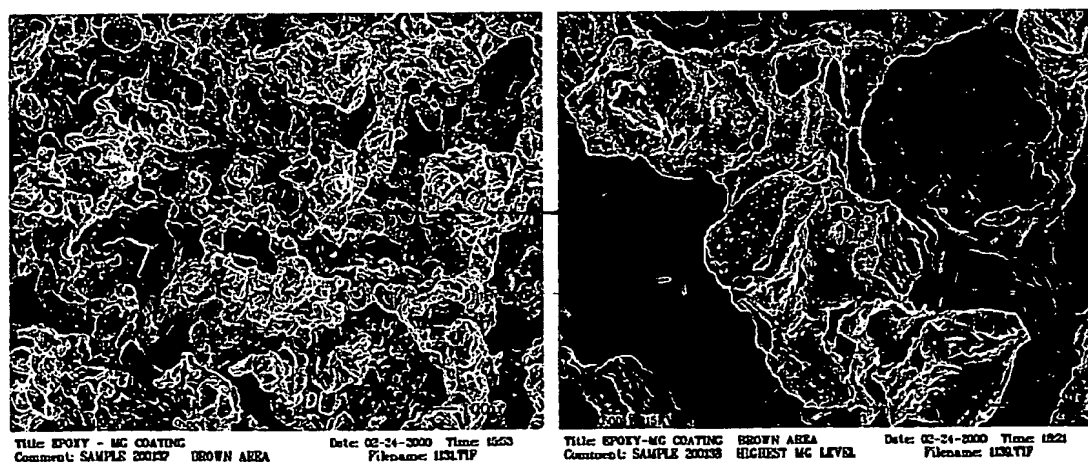


Figure-3.6: SEM image of exposed depleted area of Mg-rich coating after 1,300 hrs. Prohesion™ exposure *left* 100-% magnification and *right* 500-% magnification.

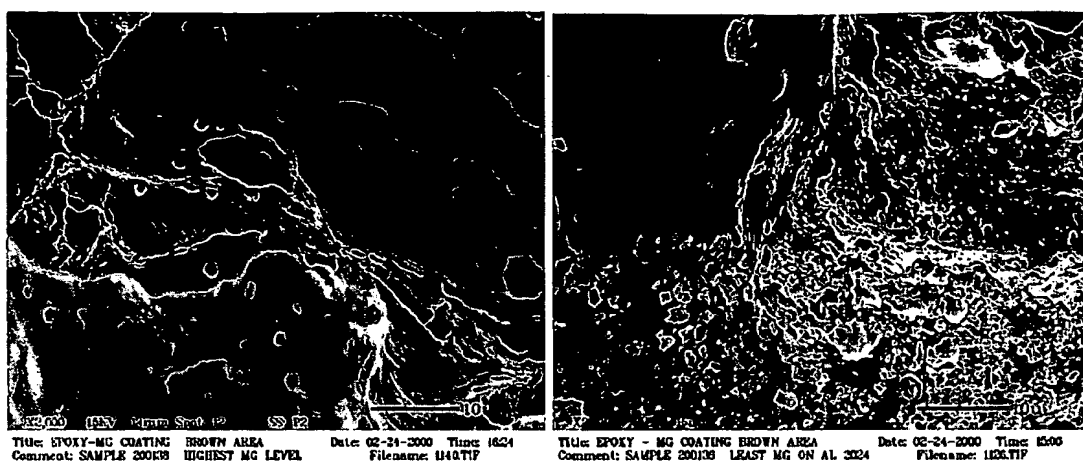


Figure-3.7: SEM image of exposed Mg rich coating depleted of Mg after 1,300 hrs. Prohesion™ exposure *left* 2,000-% magnification and *right* 3,000-% magnification.

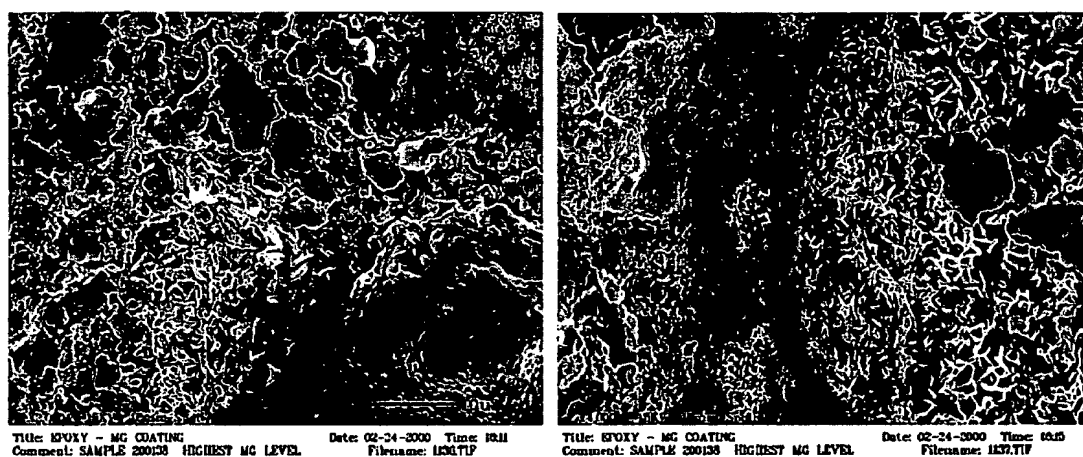


Figure-3.8: SEM image of exposed Mg rich coating development of Hexahydrite structure at the underside of Mg-rich coating after 1,300 hrs. Prohesion™ exposure *left* 2,000-% magnification and *right* 4,000-% magnification.

1) White oxide area magnesium hydroxide (brucite) formed over magnesium metal and energy dispersed X-ray analysis (EDXA) measurements indicated the presence of magnesium, oxygen and aluminum with a minimum amount of carbon detected.

2) In the scribed area with no epoxy matrix or magnesium metal originally present, EDXA spectra show carbon, oxygen, magnesium and aluminum with possible presence of dypingite (magnesium carbonate) structure over the exposed aluminum surface.

Table 3.1: Magnesium salts solubility and pH

Salt (designation)		K_{sp}	H ₂ O g/100ml	pH
Mg(OH) ₂	<i>Brucite</i>	7.1×10^{-12} *	7.8×10^{-4}	9.6 ~ 10.4 **
MgCO ₃ •H ₂ O	<i>Magnesite</i>	3.8×10^{-6} *	0.002 ***	8.0 ~ 8.8 ***
MgSO ₄ •H ₂ O	<i>Hexahydrate</i>	(soluble)	95 ***	6 ~ 9 ***

* CRC Handbook of Chemistry and Physics, 68th Ed., Boca Raton, FL (1987-88)

** Kramer, D., Magnesium, its Alloys and Compounds, US Geological Survey Open-File Report 01-341

*** Seelig, B.D., Salinity and Sodicity in North Dakota Soils, EB-57, North Dakota Extension Service, May 2000

In summary, Table 3.1, gives the relative pH, the solubility product, and the water solubility for magnesium salts identified in EDXA and SEM spectra. It was observed that the salts generated during the first 1000 hours of exposure increased in local pH according to a stratification scheme from the coating / alloy surface interface toward the external surface of the coating.

The degradation process of Mg-rich coatings exposed to the acidic environment of the dilute Harrison's solution may be described as follows. From Figure 3.8, above, SEM image of underside of exposed Mg-rich coating. The more acidic salts (i.e., hexahydrate) were identified at the alloy interface where local pH conditions may have been affected by the polarization of Al metal. While the salts found at the surface of the coating nearest to the remaining Mg(OH)₂ structure, are identified as species with a higher pH. In addition, damaged areas did not degrade either the coating polymer or the alloy surface until after the depletion of Mg(OH)₂ and the accumulation of hexahydrate salts occurred. According

to Kramer⁴⁶⁵, aqueous magnesium hydroxide acts a pH buffer that does not exceed a pH of about 10.0 even in the presence of excess $\text{Mg}(\text{OH})_2$. It would be surmised that the presence of other metal cations in solution might cause this value to be slightly higher or lower. For example, the addition of sodium hydroxide elevates the equilibrium pH of $\text{Mg}(\text{OH})_2$ to a slightly higher value depending on concentration.²⁸

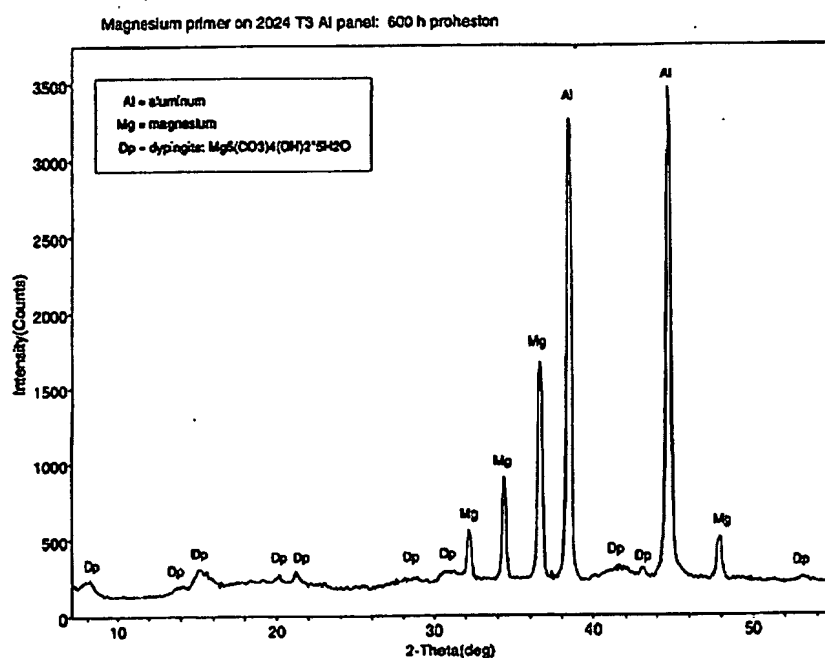


Figure-3.9: Disperse x-ray pattern of dypingite: $\text{Mg}_5(\text{CO}_3)_4(\text{OH})_2 \cdot 5\text{H}_2\text{O}$ from surface of exposed Mg rich panel at 600 hrs. ProhesionTM exposure.

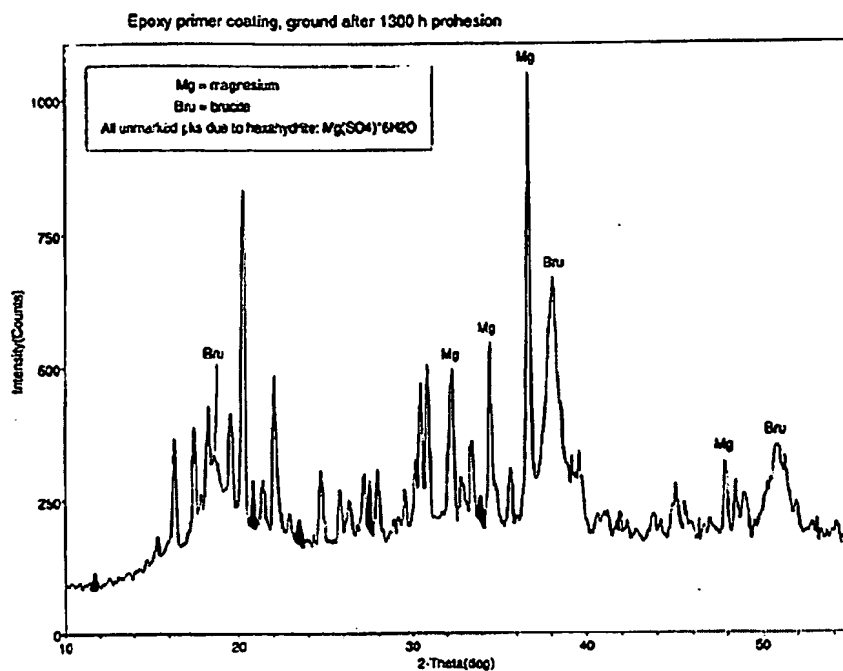


Figure-3.10: Disperse x-ray pattern of brucite: $\text{Mg}(\text{OH})_2$ from surface of exposed Mg rich panel at 1,300 hrs. Prohesion™.

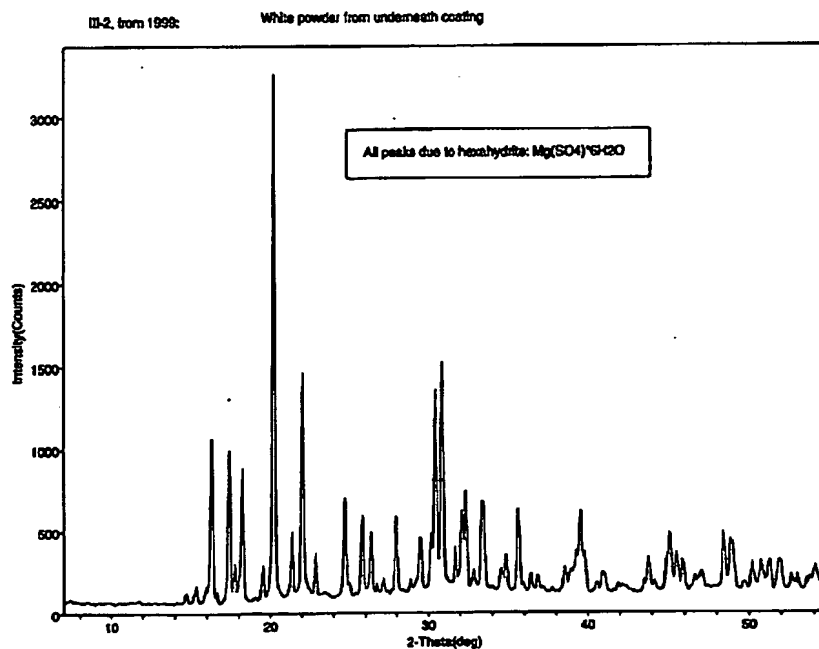


Figure-3.11 Disperse x-ray pattern Disperse x-ray pattern of hexahydrate: $\text{MgSO}_4 \cdot 6\text{H}_2\text{O}$ from underside of exposed Mg rich panel at 1,300 hrs. Prohesion™.

The corollary to these exposure studies lies in the chemical similarities between magnesium and zinc, both of which have hexagonal close packed HCP crystal structures and 2^+ valence and form similar sulphates, hydroxides and oxychlorides. What has been observed in x-ray diffraction data from Mg-rich coatings corroding in slightly acidic conditions can be contrasted to analogous Zn-rich systems that have been studied in slightly acidic conditions. The physio-chemical description of such a process was documented by Almeida *et al.*⁴⁶⁶, who found that zinc, in zinc rich polyamide primers upon exposure to salt spray in the presence of CO_2 and Chloride ion formed analogous salts. For example, a zinc carbonate $\text{Zn}_5(\text{OH})_5\cdot\text{CO}_3$ compound was observed to form at the surface during the first 24-hours of exposure. Later this salt was replaced by a more densely packed zinc chloride $\text{Zn}_5(\text{OH})_8\text{Cl}_2\cdot 2\text{H}_2\text{O}$ (pseudo-hexagonal) crystal structure. According to Evans⁴⁶⁷, this is thought due to the polarizability of the surface active chloride ions ($8.9\text{cm}^3/\text{mole}$) that displace the carbonate ions of (lower polarizability, $4.1\text{cm}^3/\text{mole}$) from the inner Helmholtz layer, leading to their preferential adsorption onto the surface of the zinc. Therefore, an overview of this adsorption cycle can be described in terms of carbonate's initial accumulation at the metal surface, as its polarizability is higher than that of water ($3.7\text{cm}^3/\text{mole}$), at which time it displaces water from the Helmholtz region with subsequent formation of zinc carbonate. Subsequently, other anions of higher polarizability such as Cl^- eventually adsorb and displace those of lower polarizability. The rosette structure observed in the SEM image Figure 3.5, above, for brucite is similar to the zinc chloride $\text{Zn}_5(\text{OH})_8\text{Cl}_2\cdot 2\text{H}_2\text{O}$ (pseudo-hexagonal) structure that is observed to form upon exposure to NaCl in sal spray testing.⁴⁶⁷

3.10 Summary Mg-rich Primer Exposure Studies

The major cause of primer adhesion failure in early stages of corrosion is disruption of the primer surface by corrosion generated by hydroxides. The rate of corrosion induced adhesion failure is apparently related to the ease of hydrolysis of polymer network. Upon initial exposure the acidic (pH~4.5) solution quickly attacks magnesium metal yielding hydrogen gas H_2 , the metal oxide MgO , and brucite the metal's hydroxide $Mg(OH)_2$. (1) Primer PVC (pigment volume concentration) was found to strongly influence integrity of exposed primer coatings. (2) High PVC metal content primers contain more surface metal available to serve as sacrificial anode, thus elevating PVC far above CPVC extends galvanic protection to both binder and alloy; however, lower available binder concentration at the metal anode surface caused poor adhesion between primer and interface. Poorly encapsulated magnesium in a sulfate solution quickly forms a high volume of interlaced hydroxide extending over the metal's surface. (3) Lower PVC metal load primers develop lower surface hydroxide coverage thus are prone to develop aluminum oxides sooner when alloy surface is damaged or exposed. Formulating primers near CPVC causing particles to pack and connect thereby increasing the coatings effectiveness to serve as a sacrificial anode. Elevating the PVC of a primer above CPVC increases the exposed anode surface area, more anode metal delivers more protection. Primers formulated far above CPVC lack sufficient binder required to effectively encapsulate the metal, as a result connectivity and volume of brucite formed over the surface is greater and more uniform. Generally, primers formulated above CPVC will perform poorly in immersion testing as they are designed to be used with a topcoat.

3.11 Primer Polymer Matrix

The first proof of concept from initial electrochemical and exposure studies⁴⁶⁸ performed on Mg-rich primers in the Bierwagen group involved a study on the effect of pigment volume concentration (PVC) on Mg-rich primers formulated at or near critical pigment volume concentration (CPVC) subjected to a three (3) percent solution of sodium chloride neutral electrolyte. This neutral electrolyte more fairly resembles Mg systems. The study involved testing primers formulated with Eckart Mg powders at pigment volume concentrations near CPVC with commercially available OTS ambient temperature cure (22°C / 72°F) epoxy/polyamines. The primer vehicle for these experiments consisted of digycidyl ether of bisphenol A (DGEBA) Epon™ 1001 with an epoxide equivalent weight (EEW \approx 450) and a popular commercially formulated polyamide Ancamid™-2353 with an amine hydrogen equivalent weight (AHEW \approx 114). The curative ratio of AHEW to EEW for these coatings was ascertained from differential scanning calorimetry (DSC) exotherm data.

3.12 Differential Scanning Calorimetry

Differential scanning calorimetry (DSC) measures the Exothermic Heat flow of a material as it is heated over a given temperature range. For ambient cure epoxy materials this heating range usually starts at 30°C and ends at about 160°C. The typical DSC scan for an exothermic reaction shows a negative heat flow assigned to exothermic event for a fixed heating rate. In all DSC experiments the sample mass must be controlled because essentially, it is the difference in energy inputs between the sample and reference or the temperature difference between the sample and reference which is related to heat flow Q in Joule/gram °C. For the epoxy / polyamide materials stoichiometric ratios of epoxy to

polyamide hardener were measured by DSC in order to obtain the mixture that yielded the maximum normalized exotherm. Figure 3.12, below, gives normalized exotherm for different mass mixture ratios of epoxy to polyamide hardener.

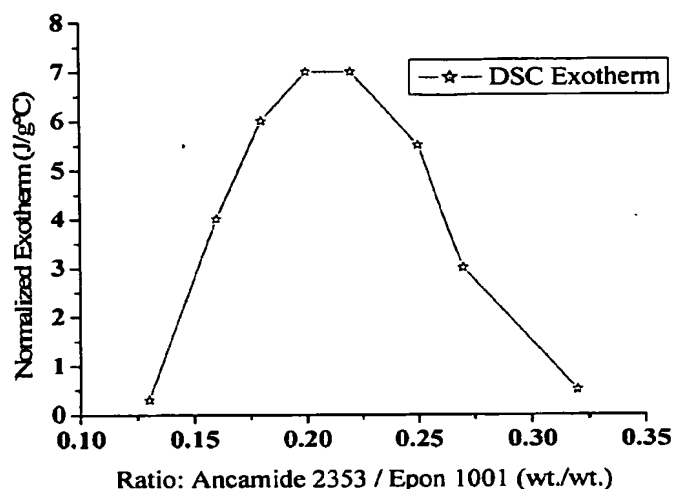


Figure 3.12: Epoxy hardener optimization ratio.

The exothermic reaction data, shown in Figure 3.12 were ascertained from differential scanning calorimetry measurements using a Perkin-Elmer Series-7 Instrument. Sample sizes were in the range of 5-10mg. This exothermic event usually signifies that the epoxy and curative are reacting. Each sample was analyzed by heating from 30 °C-160°C at a heating rate of 10 °C/minute. The sample was held at 160 °C for three minutes and cooled at a rate of 10 °C/minute and held at 30 °C for three minutes. Results from this experiment showed that a mix ratio of 0.22 Ancamide 2353 to Epon®1001 (neat) gave the maximum DSC relative exotherm. This ratio was found to be in agreement with a calculated value for Epon 1001 and Ancamide 2353 of ~0.24, derived from Air Products Co. manufacturer's product literature bulletin for Ancamide 2353 which gives

recommended ratios in parts per hundred (PPH) of Ancamide 2353 for Epon 828 which is a liquid DGBPA with an EEW ~188.

The primer pigment volume concentrations were estimated with the following PVC volume index relationship Equ. 3.3, below:

$$\text{Equation 3.3} \quad \text{PVC} = \frac{\sum_{i=1}^n \text{Pigments}_i}{\sum_{i=1}^n \text{Pigments}_i + \sum_{i=1}^n \text{Binder}} \quad (3)$$

Primers were formulated using conventional techniques, pigment was dispersed in a resin solvent mix and Bentone-Gel™ an organically modified bentonite clay thixotrope was added to the letdown mix. Viscosity was adjusted with a No. 4 Ford cup at ~24 seconds. Paints were applied to steel-wire brushed Al 2024 T3 Q-panels™ with a touch-up spray-gun and allowed to ambient cure at 22° C for seven days. The average primer film thickness was measured at 3 mils with an average coefficient of variation of 10%.

3.13 Open Circuit Potential and Early EIS Studies

The exposure time dependence of open circuit potential or (E_{corr}) measurements were used to evaluate the corrosion protection effect of Mg-rich primers on Al 2024 T-3 substrates. Immediately after immersion of the painted aluminum panels in the electrolyte E_{corr} was about -1.1 V, a value that lies in the mixed potential range of Mg / Al 2024 T-3 couple. The time dependence of E_{corr} for the different tested samples, illustrates the galvanic protection supplied to Al 2024 T-3 substrates by coatings loaded with Mg powder Figure-3.11, below. The free potential (E_{corr}) of an aluminum alloy is determined by the composition of the aluminum-rich solid solution with the dominant volume fraction of the

alloy microstructure. Measurements of free potentials of aluminum are described in ASTM G 69, using an oxygenated salt water NaCl solution. Free potentials of heat treatable uncoated commercial wrought aluminum alloys such as 2024 T-3 is -0.69 and in this experiment were measured versus a saturated calomel electrode. The open circuit potential (OCP) was monitored and the electrochemical impedance spectroscopy (EIS) spectra of the various primers as formulated in an epoxy-polyamide polymer matrix were recorded. The data presented below are for three of these primers based on ECKA 50 micron average Mg powder at 43, 46 and 50% PVC. These data indicate that the most effective protection from just the primer is about 46% PVC, which was the estimated CPVC for this system.

The electrochemical studies of Mg-rich primers formulated in our laboratory were carried out on the surface of the primed Al 2024 T-3 immersed in 3% NaCl solution.⁴⁶⁹ *Figure 3.11*, gives (OCP) vs. exposure time for Mg-rich primers, at 43, 46, and 50% PVC in a polyamide / epoxy coating polymer exposed to 3% NaCl solution at pH \approx 6.2. Interpretation of the events is as follows. Initial OCP values for the three sets correspond to a single electron reduction potential⁴⁷⁰ for Mg metal, $E_{Mg} \approx -1.50V$ to $-1.60 V_{SCE}$, and the primers appear to be acting like pure Mg⁴⁷¹. Subsequently, over a 24 hour period, Mg and the Al alloy polarize to a mixed potential, E_{mix} , corresponding to the galvanic corrosion potential, E_{corr} ,⁴⁷² at which the Mg is still sacrificially protecting the Al 2024 whose OCP is -0.68 V vs. saturated calomel electrode (SCE).

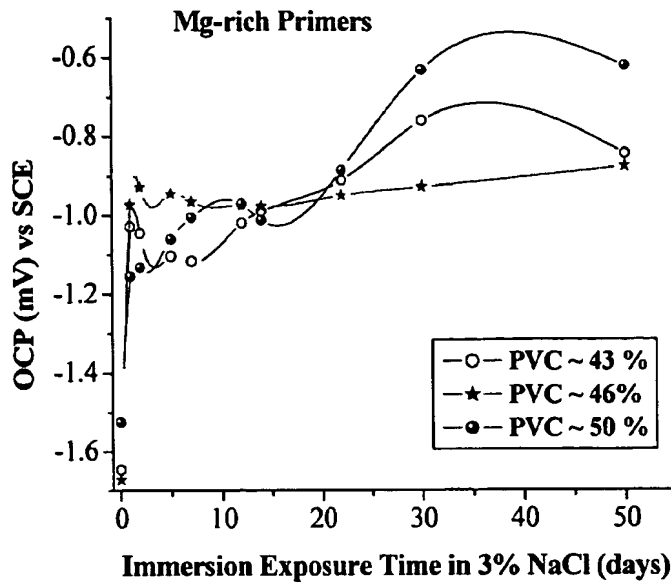


Figure 3.11: Open circuit potential SCE vs PVC Mg-rich epoxy/polyamide primers at pH \approx 6.2 in 3% NaCl ⁽⁴⁷²⁾

The observed mixed potential for Mg and Al alloy in 3% NaCl was found to be about $E_{\text{mix}} \approx -0.90 \text{ V}$ to $-1.00 \text{ V}_{\text{SCE}}$. OCP values extending beyond the initial 24-hour period varied according to primer PVC. The initial lower mixed potential value, E_{mix} , (Figure 3.11), for the 43% PVC sample is thought to be due to the lower effective active metal area as a result of higher polymer coverage at the Mg/Al alloy interface. Initially, the Mg-anode dominates the OCP. The gradual change in OCP for the 43% PVC sample toward $E_{\text{Al-2024}_T3} \approx -0.68 \text{ mV}_{\text{SCE}}$ is assumed to be due to reactive consumption of the exposed Mg in this system and the disbonding of epoxy coating polymer from the cathode surface. The observed change in OCP of the 43% PVC sample toward $E_{\text{mix}} \approx -0.90 \text{ V}$ to $-1.00 \text{ V}_{\text{SCE}}$ is thought to be due to resistance polarization by the formation and packing of Mg oxides in the coating. The initial and continuous change in OCP of the 50% PVC

sample is concluded to be due to a higher void volume in the primer as well as a higher cathode area at the primer alloy interface. The OCP of the 46% PVC sample quickly arrives at the $E_{\text{mix}} \approx -0.90 \text{ V}$ to $-1.00 \text{ V}_{\text{SCE}}$ value and remains constant for the duration of the test time period. Thus, it is assumed that the 46% PVC primer corresponds to the critical pigment volume concentration for the primer. Therefore, suggesting cathodic protection of the Al alloy due to Mg metal occurs most effectively at or near CPVC.⁴⁶⁹ Trends in OCP data suggest three distinct periods that distinguish the evolution and effectiveness of cathodic protection in the Mg-rich primers as a function of exposure time. These are as follows:

Period I. Initial immersion day one, the “activation” period when the value of the corrosion potential shifts to a cathodic value 1.1 V vs SCE, corresponding to the Mg metal / Al-2024 T-3 mixed potential in the electrolyte. Magnesium immediately begins to react with the sodium-chloride solution, it is “activated” leading to better metal-to-metal electrical contact being established between magnesium particles and Al surface.

Period II. Once initially past the “activation” period, the cathodic protection mechanism reaches its peak due to a maximum in the ratio of magnesium-to-aluminum area ratio. This occurs around day 5~7 when the corrosion potential shifts to a more anodic value of about -0.9 V vs SCE; it is where a relative stabilization called the “transition” period occurs.

Period III. After the transition period, and up to day 21, the corrosion potential shifts out of the cathodic protection domain, and the potential fluctuates as the film’s solution chemistry begins to change. At which time oxygen reduction begins

to occur on the upper part of the film causing a local increase in pH that changes the corrosion products from magnesium hydroxychlorides to magnesium hydroxides, the same as at the interface.

Figure 3.12, below, gives the $|Z|$ modulus versus exposure time as measured in 3% NaCl solution at $\text{pH} \approx 6.2$ on 43, 46, and 50% PVC Mg-rich primers. This figure demonstrates the effect of PVC at CPVC for Mg-rich primers. The Z modulus values for the 46 PVC samples yielded a higher impedance modulus over the 28-day period suggesting proper formulation at or near the critical pigment volume concentration, which is required to ensure close packing of Mg pigment with minimum resistance from the polymer matrix of the system, but with polymer matrix content sufficient enough to ensure good substrate wetting and reasonable physical properties from the primer.

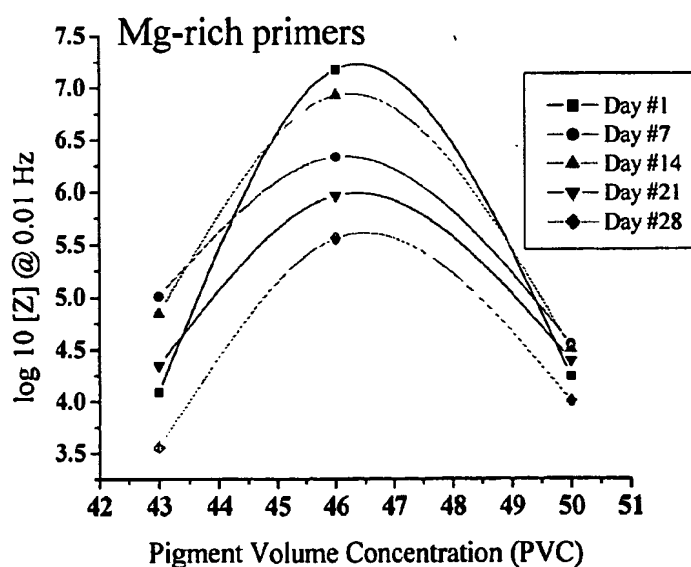


Figure 3.12: $|Z|$ at 0.01Hz vs PVC for Mg-rich epoxy /polyamide primers at $\text{pH} \approx 6.2$ in 3% NaCl .⁽⁴⁷²⁾

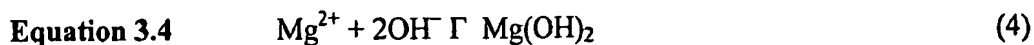
3.14 Summary and Conclusions of Preliminary Feasibility Studies

The studies presented in this chapter demonstrate close similarities in the chemical and electrochemical behavior of Mg-rich primers used in cathodic coatings for corrosion control of aluminum contrasted to similar Zn-rich coatings reported in the literature for steel. The initial hypothesis regarding developing such analogous systems was that like zinc, magnesium must deliver two essential components to validate the assumptions made regarding these metal coatings:

1. A sacrificial anode or galvanically negative electrode, where excess electrons accumulate due to the release of positively charged ions into an electrolyte.
2. A cathode or galvanically positive electrode where electrons are consumed by discharge of ions into an electrolyte.

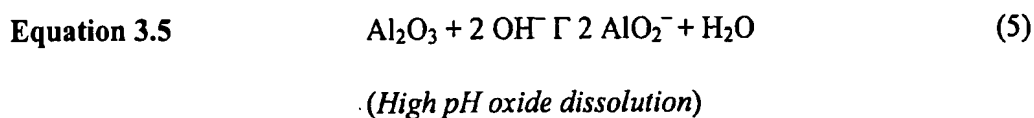
It has also been shown that like commercially available inhibitive metal containing coating systems formulated with active metal pigments the polymeric binder systems must synergistically moderate the dissolution of the pigment to yield voluminous metal oxides or carbonates that in turn block further corrosion attack.⁴⁷³

The general reaction for corrosion of magnesium in water, *Equ. 3.3*, shows that Mg(OH)_2 is formed from available hydroxyls in electrolyte solution according to the cathodic reaction accompanying the anodic dissolution of Mg *Equ. 3.4*:

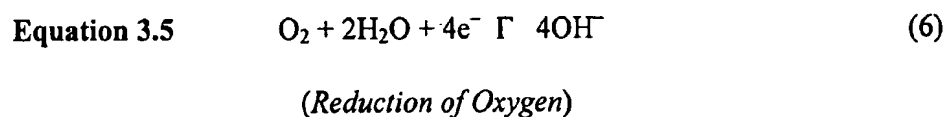


So long as there is sufficient magnesium metal present the destruction of Al native oxide reaction, *Equ. 3.5*, below, is not energetically favored. Given Mg metal's higher standard

electromotive force, the reduction potential of Mg metal at -2.36 V vs SHE would favor the anodic reaction, Equ. 3.4 with the liberation of Mg^{2+} into the electrolyte solution.



The corollary to these observations is that the presence of magnesium metal effectively reduces the concentration of solution hydroxyl from the reduction of O_2 , Equ. 3.6, below.



Since cathodic disbonding is attributed to the build up of hydroxide at the Al coating interface the reaction with Mg metal, *Equ. 3.4*, above, may therefore decrease the rate of disbonding as hydroxide will first appear on the surface of the pigmentary Mg metal as opposed to at the Al coating interface, thus preserving the metals passive native oxide Al_2O_3 layer.

These results were obtained from a simple Mg-rich coating based on an off-the-shelf (OTS) polymer system with no optimization efforts. They showed that the oxidation products of the Mg pigment in an exposure environment, fairly typical of what an actual system might see in field exposure, did not cause basic corrosion of the Al 2024 T-3 alloy. Further, the Mg-rich system did provide a type of cathodic protection to the Al 2024 T-3, giving the system significant corrosion protection properties in a completely Cr-free system. The research studies now proceed to the improvement of the coating polymer system and additional formulation studies.

References / Bibliography

- ⁴³⁸ Janata, J., Baer, D., Bierwagen, G.P., Birnbaum, H., Buchheit, R., Davenport, A., Isaacs, H., Hedberg, F., Kendig, M., Mansfeld, F., Miller, B., Wieckowski, A., and Wilkes, J., "Issues Related to Chromium Replacement," presented at 187th Meeting of The Electrochemical Society, May pp. 21-26, Reno, Nevada (1995)
- ⁴³⁹ Twite, R.L. and Bierwagen, G.P., "Review of Alternatives to Chromate for Corrosion Protection of Aluminum Aerospace Alloys," *Prog. Org. Coatings*, Vol. 33 pp. 91-100 (1998)
- ⁴⁴⁰ S. Felix, R. Barajas, J.M. Bastidas, M. Morcillo and S. Feliu, "Study of Protections Mechanism of Zinc-Rich paints by Electrochemical Impedance Spectroscopy," in *Electrochemical Impedance Spectroscopy, ASTM STP 1188*, J.R. Scully, D.C. Silverman, & M. Kendig, eds., Amer. Soc. Testing and Materials (ASTM), Philadelphia, PA pp. 438-449 (1993)
- ⁴⁴¹ Hare, C., "Corrosion Control of Steel by Organic Coatings," Ch. 55 in *Uhlig's Corrosion Handbook*, 2nd Edition. R. W. Revie, Editor, John Wiley & Sons, New York pp. 1023-1038 (2000)
- ⁴⁴² Böhm, S., Holness, R.J., McMurray, H.N., and Worsley, D.A., "Charge percolation and sacrificial protection in zinc-rich organic coatings," Eurocorr 2000, Queen Mary and Westfield College, London, 10th-14th September (2000)
- ⁴⁴³ H.K. Yasuda, C.M. Reddy, Q.S. Yu, J. Deffeyes, G.P. Bierwagen & L. He, "Effect of Scribing on Corrosion Test Results," *Corrosion*, Vol. 57, pp. 29-34 (2001)
- ⁴⁴⁴ He, J., Johnston Gelling, V., Tallman, D.E., Bierwagen, G. P. and Wallace, G.G., "Conducting Polymers and Corrosion III: A Scanning Vibrating Electrode Study of Poly(3-Octyl Pyrrole) on Steel and Aluminum," *J. Electrochem. Soc.*, Vol. 147, pp. 3667-3672 (2000)
- ⁴⁴⁵ Tallman, D.E., Pae, Y., and Bierwagen, G.P., "Conducting Polymers and Corrosion 2: Polyaniline on Aluminum Alloys," *Corrosion*, Vol. 56, pp. 401-410 (2000)
- ⁴⁴⁶ Information from Eckart GmbH, Kaiserstrasse 30, Fürth D-90763, Germany and technical references therein.
- ⁴⁴⁷ Jones D. A. Jones, *Principles and Prevention of Corrosion*, 2nd Ed., Prentice-Hall, Upper Saddle River, NJ (1996), Ch. 2
- ⁴⁴⁸ Perrault, G.G., in *Encyclopedia of the Elements*, Vol. VIII, Ed. A.J. Bard, pp. 262, Marcel Dekker, New York, NY (1978)

- ⁴⁴⁹ Kramer, D.A., Magnesium, its Alloys and Compounds, U.S. Geological Survey Open-File Report 01-341
- ⁴⁵⁰ Perrault, G.G., *Electroanal. Chem., Interface Electrochem.* Vol. 27, pp. 47 (1970)
- ⁴⁵¹ Censullo, A., C., Jones, D. R. and Wills, M. T. : "Investigation of Low Reactivity Solvents," Final Report for California Air Resources Board Contract 98-310, May 10 (2002)
- ⁴⁵² Hare C.H., and Wright S.J., Anti-Corrosive Primers Based on Zinc Flake, *J. Coatings Technology*, Vol. 54, No. 693, Pp. 65 to 76, Oct. (1982)
- ⁴⁵³ Abreu, C. M, Izquierdo, M., Keddah, M., Nóvoa, X. R. and Takenouti, H., *Electrochim. Acta*, Vol. 41, pp. 2405 (1996)
- ⁴⁵⁴ Song, G.L., and Atrens, A, Corrosion Mechanisms of Magnesium Alloys, *Adv. Eng. Matl.*, Vol. 1, No.1, Pp.11-33 (1999)
- ⁴⁵⁵ Froats A., Aune, T. K., Hawke, D. Unsworth, W., Hillis, J., in Metals Handbook, 9th ed., Vol. 13, ASM Int., Materials Park, OH, pp.740-754 (1987)
- ⁴⁵⁶ Petty, R.L., Davidson, A.J., and Kleinberg, J., *J. Am. Chem. Soc.*, Vol. 76, pp.363 (1954)
- ⁴⁵⁷ Tunhold, R., Holtan, H., and Hagg-Berg, M.B., *Corros. Sci.*, Vol. 17, pp. 353 (1977)
- ⁴⁵⁸ Rausch, M.D., McEwan and Kleinberg, *J. Am. Chem. Soc.*, Vol. 76, pp.3622 (1954); Vol. 77, pp. 2093 (1955)
- ⁴⁵⁹ Kokoulina, D.U., and Kabanov, B.N., *Dokl. Akad. Nauk.*, SSSR, Vol. 112, pp 692 (1957)
- ⁴⁶⁰ James, W.J., Straumanis, M.E., Bhatia, B.K., and Johnson, J.W., *Ibid*, Vol. 110, pp. 1117 (1963)
- ⁴⁶¹ López-Buisán Natta, M.G., *Corrosion*, NACE International, Vol. 57, No8., pp. 712-720 (2001)
- ⁴⁶² Epoxy Curing Agents and Diluents, Air Products Performance Chemicals, product guide, <http://www.airproducts.com/chemicals>, (2002)
- ⁴⁶³ Adams, R., Johnson, J.R., and Wilcox, C.F., Laboratory Experiments in Organic Chemistry, Organic Chemistry, Fifth Ed., The Macmillan Co, New York, NY, pp. 25-30 (1963)

⁴⁶⁴ Vanlandingham, M.R., Eduljee, J.W., and Gillespie, J.W., JR., *J. Appl. Polym. Sci.*, Vol. **71**, pp. 699-712 (1999)

⁴⁶⁵ Kramer, D., Magnesium, its Alloys and Compounds, US Geological Survey Open-File Report 01-341

⁴⁶⁶ Almeida, E., Pereira, D., and Figueredo, O., *Progress in Organic Coatings*, Vol. **17**, pp. 175 – 189 (1989)

⁴⁶⁷ Evans, U.R., *The Corrosion and Oxidation of Metal*, Arnold, London, (1960)

⁴⁶⁸ Ellingson, L., "Corrosion Studies for the Protection of Aluminum Alloys and Outdoor Bronze," Masters Thesis, North Dakota State University, June 2001

⁴⁶⁹ Balbyshev, V. N., Bierwagen G. P., and Berg, R.L., "Electrochemical Studies of Vinyl Ester Coatings for Fuel Tanks," ACS Symposium Series 689, Organic Coatings for Corrosion Control, G.P. Bierwagen, ed., pp. 292 (1998)

⁴⁷⁰ Genesca, J., Betancourt, L. and Rodriguez, C., Electrochemical Behavior of a Magnesium Galvanic Anode Under ASTM Test Method G-97-89 Conditions, *Corrosion*, pp. 502 – 507 July (1996)

⁴⁷¹ Song G., Atrens A., StJohn D., Nairn J., Li Y., "The Electrical Corrosion of Pure Magnesium in 1N NaCl," *Corrosion Science*, Vol. **39**, Pp 5, 855-875, (1997)

⁴⁷² Ellingson, L., "Corrosion Studies for the Protection of Aluminum Alloys and Outdoor Bronze," Masters Thesis, North Dakota State University, June (2001)

⁴⁷³ Pfeifer, A., "Dacromet and Geomet Environmentally Compliant Cadmium Replacement Coatings," U.S. Navy & Industry Corrosion Technology Information Exchange, Louisville; July 19-22, (1999)

Chapter 4 Silane Modified Hybrid Epoxy-Urea Materials

Abstract

A hybrid polymeric material was synthesized and developed for use in pigmented Mg-rich coating systems for corrosion control of Al alloys. The hybrid polymeric material was derived from a novel (silane modified quinoxalinol) crosslinking agent that functions as an organic / inorganic surface and bulk crosslinker for epoxy / polyisocyanate polymeric matrices. A suitably reactive starting material for crosslinker synthesis was obtained from an improved oxidation method of phenyl-hydroquinone to 6-phenyl-*p*-1,4-benzoquinone. The oxidation process yielded an α - β unsaturated ketone (6-phenyl-*p*-1,4-benzoquinone) product mixture that was subjected to further reaction with *N*-beta-(aminoethyl)- γ -aminopropyltrimethoxysilane to yield the 7-phenyl-1-[4-(trimethyl- silyl)-butyl]-1,2,3,4-tetra-hydro-quinoxalin-6-ol (7-PQ-6-ol) crosslinker. The silane modified quinoxalinol crosslinker was added to a mixture of polymeric epoxy and polyisocyanate materials to form a silane modified epoxy-urea polymeric matrix that was subsequently developed into multi layer pseudo-IPN coating matrix for a Mg-rich primer.

4.1 Introduction

The literature is replete with organic-inorganic hybrid polymers that can be used as polymeric materials for coatings. Most accounts describe short organic polymer chains directly linked to the inorganic backbone of a siloxane structure that have been obtained by appropriate choice of starting materials. Generally, these coatings show excellent adhesion to Al substrates and due to their high three dimensional crosslinking they act as diffusion

barriers which helps minimize then need for active corrosion protection pigments. The most widely used method for developing such organic modification has been through the use of epoxy systems in which the inorganic network is made by polysiloxane hydrolytic silanol condensation reaction coupled with epoxy – amine reaction.^{474, 475} Other reactions have also been reported that involve development of urethane modified polysiloxanes⁴⁷⁶ that involves modification of polyisocyanates with silanes bearing an H-active functional group.⁴⁷⁷ The resulting films have dry thickness of anywhere from 4 -80 μm (clear coatings) and up to 150 μm when pigmented. They can also be applied, (e.g., as single-coat metallic paints.) Coatings of up to 50- μm thickness have been reported to yield very good salt spray resistance on aluminum without chromating.

4.2 Design of Hybrid Coating Polymeric Materials

Several researchers^{478, 479, 480} have proposed IPN combinations to improve properties of (PUs) and (ERs)^{481, 482, 483, 484} with most have focused on improving the brittleness of ERs by modification with a PU elastomer.^{485, 486, 487, 488, 489, 490, 491} Interpenetrating polymer networks (IPN's) as polymer alloys have been characterized as two or more distinct crosslinked polymer networks held together by permanent entanglements.⁴⁹² Frisch *et al.*⁴⁹³ first reported simultaneous interpenetrating networks (IPNs) composed of polyurethane / polyisocyanate (PU) combined with an epoxy resin. Generally, the epoxy backbone promotes toughness and flexibility to cured films while the carbon-carbon and the urethane bonds of the same improve solvent resistance, and adhesion. Polymeric materials derived from the reaction of epoxy hydroxyls with polyisocyanates occurs when the secondary hydroxyl group in the epoxy backbone is reacted with an isocyanate that gives rise to a hybrid structure.

Traditionally, two-pack zinc epoxy primers based on epoxy / polyamide binder have been used for cathodic protection of steel as they result in crosslinked matrices with a good adhesion and resistance against alkalies, so that any alkaline reaction involving zinc does not affect the binder itself.⁴⁹⁴ More recently, epoxy siloxane hybrid coatings with excellent compatibility with most zinc epoxy and zinc silicate primers have been reported⁴⁹⁵ to represent a significant advancement compared to epoxy, epoxy acrylic and polyurethane coatings. The principle reason epoxy resins are used in such hybrid /interpenetrating network (INP) systems is because they possess good adhesion strength to metals and their crosslink density can be adjusted. Therefore, “hybrid” polymeric matrices, for high performance primers, must be designed as polymer composites or alloys that contain a polymer backbone with at least two types of reactive groups that can take part in crosslinking and network formation under at least two different mechanisms.

Organofunctional silanes are commonly used as coupling agents and adhesion promoters in epoxide and urethane paints to improve their initial, wet, and recovery adhesion (latent adhesion) to aluminum surfaces, discussed in Chapter 2.4. It has been well documented that the best deterrent to adhesion failure in organic coatings lies in developing the right chemical interactions between the coating polymer, pigment, coating layers, and their metallic substrates.⁴⁹⁶ The most effective strategy, thus far, has been to develop coatings whose polymer matrix hydrophilicity decreases during cure as the polymer matrix coating undergoes film formation and solidifies.

4.3 Design of Silane Modified Quinoxalinol Crosslinker

The purpose of the silane modified bulk crosslinker is to facilitate the formation of a moisture cure polymer alloy (IPN) composed of a polymer network made up of: 1)

polyisocyanate / polyurea; 2) epoxy / amine; 3) organic / inorganic silane functionalities.

The criteria for the crosslinker was that it not contain primary amine functionality (minimum water sensitivity), possess hydrophobicity, solubility in oxygenated solvent such as aliphatic ketones and carbonates, cost effective, relatively low equivalent weight, autocatalytic effect at opening both epoxide ring and isocyanate reactions (best achieved with heterocyclic ring structure involving nitrogen). The resulting polymeric material must be unsaponifiable and relatively insensitive to the effect of alkaline oxidation products from Mg particles. Therefore, the most suitable crosslinker would be one that was not sensitive to acid / base hydrolysis, (i.e., formation of carboxylate ion under elevated pH conditions) that promotes deposition of water sensitive salts at the coating / metal interface.

The application of a polymer that minimized water's effect at a metal's interface was reported by Erhan⁴⁹⁷ who observed that polymers containing the 2,5-diamino-1,4-benzoquinone functional group have a strong affinity for metal surfaces and can protect some metals against corrosion as a result of the polymer's ability to adsorb onto metal surfaces through a surmised coordination complex.^{498,499,500,501,502,503,504} In light of these observations much interest has been generated in this class of polymer / functionality as a means to improve coatings for corrosion control of metals.^{505,506} Similarly, Nikles *et al.*⁵⁰⁷, claim that amine-quinone polymers can displace moisture from the surface of metals, making them more hydrophobic once the polymer has adsorbed through imine acceptor interactions between the *p*-electrons of the polymer and the vacant *d*-orbitals of a metal's surface atoms.

However, what appears to be missing from these authors studies on quinonoidal polymers is data demonstrating the effect of aqueous equilibrium on the quinone moiety as

a function of pH under conditions where significant corrosion actually occurs. As of yet, no study has described the effect of quinone polymers and polymer adhesion due to the effect of the hydroquinone monophenolate ion as a function of pH. Especially at high pH conditions where corrosion for actually occurs aluminum. Figure 4.1, below, shows the Pourbaix pH stability diagram for magnesium and aluminum superimposed over the reduced form of *p*-1,4-benzoquinone, which has two hydroxyl groups, that are subject to deprotonation resulting in three reduced species: 1) hydroquinone; 2) the monophenoxide anion; 3) the diphenoxide dianion. The relative stabilities of these species are represented as a function of potential (E) and pH in Figure 4.1 the lines that suggest boundaries should be interpreted as continuous transitions from one species to predominance of another. Figure 4.1 shows aqueous equilibria for two metals Al and Mg and quinone / hydroquinone as a function of pH and potential (E) in volts.

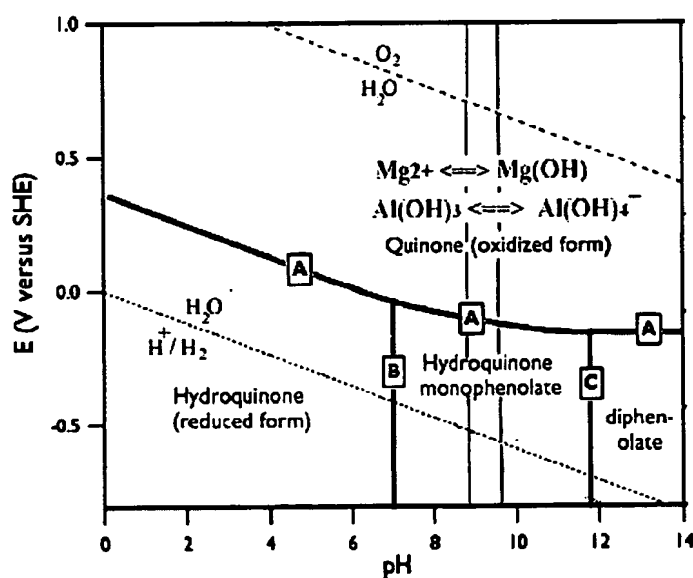


Figure 4.1: Pourbaix diagram for Al, Mg and quinone with stability boundaries for species as a function of $E(V)$ vs pH.

What is clear from Figure 4.1, above, is that in the pH range between 6.5-to-12 and with a potential difference less than zero, the monophenolated ion is the dominant species. Therefore, it may also be surmised that observed anti-corrosive properties attributed to quinone-amine polymers on metal surfaces may in part be attributed to the presence of the hydroquinone monophenolate moiety participating in what Funke⁵⁰⁸ described as effect of cooperative functional group interactions that promote good interactions between polymeric material and metallic substrate, see Chapter 2.2.

4.4 Materials from 2- phenyl-1,4-benzoquinone

A review of the literature on quinonidal polymeric materials used in coatings for corrosion control, Chapter 2.8, generally involves a Michael Addition reaction by nuclear substitution or amination.^{509, 510} This synthesis scheme, that involves addition of primary amines to quinone, takes place by replacement of hydrogen from an alkyl group on the quinonoid ring by an amine and is the method pertaining to the reactions described in the preparation of quinone-amine polymeric materials. Even in the earliest accounts of these polymerization schemes, given by Erhan *et al.*⁵¹¹, much work has been devoted to the oxidation of the hydroquinone moiety after the initial substitution reaction occurs. Initially, excess free quinone was used; see Chapter 2.8, followed by addition of sodium hypochlorite. An improved, more reproducible oxidation scheme was reported by Nickles *et al.*⁵¹², that utilizes an oxygen / CuO oxidation procedure to reoxidize the quinonoidal ring after the initial substitution. Nikles *et al.*⁵¹² were also the first to report a successful methodology for incorporation of the quinonoidal oligmer into a polyisocyanate prepolymer to yield a quinone modified polyimine used in coatings for corrosion control.

In summary, the most significant aspects of the work reported on quinone-amine polymers by Erhan *et al.*⁴⁹⁸ and Nikles *et al.*⁵¹³ that can be applied to developing coatings for corrosion control are that: 1) incorporation of quinone functionality or quinonal derivatives into prepolymers of polyisocyanates or epoxy resins yields a more corrosion resistant polymeric material; 2) functionalized oligomeric quinonoidal materials can be designed as as moisture cure (MC) polymeric coating systems that are easily prepared and applied.

Initially, work in developing quinone-amine oligomers was undertaken in these laboratories with both Erhan's and Nikle's oxidizers. However, the results obtained from each were not satisfactory. In the first case Erhan's calcium hypochlorite oxidizer⁴⁹⁸ was too moisture sensitive and presented a safety hazard as well; in the second case Nikle's O₂ / CuO scheme reacted immediately with primary amines causing thee solution to change to a copper patina green. Instead, the oxidizer material chosen for the work done in these experiments was trichloroisocyanuric acid (TCCA) where it was used to oxidize 2-phenylhydroquinone Figure 4.2, below, to 2-phenylbenzoquinone. In this synthesis scheme it was desire that only one a side-chain substitution reaction occur per 2-phenyl-1,4-benzoquinone molecule, as discussed in Chapter 2.8.

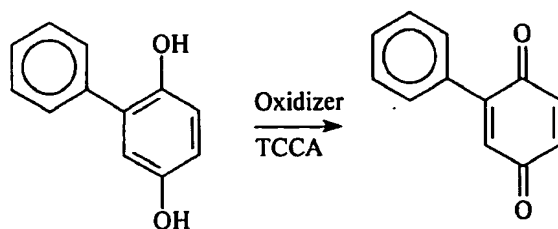


Figure 4.2: 2-phenylhydroquinone, oxidized with (TCCA) trichloroisocyanuric acid to 2-phenyl-1,4-benzoquinone.

In light of the aforementioned advances in designing polymeric materials from quinonoidal structures the first problem to be resolved was choosing an inexpensive but effective oxidizer that did not interfere with the overall synthesis scheme. Hydroquinone can be oxidized relatively easily compared to secondary alcohols, as reviewed in Chapter 2.8, but most oxidation methods reviewed were not simple to perform nor convenient to recover, nor are they environmentally acceptable on a large scale, or always efficient when applied. From Figure 4.2, the 2-phenylhydroquinone product was the starting material for the preceding crosslinker synthesis.

4.5 Oxidation of phenylhydroquinone

Experimental

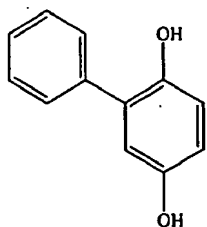
The starting materials for this reaction were phenyl-hydroquinone, trichloroisocyanuric acid, and dichloromethane (solvent). The apparatus for the reaction was a 400-ml, triple neck flask with nitrogen purge, and Vigreux column attachment. The reaction was run as follows: 1) a solution (CH_2Cl_2) and phenylhydroquinone was heated to 37°C ; 2) subsequent gradual addition of TCCA oxidizer to the solution, the oxidizer was added gradually to avoid bumping due to the exothermic nature of the reaction. Note, this reaction is exothermic and will occur at 0°C with evolution of HCl gas.

Table 4.1: Materials for oxidation of 2-phenyl-hydroquinone

Material	supplier	grams	mmoles
2-phenylhydroquinone	(Aldrich)	5.0	26.45
Trichloroisocyanuric acid	(Aldrich)	2.2	9.55
Dichloromethane	(Aldrich)	(300-ml)	(solvent)

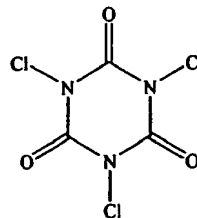
The oxidation reaction can be followed by a color change where initially the phenylhydroquinone solution is a dull gray / green and changes color to a bright canary yellow upon oxidation. Once all of the oxidizer has been added the solution is kept at 36°C under nitrogen purge for an additional 30 minutes. Thereafter, it is allowed to set for 60 minutes to allow the now insoluble spent oxidizer isocyanuric acid (IA) to settle out. Finally, the solution is filtered through two fluted filter papers and the (IA) is separated out. The filtration process is repeated twice, presence of (IA) is readily apparent in the form of particle precipitate.

Results from this oxidation process shown in Figure 4.2, above, yields an approximate 60% conversion to phenyl-hydroquinone with a remainder of 40% starting material (phenyl hydroquinone). According to spectroscopic results the product is surmised to be a mixture of 2-phenyl-1-,4-benzoquinone and phenyl-quinhydrone, see Figure 4.4, below.



$C_{12}H_{10}O_2$
Exact Mass: 186.07
Mol. Wt.: 186.21
C, 77.40; H, 5.41; O, 17.18

2-phenyl-hydroquinone



$C_3Cl_3N_3O_3$
Exact Mass: 230.90
Mol. Wt.: 232.41
C, 15.50; Cl, 45.76; N, 18.08; O, 20.65

Trichloroisocyanuric acid (TCCA)

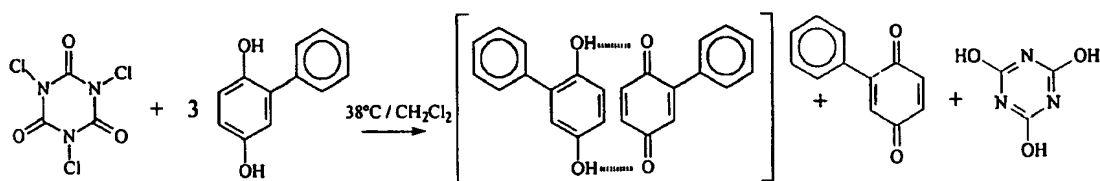


Figure 4.3: 2-phenyl-hydroquinone, oxidized with (TCCA) to product mixture consisting of about 60 percent (6-phenyl-*p*-1,4-benzoquinone) with a remaining ~ 40 percent unoxidized or partially oxidized starting material.

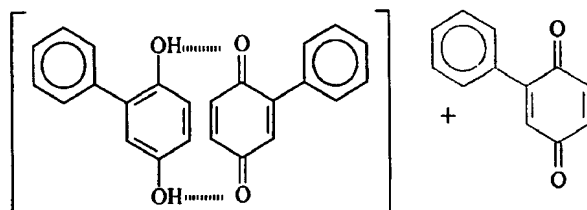


Figure 4.4: oxidation products: 2-phenyl-hydroquinone / 2-phenyl-1,4- benzoquinone (quinhydrone); and 2-phenyl-1,4-benzoquinone.

UV-Vis Spectroscopy* was performed on mixtures prepared in dilute tetrahydrofuran solutions ($<10^{-5}$ M) at room temperature (22°C) in quartz cuvettes. The first step of the UV-VIS analysis involved recording and obtaining spectral data for mixtures of phenylhydroquinone: hydroquinone to serve as a standard; the materials for these standards were obtained from Aldrich Chemicals. Dilute solutions of phenylhydroquinone: phenylquinone mixed in ratios ranging from: 0:100; 33:66; 50:50; 66:33 and 100:0 were analyzed in order to establish concentration absorption dependence for the functional groups characteristic to both of these molecules. Spectral data from the

* dual-beam scanning UV-vis-NIR spectrophotometer

oxidation product was compared to the standardized mixtures as shown in Figures 4.5 (a) and (b), below.

The UV-VIS acquisition procedure for this experiment involved making an initial fluorescence absorption measurement of the solvent prior to each sample absorption spectrum to ensure that the maximum absorption of the solvent was less than 0.1. The resulting UV-VIS spectra of material mixtures compared to the oxidation product are shown in Figures 4.5 (a) and (b), below. The product mix from reaction in Figure 4.3 was estimated to be a 60:40 ratio of phenylquinone to phenylhydroquinone. What is observed in the spectra for mixtures ranging from 33: 66 and 50:50 of phenyl-hydroquinone (Aldrich) are the maximum absorptions at 290nm (phenylhydroquinone), and a maximum absorbance at 245 and 365nm (phenylquinone). For unsaturated ketones, the $\pi \rightarrow \pi^*$ absorption located at 242 nm is strong, with an $\epsilon = 18,000$ while the weak $n \rightarrow \pi^*$ absorption near 300 nm has an $\epsilon = 100$.⁵¹⁴ All spectra, except phenylhydroquinone, exhibit two transitions the first a high energy $\pi \rightarrow \pi^*$ transition at $\lambda_{\text{max}} \approx 245$ nm which represents quinone; the second a lower energy, C=C, $n \rightarrow \pi^*$ transition⁵¹⁴ at $\lambda_{\text{max}} \approx 290$ to 306 nm which represents phenylhydroquinone; as well as a third, the lowest energy, C=O, $n \rightarrow \pi^*$ transition⁵¹⁵ at $\lambda_{\text{max}} \approx 365$ nm which represents phenyl-quinone.^{516,517,518}

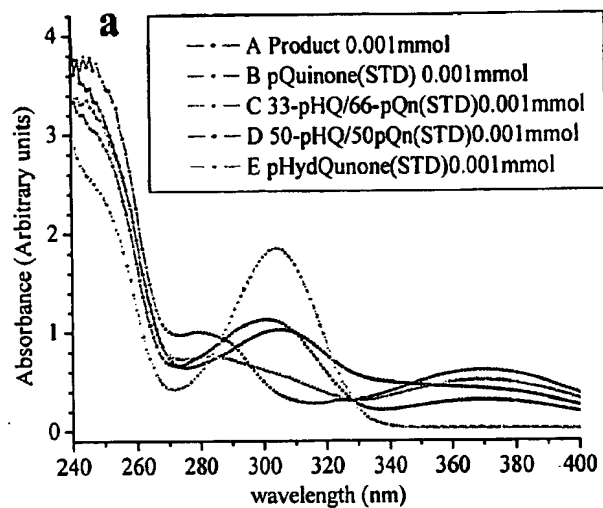


Figure 4.5 (a): UV-Vis transmission spectra of oxidation product: phenylhydroquinone / phenylbenzoquinone (quinhydrone); and phenylquinone contrast to mixtures of 1) phenylhydroquinone; 2) phenylbenzoquinone.

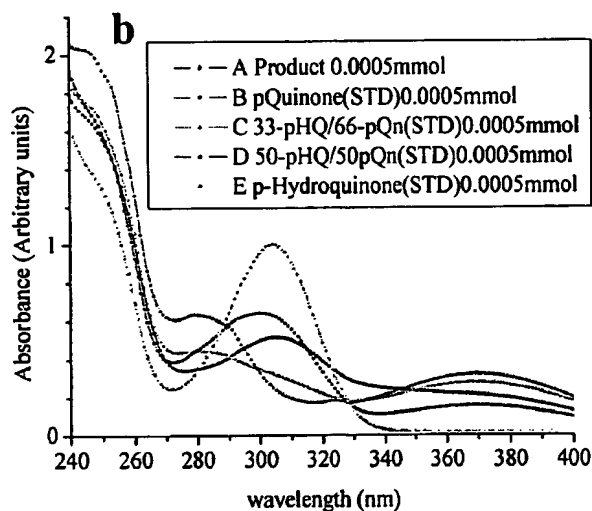


Figure 4.5 (b): UV-Vis transmission spectra of oxidation product: phenylhydroquinone / phenylbenzoquinone (quinhydrone); and phenylquinone contrast to mixtures of 1) phenylhydroquinone; 2) phenylbenzoquinone.

FTIR spectroscopy[†], Standard samples of phenylhydroquinone and phenylquinone from Aldrich Chemicals were prepared at similar mix ratios to those described, above, in UV-VIS analysis, and cast on KBr plates from solution (the solvent acetone was evaporated *in situ*). Spectral data was collected in transmission mode. Figure 4.6, below, absorption spectra for: 1) Aldrich phenylquinone (top); 2) oxidation product (center), and 3) Aldrich (bottom) phenylhydroquinone.

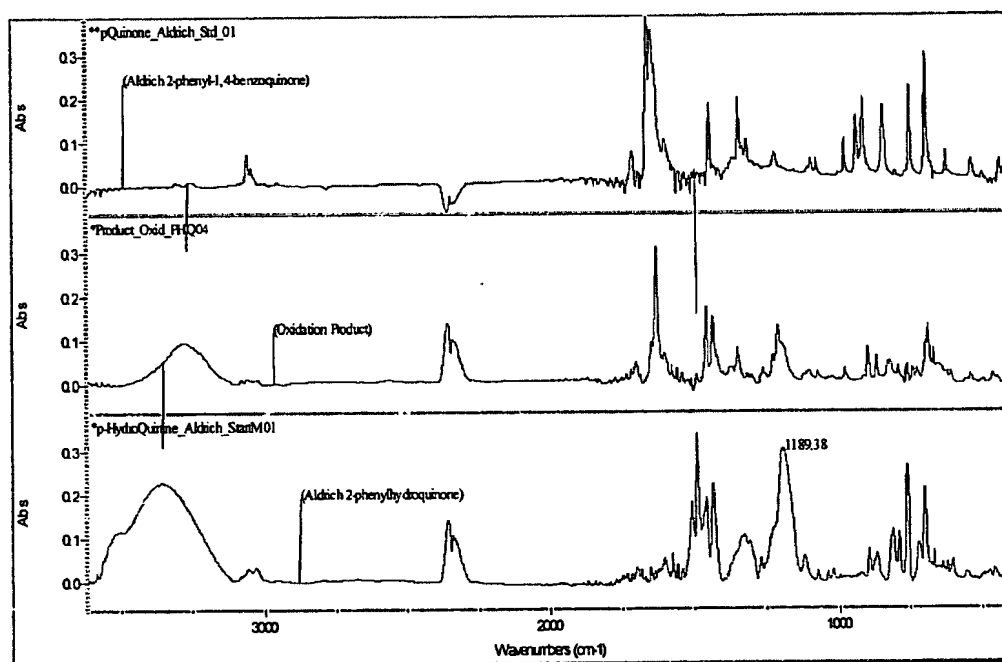


Figure 4.6: FTIR transmission spectra of oxidation products: 1) (top) phenylquinone; 2) (center) phenylhydroquinone / phenylquinone (quinhydrone); 3) product (bottom).

[†] Measurements were performed using a Nicolet 850 Series II FTIR spectrometer, data acquisition and spectral manipulations were obtained using Omnic ESP™ FTIR software (Nicolet Instruments Corp.)

The wavenumbers (ν_{\max}) for characteristic frequencies of functional groups associated with each are listed in Table 4.2, below.

Table 4.2: Characteristic group frequencies (IR) in wavenumbers for spectra in Figure 4.6

Spectrum	supplier	1) band (cm^{-1}) (OH)	2) band (cm^{-1}) (C=O)	3) band (cm^{-1}) (C-O)
2-phenyl-hydroquinone	(Aldrich)	N/A	1610	N/A
product (oxidation)	(<i>in house</i>)	3400	1610	1200
phenylhydroquinone	(Aldrich)	3600	(aromatic)	1200

Figure 4.7, below, FTIR spectra for mixtures of phenyl-hydroquinone and phenylquinone at ratios of 25:75; 50:50 and 75:25 contrasted to oxidation product. The key absorption frequencies are at: 1) group frequency values circa $\nu_{\max} \approx 3280$ and 3209cm^{-1} which gives the relative hydroxyl absorbance; 2) the $\nu_{\max} \approx 1660$ and 1630cm^{-1} which gives the conjugated C=O absorbance, as the carbonyl centers are not equal, one carbon C-1 is adjacent to a phenyl ring while the other C-4 is positioned *meta* with respect to the phenyl substituent; and 3) the $\nu_{\max} \approx 1190\text{-to-}1215\text{cm}^{-1}$ which gives the phenolic OH stretch indicating the presence of phenylhydroquinone.

With reference to Figure 4.7, below, the spectra show transmission absorbances for mixtures of phenylquinone/hydroquinone: (top) gives the absorbance spectrum for a 25:75 ratio mix of phenylhydroquinone to phenylquinone; (second from the top in black) shows spectrum of the oxidation product. The key absorbance frequencies to note are the $\nu_{\max} \approx 3280$ and 3209cm^{-1} . Note that in both of these spectra the arbitrary absorbance unit values are circa ~ 0.2 at these functional group frequencies.

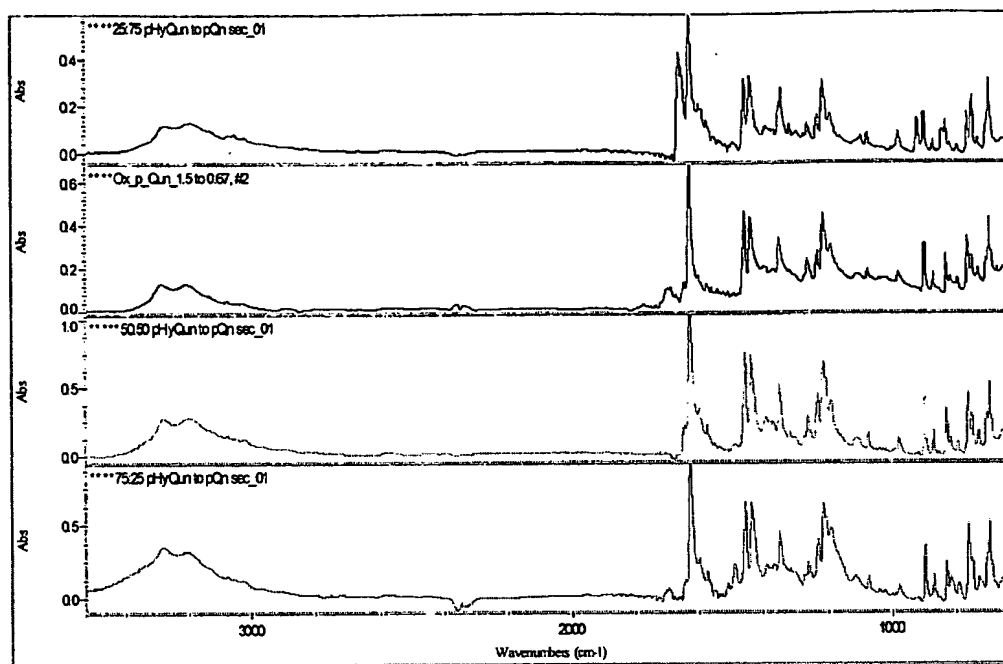


Figure 4.7: FTIR transmission spectrum of oxidation products in contrast with samples mixed at differing ratios of phenylhydroquinone to phenylquinone. 1) (top) 25:75 ratio; 2) second from top (2nd) oxidation product; 3) second from bottom (3rd) 50:50 ratio; 4) (bottom) 75:25 mix ratio.

While the two bottom spectra for the 50:50 mix and the 75:25 mix that show $\nu_{\max} \approx 3280$ and 3209cm^{-1} absorbance values of about 0.3 and above 0.3 respectively, suggesting that the ratio of phenylhydroquinone to phenylquinone in the oxidation product is closer to the ratio of 25:75 in favor of phenylquinone.

Figure 4.8, below, shows absorption spectra for the evolution of hydroxyl stretch as a function of decreased phenylhydroquinone to increased phenylquinone mix ratios. In other words the larger and broader the hydroxyl group frequency absorption the higher the relative ratio of phenylhydroquinone in the mix. The top spectrum at spectrum (100% phenylhydroquinone) shows the highest absorbance at 0.112 arbitrary units for $\nu_{\max} \approx 3300\text{cm}^{-1}$. The trend in hydroxyl absorption decrease can be observed as a function of phenylhydroquinone mix ratio. The trend in hydroxyl absorbance decrease at $\nu_{\max} \approx 3300$

cm^{-1} for the eight spectra shown in Figure 4.8, above, follows the reduction in the mix ratio of phenylhydroquinone to phenylquinone. The $\nu_{\text{max}} \approx 3300 \text{ cm}^{-1}$ absorption of the (90:10 mix) gives absorbance at 0.090 arbitrary units for $\nu_{\text{max}} \approx 3300 \text{ cm}^{-1}$. The characteristic $\nu_{\text{max}} \approx 3300 \text{ cm}^{-1}$ for the oxidation product is estimated at about 0.012 arbitrary units far less than either the 50:50 or 40:60 mixes. Figure 4.8 suggests the oxidation product mixture ratio is somewhere between a 40:60 to 20:80 mix favoring phenylquinone.

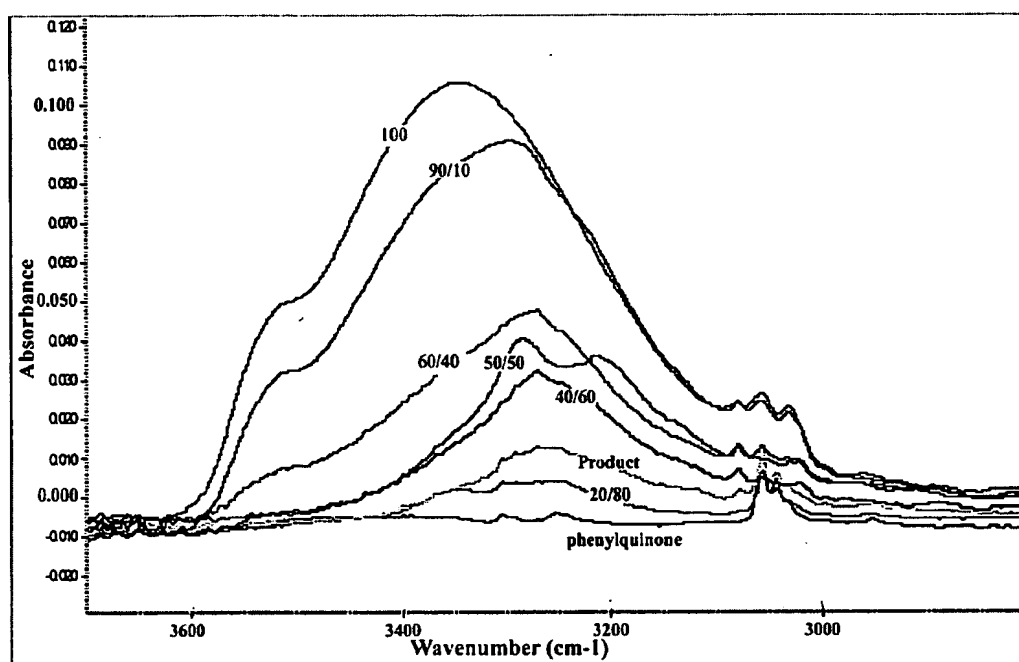


Figure 4.8: FTIR transmission spectra showing, trend in reduction of hydroxyl absorbance at $\lambda_{\text{max}} \approx 3300 \text{ cm}^{-1}$ for: 1) (top) phenylhydroquinone @100:0 ; 2) 2nd from top (90:10 mix); 3) 3rd from top (60:40 mix); 4) 4th from top (50:50 mix); 5) 5th from top (50:50 mix); 6) 4th from bottom (40:60 mix); 7) 3rd from bottom (product); 8) 2nd from bottom (20:80 mix); and bottom (0:100) 100% phenylquinone.

The following three spectra, Figures 4.9, 4.10, and 4.11, below, show IR absorbance in the “finger print” region for three mixture ratios of phenylhydroquinone / phenylquinone contrasted to the oxidation product at: 1) 25:75 ratio Figure 4.9; 2) 50:50 ratio Figure 4.10; 75:25 ratio Figure 4.11. The three characteristic IR absorbance functional group frequencies of interest occur at wavenumber values $\nu_{\text{max}} \approx 1660, 1632 \text{ cm}^{-1}$

(conjugated C=O); $\nu_{\max} \approx 1509 \text{ cm}^{-1}$, $1490, 1431 \text{ cm}^{-1}$ (aromatic C=C) benzene ring; $\nu_{\max} \approx 1280$, and 1195 cm^{-1} for (phenol-OH). Results from the fingerprint region suggest that the mix ratio of phenylhydroquinone to phenylquinone was closer to a 40:60 mix.

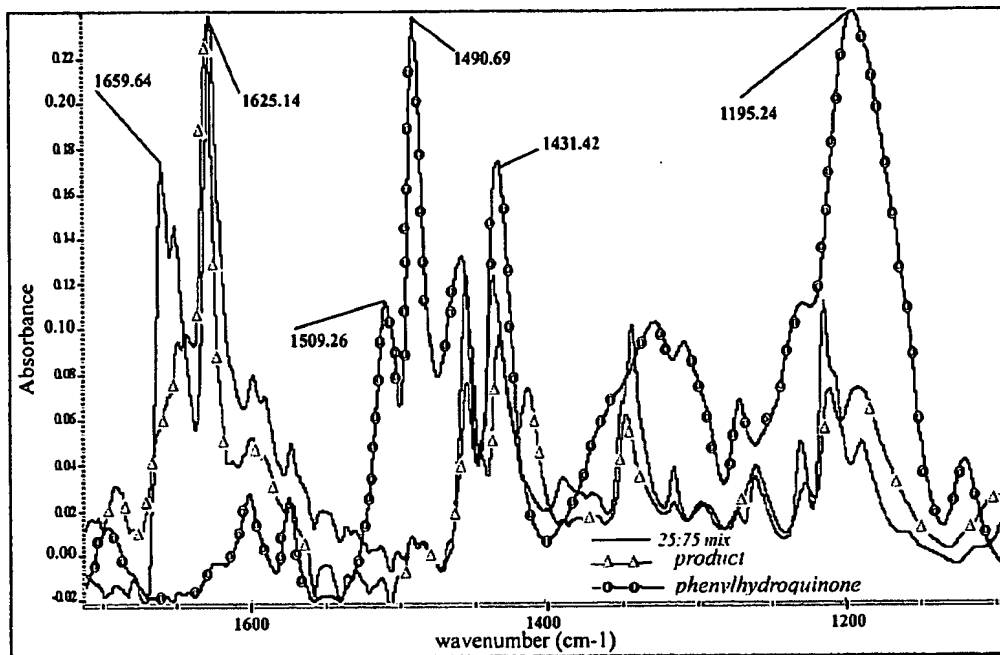


Figure 4.9: FTIR transmission spectra of : 1) 25:75 ratio mix of phenylhydroquinone /phenylquinone mix (—)contrasted with; 2) oxidation product (—Δ—); and 3) phenyl- hydroquinone (—○—).

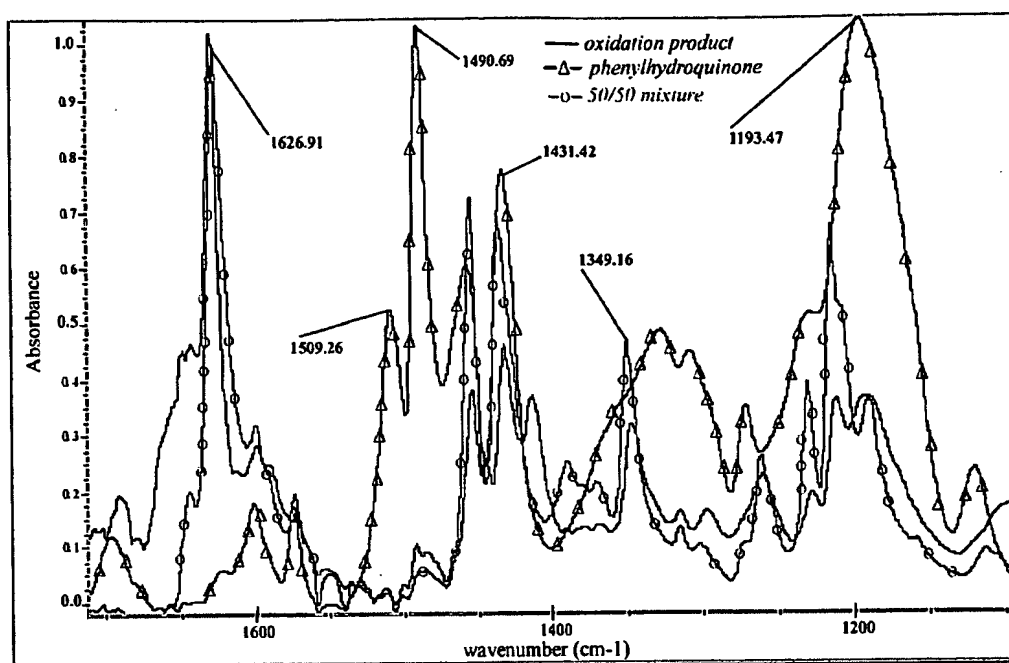


Figure 4.10: FTIR transmission spectra of: 1) 50:50 ratio mix of phenylhydroquinone / phenylbenzoquinone mix (—○—), contrasted with 2) oxidation product (—); and 3) phenylhydroquinone (—△—).

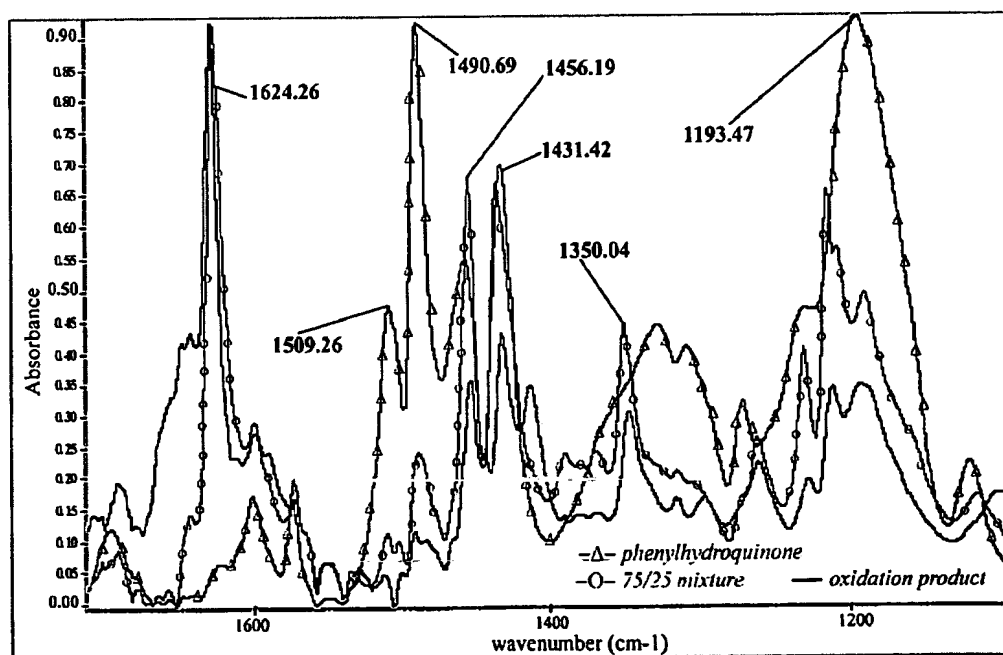


Figure 4.11: FTIR transmission spectra of: 1) a 75:25 ratio mix of phenyl hydroquinone / phenylquinone mix (red, —○—) contrasted with; 2) oxidation product (—); and 3) phenyl- hydroquinone (—△—).

4.6 Summary

The UV-Vis spectra, Figures 4.5 (a)-(b), above, show two characteristic λ_{\max} absorption values at 245 nm and 360nm that correspond to the presence and relative molar fraction of phenylquinone in the oxidized product. The observed λ_{\max} circa 290nm corresponds to the presence of phenylhydroquinone. Data from spectra, Figure 4.5 (a) and (b), show an absorption at $\lambda_{\max} = 245\text{nm}$ for the oxidation product of 3.5 at 0.001mmole and 1.75 at 0.0005mmol, which is above the absorbance for the 33:66 ratio mix product.

With reference to the FTIR absorption spectra, Figures 4.9 to 4.11, the oxidized product is surmised to consist of a mixture of phenylhydroquinone and phenylquinone at a ratio greater than 50:50 and less than 25:75. From Figure 4.9, at a ratio of 25:75, the oxidized product in (—Δ—) shows a shoulder at $\nu_{\max} \approx 1660\text{ cm}^{-1}$, with equal absorbance at 1632 cm^{-1} (conjugated C=O). In addition there is minimum absorbance at $\nu_{\max} \approx 1509\text{ cm}^{-1}$, 1490, 1431 cm^{-1} (aromatic C=C) benzene ring, confirming the transformation from benzoidal to quinonoidal, and finally, the minimized absorption at the frequencies $\nu_{\max} \approx 1280$, and 1195 cm^{-1} for (phenol-OH) which are strongest for phenylhydroquinone and weakest for phenylquinone. From Figure 4.10, the oxidized product was contrasted to the 50:50 mixture in which reveals a strong absorption at $\nu_{\max} \approx 1632\text{ cm}^{-1}$ (conjugated C=O), but no shoulder at $\nu_{\max} \approx 1660\text{ cm}^{-1}$ indicating the presence of quinone and that the 50:50 mix ratio with no shoulder may be present as quinhydrone. In addition, Figure 4.10 shows an increase in the absorbance at $\nu_{\max} \approx 1509$, 1490, and 1431 cm^{-1} (aromatic C=C) benzene ring, indicating more benzoidal alkene as opposed to quinonoidal; and finally, the absorption at the frequencies $\nu_{\max} \approx 1280$, and 1195 cm^{-1} for (phenol-OH) which are strongest for phenylhydroquinone are enhanced. Finally, absorption data from Figure 4.11,

above, follow the same trend as Figure 4.10, above, suggesting that the oxidation product consisted of a mix ratio greater than 60 % phenylhydroquinone.

4.7 Experimental Crosslinker

The crosslinker synthesis in this section is based amine-quinone chemistry where 1) phenylquinone undergoes nucleic amination by the primary amine from *N*-β-(aminoethyl)-γ-aminopropyltrimethoxysilane, (nucleophilic Michael addition) followed by 2) heterocyclic ring closure occurs by secondary amine of the *N*-β-(aminoethyl)-γ-aminopropyltrimethoxysilane moiety. This is thought to occur according to the proposed reaction Scheme 4.1, below. The molar ratio of nucleophile, βE- γ-APTMS to phenylquinone was 3.80: 2.77 leaving an additional mole of primary amine in the mix. This was done based upon the observation that phenylhydroquinone continues to be oxidized *in situ* within 24 hours after the initial side chain amination reaction, Figure 4.14 A, B, and C, below.

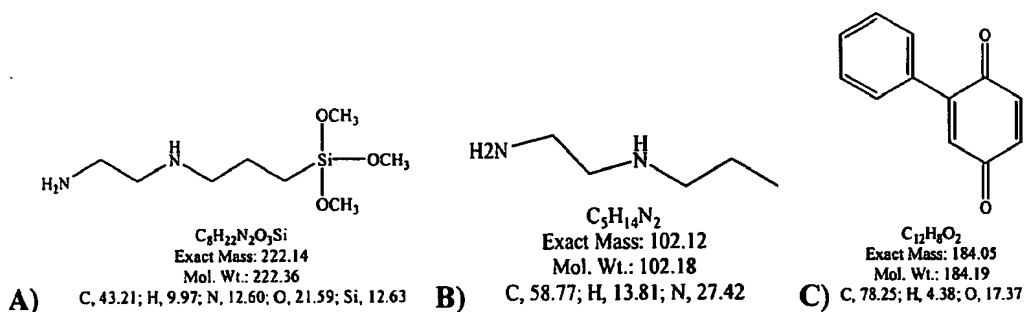


Figure 4.12: A) *N*-β-(aminoethyl)-γ-aminopropyltrimethoxysilane, Silquest™ (A-1120), Witco OSi Specialties[‡]; B) *N*-propylethylenediamine (Aldrich); C) 2-phenyl-1,4-benzoquinone or phenylquinone.

The crosslinker for this study was synthesized by starting with the oxidation product, that was determined to consist of about 60 % phenylquinone and 40%

[‡] OSi Specialties, A Crompton Corp. ,One American Lane, Greenwich, CT 06831 2559, USA

phenylhydroquinone, which was dissolved in propylene carbonate at 0.85g per 25-ml (PC) to which 0.85g SilquestTMA1200, *N*-β-(aminoethyl)-γ-aminopropyltrimethoxy silane all chemicals was added. From Table 4.3, below, the relative mass and molar quantities used in a one pot synthesis batch are reported.

Table 4.3: Materials for crosslinker synthesis

Material	supplier	grams	mmoles
Product (phenylquinone)	(<i>in house</i>)	0.50	2.77
βAE- γ-APTMS	(Witco)	0.85	3.80
Propylene Carbonate (PC)	(Aldrich)	(20-ml)	(solvent)
EEP solvent	(Aldrich)	(5-ml)	(solvent)
N-propylethylenediamine	(Aldrich)	0.28	2.74

* note: (PC) and 3-Ethoxypropionic acid ethyl ester (EEP) both non-HAPS compliant solvents.

Quinones are highly conjugated α,β unsaturated diketones that possess color due to charge separated resonance forms from *sp*² conjugation extending throughout the molecule. Color is a property that has been used to classify the effects of substitution reactions on the quinonoidal ring. Central to understanding the reactions of quinones is that that the parent, benzoquinone, is yellow and with larger conjugated systems, especially when hydroxyl groups modify the chromophore (*auxochromes*), they can be bright red.

Nikles *et al.*⁵⁰⁷, report the color change associated with the nuclear amination reaction / Michael addition involving benzoquinone and a primary amine has observed to result in the solution of benzoquinone changing from yellow to green upon addition and reaction of the amine. Thus, signifying that the more substituted quinonoidal ring has undergone a substitution reaction causing a *red shift* in the conjugated system, i.e., the color of light the substance absorbs is related to the wavelength of light, see Table 4.4, below. Conjugated systems that become more delocalized shift to absorptions at longer

wavelengths. The substitution reaction described by Nikles *et al.* results in an amino-quinone, where the lone pair electrons on the *sp*³ nitrogen extend the molecule's electron density and provide extended charge separated resonance forms as well.

However, what is observed in the reaction of phenylquinone and the β AE- γ -APTMS is a color change from yellow to green, (signifying the initial nuclear amination reaction); followed by a color change from green to red, (signifying the formation of an *auxochrome* phenolic group). From Table 4.4, the color change from green to red signifies a shift in the wavelength of light the molecule absorbs, i.e, the appearance of a red colored material signifies a *blue-shift* from the green colored material meaning the conjugated "green" system has become more localized and shifted to absorptions at shorter wavelength. The color change corresponds to the loss of extended electron density, and the reduction in the number of resonance contributors.

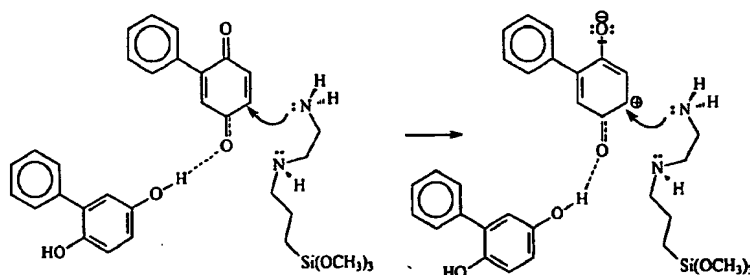
Table 4.4: Guide to wavelengths and corresponding colors ⁵¹⁹		
Wavelength of light λ (nm)	Color of light	Color of substance that absorbs at λ
400	Blue	Yellow
500	Green	Red
600	Yellow	Blue
700	Red	Green

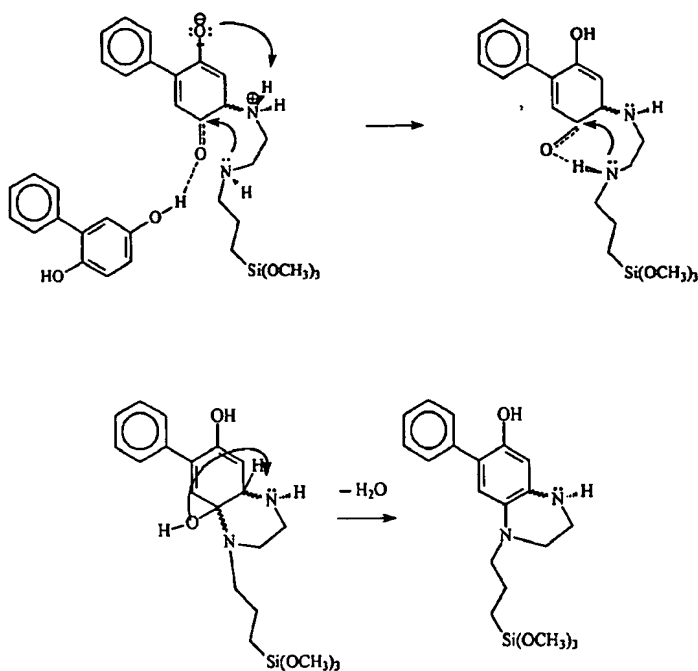
The synthesis of the crosslinker is described as follows: 1) oxidized product was first dissolved in the solvent mix at 25°C and the reaction was run in a 100 ml cup in open air at 25°C; 2) the β AE- γ -APTMS was added using a disposable pipette, added drop wise while gently swirling, and 3) A color change in solution can be observed where the phenylquinone solution changes from yellow \rightarrow green \rightarrow vermillion / red, with the

evolution of water vapor occurring during the green to red color change step. The duration of the color change from yellow to green is instantaneous, while the green to red period can last between 5 to 60 seconds, depending upon the temperature of the solution and the nature of the solvent used. It should be noted that during the green to red color change step water vapor is observed. This is important to note as water loss is required in the heterocyclic ring formation step of the proposed mechanism, Scheme 4.1, below.

Additionally, it was observed that warmer solutions, circa 25°C to 30°C changed color faster and evolved more water vapor than room temperature solutions which evolved less water vapor. Note, the pH of the water vapor was acidic, pH~2, determined with both wetted and dry pH paper. The solvent effect thought responsible for moderating the green to red transition followed a polarity effect where aliphatic ketones and carbonates act to slow the reaction while aromatic hydrocarbons such as xylene, or a polar ether such as THF act to greatly accelerate the green to red transition reaction.

The reaction is proposed to occur as follows, see Scheme 4.1, below: 1) substitution by nuclear amination via replacement of hydrogen from an alkyl group on the quinonoid ring by an amine^{520, 521}; 2) heterocyclic ring-closure to form the silane modified quinoxalinol product.





Scheme 4.1, general reaction sequence in the formation of 7-phenyl-1-[4-(trimethyl-silyl)-butyl]-1,2,3,4-tetra-hydro-quinoxalin-6-ol crosslinker (7-PQ-6-ol).

The spectroscopic data shown in Figure 4.12 is for the product of Scheme 4.1, top spectrum in (green) contrasted to the product from an analogous compound N-propyl-ethylenediamine (Aldrich Chemicals) added to the oxidation product (top) that appears to undergo a similar reaction similar reaction to the homologue β AE- γ -APTMS.

The most readily observed differences between the two spectra is that the spectrum in red lacks the methoxysilane absorbance at $\nu_{\max} \approx 1090$, and 954 cm^{-1} and it shows a more prominent $\nu_{\max} \approx 1260 \text{ cm}^{-1}$ for phenol Ar-OH possibly due the observation that silation of the methoxy silane occurs in the case when β AE- γ -APTMS is present. The hydrosilation reaction, which begins immediately in the presence of Ar-OH, tends to reduce the hydroxyl absorption and lead to a broadening of the characteristic $\nu_{\max} \approx 1090 \text{ cm}^{-1}$ region as depicted in Figures 4.12, 4.13, 4.14 and 4.26, below.

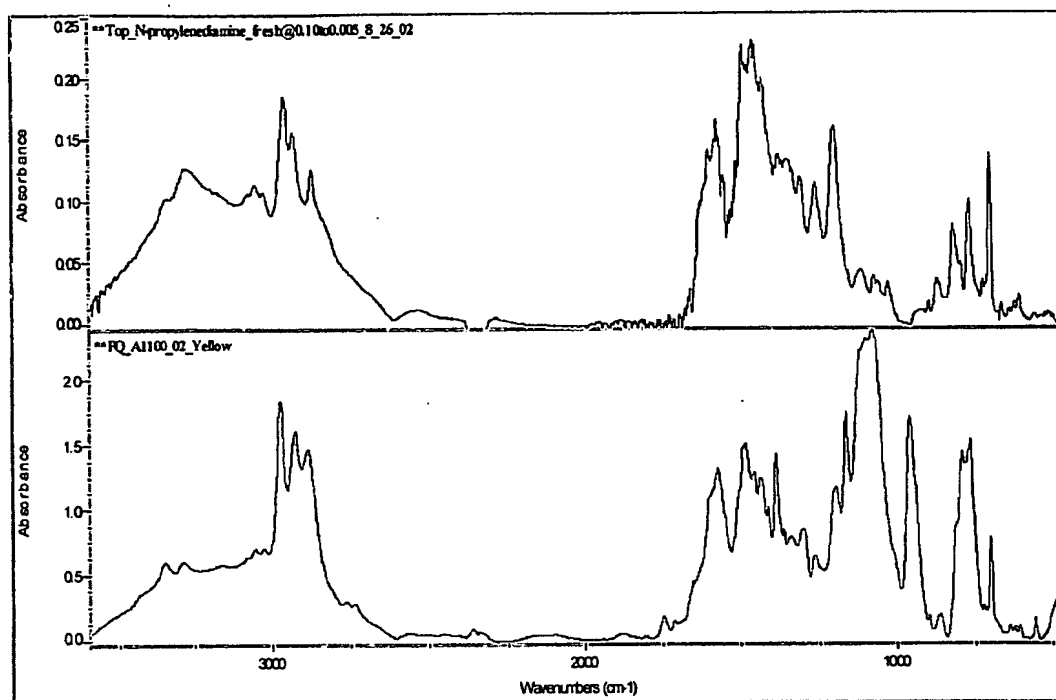


Figure 4.13: FTIR transmission spectra of products formed from 1) phenylquinone and diamine (top) in blue: β AE- γ -APTMS product and 2) (bottom) in red: N-propylethylenediamine product.

Table 4.5, below, gives reference absorption frequencies of ν_{\max} for functional groups relative to spectra shown in Figures 4.13-to- 4.15. The structure of the proposed (7-PQ-6-ol) crosslinker appears to match group IR frequency absorbance data in Figures 4.13-to- 4.15. However, due to some overlap of select group frequencies in complex spectral data, not all group frequency absorptions can be substantiated at more than two characteristic ν_{\max} group frequencies. In particular, with reference to Figure 4.14, for the β AE- γ -APTMS product, group frequency absorptions for (C-N) stretch for secondary and tertiary amines is obfuscated in the $1120\text{--}1150\text{ cm}^{-1}$ wavenumber range is hidden due to the presence of strong Si-O-Si absorption. On the other hand, for the N-propylethylenediamine product, the characteristic group frequency absorptions do appear thus confirming the presence of Aryl-N and the formation of the proposed (7-PQ-6-ol) structure.

Table 4.5: Characteristic (IR) functional group frequency ν_{\max} in fingerprint region.

Functional group	1) band (cm^{-1})	2) band (cm^{-1})	3) band (cm^{-1})
N-H (sec amine bend)	1660	1509	1463
Ar-N (C-N stretch)	N/A	1250 -1310	1210-1150
C=C (aromatic bend)	1605	1489	790
C-N (stretch)	1576	1380 & 1296	1090-1020
C-O-H (phenol bend)	1326	1270	1200
Si-O-CH ₃	N/A	1090	813

* Coates, J., Interpretation of IR spectra⁵²²

A brief summary of the spectral data in Figure 4.13, above, reveals an apparent difference in relative absorbance units for the two spectrum and the amount of secondary amino stretch circa $\nu_{\max} \approx 3280 \text{ cm}^{-1}$ for the N-propylethylenediamine product (spectrum, top) as opposed to the β AE- γ -APTMS product (spectrum, bottom) with amino group absorptions at $\nu_{\max} \approx 3347$ and 3290 cm^{-1} which fall into the range of secondary amino absorption $3360\text{-}3310 \text{ cm}^{-1}$ for aliphatic secondary amines, or possibly primary amino at 3347 cm^{-1} .⁵²²

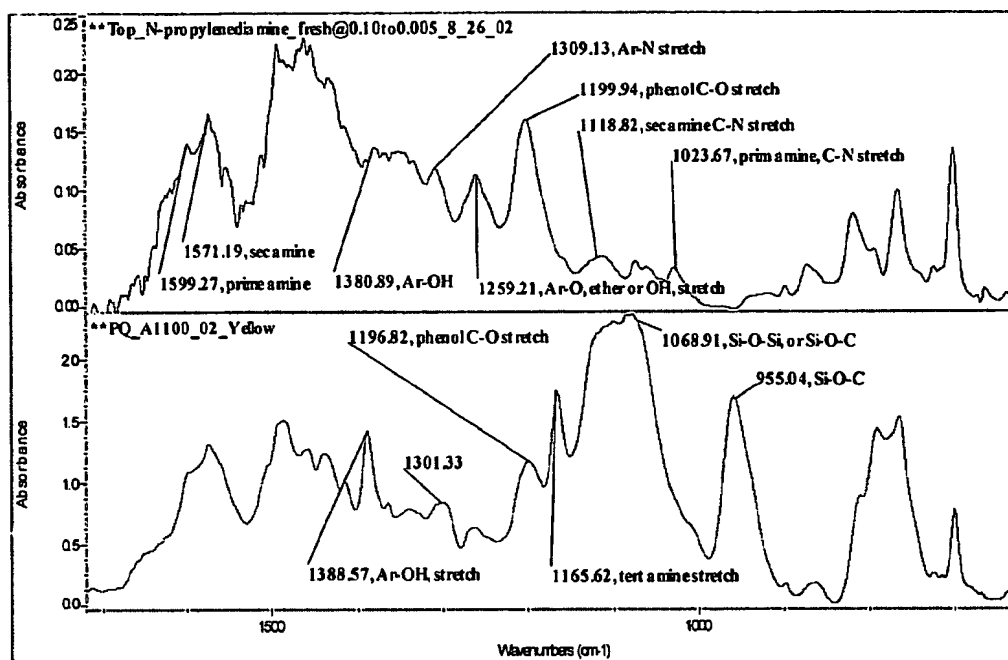


Figure 4.14: FTIR transmission spectra of frequency group absorbance in the spectral finger print region for the two products; 1) above N-propylethylenediamine product; 2) below β AE- γ -APTMS product. Characteristic ν_{\max} given in wavenumbers.

Observations from preliminary work done on formulating polymeric coatings from crosslinker prototypes, such as those described here, showed that when the crosslinker was used as a curative for epoxy / polyisocyanate coatings, those coatings that contained crosslinker formulated with a phenylhydroquinone / phenylquinone mix cured faster than those with just phenylquinone. It may be surmised that the phenolic hydroxyls work in conjunction with heterocyclic tertiary amines to promote full cure. In addition, it was observed the crosslinker takes on a deeper color vermilion / red with time. This color change was investigated using FTIR spectroscopy.

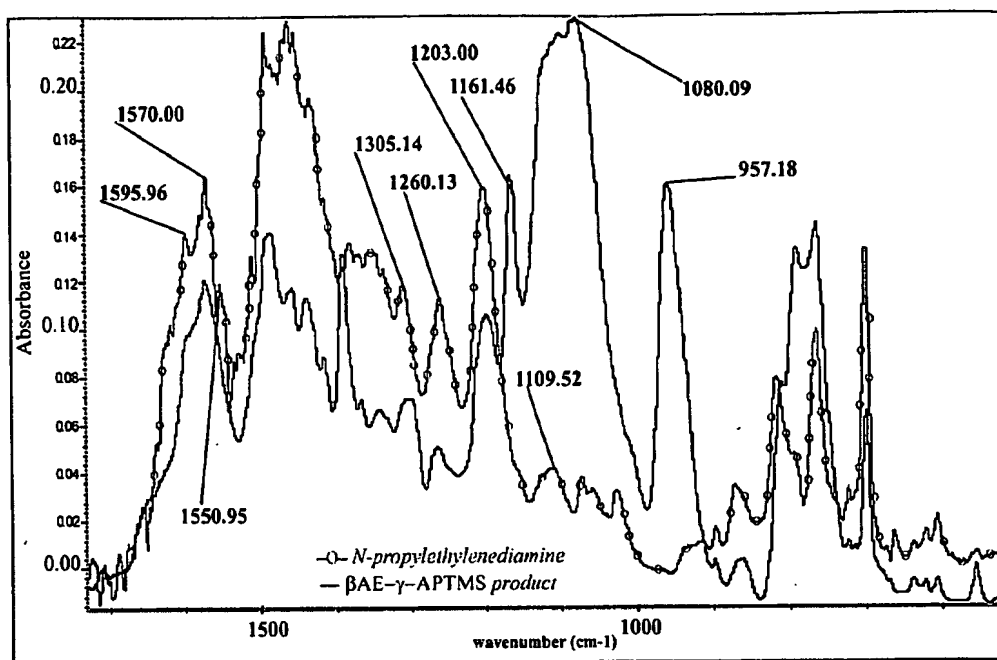
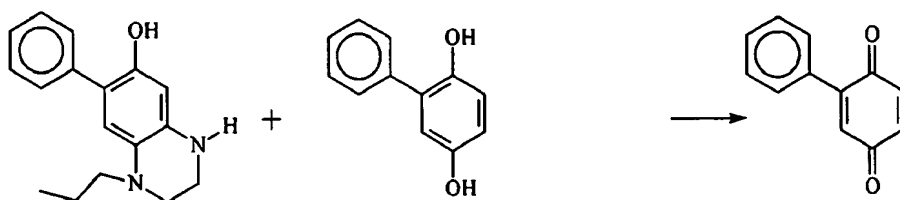


Figure 4.15: FTIR transmission spectra for frequency group absorbance in the spectral finger print region for the two products, 1) above in (—○—), N-propylethylenediamine product; 2) below in (—), β AE- γ -APTMS product.

A potentially beneficial side reaction that was surmised to have occurred as a result of an excess of phenylhydroquinone in the 40:60 mix was the latent oxidation of phenylhydroquinone to phenylquinone. Figure 4.15, below, depicts the product mix, hydroquinoxalinol product and phenylhydroquinone. What was observed, Figures 4.17 and 4.18 in the spectroscopic data, was the conversion / oxidation of phenylhydroquinone into phenyl quinone *in situ* as can be seen in the appearance of group frequency $\nu_{\max} \approx 1654 \text{ cm}^{-1}$ for conjugated ketone quinone and the decrease in the $\nu_{\max} \approx 1200 \text{ cm}^{-1}$ (Ar-O stretch) for phenol as well as a reduction in the relative absorbance in the broad hydroxyl (O-H stretch) at $\nu_{\max} \approx 3200 \text{ cm}^{-1}$.



(hydroquinoxininol product) (phenylhydroquinone) oxidized *in situ* → 72-hours

Figure 4.16: Fresh product mix with plus 2-phenyl-1,4-benzoquinone oxidized, under nitrogen, *in situ*, at room temperature~ (70°F / 22°C) after 72 hours.

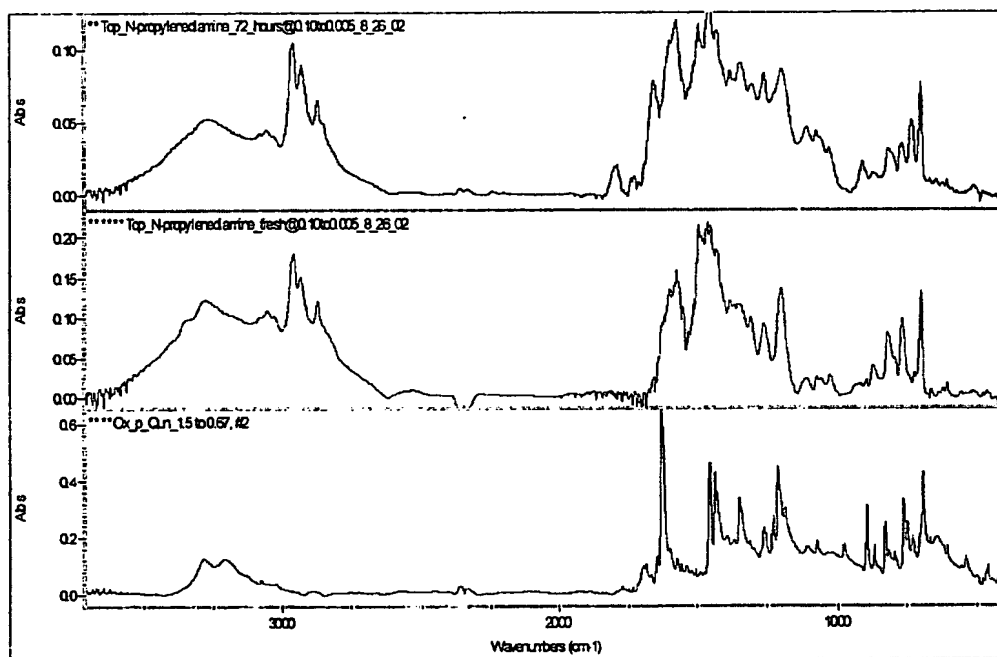


Figure 4.17: FTIR transmission spectrum of 1) hydroquinoxininol product from N-propylethylenediamine; (top) blue aged 72 hours under nitrogen; 2) (middle) red initial, and 3) starting material (bottom) pink no amine present, group frequency $\nu_{\text{max}} \approx 1654 \text{ cm}^{-1}$ typical of conjugated quinone.

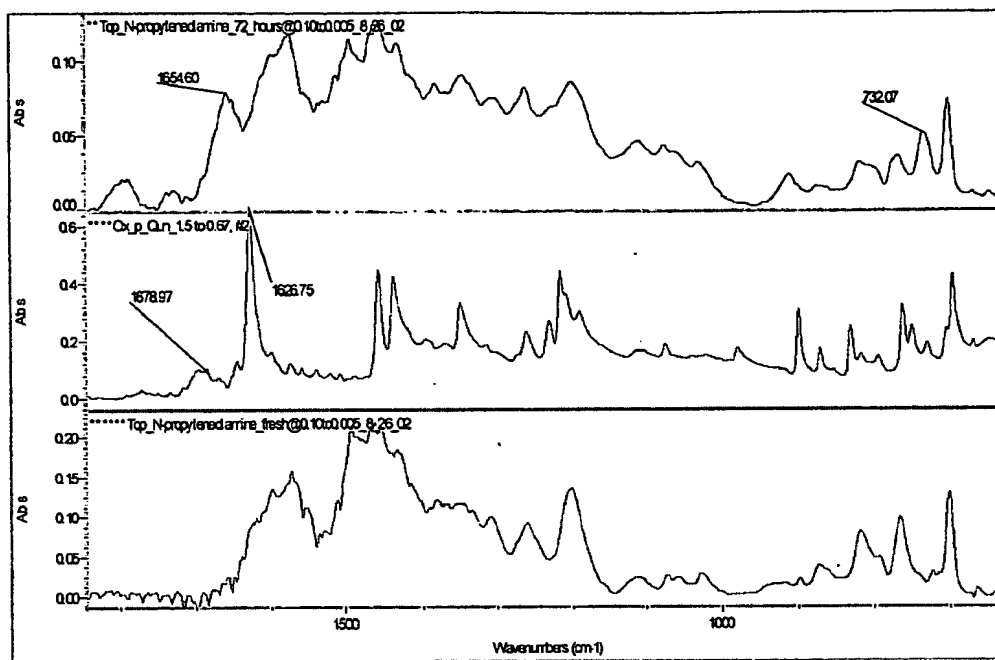


Figure 4.18: FTIR transmission spectrum of: 1) hydroquinoxininol product from N-propylethylenediamine, (top) red aged 72 hours under nitrogen; 2) (middle) green initial, and starting material (bottom) gray; no amine present, group frequency $\nu_{\max} \approx 1654 \text{ cm}^{-1}$ typical of conjugated quinone.

Spectroscopic evidence strongly suggests that latent oxidation of free phenylhydroquinone occurs in the presence of the product (7-PQ-6-ol). What is not believed to occur is the oxidation of the (7-PQ-6-ol) product for the following reasons: 1) loss of aromaticity; 2) formation of imine at C-1; formation of C=O at C-6 are all unlikely to occur. Therefore, the observed change is surmised to be due to the oxidation of free phenylhydroquinone.

The following analysis[§] given in reference to Figures 14.19 –to– 4.25, below, show group frequency absorption characteristics, for select functional group absorbance ν_{\max}

[§] Spectral characterization group frequency standards were obtained using Bio-Rad laboratories IR MentorPro™ version 2.0 software.

superimposed over spectrum of β AE- γ -APTMS product, proposed (7-PQ-6-ol) structure.

Overall, it can be seen that group absorption frequencies for the proposed structure coincide with the corresponding reference standards.

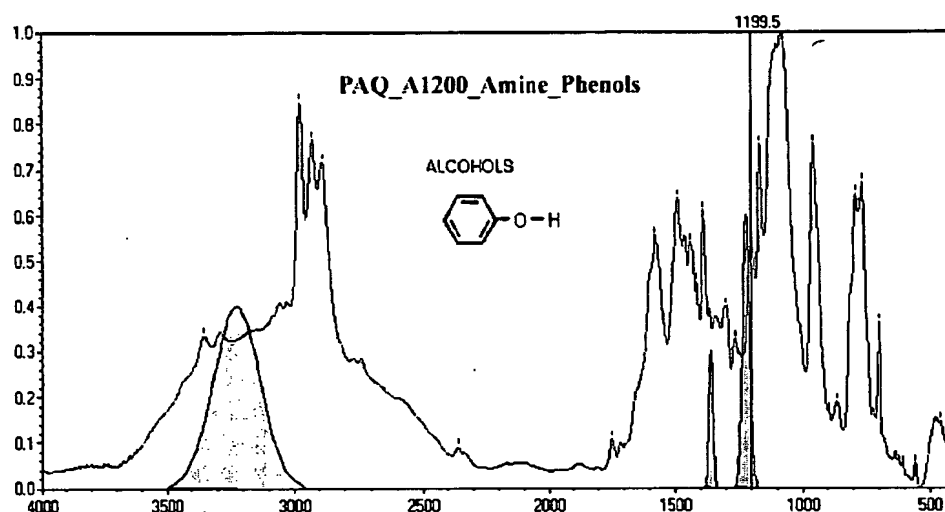


Figure 4.19: FTIR transmission spectrum with group frequency absorption ν_{\max} for phenol superimposed over product FTIR spectrum, illustrating function absorptions that coincide.

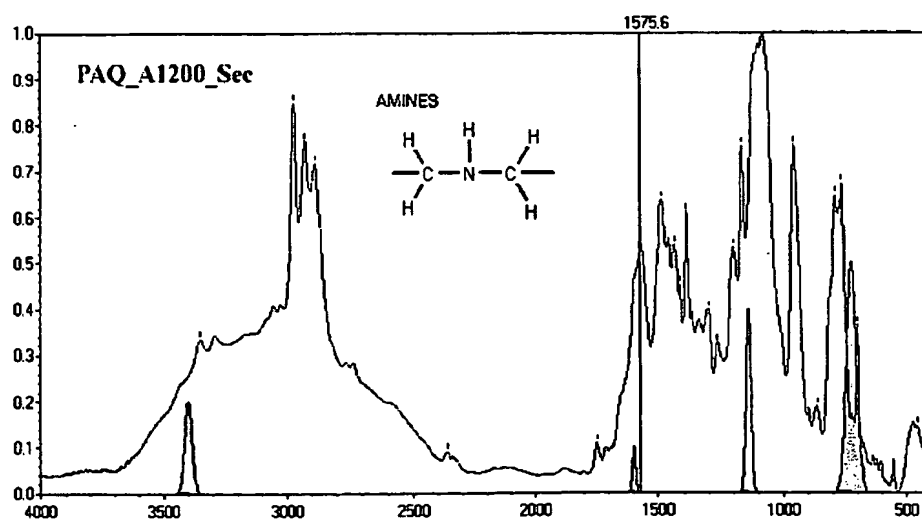


Figure 4.20: FTIR transmission spectrum with group frequency absorption ν_{\max} for secondary amino superimposed over FTIR product spectrum, illustrating function absorptions that coincide.

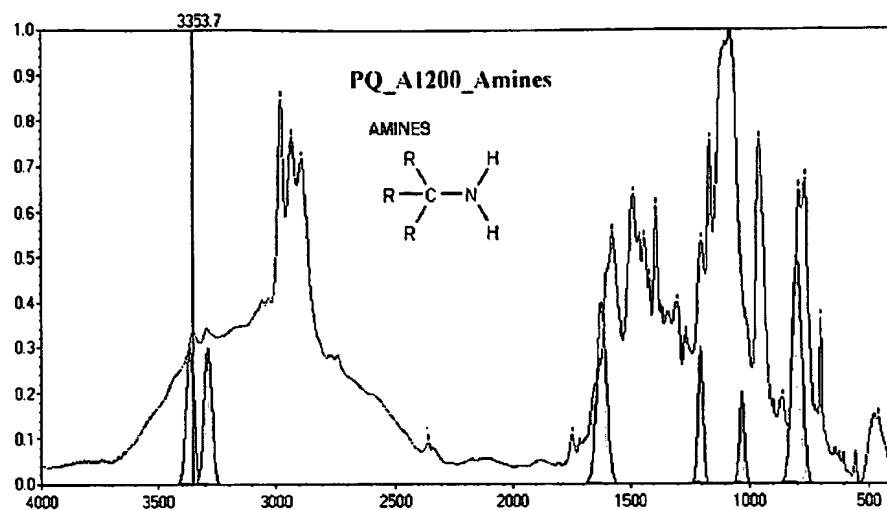


Figure 4.21: FTIR transmission spectrum with group frequency absorption ν_{\max} for primary amino superimposed over product FTIR spectrum, illustrating function absorptions that coincide.

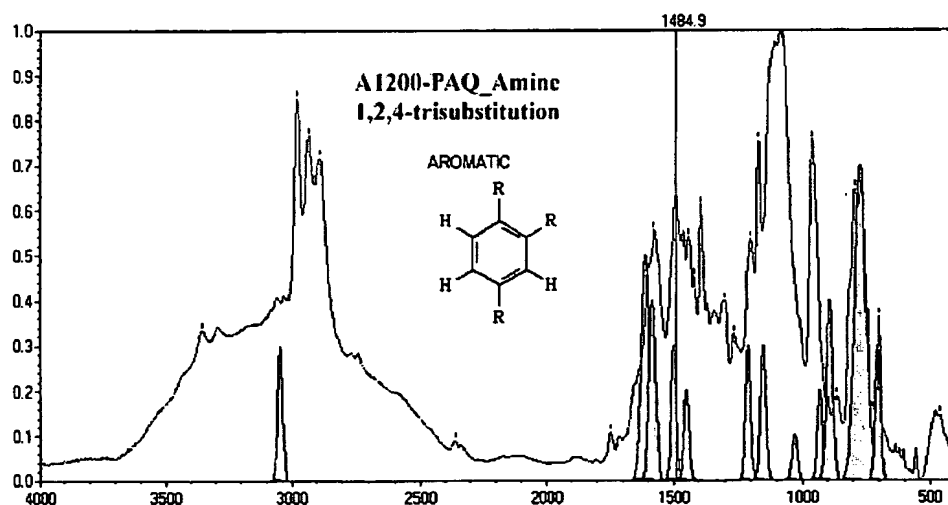


Figure 4.22: FTIR transmission spectrum with group frequency absorption ν_{\max} for 1,2,4-substitution of benzene ring superimposed over product FTIR spectrum, illustrating function absorptions that coincide.

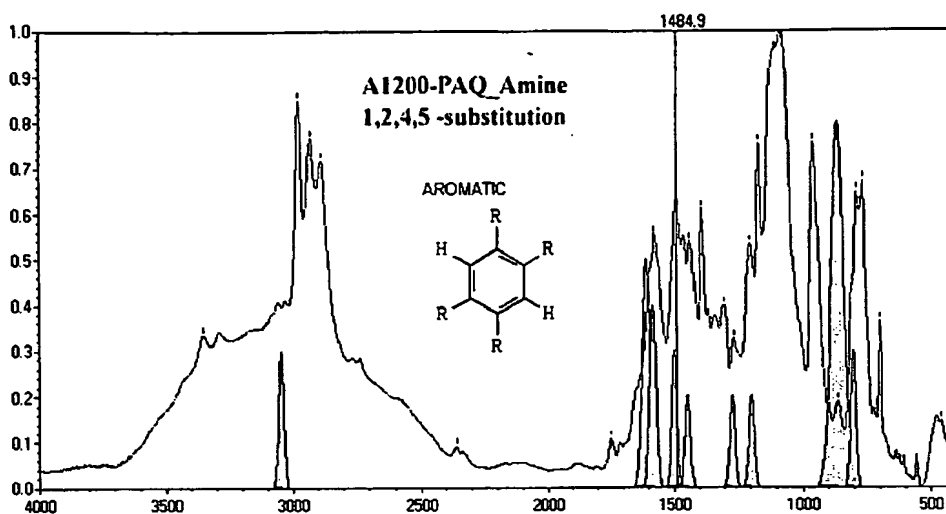


Figure 4.23: FTIR transmission spectrum with group frequency absorption ν_{\max} for 1,2,4,5-substitution of benzene ring superimposed over product FTIR spectrum, illustrating function absorptions that coincide.

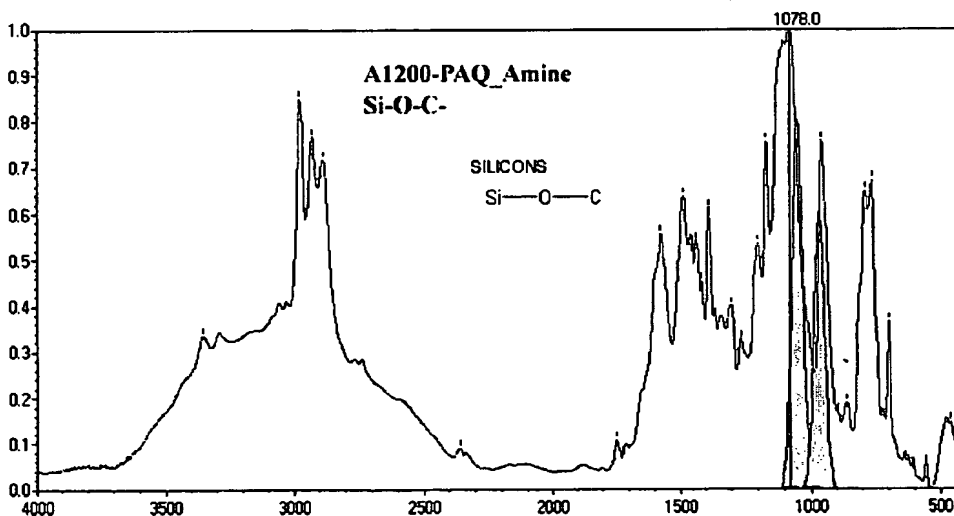


Figure 4.24: FTIR transmission spectrum with group frequency absorption ν_{\max} for Si-O-C superimposed over product FTIR spectrum, illustrating function absorptions that coincide.

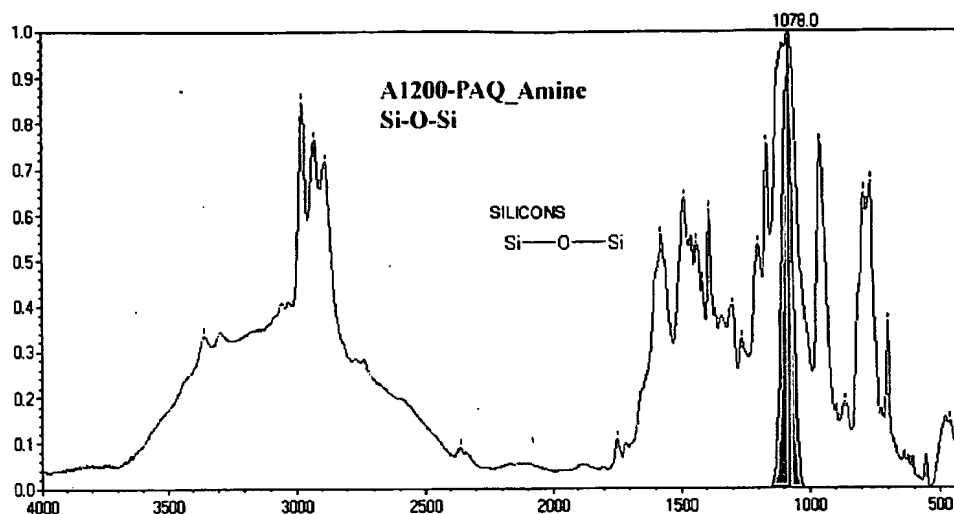


Figure 4.25: FTIR transmission spectrum with group frequency absorption ν_{\max} for phenol superimposed over product FTIR spectrum, illustrating function absorptions that coincide.

4.8 Summary Crosslinker Synthesis

Complex FTIR spectra were used to identify the formation of the 7-phenyl-1-[4-(trimethyl-silyl)-butyl]-1,2,3,4-tetra-hydroquinoxalin-6-ol (7-PQ-6-ol) structure. In addition, a homologous product, (7-PQ-6-ol) structure was examined and contrasted as shown in the spectral data presented in Figures 4.13-to-4.25. Spectra of both products show similar results, thus indicating a similar reaction mechanism for both. Due to the occurrence of *in situ* hydrosilation reactions with dissolution / precipitation of silyl modified product, *N*-propylethylenediamine was used as a nucleophile to form an analogous product that could be analyzed without complications arising from hydrosilation reactions. From this it was observed that phenylhydroquinone was further oxidized *in situ*, in the presence of the (7-PQ-6-ol) product. Therefore, an excess of primary amine functionality, Table 4.4, above was added for the purpose of promoting latent sidechain substitution reactions between labile amine and the latent forming α - β unsaturated diketone

(phenylquinone). It is surmised that facile formation of quinone-amine oligomers would occur under such circumstances, as reported by Erhan⁵⁰³, Nikles⁵⁰⁷, etc. that in turn may confer similar beneficial performance properties to the polymeric material formed in these systems.

4.9 Crosslinker hydrosilation reaction

The purpose of the following study was to ascertain whether the hydrosilation mechanism, though responsible for contributing to IPN structure in this polymeric material could be substantiated and verified using Fourier transform infrared spectroscopy (FTIR) methodology through identifying characteristic group frequency absorptions that occur in the course of the hydrosilation reaction. In developing the crosslinker, Silquest™ A1200 β AE- γ -APTMS (methoxysilane) was chosen as opposed to Silquest™ A1100 β AE- γ -APTMS (ethoxy silane) due to the higher reactivity of the methoxy silane functionality at lower temperatures. See literature review Chapter 2.4 for adjunct references. Results from studies on a prototype crosslinker formulated with β AE- γ -APTMS (ethoxy silane) showed that β AE- γ -APTMS (ethoxy silane) was not suitable as it did not come to full cure, over hybrid epoxy / polyisocyanate systems and required extended cure times and elevated temperature to yield proper crosslinking.

Figures 4.26– 4.27, below, show FTIR spectral data for the proposed *in situ* hydrosilation reaction occurring between methoxysilane moieties and the (7-PQ-6-ol) crosslinker in open, air and under ambient conditions. This experiment was performed on KBr salt plate.

The crosslinker was deposited on the plate from an acetone solution and allowed to cure on the salt crystal enclosed in the sample compartment of the spectra photometer. The

duration of the reaction was one hour during which time significant changes in the spectral data occurred from which it was observed that the formation of silane linkages occurred as measured by an increase in functional group frequency absorbance attributed to the presence of Si-O-Si and by a relative decrease in functional group frequency absorbance attributed to -Si-O-C-, the methoxy silane component that reacts with atmospheric moisture to liberate methanol. See Chapter 2.4 regarding the hydrosilation reaction.

Equation 4.1 hydrosilation:

(1)

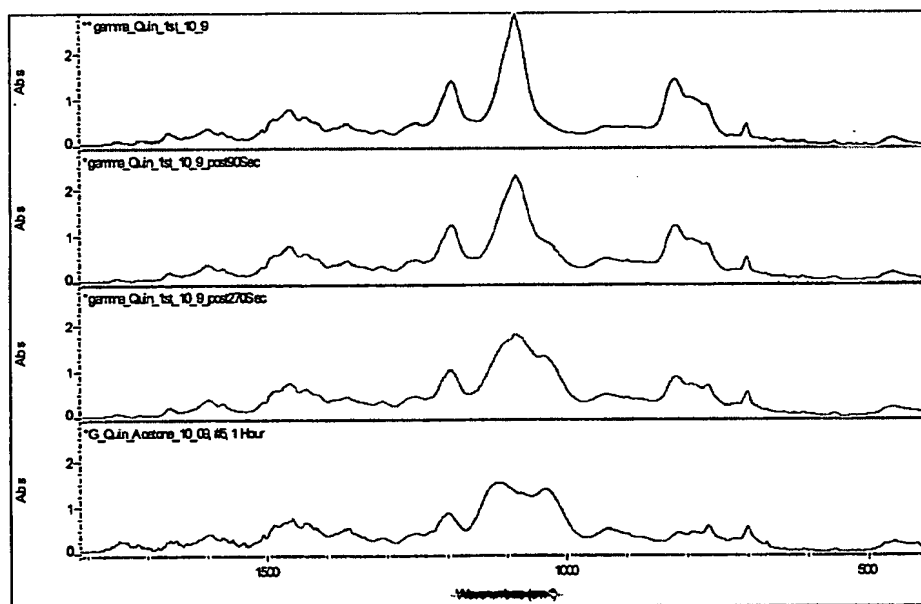


Figure 4.26: FTIR transmission spectra finger print region for crosslinker undergoing *in situ* hydrosilation. (blue) spectrum at time zero; (green) at 90-seconds; (pink) at 270- seconds; and (red) at 60-min. Note reduction of $\nu_{\max} \approx 1082 \text{ cm}^{-1}$ with splitting of absorption into $\nu_{\max} \approx 1117$ and 1034 cm^{-1} after 60 minute duration.

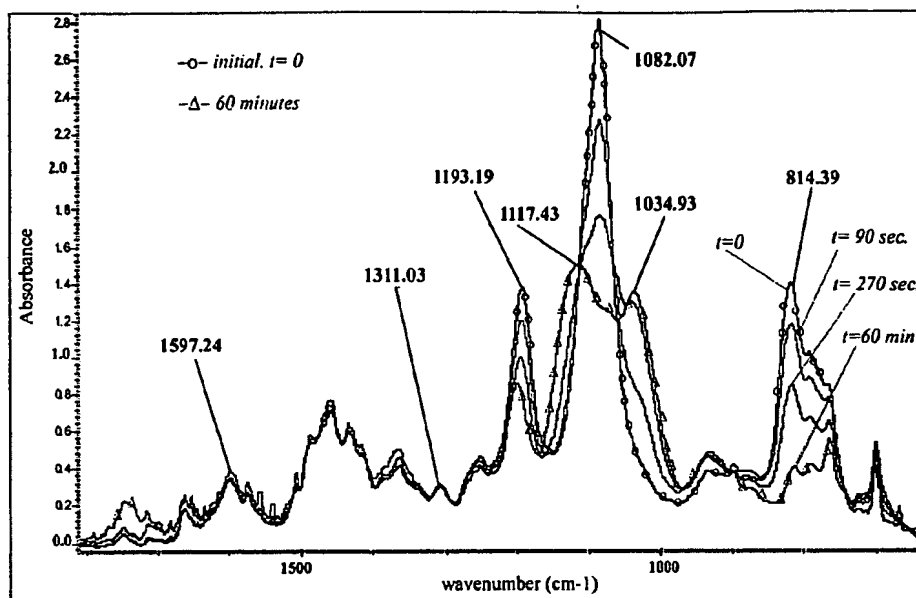


Figure 4.27: FTIR transmission absorption spectra in finger print region illustrating hydrosilation reaction: 1) (—O—), initial at $t = 0$; 2) (—) at $t = 90$ -seconds; 3) (—) at $t = 270$ -seconds; and 4) (—Δ—) post one hour cure, Si—O—CH₃ stretch $\nu_{\max} \sim 817\text{cm}^{-1}$; asymmetric stretch $\nu_{\max} \sim 1087\text{cm}^{-1}$; Aryl—NH— stretch $\nu_{\max} \sim 1320\text{cm}^{-1}$; Si—O—Si Asymmetric stretch, chain length, band splits into two group ν_{\max} absorption frequencies $\nu_{\max} \sim 1112$ and 1038cm^{-1} .

4.10 Crosslinker: Epoxy-Amine Reaction

The purpose of the following study was to determine the effectiveness and of the (7-PQ-6-ol) crosslinker as a curative for an epoxy diglycidal ether of bisphenol A (DGEBA). Even though this study examines the epoxy-amine reaction, the DGEBA epoxy system was chosen for the simple reason that if it will not cure in an epoxy-amine system, it probably would not be suitable for promoting a pseudo IPN structure in a hybrid modified epoxy-polyurea system.

The spectroscopic data, Figures 4.29 and 4.30 is referenced to Figure 4.28, below, FTIR transmission spectrum with characteristic group frequency ν_{\max} absorption for commercial grade liquid diglycidyl ether of bisphenol A, Epon® 828.⁵²³ What is clearly

missing in the spectrum is the characteristic hydroxyl (O-H) stretch commonly observed at group frequency absorptions in the $\nu_{\max} \sim 3400 - 3200 \text{ cm}^{-1}$ region indicating chemical conversion by the opening of the epoxide ring.

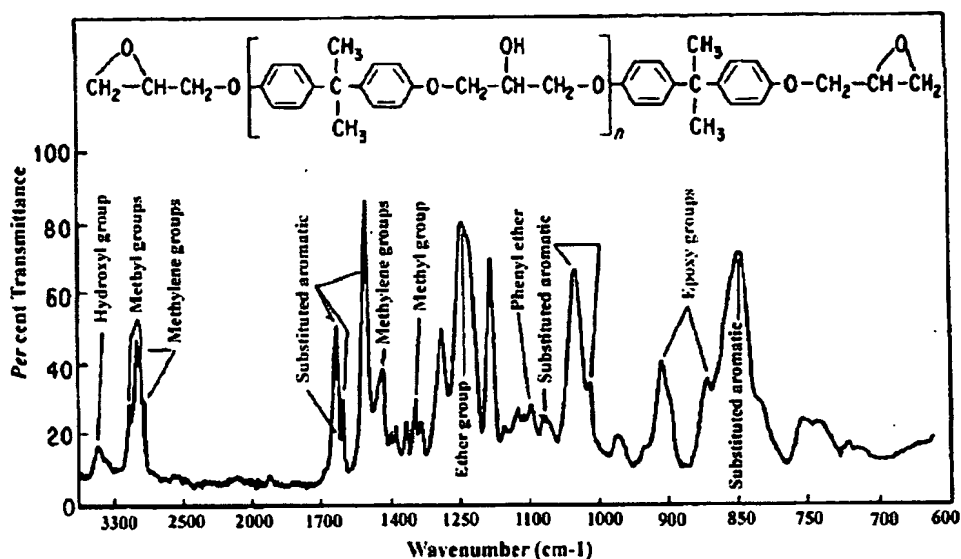


Figure 4.28: FTIR transmission spectra for characteristic epoxide functional group absorption appearing at $\nu_{\max} \sim 914$ and 876 cm^{-1} .

Figures 4.28 –to- 4.29, below, show FTIR spectra for the epoxy amine reaction product between Epon™ 1001-X, with epoxide equivalent weight (EEW)~500 and 7-phenyl-1-(4-propyl)-1,2,3,4-tetra-hydroquinoxalin-6-ol crosslinker. Regarding the chemical structure of Epon™ 1001-X, it is a Taffy process resin⁵²⁴ that possesses hydroxyls and a higher EEW (lower concentration of oxirane) in contrast to the liquid diglycidyl ether of bisphenol A, Epon 828 material depicted in Figure 4.28. Therefore, the characteristic hydroxyl (O-H) stretch commonly observed in the in the at $\nu_{\max} \sim 3400 - 3200 \text{ cm}^{-1}$ region is present and the resulting measure of chemical conversion has been based upon a relative increase in the $\nu_{\max} \sim 3400 - 3200 \text{ cm}^{-1}$ region as well as a concomitant decrease in the at $\nu_{\max} \sim 914$ and 876 cm^{-1} peaks of the glycidal ether epoxide group, Figure 4.29, below.

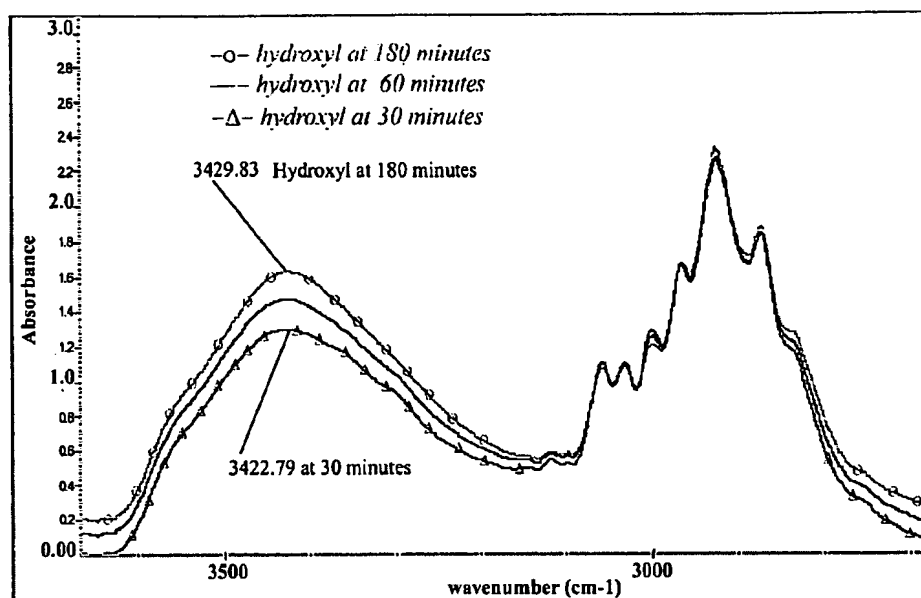


Figure 4.29: FTIR transmission spectra for 30, 60, and 180 minute cure of Epon 1001X and crosslinker red spectrum at times: 1) $t=30$ minutes (bottom); 2) $t=60$ min (middle); 3) $t=180$ min (top). Increase in Hydroxyl (O-H) stretch indicating chemical reaction / conversion of oxirane into an amino hydroxy alcohol.

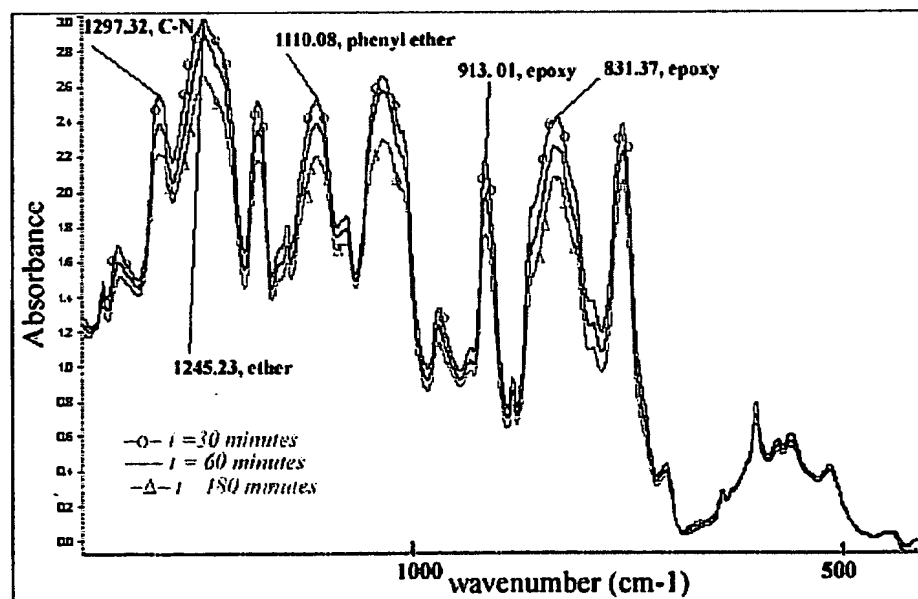


Figure 4.30: FTIR transmission spectra in the "finger print" region, IR spectra for 30, 60, and 180 minute cure of Epon 1001X and crosslinker (top) spectrum at time: $t=30$ minutes; (middle) $t=60$ min; (bottom) $t=180$ minute. Decrease in $\nu_{\max} \sim 914$ and 876 cm⁻¹ peaks of the glycidal ether epoxide group indicating chemical conversion / reaction.

4.11 Summary Reactivity

The crosslinker developed for this proposed psuedo IPN system was designed with two functional groups that support ambient temperature curing. Namely: 1) trimethoxy-silane moiety that undergoes hydrosilation with itself and other hydroxyl bearing moieties; 2) a heterocyclic secondary amino group with labile secondary amino "H" proton, and the presence of a heterocyclic tertiary amine which acts as a catalyst to promote nucleophilic addition reactions with such functional groups as epoxies and isocyanates. The action of which may be contrast to an analogous compound 1-piperazineethanamine or aminoethylpiperazine (AEP) that consists of an aliphatic primary amine attached to a heterocyclic ring containing a secondary and tertiary amine. AEP is often used as a room temperature curative for 2K epoxy systems.⁵²⁵ However, due to the presence of the heterocyclic ring and unlike other primary aliphatic amines it does not require the addition of a hydroxyl bearing catalyst, such as nonylphenol, propylene carbonate, or an auxiliary tertiary amine to effect full cure at low temperatures.

The focus of these studies has centered on elucidating the reactivity of the proposed crosslinker relative to formation of 1) an inorganic-organic, lower mole fraction component, that acts to develop bulk organo-silane structure; 2) an organic-organic component based upon an epoxy-amine reaction that contributes, the higher mole fraction component to the polymeric structure. Based upon the spectroscopic results that clearly show the development of siloxane functionality and the curing of a diglycidyl ether of bisphenol A, Epon 1001X though an epoxy amine reaction, it may be surmised that the crosslinker acts to form a hybrid silane modified pseudo IPN. What the results from the first study suggest is that: 1) the silane functionality may also undergo hydrolysis under

optimized pH conditions to yield a covalent bond to a metal oxide surface; 2) in turn it may further react with an organic functional group that is part of the pseudo IPN. Secondly, the results also imply that due to the presence of labile secondary amino group attached to a heterocyclic ring, the crosslinker can also be used to promote formation of a polyurea linkage when formulated with a polyisocyanate prepolymer.

One of the key performance features of this silane modified polymeric material is its ability to contribute network structure from three different chemical moieties: 1) silane linkages; 2) polyurea linkages, and 3) epoxy-amine linkages. On a hierarchical scale, the first reaction to develop an significant crosslink density in the proposed system is the formation of polyurea linkages between the secondary amino group of the heterocyclic ring and polyisocyanate prepolymer. This polyurea reaction has been observed to occur relatively fast and must be moderated by addition of polar solvents such as 3-ethoxypropionic acid ethyl ester (EEP) or propylene carbonate (PC) that acts both as a urethane retarder and epoxy-amine reaction promoter.

Reference / Bibliography

- ⁴⁷⁴ Kasemann R., Burkhart T., Schmidt H.; *Ceram. Trans.* Vol. 55, pp. 307 (1995)
- ⁴⁷⁵ Wagner G.; *Proc. European Coatings Conference*, Zurich, Switzerland, 3rd – 4rd, pp. 223-228, September (2001)
- ⁴⁷⁶ Hoppe D., Lomölder R., Plogmann F. and Speier P.; *Proc. European Coatings Conference*, Zurich, Switzerland, pp. 163-177, 3rd – 4th September (2001)
- ⁴⁷⁷ Ni., H., Skaja, A., Soucek, M., *Progress in Organic Coatings*, Vol. 40, pp. 175–184 (2000)
- ⁴⁷⁸ Sperling, L.H., *Interpenetrating Polymer Networks and Related Materials*, Plenum, New York (1981)
- ⁴⁷⁹ Frisch, K. C., Klempner, D., and Mukherjee, S. K. *J. Appl. Polym. Sci.*, Vol. 18, pp. 689 (1974)
- ⁴⁸⁰ Cassidy, E. F., Xiao, H. X., Frisch, K. C., and Frisch, H. L. *J. Polym. Sci. Polym. Chem. Ed.*, Vol. 22, pp. 2667 (1984)
- ⁴⁸¹ Pernice, R., Frisch, K. C. and Navare, R., *J. Cell. Plast.*, Vol. 18, pp. 121 (1982)
- ⁴⁸² Klempner, D., Berkowski, L., Frisch, K. C., Hsieh, K. H., and Ting, R., *Rubber World*, Vol. 192, pp. 16 (1985)
- ⁴⁸³ Klempner, D., Muni, B., Okoroafor, M., and Frisch, K. C., *Advances in Interpenetrating Polymer works*, Vol. II, Technomic Publishing, pp. 1 (1990)
- ⁴⁸⁴ Lee, Y., Ku, W., Tsou, J., Wei, K. and Sung, P., *J. Polym. Sci.: Part A: Polym. Chem.*, Vol. 29, pp. 1083 (1991)
- ⁴⁸⁵ Sperling, L.H., *Interpenetrating Polymer Networks and Related Materials*; Plenum Press: New York, NY (1981)
- ⁴⁸⁶ Hsieh, K. H., Chiang, Y. C., Chern, Y. C., Chiu, W. Y. and Ma, C. C. M., *Angew. Makromol. Chem.*, Vol. 193, pp. 89 (1991)
- ⁴⁸⁷ K. H. Hsieh, Y. C. Chiang, Y. C. Chern, W. Y. Chiu, C. C. M. Ma, *Angew. Makromol. Chem.*, Vol. 194, pp. 15 (1992)
- ⁴⁸⁸ Chern, Y. C., Hsieh, K. H., Ma, C. C. M. and Gong, Y. G., *J. Mater. Sci.*, Vol. 29, pp. 5435 (1994)

- ⁴⁸⁹ Prakash, N. A., Liu, Y. M., Jang, B. Z. and Weng, J. B., *Polym. Comp.*, Vol. 15, pp. 479 (1994)
- ⁴⁹⁰ Thomas, D.A., and Sperling, L.H., in *Polymer Blend*, Vol. 2: Paul, D.R., Newman, S., Eds., Academic Press, New York, NY (1978)
- ⁴⁹¹ Funke, W., "Problems and Progress in Organic Coatings Science and Technology," *Progress in Organic Coatings*, Vol. 31, pp. 5-9 (1997)
- ⁴⁹² Sperling L.H., *Interpenetrating Polymer Networks and Related Materials*, New York: Plenum, (1981)
- ⁴⁹³ Frisch H.L., Klempner D., *Polymer Engineering Sci.*, Vol. 14, (9), pp. 646 (1974)
- ⁴⁹⁴ Van Vliet, C.H., *Progress in Organic Coatings*, Vol. 34, pp. 220-226 (1998)
- ⁴⁹⁵ Keijman, J.M. - High Solids Coatings: Experience in Europe and USA - Paper 40, *Proceedings PCE Conference in The Hague, The Netherlands "Protecting industrial and marine structures with coatings"*, March (1997)
- ⁴⁹⁶ Funke, W., "Problems and Progress in Organic Coatings Science and Technology," *Progress in Organic Coatings*, Vol. 31 pp. 5-9 (1997)
- ⁴⁹⁷ Nithianandam, V. S.; Erhan, S., *J. Appl. Polym. Sci.*, Vol. 42, pp. 2387-2389 (1991)
- ⁴⁹⁸ Kaleem, K.; Chertok, F.; Erhan, S., *Prog. Org. Coat.*, Vol. 15, pp. 63-71 (1987)
- ⁴⁹⁹ Nithianandam, V. S.; Erhan, S., *Polymer*, Vol. 32, pp. 114 (1991)
- ⁵⁰⁰ Kaleem, K.; Chertok, F.; Erhan, S., *J. Polym. Sci. Part A: Polym. Chem.*, Vol. 27, pp. 865-871 (1989)
- ⁵⁰¹ Nithianandam, V. S.; Chertok, F.; Erhan, S., *J. Appl. Polym. Sci.*, Vol. 42, pp. 2899-2901 (1991)
- ⁵⁰² Nithianandam, V. S.; Chertok, F.; Erhan, S., *J. Appl. Polym. Sci.*, Vol. 42, pp. 2893-2897 (1991)
- ⁵⁰³ Reddy, T. A.; Erhan, S., *J. Polym. Sci. Part A: Polym. Chem.* Vol. 32, pp. 557-565. (1994)
- ⁵⁰⁴ Nithianandam, V. S.; Chertok, F.; Erhan, S., *J. Coat. Technol.*, Vol. 63, pp. 47-49 (1991)

- ⁵⁰⁵ Phani, K. L. N.; Pitchumnani, S.; Muralidharan, S.; Ravichandran, S.; Iyer, S. V. K. *J Electroanal. Chem.*, Vol. **353**, pp. 315. (1993)
- ⁵⁰⁶ Muralidharan, S.; Phani, K. L. N.; Pitchumnani, S.; Ravichandran, S.; Iyer, S. V. K., *J Electrochem. Soc.*, Vol. **142**, pp. 1478 (1995)
- ⁵⁰⁷ Han, M., and Nikles, D., *J. Polymer Science: Part A: Polymer Chemistry*, Vol. **38**, pp. 3284–3292 (2000)
- ⁵⁰⁸ Funke, W., *Progress in Organic Coatings*, Vol. **28**, pp. 3-7 (1996)
- ⁵⁰⁹ Cameron, D.W., Scott, P.M., and Todd, L., *J. Chem. Soc.*, pp. 42 (1964)
- ⁵¹⁰ Cameron, D.W., Cromartie, R.I.T., Hameid, Y.K., Scott, P.M., and Todd, L., *J. Chem. Soc.*, pp. 62 (1964)
- ⁵¹¹ Kaleem, K., Chertok, F., and Erhan, S., *J. Polym. Sci., Part A: Polym. Chem.*, Vol. **27**, pp. 865 (1989)
- ⁵¹² Vaideeswaran, K., Bell, J.P., and Nikles, D.E., *J. Appl. Polym. Sci.*, Vol. **76**, pp. 1338-1350 (2000)
- ⁵¹³ Vaideeswaran, K., Bell, J.P., and Nikles, D.E., *J. Appl. Polym. Sci.*, Vol. **76**, pp. 1338-1350 (2000)
- ⁵¹⁴ Crews, P., Rodríguez, J., and Jaspars, M., *Organic Structure Analysis*, Oxford University Press, pp. 349-363, (1998)
- ⁵¹⁵ Crews, P., Rodríguez, J., and Jaspars, M., *Organic Structure Analysis*, Oxford University Press, pp. 352, (1998)
- ⁵¹⁶ Reddy, T.A., Macainoe, D., and Erhan, S., *J. Polym. Sci., Part A: Polym. Chem.*, Vol. **32**, pp. 1977-1982 (1994)
- ⁵¹⁷ Nithianandam, V.S., Kaleem, K., Chertok, F., and Erhan, S., *J. Appl. Polym. Sci.*, Vol. **42**, pp. 2893-2897 (1991)
- ⁵¹⁸ Reddy, T.A., and Erhan, S., *Intern. J. Polymeric Matter*, Vol. **19**, pp. 109-116 (1993)
- ⁵¹⁹ *Color Physics for Industry*, Ed. by Roderick McDonald, Society of Dyers and Colourists, pp. 31 (1987)
- ⁵²⁰ Finely, K.T., *The Chemistry of Quinonoid Compounds*, Patai, S., Ed.; John Wiley & Sons: New York, NY, pp. 900-1101 (1974)
- ⁵²¹ Crosby, A.H., and Lutz, R.E., *J. Am. Chem. Soc.*, Vol. **78**, pp.1233 (1956)

- ⁵²² Coates, J.P., The Interpretation of Infrared Spectra: Published Reference Sources, *Appl. Spectrosc. Rev.*, **31**(1-2), 179-192 (1996)
- ⁵²³ George, G. A., Cole-Clarke, P., St. John, N., Friend, G., *J. Appl. Polym Sci.* Vol. **42**, pp. 643 (1991)
- ⁵²⁴ Wicks, Z.W., Jones, F.N., and Pappas, S.P., Organic Coatings: Science and Technology, Vol. I: Film Formation, Components, and Appearance, pp. 162-164, Wiley and Sons Inc., New York, NY (1992)
- ⁵²⁵ The Use of Aminoethylpiperazine in Curing Epoxy Resins, Huntsman Technical bulletin, N-Aminoethylpiperazine or 1-Piperazineethanamine, [CAS 140-31-8], Huntsman Corp. (1994)

Chapter 5 Mg-rich Coatings Design and Formulation

5.1 Introduction

As reviewed in chapter two, active metal coating systems can be represented in terms of a convenient model that facilitates the design and evaluation of coatings for corrosion control. Zinc-rich systems have been the active metal system of choice for protecting ferrous substrates; however, zinc is not the only active metal used in these systems. More recent formulation designs have been reviewed by Hare⁵²⁶ that include the addition of aluminum flakes and powders to yield mixed metal-rich systems that deliver highly effective cathodic coatings for corrosion control of steels. However, the technology proceeding from these systems has not been seriously investigated, developed, and applied to an analogous metal rich cathodic coating system for corrosion control of aluminum and its alloys. Traditionally, chromates and chromate pretreatments have gained the widest acceptance in corrosion control of aluminum and its alloys.

In considering a parallel approach to the design of an analogous metal-rich system, for cathodic protection of aluminum there is only one engineering metal more usable than aluminum itself that may be used as a sacrificial anode, namely magnesium. The major concern associated with designing such an active metal coating system comprised of magnesium powder, which would be analogous to zinc, is the issue of the metal's reactivity and stability. It presents both a fire potential in manufacture of the pigment itself as well as and the generation of potentially corrosive salts when coupled galvanically to Al. Fortunately, the first concern can be completely allayed due to the advanced production technology employed by Eckart GmHB, Velden Germany in the manufacture of their magnesium powders. These micron sized powders are commercially available from Eckart

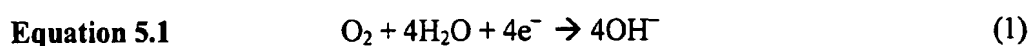
GmbH, ECKA™ metallic magnesium powder produced from *p*-magnesium 99.95 % and conform to (Deutsches Institut für Normung) DIN 17800 part-7 standards with Mg content @ 96% and MgO (magnesium oxide) content @ 4%. Formation of this stable oxide layer greatly reduces the metal powders potential reactivity. The second concern addresses the oxidation products of Mg, MgO and its various hydroxides in hydrated form, that they would create such basic conditions that Al would undergo basic corrosion as is indicated in its Pourbaix diagram.⁵²⁷ Fe is mostly passive under basic conditions, so this is not a valid consideration for Zn over steel, and the natural Mg oxidation products do not yield a pH high enough to corrode and dissolve Al, so this concern was also alleviated.

In light of the above mentioned concerns regarding incorporation of pigmentary magnesium into a coating, the issue of reactivity of the cathodic material i.e., aluminum and its alloys is of primary concern. It is well known that the overall excellent corrosion resistance of aluminum is attributed to the passive layer of oxide film that forms over its surface.⁵²⁸ But the major fault with respect corrosion control of Al and its alloys manifests itself in the form of corrosion by pitting which is generally described as complex processes that can be mitigated or exacerbated by variable environmental conditions.^{529,530}

5.2 The Generic Corrosion Model

The problem with Al 2024 T-3 is its heterogeneous nature due to the artificial aging process used to temper the alloy. The most general model applied to describe corrosion of Al 2024 T-3 is the pitting of aluminum, i.e., localized breakdown of the passive oxide film, is the “point defect” model for pitting.^{531, 532} According to *Figure 5.1*, below, the principle of point defect is based upon anodic polarization conditions driving anionic defects, such as aluminum vacancies through the film to the Al₂O₃: Al interface, while cationic species

such as oxygen vacancies are driven to the solution Al_2O_3 : solution interface. For example, this is equivalent to moving Al^{3+} toward the solution interface while O^{2-} ions are driven towards the Al: interface. Pitting has been hypothesized to occur when the flux of aluminum vacancies reaching the Al_2O_3 : Al interface exceeds the rate at which Al is oxidized to Al^{3+} to fill the resulting vacancies. The imbalance in the number of vacancies causes a nucleation process to occur which is assumed to promote void formation that undermines the overlaying protective oxide layer and contributes to the growth of localized pits according to Equ.(s) 5.1 to 5.2.⁵³³



(Cathode reaction, occurs most favorably on Cu)



(Anode reaction)

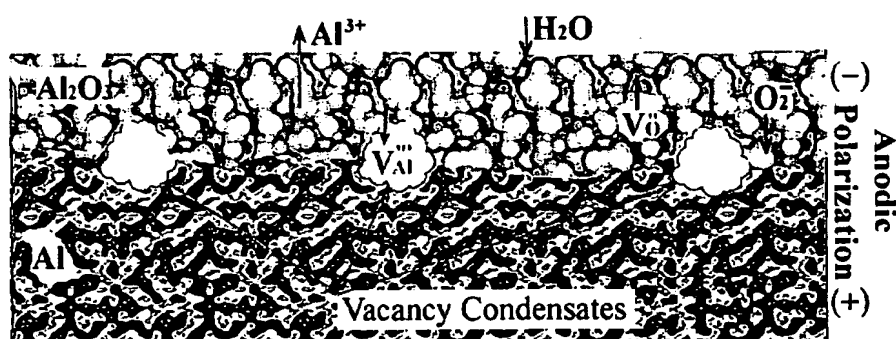


Figure 5.1: Point defect model for pitting. Adapted from Bunker *et al.*⁸ Under anodic polarization, Al^{3+} ions migrate toward Al_2O_3 : solution Interface while V_{Al} (aluminum vacancies) are driven to the Al_2O_3 : Al Interface. Oxygen ions, O^{2-} , are driven toward the Al_2O_3 : Al interface. While V_{O} (oxygen vacancies) migrate toward the Al_2O_3 : solution interface that is occupied by water molecules.

Another model which has been likened to hydrolysis of Al under anodic polarization conditions is the model for “uniform corrosion” of Al in hot water.⁵³⁴ This

model, *Figures 5.2 and 5.3 below*, describes the formation of a pseudoboehmite (AlOOH) layer over the Al_2O_3 surface when it is subjected to hot water. According to this model, hydration of the Al_2O_3 : solution occurs over a given time period or under an imposed anodic potential which leads to rapid film growth of a “hydrated front” layer of pseudoboehmite on top of which a layer of $\text{Al}(\text{OH})_3$ grows.

Stage 1: Introduction (no film growth) $\text{Al}_2\text{O}_3 + \text{H}_2\text{O} \rightarrow 2\text{AlOOH}$

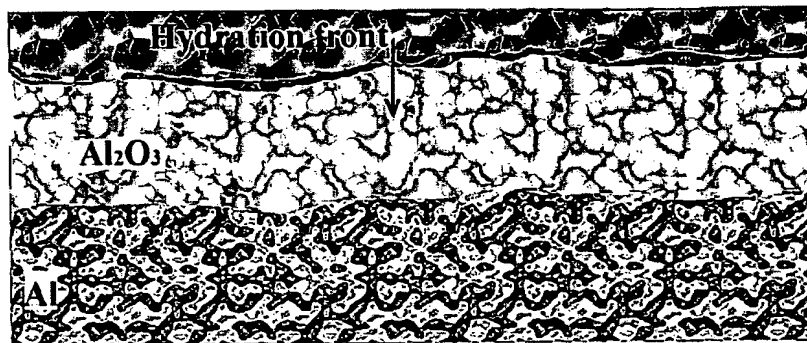


Figure 5.2: Uniform corrosion model. Adapted from Bunker *et al.*⁸ Under hot water / anodic polarization the Al_2O_3 : solution interface becomes hydrated and develops a “hydration front” layer of pseudoboehmite.

Stage 2: (film growth) $2\text{Al} + 4\text{H}_2\text{O} \rightarrow 2\text{AlOOH} + 3\text{H}_2$

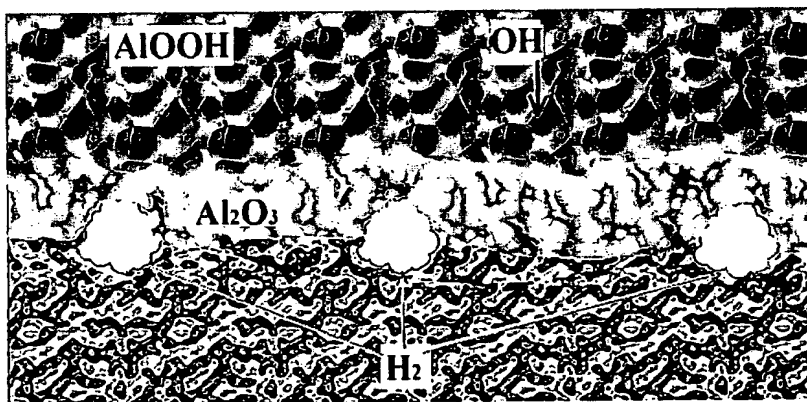


Figure 5.3: Uniform corrosion model. Adapted from Bunker *et al.*⁶ Under anodic polarization, OH^- ions migrate toward Al_2O_3 : solution Interface (through the AlOOH gel) while H_2 is driven toward V_{Al} (aluminum vacancies) at the Al_2O_3 : Al interface.

Once the hydrated layer has been established, Figure 5.3, below, hydroxide ion (OH^-) migrates to the Al_2O_3 : Al interface where the it is reduced by Al to regenerate the oxide and generate H_2 gas.

Pitting, in either case involves some mechanism that accounts for the oxidation of Al metal anode once water has been introduced. On the other hand, under cathodic polarization conditions, see Figure 5.4 below, anionic species in the film such as O^{2-} and Cl^- are driven toward the Al_2O_3 : solution interface, while cationic species, such as Al^{3+} are driven from solution towards the Al interface. According to Bunker *et al.*⁸, cathodic polarization causes Al_2O_3 oxide film dissolution and H_2 evolution to occur. Where the total current passed through the film is sufficient to dissolve either 2 nm of Al_2O_3 oxide film, or to generate 2×10^{-8} mol of H_2 via the reactions according to Equ(s) 5.3 to 5.4:

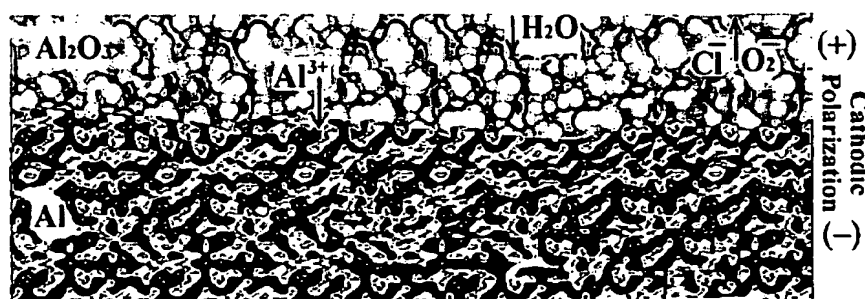
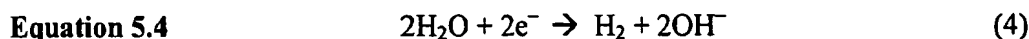
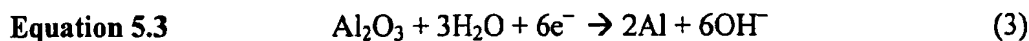


Figure 5.4: Cathodic polarization, under anodic polarization, Al^{3+} ions migrate toward Al_2O_3 : Al interface while oxygen ions, O^{2-} are driven toward the Al_2O_3 : solution interface that is occupied by water molecules.

Generally, the hydroxide content within the passive film adjusts to environmental changes depending on the extent of hydration. Under water, the films tend to hydrate and dehydrate

when dried. Extensive hydration leads to enhanced diffusion and faster hydroxide migration at the Al_2O_3 : Al interface.⁸

5.3 Copper Redistribution in Al 2024 T-3

The corrosion of Al 2024 T-3 has been ascribed to enhanced cathodic activity of intermetallic particles⁵³⁵ that serve as preferential sites for oxygen reduction as the conductivity of the mixed oxide from these areas is higher than that of the passive Al_2O_3 oxide film. The key issue associated with coatings for corrosion control of Al-Cu-Mg alloys such as Al 2024 T-3 is the redistribution of copper that occurs during painting / depainting processes and subsequent corrosion. According to Dimitrov *et al.*,⁵³⁶ most of the copper that accumulates over the surface of the alloy originates from the dealloying of intermetallic S-phase particles ($\text{Al}_2\text{-Cu-Mg}$) which account for ~60 percent of the particle population over the surface of the alloy. The dealloying process has been shown to result in the formation of nanoporous Cu-rich remnants that contribute to pitting around the periphery.⁵³⁷ Figure 5.5, below, schematic depicting micron scale surface of Al-2024 T-3 with ($\text{Al}_2\text{-Cu-Mg}$) intermetallic S-domains dispersed over the metal surface.



Figure 5.5: Illustration depicting heat treated Al 2024 T-3 with cathodic ($\text{Al}_2\text{-Cu-Mg}$) intermetallic S-domains on a micron scale.

According to Vukmirovic *et al.*⁵³⁷ above oxide on the surface of the S-phase is not very protective and is susceptible to breakdown when exposed to an electrolytes such as a neutral chloride solution. The breakdown process involves dissolution and release of the Mg^{2+} cation, leaving the remaining copper in the depleted S-phase to form a high surface area, porous, sponge-like structure.⁵³⁸ Initially, this depleted S-phase is anodic but changes into a high surface area cathode for oxygen reduction, see *Figure 5.6*, below.

The dealloyed, cathodic Cu sponge-like S-phases have been reported¹² to range in size from 250nm up to 6 μ m and as long as these remnants remains mechanically and electrically connected to the Al matrix the corrosion potential remains too low to promote dissolution of Cu by electrochemical means. Although, once a copper remnant becomes detached from the matrix it will dissolve in the presence of Cl^- ion and electrolyte, at its corrosion potential, and electrochemically replating back onto the aluminum alloy surface. The process is pH sensitive and as pH increases in the range of ~ 9 to 9.5,^{539,540} the passive (anodic)oxide on the surface of the alloy matrix begins to dissolve and the bare aluminum will dissolve as the soluble AlO_2^- anion.

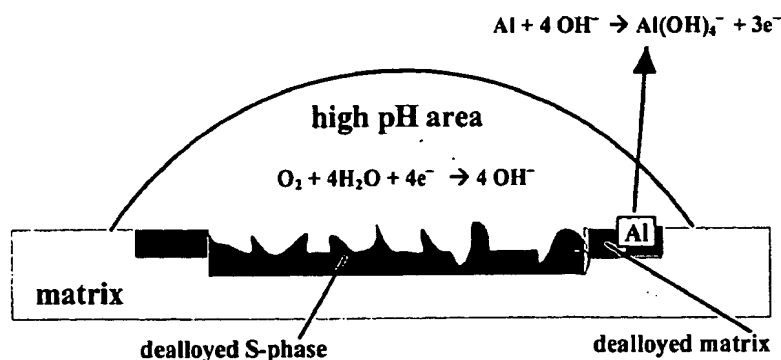


Figure 5.6: Illustration, adapted from Vukmirovic *et al.*⁵³⁷ depicting matrix dealloying in the vicinity of an S-phase particle, under high pH conditions, over surface of Al 2024 T-3.

According to the previously described corrosion models the corrosion of aluminum metal is most likely to occur under anodic polarization conditions in the presence of Cl^- ion, and electrolyte. The corrosion of the precipitation grade alloy Al 2024 T-3 is exacerbated by the presence of (Al-Cu-Mg) S-phases that are readily dissolved in of Cl^- and O^{2-} ions in an electrolyte solution liberating Cu for redistribution as a cathodic site for further reduction of oxygen. Therefore, any attempt to preserve the alloy must address 1) retarding or stopping dissolution of (Al-Cu-Mg) S-phases, and 2) maintaining a low corrosion potential to retard dissolution of Cu in the presence of Cl^- ion.

5.4 Introduction to Prima Facia Study

A *prima facia* study was conducted to examine the gross nature of the corrosion process acting on Al 2024 T-3 when subjected to Prohesion™ exposure according to ASTM D5894-96 emulating an acid rain environment. In addition, the effect of corrosion mitigation by application of an organo-silane, 7-phenyl-1-(4-propyl)-1,2,3,4-tetrahydroquinoxalin-6-ol, (7-PQ-6-ol sol treatment over the surface of the Al 2024 T-3 alloy was examined. Panels were exposed up to 1,000 hours and visually assessed for physical changes over the surface due to pitting corrosion. The results of this study show that on unscrubbed panels, extensive uniform pitting begins to develop over the surface of the Al 2024 T-3 alloy during the first 500 hours exposure while panels treated with the (7-PQ-6-ol) crosslinker developed a glassy-gel coating over the surface that forestalled the onset of pitting corrosion for up to 1,000 hours. The results demonstrate that the most probable corrosion mechanism affecting this alloy is the to formation of localized pits that promote anodic dissolution of the material in a manner that is consistent with the previously described model for uniform pitting. In addition, the study demonstrates that organo-silane

gel films formed over the surface of the alloy from the (7-PQ-6-ol) crosslinker can provide a measure of corrosion resistance, possibly due to the presence of the monophenolate ion.

5.5 Panel and Film Preparation (Experiment)

The primers formulated from materials in Table 5.2-B, below, were prepared using conventional techniques such as manual scrub panel prep and coating spray application. Panel preparation of stock 6" x 3" Al 2024 T3 Q-panels™ was done by lightly wire brushed to normalize the surface of all panels. It should be noted that for about every one out of every twenty panels, the surface hardness of the 6" x 3" Al 2024 T3 Q-panel™ varies and has noted to be dramatically harder than the others.

Lightly wire brushing the panels with a steel brush quickly reveals those panels with dramatically harder surfaces so they may be discarded. It should also be noted that wire brushing is preferred to the use of sand paper as sand paper is loaded with stearates (soap) and phthalates that serve as sanding-aids or lubricants that strongly adsorb onto metallic surfaces. After wire brushing, the panels are scrubbed with a Scotch Brite™ pad followed by rinsing / degreasing in 3 -ethoxypropionic acid ethyl ester (EEP) solvent. Once the EEP solvent had been rinsed with distilled (DI) water, it was subsequently immersed in a 10% phosphoric acid solution for 60 seconds followed by a rinse with DI water. The freshly prepared Al panels were subsequently coated with a surface modifier according to methodology described in Chapter 4, thesis^{Error! Bookmark not defined.}, where a 2% mixture of Silwet®1120 in acetone / water mix as described in the literature⁵⁴¹ was applied via foam brush. Panels were subsequently placed into a BigBlue over at 30°C for 60 minutes.

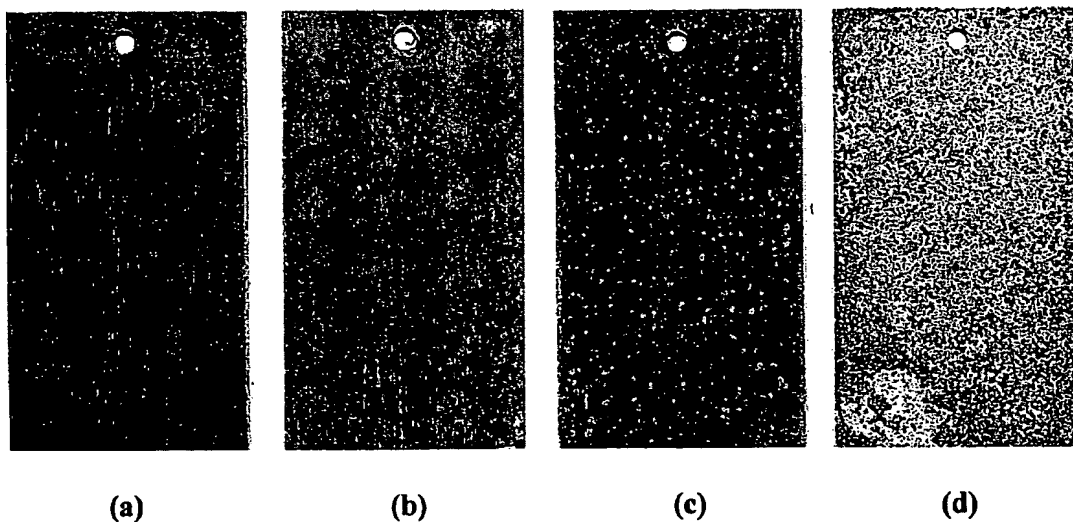
Mg-rich primer preparation and application involved slowly dispersing the magnesium pigment into a mixture of epoxy / polyisocyanate and solvents. This was accomplished with a 1" -diameter propeller blade connected to an electric mixer set which was set at speed of approximately 1,000 rpm. The rheology control agent(s) Aerosil®R202 was gently blended into the pigment / binder-resin / solvent mix after the Mg pigment was added; while in the case of the rheology control agent Bentone®39, a pre-gel was made according to reference⁵⁴² and then blended into the mix. The primers were applied with a touch-up spray gun, at a pressure setting of 60psi. Multi-coat passes were required to apply the mg-rich primer taking care to avoid paint running. The coatings were subsequently allowed to cure at 30° C for 14 days before topcoat application. Note, all primed panels were subsequently top coated with Extended Lifetime™ topcoat. The average film thickness (FT) estimated from EDAX photos reveal primer film thickness to be on the order of ~50 +/- 20 microns with topcoat film thickness at~ 100 +/- 40 microns.

The question with regard to the preponderance of dealloying the Al 2024 T-3 by passing a wire brush over it was addressed by comparing the "flatness" of the wire brushed panel versus a sand blasted panel. Al 2024 T-3 panels should not be sandblasted as a means of preparation as it causes the panel to bow considerably which signifies the dealloying of the material on the side that was sandblasted. In this experiment, it was observed that wire brushing the panels did not cause them to bow, nor was there any observed difference between the brushed side of the panel or the non-brushed when laid out flat.

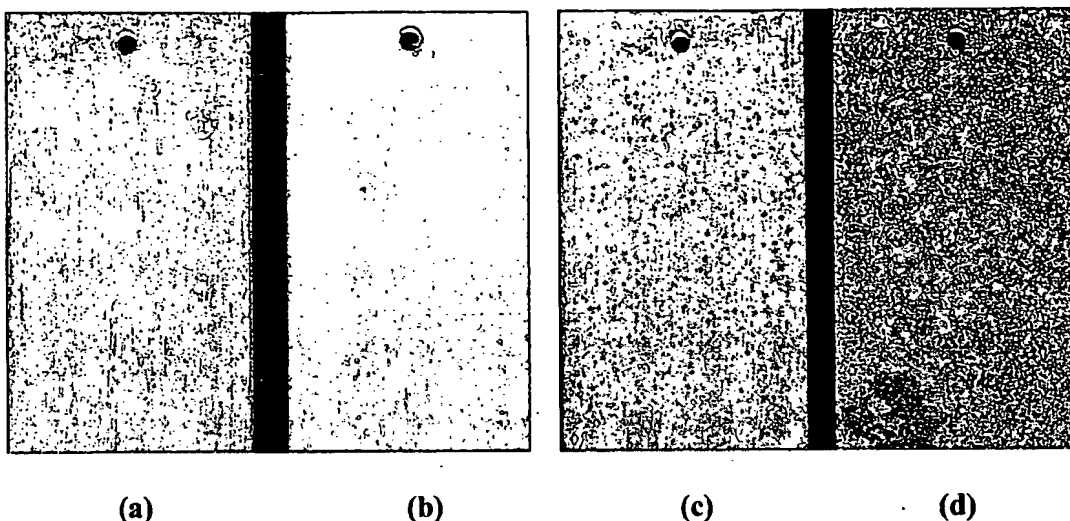
Preparation of the panels with organo-silane 7-phenyl-1-(4-propyl)-1,2,3,4-tetrahydroquinoxalin-6-ol (7-PQ-6-ol). A two percent solution of 7-PQ-6-ol in EEP was prepared and applied to the surface of the prepared panels with a sponge brush. The

thickness of the coating was measured with a Gardner wet film thickness gauge and found to be about 2-mils wet. The coatings were allowed to cure overnight to develop into a hard, glassy coating. Panels were subsequently placed into Prohesion™ chamber and exposed for 1,000 hours.

Results shown below, Figures 5.7 to 5.8 below, for 5.7(a) (treated) and 5.7(b) (untreated) Al 2024 T-3 panels compared to exposed panels 5.7(c) and 5.7 (d) after 1,000 hours Prohesion™. Panel, Figure 5.7 (d) (bare Al 2024 T-3) after 1,000 hours shows extensive pitting while panel, Figure 5.7 (c) (treated Al 2024 T-3) shows gray spotted areas presumed to be cathodic areas possibly sites where the dissolution of (Al-Cu-Mg) S-phase occurred.



Figures 5.7a, b, c, and d: Panels (a) treated and (b) bare Al before exposure; (c) and (d) after 1,000 hours Prohesion™ exposure.



Figures 5.8 a, b, c, and d: Inverted color image of panels (a) treated and (b) bare Al before exposure; (c) and (d) after 1,000 hours Prohesion™ exposure. Inverted image revealing features due to absorbed light as opposed to reflected in figures 5.7 a) to d).

5.6 Conclusion General Corrosion Model

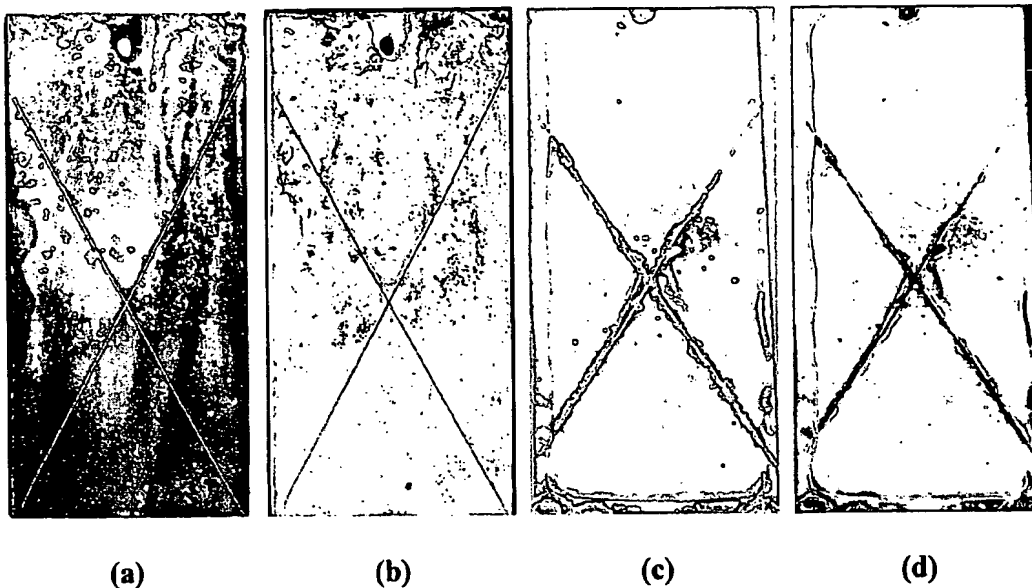
Results from this study demonstrate that the generic corrosion mechanism of Al 2024 T-3, in a simulated acid rain environment i.e., Prohesion™ exposure, follows an initial point defect model for pitting, under anodic polarization, where dealloying and dissolution of (Al-Cu-Mg) S-phase occurs generating pits, as depicted in Figure 5.6 , above, that leads to the depletion of the passive Al_2O_3 oxide film leaving the bare Al prone to dissolve as the soluble Al O^{2-} anion. Coating the Al 2024T-3 with the organo-silane gel coat appears to forestall or modulate the onset of corrosion by isolating and insulating the alloy from soluble Al O^{2-} anion and Cu that may rapidly promote the matrix dealloying in the vicinity of an S-phase particles over the surface of the alloy. Overall, it can be surmised that the presence of the organo-silane coating modulates the corrosion process by protecting anodic sites through Al-O-Si-R / Al-O-Si-O-Si-R , where R is the organic species containing the monophenolate ion.

5.7 Introduction to Al 2024 T-3 Silane Modification

The previous experiment provided insight into the generic corrosion mechanism affecting Al 2024 T-3 in an acid rain environment, as it served to illustrate how cathodic pitting sites appeared and developed over the coated surface of the alloy. The proceeding study addresses the integrity of the Al-O-Si-R / Al-O-Si-O-Si-R coating structure at forestalling the corrosion process when the panel is scribed.

Experiment

6" x 3" Al 2024 T3 Q-panels™ were degreased with 3-ethoxypropionic acid ethyl ester (EEP) solvent and lightly wire brushed to normalize the surface of all panels. Three panels were coated with a two percent solution of (7-PQ-6-ol) in EEP was prepared and applied to the surface of the prepared panels with a sponge brush. However, in this experiment the panels were coated with two coats of the solution containing the organo-silane. Three panels were spray coated, at 2 mils dry film thickness, with Deft GY-001, extended lifetime topcoat (ELT) and allowed to cure for 10 days at room temperature. Both sets of panels were scribed with an X using a carbide tipped glass scribe. The coatings painted with ELT™ were covered on the back and edges with electroplater's tape and sealed with a 2-K epoxy / amine from Aldrich chemicals. Both sets of panels were placed into Prohesion™ exposure for up to 1,200 hours, Figures 5.9 (a), (b) and (c), (d), below. Note, that ELT™ is strictly a topcoat and not intended to used alone. The Al 2024 T-3 panel prepared in Figure 5.9 (d) was treated with a non-pigmented epoxy / polyamide(Epon 1001/Ancamide 2353, see Chapter 3 this thesis) tie-coat, FT< 0.5 mils, to promote adhesion between the ELT™ topcoat and Al 2024 T-3 substrate.



Figures 5.9 a, b, c, and d: Scribed panels Al 2024 T-3: on left (a) and (b) after 1,200 hours Prohesion™ exposure; panels (c) and (d) on right Deft ELT™ after 1,200 hours exposure.

5.8 Conclusion Al 2024 T-3 Silane Modification

After 1,200 hours Prohesion™ exposure a qualitative assessment was made and the panels with two coats of the organo-silane treatment showed far less oxide in the scribed areas than the panels with the organic coating alone. The pictures in Figures 5.9 (b) and (d) were inverted to their negative, in order to enhance the visual effect from the surface of light that was absorbed as opposed to reflected. The black scribes in the inverted Figure 5.9 (d), above, reveal qualitatively more oxide in the scribed areas when contrasted with the scribes in Figure 5.9 (b) above. In addition, the inverted panel Figure 5.9 (b), above, shows a darkened area at the top of the panel where the top layer of the coating has been affected by the accumulation of an insoluble salt that appears to be causing the coating to spall off the surface. However, the absence of initiation sites for pits suggests that two coats of the organo-silane coating served as an effective barrier to retard migration of electrolyte to the surface of the alloy where it might initiate pitting.

The conclusion derived from this study was that the 7(7-PQ-6-ol) organo-silane treatment probably forms Al-O-Si-O-Si-R linkages due to hydrosilation reactions, as previously described in Chapter 4 this thesis, that prevents the alloy from developing pits and corroding via the afore mentioned general corrosion mechanisms. In addition, it can be surmised that the presence of the monophenolate ion, as described in *chapter 4*, may have influenced or retarded the anodic polarization mechanism that acts to promote dissolution of Al₂O₃ oxide film leaving the bare Al prone to dissolve as the soluble Al O²⁻ anion.

5.9 Coating System Design

Results from the previous studies show that significant corrosion resistance can be designed into a coating system by simply applying a organo-silane treatment to the surface similar to those techniques reviewed previously in Chapter 2.4, this thesis. In addition, the appearance of surface pits in Figures 5.7 (c) and 5.8 (c) reveals the origin of cathodic sites which appear to initiate on a localized micro scale, under anodic polarization conditions, and develop into macro-scale pitting. Therefore, the primary design of a coating system must address the issue of heterogeneity of the metals and their galvanic activity when exposed to an electrolyte as well as arrest conditions that promote dissolution of the (Al-Cu-Mg) S-phase.

The approach taken to solve this problem is the application of a metal rich coating, prime, to cathodically protect the Al alloy by providing a sacrificial anode, magnesium, which serves to retard formation of point defects, that occur under anodic polarization conditions, thereby preserving the protective Al₂O₃ oxide film and forestalling corrosion of the structural alloy. Therefore, the design of such a coating system must 1) provide a pigmentary active metal that act to cathodically protect the substrate; 2) be comprised of a

suitable polymeric matrix that possesses an inherent resistance to hydrolysis, in the presence of magnesium degradation products, and 3) involve a simple and relatively easy application technique.

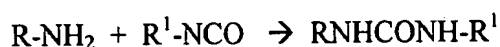
The focus of this formulation effort was to develop a magnesium powder primer / coating system that does not contain chemicals or materials that are hazardous, toxic, or give rise to health and safety concerns. The design of this Mg-Rich coating centered on developing an ambient temperature, moisture cure, spray application primer, with short treatment times and good compatible with existing cleaning and pretreatment procedures. The system was to be comprised of only commercially available chemicals and materials which do not require special storage provisions and can be easily adapted into existing application methods.

5.10 Coating Polymeric Materials

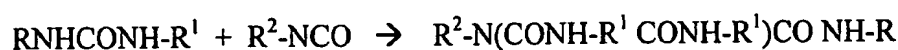
Adhesion is the most important property of an organic coating, when a coating's adhesion fails it becomes worthless. It has been well documented that the best deterrent to adhesion failure in organic coatings lies in developing the right chemical interactions between the binder, pigment, coating layers, and their metallic substrates.⁵⁴³ The most effective strategy, thus far, has been to develop coatings whose vehicle's hydrophilicity decreases during cure as hydrophilic groups are converted to crosslinks as the vehicle solidifies. Organo-functional silanes are commonly used as coupling agents and adhesion promoters in epoxide and urethane paints to improve their initial, wet, and recovery adhesion to aluminum surfaces.

The "Reversible Hydrolytic Bond Mechanism Theory" discussed by Walker^{Error!} Bookmark not defined. describes the reversible breaking of and reformation of stressed bonds

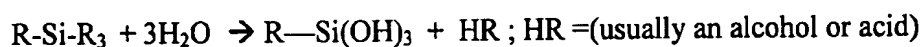
between a coupling agent and the substrate and allows stress relaxation without the loss of adhesion when water is present. It is argued that when Si-O-metal bond is broken by intrusion of water, the bond is capable of reforming with some recovery in adhesion.⁵⁴⁴ Chemical reactions between organofunction silanes and some component of a functional polymeric material occur between a N-beta-aminoethylamino propyl trimethoxysilane (A-1120), $\text{NH}_2(\text{CH}_2)_2 \text{NH}(\text{CH}_2)_3 \text{Si}(\text{CH}_3)_3$ and a substituted isocyanate group to form initially a substituted urea



then further reacted with another isocyanate group to form a biuret.⁵⁴⁵



The reactions between an amino-silane and organic binder components have been shown to be multiple in nature, and therefore it may be speculated that the degree of bonding to a metallic surface is strongly influenced by the number of hydroxyls present. Alkoxy silanes can hydrolyze with water to form silane triols.⁵⁴⁶



Silane triols condense readily to form higher molecular weight complex oligomers and lose their ability to act as adhesion promoters in the presence of water. Silanes such as γ -aminopropyltrimethoxy silane will react with solvents like methyl ethyl ketone (MEK) to form the ketimine plus water according to the reaction.⁵⁴⁴



Therefore, incorporation of organo-functional silanes requires judicious solvent selection to minimize side reactions that can occur between the organic binder, water and organo-functional silane. The solvent must effectively reduce vehicle viscosity and

promote good wetting of the Al metal substrate. Propylene Carbonate is a low vapor pressure, non-volatile, HAPS compliant, liquid with low toxicity that is completely miscible with many organic solvents such as glycol ethers and is often used as urethane viscosity reducer. In addition, 2-ethyl-3-ethoxypropionate (EEP) is another non-HAPs solvent that has been found effective at retarding isocyanate reactions. Both of these solvents have are suitable in the hybrid epoxy/urea polymer systems as formulated with organo-functional silanes and reactive polyisocyanates.

The polymeric materials chosen for the primer was a mixture of DGBA epoxy prepolymer Epon 1001F type, as reviewed in Chapter 2.9, and a polyisocyanate, (both aromatic MDI and aliphatic HMDI), prepolymers were used. Essentially what remains to be investigated is the effect of aliphatic (HMDI) versus aromatic (MDI) prepolymers used in these hybrid systems. For example, aromatic polyisocyanates such as MDI prepolymers do not require an added catalyst in order to react according to the Hoffmann rearrangement where an isocyanate is transformed into an amine. The the polyisocyanates used were Desmodure E-23A, a prepolymer of diphenylmethane diisocyanate (MDI), and Desmodure N3300 a hexamethylene diisocyanate (HMDI).

As previously reviewed, chapter 4, the moisture cure mechanism involves isocyanate functionality contributed by either HMDI or MDI prepolymers, converted into primary amine, forming both amines and carbon dioxide, that are intermediates in the Hoffmann rearrangement of an isocyanate with water to yield a reactive / reaminated labile amino functionality. Most accounts in the literature^{547,548} describe reactivity of aromatic polyisocyanates with water as much faster than corresponding aliphatics such as HMDI. Therefore, the use of an acid catalysis^{549,550} is an option when HMDI polyisocyanates are

involved. In these experiments the acid catalyst used to expedite the Hoffman rearrangement with aliphatic polyisocyanates was a 0.05% solution of the 2-phenylhydroquinone, oxidized with (TCCA) to product mixture see Figures 4.3 and 4.4.

According to this scheme the resulting Hoffman rearrangement generates the amino functionality that further facilitates the cure of epoxide functionality as well as any remaining isocyanate to yield an epoxy-urea polymeric material. An analogous system utilizing a moisture cure ketimine curative Epicure 3502 (the reaction product of ethylenediamine and methyl isobutyl ketone and which is recommended for low VOC coatings)⁵⁵¹ can be combined with either of the above mentioned polyisocyanates, and the type 1001X epoxy resin yields a coating with similar properties and improved application potential.

The advantage of such an epoxy-polyurea system lies in: 1) the relatively low concentration of amine MEK Schiff base required to cure mixtures of epoxy / polyisocyanate, and 2) improved solubility of epoxy 1001X epoxy resin in liquid polyisocyanate. Both effects contribute to improved pigment dispersion in the formulated coating which will be discussed in the following sections.

Interpenetrating polymer networks (IPN's) as polymer alloys consists of two or more distinct crosslinked polymer networks held together by permanent entanglements.⁵⁵² Frisch *et al.*⁵⁵³, first reported simultaneous interpenetrating networks (IPNs) composed of a polyurethane (PU) combined with an epoxy polymers. The epoxy backbone promotes toughness and flexibility to cured films while the carbon-carbon and the urethane bonds of the same improve solvent resistance, and adhesion. The epoxy-urethane reaction occurs

when the secondary hydroxyl group in the epoxy backbone is reacted with an isocyanate which gives rise to the hybrid structure of such IPNs.⁵⁵⁴

2-ethyl-3-ethoxypropionate (EEP) is primarily used as a retarder in coatings containing polyisocyanates as it possesses slight water solubility, non-toxic, has a low vapor pressure, and is not a skin irritant. In this coating system EEP has been found to be an effective retarder when used at about 10 percent total solvent. Propylene carbonate (PC) is commonly used as a urethane prepolymer viscosity reducer.⁵⁵⁵ PC is the primary carrier solvent used in this system, it is used as both an isocyanate retarder and wetting agent. Propylene carbonate wets both aluminum and magnesium powder and is an excellent solvent for both the epoxy and polyisocyanate. Both solvents have been found suitable in Mg-rich coatings with organo-functional silanes and polyisocyanates such as hexamethylene diisocyanate (HMDI). On the other hand, moisture-cure polyureas (MC-PUR's), such as those containing prepolymers of diphenylmethane diisocyanate (MDI) Desmodur™ E23-A from Bayer Corp., are recommended for use in Zinc-rich coatings applied to steel structures, but the recommended starting formulations and require photo-active aromatic solvents such as xylol that are environmentally unacceptable.⁵⁵⁶

5.11 Preparation of Silane modified Epoxy-Urea Coatings

The synthesis of the hybrid polymeric materials have been previously described in Chapter 4 this thesis. The reactions are carried out in propylene carbonate / 2-ethyl-3-ethoxypropionate (EEP) solvent mix. The crosslinker, , is thought to react with either the polyisocyanate or epoxy oxirane ring (Epon1001CX) or it may be reacted with an epoxy to form an intermediate that in turn moisture cures with either polyisocyanate MDI and

HMDI. It is surmised that both hybrid polymeric material systems in this study yield multiple organo-silicate (Al-O-Si-R-) crosslinked structures.

Materials

See appendix 5-A for Table 5.2A Magnesium Rich coating materials while Table 5.2-B, below, lists the materials used in the four coating polymer systems evaluated as primers for Mg-rich coatings: two conventional coatings and two hybrid coatings. The carrier solvent for MC-PUR and the epoxy / polyamide was xylol an aromatic hydrocarbon solvent mixture, while the carrier for the two hybrid coatings was a 90:10 mix of propylene carbonate (PC) and 3-Ethoxypropionic acid ethyl ester (EEP) both HAPS compliant solvents. The polyisocyanates used in the study were graciously supplied by Bayer Inc^{*}, Desmodure® N3300, 1,6-hexamethylene diisocyanate homopolymer (HMDI) trimer, NCO content at 21%; Desmodure® E-23A (a polyisocyanate prepolymer): 4,4'-methylenediphenylisocyanate (MDI), NCO content at 17%.

Table 5.2 B: Components of individual Mg- rich primer formulations

Formulation	Materials
A) Hyb-E23A	Desmodure® E23-A, Aerosil® R202, Eckagranules® PK51/31, Epon® 1001CX, Propylene Carbonate/EEP
B) MC-PUR ^{§§}	Desmodure® E23-A, Bentone® 34 [†] , Eckagranules® PK51/31 [‡] , Anti Terra® U [§] , Aromatic solvent Xylol
C) Hyb-N3300	Desmodure® NC-3300, Aerosil® R202, Eckagranules® PK51/31, Epon® 1001CX, Propylene Carbonate/EEP
D) Epoxy-Polyamide Eckagranules®	Epon® 828, Epicure® 3115 ^{§§} , Aerosil® R202,

^{*} Bayer Polymers, 100 Bayer Road, Pittsburgh, PA15205-9741

[†] Rheox, Inc., P.O. Box 700-T, Hightstown, NJ 08520, USA

[‡] Eckart GmbH, Kaiserstrasse 30, Furth D-90763, Germany

[§] BYK-Chemie USA, 524 South Cherry Street, P.O. Box 5670, Wallingford, CT 06492

The epoxy resin and polyamide curative Epicure® 3115 were graciously supplied by Resolution Performance Chemicals** diglycidyl ether of bis-phenol A (BPA), 1) Epon® 1001-X, with epoxide equivalent weight (EEW)~500; 2) Epon® 828 liquid BPA, EEW~188. The propylene carbonate solvent, (Propasol™ P) was graciously supplied by Huntsman Performance Chemicals†† and the EEP solvent from (Aldrich, Milwaukee, WI). Silquest® (A-1120) supplied graciously by Witco OSi Specialties‡‡, N-beta-(aminoethyl)-γ-aminopropyltrimethoxysilane all chemicals were used as received.

The crosslinker (used in both Epoxy- HMDI and Epoxy- MDI hybrids) was the (7-PQ-6-ol) synthesized in these laboratories, and described in Chapter 4, was added at a ratio of (0.25: 1) equivalent weight (Ew) crosslinker to one Ew of NCO, with the epoxy added at a ratio of 0.75 Ew (esterification value)^{§§} to one Ew of NCO. The epoxy Epon 828 / epicure 3115 (high molecular weight, polyamide, dimerized fatty acid polyamines) was mixed at a stoichiometric ratio as recommended in product bulletin.⁵⁵⁸

5.12 Preparation of Silane Modified Epoxy-Urea Polymeric Material

** Resolution Performance Chemicals, 1600 Smith Street, 24th Floor P.O. Box 4500 Houston, Texas 77210-4500

†† Huntsman Performance Chemicals, 3040 Post Oak Blvd., Houston, TX 77056

‡‡ OSi Specialties, A Crompton Corp. ,One American Lane, Greenwich, CT 06831 2559, USA

§§ Product Bulletin: RP:3062-01 / EPON™ Resin 1001F, ©2001 Resolution Performance Products

Experimental

The materials used in this study were graciously supplied by the following: Bayer Inc^{***}, Desmodur® N3300, 1,6-hexamethylene diisocyanate homopolymer (HMDI) trimer, NCO content, % ~21. The epoxy resins Resolution Performance Chemicals^{†††}, was diglycidyl ethers of bis-phenol A (BPA); 1) Epon® 1001-X, with epoxide equivalent weight (EEW)~500. Propasol P® propylene carbonate solvent Huntsman Performance Chemicals^{‡‡‡}, and the EEP solvent from (Aldrich, Milwaukee, WI). Silquest™ (A-1120), Witco OSi Specialties^{§§§}, N-beta-(aminoethyl)-γ-aminopropyltrimethoxysilane all chemicals were used as received The crosslinker (used in both Epoxy- HMDI and Epoxy-MDI hybrids): 7-phenyl-1-[4-(trimethyl-silyl)-butyl]-1,2,3,4-tetra-hydro-quinoxalin-6-ol (scheme 4.1, above) was added at a ratio of (0.25: 1) equivalent weight Ew crosslinker to 1 Ew NCO, with the epoxy added at a ratio of 0.75 Ew (esterification value)^{****} to 1Ew NCO. The epoxy Epon® 828 / epicure 3115 polyamide was mixed at a stoichiometric ratio. The carrier solvent for the MC-PUR and the epoxy / polyamide were xylol, aromatic hydrocarbon solvent; while the carrier for the two hybrid coatings was a 90:10 mix of propylene carbonate (PC) and 3-ethoxypropionic acid ethyl ester (EEP) both non-HAPS compliant solvents.

The polymerization reactions in this experiment were assumed to have been initiated at the Al surface where M–O–S–R–NH₂ bonds were assumed to have formed

^{***} Bayer Polymers, 100 Bayer Road, Pittsburgh, PA15205-9741

^{†††} Resolution Performance Chemicals, 1600 Smith Street, 24th Floor P.O. Box 4500 Houston, Texas 77210-4500

^{‡‡‡} Huntsman Performance Chemicals, 3040 Post Oak Blvd., Houston, TX 77056

^{§§§} OSi Specialties, A Crompton Corp. ,One American Lane, Greenwich, CT 06831 2559, USA

upon application of the N-beta-(aminoethyl)-γ-aminopropyltrimethoxysilane, from which it is assumed a (M~Al, and R-NH₂) structure formed at the surface of the substrate and was extending into the bulk upon addition of 1) MC-PUR; 2) (7-PQ-6-ol) crosslinker according to Figures 5.10 –to– 5.12, below :⁵⁵⁹

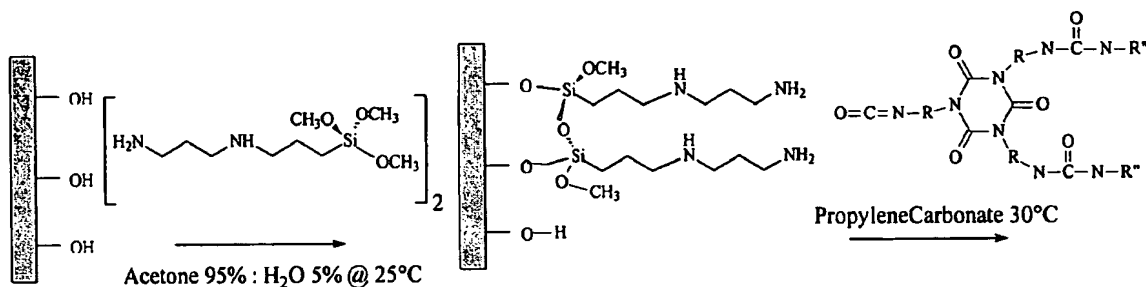


Figure 5.10: Initial sol reaction with surface hydroxyls and β-(aminoethyl)-γ-amino propyl trimethoxysilane.

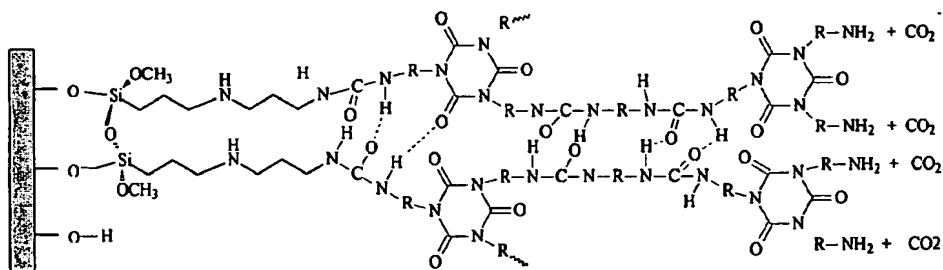


Figure 5.11: Terminal surface amines reacting with MC-PUR isocyanates in solution phase (HMDI or MDI prepolymers) to form second layer over M~Al, and R-NH₂).

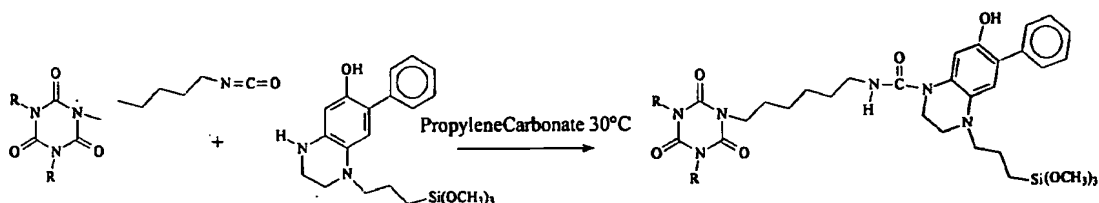


Figure 5.12: Development of bulk structure: A) to B) amino-silane sol-layer at Al surface; B) to C) isocyanate-functionalized monomers and hydrolysis to achieve high molecular weight conversion.

5.11 Bulk reactions with crosslinker

The crosslinker (used in both Epoxy- HMDI and Epoxy- MDI hybrids) (7-PQ-6-ol) (Figure 5.12, center) synthesized in these laboratories, was added to promote bulk polymerization throughout the IPN matrix. In addition, from spectroscopic analysis Chapter 4 the reaction depicted in Figure 5.13, below, is surmised to occur in the bulk between silanol and silane functionalities.

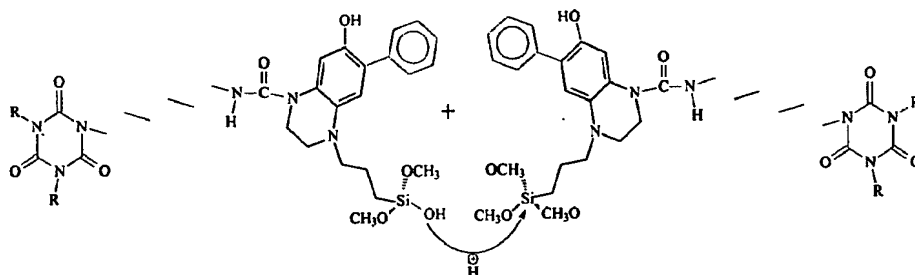


Figure 5.13: Bulk reaction of (7-PQ-6-ol) to achieve bulk pseudo IPN growth.

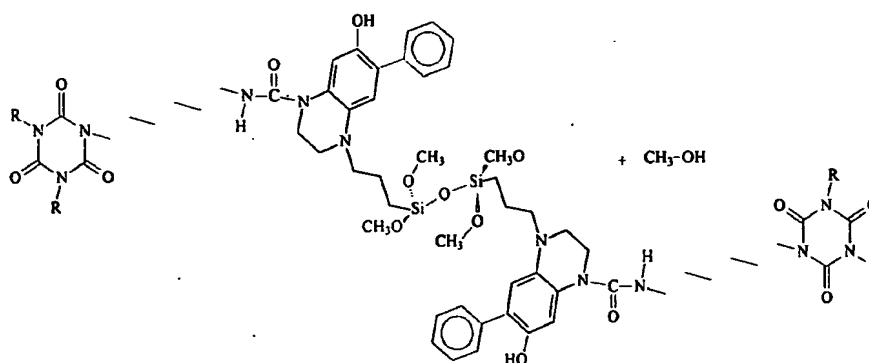


Figure 5.14: Isocyanates in solution phase (HMDI or MDI prepolymers) may further react with crosslinker and undergo further hydrosylation.

5.13 Summary Multi-layer Surface

The multi layer silane modified polyurea provides a means whereby the properties of polymers/ macromolecules adsorbing at a metal surface can be tailored to match those of the polymer in bulk. Based upon this assumption, a conformation approach, involving pretreatment with a dilute polymeric material, as suggested by Funke⁵⁴³, was pursued as a means by which to improve the adhesive properties of a coating.⁵⁴³ In addition, two other methods have been suggested and incorporated into this scheme as well: 1) use of reactive molecules of low molecular weight organ-silane (N-beta-(aminoethyl)-gamma-aminopropyl trimethoxysilane), which after physical or chemical adsorption can be connected by crosslinking or improving the molecular adaptation to the metal surface structure; 2) by incorporating small reactive, mobile binder molecules, (polyisocyanate prepolymer) which may be crosslinked after adsorption, i.e., polyurea multi layer. Figure 5.15, below, depicts the effect of cooperative functional groups at promoting good interactions between polymeric material and areas surrounding a potentially flawed metallic surface that have been filled in with polymeric material.

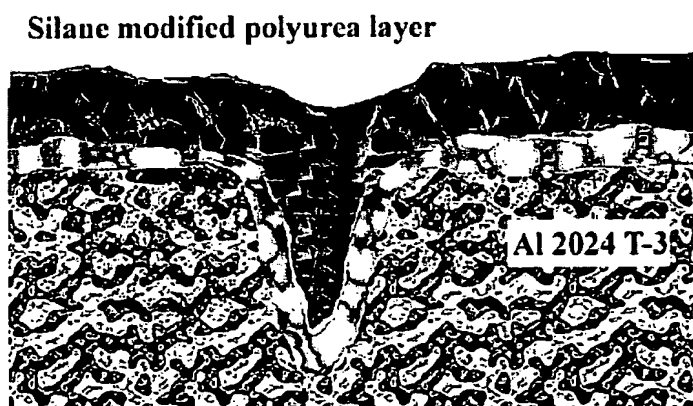


Figure 5.15: Illustration, modified micro surface depicting proposed improved interfacial area at flawed site by filling with inorganic-organic multi-layer coating.

Moreover, it is hypothesized that the most effective approach to be taken in the development of Mg-rich coatings for corrosion control of aluminum alloys is to prepare a micro-smooth, high energy surface with a dilute solution of low molecular weight oligomer containing reactive or crosslinkable functional groups that can be crosslinked from the Al_2O_3 surface up in a multi-layer technique and into the bulk where an applied metal-rich primer later can later be deposited.

5.14 Critical Pigment Volume Concentration Estimates for Mg-rich Primers

CPVC is a function of the random dense packing efficiency of the pigment plus adsorbed layer thickness (δ), which must be experimentally determined. This has been discussed extensively in the literature and a recent review considers new developments.⁵⁶⁰ The procedure for obtaining CPVC's for these Mg-rich systems is described has been described.⁵⁶¹ In this experiment two magnesium powders, (Eckagranules™ PK 31~ 30 μm , and PK-51~70 μm used as received), with different mean particle size distributions, see Figure- 5.16, below, were mixed at a 52%-PK31: 48%-PK51 volume. A 52:48 volume mix of the two powders was found to yield a higher bulk density value than that of either powder alone. Aerosil R202™ a hydrophobically modified fumed silica, containing no microcrystalline silica, was used as the rheology control agent due to its effectiveness in epoxy related systems. Due to the nature of the solvents used PC and EEP, both with low vapor pressures, appreciable solvent is not volatilized when atomized via spray application, and as a result, rheology control, via an efficient agent, is necessary to ensure uniform film formation during application.

The critical pigment volume concentration (CPVC) of the primers was first approximated by obtaining a resin / powder rub-up value with Aerosil R202™ at 2% vol. on total pigment, and the final CPVC was calculated from PSDs of the three pigments, assuming spherical geometry, combined with the experimentally determined resin rub-up values.⁵⁶¹ Figure-5.17, below, shows the calculated CPVCs that coorespond to shaded areas in the ternary diagram for the three pigment mixtures.

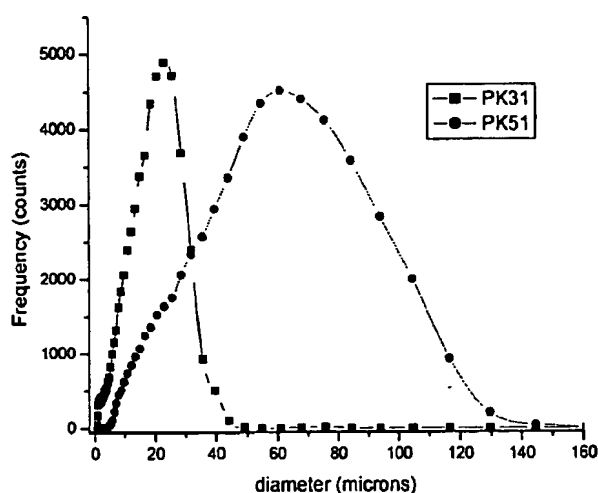


Figure 5.16: Particle size distributions for Mg for powders Eckagranules™ PK31 and PK51.

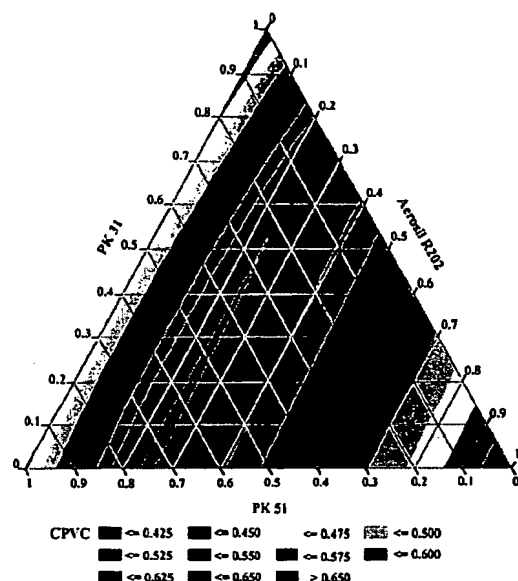


Figure 5.17: Ternary mixture diagram for powders Eckagranules™ PK31 and PK51 with calculated CPVCs and shaded areas for mixtures of PK31, PK-51 and Aerosil™ R202.

The volume fraction coordinates (PK-31 = 0.51, PK-51 = 0.47, and R-202 = 0.02) yields a calculated CPVC value in the region @ $PVC \leq 0.475$. Magnesium rich coatings may be viewed analogously to zinc rich systems, in that, as long as there is sufficient electrical contact within the continuous film the interface of the aluminum alloy will remain protected. However, unlike zinc, magnesium metal has a relatively low density of 1.738 g/cm^3 . This is in sharp contrast to zinc metal with density of 7.133 g/cm^3 , a denser pigment.



Figure 5.18: Eckagranules™ PK51 Mg powder at 50% magnification.

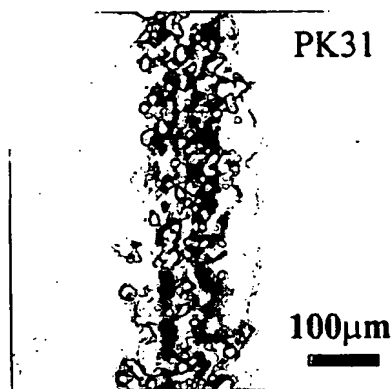


Figure 5.19: 20% Eckagranules™ PK31 Mg powder contrast with a 4-mil human hair at 20% magnification.

5.15 Panel and Film Preparation

The primers formulated from materials in Table 5.2-B, above, were prepared using conventional techniques. Primers were applied to 6" x 3" Al 2024 T3 Q-panels™, scrubbed with a Scotch Brite™ pad, rinsed and degreased with EEP, then immersed in a 10% phosphoric acid solution for 60 seconds, then rinsed with distilled water. Al panels were surface modified according to methodology described in Chapter 4, this thesis, where a 2% mixture of Silwet®1120 in acetone / water mix as described in the literature.¹⁶ The magnesium pigment was mixed slowly into a mixture of epoxy / polyisocyanate solvent with a 1" -diameter propeller blade mixer at 1,000 rpm. The rheology control agent Aerosil®R202 was added slowly to the pigment/binder-resin/solvent mix after the Mg pigment was added. The resulting paint was applied with a touch-up spray gun, at a pressure setting of 60psi. The coatings were cured at 30° C for 14 days. Primed panels were subsequently top coated with Extended Lifetime™ topcoat. The average film thickness (FT) estimated from EDAX photos reveal primer film thickness to be on the order of ~50 +/- 20 microns with topcoat film thickness at ~ 100 +/- 40 microns.

5.16 Coating Morphology

The resulting primed and topcoated panels from the four formulations given in Table 5.2-B, were observed to develop differing surface textures which are surmised to be related to: 1) pigment dispersion and the polymeric material's ability to wet the magnesium pigment; 2) the solvent evaporation and the type of thixatrobe used in the study. Early on it was observed that hydrophobically modified fumed silicas such as AerosilTMR202⁵⁶² which has polydimethylsiloxane groups anchored to the surface are not wet by aromatic polyisocyanate resins. According to Schwindt⁵⁵⁶, the recommended thixatrobe for these systems are the organically modified Bentone® clays from Rheox Corp., such as Bentone® 39, which is a hydrophobically modified bentonite clay.

The Mg-rich coating systems in this study were comprised of a highly pigmented Mg-rich primer coat followed by a ELTTM, see Figures 5.20 – 5.15, below. The film formation process which is related to the ultimate performance of the coating system is dependent on the coating's morphology as applied to the alloy surface. As discussed previously, the CPVC is related to the maximum packing efficiency of the pigmented material in a coating.⁵⁶¹

Factors leading to pigment agglomeration are known to result in coatings with inefficient particle packing which is related to the coating's CPVC. Generally, when pigment agglomeration occurs the larger the agglomerate the higher the formulated PVC must be to reach a coating's CPVC. Therefore, as a result of poor dispersion or agglomeration, the actual PVC of a poorly dispersed or agglomerated system will be formulated far above the PVC value of a well dispersed system at its CPVC. Thus, this raises the value of λ PVC/CPVC for poorly dispersed systems. Agglomeration of

pigments, in such a case, leads to a coating below its CPVC and as a result its performance properties, as a cathodic coating, will not be equal relative to the analogous well dispersed coating system formulated at the same PVC.

5.17 Micrographs SEM and EDAX

Samples were assembled on aluminum mounts and coated with gold using a Technics Hummer II sputter coater. Images were obtained using a JEOL JSM-6300 Scanning Electron Microscope. X-ray information was obtained by a ThermoNoran EDX detector using a VANTAGE Digital Acquisition Engine. Figures 5.20 –to– 5.26, below, show SEM and EDAX cross sections of the four 50 PVC Mg-rich primers, with pigmentary Mg showing the distribution / alignment of Mg powder at the Al interface and its distribution in the polymer matrix which is thought to be related to its dispersion in the coating's polymer matrix and ultimately to its effectiveness as a coating for corrosion control.

Data collected for four coating systems in SEM lateral profiles, Figures 5.20 (a) and (b), and 5.21(a) and (b), show Al 2024 T-3 substrate, Mg-rich primer, and Deft ELT™ coating contrasted to a 50 micron scale. The appearance of voids in the coating or at coating interface can be used as a rough qualitative measure of the integrity of the coating system. Those coatings with visible void area may be considered inherently flawed and most prone to failure when subjected to performance testing conditions.

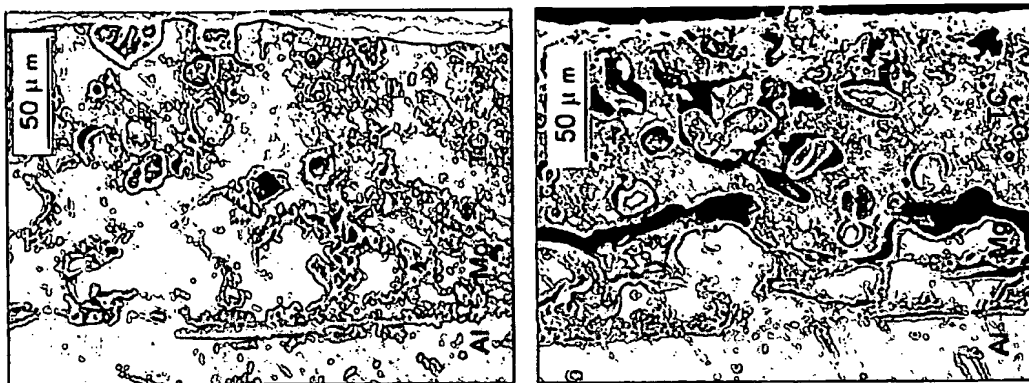


Figure 5.20 (a) and (b): SEM lateral profile Mg-rich primers at 50 PVC with ELT™ (a) left silane modified MDI-polyisocyanate / epoxy-urea; (b) right, MC-PUR, MDI polyisocyanate. With (+/-) 70 micron film thickness (FT) ELT™ topcoat. Al 2024 T-3 alloy, (base), Mg powder matrix (middle); ELT™ coating (top).



Figure 5.21 (a) and (b): SEM lateral profile Mg-rich primers at 50 PVC with ELT™ (a) left silane modified HMDI-polyisocyanate / epoxy-urea; (b) right Epoxy/ polyamide. with (+/-) 70 micron film thickness (FT) ELT™ topcoat. Al 2024 T-3 alloy, (base), Mg powder matrix (middle); ELT™ coating (top).

Figures 5.22 and 5.23, below, show EDAX images for lateral profiles of Mg-rich coatings with X-ray fluorescence (XRF) counts for magnesium, in red, and silicone, in blue, corresponding to SEM images Figures 5.20 and 5.21, above. Figures 5.22 and 5.23 (a) and (b) EDAX images that show the structure of Mg-rich coating primer with ELT™ topcoat for the 50%PVC silane modified epoxy-urea. In reference to Figure 5.22 (a) the carrier solvent was propylene carbonate / EEP, with Aerosil® R202 hydrophobically modified silica rheology agent. The Mg XRF counts, in left, show that Mg particles have

attained good particle-particle contact. While Figure 5.22 (b) gives an image from XRF Si counts, right, (lighter phase) and reveal presence of silicate structure in the ELT™, due to the presence of polymer beads that can be observed also in Figure 5.23(b). The XRF Si count, Figure 5.23(b) (light area / phase) appears slightly higher in the bulk of the primer than that on the surface which may have implications to the coatings adhesion to the substrate.

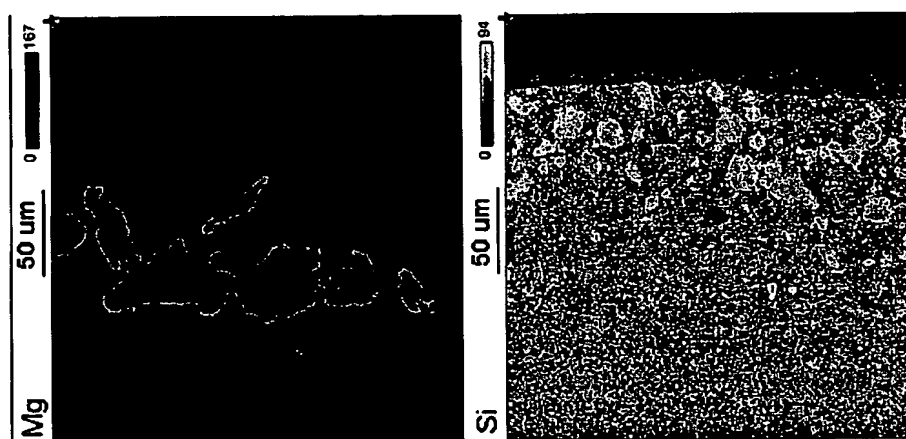


Figure 5.22 (a) and (b): EDAX cross section of 50% PVC MDI, Desomdur E23A polyisocyanate, silane modified epoxy-polyurea with ELT™ topcoat: (a) left, Mg XRF counts and (b) right, silicon XRF counts.

Figures 5.23 (a) and (b), below, show EDAX and SEM images for the MC-PUR at 50% PVC, where the carrier solvent was xylol (commercial mixture of xylenes), and the rheology modifier was Bentone®39 / bentonite clay activated with propylene carbonate. Note that the bentonite clay solids in the formulation were approximately ~ 2% by volume, similar to that of the hydrophobically modified fumed silica. However, it should be noted that for the MC-PUR / xylol vehicle the Bentone®39 is far more efficient than hydrophobically modified silicas such the Aerosil® R202. In addition, it was noted that a phase separation occurs when Aerosil® R202 is used in the MC-PUR / xylol vehicle with the resulting coatings having no adhesion to the AL 2024T-3 substrate.

Overall, the primer coating in Figures 23 (a) and 5.24 shows good alignment and packing of Mg-powder but with the exception of the void formed between the topcoat and primer. The void formation at the interface observed between primer and ELT™ topcoat was not a local defect but rather a flaw resulting from a wetting problem in adhesion to PUR. It has also been observed in other SEM images of identical coating samples analyzed in previous studies.

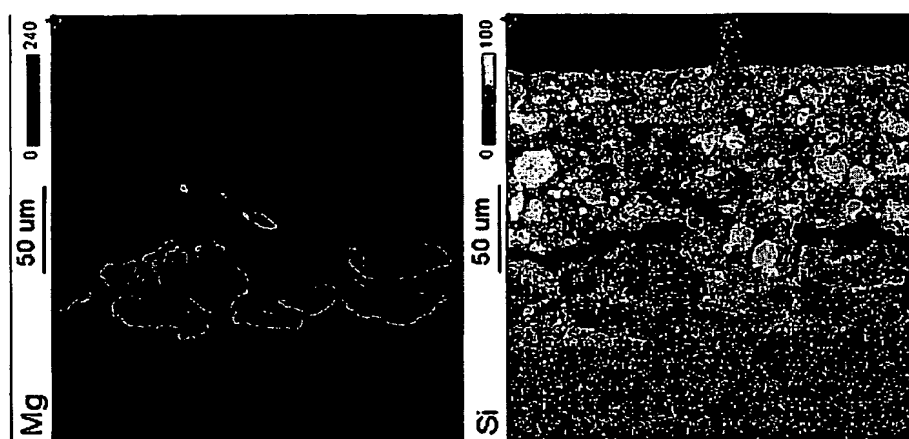


Figure 5.23 (a) and (b): EDAX cross section of 50% PVC Desomdur E23A, MDI, MC-PUR, with ELT™ topcoat: (a) left, Mg XRF counts and (b) right, silicon XRF counts.

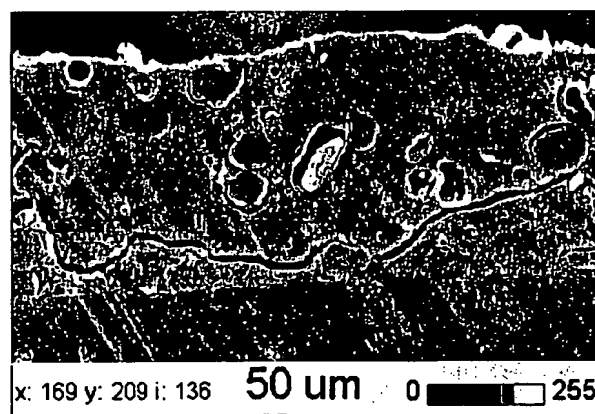


Figure 5.24: SEM lateral profile Mg-rich primer at 50 PVC (MDI) Desomdur E23A, MC-PUR, with ELT™ topcoat. Results from previous study, shows formation of void defect at interface between topcoat and Mg-rich primer.

The EDAX images, Figures 5.25 (a) and (b), below, show lateral profile of the 50% PVC HMDI, Desomdur™ N3300 polyisocyanate, silane modified epoxy-polyurea system. The primer coating shows good alignment and packing of Mg-powder horizontal to the surface. Figure 5.25 (b) Si XRF counts for Si (lighter area) show a more extensive network of silicon extending from the ELT™ topcoat to the surface of the Al 2024 T-3. The absence of voids at the primer / topcoat interface suggests good topcoat adhesion to the primer. The coating system appears more as a one phase system as opposed to a two phase system, i.e., Figure 5.23 (a) and (b) above.

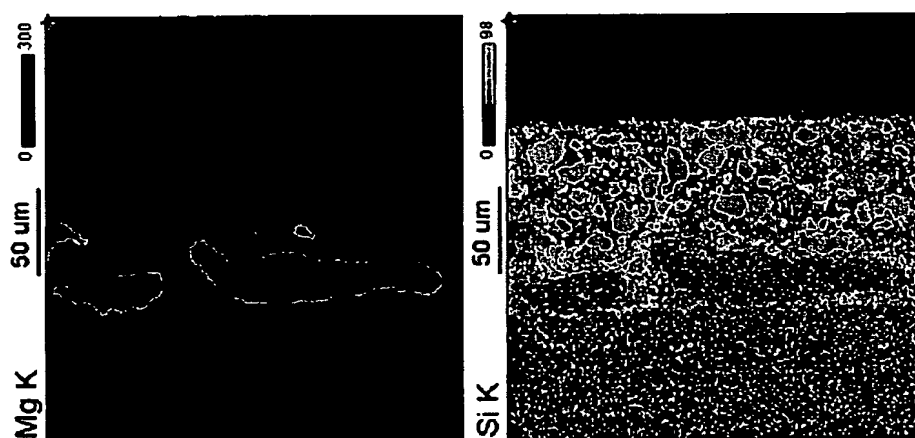


Figure 5.25 (a) and (b): EDAX cross section of 50% PVC HMDI, Desomdur N3300 polyisocyanate, silane modified epoxy-polyurea with ELT™ topcoat: (a) left, Mg XRF counts and (b) right, silicon XRF counts.

The EDAX images, Figures 5.26 (a) and (b), below, show lateral profile for of 50% PVC epoxy / polyamide, the rheology control agent used was Aerosil™ R202 and the carrier solvent was xylol. The primer coating in Figure 5.26(a) compared to 5.25 (a) shows poor alignment and packing of Mg-pigment, in gray, near the Al substrate with the appearance of a void at the primer / Al 2024 T-3 interface. Note Aerosil™ R202 is the Silicon component in the Mg-rich coatings.

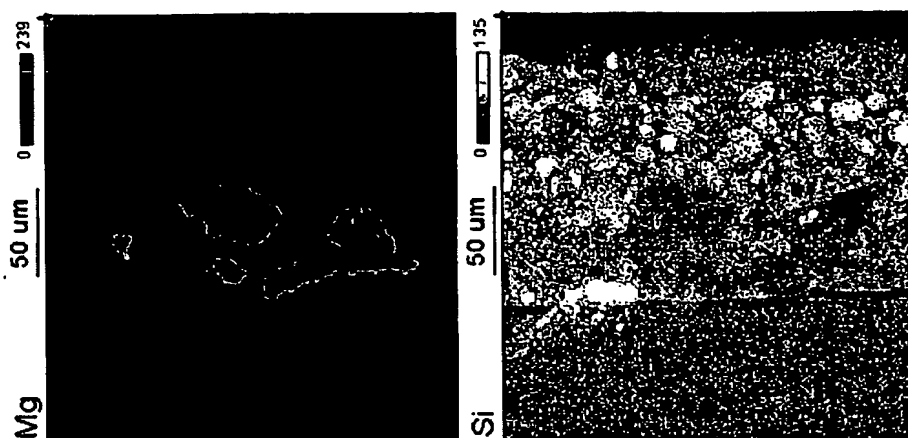


Figure 5.26 (a) and (b): EDAX cross section of 50% PVC epoxy/polyamide, with ELT™ topcoat: (a) left, Mg XRF counts and (b) right, silicon XRF counts.

5.18 Topographic Profiles

The following SEM pictures Figures 5.27 to 5.35 consist of topographic profiles of the individual coating systems as applied, primer plus topcoat at two different PVCs, 43 % and 50% PVC. Figures 5.27 to 5.30, below, contrast 43 % versus 50% PVC at 50-% magnification; while Figures 5.31 to 5.35, below, contrast 43 % versus 50% PVC at 200-% magnification.

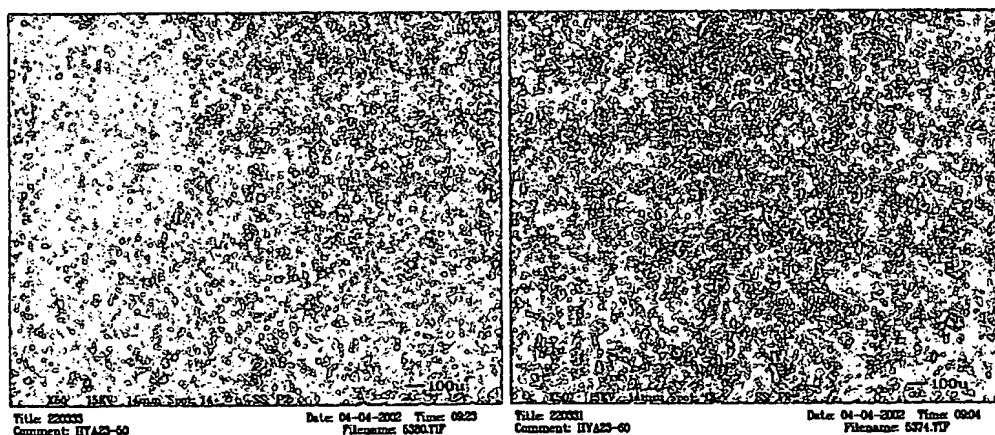


Figure 5.27 (a) and (b): SEM of (a) 43% PVC and (b) 50%PVC MDI, Desomdur E23A polyisocyanate, silane modified epoxy-polyurea with ELT™ topcoat at 50-% magnification.

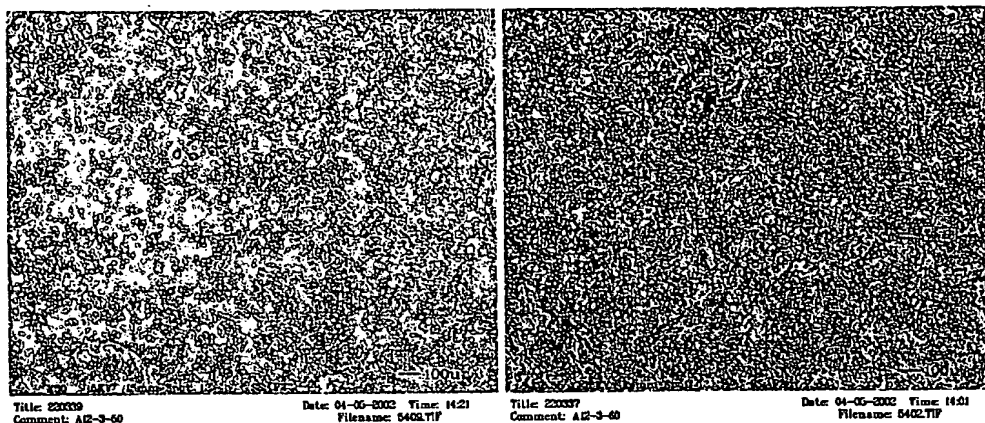


Figure 5.28 (a) and (b): HMDI, Desomdur N3300 polyisocyanate, silane modified epoxy-polyurea with ELT™ topcoat 43% PVC and (b) 50%PVC with ELT™ topcoat at 50-% magnification.

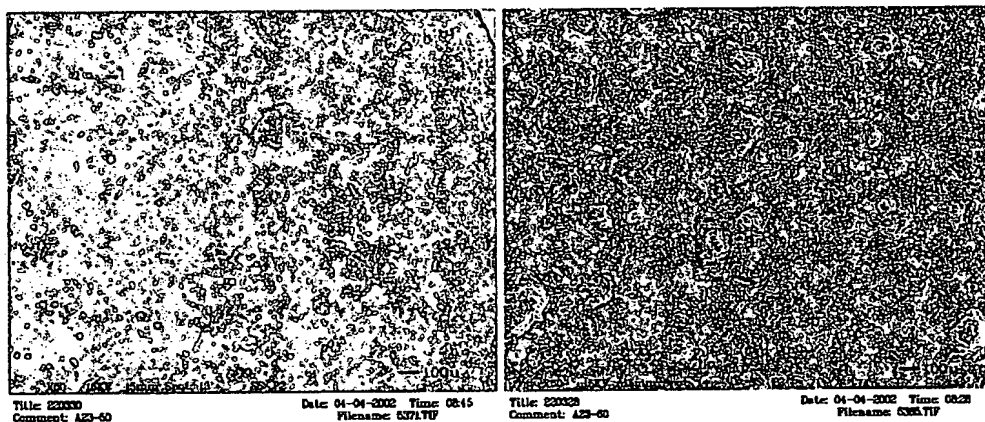


Figure 5.29 (a) and (b): SEM of (a) 43% PVC and (b) 50%PVC MC-PUR, MDI, Desomdur E23A polyisocyanate at 50-% magnification.

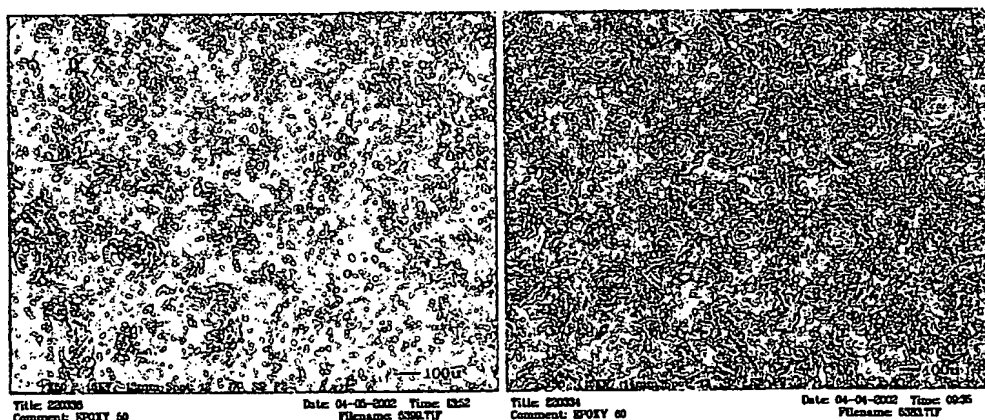


Figure 5.30 (a) and (b): SEM of (a) 43% PVC and (b) 50%PVC epoxy at /polyamide, with ELT™ topcoat, at 50-% magnification.

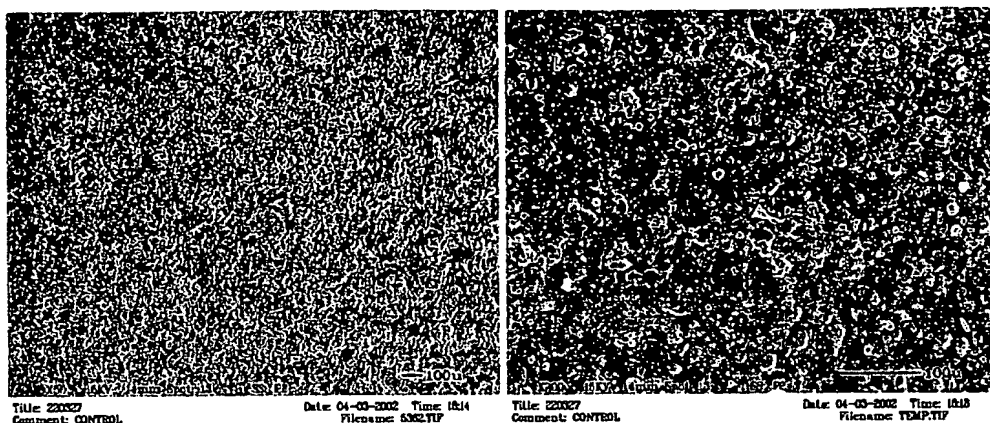


Figure 5.31 (a) and (b): ELT™ surface of control at 50-% magnification.

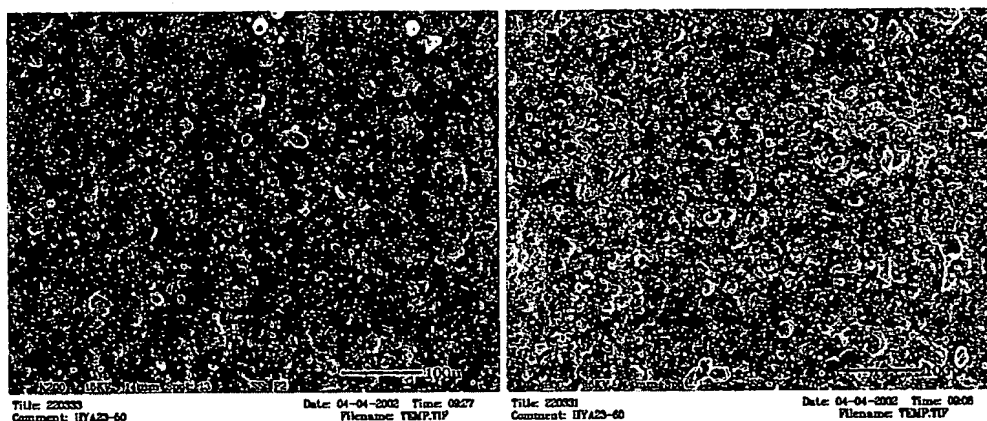


Figure 5.32 (a) and (b): SEM of (a) 43% PVC and (b) 50%PVC, Desomdur MDI, E23A polyisocyanate, silane modified epoxy-polyurea with ELT™ topcoat at 200-% magnification.

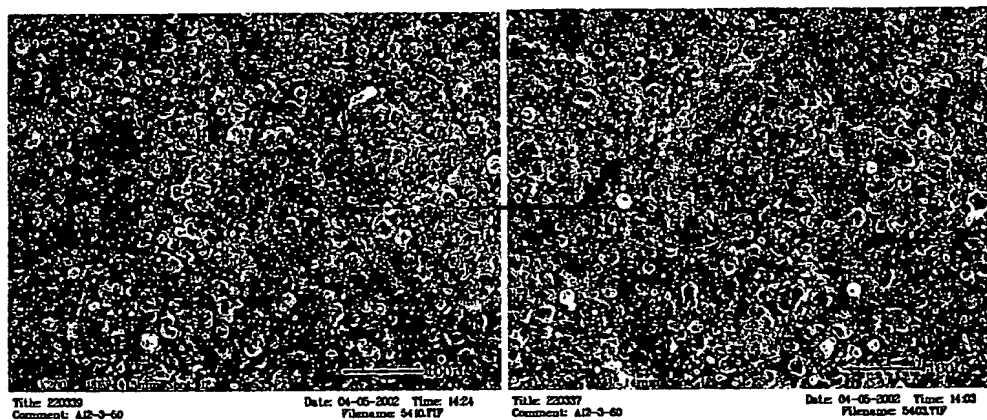


Figure 5.33 (a) and (b): HMDI, Desomdur N3300 polyisocyanate, silane modified epoxy-polyurea with ELT™ topcoat 43% PVC and (b) 50%PVC with ELT™ topcoat at 200-% magnification.

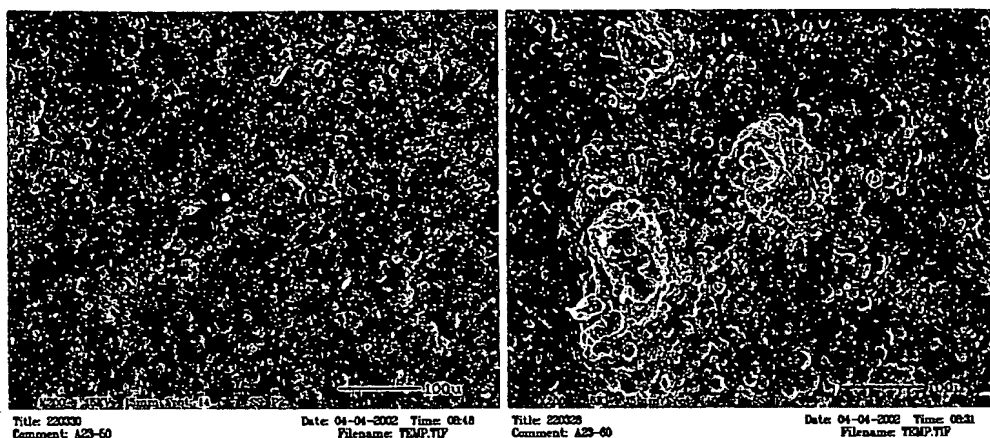


Figure 5.34 (a) and (b): SEM of (a) 43% PVC and (b) 50%PVC MC-PUR, MDI, Desomdur E23A polyisocyanate at 200-% magnification.

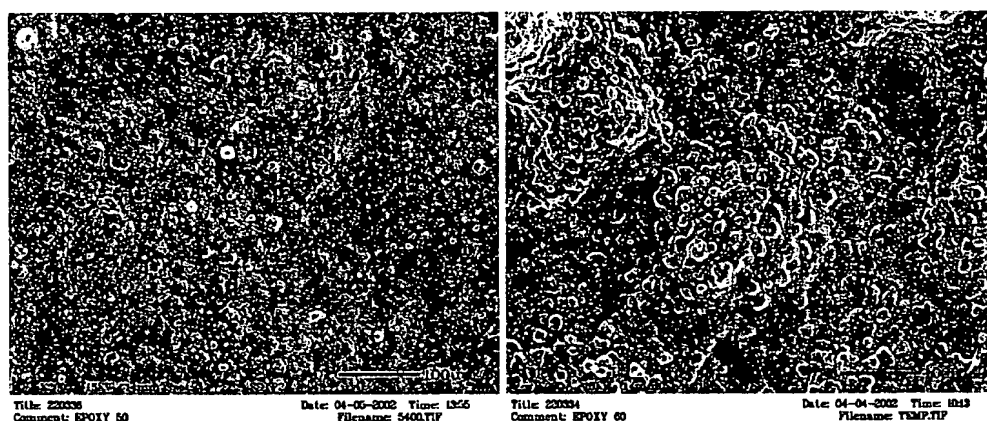


Figure 5.35 (a) and (b): SEM of (a) 43% PVC and (b) 50%PVC epoxy /polyamide with ELT™ topcoat, at 200-% magnification.

5.19 Summary

In reference to Figures 5.27 to 5.35, above, the overall quality of the coating systems can be assessed according to the observed difference in surface roughness, as transmitted through to the topcoat by the underlying primer as a function of PVC. The difference in the quality of the coatings formulated at 43% PVC where $\lambda < 1$ *versus* formulations at 50% PVC where $\lambda > 1$ becomes apparent due to the increased surface roughness contributed by the more aggregated pigment conformations for those systems that did result in good pigment dispersion. Overall, the silane modified epoxy /

urea hybrid systems yielded primers with less roughness at higher PVCs than the primers formulated by conventional systems, i.e., the moisture cure polyurea (MC-PUR) and the epoxy / polyamide lacquer with the xylol solvent system.

The initial assumption regarding these Mg-rich systems was that their CPVC lie somewhere in the 43% to 50% PVC range, and according to theoretic calculations as described above, it was determined to be about 47% PVC. The above results shown for the 43 and 50% PVC samples emphasizes the effect agglomeration exerts on the coatings morphology. Where Figures 5.27(a) and (b) contrasted to both Figures 5.29 (a) and (b); 5.30 (a) and (b) show dramatic differences in surface morphology between primers at 43% PVC *versus* 50% PVC. Especially in the case of Figures 5.29 (a) and (b) the MC-PUR, where at 43% PVC the coating appears very smooth while at 50% PVC the surface roughness has increased dramatically over that of the Silane modified (MDI) epoxy / urea hybrid at 50 %PVC in Figure 5.27(b). This trend can also be observed at a higher magnification, 200-% as shown in Figures 5.31 to 5.35.

The results from these topographic studies reveal that the effective CPVC of a magnesium rich primer coating is sensitive to agglomeration and may be very formula specific. Considerable variation in the coating's morphology results according to the nature of the polymeric material, solvent system, and thixotrope used. It may also be surmised that such coating systems displaying a minimum increase in surface roughness over a PVC range that includes PVCs $< (\Lambda)$ to PVCs $> (\Lambda)$ yield a more effective metal-rich coating system by virtue of pigment dispersion, packing and distribution in the primer coat.

References / Bibliograph

- ⁵²⁶ Hare, C.H., and Kurnas, J.S., *J. Coatings Technology*, Vol. 72, No. 910, pp. 21 – 27 (2000)
- ⁵²⁷ Jones D. A. Jones, *Principles and Prevention of Corrosion*, 2nd Ed., Prentice–Hall, Upper Saddle River, NJ (1996), Ch. 2
- ⁵²⁸ Szklarska-Smialowska, Z., *Corrosion Science*, Vol. 41, pp. 1743-1767 (1999)
- ⁵²⁹ McCafferty, E., *Corrosion Science*, Vol. 45, pp. 1421-1438 (2003)
- ⁵³⁰ Kreuner, K-D, *Chem. Mater.*, Vol. 8, pp. 610 (1996)
- ⁵³¹ Chao, C.Y., Lin, L.F., and Macdonald, D.D., *J. Electrochem. Soc.*, Vol. 128, pp. 1187 (1981)
- ⁵³² Macdonald, D.D., *J. Electrochem Soc.*, Vol. 139, pp. 3434 (1992)
- ⁵³³ Bunker, B.C., Nelson, G.C., Zavaldil, K.R., Barbor, J.C., Wall, F.D., Sullivan, J.P., Windlisch, C.F. Jr., Englehart, M.H., and Baer, D.R., *J. Phys. Chem. B*, Vol. 106, pp. 4705 – 4713 (2002)
- ⁵³⁴ Alwitt, R.S., The Aluminum-Water System, In *Oxides and Oxide Films*; Diggle, J.W., and Vijh, A.K., Eds.; Marcel Dekker: New York, NY, Chapter 3 (1976)
- ⁵³⁵ Buchheit, R.G., *J. Electrochem. Soc.*, Vol. 142, pp. 3994 (1995)
- ⁵³⁶ Dimitrov, N., Mann, J.A., and Sieradzki, K., *J. Electrochem. Soc.*, Vol. 146, pp. 96-102 (1999)
- ⁵³⁷ Vukmirovic, M.B., Dimitrov, N., and Sieradzki, K., *J. Electrochem. Soc.*, Vol. 149, pp B-428-B439 (2002)
- ⁵³⁸ Dimitrov, N., Mann, J.A., Vukomirovic, M.B., and Sieradzki, K., *J. Electrochem. Soc.*, Vol. 147, pp. 3283 (2000)
- ⁵³⁹ Alodan, M.A., and Smyrl, W.H., *J. Electrochem. Soc.*, Vol. 145, pp. 1571 (1998)
- ⁵⁴⁰ Park, J.O., Paik, C.H., Huang, Y.H., and Alkire, R.C, *J. Electrochem. Soc.*, Vol. 146, pp. 517 (1999)
- ⁵⁴¹ Walker, P., “Organo Silanes As Adhesion Promoters for Organic Coatings,” *Journal of Coatings Technology*, Vol. 52, No. 670, November, pp. 49-61 (1980)

- ⁵⁴² Schwindt, J., "Moisture-Cured, Polyurethane-Based, Surface Tolerant Coatings: An Economical Alternative for Corrosion Control," Technical literature from Bayer AG, Leverkusen, Germany, (2000)
- ⁵⁴³ Funke W., Problems and Progress in Organic Coatings Science and Technology, *Progress in Organic Coatings*, vol. 31, Pp 5–9, (1997)
- ⁵⁴⁴ Rosen M.R., *Journal of Coatings Technology*, Vol. 50, No.644, pp. 70, (1978)
- ⁵⁴⁵ Vanderbuilt, B. M., and Clayton, R.E., *Ind. Eng. Chemistry.*, No 4, pp. 18, (1965)
- ⁵⁴⁶ Bjorksten, J., and Yalger, L.L., *Mod. Plastics*, Vol. 29, 124, (1952)
- ⁵⁴⁷ Seneker , S.D, and Potter, T.A, *Journal of Coatings Technology*, Vol. 63 , No. 793 pp. 19 (1991)
- ⁵⁴⁸ Kakabe, Y., and Bailey, R.E., *Environ. Sci. Technol.*, Vol. 33, pp. 2579-2583, 1999
- ⁵⁴⁹ Major J.S., and Blanchard, G.J., *Chem. Mater.*, Vol. 14, pp. 4320-4327 (2002)
- ⁵⁵⁰ Ni, H., Nash, H.A., and Worden, J.G., *J. Polymer Science: Part A: Polymer Chemistry*, Vol. 40, pp. 1677–1688 (2002)
- ⁵⁵¹ Product Bulletin, Epi-Cure™ Curing Agent 3502, SC:1724-01, ©2001 Resolution Performance Products.
- ⁵⁵² Sperling L.H., *Interpenetrating Polymer Networks and Related Materials*, New York: Plenum, (1981)
- ⁵⁵³ Frisch *et al.*: Frisch H.L., Klempner D., *Polymer Engineering Sci.*, Vol. 14, (9), pp. 646 (1974)
- ⁵⁵⁴ Hseih K.H., Han, T.H., *J.Polymer Sci.*; Part B: Polymer Physics; Vol. 28, pp. 623, (1990)
- ⁵⁵⁵ BASF Tech data sheet, BASF Co. Chemicals Division 3000 Continental Drive–North Mt. Olive, NJ, (www.basf.com)
- ⁵⁵⁶ Schwindt, J., "Moisture-Cured, Polyurethane-Based, Surface Tolerant Coatings: An Economical Alternative for Corrosion Control," Technical literature from Bayer AG, Leverkusen, Germany, (2000)
- ⁵⁵⁷ Adapted from: Bayer Desmodure™ E-23A Moisture Cure Urethane, Zinc Rich Primer, Formulation # 294-35

⁵⁵⁸ Product Bulletin, Epi-Cure™ Curing Agent 3115, SC:1714-01, ©2001 Resolution Performance Products.

⁵⁵⁹ Kohli, P., and Blanchard, G.J., *Langmuir*, Vol. 16, pp. 4655-4661 (2000)

⁵⁶⁰ G. P. Bierwagen, R.S. Fishman, T. Storsved, and J. Johnson, "Recent Studies of Particle Packing in Organic Coatings," *Prog. Organic Coatings*, Vol. 35 pp. 1-10 (1999)

⁵⁶¹ Johnson, J.A., Computer Assisted Coatings Design – Critical Pigment Volume Concentration Issues, Ph.D. thesis, North Dakota State University, May (2000)

⁵⁶² Degussa, Technical bulletin No. 27, Aerosil® for solvent free-epoxy resins.

Chapter 6 Coating Systems Performance Evaluation

6.1 Thesis

The polymeric materials developed in this study have been devised specifically for a Mg-rich primer system. According to general consensus⁵⁶³ polyureas are the reaction products of a primary or secondary amino group with an isocyanate where the amine reaction with a prepolymer containing about 13-to-16 percent isocyanate content that yields a polyurea. The polyurea reaction, in itself, does not constitute a hybrid polymeric system, such as those polyisocyanate / polyol or other hydroxyl containing materials that are reported⁵⁶⁴ to lead to two step reactions with questionable physical properties.

The central feature of the polyurea reaction^{565,566,567} is that it can be accelerated by the presence of humidity / water, and as a result the reaction is carried to completion yielding a high molecular weight more hydrolytically stable product compared to most so called hybrid systems. The problem associated with most hybrid systems, containing polyols or other hydroxyl containing materials, is that these hydroxyl containing components can adversely retard the autocatalytic effect of the polyurea reaction which in turn promotes a second step reaction that yields a material that is more reactive than the polyurea. The end result is a material with a lower conversion and poor hydrolytic stability and film quality. The emphasis of the mechanical testing presented in this section is to show by appropriate means that the quality of the hybrid polymeric materials developed is comparable or better than that of the polyurea and epoxy-amine starting materials themselves.

Another objective of this research has been to establish that metal rich coating systems comprised of particulate magnesium powder, in an appropriate polymeric binder matrix, will impart acceptable performance properties to a coating for use in corrosion control of precipitation grade hardened aluminum alloys. The system under investigation has been designed to function as primer plus a topcoat. The topcoat used in these studies was a commercially available fluoropolymer product from Deft Inc., formulated specifically for spray application use over primed aerospace alloy substrates. The following generic evaluations serve to demonstrate that the choice of polymeric materials used in the primer coat have a direct influence on the corrosion control performance of the integral system primer plus topcoat.

6.2 Testing the Polymeric Material systems

Synthesis of the hybrid polymeric materials for this system was described in Chapter 4. Since these hybrid polymeric materials are derived from an epoxy and select polyisocyanate prepolymer, a generic epoxy and polyisocyanate/polyurea system, respectively, were chosen to contrast the effectiveness of the hybrid polymeric matrices developed in these studies. The solvents used in the primers formulations, propylene carbonate (PC) and 2-ethyl-3-ethoxypropionate (EEP) are low vapor pressure / higher boiling point solvents that do not readily evaporate at temperatures below 25°C / °F from films with thicknesses greater than 2 mils. It is surmised that the ambient cure mechanism for thick films differs from that of thinner films, i.e., film thickness (FT) < 0.5 mils, in that thicker films retain the solvents over a longer period of time which causes the polyisocyanate reaction to be retarded, as propylene carbonate acts as an isocyanate retarder and on the other hand as an epoxy-amine catalyst, thus promoting the epoxy /

amino reaction. Experimental observation has also shown that as drawdown film thickness increases the film tends to exude or “sweat-out” the solvent causing it to bead-up over the surface of the quasi-cured coating. Another factor that was not investigated, but thought to be related to film thickness/solvent retention, is the difference in the extent of hydrosilation between surface hydroxyls, contributed by the magnesium metal and aluminum alloy surfaces versus hydrosilation between silanol groups in the bulk of the matrix. It might be surmised that as film thickness increases, for example given a thick film FT >2 mil, bulk hydrosilation reactions would eventually contribute to a higher degree of crosslinking in the interpenetrating network structure than if the film were part of a thin film in a pigmented matrix adsorbed onto pigment particles near or at the coating’s CPVC. In the later case, the polymeric material would show a different set of mechanical properties than in the former, i.e., the resulting viscoelastic properties such as the glass transition temperatures (T_g s), or mechanical properties such as elastic modulus and tensile strength may all differ considerably.

6.3 Mechanical Properties of Polymeric Materials

All mechanical testing was performed according to the following ASTM standards: reverse impact resistance (ASTM D 2794-84), pull-off adhesion (ASTM D 4541-85), and tensile properties (ASTM D 2370-82). For reverse impact and pull-off adhesion, three sets of measurements were made per sample and at least six per sample in tensile tests. Tensile properties were measured using an Instron™ model 5542 with Merlin (2) software. The dimensions of films in tensile test were 0.06 to 0.20 mm in thickness, 12 mm in width and at least 40 mm in length. A crosshead speed of 20mm / min was used to determine elongation-at-break, tensile modulus, and tensile strength. The mean and standard deviation

for each polymer sample set is reported. DMTA measurements were made with a Rheometrics model 3-E dynamic mechanical analyzer.

6.4 Viscoelastic Polymeric Materials

In sinusoidal deformation a polymer's modulus is expressed in terms of a complex quantity that is composed of two components the storage modulus (E') that accounts for the polymer's recoverable elasticity, and the loss modulus (E'') the dissipative energy loss. The material's mechanical loss or damping is given by the quantity $\tan \delta$ which is the ratio of its out of phase deformation to in phase deformation (E''/E') taken at the maximum in the $\tan \delta$ signifying the material's glass transition temperature T_g at an α -transition.⁵⁶⁸ The crosslink density was calculated from elastic modulus (E') at $T_g + 50^\circ\text{C}$, where ν_e is the elastically effective crosslink density. The measured viscoelastic properties for five polymer systems, in Table 6.1, below, gives T_g , elastic storage modulus E' (*minimum*), and calculated crosslink density. The significant differences in reported glass transition temperatures are assumed to be related to the individual coating's chemical properties at full cure. Crosslink density was calculated from (E'): ($T = T_g + 50^\circ\text{C}$) at which the materials were in the rubbery state; where ν_e is the elastically effective crosslink density, Equ. 6.1.⁵⁶⁹

Equation 6.1
$$\nu_e = 3 E' / RT (T + T_g) \quad (1)$$

The reported T_g s, elastic modulus, crosslink density, properties of films from the formulations are given in Table 6.1, below. While the percent elongation, and tensile properties of these samples are shown Table 6.3, below. As a cross reference to the film cast from the moisture cure PUR of HMDI Desmodur® N3300, Table 6.3, below, shows

good agreement with a similar polyurea film derived from Desmodur N3300 (HMDI)

reported in the literature.⁵⁷⁰

Table 6.1: Viscoelastic properties of polymer films

Polymer film	Tg (°C)	Crosslink density (mol/cm ³)	E' (Pa) minimum
N3300 (MC-PUR)	122	3.4 %10 ⁻³	2.6 % 10 ⁷
E23A (MC-PUR)	159	5.8%10 ⁻⁴	6.6 % 10 ⁵
Epoxy-polyamide	65	2.1% 10 ⁻³	2.0 % 10 ⁷
Hyb-N3300	96	1.3 % 10 ⁻³	1.3 % 10 ⁷
Hyb-E23-A	100	6.9 % 10 ⁻⁴	6.9 % 10 ⁶

Table 6.2 : Properties of polymer films HMDI, MC-PUR, Desmodur N3300

Polymer film	Tg (°C)	X-link density (mol/cm ³)	E' (Pa) min.	(%) elong
N3300 (MC-PUR)	122	3.4 %10 ⁻³	2.6 % 10 ⁷	8.0
POC, 38 (2000)	130	2.3 %10 ⁻³	2.2 % 10 ⁷	4.6

Generally, Desmodur N3300 prepolymer is characterized as an elastomer, while Desmodur E23A a pentamer of MDI, is characterized as a more rigid aromatic system characterized with a higher Tg, tensile strength and lower elongation than that of the polyurea from HMDI.⁵⁷¹ The results in Table-6.1 also suggest that some difference in chemical composition of crosslinks formed may lead to observed differences in T_gs.

According to Hale and Macosko,⁵⁷² changes in T_g arise both from disappearance of chain ends and the formation of chemical crosslinks that yield elastically effective chain density at higher levels of branching. The measured viscoelastic properties for the three coating polymers in Table-6.1 reveals a wide range of variation in T_g and elastic storage modulus E' (minimum). The significant differences in reported glass transition temperatures are assumed to be related to the individual coating polymer's composition and free-volume. The epoxy-polyamide yields the highest E' (min.) which would be directly

proportional the coating polymer's crosslink density. However, the lower glass transition temperature indicates more available free volume in which diffusion related processes to occur over a shorter time scale.

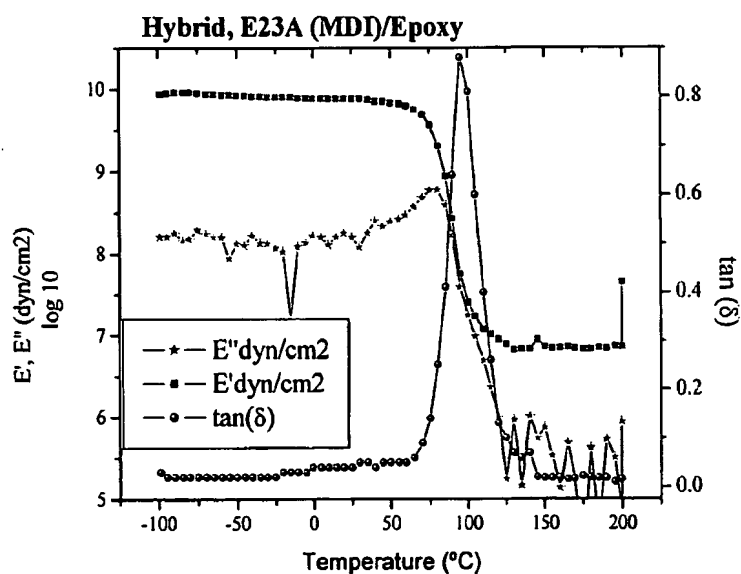


Figure 6.1: Dynamic mechanical properties of sample hybrid (MDI)/epoxy; E' , storage modulus; E'' , loss modulus; $\tan \delta = E''/E'$.

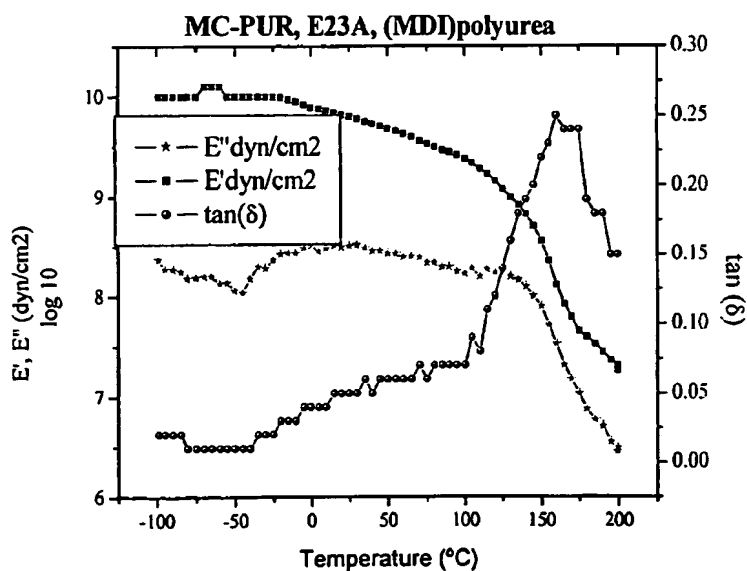


Figure 6.2: Dynamic mechanical properties of sample MC-PUR

(MDI): E' , storage modulus; E'' , loss modulus; $\tan \delta = E' / E''$.

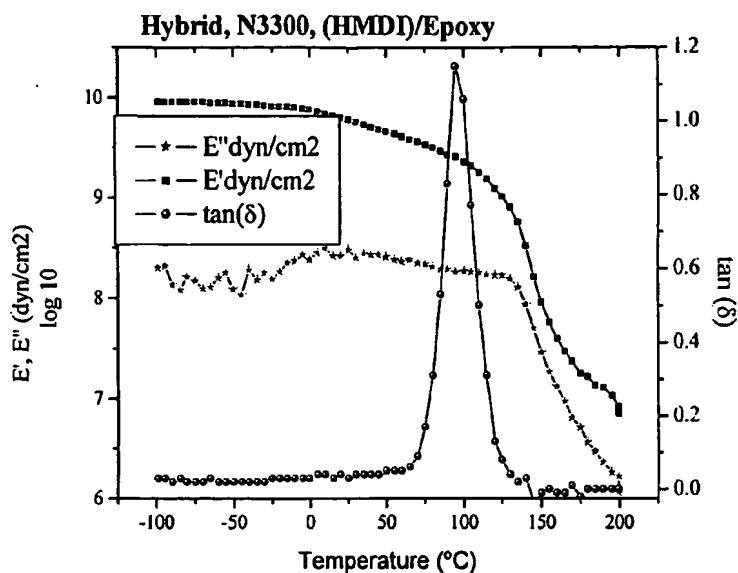


Figure 6.3: Dynamic mechanical properties of sample hybrid (HMDI)/epoxy; E' , storage modulus; E'' , loss modulus; $\tan \delta = E' / E''$.

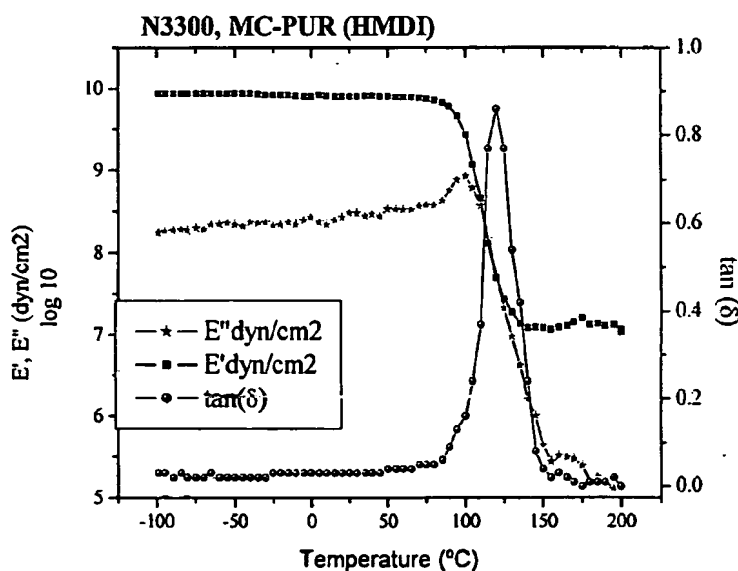


Figure 6.4: Dynamic mechanical properties of sample MC-PUR (HMDI); E' , storage modulus; E'' , loss modulus; $\tan \delta = E' / E''$.

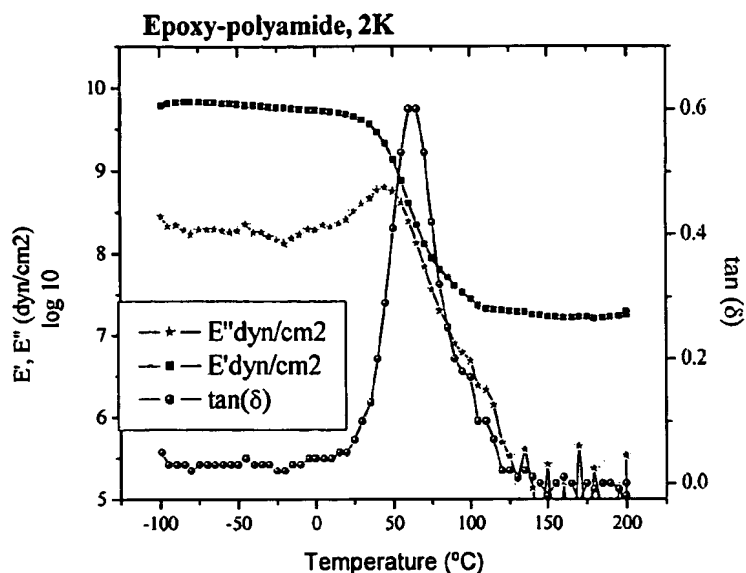


Figure 6.5: Dynamic mechanical properties of sample 2-K
Epoxy-polyamide. E' , storage modulus; E'' , loss modulus; $\tan \delta = E' / E''$.

6.5 Mechanical Properties of Polymeric films

Table 6.3, below, shows the measured tensile properties of the cured polymer films used in these coatings. Tensile tests were conducted on coating polymer film- strips with no visible voids. The mechanical properties in Table 6.3, suggest that an improvement in both hybrid systems in tensile strength and tensile modulus properties over parent materials. The tensile modulus is known to be a good measure of a film's mechanical properties, as its measurement is less defect dependent than the film's tensile strength.

Table 6.3: Mechanical properties of coating polymer films			
Polymer film	Elongation at-break (%)	Tensile strength (MPa)	Tensile modulus (MPa)
N3300 (MC-PUR)	8.0 ± 0.1	45 ± 7	1250 ± 90
E23A (MC-PUR)	5.0 ± 0.3	25 ± 6	825 ± 110
Epoxy-polyamide	18.0 ± 0.1	5 ± 0.9	150 ± 50
Hyb-N3300	6.0 ± 0.3	56 ± 9	1800 ± 50
Hyb-E23-A	5.5 ± 0.2	50 ± 5	1500 ± 50

Generally, the high tensile modulus also suggests that the material is more elastic which implies a higher degree of cure or conversion. The hybrid silane modified epoxy-urea/urethane analogs both show lower T_g s than parent materials with no significant difference in crosslink density, suggesting the presence of $(-N-R-Si-O-Si-R-N-)$ bonds throughout the IPN matrix. In addition, the higher tensile modulus and tensile strengths for both hybrid materials, over parent, suggest the formation of elastically effective IPN structure.

6.6 Pull-Off Adhesion ASTM D 4541-85

Table 6.4, below, gives the pull-off adhesion for primed coatings as a function of PVC and five week exposure in a solution of 3 % NaCl. Table 5, below, shows mechanical properties of the coatings as a function of Mg-powder PVC and pull-off adhesion as a function of exposure time in a 3 percent sodium chloride solution for a duration of 4 weeks. The pull-off adhesion is a sensitive measurement that can differentiate between coatings that developed the reversible breaking and reformation of stressed bonds between a coupling agent and the substrate without the loss of adhesion when water is present. The reverse impact results suggest coatings formulated near CPVC require a polymeric material with more elastomeric / rubbery qualities such as one formulated with an aliphatic polyisocyanate HMDI prepolymer as opposed to an aromatic MDI prepolymer.

In the conventional, high VOC coatings MC-PUR and epoxy-polyamide initial pull-off adhesion was comparable to the hybrid coatings. However, without the silane coupling agent these two coating systems failed wet adhesion in spite of the vehicle's hydrophobic nature. The reverse impact results suggest coatings formulated near CPVC require a vehicle material with a high tensile modulus.

Table 6.4: Mechanical Properties of Mg-rich Primers

Coating	PVC	MC-PUR	Epoxy-Polyamide	HyE23-A	HyN3300
Pull-off adhesion (lb _f /in. ²)					
(initial)	(43% PVC)	150	90	175	100
	(46% PVC)	200	80	150	175
	(50% PVC)	140	50	150	175
(5 week exposure 3% NaCl)					
	(43% PVC)	80	25	400	200
	(46% PVC)	30	35	300	225
	(50% PVC)	90	25	350	400
Reverse Impact (inch-lb.)					
	(43% PVC)	30	0	30	60
	(46% PVC)	30	10	10	60
	(50 %PVC)	30	20	0	60

6.7 Mechanical Property Results

Viscoelastic DMTA measurements of polymer films revealed that hybrid silane modified Epoxy- ureas displayed lower T_gs at equal crosslink densities from those of the parent materials suggesting the formation of bulk (-N-R-Si-O-Si-R-N-) bonds throughout the IPN matrix. The increase in pull-off adhesion, for the hybrid coatings, after 5-weeks exposure to 3% NaCl solution, suggests latent hydrolysis and gel formation in bulk due to unreacted silanol moieties in the 7-phenyl-1-[4-(trimethyl-silyl)-butyl]-1,2,3,4-tetra-hydro-quinoxalin-6-ol crosslinker (7-PQ-6-ol). According to Walker 1980⁵⁷³, it may be surmised that latent silanol may be drawn toward a substrate that has corroded or become anodically polarized thus enabling it to inhibit corrosion via formation of organo-functional silicate. The tensile properties of the Hyb-N3300 / epoxy were improved over that of its parent moisture cured Desmodur®N3300 film, and to the epoxy-polyamide. Overall, it is surmised that the presence of the crosslinked silanol structure in the bulk of

the polymeric material that accounts for the higher observed crosslink density in the slightly lower T_g film samples. All of which implies a polymeric materials containing domains of differening composition and therefore evidence of a pseudo interpenetrating network.

6.8 Electrochemical Impedance Spectroscopy (EIS) and Open Circuit

Potential OCP/ E(corr) Testing

AC impedance spectra of coated metals can be analyzed in terms of a simplified electrochemical circuit (EC) that predicts the corrosion mechanism occurring in potentially defective coatings.⁵⁷⁴ The associated corrosion processes, see *Figure 6.6* below, can be attributed to metals exposed to electrolytes modeled by simple equivalent circuits with the following associated parameters; R_e denotes the corrosive electrolyte solution resistance, R_{po} the resistance due to pores in the coating, R_{t1} the charge-transfer resistance in the pores, R_{i2} the interfacial resistance due to blistering at the coating-metal interface, C_c the organic coating's capacitance (not assumed to be unaffected), C_{dl} the double layer capacitance at the interface and W the impedance associated with diffusive mass transfer occurring at the interface (Warburg impedance).⁵⁷⁵ These electrochemical parameters are related directly to characteristics of the organic coating-metal system are R_{po} and C_c both related to a coating's overall protective properties for example, R_{po} is directly related to porosity, an initially high impedance modulus value, reflected in high frequency measurements, may be indicative of a non-porous coating.

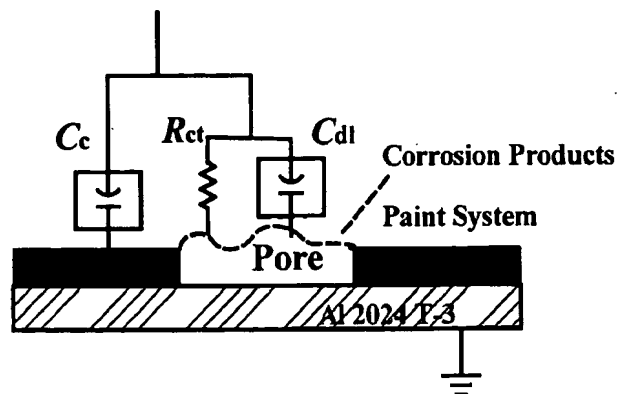


Figure 6.6, Schematic of the corrosion process occurring in coating pores that may eventually be blocked by magnesium corrosion by-products.

Whereas, R_{ct} and C_{dl} derived from low-frequency data are influenced by corrosion reactions and the byproducts generated, a gradual increase in impedance modulus over time, for a Mg or Zn-Rich coating, may be indicative of the filling of pores with hydrated metal oxides. Low-frequency impedance measurements, $Z_{1-100\text{mHz}}$ have been identified as the most reliable estimate of charge-transfer resistance due to a coating's barrier effect.⁵⁷⁶

Generally, polymer hydration has been noted as the first step in the corrosion mechanism of coated metals. Hydration with subsequent water penetration can affect a coating's measured capacitive values where the change in measured capacitance values implies the barrier properties of the coating are failing as water penetrates and swells the coating capacitance increases with increased water content.⁵⁷⁷ In general, the EIS test method is applicable for use in situations where salt spray test methods would be used to evaluate corrosion resistance of chemically passivated surfaces. These include evaluation of closely related materials, quality acceptance, evaluation of coating process control, and

coating process qualification. This test is appropriate for all coatings and oxide films produced by chemical passivation provided that intact portions of the coating exhibit a high degree of electrical resistivity. The test is applicable to all aluminum alloy substrates and nearly all product forms. The result from this test is subject to some of the same limitations as salt spray exposure test results. Results can not be extrapolated to predict performance in other environments. Results cannot be used for design purposes since the test solution may not be representative of various real world exposure conditions. Finally, EIS method permits measurement and calculation of a numerical measure of coating corrosion resistance, R_c , which has been found to correlate with probability of achieving passing result after 168 hours of exposure to ASTM B117 salt spray exposure.⁵⁷⁸

6.9 Apparatus OCP and EIS Measurements

Test Cell - The test cell contained the test solution which was composed of a (0.5 M NaCl solution using reagent grade sodium chloride and deionized water). The cell sealed the test surface in a way that did not permit leakage or crevice corrosion. The area of the sample exposed to solution for testing shall be 20 cm² at a minimum). The cell should be constructed to permit insertion of an auxiliary electrode and a reference electrode, in addition the cell should be constructed of material, such as glass or polyvinyl chloride pipe, to avoid contaminating the solution.

Generally, after filling the cell it should be checked for leaks at the cell-sample junction, solution evaporation and bubbles on the sample surface. If the cell doesn't leak then the reference electrode is inserted and the necessary electrical connections between cell electrodes and the potentiostat are made. Then check the open circuit potential to ensure the measurement circuit is closed, and finally initiate and EIS measurement.

Usually, the parameters associated with the EIS measurement can be set with the Gamry software. The most common acquisition parameters are: 1) voltage sine wave with an amplitude of 10 mV, A.C.; 2) scan from 10 kHz to 10 mHz frequency; 3) sampling at minimum rate of 5 points per decade frequency; 4) collect a minimum of 3 cycles per point.

6.10 Data Analysis

Generally, EIS spectra are suitable for analysis when they exhibit a well-defined DC limit such as in a Bode magnitude plot, and a broad minimum in a Bode Phase Angle plot. The three most generally encountered graphical representations of EIS data are presented in the form of : 1) Nyquist plot; 2) Bode magnitude plot, and 3) Bode phase angle plot.

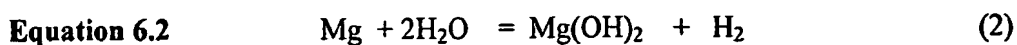
The literature on metal-rich paints as studied by EIS provides good insight into the metal-rich coatings that have not been topcoated, but are exposed directly to the immersion electrolyte.^{579, 580} Essentially, what these authors have seen is the lifetime of the reactive metal in the coatings and the transition of cathodic protection behavior when sufficient metal is present to protect the substrate, to a more barrier-like system as metal oxides formed in the originally porous metal rich primer and reduced the porosity to give a higher resistance film. The exposure time dependence of the open circuit potential (E_{corr}) was used to evaluate corrosion protection by Mg-rich coatings due to their conductive nature.

6.11 EIS of Mg-rich Primers

The mechanism⁵⁸⁰ of cathodic protection for zinc-rich primers (ZRP) was reviewed in Chapter 2.5 and based upon similarities, discussed in Chapter 3, serves as a model for

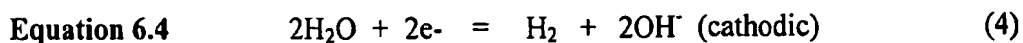
the following study. In these studies performed on Mg-rich primers formulated from the four above mentioned polymeric materials, at 43, 46, and 50% PVC. These samples were subject to EIS testing in 3% NaCl solution for up to 21 days, and the resulting $|Z|$ modulus and open circuit potential measurements were recorded. Initial observations, immediately after immersion, showed that the painted aluminum panels in electrolyte attained an (E_{corr}) of about -1.1 V, a value that lies in the mixed potential range of Mg / Al 2024 T-3 couple. The time dependence of (E_{corr}) for the different tested samples, illustrated that galvanic protection was supplied to Al 2024 T-3 substrates by the coatings that were loaded with Mg powder Figures 6.6 A-D. This is believed to be attributed to the relative permeability of the Mg-rich coatings to the electrolyte solution. These observations were consistent with those described by Abreu *et al.*⁵⁸⁰ for analogous zinc-rich primer systems tested with EIS in 3% NaCl solution.

In this experiment the duration of the cathodic protection effect was similar for all of the samples tested, but the performance of the coatings after the cathodic protection period differed according to the integrity of the primer. Sacrificial coatings, such as Zn-rich or Mg-rich primers contain high volume fractions of metal particles that act to prevent anodic areas from developing over cathodic sites. In the presence of an electrolyte, such as NaCl, both zinc and magnesium corrode in the presence of acid. The overall reaction for the corrosion of pure magnesium is given by Equ.(s) 6.2-to-6.5:⁵⁸¹

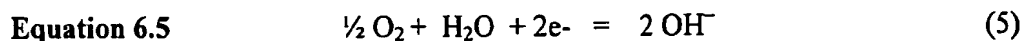


and can be written in terms of the following anodic and cathodic partial reactions:





while the dominant cathodic reduction reaction:

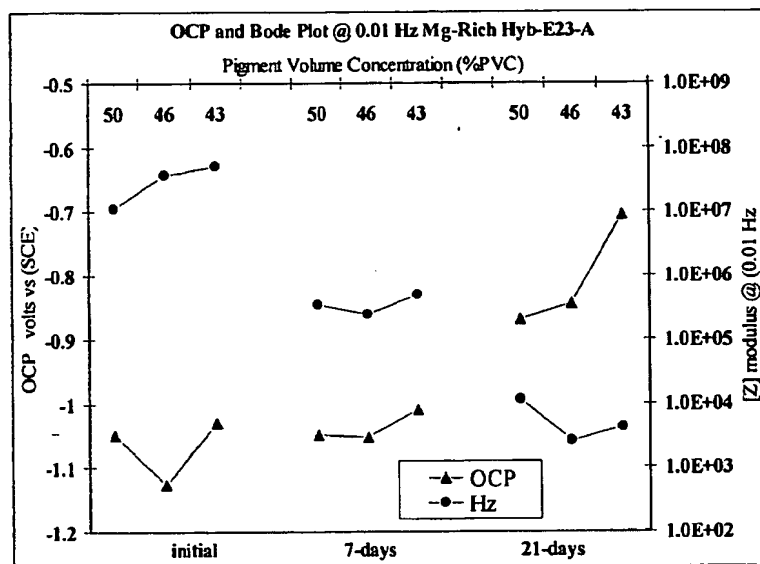


In the presence of corrosive metals, it is the interaction between water, polymer coating, and metal(s), that which is reflected in capacitance measurements, rather than just the water concentration in the polymer.^{582, 583} Figures 6.6-A-D are Bode plots, at $f = 0.01$ Hz, and open circuit potentials (OCP) obtained for topcoated Mg-Rich coatings exposed to percent NaCl solution for up to 3-weeks. Initially, the OCP values of the coating are near – 1.1 volts which is close to the mixed potential value of –1.2 volts for the galvanic couple.

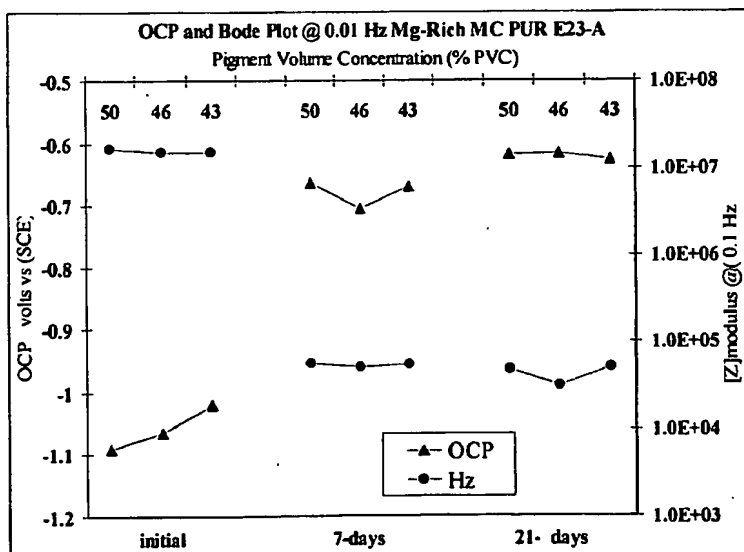
Generally, all of the unscribed coatings possess a relatively high initial $|Z|$ modulus $> 10^7 \Omega \text{ cm}^2$ signifying the presence of a barrier to water and oxygen. The general trend over the first seven days of exposure showed an increase in OCP to values slightly more anodic than the Al 2024 T-3 alloy ≈ -0.65 volts, while $|Z|$ modulus values fell dramatically modulus $10^7 \Omega \text{ cm}^2$ signifying a weak barrier effect, the consumption of Mg anode, the presence of water in the coating, and a corrosion reaction occurring between the coating and the metal substrate interface. After three weeks exposure, most of the coating OCP values reflect the open circuit potential of the Al 2024 T-3 alloy, signifying the depletion of Mg anode.

However, some of these unscribed Mg-primers coatings tested showed a latent increase in $|Z|$ modulus values possibly due to the filling of pores with oxides yielding an increase in R_{ct1} . This latent increase in capacitance was observed to occur around the 3rd week of testing where it is surmised that such a shift in impedance $|Z|$ modulus values PVC may be due to vehicle system corrosion behavior. For example, polymeric materials that

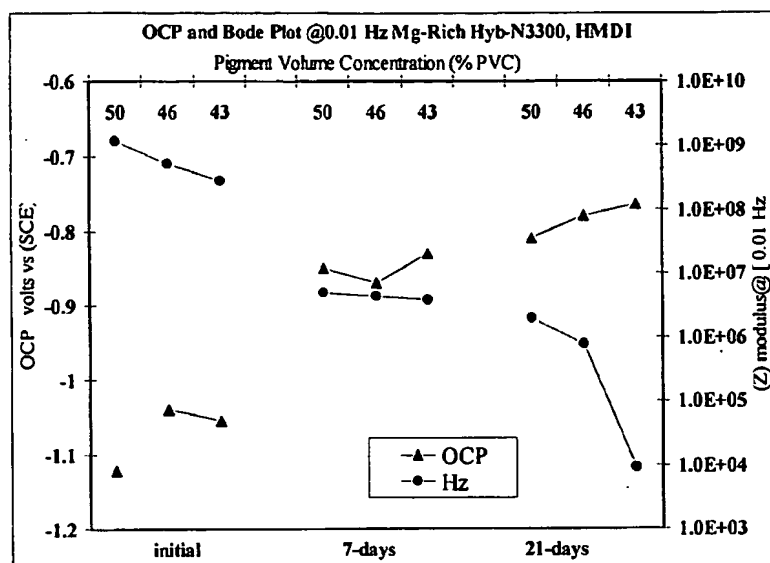
showed poor adhesion to the substrate as a function of immersion time, see Table 6.4, above, may have been susceptible to corrosion reactions, Equ.(s) 6.2 –to– 6.5, above, which deteriorated the polymeric binder material.



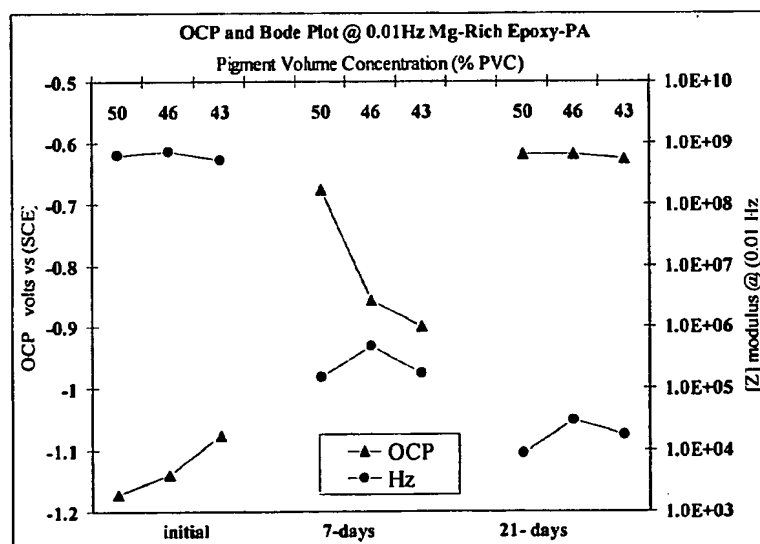
Figures 6.6-A: Mg-rich primer, E-23A, MDI silane modified Epoxy-urea hybrid.



Figures 6.6-B: Mg-rich primer, E-23A, MDI, PC-PUR.



Figures 6.6-C: Mg-rich primer, N3300, HMDI silane modified Epoxy-urea hybrid.



Figures 6.6-D: Mg-rich primer, epoxy / polyamide

Figures 6.6-A, B, C, and D: above, effect of exposure in 3% NaCl solution on open circuit / E_{corr} and low frequency impedance $|Z|$ at (0.01 Hz) for Mg-rich primers at 43, 46, and 50 % PVC for the four coating systems: A) *top*, (MDI)hybrid Desmodur®E23A/Epon1001®; B) MC-PUR *second from top*, Desmodur®E23A; C) *second from bottom*, (HMDI)hybrid Desmodur® N3300/Epon1001®; D) *bottom*, Epoxy-polyamide, Epon® 828 / Epi-Cure® 3115.

Overall, the silane modified coatings displayed higher $|Z|$ modulus values for the 50 % PVC samples, and even showed latent increase in $|Z|$ modulus values, whereas the conventional / non-silane coatings formulated at 43% -to- 50% PVC were observed to show relatively lower $|Z|$ modulus values after 21 days constant immersion.

6.12 (EIS) and E_{corr} Opencircuit Potential (OCP) Results

Irregardless of the overall performance observed in any of the above systems, from the OCP data, presented in Figures 6.6 A-D, there are three distinct periods that clearly distinguish the performance of cathodic protection in the Mg-rich coatings as a function of exposure time.⁵⁸⁴

Period I. Initial immersion day one, the “activation” period when the value of the corrosion potential shifts to a cathodic value 1.1V vs SCE, corresponding to the Mg metal / Al-2024 T-3 mixed potential in the electrolyte. Magnesium immediately begins to react with the sodium-chloride solution whereby it becomes “activated” leading to better metal-to-metal electrical contact being established between magnesium particles and Al surface.

Period II. Once initially past the “activation” period, the cathodic protection mechanism reaches its peak due to a maximum in the ratio of magnesium-to-aluminum area ratio.⁵⁷⁴ This occurs around day 1~2, see Figures 6.6 A-D, above, (*initial*) and Figure 3.1, Chapter 3, (initial 24-hour exposure) when the corrosion potential shifts to a more anodic value of about -0.9V vs SCE; it is where a relative stabilization called the “transition” period occurs.

Period III. After the transition period, and up to day 21, the corrosion potential shifts out of the cathodic protection domain, and the potential fluctuates as the film’s solution chemistry begins to change.

6.13 Electrochemical Impedance Spectroscopy (EIS) Scribed Panels

EIS studies of the Mg-rich primer at 50%PVC (above CPVC) with topcoat, under conditions of high, neutral, and low pH were performed. An EIS test method was used that involved subjecting circularly scribed Mg-rich coatings to immersion varying the pH conditions in 3% NaCl solutions. This method was utilized to help differentiate among the various primer formulations developed in this work. Subjecting the system to acid pH = 2.8, neutral and basic pH=12.0 3% NaCl immersion under scribed conditions allowed comparison of the formulations in a wide range of exposure conditions. The Mg-rich Al 2024 T-3 panels were topcoated with Deft 99 GY-001 ELT™, a very chemically resistant coating, scribed, and then subjected to continuous immersion.

Three coating systems were evaluated as Mg-rich coatings, two commercially available OTS products and one hybrid silane modified epoxy-urea developed in this laboratory. Error! Bookmark not defined.

1. Moisture cure (MC-PUR) aromatic polyisocyanate, Desmodur™ E23A, polyurea.⁵⁸⁵
2. Epoxy/polyamine consisting of Epon™ 828 with a Mannich base polyalkylamine curative Epicure™ 3251.
3. Hybrid silane modified epoxy-urea consisting of Epon 1001 and Desmodur™ N3300 aliphatic polyisocyanate, the silane was Silquest™ A-1120 (N-β-(aminoethyl)-γ-aminopropyl trimethoxysilane) see *Table 2* formulation C.
4. The topcoat was Deft GY-001 ELT fluorinated polyurethane.

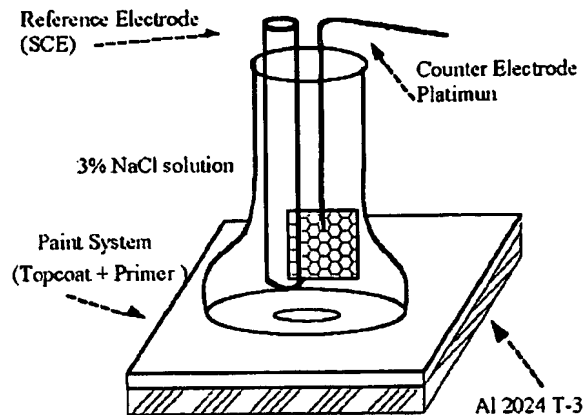


Figure 6.7 Cylindrical electrode cell for scribed EIS.

Cylindrical electrode cells, Figure 6.7, above, were mounted over samples with 1.0 cm diameter circular scribes cut through the coating exposing Al 2024 T-3 surface. Cylinders were filled with electrolytes of the following compositions: 1) basic at 3 percent weight NaCl adjusted to pH= 12.0 with NaOH; 2) acidic at 3 percent weight NaCl adjusted* to pH=2.8 with HCl; 3) near neutral at 3.0 percent weight NaCl at pH=6.2. Impedance measurements were carried out over an 11-day time period pH adjusted at each test interval.

The experimental set-up consisted of a three-electrode cell containing 40 ml of 3.0 percent weight NaCl aqueous solution, open to air, held at room temperature. A saturated calomel electrode (SCE) was used as the reference electrode and a stainless steel plate served as the counter-electrode. All measurements were performed at the open circuit potential of the system. EIS measurements were performed with a Gamry Instruments Framework™ potentiostat-galvanostat. Impedance spectra were recorded in the 1 mHz–100 kHz frequency range and Gamry 3.1 software was used to acquire and analyze the data in terms of both Bode plots.

EIS of Scribed panels

Cylindrical electrode cells were mounted over samples with 1.0 cm diameter scribes cut through the coating exposing Al 2024 T-3 surface. Cylinders were filled with electrolytes of the following compositions:

- 1) Basic at 3 percent weight NaCl adjusted* to pH~ 12.75 with NaOH
- 2) Acidic at 3 percent weight NaCl adjusted* to pH ~ 2.2 with HCl
- 3) Neutral at 3.0 percent weight NaCl at pH ~6.2

Impedance measurements were carried out using a Gamry instruments PC4/300TM electrochemical measurement system. The amplitude of the signal perturbation was 10mV (rms) with frequency sweep from 0.01Hz to 10 kHz. Measurements were made over an 11-day time period with test intervals on the 1st, 2nd, 4th, 7th, and 11th day. *(pH adjusted at each test interval).

Basic Conditions: Scribed Panels Mg-Rich & Topcoat

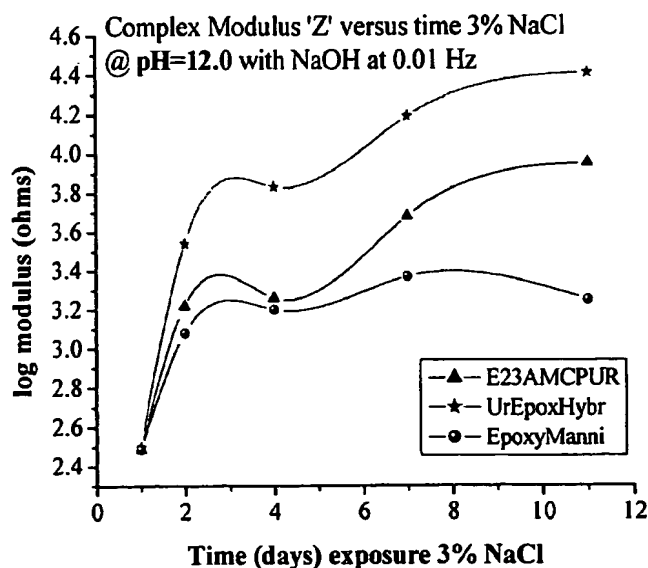


Figure 6.8-A: Complex modulus vs time (days), pH~ 12

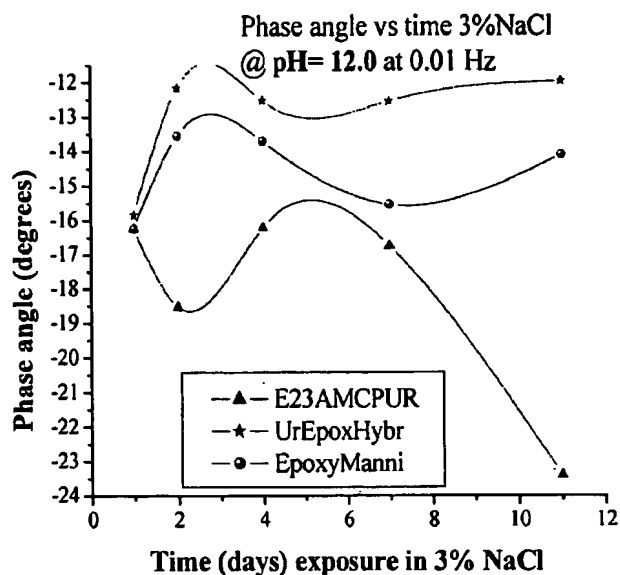


Figure 6.8-B Phase angle vs time (days), pH~ 12.

Changes (decrease) in the low frequency end of the spectrum, purely resistive, is usually indicative of electrolyte penetration and / or the formation delamination or pitting corrosion. Phase angle (decrease) indicating diminished capacitive effect due to water uptake and related charge transfer effects. The Mannich base epoxy blistered and delaminated to the same extent as it did in basic conditions. Hybrid epoxy-urea was similar to that of the sample in basic conditions best overall.

Acidic Conditions: Scribed Panels Mg-Rich & Topcoat

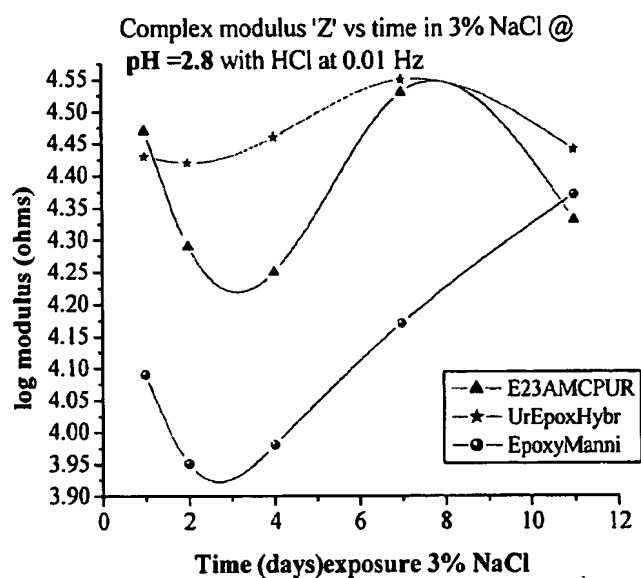


Figure 6.9-A. Complex modulus vs time (days), pH~ 2.8

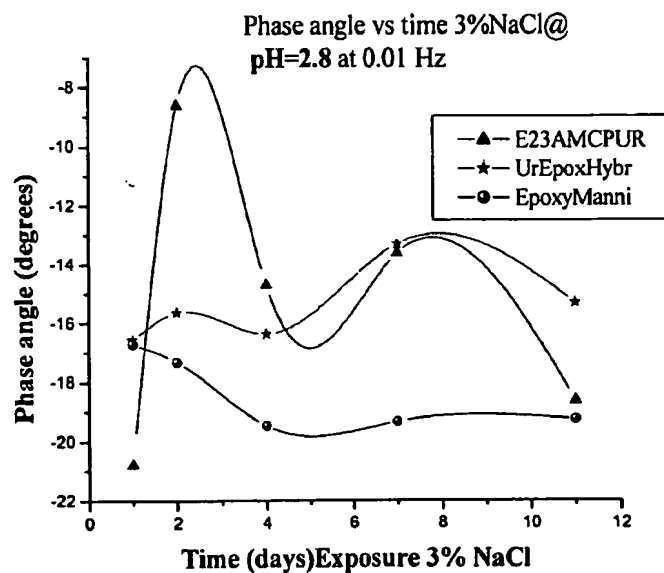


Figure 6.9-B Phase angle vs time (days), pH~ 2.8

Near Neutral Conditions: *Scribed Panels Mg-Rich & Topcoat*

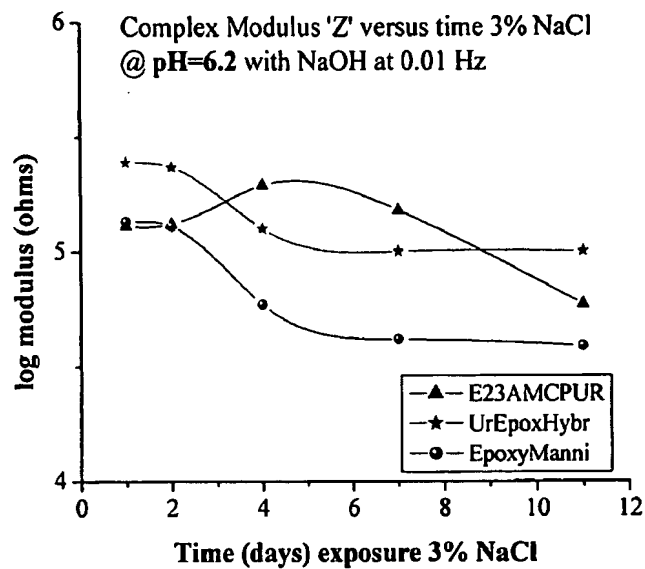


Figure 6.10-A Complex modulus vs time (days), pH~ 6.2.

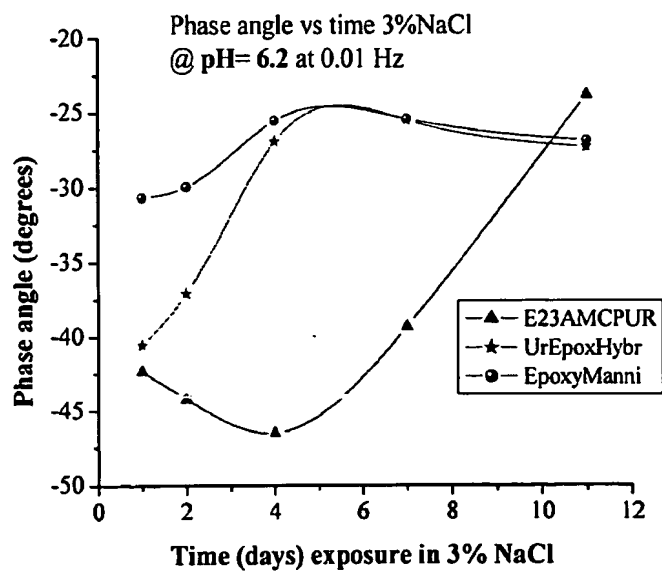


Figure 6.10-B Phase angle vs time (days), pH~ 6.2.

Near Neutral 3% NaCl solution at pH~ 6.2

At pH = 6.2, no “protective hydroxide” skin forms on magnesium surface. EIS spectra, *Figure 6.11-A*, below, data collected at 0.01Hz, show hydroxide accumulation at the surface.

Basic conditions: pH~12.75, (Al most prone to dissolve)

- A) MC-PUR (isocyanate) phase angle change: (–16 to –24) observed minute blistering about concentric.
- B) Hybrid Epoxy-urea phase angle change (–17 to –15) observed salt accumulation over topcoat.
- C) Epoxy-Mannich base, phase angle no net change, observed severe blistering and delamination.

Basic conditions: pH=12.0, (Al most prone to dissolve)



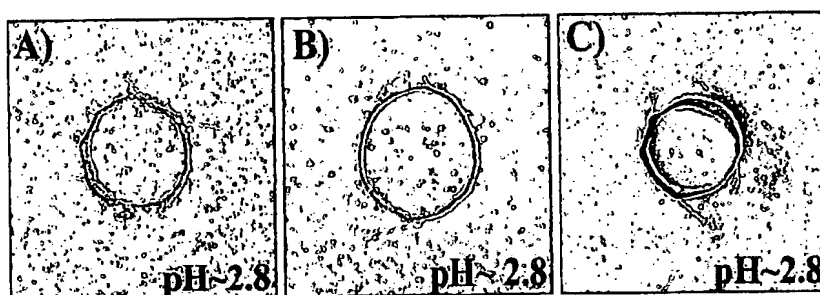
Figures 6.11: 50% PVC Mg-rich primer with ELT™ A) E23A, MC-PUR; B) Hybrid Epoxy-urea; C) Epoxy-Mannich base. Scribed samples after 11-days immersion and EIS testing at pH=12.0.

Acidic conditions: pH~2.2, (Mg most prone to dissolve)

- A) MC-PUR (polyisocyanate/ polyurea) phase angle no net change observed delamination concentric scribe ring.
- B) Hybrid Epoxy-urea phase angle changes from (–16 to –12) observed salt accumulation over topcoat.

C) Epoxy-Mannich base, phase angle change (–17 to –20) observed severe blistering and delamination (very little change).

Acidic conditions: pH=2.8, (Mg most prone to dissolve)



Figures 6.12: A) E23, AMC-PUR; B) Hybrid Epoxy-urea; C) Epoxy-Mannich base. Scribed samples after 11-days immersion and EIS testing at pH=2.8.

Neutral conditions: pH~6.2, (Al stable, Mg meta-stable)

A) MC-PUR (isocyanate) phase angle change: (– 40 to –27) no observable defects developed.

B) Hybrid Epoxy-urea phase angle change (– 40 to – 25) no observable defects developed.

C) Epoxy-Mannich base, phase angle no net change; no observable defects developed.

No observable difference between scribed areas of any of the samples after 11-days testing at pH~6.2; conditions for maximum coating/interface stability.

6.14 Results from Scribed Study

The visual results from the scribed exposure tests Figures 6.11-12, above, give indication that under conditions of both high and low pH the Mg-rich coating formulated with traditional coating polymers, i.e., MC-PUR and the epoxy/Schiff base have weakness at these pH extremes. At high pH =12 samples (A) and (C) blistered after immersion

exposure. At low pH = 2.8, immersion exposure caused the film to disbond and lift from the substrate. The amino-silane modified hybrid polymer matrix provides a much more pH resistant system in an Mg-rich coating in adhesion and reactivity than the more traditional polymers. As Zhu and van Ooij⁵⁸⁶ have noted that protonated amine ($--NH_3^+--$) from γ -APS (γ -aminopropyltriethoxysilane) in films on Al 2024 T-3 promotes the ingress of corrosive chloride ions into the film. No visible difference in scribed samples after 11-days testing suggests conditions at pH = 6.2 yield higher stability at the primer coating/interface.

A general examination of the scribed systems gave similar results, as shown in Figures 6.8 – 6.10, above. The results essentially show the low frequency impedance modulus, $|Z|_0$ vs. time as this tracks the resistance of the coating system vs. time quite well.⁵⁸⁷ Impedance data from damaged/scribed systems is notoriously difficult to interpret, as the damaged area of the coating dominates the electrochemical behavior of the system when its surface area is large. The impedance measurement in this case is averaging over the entire surface area under study.⁵⁸⁸ The low $|Z|$ modulus values seen in Figures 6.8 – 6.10 indicate conductive pathways are dominating the measurements in scribed areas. Comparison to the $|Z|_0$ data from undamaged neutral systems as shown in *Figure 16* demonstrates this further. In this case, all of the coatings are in excess of $10^6 \Omega$, some as high as $10^{10} \Omega$, while all of the scribed systems exhibit $|Z|_0$ values below $10^5 \Omega$, some as low as $\sim 150 \Omega$.

6.15 EIS of Non-Scribed Mg-rich Coatings

Generally, it is reported⁵⁸⁹ that low frequency impedance values less than 10^7 ohms/cm² result in coatings with a short service lifetime, and coatings with low frequency impedances greater than 10^7 ohms/cm² result in longer lifetimes. All of the electrochemical

data, especially that shown in Figures 6.13 A-C, below, seem to corroborate that the coating system with the Mg-rich primer based on the hybrid polymers system performed the best. Unscribed, topcoated films were also examined electrochemically to determine what is happening in undamaged coatings due to immersion in neutral 3% NaCl solution. The corrosion protection properties of primed / topcoated panels were evaluated by (EIS) and open circuit potential (OCP).

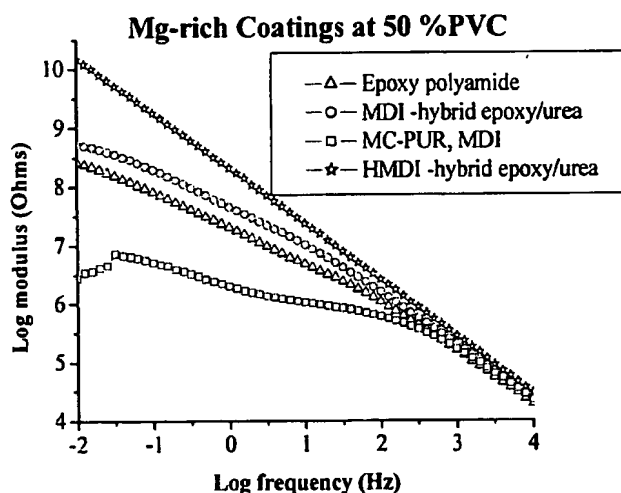


Figure 6.13 A: Bode plot of topcoated Mg-rich coatings after 3 weeks continuous immersion in 3% NaCl at 50% PVC: Epoxy / polyamide (8); Epoxy-MDI hybrid (—); MDI Polyurea MC-PUR (∇) ; Epoxy-HMDI hybrid (ψ).

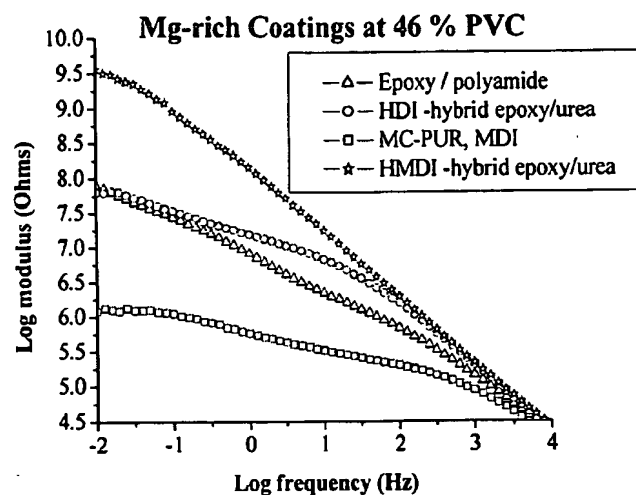


Figure 6.13 B: Bode plot of topcoated Mg-rich coatings after 3 weeks continuous immersion in 3% NaCl at 46% PVC: Epoxy / polyamide (8); Epoxy-MDI hybrid (–); MDI Polyurea MC-PUR (∇) ; Epoxy-HMDI hybrid (ψ).

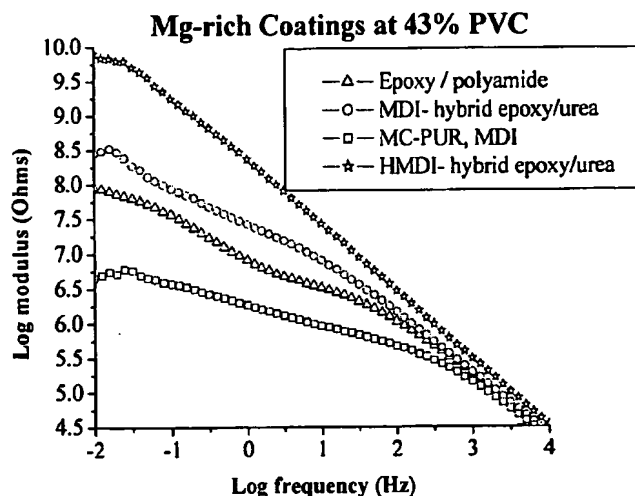


Figure 6.13 C: Bode plot of topcoated Mg-rich coatings after 3 weeks continuous immersion in 3% NaCl at 43% PVC: Epoxy / polyamide (8); Epoxy-MDI hybrid (–); MDI Polyurea MC-PUR (∇) ; Epoxy-HMDI hybrid (ψ).

The EIS data for the damaged / scribed systems in Figures 6.8 – 6.10 seem to indicate that the Mg-rich primers are providing active, cathode protection of Al 2024 T-3,

and that the mode of protection of these systems is similar to Zn-rich primers for steel. The undamaged coatings (see Figures 6.13-A-C) yield EIS data in Bode format after three weeks of 3%NaCl immersion for Mg-rich primers plus topcoat that shows no clear trend in PVC of Mg in the systems. The performance of the hybrid polymers system exceeds the other samples among the four coating systems studied and maintained the highest $|Z|_0$ throughout the study. Further, the behavior of this coating system was almost purely capacitive with only one time constant throughout this exposure, indicating an excellent coating system. However, the low frequency impedance $[Z]$ modulus in the (0.01 to 0.1Hz) range for the MC-PUR coatings is observed in the range of 10^6 ohms/cm² which is two orders of magnitude below the average for the other systems. This behavior is thought to be due to poor wetting of the primer by the ELT™ topcoat as revealed in SEM profiles, similar to those in Figures 5.14b and 5.18, previous chapter, in which numerous air channels and voids were observed to have formed at the primer/topcoat interface. Aside from this discrepancy the other coating systems displayed impedances that correspond to long lifetimes.

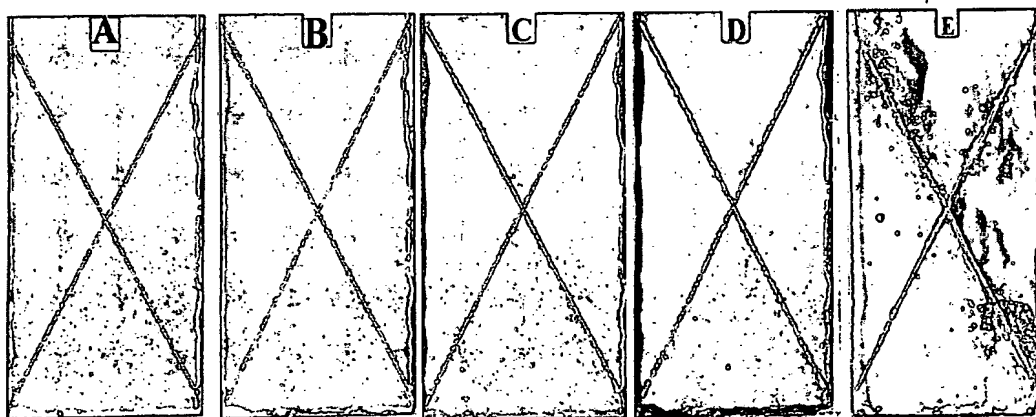
6.16 Prohesion™ Exposure Results

Prohesion™ exposure in dilute Harrison solution, (NH₄SO₄) acid rain emulation, resulted in Mg-rich coatings with conventional binders maintaining clean scribes for up to 1,000 hours, and those formulated with hybrid binders realized unattacked scribes from 3,000 to 4,800 hours exposure. The topcoat only slows diffusion and primer / metal adhesion is apparently very important.

6.17 Exposure Testing Topcoated Mg-rich Coatings

Prohesion™ exposure was performed according to ASTM test method D5894-96.

This method uses a time cycle of one hour dry air at 35°C and one hour of salt fog at 25°C. The fog solution consists of 50 grams of NaCl and 350 grams of (NH₄)₂SO₄ per 100 liters of water. Top-coated Mg-rich panels were prepared by covering panel backside and edges with 3M electroplater's tape and edges were then sealed with a 2K industrial epoxy form Aldrich. Top-coated panels were scribed through the entire coating with a carbide tip glass scribe, forming an X pattern in the aluminum, approximately 4-mils in depth, thus directly exposing the Al surface.



Figures-6.14 A, B, C, D and E: Prohesion™ (ASTM D5894-96) results for Al 2024 T-3 panels from formulation (C) Table-2, Mg-Rich primer Hybrid N3300 at 50% PVC with ELT™ topcoat at A) 0-hrs.; B) 1,200 hrs.; C) 3,000-hrs.; D) 4,800-hrs. and contrasted with E) an epoxy Epon™828 /Ancamide™ 2353 polyamide (non Mg pigmented primer) with ELT™ topcoat at 1,800-hrs.

6.18 Flammability Topcoated Mg-rich Coatings

Two classes of “fire protection / minimization” coatings have been reviewed.^{590,591,592,593,594,595,596} The first class is generally referred to as flame retardant (FR) coatings that describe coatings that delay ignition and hinder flame spread. The

second class consists of all coatings that protect the substrate by formation of an insulation layer during its combustion also referred to as intumescent coating.^{597,598,599,600} The common test method for evaluating flammability is the Limiting Oxygen Index (LOI) test (ASTM D 2863), that measures the minimum concentration of oxygen in a flowing mixture of oxygen and nitrogen that just supports flaming combustion of a sample.⁶⁰¹ According to *Equ. 6.6*, a material is normally considered as flammable if the LOI is less than 26.⁶⁰²

Equation 6.6 Limiting Oxygen Index:
$$LOI = \frac{[O_2]}{[O_2] + [N_2]} \times 100 \quad (6)$$

The thermal decomposition of polymers has been described to follow a series-parallel reaction model^{603,604} Figure 6.15 with a reversible primary, rate –limiting, decomposition first step k_p involving main-, end-, or side-chain scission of the polymer to form free-radical intermediates.⁶⁰⁵ The subsequent mass loss processes proceed through hydrogen transfer and / or recombination of intermediates leading to primary volatiles k_g (gas and tar) and char k_c1 ; k_c2 leads to secondary char formation.⁶⁰⁶ Flame retardant (FR) coatings describe coatings that delay ignition and hinder flame spread.

Theses coatings were all coated with a fluorinated ELT™ topcoat that may have contributed in some measure to the coatings non-flammability Figure 6.16 A-D. The most often reported parameter associated with coating flammability is the material's limiting oxygen index (LOI) value. Epoxy / polyamine systems, vary from a low of 24 to a high of 32 for silane modified ceramer epoxies⁶⁰⁷ while fluorinated polyurethanes are rated up to 50. Another contributing factor to improved non-flammability is the presence of the isocyanurate linkage. HMDI has been reported⁶⁰⁸ to possess an inherently higher thermal stability than that of other urethane linkages, such as MDI, as the latter is reported to

dissociate at about 200°C. In general, flammability decreases as the proportion of isocyanurate trizine ring increases.^{609, 610, 611}

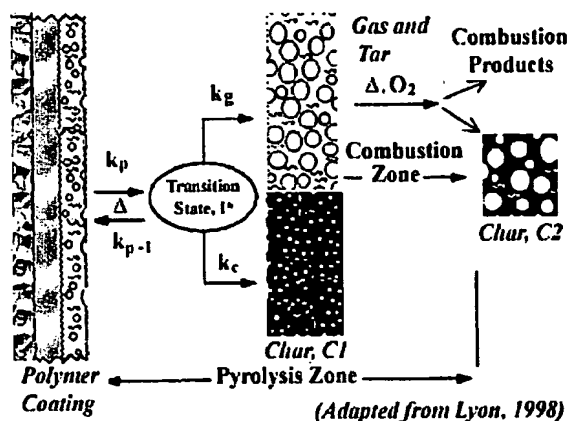


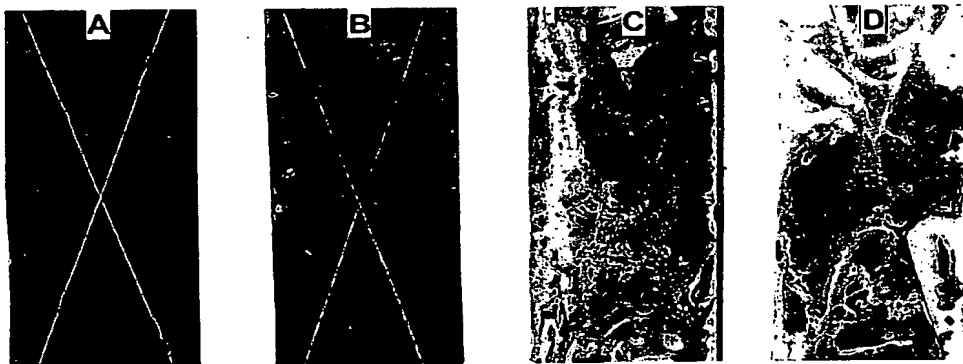
Figure 6.15, Kinetic model for polymer / coating flaming combustion adapted from Lyon 1998.⁶¹²

6.19 Flammability Testing of Mg-Rich Coatings

Six inch strips were cut from top-coated Mg-rich Al panels and subjected to a modified flammability test, referenced in document IPC-SM840B (International Printed Circuit). Also refer to test method 2.3.10.1 and the U.L.-94 flammability specification using a Bunsen burner, tube length 4", with an inside diameter (I.D.) of 0.37" with methane gas at equivalent 1000 BTU/Ft³. A propane torch with flame temperature of about 1120 °C (or 2048°F)⁶¹³ was applied for thirty seconds to the back side of the aluminum panel covered with coatings of thickness ~1.5 mils. The test was further modified by scribing an X over the face of each panel to directly expose magnesium metal in the primer to air.

6.20 Flammability Results

The results in Figures 6.14-A-D, the two hybrid and two conventional coatings can be analyzed in terms of the flammability Schematic Figure 6.15, above. The two conventional coatings, when heated, disbonded, liquefied, and incinerated with subsequent magnesium incineration; they followed the path of combustion products and char 2 ~C2. The Hybrid-E23A, MDI, did not liquefy or disbond, but formed a limited amount of char 1, C1, without incinerating the magnesium metal. Finally, the Hybrid N3300, aliphatic, evolved non-flammable gas and did not char. It may be surmised that coatings covalently bonded to the Al substrate through (-Si-O-Si-) linkages act to increase the effective LOI. The effectiveness of the aliphatic hybrid system may be due to a combination of factor such as the higher LOI of the fluorinated topcoat and the presence of the trimer N-alkylisocyanurate.⁶¹⁴



Figures-6.16 A, B, C, and D Results from modified UL-94 flammability test. From least affected 50 %PVC Hybrid epoxy/urea/urethaneN3300; B) 50 %PVC Hybrid E23A to most affected C) 50% PVC MC- PUR; D) 50% PVC Epoxy-polyamide. polyamide.

Results from each flammability test can be interpreted in terms of a relative LOI that corresponds to the parent material. For example, polymeric materials such as epoxies can vary from a low of LOI~ 24 for typical pure epoxy amine / amide systems to a high of

LOI~ 32 for silane modified ceramer epoxy.⁶¹⁵ Thus by simply modifying the epoxy system with a organo-silane, i.e., ceramer, the LOI value is shifted to above the flammability # of 26. In addition, fluorinated polyurethanes are described as relatively flame resistant and have been rated up to LOI~ 50.⁶⁰⁶ Finally, the isocyanurate linkage in HMDI has been reported⁶¹⁶ to possess an inherently higher thermal stability than that of the urethane linkage, the latter dissociates easily at about 200°C and that in general, flammability decreases as the proportion of isocyanurate triazine ring increases.^{617,618,619}

6.21 Summary

Two hybrid polymeric materials were formulated as coating matrices for Mg-rich coatings. Select mechanical and viscoelastic properties of these materials were tested and compared to similar polymeric materials used in zinc-rich coating systems. Overall, the hybrid polymeric materials possessed good mechanical properties and the results from viscoelastic testing demonstrated that the films tested showed similar T_g s, elastic modulus (E'), and elastically effective crosslink densities to their parent materials. Moreover, both hybrid polymeric materials showed marked improvements over the parent materials. In turn, these four polymeric materials were formulated into coating primers for Mg-rich coating systems on Al 2024 T-3 and tested for corrosion control. They included the two hybrid polyurea / epoxy systems, one MC-PUR and one epoxy-polyamide. These studies were conducted to determine the corrosion protection potential of select Mg-rich coating systems on Al 2024 T-3.

The primary testing methodology applied to the corrosion control investigation involved monitoring of painted panels with electrochemical impedance spectroscopy. Three different experimental situations were investigated. The first, where Mg-rich

primers formulated from the four above mentioned polymeric materials were subject to EIS testing in 3% NaCl solution for up to 21 days. Second, topcoated Mg-rich primers, formulated from 1) MC-PUR from MDI; 2) silane modified epoxy/polyurea (HMDI) hybrid; 3) epoxy-Mannich base system were topcoated with a fluorinated polyurethane topcoat Deft ELT™. Testing protocol for these coatings involved EIS over circularly scribed coatings. The third, involved EIS testing of non-scribed topcoated Mg-rich primers formulated from the four above mentioned polymeric materials in 3% NaCl solution for up to 21 days.

Results from these tests illustrate 1) cathodic coatings formulated from Mg-rich systems function and protect Al alloy 2024 T-3 analogously to those Zn-rich systems formulated for steel; 2) if the coating system, primer plus topcoat sustains localized damage, in either an acidic or basic environment, the integrity of the primer's polymeric material determines the corrosion control properties of the coating; 3) even when non-damaged, topcoated Mg-rich coatings over Al 2024 T-3 are exposed to a mild electrolyte solution, the effect of the polymeric material used in the Mg-rich coating exerts a significant effect on the extended service life and corrosion control of the coating system.

Flammability, and incineration resistance of the coating system was demonstrated by primer polymeric material selection. Those primers formulated with the silane modified coatings did not incinerate when exposed to direct flame for a significant period of time. From these studies it has been ascertained that polymeric materials that soften and melt when exposed to flame, i.e., liquefy above their T_{gs}, decompose and evolve combustible gasses were the most prone to incineration. While the coating systems whose polymeric materials did not liquefy when heated did not incinerate.

In light of these findings it can be surmised that the general effect of adding pigmentary Mg metal to a coating was that preferential dissolution of Mg metal occurred as opposed to the Al metal/ Al_2O_3 metal oxide layer, even at slightly elevated pH conditions. Thus, the coating remained cathodically protected, and in addition cathodic disbonding of the coating from the coating from the Al surface did not occur when hybrid polymeric materials were used. Moreover, the Al metal remained cathodically protected in acidic conditions for a significant period of time. Finally, in terms of devising and implementing sacrificial metal-rich coating systems comprised of pigmentary magnesium, it was shown that the multi-layer surface preparation modification technique, as demonstrated in this thesis, has shown to be a simple, environmentally acceptable, and versatile corrosion control tool for protecting structural Al 2024 T-3.

References / Bibliography

- ⁵⁶³ Klockmann, K., and Hayden, K.E., Polyurea: The slower dimension of a fast reaction, Performance Chemical Intl. Co., (2001) < www.nitroil.net/html/download/Polyurea.PDF >
- ⁵⁶⁴ Bader, M., Polyurea Systems for Casting and Adhesives, Inst. For Polyurethane Technology, by R. Milan at (2001) PDA meeting.
- ⁵⁶⁵ Baker, J. W. and Bailey, D. N., *J. Amer. Chem. Soc.*, Vol. 79, pp. 4652 (1957)
- ⁵⁶⁶ Luo, N., Wang, D-N, and Ying, S-K, *J. Appl. Polym. Sci.*, Vol. 61, pp. 367 -370 (1996)
- ⁵⁶⁷ Ni, H., Nash, H.A., Worden, J.G., Soucek, M.D., *J. Polymer Science: Part A: Polymer Chemistry*, Vol. 40, pp. 1677-1688 (2002)
- ⁵⁶⁸ Heijboer J., Modulus and Damping of Polymers in Relation to Their Structure, *Br. Polymer J.*, Vol. 1, January (1969)
- ⁵⁶⁹ Hill, L.W., *Prog. in Organic Coatings*, Vol. 31, pp. 235-243 (1997)
- ⁵⁷⁰ Ni, H., Simonsick, W.J., Jr., Skaja, A.D., Williams, J.P., Soucek, M.D., *Prog. in Organic Coatings*, Vol. 38, pp. 97-110 (2000)
- ⁵⁷¹ Roesler, R., Bayer Corp., Personal Communication, [Industrial Advisory Board (IAB) Meeting, NDSU], May (2002)
- ⁵⁷² Hale, A., Macosko C. W., and Bair, H. E., *Macromolecules*, Vol. 24 (9), pp. 2610 (1991)
- ⁵⁷³ Walker, P., "Organo Silanes As Adhesion Promoters for Organic Coatings," *Journal of Coatings Technology*, Vol. 52, No. 670, November, pp. 49-61 (1980)
- ⁵⁷⁴ Feliu S., Galvan J.C., Morcillo M., *Progress in Organic Coatings*, Vol. 17, pp. 143 - 153, (1989)
- ⁵⁷⁵ Kern, P., Baner, A. L., Lange, J., , *Journal of Coatings Technology*, Vol. 71, No. 899, pp. 67 - 74 (1999)
- ⁵⁷⁶ Bautista A., Gonzalez, J.A., Otero E., Morcillo, M., *Journal of Coatings Technology*, Vol. 71, No. 893, pp. 61 - 68 , (1999)
- ⁵⁷⁷ Kouloumbi, N., Tsangaris, G.M., and Kyvelidis, S.T., *Journal of Coatings Technology*, Vol. 66, No. 839, pp.83 - 88, Dec. (1999)

- ⁵⁷⁸ Buchheit, R.G., Cunningham, M., Jensen, H., Kendig, M.W., and Martinez, M.A. , Corrosion, Vol. 54, pp. 61 (1998)
- ⁵⁷⁹ Vilche, J.R., Bucharsky, E.C., Guidice, C.A., *Corr. Sci.*, Vol. 44 , pp. 1287-1309 (2002)
- ⁵⁸⁰ Abreu, C. M, Izquierdo, M., Keddah, M., Nóvoa, X. R. and Takenouti, H., *Electrochim. Acta*, Vol. 41, pp. 2405 (1996)
- ⁵⁸¹ Song, G., Atrens, A, StJohn, D., Nairin J., Li, Y., Corrosion Science, Vol. 39, No. 5, pp. 855-875, (1997)
- ⁵⁸² Leidheiser, H. Jr, *Corrosion Control by Coatings*, Science Press, Princeton, NJ, (1979)
- ⁵⁸³ Giminez , P., Petit, D., and Badia, M., Water Uptake of Polymer Coatings: New Investigation of Early Stages by the Electrochemical Impedance Methods, from Electrochemical Methods in Corrosion Research, Materials Science Forum , 8, 315, (1986)
- ⁵⁸⁴ Ellingson, L., "Corrosion Studies for the Protection of Aluminum Alloys and Outdoor Bronze," Masters Thesis, North Dakota State University, June (2001)
- ⁵⁸⁵ Schwindt, J., Moisture-Cured, Polyurethane-Based Surface Tolerant Coatings: An Economical Alternative for Corrosion Control, Leverkusen, Germany, Bayer Co., Formulation # 294-35 (2001)
- ⁵⁸⁶ Zhu, V., and van Ooij, W.J., *J. Adhesion Sci. Tech.*, Vol. 19 (2002) 1235-1260
- ⁵⁸⁷ Bierwagen, G.P., Tallman, D. E., Li, J., and He, L., *Prog. Organic Coatings*, Vol. 46, pp. 148-157 (2003)
- ⁵⁸⁸ Phillipe, L.V.S., Walter, G. and Lyon, S.B, *J. Electrochem. Soc*, Vol. 150, (2003) in press
- ⁵⁸⁹ Bierwagen, G.P., Jeffcoat, C.S., Li, J., Balbyshev, S., Tallman, D.E., and Mills, D.J., *Prog. Organic Coatings*, Vol. 29, pp. 21-20 (1996)
- ⁵⁹⁰ Cagliostro, D. E., Riccitiello, S. R., Clark, K. J. and Shimizu, A. B., *J. Fire & Flammability*, Vol. 6, pp. 205 (1975)
- ⁵⁹¹ Lyons, J.W., The Chemistry and Uses of Fire Retardants, Wiley/Interscience, New York, (1970)
- ⁵⁹² Anderson, C. E. and Wauters, D. K., *Int. J. Eng. Sci.*, Vol. 22, pp.881 (1984)
- ⁵⁹³ Mamleev, V. Sh., and Gibov, K. M., *J. Appl. Polym.Sci.*, Vol. 66, pp. 319 (1997)
- ⁵⁹⁴ Gibov, K. M. and Mamleev, V. Sh., *J. Appl. Polym. Sci.*, Vol. 66, pp. 329 (1997)

- ⁵⁹⁵ Buckmaster, J., Anderson, C. E., and Nachman, A., *Int. J. Eng. Sci.*, Vol. 24, pp. 263 (1986)
- ⁵⁹⁶ Anderson, C. E., Dziuk, J. J., Mallow, W.A., and Buckmaster, J., *J. Fire Sci.*, Vol. 3, pp. 161 (1985)
- ⁵⁹⁷ G. Camino, L. Costa, Mechanism of Intumescence in Fire Retardant Polymers, *Rev. Inorg. Chem.* 8, pp. 69–100 (1986)
- ⁵⁹⁸ Camino, G., Costa, L., Martinasso, G., Intumescent Fire Retardant Systems, *Polym. Degrad. Stab.* 23, pp. 359–376 (1989)
- ⁵⁹⁹ Troitzsch, H.J., Flame Retardants, in Polymer Additives, ed. Gächter and Müller 3rd Ed. Hanser Publishers pp. 712–730 (1990)
- ⁶⁰⁰ Green, J., Flame-retardants and smoke suppressants in Thermoplastic Polymer Additives – Theory and Practice, ed. John T. Lutz Marcel Dekker (1989)
- ⁶⁰¹ Tewarson, A., and Pion, R. F., *Combust. Flame*, 26 pp. 85–103 (1976)
- ⁶⁰² Tewarson, A., and Pion, R. F., *Combust. Flame*, Vol. 26, pp. 85–103 (1976)
- ⁶⁰³ Brodio, A. and Nelson, M.A., *Combustion and Flame*, Vol. 24, pp. 263 (1975)
- ⁶⁰⁴ Wichman, I.S., and Melaan, M., In Advances in Thermochemical Biomass Conversion, ed. T. Bridgewater. Chapman and Hall, London (1993)
- ⁶⁰⁵ Suuberg, E.M., Milosavljevic, I., and Vahur, O., Proc. 26th Symposium (*International*) on Combustion, The Combustion Institute, pp. 1515 (1996)
- ⁶⁰⁶ Van Krevelen, D.W., *Polymer*, Vol. 16, pp. 615–620 (1975)
- ⁶⁰⁷ Chiang, C-L., Wang, F-Y., Ma, C-C., M., and Chang, H-R., *Polym. Degrad. Stab.*, Vol. 77 pp. 273–278 (2002)
- ⁶⁰⁸ Reymore HE, Lockwood RJ, Ulrich H., *J. Cell. Plast.*, Vol. 14, pp. 332 (1979)
- ⁶⁰⁹ Dick C, Dominguez-Rosado E, Eling B, Liggat JJ, Lindsay CI, Martin SC, *Polymer*, Vol. 42 pp. 913–23 (2001)
- ⁶¹⁰ Fabris, H.J., “Thermal and oxidative stability of urethanes,” *Advances in Urethane Science and Technology*, Vol. 4, pp. 891–911 (1976)
- ⁶¹¹ Singh, LW, and Mollica, J.C., *Rubber Age*, Vol. 98, pp. 12 (1966)

- ⁶¹² Lyon, R.E., *Polymer Degredation and Stability*, Vol. 61, pp. 201-210 (1998)
- ⁶¹³ Bhargava, A., and Griffin, G.J., *J. Fire Sciences*, Vol. 17, May/June, pp. 188-208 (1999)
- ⁶¹⁴ Levchek, L.V., Levcheck, G.F., Balabanovich, I.A., Gambino, G., and Coasta, L., *Polym. Degr. and Stab.*, Vol. 54, pp. 217-222 (1996)
- ⁶¹⁵ Chiang, C-L., Wang, F-Y., Ma, C-C., M., and Chang, H-R., *Polym. Degrad. Stab.*, Vol. 77, pp. 273-278 (2002)
- ⁶¹⁶ Reymore HE, Lockwood RJ, Ulrich H., *J. Cell. Plast.*, Vol. 14, pp. 332 (1979)
- ⁶¹⁷ Dick C, Dominguez-Rosado E, Eling B, Liggat JJ, Lindsay CI, Martin SC, *Polymer*, Vol. 42 pp. 913-23 (2001)
- ⁶¹⁸ Fabris, H.J., Thermal and oxidative stability of urethanes. *Advances in Urethane Science and Technology*, Vol. 4, pp. 891-911, (1976)
- ⁶¹⁹ Singh, LW, and Mollica, J.C., *Rubber Age*, Vol. 98, pp.12 (1966)

Chapter 7 Summary

7.1 Summary of the Research Problem and Procedure Results

Currently, coating systems for corrosion control of aluminum alloys are evaluated by ease of processing and application, efficiency, performance, price, reproducibility, safety, stability, service life, and toxicity. The effectiveness of these organic coating depends primarily on the interfacial adhesion strength between the metal and polymer. Thus far the state of the art coatings for corrosion control of Al 2024 T-3 aluminum alloy are based upon a chromate-conversion coating system. Starting from the beginning the whole process must be simple and easy to apply. For example, the quickest easiest application method has been spray application of an organic primer (epoxy), followed by the final (polyurethane) topcoat, consisting of the highly pigmented chromate corrosion inhibitor.

The alternative approach to the chromate process has been presented in this thesis by the incorporation of pigmentary Mg particles into a coating where it was shown that they act as a sacrificial anode / inhibitory pigment. A problem associated with developing coatings containing pigmentary magnesium is that magnesium metal is a thermodynamically reactive metal, even more so than aluminum, which on one hand, makes it a suitable sacrificial anode for Al alloys, but on the other hand, being more active than aluminum has caused it to be viewed with a great deal of skepticism when considered for use in an engineering applications. The problem thus perceived has been that in a galvanic couple between Mg and another more cathodic metal, the resulting caustic corrosion byproducts generated in the process would lead to the rapid disintegration /

deterioration of a coatings polymeric binder material; thus accelerating coating failure. In addition, it has been asserted that the potential difference developed in a galvanic couple between Mg and Al, would not be sufficient to provide cathodic protection. However, what was observed in these studies is that in a galvanic couple Mg is about (-1 volt) more anodic than the Al 2024 T-3 alloy and that cathodic coatings could be designed and formulated according to methodologies used in zinc-rich coating systems for steel. The basic principles of Mg-rich coating formulation are as follows:

1. The coating's matrix consists of a polymeric material
2. It is pigmented with a surface treated particulate Mg, in either spherical or flake form.
3. The PVC of the Mg pigment in the coating should be near the CPVC in order for the coating to properly provide sacrificial / cathodic protection to the underlying steel substrate. Under these conditions, the Mg particles are all in mutual contact as well as in electrical contact with the steel substrate.
4. The mode of protection by these coatings is sacrificial as long as the Mg is electrically connected to the Al alloy as the Mg is more anodic (reactive) than Al or Cu (major constituents of Al 2024 T-3) in the electrochemical series, and then the mixed Mg oxides formed in the sacrificial oxidation fill damaged areas and tend to slow transport in the film.
5. The organic or inorganic matrix of the coating must be stable under the basic environment created by the magnesium oxide, hydroxide, etc., formed from the oxidation of Mg in the presence of electrolyte. It must also adhere well to the Aluminum alloy and be stable in a corroding environment.
6. These primer coatings must be top-coated to function properly and have a long field lifetime. When used properly, these primers provide better protection to Al 2024 T-3 than

chromating with a fraction of the labor. With a topcoat, they provide both barrier and damage (sacrificial / cathodic) protection to Al alloy substrates.

Previous studies have show that both polyamine/polyamide and fatty acid polyamide cured epoxy lacquers used as vehicles for Mg-rich primers were susceptible to acid degradation, and that epoxy resins cured with amine-quinone curatives greatly increased acid resistance of the polymer matrix.

7.2 The Model

The research procedure in this thesis consisted of constructing a model for the Mg-rich coating system based upon information derived from previous studies on actual precursor Mg-rich coating systems and comparing them to analogous systems discussed in the literature reviewed sections, and then applying to experimental formulation and evaluation techniques. The coating system was designed starting at the Al substrate and working up to the final topcoat. The following topics were reviewed and integrated into the design of this system:

1) Factors affecting coating systems for corrosion control of metals starting with a total system application approach; see literature review Chapter 2.1. The purpose of this section was to review the basic principles of coating systems used in corrosion control and the underlying mechanisms associated with each.

2) The relationship between metal surface energetics and polymeric coatings; see literature review Chapter 2.2. The purpose of this section was to establish the status of the substrate and the necessary conditions required to promote improved film formation.

3) Surface treatments of Al metals and improving surface bonding at the adherend-adhesive interface, the adherend surface can be enhanced by some method of pretreatment

prior to adhesive bonding via chemical modification; see literature review Chapter 2.3. The purpose of this section was to define the nature and extent of treatment required to prepare an Al alloy surface for improved adhesion.

4) Silanes used to enhance adhesion of polymers are known as coupling agents. Organosilane coupling agents function by forming covalent bonds between an inorganic metal oxide and an organic molecule / polymer through an intermediate organo-silicate (Al–O–Si–C-) bond; see literature review Chapter 2.4. The purpose of this section was to illustrate the application of organo-silane coupling agents and the chemistry of silicate formation.

5) An overview of the mechanistic aspects of zinc rich coatings (ZRC) and the generic description of the electrochemical processes involved in a zinc-rich / active metal cathodic protect anti-corrosive coating systems designed to protect a steel substrate; see literature review Chapter 2.5. The purpose of this section was to identify the key features of an analogous cathodic corrosion system for metals, zinc-rich, and illustrate the accepted protection mechanism and measurement techniques used to classify it.

6) An overview of pigmented coating systems that can be represented as a mass of particles consolidated to various degrees in a given polymeric vehicle. Where the focus was on pigmentation in metal-rich coatings systems, such as the popular zinc-rich systems; see literature review Chapter 2.6. The purpose of this section was to illustrate the volume relationships involved with pigmented coating systems and how they can be used to establish parameters that lead to optimization of the metal rich coating system's corrosion control potential.

7) The corrosion behavior of magnesium metal and magnesium alloys; see literature review Chapter 2.7. The purpose of this section was to illustrate the electrochemical behavior of magnesium metal and relate its physio-chemical properties to a cathodic coating system involving aluminum alloys, and justify the utility of pigmentary magnesium for use as a sacrificial anode in active metal coatings.

8) Design and synthesis of a novel polymeric material crosslinker derived from benzoquinone and quinonoidal substitution reactions; see literature review Chapter 2.8. The purpose of this section was to illustrate the specific chemical reaction mechanisms applicable to the synthesis of oligomeric amino-quinone and amino-quinonoidal compounds, and to reveal the pertinent features of quinone / hydroquinone red-ox equilibria as applied to Fe metal. In addition, the general features of TCCA as an oxidizer were reviewed.

9) “Hybrid” polymeric systems starting from the parent polymeric systems and proceeding to hybrid systems see literature review Chapter 2.9. The purpose of this section was to illustrate the chemical nature of the epoxy-amine and polyisocyanate polymeric materials and discuss underlying features that contribute to their effective use in coating systems. In addition, so called “hybrid” polymeric coatings from these materials were defined and reviewed in terms of structure and reactivity.

10) Flame retardance in polymeric coatings, arresting the incineration of magnesium rich coatings; see literature review Chapter 2.10. The purpose of this section was to illustrate the definition of fire retardant coatings and review the generic model and mechanism of coating combustion and pyrolysis of Mg metal. This section provides

rational for the combustion behavior of polymeric materials and its application to established testing protocol.

7.2 Summary of Findings the Data Interpretation; Hypothesis Verification

The impetus for this research was to deliver a simple but effective coating system for cathodic protection of aluminum alloy structures comprised of environmentally acceptable components. The overall objective of these foregoing studies has been to examine magnesium pigmentation as a potential raw material for use in anticorrosive metal-rich primers for aerospace aluminum alloys and determine the underlying relationships between primer polymer material, Mg powder pigmentation PVC, and the corrosion by-products formed. It also established how and if the use of Mg may detrimentally affect the aluminum alloy during service.

These studies produced a more extensive knowledge base founded on materials testing, formulation techniques for coatings formulated with magnesium powders for cathodic protection of aluminum alloys. The most important aspect of this work is that proceeds from it can be compared and contrasted to coatings that both parallel and differ from existing zinc-rich coating systems, which have been used extensively to provide cathodic protection of steel structures. In summary, while the full optimization of Mg-rich technology for corrosion control is yet to be realized, a wide range of possibilities and variations in coating polymer components exist, making this a most interesting and valuable raw material for use in achieving corrosion control with environmentally benign coating systems.

Based upon the underlying principles that apply to protecting steel with zinc-rich coatings it has been shown that aluminum alloys can be protected in an analogous manner

by using a magnesium-rich coating system. Investigations proceeding from this thesis into the chemistry, physics and metallurgy of Mg-rich systems have shown that the Zinc-rich model is valid for Mg-rich systems as well. The polymeric binder matrices traditionally used in zinc-rich system have been found to be somewhat weak, because the magnesium hydroxides form more basic conditions than the corresponding Zn hydroxides.

Surface Preparation / Organo-Silane Modification

Due to the fact that the energetics of passive oxide formation are favorable at the metal / γ -alumina interface and that the energetics at the β -Al(OH)₃ bayerite / γ -AlOOH(s) boehmite interface allow for hydration and dissolution of the native oxide layer, the focus of a surface preparation technique was on promoting a reaction with organo-silanes that yielded a more stable hydrophobic organo-silicate that aided in preserving the Al 2024 T-3 passive metal oxide matrix. The preparation of the Al 2024 T-3 surface for deposition of Mg-rich coatings for corrosion control was performed by preparing a high-energy surface obtained by means of treatment with amino-silane where upon subsequently a dilute solution of low molecular weight polyisocyanate containing reactive or crosslinkable functional groups that can be crosslinked to a bulk layer was applied. The feature of this surface enhancement technique was that it appeared to promote enhanced interactions, such as those between acid-base interactions of surface and polymer. In this case such acid base interaction are surmised to occur as a result of a hydrophobic polymeric material associated with the monophenolate ion at the Al metal oxide surface. This surface preparation modification technique appears to be valid and serves as a corrosion control utility tool when applied directly to the surface of the Al 2024 T- for the purpose of arresting the

ingression and migration of both Cu^{2+} and Cl^- , which have been implicated in the destruction of the $\text{Al}_2\text{O}_3/\text{Al}(\text{OH})_3$ protective oxide layer.

Analogous Metal-rich System

It was determined that a similar testing protocol, such as that applied to conventional Zn-rich systems, was effective at examining similar aspects of Mg-rich coatings formulated for corrosion control of Al alloy. The preponderance of the galvanic couple between the two metals was examined, via EIS and OCP techniques, and found to yield a significant mixed potential difference between that of the Al-2024-T-3 and the magnesium metal to validate such an assumption, i.e., that the cathodic protect mechanism was indeed valid. For example, in zinc-rich systems a potential difference of about (- 1.0 volt) vs SCE, is required in order to promote an effective cathodic current between the anode and cathode. What was observed in these Mg-rich systems was that they developed a potential difference, OCP, of the same magnitude. Secondly, the corrosion of magnesium metal was found to be similar to that of zinc metal used in zinc-rich systems. In addition, it was also observed that the magnesium hydroxide corrosion byproducts, like zinc hydroxides, produced as a result of exposure to sodium chloride solution, the hydroxides serve to influence the electron transfer processes, by neutralization of acid moieties, in the coating as it fills with corrosion byproducts. Finally, it was also determined by such electrochemical measurement processes that corrosion byproducts, contributed by corrosion of pigmentary magnesium anode were excessively corrosive, in some cases, and influenced the stability of the polymeric materials used in the coating matrix.

Pigment Volume Relationship

Pigment volume concentrations (PVCs) are important due to their ability to predict and relate corrosion related phenomenon such as blistering, rusting, and permeability to actual coating formulation. Volume relationships are much more convenient to use as in any pigmented coating system they can be normalized in terms of the PVC/CPVC ratio (Λ). Such an index allows one to compare metal-rich systems formulated from zinc or magnesium on a common scale, and classify/ascribe such corrosion related phenomenon to a measured number that can be associated with a similar relative error distribution.

Magnesium Metal

Mg metal is attractive from the point of view that: 1) the Mg metal itself constitutes an effective sacrificial anode when coupled to Al, and 2) the general corrosion byproduct $\text{Mg}(\text{OH})_2$ also may serve as a corrosion inhibitor (such as used in steel systems) and is available in several commercial grades such as, MHT 60 S Magnesium Hydroxide Premium Grade and MHT 100 Magnesium Hydroxide Technical Grade Powder Dow Chemicals, which are sold as filler additives used in coatings for corrosion control, as $\text{Mg}(\text{OH})_2$ is noted for its effectiveness at neutralizing acids and acts as a buffer system in the coating.

Oxidation of phenylhydroquinone

A class of reactive materials *N*-chloroamines, such as cyanuric acid, was described as the parent material for the synthesis of trichloroisocyanuric acid, TCCA. TCCA has been described as an inexpensive, mild but efficient oxidant, and in the context of this

thesis has been selected as the preferred oxidant for the oxidation of 2-phenyl-hydroquinone to 2-phenyl-1,4-benzoquinone.

Hybrid Polymeric Materials

Hybrid polymeric systems derived from polyisocyanates and hydroxyl containing materials have been characterized as systems that usually involve an elastomeric polyisocyanate and labile hydroxyls from diglycidyl ethers of bisphenol-A. At this point, there has been no autocatalysis mechanism ascribed to facilitating these reactions; however, these reactions are believed to be promoted by the presence of PU elastomer. What remains to be determined is the influence of each of these mechanisms on the cure of “hybrid” polymeric systems comprised of two or more of these functional groups and whether the “hybrid” system can achieve near or full conversion as compared to that of either of the parent materials. In the case of this study it was determined that silane modified hybrid epoxy-polyurea materials achieved mechanical properties equal to or surpassing the parent materials. However, results from mechanical testing i.e., T_g , crosslink density, elastic modulus do not indicate that hybrid polymeric materials based on the more elastomeric polyisocyanate HMDI cured to any greater extent than those derived from MDI.

Pyrophoric Magnesium

The most significant aspect of the following review is that it demonstrates the pyrolytic nature of both polymeric materials and magnesium metal. Most important is the fact that by virtue of its charge density Mg metal does not form highly combustible metal peroxides upon heating in oxygen which implies that combustion control of this metal can be achieved by means other than those associated with cooling of the solid by conduction,

convection, and radiation. Another important aspect of the following review is that it demonstrates essential principles involved with the development of flame retardant polymeric materials used in coatings for two general classes of polymeric materials: 1) polymers synthesized via chain reaction or step-growth and 2) polymeric materials via sol-gel or ceramer modified hybrids.

Conclusions Summary and Findings

As a result of this study it can be concluded:

1. The (Mg-rich primers + Extended Life Topcoat) coatings systems are the first non-chromated coatings systems to satisfy 3,000 hours of such exposure and remain shiny and undamaged in the scribe area, only showing damage at about 4800 hours.
2. The degradation of Mg-rich coatings in simulated acid-rain atmospheres was found to be controlled by the nature of the salts formed and was found not to be deleterious to the Al substrate. As a result of this finding it may be concluded that coating systems pigmented with magnesium and applied to aluminum alloy can protect the Al metal without causing subsequent high pH corrosion.
3. A novel, room temperature cure, polymer matrix was synthesized by first reacting an amino-functional silane with an α,β unsaturated phenyl quinone. The silane modified quinoxalinol serves as the effective intermediate which can be incorporated into both the epoxy and urethane portions of the polymer's organic matrix.
4. Incorporation of a silane modified organic-inorganic IPN with multi-functional crosslink potential yields an acceptable polymer material system adding many desired properties including burn-flame resistance, adhesion, mechanical properties, total system performance, and durability.

This study has shown that these pigmentary Mg systems provide sacrificial cathodic protection of Al aerospace alloys in a mode analogous to that of zinc-rich systems. It was also found that coatings formulated with conventional binders and conventional HAP solvents performed poorly in contrast with the hybrid silane modified epoxy-urea IPNs derived from non-HAP solvent systems. Thus it is crucial that this new paradigm for corrosion protection of Al by Mg-rich pigmentation be obtained in a coating polymer system that provides proper film properties for use as an aerospace primer coating.

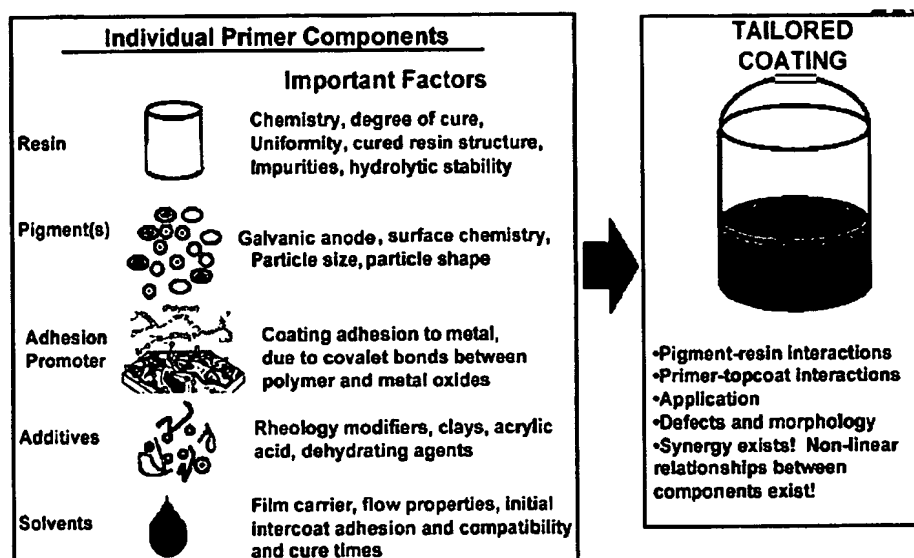


Figure 7.1, Individual paint components of the Mg-rich primer system
Synergy exists, non-linear relationships among components.

Another objective of this study was to develop a polymeric material suitable for use in active-metal rich systems. The primary focus was on developing a “hybrid” system involving a moisture cure polyisocyanate / polyurea (MC-PUR). The problem encountered in developing most “hybrid” polymeric systems, derived from polyisocyanate- polyureas, has been overcoming the retardation of the polyurea “autocatalysis” mechanism that is

responsible for driving the polymerization reaction to completion, thus yielding a higher molecular weight polymeric material.

It has been well documented that the best deterrent to adhesion failure in organic coatings lies in developing the right chemical interactions between the coating polymer, pigment, coating layers, and their metallic substrates. The most effective strategy, thus far, has been to develop coatings whose polymer matrix hydrophilicity decreases during cure as the polymer matrix coating undergoes film formation and solidifies. Organo-functional silanes are commonly used as coupling agents and adhesion promoters in epoxide and urethane paints to improve their initial, wet, and recovery adhesion to aluminum surfaces.

Mechanical Property Results

The mechanical properties of the “hybrid coatings” were equal to or better than the conventional coating systems. Starting with pull-off adhesion, results show that after 4-weeks exposure to 3% NaCl solution the hybrid coating systems were better. The tensile properties of the Hyb-N3300 and Hyb-E23A were both superior to their parent moisture cure Desmodure® N3300 and E-23A films in addition to the epoxy-polyamide coating. These results suggest an improved hybrid silane modified poly(ureoxy) binder to be a more suitable vehicle for active metal filled primers. Viscoelastic DMTA measurements show the Hyb-N3300 and E-23A both possess higher (E') elastic modulus while retaining a moderate T_g , thus supporting the formation of elastically effective crosslink networks with good chemical resistance and modulus.

Corrosion Resistance

Results from these tests illustrate; 1) cathodic coatings formulated from Mg-rich systems function and protect Al alloy 2024 T-3 analogously to those Zn-rich systems formulated for steel; 2) if the coating system, primer plus topcoat sustains localized damage, in either an acidic or basic environment, the integrity of the primer's polymeric material determines the corrosion control properties of the coating; 3) even when non-damaged, topcoated Mg-rich coatings over Al 2024 T-3 are exposed to a mild electrolyte solution, the effect of the polymeric material used in the Mg-rich coating exerts a significant effect on the extended service life and corrosion control of the coating system.

Flammability

The utility of a coating lies in its inherent ability to protect a substrate from environmental degradation. A coating that supplies the potential to incinerate the very structure it has been designed to protect is undesirable. Early in this work it was realized that conventional binder systems only promoted magnesium powder incineration when subjected to flammability exposure, which resulted in emphasis on developing a non-incinerating Mg-rich polymer vehicle. Results from the flammability tests revealed that once the conventional coating had disbonded from the Al substrate the paint burned with magnesium incinerating. Both hybrid coatings were found to firmly adhere to Al substrate even after 30 seconds exposure to direct flame, thus preventing incineration. Conventional binders evolved black soot when burned while hybrid binders did not evolve soot.

Cost analysis

An estimate of the total cost of Mg-rich coating applied is based upon a primer formulated with 2.5-lbs per gallon Mg Powder at 50-PVC RMC and manufacturing cost of about \$450.00/ gallon, assuming \$160.00/lb for pigmentary Mg and silane modified polymeric material. The estimate cost for the ELT topcoat at \$100/gallon with a given a spread rate (SR) at 200 ft²/gal (topcoat). Total cost for primer and topcoat at \$550 per /gallon, yielding approximately 200 ft²/gal primer and topcoat.

	<u>Mg-Rich System</u>	<u>Chromated System</u>
<i>Paint</i>	\$2.75 / ft ²	\$14.50 / ft ²
<i>Application cost</i>	< \$11.20 / ft ²	

In addition, the following value added *Reduced HAZMAT disposal costs * Greatly reduced hazardous materials * Reductions in medical claims * All non HAPs listed Solvents* Landfill disposable * Reduction of paint facilities * Shirt environment * No HAZMAT protective gear.

Note: cost of Mg powder~ 80nm PSD estimated at \$160.00/lb may eventually approach the cost of atomized Mg powder with PSD less than 5 µm @ \$13.00 per pound.

7.3 Conclusion implications of the Study:

The underlying hypothesis stated earlier was the purpose of this investigation was to determine whether aluminum alloys could be protected with an active metal coating system, comprised of magnesium powder, in an analogous manner to those zinc-rich systems that protect steel. Overall, this study has shown that these pigmentary Mg systems provide sacrificial cathodic protection of Al aerospace alloys in a mode analogous to that of

zinc-rich systems. It was also found that coatings formulated with conventional binders and conventional HAP solvents performed poorly in contrast with a hybrid silane modified epoxy-urea IPNs derived from non-HAP solvent systems.

In addition, through exploring the siloxane chemistry and combining polysiloxanes with organic binder systems, epoxy siloxane hybrid coatings have been developed with performance properties than surpass conventional technology. By the combination of the inorganic polymeric structure of the polysiloxanes with the organic epoxy binder system, a coating has been developed that combines the corrosion resistance of high build epoxy polymers and exceeds the weatherability of the best aliphatic polyurethane finish coats. This allows the replacement of traditional anti-corrosive systems with three or four coats by a two coat system.

The final implication of all of these studies is that the development of this technology is convenience as these systems can be applied at room temperatures with a minimum requirement of surface preparation. The coating system can be spray applied with existing technology that can be modified through process engineering to optimize the heat, pressure, time required to apply the coatings. An unanticipated benefit of this coating system is the element of convenience that it delivers to those who chose to employ it. It may be surmised that this coating system may not be appropriate for providing corrosion control to all structural aluminum alloy systems.

Chapter 8 Recommendations for Future Work

8.1 Mg-Al-Zn Alloy Cathode *versus* Mg metal

Pigmentary forms AZ-63, AZ-91 and M1A magnesium alloys may possess distinct advantages over the pure metal in a cathodic coating system. The high purity alloy, for example, AZ91E, has salt water corrosion resistance 10-100 times better than the standard purity alloy, and equal to or better than mild steel and the die cast aluminum alloy 380.⁶²⁰ ⁶²¹ Tunold *et. al.*,⁶²² reported that corrosion of commercial purity magnesium was usually transgranular, while the corrosion of the alloys was more uniform. Similarly, Makar and Kruger⁶²³ reported that the corrosion of pure magnesium was non-uniform, giving an etched appearance, but corrosion of AZ61 appeared to undergo uniform attack and rapidly solidified alloys were attacked more uniformly than the conventional alloys.

In a recent study, Inoune *et al.*⁶²⁴, investigated the corrosion rate of cast pure (>99.95 mass %) and high purity (>99.999%) magnesium, and AZ31 and AZ91 Mg alloys in buffered chloride solutions. According to Inoue *et al.*⁶²⁴, in a conventional (buffered chloride ion) solution, 3 N-Mg had a significantly higher corrosion rate than 6N-Mg (*Figure 8.1* below). This rate was also higher in the pH~9 buffer, although the pH of solution in which it was immersed was ~ 9 or more. The reasoning given is that the 3N-Mg contains certain amounts of cathodic impurities⁶²⁵, such as Fe or Cu, but no alloying elements like Mn or Zn that make the impurities inactive.⁶²⁶ The cathodic impurities are believed to accelerate the cathodic reaction, hydrogen gas evolution at the material's surface. According to Inoue *et al.*⁶²⁴, the pH of the solution near the cathodic areas is observed to increase due to the consumption of hydrogen ions, while that (pH) in the

anodic areas is observed to decrease as a result of metal ions hydrolyzing from the corrosion reaction.

H. Inoue et al. / Corrosion Science 44 (2002) 603–610

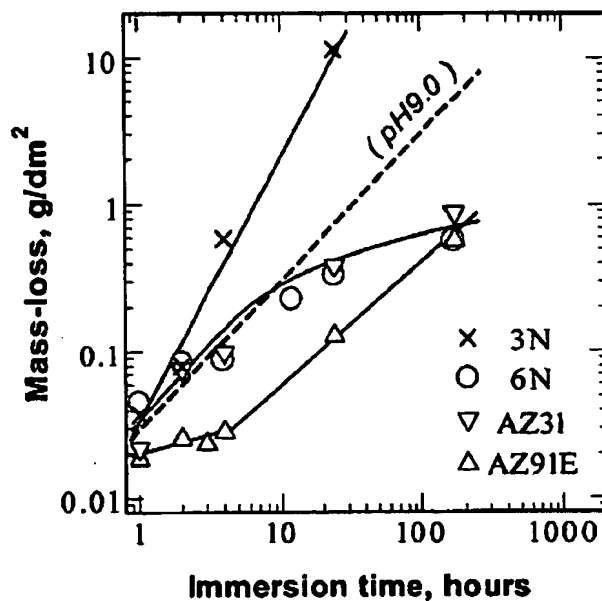


Figure 8.1, Mass-losses of cast pure magnesium (3N), high purity magnesium (6N0, AZ31, and AZ91 in conventional 10 g/dm³ NaCl solution as a function of immersion time. The dashed line represents typical mass-losses with time of all examined materials in the pH ~9 borate buffer.⁶²⁴

8.2 Smaller Particle Size Distribution Mg Alloy Powders and ICPs

It has been observed that relatively pure Mg powders, with particle size distributions (PSD) < 20 micron, are far too reactive when formulated as a high PVC active metal primer in conjunction with a non-conductive polymer material. When damaged, the metal in these coatings is quickly oxidized and develop a higher ratio of surface hydroxides to metal than larger PSD Mg powders which limits their utility to provide cathodic protection. Based upon the above mentioned difference in reactivity of the Mg alloy versus that of the pure metal, a PSD<20 micron Mg alloy powder, used in conjunction with an

inherently conductive polymer (ICP) may act to form a more electrically continuous coating whose anode is not quickly consumed about a localized defect. The emphasis would be to take advantage of the above mentioned reactivity characteristics, such as reduced reactivity of the alloy powder over that of the pure metal in a conductive polymer matrix.

8.3 Particle Shape Mg-powder *versus* Flake

The so called magnesium powder, Eckagranules™, used in these experiments was not originally intended for use in pigmented Mg-rich coating systems. The particle shape of these powders both PK-31 and PK51 has been observed to spherical up to about 20microns, and somewhat more of a flake shape after about 80microns. Hare, *et al.*⁶²⁷, discuss zinc-rich coating systems that impart cathodic protection via the packing of spherical pigment particles, as depicted in *Figure 8.2-A*, below *versus* zinc flake inhibitory systems, as depicted in *Figure 8.2-B*, below.

(A)

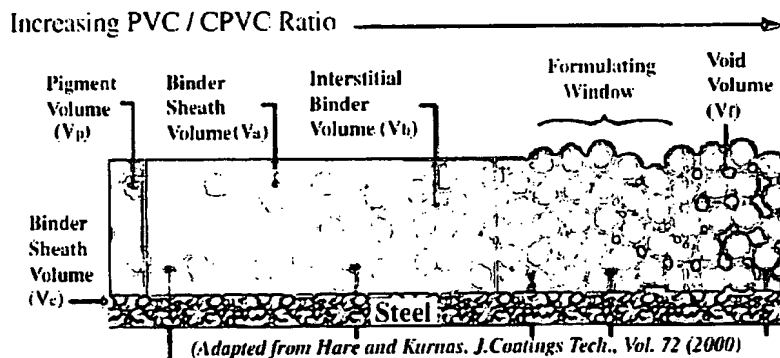
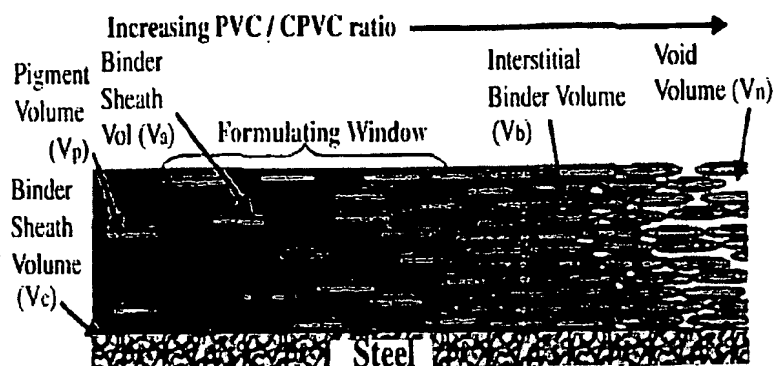


Figure 8.2-A: Zinc-rich: powder coating and PVC relationship.

(B)



(Adapted from Hare and Kurnas, *J.Coatings Tech.*, Vol. 72 (2000))

Figure 8.2-B: Zinc-rich flake coating and PVC relationship.

According to Hare, *et. al.*⁶²⁷, both systems, described in *Figures 8.2 (A) and (B)* below, provide a reliable means by which to protect the substrate. However the means by which one chooses to modify either, for example, by combining the metal flake with the powder, must be done according to variations in PVC/CPVC ratios that yield best performance. Therefore, pigment geometries and particle size distribution data must be ascertained and CPVC calculations must be performed so that variations in PVC/CPVC may be correlated to a coating's performance.

In a recent study Kalendová *et al.*⁶²⁸, describe the difference between the two types of zinc particles, lamellar vs spherical, to act as an effective barrier to arrest water vapor transmission. They measured water vapor diffusion resistance values for pigmented coatings at a constant 50 % PVC for both types of pigment particles and concluded that "lamellar pigmented zinc coatings create a more efficient barrier to water vapor transmission than isometric spherical zinc particles." See *Figure 8.3* below:

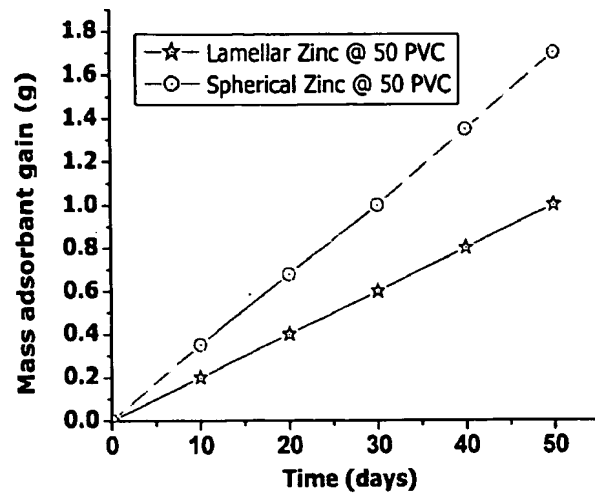
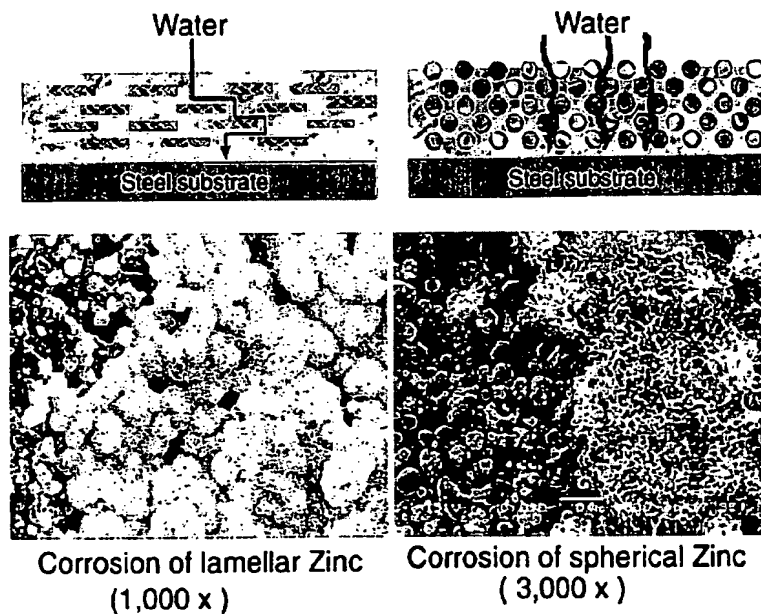


Figure 8-3: Time dependence of mass adsorbent gain in grams vs time for coatings pigmented at 50 %PVC with (.) spherical zinc: (ζ) lamellar zinc.



(Adapted from Kalendova et al., 2002)

Figure 8.4, Illustrative scheme of water vapor transmission / Penetration through coatings composed of different particle shapes: lamellar zinc (top-left); spherical zinc (too-right). SEM results of corrosion products coatings after 800-hr exposure to salt chamber conditions. (Adapted from Kalendová et al., 2002)

The significance *Kalendová's* work, Figure 8.4 above, is that it relates easy to observe morphological changes occurring as a function of exposure conditions and relates them to the pigment's particle shape. Such information can be readily observed with SEM and EDAX techniques and the general corrosion mechanism, as a function of exposure, ascertained from the morphology of the observed surface oxides. In addition, the effect exposure in different electrolytes can be correlated to water vapor transmission / penetration through coatings composed of different particle shapes through gravimetric methodology. This may also reveal information regarding the corrosion rate via evolution of H₂ gas with respect to the type of Mg metal / alloy used in the study, see work done by Inoue *et al.*⁶²⁴

8.4 Cerium Nitrate Modified Magnesium-Silicates

It has been well established that chromate conversion coatings are noted for their ability to "self-heal" if damaged by mechanical or chemical action, provided the damage is local and not severe. Self-healing, or active corrosion protection, involves release of chromate from the coating, transport through the solution and action at the site of damage, namely pits. A similar scheme for active corrosion protection has been devised through the use of rare earth metals whereby the introduction or modification of the aluminum alloy surface with Ce and Mn oxides has shown to result in a "self-healing effect".⁶²⁹ The key to understanding the ACP in these systems appears to be that these metals exhibit soluble high oxidation state forms and lower oxidation forms with lower solubility. When high oxidation state oxides are introduced to hydrocalcite, they can be dissolved by a contact solution transported to a defect site on bare Al samples where they are reduced and precipitated to inhibit further corrosion.

In a more practical application, Aramaki⁶³⁰, describes the self-healing protective effect of 1,2-bis(triethoxysilyl)ethane ($(\text{C}_2\text{H}_5\text{O})_3\text{Si}(\text{CH}_2)_2\text{Si}(\text{OC}_2\text{H}_5)_3$ (abbreviated to BTESE) polymer containing sodium silicate $\text{Na}_2\text{Si}_2\text{O}_5$ (water glass) and cerium(III)nitrate $\text{Ce}(\text{NO}_3)_3$ in zinc-rich systems. The synergistic inhibition effect of $\text{Na}_2\text{Si}_2\text{O}_5$ and CeCl_3 mixtures has also been examined on zinc corrosion in 0.5 M NaCl by polarization measurements indicating high inhibition efficiencies of the equimolar mixture. Surface analyses have demonstrated that the zinc surface is covered with a layer of the hydrated or hydroxylated cerium-rich oxide mostly and small amount of zinc silicate precipitates at a defect of the layer to prevent the cathodic and anodic processes, respectively.⁶³¹

As discussed previously, smaller sized Mg particles react faster and therefore limit the effective life of the coating. Aramaki⁶³⁰, describes the modification of zinc metal surface with cerium-silicates, which have been implicated to self healing ACPs. It has always been an overall objective to formulate metal-rich coatings at thinner film thicknesses. Modification of the magnesium metal's surface via treatment with 1,2-bis(triethoxysilyl)ethane ($(\text{C}_2\text{H}_5\text{O})_3\text{Si}(\text{CH}_2)_2\text{Si}(\text{OC}_2\text{H}_5)_3$ (abbreviated to BTESE) polymer containing sodium silicate $\text{Na}_2\text{Si}_2\text{O}_5$ (water glass) and cerium(III)nitrate $\text{Ce}(\text{NO}_3)_3$ in to form a modified pigment may be an effective way to combine the micron sized powder with a conductive polymer matrix that does not “burn-out” due to localized depletion of Mg metal in the area a coating has been damaged.

8.5 Cerium and Cerium Oxides/Hydroxides

As previously discussed in Chapter 2.3, central to the preservation of the $\beta\text{-Al}(\text{OH})_3$ bayerite / $\gamma\text{-AlOOH(s)}$ boehmite interface in the presence of copper cathodic sites has been the application of REMS such as cerium. These REMS, when incorporated as a film or

coating, have also shown to inhibit the primary reduction reaction occurring on the surface of Al alloys containing copper at pH's circa ~ 8.5 , (which is at the upper stability limit for Al according to Pourbaix diagrams previous section 2.1), by precipitation of rare earth hydroxides/oxides. In addition, when used in conjunction with magnesium, they also show a similar activity by the precipitation of rare earth hydroxides/oxides at the surface of magnesium thus inhibiting corrosion of the magnesium metal by preferentially forming oxides/hydrides.

As a means by which to control the afore mentioned "burn-out" due to localized depletion of micron sized Mg powder in the vicinity of cathodic sites of the Al alloy, nano-particle cerium should be incorporated into the primer interface as a means by which to moderate excessive magnesium consumption directly at the Al / primer interface, as depicted in Figure 8.5, below.

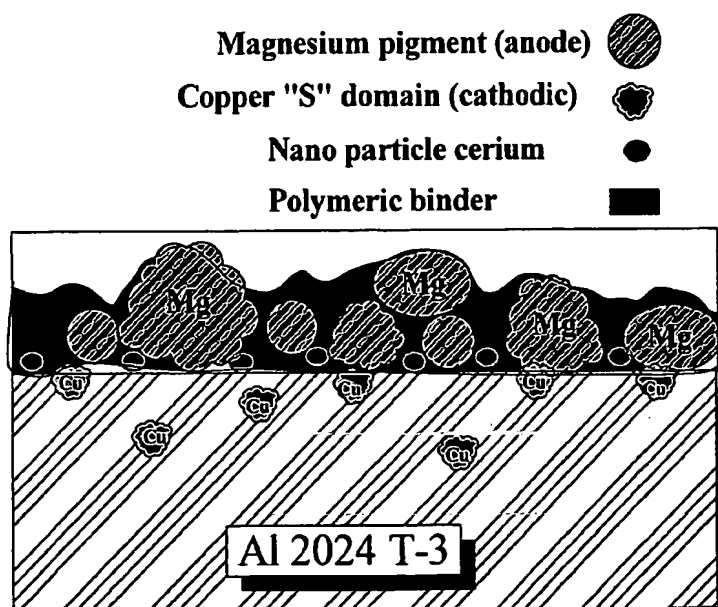
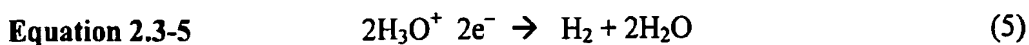


Figure 8.5, Illustrative scheme for proposed Mg-rich coating system with nano particle cerium incorporated at Al / Coating interface.

Figure 8.5, above, depicts a Mg-rich coating over Al 2024 T-3 with nano-particle cerium incorporated into the interface. It is surmised that the presence of cerium would forstall the consumption of micron sized Mg powder, (particle sizes < 20µm), and in so doing extend the actual period the coating functions as a cathodic coating, i.e., the potential difference due to cathodic current, as depicted in Figure 3.11 , would be extended.

Therefore, the effect of moderating consumption of Mg-powder closeset to the Cu-cathodic sites should be similar to that of formulating the coating at the PVC which was shown to best extend the coating's cathodic lifetime. This was shown to occur in Chapter 3, i.e., the magnitude of the negative potential (OCP) remained larger over an extended period for the Mg-rich primer that was formulated at its CPVC. The electrochemical interpretation ascribed to such to effect would be that extended cathodic protection would be due to the more even distribution and consumption of sacrificiaial anode that feeds the hydrogen evolution reaction, Equ. 2.3-5, which has been implicated as the major reduction reaction occurring in such an alkaline environment.⁶³²



It would also be surmised that another approach taken to achieve a similar effect would be to simply treat the Al 2024 T-3 surface with cerium(III)nitrate $\text{Ce}(\text{NO}_3)_3$, as described in the literature by Yu and Cao⁶³³ and then apply the Mg-rich coating. In this approach the Al surface would receive an anodization treatment, by any such means previously described in Chapter 2.3, and then the cerium(III)nitrate solution applied followed by application of Mg-rich primer according to the methodology described in this thesis.

8.6 Mg-powders with Cerium (III) nitrate Treatment

This section proposes a methodology for preferential treatment of the smaller particle size distribution fraction of Mg powder, i.e. PSD < 20 μ m, used in conjunction with a larger PSD > 20 μ m, similar to the pigmentary Mg powders used in Chapter 5 this thesis. For example, the PK-31 (PSD < 30 μ m) would be treated with cerium(III)nitrate solution, while the PK-51 (PSD > 30 μ m) would not receive treatment. Based upon the observation by Mansfeld that Mg treated with cerium(III) preferentially formed hydroxides before the Mg metal did when exposed to a NaCl environment. Mansfeld *et al.*^{Error! Bookmark not defined.}, showed that the corrosion protection of cerium conversion coatings formed on pure magnesium and a magnesium alloy, WE43, was studied by D.C. polarization and A.C. impedance techniques. REMS coatings were observed to show reduced dissolution of magnesium in a pH 8.5 buffer solution. This was ascribed to the formation of protective magnesium hydroxy corrosion products and mixed rare earth/magnesium oxide/hydroxides. It was observed that protection continued until REMS coatings were consumed by the formation of magnesium corrosion products.

The importance of this methodology lies in its ability to reduce the overall PSD of the Mg-powder incorporated into the primer coating which is important for the following reasons: 1) a reduced PSD yields a primer with a thinner film thickness and more uniform coating; 2) flammability / fire retardance of the coating is increased by reducing the mass of Mg metal that may incinerate, (smaller PSD Mg-powders are better wet by due to more even distribution of silane modified polymeric binder than large PSDs), and 3) formulation and application of smaller PSD Mg-powders are easier due to the more spherical geometry of the powders. Recalling that the model used to approximate CPVC relies on the volume

of a sphere which more accurately represents the geometry of the fine PSD Mg-powders as opposed to a more “oblongated-swarf” geometry observed in the larger PSD, (PSD>80µm) powders.

8.7 Testing Protocol

Thus far, above, it has been shown how zinc particle morphology and related electrochemical mechanisms involving physico-chemical aspects of zinc powder are closely tied to corrosion-inhibition efficiency of ZRCs used in cathodic protection systems.⁶³⁴ Formulation of efficient ZRCs has recently been studied by Kalendová *et al.* who examined the effect of select parameters such as zinc pigment particle size and shape, PVC, and polymeric binder matrix on the performance of zinc-metal coatings used to provide sacrificial protection for corrosion control.

The testing protocol, for corrosion control, applied to the Mg-rich coatings in these studies was based upon electrochemical impedance spectroscopy (EIS) which is valid for modeling or providing a means to assess the protective ability of an inorganic coating formed by chemical means on an aluminum alloy substrate. This test measures passive corrosion protection, and results may not reflect corrosion protection due to electroactive substances in the chemically passivated surface and electrochemical noise methods (ENM) provide insight into the global properties of a coating system, and both techniques are being used on a limited basis. However, there is a need to investigate corrosion events with improved dimensional resolution under the coating or at the metal/coating interface.

Based upon the previous discussion the measurement of CPVC in zinc-rich coatings is a highly subjective and dependent upon a complex array of parameters associated with the physical behavior of the pigments and polymeric material mixtures. Consequently,

according to Beirwagen⁶³⁵ coatings "...in which there is an incentive to have a high pigment volume concentration (PVC) for performance or economic reasons" the measurement and determination of a coating's CPVC is not a straightforward process due to issues involving origin of the measurement made, sensitivity of the measurement, and the nature of the associated experimental error of the individual property measured.

Bierwagen⁶³⁵ (1992), emphasizes the importance of film application and formation that is controlled by random packing connectivity events occurring in the film, on a microscopic scale, that can cause particles to either act independently of other components in the film or to act in conjunction with two or more components to form an undesirable non-random or flocculated matrix structure. The scanning vibrating electrode technique (SVET) is a high spatial resolution investigation technique whereby localized corrosion activity that may be associated with coating defects or galvanic coupled regions of the metal surface.⁶³⁶ The SVET technique may be applied to monitoring high resolution current measurements due to the onset of percolation in a metal rich coating. This in turn would yield a parameter associated with coating's morphology and its PVC/CPVC ratio.

8.8 Further Considerations

The essentials of these hybrid coating systems have been reviewed and tested according to methodology described. Further refinements can be brought to bear on the system through formulation refinement and material selection. For example, first, the crosslinking action of the silane modified quinoxalin crosslinker synthesized *in House* was described in terms of its ability to develop polymeric structure through both the organo-silane and amino moieties. Since this reaction scheme has shown to possess utility other commercially available products might be investigated for similar results. Second, the

“hybrid” polymeric material developed in these investigations was derived from polyisocyanates based on HMDI and MDI, and each was formulated into an epoxy-urea system and tested. What remains to be done is experimentation and formulation of new polymeric hybrids with either new polyisocyanates, of differing reactivity and chemical composition, or a mixture of any two polyisocyanate prepolymers, such as HMDI plus MDI. Third, the film forming properties of polyisocyanate systems can be improved by incorporation of a polyol to yield a urethane linkage. An aromatic polyisocyanate, such as Desmodur E23A could be modified with a polyol, such as butanediol, to yield a more flexible oligomer and then end-capped with any choice of polyisocyanate to yield a urethane modified polyurea.

Pigment surface modification would be the second area to be identified for overall coating system / performance improvement. As received the magnesium powder has a surface oxide that makes up about 4 percent of its total mass. The magnesium powder should be roller milled with steel spheres to remove the oxide and polish the surface of the metal. Once polished the powder could be modified with a dilute solution of water soluble polymer that would prevent adsorption of the hybrid polymeric material to the surface of the metal powder. Thus, when the metal rich coating was damaged, the thin water soluble polymer would dissolve leaving the pigment particle in the coating without a dielectric sheath which has been described as an impediment to cathodic connectivity of the anode on a global scale. Thus far, no study has been undertaken to establish whether or not adsorption of the silane modified polymeric material onto the surface of pigmentary magnesium metal/ oxide, through silicate bonds, either retards or promotes the corrosion control effectiveness of these coatings.

8.9 Further Polymeric Binder Material Study

Panel and Film Preparation

The primers formulated from materials in Table 8.2-B, below, were prepared using conventional techniques such as manual scrub panel prep and coating spray application.

Panel preparation of stock 6" x 3" Al 2024 T3 Q-panels™ was done by lightly wire brushing the surface to normalize the surface of all panels. It should be noted that for about every one out of every twenty panels, the surface hardness of the 6" x 3" Al 2024 T3 Q-panel™ varies and has noted to be dramatically harder than the others.

Lightly wire brushing the panels with a steel brush quickly reveals those panels with dramatically harder surfaces so they may be discarded. It should also be noted that wire brushing is preferred to the use of sand paper as sand paper is loaded with stearates (soap) that serve as sanding-aids or lubricants that strongly adsorb onto metallic surfaces.

After wire brushing, the panels are scrubbed with a Scotch Brite™ pad followed by rinsing / degreasing in 3 -ethoxypropionic acid ethyl ester (EEP) solvent. Once the EEP solvent had been rinsed with distilled (DI) water, the panel was subsequently immersed into a 10% phosphoric acid solution for 60 seconds, followed by a rinse with DI water. The freshly prepared Al panels were subsequently coated with a surface modifier according to methodology described in Chapter 4, where a 2 percent mixture of Silwet® 1120 in acetone / water mix as described in the literature⁶³⁷ was applied via foam brush. Panels were subsequently placed into a BigBlue oven at 30°C for 60 minutes.

Mg-rich primer preparation and application involved slowly dispersing the magnesium pigment into a mixture of epoxy / polyisocyanate and solvents. This was accomplished with a 1" dia. propeller blade connected to an electric mixer set which was

set at speed of approximately 1,000 rpm. The rheology control agent(s) Aerosil®R202 was gently blended into the pigment / binder-resin / solvent mix after the Mg pigment was added; while in the case of the rheology control agent Bentone®39, a pre-gel was made according to reference⁶³⁸ and then blended into the mix. The primers were applied with a touch-up spray gun, at a pressure setting of 60psi. Multi-coat passes were required to apply the mg-rich primer taking care to avoid paint running. The coatings were subsequently allowed to cure at 30° C for 14 days before topcoat application. Note, all primed panels were subsequently top coated with Extended Lifetime™ topcoat. The average film thickness (FT) estimated from EDAX photos reveal primer film thickness to be on the order of ~50 +/- 20 microns with topcoat film thickness at~ 100 +/- 40 microns.

Collected/Computed Data in Appendix

The general description of procedures and materials used in the formulation, application, and testing of such Mg-rich coatings has been described above and for a more extensive account see thesis² Chapters 3-6. Moreover, from this work a subsequent study was undertaken involving a more comprehensive study of polymeric materials used as vehicles for Mg-rich coatings. In this study a total of eight polymeric binder systems were formulated and tested, see Table 8.7-1, below, for generic description. The preparation and application procedures are the same as previously described above.

Mg-rich Primer Formulations

Below, Formulas I –to–IV, see Appendix 8-A, with material description and quantities used in the formulation of Mg-rich primers. Note, all primers were subsequently topcoated with Deft ELT™ fluorinated polyurethane topcoat.

Table 8.7-1: Polymeric binder systems for recent Mg-rich study.

- 1) 7-PQ-6-ol modified Demodur N3300/Epon 1001 hybrid
- 2) 7-PQ-6-ol modified Demodur E23A /Epon 1001 hybrid
- 3) 7-PQ-6-ol modified Demodur N3300/Epon 1001 hybrid
- 4) 7-PQ-6-ol modified Demodur E23A /Epon 1001 hybrid
- 5) Epon 1001/DesmodureN3300/Epicure 3255, (Epoxy/urea)
- 6) Epon 1001/Desmodur E23A/Epicure 3255, (Epoxy/urea)
- 7) MC-PUR, Desmodur E23A, (MDI polyurea)
- 8) Epon828/Ancamide 75-B-70 (epoxy-polyamide)

See adjunct Appendix 8-A for spread sheet formulations.

Interpretation of Spread sheet Data

The attached spreadsheets, see Appendix 8-A, contain the formulations for Mg-rich primers used in the study and are set up according to raw materials in the left column with the Formula # No. adjacent. The columns with numbers are headed accordingly: 1) [mass] which is the mass in grams of the material volatile plus non-volatile; 2) [mass (Adj)] which is the non-volatile mass; 3) [Vol] which is the non-volatile volume component; 4) [Batch (Lab/mass)], this is the actual amount of the raw material the mixologist will weigh out when blending / mixing up the paint. Note that lab mass calculations and numbers are based on the volatile components include and are derived from the [Batch (Lab/mass)] column and differ only by an arbitrary scaling factor used to normalize each individual formula according to a batch of paint that will be charged to the spray gun for application.

Appendix 8-A

Formulas I: 1-4 for 40% PVC Mg-rich

Mg-rich Formulations for panels by Mike Nanna @ 40 %PVC

Sept_29_02	Mg Rich Coatings Sept_Eight				PVC @ 40% PVC (low)				Sept_29_02
	Mg-pow	Pk51/31	1 density	2 density	3 density	4 density	atom	2	
Mike_Nanna			1.74	2.3	1.14				Mike_Nanna
Formula # 1		40% PVC			Batch				Formula # 3
Material	Mass(g)	Mass(Adj)	Vol	Mass Lab	Material	Mass(g)	Mass(Adj)	Vol	Batch
p-Quin	0.24	0.24	0.2777778	0.96	p-Quin	0.24	0.24	0.2777778	0.768
PropylCarb	12			48	PropylCarb	12			38.4
Si-A1120	0.46	0.46	0.4181818	1.84	Si-A1120	0.46	0.46	0.4181818	1.472
1001EEP	2.69	2.6175	1.7697368	10.76	1001EEP	3.8	2.85	2.5	12.16
N3300	2.69	2.7731959	2.6665345	10.76	N3300	1.9	1.9	1.958763	6.08
AcrR202	0.5	0.5	0.2173913	2	AcrR202	0.6	0.6	0.26687	1.92
Mg Pk51/31		5.6	3.2183208	12.873563	Mg Pk51/31		5.6	3.218391	17.92
% PVC			0.401001	87.102563	% PVC			0.402973	78.72
40.10010362					40.29728144				
Mike_Nanna		40% PVC		Batch	Mike_Nanna		40 PVC		Batch
Formula # 2	Mass(g)	Mass(Adj)	Vol	Mass Lab	Formula # 4	Mass(g)	Mass(Adj)	Vol	Mass Lab
Material					Material				
p-Quin	0.12	0.12	0.277778	0.408	p-Quin	0.12	0.12	0.27778	0.408
PropylCarb	12			40.8	PropylCarb	12			40.8
Si-A1120	0.23	0.23	0.209091	0.782	Si-A1120	0.23	0.23	0.20909	0.782
1001EEP	3.15	2.3625	2.3625	10.71	1001EEP	3.15	2.3625	2.07237	10.71
E23-A	2.56	2.56	2.461538	8.704	E23-A	2.3	2.3	2.3	7.82
AcrR202	0.5	0.5	0.217391	1.7	AcrR202	0.5	0.5	0.21739	1.7
Mg Pk51/31		5.9	3.390805	20.06	Mg Pk51/31		5.3	3.04598	18.02
% PVC			0.404547	83.164	% PVC			0.40176	80.24
40.45169462					40.17637378				

Formulas II: 5-8 for 40% PVC Mg-rich

Mg-rich Formulations for panels by Mike Nanna @ 40 %PVC

Mike_Nanna		Sept_29_'02				Mike_Nanna		PVC @ 40%			
Formula # 5		40 PVC %				Formula # 6		Batch			
8/2		Batch									
Material		Mass(g)	Mass(Adj)	Vol	Mass Lab	Material		Mass(g)	Mass(Adj)	Vol	Mass Lab
PropylCarb		12			43.2	PropylCarb		12			40.8
1001EEP	1.19	4.05	3.0375	2.552521	14.58	1001EEP	1.85	1.3875	1.16597	6.29	
N3300	0.97	1.72	1.72	1.7731959	6.192	E23-A	3.8	2.85	3.91753	12.92	
Epi-3255	0.96	0.44	0.44	0.4583333	1.584	Epi-3255	0.25	0.25	0.26012	0.85	
AcR202		0.5	0.5	0.2173913	1.8	AcR202	0.55	0.55	0.23913	1.87	
Mg Pb51/31			5.2	2.9885057	18.72	Mg Pb51/31		5.8	3.33333	19.72	
% PVC				0.4012413	86.076	% PVC			0.40066	82.45	
40.12413278						40.06633561					

Mike_Nanna		Sept_29_'02				Mike_Nanna		Sept_29_'02			
Formula # 7		40% PVC				Formula # 8		40% PVC			
		Batch						Batch			
Material		Mass(g)	Mass(Adj)	Vol	Mass Lab	Material		Mass(g)	Mass(Adj)	Vol	Mass Lab
Xylol		12			43.2	Xylol		12			40.8
E23-A		5	3.75	5.1546392	18	Epoxy 828	3.2	3.2	2.68908	10.68	
Bentone 34 Gel		0.5	0.5	0.2272727	1.8	Ac 75-15-70	2.88	2.16	2.25	9.792	
						AcR202	0.5	0.5	0.21739	1.7	
Mg Pb51/31		5.6	5.6	3.2183908	20.16	Mg Pb51/31	5.4	5.4	3.10345	18.36	
% PVC				0.4006444	83.16	% PVC			0.40204	81.532	
40.06444481						40.20428171					

Appendix 8-A

Formulas III: 1-4 for 50% PVC Mg-rich

Mg-rich Formulations for panels by Mike Nanna @ 50 %PVC

Mg Rich Coatings Sept_Eight					PVC @ 50 high				
		Mg	R2o2	E1001828					
		1 density	2 density	3 density					
		1.74	2.3	1.14					
		1 density	2 density	3 density					
		1.74	2.3	1.14					
Mike_Nanna					Mike_Nanna				
Formula # 1		50% PVC			Formula # 2		50% PVC		
Material	Mass(g)	Mass(Adj)	Vol	Batch	Material	Mass(g)	Mass(Adj)	Vol	Batch
p-Quin	0.24	0.24	0.277778	0.72	p-Quin	0.24	0.24	0.27778	0.72
PropylCarb	12			36	PropylCarb	12			36
Si-A1120	0.46	0.46	0.46	1.38	Si-A1120	0.46	0.46	0.46	1.38
1001EE2P	3.19	2.3925	2.098684	9.57	1001EE2P	2.76	2.07	1.81579	8.28
N3300	2.69	2.69	2.663366	8.07	E23-A	2.76	2.76	2.73267	8.28
AcR202	0.65	0.65	0.282609	1.95	AcR202	0.65	0.65	0.28261	1.95
Mg PK51/31		9.2	5.287356	27.6	Mg PK51/31		8.8	5.05747	26.4
% PVC			0.503168	85.29	% PVC			0.50253	83.01
50.31679314					50.25333059				
Mike_Nanna					Mike_Nanna				
Formula # 3		50%PVC		Batch	Formula # 4		50% PVC		Batch
Material	Mass(g)	Mass(Adj)	Vol	Mass Lab	Material	Mass(g)	Mass(Adj)	Vol	Mass Lab
p-Quin	0.12	0.12	0.12	0.36	p-Quin	0.12	0.12	0.25	0.36
PropylCarb	12			36	PropylCarb	12			36
Si-A1120	0.23	0.23	0.209291	0.69	Si-A1120	0.23	0.23	0.65455	0.69
1001EE2P	4.3	3.225	2.828947	9.675	1001EE2P	3.45	2.5875	2.26974	10.35
N3300	1.8	1.8	1.85567	5.4	E23-A	2.2	2.2	2.2	6.6
AcR202	0.65	0.65	0.282609	1.95	AcR202	0.65	0.65	0.76471	1.95
Mg PK51/31		8.4	4.827586	25.2	Mg PK51/31		8.2	4.71261	24.6
% PVC			0.504765	79.275	% PVC			0.50475	80.55
50.47652827					50.47489292				

Formulas IV: 5-8 for 50% PVC Mg-rich

Mg-rich Formulations for panels by Mike Nanna @ 50 %PVC

Mike_Nanna	Sept_29_'02				Mike_Nanna	Sept_29_'02			
Formula # 5	50% PVC			Batch	Formula # 6	50 PVC			Batch
Material	Mass(g)	Mass(Adj)	Vol	Mass Lab	Material	Mass(g)	Mass(Adj)	Vol	Mass Lab
PropylCurb	12			37.2	PropylCurb	12			36
1001E13*	4.05	3.0375	2.664174	12.555	1001E13P	1.85	1.3875	1.21711	5.55
N3300	0.97	1.72	1.773196	5.332	E23-A	3.8	2.85	3.91753	11.4
Epi-3255	0.96	0.44	0.458333	1.364	Epi-3255	0.25	0.25	0.26042	0.75
AcrR202	0.65	0.65	0.282669	2.015	AcrR202	0.65	0.65	0.28261	1.95
Mg Ph51/31		8.1	4.655172	25.11	Mg Ph51/31		9.1	5.22989	27.3
% PVC			0.502124	83.576	% PVC			0.50538	82.95
50.21242187					50.53837086				

Mike_Nanna	Sept_29_'02				Mike_Nanna	Sept_29_'02			
Formula # 7	50 PVC			Batch	Formula #8	50 PVC			Batch
Material	Mass(g)	Mass(Adj)	Vol	Mass Lab	Material	Mass(g)	Mass(Adj)	Vol	Mass Lab
Xyrol	12			36	Xyrol	12			33.6
E23-A	5.5	5.5	5.670103	16.5	Epon 828	3.6	3.6	3.15789	10.08
	0		0	0	Aue 75-13-70	3.2	2.4	2.5	8.96
Hexone 34 Gel	0.8	0.8	0.363636	2.4	AcrR202	0.8	0.8	0.34783	2.24
Mg Ph51/31	9.6	9.6	5.517241	28.8	Mg Ph51/31	9.3	9.3	5.34483	26.04
% PVC			0.509124	83.7	% PVC			0.50153	80.92
50.91236689					50.15311567				

References / Bibliography

- ⁶²⁰ Reichek, K. N. , Clark, K. J., Hillis, J. E. , Controlling the Salt Water Corrosion Performance of Magnesium AZ91 Alloy, SAE Technical Paper Series #850 417, Detroit (1985)
- ⁶²¹ King, J. F., in Advanced Materials Technology International (Ed: G. B. Brook), Sterling, London, pp. 12 (1990)
- ⁶²² Tunold, R., Holtan, H., Hagg Berfe, M.-B., Lasson, A., Steen-Hansen, R., *Corr. Sci.*, Vol. 17, pp. 353 (1977)
- ⁶²³ Makar, G. L., Kruger, J., Joshi, A., in Advances in Magnesium Alloys and Composites (Eds: H. G. Paris, W. H. Hunt), International Magnesium Association and the Non-Ferrous Metals Committee, TMS, Phoenix, Arizona, January 26, pp. 105 -121 (1998)
- ⁶²⁴ Inoue, H., Sugahara, K., Yamamoto, A., and Tsubakino, H., *Corrosion Sci.*, Vol. 44, pp. 603 – 610, (2002)
- ⁶²⁵ Hanawalt, J.D., Nelson, C.E., and Peloubet, J.A., Trans. AIME, Vol. 147, pp. 273, (1942)

- ⁶²⁶ Hawke, D.L., Hillis, J.E., Pekguleryur, M., and Nkatsugawa, I., in: Avedesian, M.M., and Baker, H., (Eds.), *Magnesium and Magnesium Alloys*, ASM International, Materials Park, pp. 194-210, (1999)
- ⁶²⁷ Hare, C.H., and Kurnas, J.S., *Journal Coatings Technology*, Vol. 72, No. 910, pp. 21-27, (2000)
- ⁶²⁸ Kalendová, A., Kuckačová, A., *Macromol. Symp.*, Vol. 187, pp. 377-386 (2002)
- ⁶²⁹ Rudd, A.L., Breslin, C., B., and Mansfeld, F., *Corrosion Science*, Vol. 42, pp. 275-288 (2000)
- ⁶³⁰ Aramaki, K., *Corrosion Science*, Vol. 44, pp. 1375 -1389 (2002)
- ⁶³¹ Aramaki, K., *Corros.Sci.* in press; Proc. *JSCE Materials and Environments 2001*, Japan Society of Corrosion Engineering, Tokyo, pp. 235 (2001)
- ⁶³² Emley, E.F., *Principles of Magnesium Technology*, Pergamon Press, Oxford, (1966)
- ⁶³³ Yu, X., and Cao, C., *Thin Solid Films*, Vol. 423 Pp. 252-256 (2003)
- ⁶³⁴ Leclercq, M., *Eur. Coat. J.*, No.3, pp.106 (1991)
- ⁶³⁵ Bierwagen, G.P., *Journal of Coatings Technology*, Vol. 64, No. 806, pp. 71-75 (1992)
- ⁶³⁶ Khobaib, M., Rensi, A., Matakis, T., and Donely, M.S., *Prog. in Organic Coatings*, Vol. 41, pp. 266-272 (2001)
- ⁶³⁷ Walker, P., "Organo Silanes As Adhesion Promoters for Organic Coatings," *Journal of Coatings Technology*, Vol. 52, No. 670, November, pp. 49-61 (1980)
- ⁶³⁸ Schwindt, J., "Moisture-Cured, Polyurethane-Based, Surface Tolerant Coatings: An Economical Alternative for Corrosion Control," Technical literature from Bayer AG, Leverkusen, Germany, (2000)

Appendices

Appendix 1-A Aluminum Alloy 2024 T-3

Aluminum entered the world of structural engineering materials toward the end of the 19th century. Its use grew significantly following the emergence of three important industrial developments: 1) the internal combustion engine; 2) the long-distance transmission of electricity, and 3) the activities of Orville and Wilbur Wright (1903) in the U.S. at developing sustained and controllable flight aircraft. Since then the unique and utilitarian properties of aluminum and its alloys have put the metal into widespread usage. Some salient features of aluminum are that it is electrically conductive, relatively corrosion resistant, low density, high strength to weight ratio, and its alloys are made available in a wide range of strength value from pure aluminum with high toughness and a low tensile (13 ksi, 90 MPa), to high strength alloy with tensile strength approaching (100 ksi, 720MPa).⁶³⁹ All of these properties have contributed to aluminum's widespread use in electrical appliances, consumer durables, machinery and equipment, and countless other applications. However, and most importantly, aluminum has been used in virtually all segments of the aircraft / aerospace industry in the manufacture of airframes, engines, fuel-tanks, and accessories well into the 21st century.

Pure aluminum is resistant to weathering in many environments, corrosion resistant to many acids, but susceptible to alkalis that act to destroy the self-healing protective oxide layer that develops as a result of anodic process.⁶⁴⁰ Aluminum possesses a native oxide layer that serves as a barrier oxide film that strongly adheres to the metal surface. The dimensions of the oxide are described as non-uniform with a nominal thickness of about 5 nm or (50Å).⁶⁴¹

Aluminum anodization was first described and likened to the Faraday paradox⁶⁴² as the deliberately controlled corrosion of the aluminum surface in sulfuric acid to yield a uniform, continuous protective oxide film.^{643, 644} The anodizing process occurs in aqueous solution when a current is discharged through an electrolyte in the presence of an aluminum anode. As anodization proceeds, the resulting micro-structure that emerges is described as a contiguous columnar film of aluminum oxide Al_2O_3 that forms and continues to grow over the surface. Film growth continues only slowly after internal electrical resistance developing within the film begins to develop.⁶⁴⁵

Aluminum alloy 2024 T-3 (Cu 4.5, Mg 1.5, Mn 0.6, Si 0.5 max., Cr 0.1 max., Ti 0.1 max., balance Al percent by weight) is classified as a precipitation grade hardened heat-treatable wrought alloy. Heat-treatable wrought alloys are materials that derive their strength from a heat-aged, strain hardened, solid solution dispersion of intermetallic copper compounds⁶⁴⁶. Age hardening or precipitation hardening is designed to produce a fine hard coherent precipitate in a softer, more ductile matrix. The Al- 4% Cu alloy is common age hardenable alloy. The hardening mechanism is described⁶⁴⁷ is described to occur in three steps, see (Figure 1.1-1).

Step1: solution treatment The alloy is heated to a temperature above the solvus temperature until a homogeneous solid solution (α) is formed. This step dissolves the (θ) phase precipitate and reduces any segregation in the alloy.

Step2: quench After solution treatment, the alloy that is rich in (α) phase is rapidly quenched, which causes a (θ) phase precipitate to form. At this point the (α) rich phase becomes a supersaturated solid solution containing excess copper, which is not an equilibrium structure.

Step 3: aging The supersaturated (α) solution is heated to a temperature below the solvus temperature. Eventually, the copper diffuses to nucleation sites and a precipitate forms and eventually an equilibrium (α) and (θ) structure is produced.

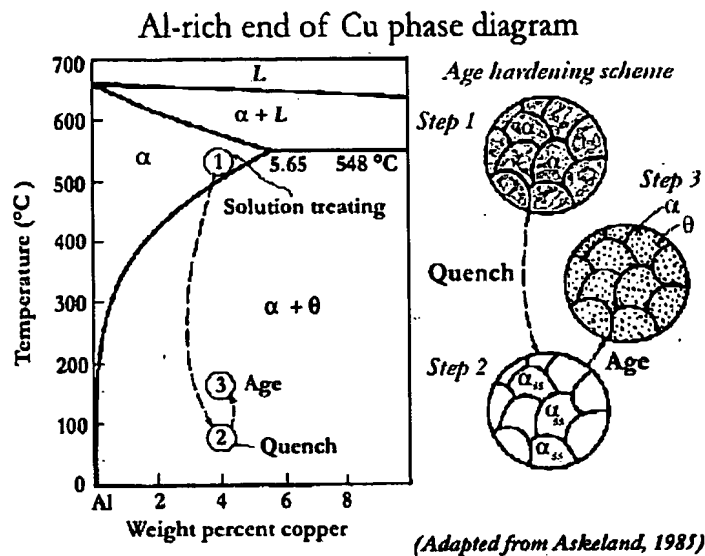


Figure A.1-1, The aluminum-rich end of the aluminum-copper diagram showing the three steps in the age hardening process with relevant micro-structure.

The temper designation of this alloy is “T” for thermally treated, and the alloy series is designated as 2xxx (copper), in contrast to 7xxx (zinc) that denotes a description of the major alloying elements. For example, 2024-T3 (Al-Cu-Mn-Mg) is a solution treated, cold worked and naturally aged.⁶⁴⁸ The effect of alloying elements on the strength of annealed aluminum is dramatic with strength ranges from (55-75ksi, 380-520MPa) for 2xxx series and (75-90 ksi, 520-620MPa) for 7xxx series.⁶⁴⁹ Table 1.1.1 demonstrates the effect of alloy element on the mechanical properties of the 2024-Tx alloy. It should be noted that there is no relationship between strength and increasing amount of alloy additions for the heat treatable 2xxx and 7xxx series.⁶⁵⁰ In other words, adding more of a particular alloying element does not necessarily impart additional strength to the alloy.

Table 1.1.1: Mechanical Properties of Heat Treated AA 2024 T-x

Alloy	Nominal Composition	Temper x	Tensile ksi	Elongation % in 2 in.	Hardness Bhn
2024	4.4% Cu	0	27	20	47
	1.5% Mg	T4	68	20	120
	0.6% Mn	T6	69	10	125
	0.5% Si	T3	75	6	135

The effects of aging temperature and time on Al-4% Cu alloy have been found to significantly influence and alter the yield strength of the alloy. In reference to figure 1.1-2, the effect of heat and time on the ultimate yield strength of an Al-4% Cu alloy is described in terms of the formation of non-equilibrium copper precipitates^{Error! Bookmark not defined.} in GP-I and GP-II (*Guinier-Preston*) zones as the alloy is aged. The formation of non-equilibrium GP-I and GP-II and (θ') structure corresponds to the growth of desirable, coherent phase precipitate that grows in size during the initial stages of heat treatment.

The strength of the alloy is observed to increase with aging time as a function of coherent phase accumulation. At 190°C, the alloy is said to undergo *artificial aging* because it has been heated to produce precipitation, as depicted in figure 1.1-2. As the alloy is aged, a dynamic equilibrium is established between the existing coherent non-equilibrium (θ') phase and newly emerging (θ) noncoherent, equilibrium phase. The thermodynamically favored noncoherent, equilibrium phase (θ) begins to precipitate right after the alloy has passed through its strength maximum. However, when the stable noncoherent (θ) precipitates, the strength of the alloy begins to decrease because the alloy has been *overaged*. The (θ) phase still provides dispersion strengthening, but with time the (θ) particles grow larger and less numerous all the while diminishing the strength of the

alloy. Finally, the (θ') phase is dissolved and the strength value of the alloy approaches that of the unalloyed aluminum metal circa 13,000 ~ 20,000 psi.

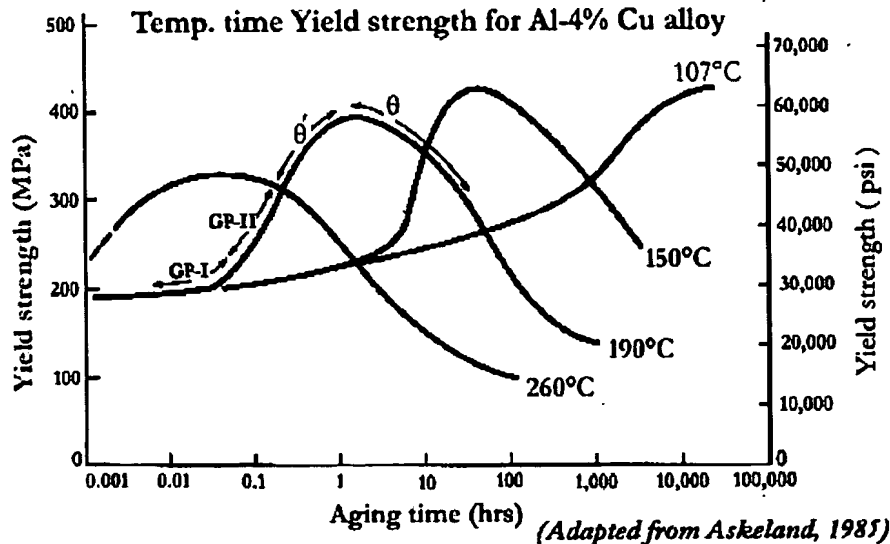


Figure 1.1-2: Effect of aging, temperature and time on yield strength of Al-4% Cu.

The nominal bulk value of copper in Al 2024 T-3 is reported at 4.4 % (w/w)⁶⁵¹ and McDevitt, *et al.*⁶⁵² who reported such results in their assay, but hypothesized that the difference in metallic copper structure at the alloy's interface versus bulk indicated that temperature gradients incurred during heat aging that may cause copper redistribution at surface to occur. Regarding the nature of the copper metal at the surface, Sun, *et al.*⁶⁵³ measured oxidation potential and report a lower oxidation potential of Cu^0 relative to Al^0 which was attributed to Cu^0 enrichment at the metal / oxide interface as a result of slower diffusion of Cu^0 , compared to Al^{3+} through the Al_2O_3 layer at the surface. Therefore Sun, *et al.* concluded that the Cu^0 did not plate out on the surface from Cu^{2+} in solution, and that the amount of Cu^0 enrichment at the interface was a function of the amount of Cu^0 in the alloy. Pocius⁶⁵⁴, in a similar study, speculated that the presence of Cu^0 at the oxide / metal

interface was due to Cu^0 being plated out due to a ($\sim 2\text{eV}$) difference in oxidation potentials of Al^0 and Cu^0 . Furthermore, in their study on chemical etching of AA 2024 T-3, Pocius speculated that Cu^0 undergoes dissolution and reprecipitation during chemical etching and that an oxide layer forms on top of the plated Cu^0 during a rinsing step in which the acidic solution is removed from the surface.^{Error! Bookmark not defined.}

It is widely agreed that the presence of the metallic Cu^0 at the metal/oxide interface is the source of many corrosion resistance problems of AA 2024 T-3. Yet, another problem with the alloy, as a structural material, occurs when it is anodized, copper is dissolved, liberated, and replated as in copper-rich / domains at the alloy's interface. These domains act to further retard the oxidation and repassivation of aluminum.⁶⁵⁵ It has been reported that this enrichment of copper on the alloy surface leads to a dealloying of intermetallic copper particles, with size on average 9-micon clusters, in particular the S-phase ($\text{Al}_2\text{-Cu-Mg}$) that account for ~ 60 percent of the particle population on the alloy surface.⁶⁵⁶ The structure of the AA 2024 T-3 has been reported to be weakened after any kind of dealloying process, and its morphology is described as one of a nano-porous matrix with copper rich remnants left behind in a periphery that is highly susceptible to pitting.⁶⁵⁷

Magnesium is the other significant alloying element reported to be associated with poor adhesive bond durability in AA 2024 T-3.^{658, 659} According to Wefers⁶⁶⁰, Al_2O_3 is stable in the pH range of about 4-to-9, while MgO is not stable in solutions with a $\text{pH} < 10$, implying that the presence of MgO on the Al_2O_3 oxide layer renders the oxide susceptible to moisture attack and depassivation. Weffers⁶⁶¹, further observed that Mg^{2+} segregates at the surface of the alloy following thermal treatment and exists as MgO or Mg(OH)_2 . It is commonly accepted in the literature that Mg^{2+} is detrimental to adhesive bond durability⁶⁶²,

and more recently Critchlow and Brewis⁶⁶³ reported little effect of Mg^{2+} on adhesive joint durability. Overall, the reported results indicate that a more generally accepted phenomenon for the alloy's corrosion susceptibility lies in the presence of enriched copper domains in the alloy's microstructure that in turn act as cathodic sites to initiate corrosion of the aluminum matrix.²⁰ Therefore, surface treatments are the only means available by which to moderate the effects of corrosion on AA 024 T-3.⁶⁶⁴

Appendix 1.2 Coating Systems

The term given to an organic binder is always taken to mean the non-volatile portion that holds the coating on the surface and gives the material its characteristic properties. The mantle of any coating system is always specified by its binder as on one side of the coating the substrate is bound and on the other side the substances in the coating are also bound.³⁴ The binder governs, to a large extent, the properties of the film and conveys information regarding characteristics of toughness, durability, application, cure time and conditions of a given coating. Some specific classes of polymeric binders found in paint and coating vehicles are acrylics, alkyds, oils, latex emulsion, powders, epoxies, urethanes, silicones, etc. Some of the key properties used to characterize polymeric binders used in paint and coating vehicles are:

1. Viscosity: a measure of the liquid resin binder and curing agent's flow properties which determine ease of processing, mixing, or application.
2. Ease of application: required substrate preparation, and relative cure conditions such as temperature or curing agent selection.
3. Low shrinkage: the amount of volume change, stress, or rearrangement that occurs as a function of cure, as most polymeric binders are low molecular weight oligomers that react through functional groups to expel volatile by-products.
5. High adhesive strength and mechanical properties: chemical resistance, electrical

insulation or conduction, and most important adhesion.

6. Glass transition temperature (T_g): which is proportional to its minimum film forming temperature (MMFT) and blocking.

Coatings of any given binder classification may be used as either primers or topcoats for corrosion control of metals. Coating systems for most metals consist of multiple composite layers such as a primer with a topcoat or a tie-coat and they are designed for a particular metal and service environment. Polymeric binders with good adhesion to metal substrates are often used as primer coats to provide good surface adherence for topcoat layers. A liquid applied coating system, primer and topcoat is expected to limit corrosion to less than 1.3 mm / year (50 mpy).⁶⁶⁵ Organic coating systems are classified according to the nature of the polymeric binders which largely governs its overall application, protectiveness, and resistance to degradation.

Appendix 2.1-A

It is well established that paints / coatings with superior adhesion properties provide metallic substrates with a high degree of protection thus significantly extending the lifetime of the structure they service. The overall effectiveness of any formulated protective layer treatment depends directly on several factors, such as application technique, environmental conditions, and mainly the relationship between the metallic substrate and the coating itself. Therefore, of the numerous combinations of materials used to protect metals, organic coatings have often been chosen, simply out of convenience, and due to their ability to be applied as liquids that favorably wet out over a metal's surface, Figure 2.1-1, below. The

wetting by the polymer coating is directly related to the coating's adhesion properties and therefore to its ultimate durability.⁶⁶⁶

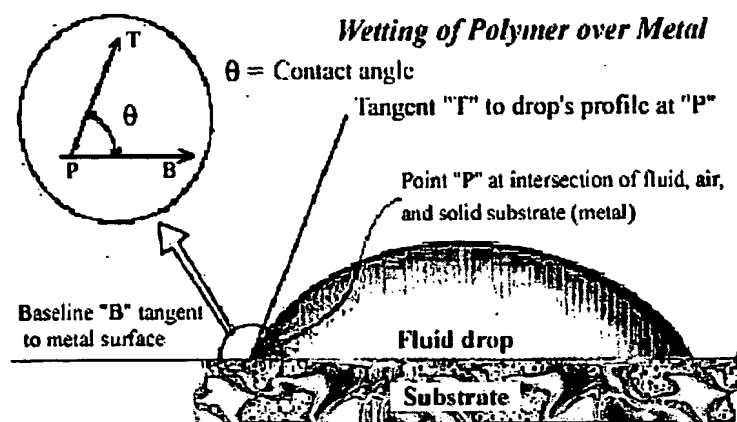


Figure 2.1-1: Wetting out of a fluid polymer over a metallic surface
mechanicalequilibrium at polymer / metal interface according to Young's
equation. Error: Bookmark not defined.

As a result of the wetting process, adhesive and cohesive interactions of polymeric coatings with their substrates evolve resulting in characteristic physicochemical properties that translate into coating performance. Cohesive interactions between polymer molecules and other components of coatings, e.g. pigments, fillers and additives, are factors correlated with the mechanical properties of coatings, such as their hardness, porosity and water permeation resistance. Adhesive interactions, on the other hand, are correlated to the durability and lifetime performance of coatings.⁴³

Most polymeric coating systems devised to protect metal surfaces suffer deficiencies to some extent, and the effectiveness of any organic coating can only be as good as the polymeric material that it is composed of. Polymers, used in liquid organic coating systems, either are, or become amorphous solids whose physical properties change

with time as a result of structural relaxation, according to a phenomenon known as (physical ageing). Coating systems on metal are known to undergo cyclic thermal related loading, to various extents, that are directly proportional to environmentally induced temperature fluctuations. Such environmentally induced temperature changes can affect a coated metal in two ways: 1) by inducing thermal stresses in the coating system, and 2) by causing gradual changes to occur in the coating that affect its viscoelastic mechanical properties.

Initially, the viscoelastic component of a given polymeric coating material has the ability to respond to stress by molecular rearrangement, as related to its glass transition process (T_g). The glass transition temperature is described⁶⁶⁷ as a phase transition process in which spontaneous changes occur in amorphous polymeric materials related to changes in the density, elastic modulus of the polymer, impact strength, fracture energy decreases; creep and stress relaxation rates decrease.⁶⁶⁸ Such changes are known to be a result of non-equilibrium state, in which polymer slowly attempts to reach equilibrium, and on a molecular scale, this phenomenon is connected with spontaneous changes in atomic structure to a lower-energy state.

Temperature and time dependent behavior of polymeric materials subjected to thermal changes are dependent on the conformational changes of the polymer backbone and are related to physical ageing.^{669, 670} Temperature cycling accelerates self-diffusion and additionally accumulates changes in the physical properties of the coating, and this effect in turn results in memory of past cycling.^{671, 672} In the physical aging process, temperature determines both the stress level and the rate of viscoelastic response of a coating subjected to a given stress level. Overall, loss of the coating's ability to relax to induced stress is the

result of physical ageing and chemical degradation. The physical manifestation of such damage due to stress ageing, Figure 2.1-2, below, results in the development of (microcracks) in the coating and eventual rupture of polymeric material and delamination from the metal substrate.^{673, 674}

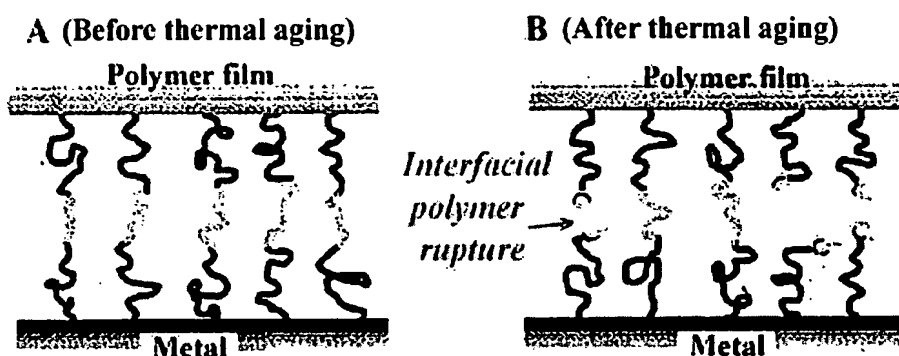


Figure 2.1-2: Manifestation of physical aging at the coating / metal Interface, before (*left*) and afterwards (*right*) thermal ageing.

An example, of such a material property that limits the utility of a protective coating over a metal is the materials coefficient of thermal expansion (CTE). An example of a coating's response to material CTE effects is shown below in Figure 2.1-3, adapted from Funke *et al.*⁴³, illustrating the modes a coating may be subjected to on a substrate while undergoing temperature / stress effects. Materials with low or similar CTEs develop less out of plane stress and are not as prone to failure during thermal cycling. This is due to the fact that induced thermal stresses tend to concentrate at coating / metal interface areas and consequently, significant differences in the coefficients of thermal expansion (CTE), between the coating and substrate develop. (i.e., for an epoxide resin from 45 to $65 \times 10^{-6} \text{ deg}^{-1}$; for alkyds @ 55 - $60 \times 10^{-6} \text{ deg}^{-1}$ and for the metal base: steel @ $16 \times 10^{-6} \text{ deg}^{-1}$, zinc @ $23 \times 10^{-6} \text{ deg}^{-1}$; aluminum @ $23 \times 10^{-6} \text{ deg}^{-1}$.⁶⁷⁵

Therefore, as a result of the coating's ability to sustain and evenly distribute stress response over an interface affects its capability to resist forming and diminishing of induced stresses without mechanical damage to the coating and the coating/metal interface. Consequently, the protective properties of such organic coatings are strongly connected to the existence of a barrier which acts to enhance and preserve adhesion to the substrate and thus forestall deterioration.⁶⁷⁶

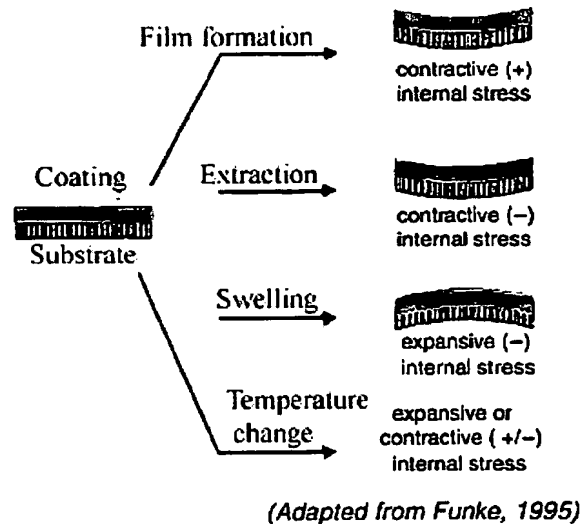


Figure 2.1-3: Development of internal stress (IS) in a coating due to solvent loss or temperature change effects dimensional stability of the substrate. The CTE of the substrate determines the coating's stability response as a function of temperature.

Corrosion of structural metals has historically been moderated by painting, galvanizing or electroplating them with some protective coating layer. The nature of a metal's surface, such as aluminum, when it is exposed to atmospheric conditions containing water, salts, and oxygen causes it to be readily oxidized. Even though aluminum is known to form a protective passive layer, the stability of the resulting passive metal oxide layer can be consumed in both acid and weakly alkaline solutions and even more

dramatically in chloride solutions. The chemical reactions occurring in these solutions usually cause breakdown of the passive film followed by pitting corrosion of Al.

Therefore, the stability of any polymeric coating at a metal-polymer interface depends on the interaction between metal surface and polymer in the presence of water, oxygen and aggressive anions.

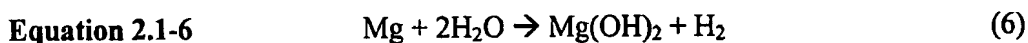
Covering a reactive metal's surface with a coating has long been a way of introducing one or more surface properties. Replacing an air-metal interface with a coating-metal interface serves to greatly reduce corrosion and preserve the metal's mechanical properties.⁶⁷⁷ It has been noted by Funke⁶⁷⁸ that the most important property of a coating, its adhesion to a substrate, is the primary factor associated with corrosion mechanisms (coating failure) and that the adsorption of binder molecules on a molecular scale plays the decisive role in determining the adhesion of a coating to a substrate. It is reported that the wetting and spreading process of a coating over a metallic substrate is strongly influenced by surface features such as geometry-shape or roughness, chemical functionality, and polarity.⁶⁷⁹ In general, the criterion for chemisorption / physisorption processes to occur across an interface requires that an adsorbate, liquid, wet a substrate such as a metal. The creation of such an interface requires that the surface energy of the solid metal be greater than that of the liquid coating. The thermodynamic work of adhesion (W_A) between the solid metal and its liquid coating can be expressed as Equ. 2.1-1:

Equation 2.1-1
$$W_A = \gamma_s + \gamma_L - \gamma_{SL}, \quad (1)$$

where γ_s is the surface energy of the solid, γ_L is the surface energy of the liquid, and γ_{SL} is the solid / liquid interfacial tension.⁶⁸⁰

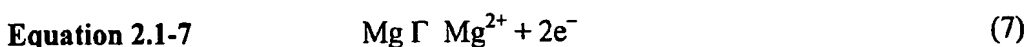
For organic coatings, the most common failure mode reported is due to the diffusion and adsorption of water at the metal-polymer interface, where water molecules break the adhesive bond between metal and the polymer.^{681, 682, 683} The mechanistic scheme involves water diffusing through the coating and adsorbing at the metal interface, creating an electrolyte for the reduction of oxygen or other reductive processes to occur, whereby the metal is oxidized with a concomitant establishment of anodic and cathodic domains. As a further result of this oxidation process the metal becomes undercut causing the polymeric coating to yield and disbond, leaving even more of the metal surface exposed to corrosion. At this point, the corrosion process becomes causal and continues on until finally the coating fails.

The general sequence of the corrosion reactions are follows:

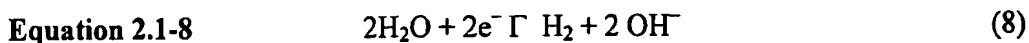


(Overall reaction)

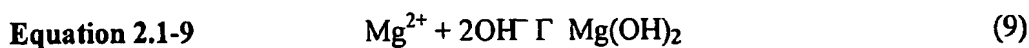
This overall reaction may be expressed as the sum of the following partial reactions:



(Anodic reaction)



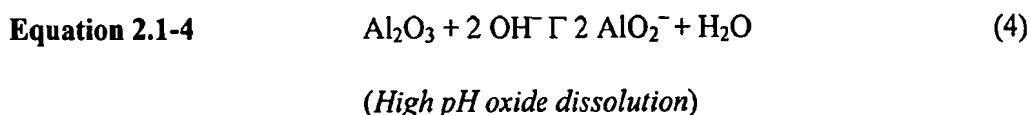
(Cathodic reaction)



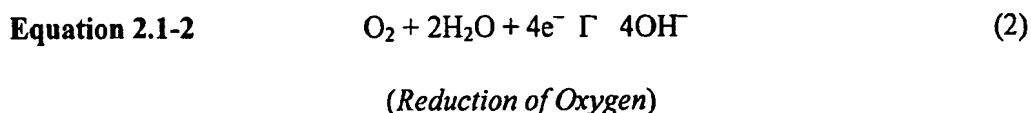
(Product formation)

According to the general reaction for magnesium in water, as given in Equ. 2.1-9, $\text{Mg}(\text{OH})_2$ is formed from available hydroxyls in electrolyte solution according to the

cathodic reaction accompanying the anodic dissolution of Mg Equ. 2.1-7. So long as there is sufficient magnesium metal present the destruction of Al native oxide reaction, Equ. 2.1-4, below, is not energetically favored. Given Mg metal's higher standard electromotive force, the reduction potential of Mg metal at -2.36 V vs SHE would favor the anodic reaction, Equ. 2.1-7 and the liberation of Mg^{2+} into the electrolyte solution.



The corollary to these observations is that the presence of magnesium metal effectively reduces the concentration of solution hydroxyl from the reduction of O_2 , Equ. 2.1-2, below.



Since cathodic disbonding is generally implicated to the build up of hydroxide at the Al coating interface, the reaction with Mg metal, Equ. 2.1-6, above, may therefore decrease the rate of disbonding as hydroxide will first appear on the surface of the pigmentary Mg metal as opposed to at the Al coating interface, thus preserving the metals passive native oxide Al_2O_3 layer.

Appendix 2.2 Adhesion

There are numerous theories to explain the adhesion of polymeric materials to inorganic surfaces, but the generalities of the mechanisms all relate to a set collective of parameters separated into various components contributing to the thermodynamic work of adhesion (W_A).⁶⁸⁴ Fowkes⁶⁸⁵ and Brokman *et al.*⁶⁸⁶, proposed a separation in according to:

London dispersion force (d), hydrogen-bonding force (h), acid-base force (ab), dipole-dipole forces (dd), and induced dipole forces (i).

Equation 2.2-1
$$W_A = W_A^d + W_A^h + W_A^{ab} + W_A^{dd} + W_A^i \quad (1)$$

Poor wetting of polymers is usually attributed to unfavorable thermodynamic conditions between surface energies of adhesive and substrate, or because there was insufficient time for equilibrium to be established before the polymer set. According to Packham⁶⁸⁷ the manifestation of poor adhesion is likely to be the result of a reduced area of contact and because of stress concentrations associated with interfacial voids. In terms of Equ. 2.2-1, above, W_A is low (part of the interface is air) and for thermodynamic or kinetic reasons poor penetration of adhesive into the interstices of the surface may result. ^{Error!}

^{Bookmark not defined.} If wetting is complete, adsorption of the adhesive is considered to occur whether the surface is smooth or rough, but poor adhesion may result from low work of adhesion, a result of low surface energy. According to Bell *et al.*⁶⁸⁸, adhesion may be enhanced by surface treatments some of which increase the surface energy and thence W_A . In addition according to Packham^{Error! Bookmark not defined.}, the treatment that raises W_A may be one that essentially alters the chemical groups in a smooth surface (although some topographical change will usually accompany it), or it may drastically alter the topography of the surface (although some chemical change will usually accompany it).

Practically all adhesion models can be grouped into one of the four major adhesion theories that have developed: 1) mechanical interlocking theory^{689, 690}, according to the mechanical interlock theory, the physical interlocking (mechanical keying) between the adhesive and the adherend surface is primarily responsible for adhesion; 2) adsorption

theory^{691, 692, 693}, according to the adsorption theory, the formation of primary and / or secondary bonds (molecular level forces) between two interacting surfaces is primarily responsible for adhesion; 3) diffusion theory^{694, 695} according to the inter-diffusion theory, polymer segments or chains between the two polymers at the interface is responsible for adhesion, and 4) electronic theory^{696, 697} according to the electronic theory, the adhesion between two different materials is due to the differences in their electronic band structure.

Overall, the most significant contribution to the development of modern adhesion theories is considered to be the classic paper⁶⁹⁸ 'On adhesives and adhesive action' published by McBain and Hopkins in 1925.^{Error! Bookmark not defined.} The paper claimed to be the first systematic study of the action of adhesives and elucidated the concept of 'mechanical adhesion'. McBain and Hopkins resolved that there were two kinds of adhesion, *mechanical* and *specific*. As described the authors, specific adhesion involved 'some species of interaction' between the smooth non-porous surface and the adhesive. The interpretation of this interaction was speculated to be either chemical or adsorption by plain wetting. The specific adhesion regime has since been developed into a model that can be described in terms of an adsorption theory. In contrast, mechanical adhesion was considered possible only with porous materials, and it occurred whenever any liquid material solidifies *in situ* to form a solid film in the pores. McBain and Hopkins^{Error! Bookmark not defined.}, further distinguished adhesion to porous surfaces from adhesion to surfaces which were merely rough. Roughness, they reported as having little influence on adhesion, "provided that the roughening has been carried out without pitting the surfaces appreciably", and that if metal surfaces were "rather deeply furrowed" the joints were found to be weaker than those obtained with smooth surfaces. Their conclusion was that

the observed reduction in adhesion was the result of either an increase in average adhesive film thickness, or an insufficient quantity of adhesive to bridge the gap between surfaces. Error! Bookmark not defined.

In 1969 Packham⁶⁹⁹, demonstrated the importance of pore structure in the adhesion of polyethylene to anodized aluminium by demonstrating that the polymer entered and penetrated pores on an anodized aluminum surface. In a similar study, Arrowsmith⁷⁰⁰, worked with electroformed copper and nickel, and asserted that mechanical adhesion was 'the main mechanism of adhesion of these surfaces to epoxide laminates.' Since then, some of the most significant research work has been carried out in the United States, for example, by Boeing^{701, 702} whose results on adhesion development have since prompted the company to adopt a standard phosphoric acid anodizing pretreatment for treating structural bonding of aluminum⁷⁰³. Further significant work was contributed by Venables⁷⁰⁴ and his colleagues at the Martin Marietta Laboratories who, from the mid-1970's, undertook a study of the influence of pretreatment variables on the structure and adhesion properties of film formation.^{705, 706} The general results of this work illustrate that strong bonds, and specifically bonds of high durability, tend to be associated with a highly porous surface oxides, providing that the values of viscosity and surface tension of the liquid polymer allows penetration into the pores.⁷⁰⁷

Porosity was again brought to light in a 1984 review by Venables⁷⁰⁸ who concluded that 'certain....pretreatment processes produce oxide films on metal surfaces which, because of their porosity and microscopic roughness, mechanically interlock with the polymer forming much stronger bonds than if the surface were smooth'. In addition, he stated, that for aluminum and titanium 'certain etching or anodization pretreatment processes produce

oxide films on the metal surfaces, which because of their porosity and microscopic roughness, mechanically interlock with the polymer forming much stronger bonds than if the surface were smooth'. In summation, the 'mechanical theory' has been accepted within the scope of general adhesion theories^{709,710,711} even though there is still no satisfactory universal adhesion model to explain adhesion properties of polymer coatings involving different combinations of metal substrates and coatings exposed to various environments.

2.2-2 Adhesion of Coating to Metals

Adhesive strength⁷¹², commonly expressed as the force needed in energy per unit area, to pull the coating away from the substrate, is the sum total of several components, according to Equ. 2.2-1. The "surface energy" expression, according to Fowkes⁷¹³, is widely recognized as the thermodynamic work of adhesion W_a or of cohesion W_c , depending on whether fracture occurs at the interface or cohesively within one phase.⁷¹⁴ The relationship between the forces acting at the interface between the bonded phases (polymeric matrix / metal) and, reflects the properties of the interfacial region and, the adhesive attachment between coating and metal surface.⁷¹⁵ This interdependent relationship has been expressed in simple mathematical form by Good⁷¹⁶ when he applied the Griffith-Irwin theory of fracture to a joint comprising a bond between two phases. The fracture stress, S_f , is given by

$$\text{Equation 2.2-2} \quad S_f = k(EG/l)^{1/2} \quad (2)$$

where k is a constant, l is the length of the critical crack which leads to fracture and E is the modulus and G the fracture energy.^{717,718} The value of the modulus in the Griffith theory determines the amount of elastically stored energy at a given strain. It is this stored energy

that is ultimately released, providing the fracture energy, G when fracture occurs. It should be noted that both of these parameters originate from within the adhesive joint, E and G are both semi-empirical properties.⁷¹⁹ Ultimate fracture, leading to delamination between polymer and metal occurs where the term EG/l is lowest, whether at or near the interface or solely within one of the bulk phases. Factors that alter E or G or l locally at the interface may alter its strength and other properties accordingly. Aside from the influence of interfacial forces on adhesion performance of an adhesive bond, another important factor is the consequence of the interface attributed to the bulk phases and the interactions between interface and bulk phases joined.⁷²⁰

The fracture energy^{Error! Bookmark not defined.} “ G ” contains a term associated with the energy required for bond breaking at the interface when the adhesive bonding fails. These may be primary or secondary bonds. As a result, a surface energy term must be added a term ‘ y ’ representing other energy absorbing processes - for example plastic deformation that occurs during fracture:

$$\text{Equation 2.2-3} \quad G = W_a \text{ (or } W_c) + y \quad (3)$$

where the fracture energy G contains the term associated with the energy required for bond breaking at the interface when the adhesive bond fails. It is this stored energy that is released, that provides the fracture energy, G when fracture occurs. These may be primary or secondary bonds. Usually ‘ y ’ is very much larger than W_a (or W_c), which is why practical fracture energies for adhesive joints are almost always reported to be orders of magnitude greater than works of adhesion or cohesion.^{Error! Bookmark not defined., 721}

Overall, it is widely agreed that the major contribution to adhesion are from mechanical, polar-polar, and chemical adhesion components. Since one of the key steps in

improving long-term performance of coatings is to ensure that the coating stays on the substrate, therefore, every available method to increase the adhesive strength is explored.

Appendix 2.3

Appendix 2.3-1 Impurities at the Metal Surface

It is well known that the presence of specific chemical species, such as, phosphates, magnesium, copper and fluoride ions in the oxide coatings can detrimentally influence the stability of the aluminum oxide film in various environments.^{722,723,724} According to Packham *et. al.* Error! Bookmark not defined., the presence of phosphate ions in oxide coatings inhibits or delays hydration of oxide films of aluminum alloys when exposed to water or moisture, thus preventing the formation of a mechanically weak hydrated oxide coating on the surface. The resulting hydrated oxide film adheres poorly to the metal alloy and thus becomes a weak link in the adhesively bonded joint. Similarly, compared to the bulk of the alloy, a lower aluminum-to-magnesium ratio in the oxide coating (presence of a relatively higher concentration of magnesium ions in the oxide coatings) of an aluminum alloy results in poor joint durability.Error! Bookmark not defined. The presence of small amounts of chloride (Cl⁻) and/or fluoride (F⁻) ions in the anodization solution or etch solution decreases the height and roughness of the aluminum oxide coating.⁷²⁵ The overall decrease in the micro-roughness of the aluminum oxide coating is said to lead to the poor joint performance in a hot-humid environment as well.Error! Bookmark not defined.

2.3-4 Chemical and Physical-Chemical Treatments

Surface pretreatments for metal surfaces are usually classified into four major groups: 1) mechanical treatment; 2) chemical treatment; 3) electrochemical treatment, and

4) plasma treatment. These surface treatments either remove material from the surfaces to be treated or alter their chemical composition. Either of these effects, surface removal or chemical alteration are thought to be important in the development of corrosion resistant coatings systems. Generally, treatments that remove material, that are either organic in nature by *degreasing* or inorganic nature by *chemical pickling* are sometimes the only treatment applied in the preparation of metallic surfaces for coatings.⁷²⁶ Moreover, treatments that alter the chemical composition of the surface are known as conversion films that are protective in themselves, as is the case of the anodizing of aluminum⁷²⁷, or conversion films on metallic surfaces that contribute to increasing coating adhesion (as is the case of phosphating⁷²⁸ and passivation.⁷²⁹

2.3-5 Mechanical Cleaning

In this method, the adherend surface is mechanically roughened to remove surface contamination and to increase the macro-roughness of the adherend surface. The removal of surface contaminants helps in preparing the surface for any additional surface pretreatments that may be necessary for any specific applications. Thus, mechanical cleaning is usually the first step involved in any surface pretreatment of an adherend surface. Mechanical cleaning involves scrubbing the substrate surface with wire brushes and/or sandpaper and/or scouring materials like Scotch-Brite. (3M company). Mechanical cleaning via grit blasting the adherend surface with high speed particles, such as alumina and silica, produces a desirable macro-rough surface morphology.

2.3-6 Acid Etchants

Sulfuric acid, nitric-hydrofluoric acid mixtures and hydrochloric-orthophosphoric acid mixtures are some of the common acid pretreatments for titanium alloys.⁷³⁰ Compared to chromic acid anodization or phosphoric acid anodization, the acid etching, by itself, does not provide superior bondable surfaces. When acid etching is used as a surface pretreatment, the acid dissolves the contaminated natural oxide layers on the adherend surface and replaces the natural oxide with a new bondable oxide coating. Therefore, though acid etching may not be a good surface pretreatment by itself, acid etching forms a very important intermediate step in surface pretreatment processes.

One of the major problems associated with acid treatments is hydrogen pick up by the adherend material, which can cause embrittlement of the metal. To minimize hydrogen pick-up a special nitric-hydrofluoric acid mixture having 3% (v/v) hydrofluoric acid (47% HF) and 15% (v/v) nitric acid (Concentrated HNO_3) is used as an etching solution.⁷³¹ Ko and Wightman⁷³² demonstrated the effectiveness of anodizing aluminum-lithium alloys in either sulphuric acid or phosphoric acid. In their studies a porous surface oxide was produced into which a polysulphone adhesive was applied and penetrated yielding a 'mechanical means of adhesion'. They concluded that the bonds obtained in the porous medium were much more durable in high humidity than comparable ones made to surfaces without this high porosity. In addition, and most important, their results bore out that the pore structure of anodized aluminum was on the order of tens of nanometers in diameter, and that polymeric adhesive did actually enter into them. Since then, these results have been corroborated by various studies using electron microscopy and surface analysis techniques^{733, 734, 735} backed up by theoretical calculations on idealized models^{736, 737} that show how polymeric adhesives and primers do often penetrate microporous surface layers.

However, according to Packham⁷³⁸, the type of surface treatment has an effect and even though some polymers are able to enter the pores produced on aluminum by sulphuric acid anodizing, they are much finer than those from anodizing in phosphoric acid⁷³⁹. In a similar study, Arrowsmith and Clifford⁷⁴⁰ demonstrated that a controlled etch in phosphoric acid after anodizing in either sulphuric acid or chromic acid results in improved bond strength and durability of adhesively bonded aluminum compared with standard etching and anodizing treatments. Digby and Packham⁷⁴¹ found that the durability of bonds to phosphoric acid anodized aluminum could also be improved by controlled exposure to phosphoric acid after anodizing Figure 2.3-1, below, that shows the more open structure of the surface after such a treatment.

Appendix 2.3-2

According to Alwitt⁷⁴², the growth of oxyhydroxide and hydroxide scales occurs in three stages: 1) an induction period (of minutes to hours depending on temperature) depending on temperature during which no film growth occurs; 2) a period of rapid growth in which a pseudoboehmite (AlOOH) layer forms and grows to several microns in thickness; 3) a period of slower growth when $\text{Al}(\text{OH})_3$ grows on top of the pseudoboehmite. Formation of boehmite film on aluminum has been studied extensively as depicted in Figure 2.3-4.^{743,744,745}

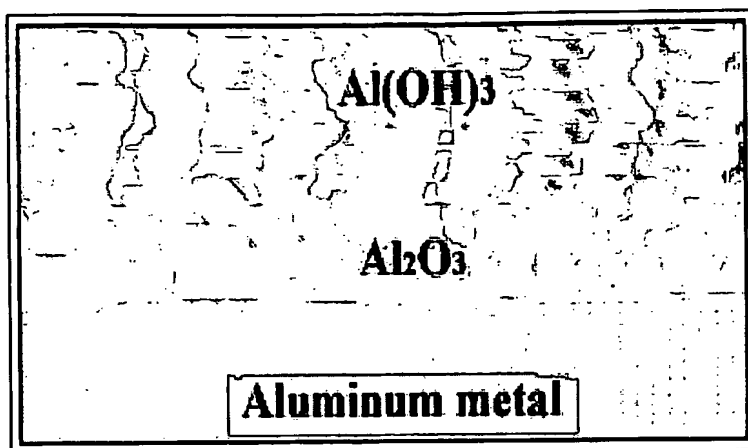
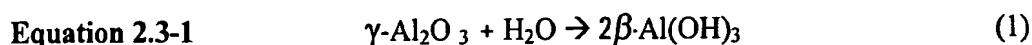


Figure 2.3-4: Al metal surface with Al_2O_3 , and $\text{Al}(\text{OH})_3$ layers.

Lefevre *et al.*^{Error! Bookmark not defined.}, discuss hydration of $\gamma\text{-Al}_2\text{O}_3$ in water and conclude that the change in the surface properties of γ -alumina during the hydration process can be explained by the superficial hydroxylation and the formation of a new phase according to a reaction such as:



In addition, Lefevre *et al.*^{Error! Bookmark not defined.}, also assert that the phenomenon that takes place during this step is not a simple hydroxylation (i.e., transformation of Al-O-Al bridges into Al-OH groups) of the anhydrous oxide surface. To help to understand the real behavior of $\gamma\text{-Al}_2\text{O}_3$ in water, its stability can be calculated from the thermodynamic constants of some chosen aluminum oxyhydroxides Table 2.3-1, below. Nordstrandite ($\gamma\text{-Al}(\text{OH})_3$), see Table 2.3-2, below, was not considered, due to its scarcer occurrence. The calculated free energies of hydration reactions of γ -alumina in water leading to the formation of bayerite, gibbsite, and boehmite are listed in Table 2.3-1 below. It has been shown in previous works^{746,747,748} that bayerite and boehmite can be identified in aged $\gamma\text{-Al}_2\text{O}_3$ suspensions.

These observations are consistent with the negative free energies found for reactions leading to these products. Gibbsite was not identified in aged suspensions, whereas its formation is possible according to the thermodynamical results which can be explained by the formation of the kinetic $\text{Al}(\text{OH})_3$ polymorph, as observed in the precipitation of bayerite from aluminate solutions⁷⁴⁹ or in the aging of amorphous alumina gels.⁷⁵⁰

Table 2.3-1: Thermodynamic properties of aluminas

species	paramineralogical name	$\Delta G_{298^\circ\text{K}}$ (kJ/mol)	reference
$\gamma\text{-Al}_2\text{O}_3(\text{s})$	γ -alumina	- 1564.2	751
$\gamma\text{-AlOOH}(\text{s})$	boehmite	-917.8	752
$\beta\text{-Al}(\text{OH})_3(\text{s})$	bayerite	-1149.8	64
$\alpha\text{-Al}(\text{OH})_3(\text{s})$	gibbsite	-1154.9	64
$\text{H}_2\text{O}(\text{g})$		-228.6	753
$\text{H}_2\text{O}(\text{l})$		-237.1	Error!
Bookmark not defined.			

Table 2.3-2: Characteristics of alumina gels.⁷⁵⁴

(pH)	Temperature and processing duration	paramineralogical name
~ 12	long reaction time, ambient temp.	gibbsite
> 10	occurs in presence of amine	nordstrandite
~ 5 – 6	ambient temp.	gibbsite (microcrystalline)
< 8	up to 80°C	pseudoboehmite
~ 4 – 6	temp > 100°C	boehmite (tabular)
~ 4	temp > 100°C	boehmite (acicular)

Appendix 2.2-3

Affrosman *et al.*⁷⁵⁵, investigated acid-base interactions, Table 2.3-3, below, of epoxy-amine systems with Lewis acid sites on aluminum oxide surfaces and concluded that

surface hydroxyl groups reacted with hydroxyls in the epoxy to form alkoxide linkages to the surface.

Table 2.3-3

Acid / Base forces

- Lewis acid-base bonds (also described as electron donor-acceptor bonds)
- A Lewis acid accepts a pair of electrons to form a covalent bond
- $A + B \rightleftharpoons A:B$ (reversible)
- Forces act over short range ($< 3 \text{ \AA}$) (force is a strong function of distance)
- Hydrogen bonding is an example, but not only type possible

(Adapted from Woodward⁷⁵⁶, 2000)

McCafferty⁷⁵⁷, investigated adhesive properties of various polymer films on metal oxide films through contact angle and maximum peel-off / pull-off force measurements and attributed energies of attraction to Lewis acid-Lewis base interactions between polymer and metal oxide surfaces above and below the metal oxide's IEP. According to McCafferty, at pH s above and below the metal oxide's IEP, as depicted in Figure 2.3-5, A and B, the water molecule interacts by ion-dipole interactions, and the interaction energy E is given by Equ. 2.3-2:

Equation 2.3-2
$$E \propto \frac{1}{r^2} \quad (\text{ion-dipole interaction}), \quad (2)$$

where r is defined as the distance of approach of the ion to the dipole moment⁷⁵⁸, and the work of adhesion W_{adh} or energy of attraction is given by Equ. 2.3-3 Young-Dupré equation:

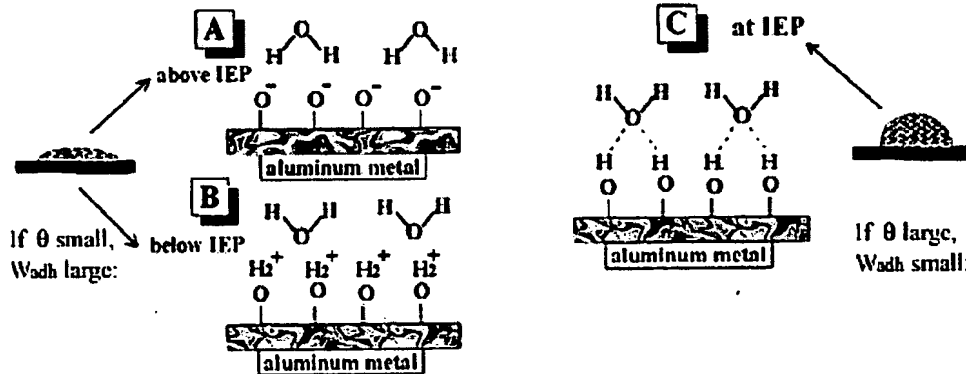
Equation 2.3-3
$$W_{adh} = \gamma_L (1 + \cos \theta), \quad (3)$$

where γ_L is the liquid surface tension.

Conversely, at a pH value corresponding to the IEP, Figure 2.3-5, (C) the energy of interaction E between water and surface hydroxyls is viewed as a dipole-dipole interaction given by Equ. 2.3-4:

$$\text{Equation 2.3-4} \quad E \propto \frac{1}{r^3} \quad (\text{dipole-dipole interaction}) \quad (4)$$

Therefore, it follows that the energy of attraction is highest (below and above the isoelectric point) as $\cos \theta$ and the W_{adh} both attain their highest values. While the attraction energy is lowest when $\cos \theta$ and the W_{adh} both attain their lowest values.



Adapted from McCafferty (2002)

Figure 2.3-5: Schematic interaction of water molecules with an oxide film: above **A**, below **B**, and at **C** the isoelectric point (IEP) of the oxide according to Young-Dupré equation.

McCafferty^{Error! Bookmark not defined.} investigated adhesion of polymers to metal surfaces considering the Lewis base-Lewis acid relationship to oxide IEP, and concluded that Lewis acid-Lewis base properties of oxide films on polymer-metal surfaces were

strongly influenced by the metal oxide's IEP and that "basic" polymers such as poly(methyl methacrylate) had the greatest (pull-off force)⁷⁵⁹ adhesion to an acidic film below the oxide's IEP; while as for "acidic" polymer or pressure sensitive adhesive films, such as (Scotch 610 Magic Tape[®]) adhesion was greatest on basic oxide films above the metal oxide's IEP.

1. acidic polymer and metal hydroxide (above IEP):



2. basic polymer and metal hydroxide (below IEP):

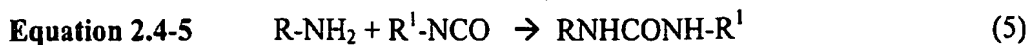


where R = organofunctional polymer chain

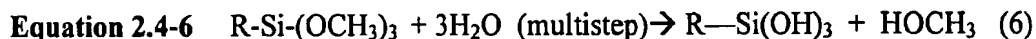
A simple analytic technique was devised by Drago⁷⁶⁰ to determine heats of acid-base complexation from IR frequency shifts of carbonyl complexes C=O. From these studies Fowkes *et al.*⁷⁶¹, combined a calorimetric analysis to conclude that the acid-base contributions to polymer adhesion were proportional to the heats of such acid-base interactions. Thus, providing a convenient means by which polymer adhesion to metal oxide surfaces might be determined spectroscopically.

Appendix 2.4-1

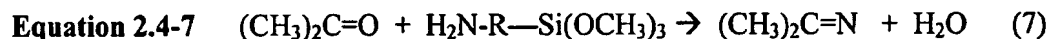
Chemical reactions between organofunction silanes and some component of a polymeric coating polymer is expected to occur between a N-beta-aminoethylaminopropyl-trimethoxysilane (A-1120): $\text{NH}_2(\text{CH}_2)_2 \text{NH}(\text{CH}_2)_3\text{Si}(\text{CH}_3)_3$ where $\text{R} \approx [(\text{CH}_2)_2 \text{NH}(\text{CH}_2)_3\text{Si}(\text{CH}_3)_3]$, and a substituted isocyanate group to form initially a substituted urea, as depicted in Equ. 2.4-5, below:



and then further react with another isocyanate group to form a biuret.^{762,763} Alkoxy silanes can hydrolyze in a multi-step process with water to form silane triols:⁷⁶⁴



Silane triols can condense readily to form higher molecular weight complex oligomers and lose their ability to act as adhesion promoters in the presence of water. Silanes such as γ -aminopropyltrimethoxy silane will react with solvents like methyl ethyl ketone (MEK) to form the ketimine plus water according to the reaction:



The extent of internal chelation / cyclization is another factor that influences these reactions and is strongly dependent on pH and therefore coupling to the metal oxide surface can only occur under conditions favoring hydrolysis. For example, above pH~9 alumina (Al_2O_3) is just above its IEP of (9.2) and substrate surfaces are rich in silanol anions. If the organic moiety is made to be a cationic group, such as a quaternary amine, the silane will orient with the silanol anions on the substrate followed by hydrolysis of the alkoxy groups. As depicted in Figure 2.4-5, below, it is the initial silanol anion rich anionic substrate that is exploited for deposition of silane coupling agents.¹⁵⁶

Van Ooij *et al.*⁷⁶⁵, studied adsorption of aminosilane coupling agents, such as γ -APS, on aluminum surfaces and found that they tend to adsorb onto metal surfaces with an inverted orientation and therefore three kinds of reactions have been shown to be found.

Figure 2.4-6, (a) and (b) shows how based upon orientation, the coating yields poor adhesion to metal resulting in poor paint adhesion and marginal corrosion protection.⁷⁶⁶

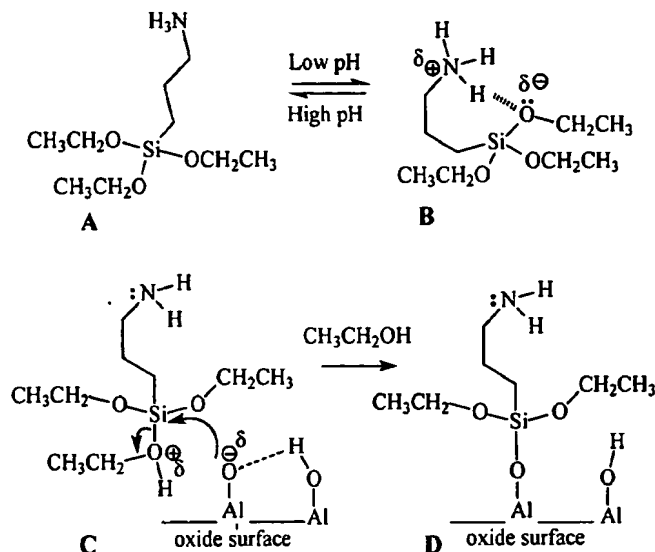


Figure 2.4-5: Interaction and formation of alkoxide bond to basic Al oxide surface at $\sim \text{pH} > 7$ with acidified (γ -APS).

The commonly used silane coupling agents described in these studies have the structure $\text{R}'(\text{CH}_2)_n \text{Si}(\text{OR})_3$, where R' represents an organofunctional group such as amine, epoxy, or mercapto, Table 2.4-1, previous, and R represents a hydrolysable group such as methoxy or ethoxy.

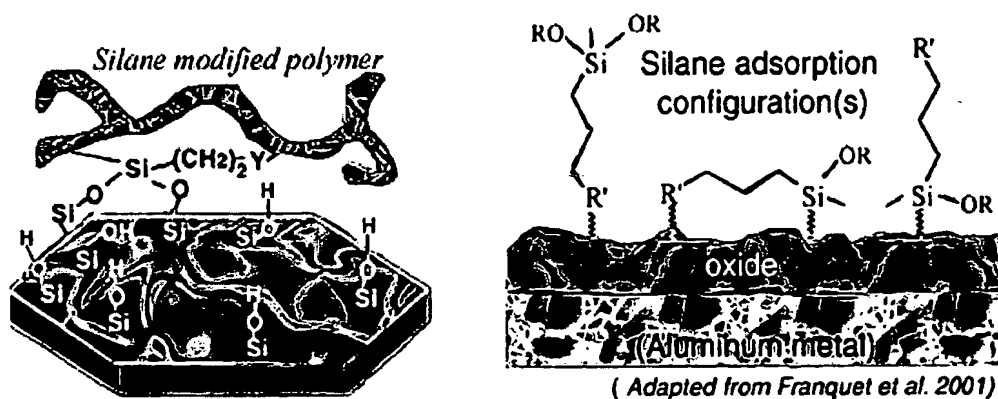
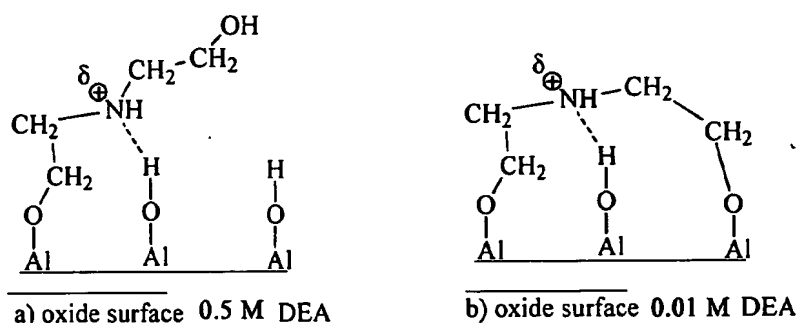


Figure 2.4-6: (a) and (b). (a) Model of possible adsorption of silane molecules on metallic surfaces. (b) surface bonding via the functional group R' ; surface bonding via the

functional and condensed silanol groups; surface bonding via the interaction between the condensed silanol group and the metallic surface.

As an example of surface bonding through functional groups, Affrosman *et al.*⁷⁶⁷ proposed the functional group interaction of DEA (diethanolamine) with an aluminum oxide surface as follows. The alcohol moieties of the molecule, Figure 2.2.6 (b) interact forming an alkoxy linkage whereas the amine side of the molecule interacts with aluminum atom via a donor-acceptor interaction or Lewis- acid-base interaction. The various conformations Figures 2.4-7 (a) and (b), below, are due to concentration differences of DEA.



Adapted from Affrossman et al. (2000)

Figure 2.4-7: (a) and (b), DEA adsorption concentration dependence;
(a) higher DEA conc. at (0.5M) and (b) lower DEA conc. at (0.01M).

According to van Ooij, *et al.*⁷⁶⁸, single step application techniques of silanes to

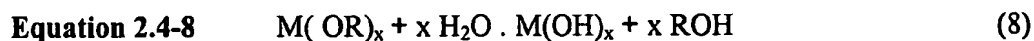
metals such as steel and aluminum lead to the presence of such unfavorable bonding interactions, as depicted in Figure 2.4-7, yielding less than maximum interfacial adhesion of paint on a metallic surface. As a result, Van Ooij, *et al.*²⁴, have recently devised a two-step application procedure which involves sequential application and rinses with non-functional silane, such as BTSE (*bis*-1,2-(triethoxysilyl)ethane), coated on metal, and then the choice of functional silane is applied in the second step.⁷⁶⁹ It has also been proposed that the non-functional silane, BTSE is a stronger acid than the organofunctional silanes

which allows it to instantaneously form covalent, hydrolysis resistant bonds with basic hydroxyl groups over the oxidized metal surface. In addition, the BTSE molecule possesses six labile silanol groups that can form covalent bonds with the surface, leaving the remainder available for silanol groups from the secondary step off the process where the organofunctional silane group is introduced for interaction with the primer coating.⁷⁷⁰ Non-functional silanes are similar to functional silanes in structure, except that they have hydrolysable Si-O-C bonds on both ends of the carbon chain and are otherwise known as cross-linking agents.⁷⁷¹

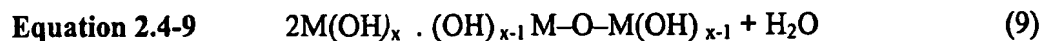
Appendix 2.4-2 Sol-gel

The sol-gel process typically involves metal alkoxides since the reaction chemistry can be easily controlled using a three step process: 1) partial hydrolysis of metal oxide to form reactive monomers; 2) the polycondensation of these monomers to form colloid-like oligomers (sol formation); 3) additional hydrolysis to promote polymerization and crosslinking of a 3-dimensional matrix (gel formation):

Monomer formation or hydrolysis :



Sol formation or polycondensation :



Sols and gels can also be obtained by controlled precipitation from soluble salts. A number of examples are given in a review by Livage *et al.*⁷⁷² In addition, a wide variety of

structures have been reported by forced hydrolysis of metal ions under carefully controlled reaction conditions by Matijevic.⁷⁷³

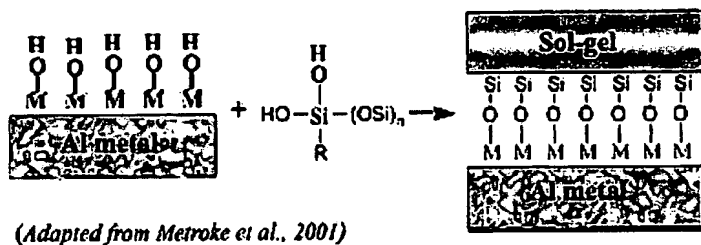


Figure 2.4-8: Hypothetical schematic of sol-gel coating applied to a metal Al-alloy surface.

Organically modified sol-gel coatings can be categorized into two major groups based on the type of organoalkoxysilane used: 1) non-functional organoalkoxysilanes; 2) organofunctional alkoxysilanes. Typical examples of group 1) are organotri- and diorganodialkoxysilanes such as $\text{CH}_3\text{-Si(OR)}_3$ and $(\text{CH}_3)_2\text{Si(OR)}_2$ ($\text{R} = \text{CH}_3, \text{C}_2\text{H}_5$), respectively. Organofunctional alkoxysilanes of group 2) are mostly acrylic, methacrylic or epoxy functional organosilanes.

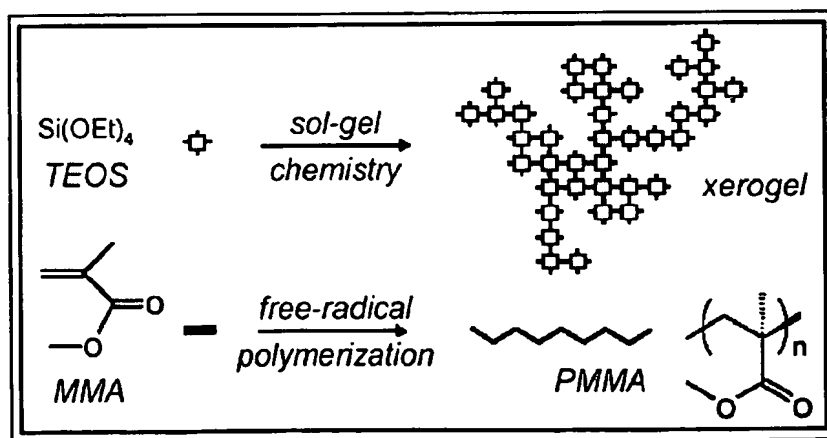


Figure 2.4-9: CERAMER scheme. (Adapted from Etienne Duguet

Document made available under the Patent Cooperation Treaty (PCT)

International application number: PCT/US04/033089

International filing date: 07 October 2004 (07.10.2004)

Document type: Certified copy of priority document

Document details: Country/Office: US
Number: 60/519,681
Filing date: 13 November 2003 (13.11.2003)

Date of receipt at the International Bureau: 17 December 2004 (17.12.2004)

Remark: Priority document submitted or transmitted to the International Bureau in compliance with Rule 17.1(a) or (b)



World Intellectual Property Organization (WIPO) - Geneva, Switzerland
Organisation Mondiale de la Propriété Intellectuelle (OMPI) - Genève, Suisse

**This Page is Inserted by IFW Indexing and Scanning
Operations and is not part of the Official Record.**

BEST AVAILABLE IMAGES

Defective images within this document are accurate representations of the original documents submitted by the applicant.

Defects in the images include but are not limited to the items checked:

- ☐ **BLACK BORDERS**
- ☐ **IMAGE CUT OFF AT TOP, BOTTOM OR SIDES**
- ☐ **FADED TEXT OR DRAWING**
- ☐ **BLURRED OR ILLEGIBLE TEXT OR DRAWING**
- ☐ **SKEWED/SLANTED IMAGES**
- ☐ **COLOR OR BLACK AND WHITE PHOTOGRAPHS**
- ☐ **GRAY SCALE DOCUMENTS**
- ☐ **LINES OR MARKS ON ORIGINAL DOCUMENT**
- ☐ **REFERENCE(S) OR EXHIBIT(S) SUBMITTED ARE POOR QUALITY**
- ☐ **OTHER: _____**

IMAGES ARE BEST AVAILABLE COPY.

As rescanning these documents will not correct the image problems checked, please do not report these problems to the IFW Image Problem Mailbox.